



AM ESGCO 2016 *AM*
biological oscillations

Programme and abstracts

April 10th-14th 2016
Lancaster, UK



Contents

- 1 Foreword** **2**

- 2 Programme** **4**

- 3 Abstracts** **26**
 - 3.1 Keynote invited talks 26
 - 3.2 Special talks 32
 - 3.3 Oral presentations 35
 - 3.4 Poster presentations 224

- 4 List of Participants** **314**

1 Foreword

The abstracts that follow include all of the presentations to be made at the Conference, both orally and as posters. Within each category, the abstracts are ordered alphabetically by surname of the expected presenter.

The ESGCO series of conferences was initiated through investigations of the reasons for the variability in the heart rhythm, including consideration of oscillations at the cellular level. The physics of complex and nonlinear systems was soon shown to be essential. A huge amount of work has been completed, showing that this variability is usually a signature of health and that it is affected by many different diseases and in other states of the body such as ageing or anaesthesia. Only recently, however, has it come to be appreciated and generally accepted that the variability can best be understood and interpreted by considering the whole circulatory system as an entity – including the cells as “end users” and their metabolism – and that the heart can be perceived as a highly intelligent pump that is able to adapt continuously to the needs of the cells. The connections between cardiovascular and brain oscillations are at the cutting edge of current research in the area.

We hardly need to convince ESGCO participants of the importance of the subject area, but it is nonetheless worth emphasising that biological oscillations occur on all scales, from cellular up to organs, organisms and whole populations. They are of *fundamental* importance for scientific understanding. It has also become apparent that cardiovascular oscillations share the same kinds of problems and opportunities as apply to all other forms of biological oscillation and that, often, the same data analysis methods can be applied to all. Hence our decision formally to widen the scope of the meeting to encompass biological oscillations quite generally, on all scales of length, time and complexity.

Consideration of oscillations means that we are encompassing dynamics, in contrast to the traditional emphases on structure and stationary states. At the same time, this approach is stimulating new theories of the physics of open systems, functioning under conditions far from thermodynamic equilibrium (like life). The clinical applications are numerous, e.g. to anaesthesia, diabetes, fetal maturation, heart failure, hypertension, malignant melanoma, sleep... The work is paving the way to new medical instruments based on biological oscillations, e.g. to quantify endothelial health or depth of anaesthesia.

We hope and believe that Lancaster University is an ideal venue for the conference. Founded in 1964 in a gale of academic innovation, idealism, and enthusiasm for interdisciplinary research, it is now, on most measures, in the “top 10” of UK universities. Physics was one of the founding departments. Including contributions from its Nonlinear and Biomedical Research Group, it has come top in the UK in two out of the last three national research assessments.

Being the 9th ESGCO, our Lancaster conference is following in an honorable and well-established tradition, and we have made every attempt to maintain the high standards set by our predecessors. In particular, the keynote invited speakers and the organisers of the Special Sessions are among the scientific leaders of their respective subfields. Each abstract, whether invited or contributed, has been refereed by a member of the Scientific Committee and/or by one or in many cases two external referees, and amended where appropriate.

The majority of the oral presentations have been invited by members of the scientific

committee, often acting as the organisers of Special Sessions. To avoid an increase in the number of parallel sessions only two additional sessions, S22 and S23, were created based on contributed abstracts. Their selection was very difficult, but was based in part on perceived quality and in part on identifying combinations of contributions leading to sessions that would be coherent and interesting.

Consequently, the majority of the contributed abstracts were designated for poster presentation. At the same time, special attention has been paid to ensuring that posters will be treated with care and accorded the full attention that they merit. They will be displayed throughout the conference, and there will be a special poster session on the Monday. Five poster prizes will be awarded on the final day of the conference. The Scientific Committee will select the prizewinning posters with great care, thus bringing additional focus and attention to the contributed presentations.

The conference is genuinely international, with 142 participants from e.g. Australia, Brazil, Canada, China, Israel, Japan, New Zealand, Russia, Taiwan, Ukraine, USA as well as from UK and 20 other European countries. It is of course also highly interdisciplinary, bringing together people from e.g. biology, biomedical engineering, complex systems, computing, data science, endocrinology, information science, integrative medicine, mathematics, microgravity, neuroimaging, neurology, obstetrics, oncology, physics, physiology, physiotherapy, psychiatry, psychology, sound & vibration, as well as from hospitals and the medical instruments industry. It promises to be an intense experience, especially as much of the programme involves three parallel sessions. We trust that the abstracts in Section 3 will help participants to optimise their choices of session.

Finally, it is a pleasure to acknowledge the valuable input from the Scientific Committee and from many colleagues in preparing for the conference, and particularly the unstinting help with the local arrangements from Gemma Lancaster and Valentina Ticcinelli and the continuing and insightful guidance of the previous ESGCO organiser Alberto Porta.

Aneta Stefanovska & Peter McClintock
Lancaster, 1 April 2016

2 Programme

**Summary Programme for the
INTERNATIONAL CONFERENCE ON
BIOLOGICAL OSCILLATIONS
and
ESGCO–2016
*George Fox Building, Lancaster University***

Sunday 10 April

| | |
|---------------|--|
| 19:00 – 21:00 | Welcome party – a running buffet in County College Bar |
|---------------|--|

Monday 11 April

| | |
|---------------|--|
| 08:00 – 08:30 | Breakfast in “Refuel @ County”, for those staying in college |
| 08:30 – 09:00 | Registration desk, in George Fox foyer |

| Times | Plenary (LT1) | Parallel 1 (LT2) | Parallel 2 (LT3) | Parallel 3 (LT4) |
|---------------|----------------------------|------------------|------------------|------------------|
| 09:00 – 09:15 | Vice-Chancellor (O) | – | – | – |
| 09:15 – 09:30 | Alberto Porta | – | – | – |
| 09:30 – 09:45 | Aneta Stefanovska | – | – | – |
| 09:45 – 10:25 | (SL1) Sandra Sünram-Lea | – | – | – |
| 10:25 – 11:10 | (P1) Martin Rasmussen | – | – | – |

| | |
|---------------|---|
| 11:10 – 11:40 | Coffee/tea/refreshments – in George Fox foyer |
|---------------|---|

| | | | | |
|---------------|---|--------------------|---------------------|-----------------------|
| | – | <u>Ivanov</u> (S1) | <u>Baumert</u> (S2) | <u>Di Rienzo</u> (S3) |
| 11:40 – 12:00 | – | Klaus Lehnertz | Niels Wessel | John Karemaker |
| 12:00 – 12:20 | – | Daniele Marinazzo | Zbigniew Struzik | Angelo Taibi |
| 12:20 – 12:40 | – | Ronny Bartsch | Riccardo Barbieri | Marco di Rienzo |
| 12:40 – 13:00 | – | Plamen Ivanov | Michal Javorka | Max Moser |

| | |
|---------------|-----------------------------|
| 13:00 – 14:00 | Lunch – in George Fox foyer |
|---------------|-----------------------------|

| | | | | |
|---------------|---------------------|------------------------|-------------------|---------------------|
| 14:00 – 14:45 | (P2) Klaus Lehnertz | – | – | – |
| | | <u>Stankovski</u> (S4) | <u>Hoyer</u> (S5) | <u>Bernjak</u> (S6) |
| 14:50 – 15:10 | – | Tomislav Stankovski | Uwe Schneider | Vilma Urbančič-R. |
| 15:10 – 15:30 | – | Nicola Toschi | Maria G Signorini | Clare Thorn |
| 15:30 – 15:50 | – | Andreas Voss | Igor Lakhno | Alan Bernjak |
| 15:50 – 16:10 | – | Vlasta Bari | Dirk Cysarz | Gemma Lancaster |

| | |
|---------------|--|
| 16:10 – 17:10 | Poster Session with coffee/tea/refreshments – in George Fox foyer |
|---------------|--|

| | | | | |
|---------------|---|-------------------------------|--------------------------|--------------------|
| | | <u>Stankovski (ctd.)</u> (S4) | <u>Hoyer (ctd.)</u> (S5) | <u>Bocchi</u> (S7) |
| 17:10 – 17:30 | – | Luca Faes | Jan Żebrowski | Vesna Vuksanović |
| 17:30 – 17:50 | – | Gaetano Valenza | Dirk Hoyer | Anne Humeau-Hert. |
| 17:50 – 18:10 | – | Zengyong Li | Lisa Stroux | Michele Sorelli |
| 18:10 – 18:30 | – | Pawel Winklewski | Fernando Andreotti | Alexei Kamshilin |

| | |
|---------------|--|
| 19:00 – 20:45 | Dinner – in Barker House Farm (Cartmel College), followed immediately by |
| 20:45 – 22:00 | Discussion: The future of the field – Stefanovska & Porta (Co-Chairs) with Niels Wessel and Andreas Spiegler |

Tuesday 12 April

| | |
|---------------|--|
| 08:00 – 08:45 | Breakfast in “Refuel @ County”, for those staying in college |
|---------------|--|

| Times | Plenary (LT1) | Parallel 1 (LT2) | Parallel 2 (LT3) | Parallel 3 (LT4) |
|---------------|-----------------------------------|-----------------------------------|--------------------------------------|--|
| 09:00 – 09:45 | (P2) Christian Aalkjaer | – – <u>Faes</u> (S8) | – – <u>Kaufman</u> (S9) | – – <u>Petkoski</u> (S10) |
| 09:50 – 10:10 | – | Gaetano Valenza | Peter McClintock | Andrea Duggento |
| 10:10 – 10:30 | – | Mathias Baumert | Bob Eisenberg | Ernest Montbrio |
| 10:30 – 10:50 | – | Roberto Sassi | U. Kleinekathöfer | Joana Cabral |
| 10:50 – 11:10 | – | Beatrice De Maria | Jiandong Feng | Spase Petkoski |

| | |
|---------------|---|
| 11:10 – 11:40 | Coffee/tea/refreshments – in George Fox foyer |
|---------------|---|

| | | | | |
|---------------|---|---|--|---|
| 11:40 – 12:00 | – | <u>Raeder/Jensen</u> (S11) Peter McClintock | <u>Kaufman (ctd.)</u> (S9) Carlo Guardiani | <u>Schiecke/Spiegler</u> (S12) Karin Schiecke |
| 12:00 – 12:20 | – | Andrew Smith | Will Gibby | Jens Haueisen |
| 12:20 – 12:40 | – | Johan Raeder | Olena Fedorenko | Robin Ince |
| 12:40 – 13:00 | – | Erik Weber Jensen | Igor Kaufman | Andreas Spiegler |

| | |
|---------------|---|
| 13:30 – 18:30 | Excursion – Packed lunch on bus to Lake District leisure, museums or walks |
| 18:30 – 22:00 | Dinner at Low Wood Hotel near Ambleside, including presentation by Antonio Colantuoni “History and discovery of vascular oscillations” |
| 22:00 – 23:00 | Bus back to Lancaster University |

Wednesday 13 April

08:00 – 08:45 Breakfast in “Refuel @ County”, for those staying in college

| Times | Plenary (LT1) | Parallel 1 (LT2) | Parallel 2 (LT3) | Parallel 3 (LT4) |
|---------------|--------------------------|-----------------------------|-----------------------------|-----------------------------|
| 09:00 – 09:45 | (SL2) Thomas Jaki | – | – | – |
| | | <u>Ben-Tal</u> (S13) | <u>Struzik</u> (S14) | <u>Ravelli</u> (S15) |
| 09:50 – 10:10 | – | Alain Nogaret | Danuta Makowiec | Richard Clayton |
| 10:10 – 10:30 | – | Julian F R Paton | Daniele Marinazzo | Ana Mincholé |
| 10:30 – 10:50 | – | Maja Elstad | Thierry Mora | Alessandro Loppini |
| 10:50 – 11:10 | – | Alona Ben-Tal | Gernot Plank | Michela Masè |

11:10 – 11:40 Coffee/tea/refreshments – in George Fox foyer

| | | | | |
|---------------|---|--------------------------------|-----------------------------|------------------------------------|
| 11:40 – 12:00 | – | <u>Stankovski</u> (S16) | <u>Javorka</u> (S17) | <u>Ravelli (ctd.)</u> (S15) |
| 12:00 – 12:20 | – | Denis Engemann | A. Daffertshofer | Frida Sandberg |
| | – | Lawrence Sheppard | Beata Graff | Valentina Corino |
| | – | | | <u>Castigl./Sassi</u> (S18) |
| 12:20 – 12:40 | – | Arina Tankanag | Dorota Wejer | Roberto Sassi |
| 12:40 – 13:00 | – | Philip Clemson | Michal Javorka | Danuta Makowiec |

13:00 – 14:00 Lunch – in George Fox foyer

| | | | | |
|---------------|----------------------------|-----------------------------|----------------------------|---------------------------------------|
| 14:00 – 14:45 | (P4) Mattias Goksör | – | – | – |
| | | <u>Edwards</u> (S19) | <u>Cysarz</u> (S20) | <u>Cas./Sassi (ctd.)</u> (S18) |
| 14:50 – 15:10 | – | Aled Jones | Dirk Cysarz | Jan Gieraltowski |
| 15:10 – 15:30 | – | Christopher George | Danuta Makowiec | Md Aktaruzzaman |
| 15:30 – 15:50 | – | Etienne Boileau | Philine Granitza | Jan Gieraltowski |
| 15:50 – 16:10 | – | Tomislav Stankovski | Claudio Mazzucco | Paolo Castiglioni |

16:10 – 16:40 Coffee/tea/refreshments – in George Fox foyer

| | | | | |
|---------------|---|---------------------------|-------------------------------------|-------------------------------|
| 16:40 – 17:00 | – | <u>Porta</u> (S21) | <u>Simpson/Colant.</u> (S22) | <u>Żebrowski</u> (S23) |
| 17:00 – 17:20 | – | Aparecida Catai | David Simpson | Chih-Wen Shih |
| 17:20 – 17:40 | – | Andreas Voss | Antonio Colantuoni | Helen Shiells |
| 17:40 – 18:00 | – | Valentina Ticcinelli | Maria Skytiti | Michele Orini |
| | – | Alberto Porta | Dmitry Postnov | Yevhen Suprunenko |

18:30 – 18:45 Reception – LICA Building foyer

18:45 – 20:00 Concert with presentation of poster prizes – LICA Building hall

20:00 – 22:00 Conference Dinner, end of ESGCO-2016 – Private Dining Room (County College South)

Thursday 14 April

08:00 – 09:00 Breakfast in “Refuel @ County”, for those staying in college

09:00 – Departure or fNIRS workshop

**Programme for the
INTERNATIONAL CONFERENCE ON
BIOLOGICAL OSCILLATIONS
and
ESGCO–2016
*George Fox Building, Lancaster University***

Sunday 10 April 2016

19:00-21:00 Welcome party – a running buffet in County College Bar

Monday 11 April 2016

08:30-09:00 Registration desk, in George Fox foyer

⊙ **OPENING SESSION (LT1)**

Peter McClintock, Lancaster University, UK (Chair)

- 09:00-09:15 **Mark Smith**, Vice-Chancellor of Lancaster University, UK: Opening of conference
 09:15-09:30 **Alberto Porta**, University of Milan, Italy: Origins and history of the ESGCO meetings
 09:30-09:45 **Aneta Stefanovska**, Lancaster University, UK: Structure and scope of conference
 09:45-10:25 **Sandra Sünram-Lea**, Lancaster University, UK: *Psychological and hormonal effects on cardiovascular regulation*
 10:25-11:10 **Martin Rasmussen**, Imperial College London, UK: *An introduction to the qualitative theory of nonautonomous dynamical systems*
- 11:10-11:40 **Coffee, tea, and refreshments**

⊙_{s1} **NETWORK PHYSIOLOGY (LT2)**

Plamen Ivanov, Boston University, USA (Chair)

- 11:40-12:00 **Klaus Lehnertz**, University of Bonn, Germany: *Seizures and chimeras in epileptic brain networks*
 12:00-12:20 **Daniele Marinazzo**, University of Ghent, Belgium: *Revealing brain-heart interactions with EEG and fMRI*
 12:20-12:40 **Ronny P. Bartsch**, Bar-Ilan University, Israel: *The novel concept of time delay stability and identifying dynamic networks of physiological systems*
 12:40-13:00 **Plamen Ch. Ivanov**, Boston University, USA: *Network Physiology: From brain dynamics and plasticity to a first atlas of organ network interactions*

⊙_{s2} **METHODS FOR EXTRACTING DYNAMICS
FROM CARDIOVASCULAR SIGNALS (LT3)**

Mathias Baumert, University of Adelaide, Australia (Chair)

- 11:40-12:00 **Niels Wessel**, Humboldt University, Germany: *Cardio-respiratory coordination during sleep*
 12:00-12:20 **Zbigniew R. Struzik**, University of Gdańsk, Poland: *Should physicists analyse heart rate?*
 12:20-12:40 **Riccardo Barbieri**, Politecnico di Milano, Italy and Harvard Medical School, USA: *Assessment of instantaneous linear and nonlinear heartbeat dynamics during seizures in untreated temporal lobe epilepsy*
 12:40-13:00 **Michal Javorka**, Comenius University, Slovakia: *Basic cardiovascular signals: Mutual interactions explored by information domain analysis*

Ⓢ3 **CARDIOVASCULAR PHYSIOLOGY IN MICROGRAVITY (LT4)**

Marco Di Rienzo, Fondazione Don Carlo Gnocchi, Milan, Italy (Chair)

- 11:40-12:00 **John M. Karemaker**, University of Amsterdam, Netherlands: *What is so special about microgravity for blood pressure and heart rate?*
- 12:00-12:20 **Angelo Taibi**, University of Ferrara, Italy: *Investigation of cerebral venous outflow in microgravity*
- 12:20-12:40 **Marco Di Rienzo**, Fondazione Don Carlo Gnocchi, Milan, Italy: *Heart rate patterns and cardiac mechanics during sleep in microgravity aboard the International Space Station*
- 12:40-13:00 **Max Moser**, Medical University Graz and Human Research Institute, Austria: *Physiological oscillations and health*
- 13:00-14:00 **Lunch**

Ⓟ2 **PLENARY SESSION (LT1)**

Aneta Stefanovska, Lancaster University, UK (Chair)

- 14:00-14:45 **Klaus Lehnertz**, University of Bonn, Germany: *Capturing time-varying dynamics – Lectures from brain dynamics*

Ⓢ4 **INTERACTIONS BETWEEN CARDIOVASCULAR OSCILLATIONS AND BRAIN WAVES (LT2)**

Tomislav Stankovski, Sts Cyril and Methodius University, Macedonia (Chair)

- 14:50-15:10 **Tomislav Stankovski**, Sts Cyril and Methodius University, Macedonia: *Cardiovascular and brain coupling functions in anaesthesia*
- 15:10-15:30 **Nicola Toschi**, University of Rome “Tor Vergata”, Italy and Harvard Medical School, USA: *Causal brain correlates of autonomic nervous system (ANS) outflow: A 7T study*
- 15:30-15:50 **Andreas Voss**, University of Jena, Germany: *Linear and nonlinear causal coupling analyses between the central and autonomic nervous system in schizophrenia*
- 15:50-16:10 **Vlasta Bari**, University of Milan, Italy: *Conditional joint transfer entropy of cardiovascular and cerebrovascular control systems in subjects prone to postural syncope*
-
- 17:10-17:30 **Luca Faes**, Bruno Kessler Foundation, Italy: *Prediction and entropy measures of brain-to-heart causal interactions in patients with sleep disorders*
- 17:30-17:50 **Gaetano Valenza**, University of Pisa, Italy and Harvard Medical School, USA: *Maximal information coefficient to estimate brain-heart dynamics during visual emotional elicitation*
- 17:50-18:10 **Zengyong Li**, Shandong University, China: *Synchronization analysis of cerebral tissue oxygenation and arterial blood pressure signals in post-stroke subjects*
- 18:10-18:30 **Pawel J Winklewski**, Medical University of Gdańsk, Poland: *Increased inspiratory resistance alters the cardiac contribution to the dynamic relationship between blood pressure and pial artery pulsation oscillations in healthy subjects*

Ⓢ5 **FETAL MATURATION AND WELL-BEING (LT3)**

Dirk Hoyer, Jena University Hospital, Germany (Chair)

- 14:50-15:10 **Uwe Schneider**, Jena University Hospital, Germany: *Fetal heart rate regulation reflecting autonomic maturation – Listening comprehension in the communication with the unborn child*
- 15:10-15:30 **Maria Gabriella Signorini**, Politecnico Di Milano, Italy: *Quantitative diagnosis of IUGR fetuses: Contributions from signal processing and prediction modelling*
- 15:30-15:50 **Igor Lakhno**, VN Karazin National University Kharkiv, Ukraine: *Fetal and maternal autonomic interaction in pre-eclampsia*
- 15:50-16:10 **Dirk Cysarz**, University of Witten/Herdecke, Germany: *Can binary symbolic dynamics of heart rate variability improve the assessment of fetal functional brain age?*

- 17:10-17:30 **Jan Żebrowski**, Warsaw University of Technology, Poland: *Recurrence plot and multifractal analysis of fetal heart rate variability – dependence on gestational age*
- 17:30-17:50 **Dirk Hoyer**, Jena University Hospital, Germany: *Validation of functional fetal autonomic brain age score fABAS developed using magnetocardiography for applicability in cardiotocography*
- 17:50-18:10 **Lisa Stroux**, University of Oxford, UK: *IUGR detection from Doppler based HRV markers in low resource environments*
- 18:10-18:30 **Fernando Andreotti**, Technical University of Dresden, Germany: *Determining factors for non-invasive fetal ECG quality: A case study*

Ⓢ6 **CARDIOVASCULAR REGULATION AND BLOOD OXYGENATION
IN HEALTH, DIABETES AND CANCER (LT4)**

Alan Bernjak, University of Sheffield, UK (Chair)

- 14:50-15:10 **Vilma Urbančič-Rovan**, University Medical Centre, Slovenia: *Diabetic foot ulcers: Improved microcirculation after low-energy laser irradiation*
- 15:10-15:30 **Clare Thorn**, University of Exeter Medical School, UK: *The role of perfusion in the oxygen extraction capability of skin and skeletal muscle*
- 15:30-15:50 **Alan Bernjak**, University of Sheffield, UK: *Cardiac repolarisation and heart rate variability during experimental hypoglycaemia in healthy subjects and patients with type 2 diabetes*
- 15:50-16:10 **Gemma Lancaster**, Lancaster University, UK: *Diagnosis of malignant melanoma based on alterations in blood flow dynamics*

- 16:10-17:10 **POSTER SESSION, with coffee, tea, and refreshments**

Ⓢ7 **TEMPERATURE REGULATION OF MICROVASCULAR FLOW (LT4)**

Leonardo Bocchi, University of Florence, Italy (Chair)

- 17:10-17:30 **Vesna Vuksanović**, University of Aberdeen, UK: *Oscillatory behaviour of skin blood flow in response to local temperature change*
- 17:30-17:50 **Anne Humeau-Heurtier**, University of Angers, France: *Temperature regulation of microvascular flow: A multi-dimensional improved EMD-based study of laser speckle contrast images*
- 17:50-18:10 **Michele Sorelli**, University of Florence, Italy: *Location-dependent microvascular response to thermal stimulation*
- 18:10-18:30 **Alexei A. Kamshilin**, ITMO University, Russia: *Blood pulsations imaging as a tool for studying thermoregulation of skin microcirculation*
- 19:00-20:45 **Dinner**
- 20:45-22:00 **Discussion: The future of the field**, Aneta Stefanovska & Alberto Porta (Co-Chairs)
- 20:45-20:50 **Aneta Stefanovska**, Lancaster University, UK: *Introduction*
- 20:50-21:05 **Niels Wessel**, Humboldt University of Berlin, Germany: *Recap: 20 years of task force heart rate variability*
- 21:05-21:20 *Discussion*
- 21:20-21:40 **Andreas Spiegler**, University of Marseille, France: *The Virtual Brain: Selective activation of resting state networks following focal stimulation*
- 21:40-22:00 *Discussion*

Tuesday 12 April 2016**P₃ PLENARY SESSION (LT1)****Plamen Ivanov**, Boston University, USA (Chair)

- 09:00-09:45 **Christian Aalkjaer**, Aarhus University and Copenhagen University, Denmark: *The origin and role of vasomotion including its potential physiological and pathophysiological relevance: From ion channels to the endothelium and smooth muscle cells*

S₈ ENTROPY MEASURES TO EVALUATE DYNAMICS (LT2)**Luca Faes**, University of Trento, Italy (Chair)

- 09:50-10:10 **Gaetano Valenza**, University of Pisa, Italy and Harvard Medical School, USA: *An instantaneous estimation of transfer entropy using point-process models with application to cardio-respiratory dynamics*
- 10:10-10:30 **Mathias Baumert**, University of Adelaide, Australia: *Assessing cardiovascular control in children with sleep disordered breathing using predictive information decomposition*
- 10:30-10:50 **Roberto Sassi**, University of Milan, Italy: *Permutation entropy and its parametric estimation in heart rate variability analysis*
- 10:50-11:10 **Beatrice De Maria**, IRCCS Fondazione Salvatore Maugeri, Italy: *Complexity of vascular control in amyotrophic lateral sclerosis patients is associated with the disease duration*

**S₉ MULTI-ION DYNAMICS AND COULOMB BLOCKADE (LT3)
OSCILLATIONS IN BIOLOGICAL ION CHANNELS****Igor Kh. Kaufman**, Lancaster University, UK (Chair)

- 09:50-10:10 **Peter McClintock**, Lancaster University, UK: *Electrostatic basis of selectivity in biological ion channels*
- 10:10-10:30 **Bob Eisenberg**, Rush University Medical Center, USA: *Multi-ion dynamics dominated by interactions*
- 10:30-10:50 **Ulrich Kleinekathöfer**, Jacobs University Bremen, Germany: *Molecular and Brownian dynamics simulations of ion transport through outer membrane channels*
- 10:50-11:10 **Jiandong Feng**, EPFL Lausanne, Switzerland: *Observation of ionic Coulomb blockade in nanopores*

-
- 11:40-12:00 **Carlo Guardiani**, University of Warwick, UK: *A simulation study of the NaChBac channel: Stability, Na⁺ binding sites and hydration*
- 12:00-12:20 **Will Gibby**, Lancaster University, UK: *Theory of alike selectivity in biological channels*
- 12:20-12:40 **Olena Fedorenko**, Lancaster University, UK: *Investigating the molecular basis of ion selectivity of NaChBac using the patch clamp technique*
- 12:40-13:00 **Igor Kh. Kaufman**, Lancaster University, UK: *Coulomb blockade oscillations and AMFE in Calcium ion channels*

(S10) NETWORKS OF BIOLOGICAL OSCILLATORS (LT4)

Spase Petkoski, University of Marseille, France (Chair)

- 09:50-10:10 **Andrea Duggento**, University of Rome “Tor Vergata”, Italy: *Reconstructing multivariate causal structure between functional brain networks through a new Laguerre-decomposition based Granger causality approach*
- 10:10-10:30 **Ernest Montbrio**, University Pompeu Fabra, Spain: *Quasiperiodic and chaotic partial synchronization in populations of inhibitory neurons with delay*
- 10:30-10:50 **Joana Cabral**, University Oxford, UK: *Metastability and collective frequencies in oscillatory brain networks*
- 10:50-11:10 **Spase Petkoski**, University of Marseille, France: *Spatial distribution of time delays determines the synchronization of coupled oscillators*
- 11:10-11:40 **Coffee, tea, and refreshments**

(S11) CARDIOVASCULAR OSCILLATIONS AND BRAIN WAVES
IN ANÆSTHESIA (LT2)

Johan Ræder, University of Oslo, Norway & **Erik Weber Jensen**, Quantum Medical S.L., Spain
(Co-chairs)

- 11:40-12:00 **Peter McClintock**, Lancaster University, UK: *Brain, respiration, and cardiac causalities in anaesthesia*
- 12:00-12:20 **Andrew Smith**, Royal Lancaster Infirmary, UK: *BRACCIA: Methodology and cardio-respiratory interactions*
- 12:20-12:40 **Johan Ræder**, University of Oslo, Norway: *The discriminatory value of combining signals from brain, cardiovascular system, respiration and skin in distinguishing awake from anaesthetised states: A randomised observational study*
- 12:40-13:00 **Erik Weber Jensen**, Quantum Medical S.L., Spain: *Perspectives on further ways to deal with EEG signals for anaesthesia depth monitoring in the future*

(S12) ANALYSING BRAIN DYNAMICS (LT4)

Karin Schiecke, Jena University Hospital, Germany & **Andreas Spiegler**, University of Marseille, France
(Co-Chairs)

- 11:40-12:00 **Karin Schiecke**, Jena University Hospital, Germany: *Advanced time-variant, non-linear approaches for analysing brain dynamics*
- 12:00-12:20 **Jens Haueisen**, Technical University of Ilmenau, Germany: *Rod driven resonance and entrainment in the visual system of the brain*
- 12:20-12:40 **Robin A. A. Ince**, University of Glasgow, UK: *Analysing brain dynamics with a novel mutual information estimator: Phase and power and their representational interactions*
- 12:40-13:00 **Andreas Spiegler**, University of Marseille, France: *Analysis of network states in large-scale brain models with an application to brain stimulation*

EXCURSION TO LAKE DISTRICT

- 13:30-18:30 **Packed lunch** on bus to Lake District; Leisure, museums or walks
- 18:30-22:00 **Dinner** at Low Wood Hotel near Ambleside, including
Antonio Colantuoni: *History and discovery of vascular oscillations*
- 22:00-23:00 **Buses** back to Lancaster University

Wednesday 13 April 2016

(SL2) PLENARY SESSION (LT1)

Alberto Porta, University of Milan, Italy (Chair)

09:00-09:45 **Thomas Jaki**, Lancaster University, UK: *Know what you know – Some guidance for efficient experimental and clinical study design*

(S13) CARDIO-RESPIRATORY INTERACTIONS (LT2)

Alona Ben-Tal, Massey University, New Zealand (Chair)

09:50-10:10 **Alain Nogaret**, University of Bath, UK: *Bioelectronic central pattern generators for cardiorespiratory disease*

10:10-10:30 **Julian F. R. Paton**, University of Bristol, UK: *Respiratory sinus arrhythmia – What is this oscillation good for?*

10:30-10:50 **Maja Elstad**, University of Oslo, Norway: *Respiratory sinus arrhythmia as buffer of systemic blood flow*

10:50-11:10 **Alona Ben-Tal**, Massey University, New Zealand: *Cardiorespiratory interactions: Looking at birds for answers*

**(S14) INTRINSICALLY MULTISCALE PHENOMENA
IN COMPLEX BIOLOGICAL SYSTEMS (LT3)**

Zbigniew Struzik, University of Tokyo, Japan (Chair)

09:50-10:10 **Danuta Makowiec**, University of Gdańsk, Poland: *Tensorial self-transfer entropy (TsTE) of R-R heart interbeat signals and healthy ageing*

10:10-10:30 **Daniele Marinazzo**, University of Ghent, Belgium: *Revealing brain-heart interactions with EEG and fMRI*

10:30-10:50 **Thierry Mora**, École Normale Supérieure and CNRS, France: *Dynamical criticality in the collective activity of a neural population*

10:50-11:10 **Gernot Plank**, University of Graz, Austria: *Stochastic spontaneous calcium release events trigger premature ventricular complexes by overcoming electrotonic load*

(S15) CARDIAC ARRHYTHMIAS (LT4)

Flavia Ravelli, University of Trento, Italy (Chair)

09:50-10:10 **Richard Clayton**, University of Sheffield, UK: *Rotors and re-entry in the human heart: Experiments and models*

10:10-10:30 **Ana Mincholé**, University of Oxford, UK: *Human whole-ventricle simulations of transmural reentry promoted by early afterdepolarizations in acute myocardial ischaemia*

10:30-10:50 **Alessandro Loppini**, University Campus Bio-Medico of Rome, Italy: *Role of temperature and tissue size on nonlinear cardiac dynamics*

10:50-11:10 **Michela Masè**, University of Trento, Italy: *Atrioventricular coupling and ventricular interval regularity during atrial fibrillation: A frequency-dependent phenomenon*

11:40-12:00 **Frida Sandberg**, Lund University, Sweden: *Characterization of ventricular response during atrial fibrillation using a network model of the AV nodal function*

12:00-12:20 **Valentina Corino**, Polytechnic of Milan, Italy: *Characterization of photoplethysmographic signal during atrial fibrillation*

11:10-11:40 **Coffee, tea, and refreshments**

S16 **EXTRACTING TIME-VARIABLE DYNAMICS AND INTERACTIONS**
(LT2)

Tomislav Stankovski, Sts Cyril and Methodius University, Macedonia (Chair)

- 11:40-12:00 **Denis Engemann**, Universit Paris-Saclay, France: *Time-resolved characterization of human brain dynamics – Noninvasive cognitive neurophysiology*
- 12:00-12:20 **Lawrence W. Sheppard**, University of Kansas, USA: *Testing and interpreting coherence in biological fluctuations*
- 12:20-12:40 **Arina V. Tankanag**, Russian Acad. Sci., Russia: *Wavelet phase coherence analysis of polyfrequency skin blood flow oscillations under normal conditions in human*
- 12:40-13:00 **Philip Clemson**, Lancaster University, UK: *Nonautonomous systems as an inverse problem: Comparison with stochastic and chaotic systems*

S17 **PHYSIOLOGICAL INTERACTIONS (LT3)**

Michal Javorka, Comenius University, Slovakia (Chair)

- 11:40-12:00 **Andreas Daffertshofer**, Vrije Universiteit Amsterdam, Netherlands: *On th relation between interacting networks and networks with multimodal frequency distribution*
- 12:00-12:20 **Beata Graff**, Medical University of Gdańsk, Poland: *Bidirectional information transfer between blood pressure and heart rate and its relation to vascular properties in hypertensive patients*
- 12:20-12:40 **Dorota Wejer**, University of Gdańsk, Poland: *Cardiovascular interactions during head-up tilt test by transfer entropy between ordinal patterns of heart rate and blood pressure*
- 12:40-13:00 **Michal Javorka**, Comenius University, Slovakia: *Basic cardiovascular signals: Mutual interactions explored by information domain analysis*

S18 **FRACTAL METHODS IN COMPLEXITY ANALYSIS (LT4)**

Paolo Castiglioni, Fondazione Don Carlo Gnocchi, Milan, Italy & **Roberto Sassi**, University of Milan, Italy (Co-Chairs)

- 12:20-12:40 **Roberto Sassi**, University of Milan, Italy: *Risk stratification by means of HRV fractal methods: Where we are*
- 12:40-13:00 **Danuta Makowiec**, University of Gdańsk, Poland: *Multifractality of R-R interval signals and healthy ageing*

- 14:50-15:10 **Jan Gieraltowski**, Politechnic of Warsaw, Poland: *Multiscale multifractal analysis - screening examination method presenting highly repetitive HRV multifractal pattern*
- 15:10-15:30 **Mid Aktaruzzaman**, University of Milan, Italy: *Use of detrended fluctuation analysis for sleep vs wake classification from heart rate variability*
- 15:30-15:50 **Jan Gieraltowski**, Politechnic of Warsaw, Poland: *Modeling linear and nonlinear properties of night-time heart rate variability*
- 15:50-16:10 **Paolo Castiglioni**, Fondazione Don Carlo Gnocchi, Milan, Italy: *Altered HRV fractal dynamics after spinal cord injury as function of lesion level*

13:00-14:00 **Lunch**

P4 **PLENARY SESSION (LT1)**

Aneta Stefanovska, Lancaster University, UK (Chair)

14:00-14:45 **Mattias Goksör**, University of Gothenburg, Sweden: *Glycolytic oscillations in isolated yeast cells*

(S19) SINGLE AND MULTIPLE CELL OSCILLATIONS (LT2)

David Edwards, Cardiff University, UK (Chair)

- 14:50-15:10 **Aled Jones**, Cardiff University, UK: *Induced pluripotent stem cell derived cardiomyocyte monolayers as a model of cardiac excitable networks*
- 15:10-15:30 **Christopher George**, Cardiff University, UK: *Crisis and stasis: A cellular model of the progressive nature of heart disease-linked Ca^{2+} release dysfunction*
- 15:30-15:50 **Etienne Boileau**, Swansea University, UK: *Human cardiac systems electrophysiology: From generic models to human stem-cell-derived cardiomyocytes*
- 15:50-16:10 **Tomislav Stankovski**, Sts Cyril and Methodius University, Macedonia: *Interactions between oscillatory cardiac muscle cells*

(S20) ANALYSIS OF SHORT AND NON-STATIONARY
CARDIOVASCULAR TIME SERIES (LT3)

Dirk Cysarz, University of Witten/Herdecke, Germany (Chair)

- 14:50-15:10 **Dirk Cysarz**, University of Witten/Herdecke, Germany: *Nonstationary heart rate dynamics of short time series assessed by symbolic dynamics analysis*
- 15:10-15:30 **Danuta Makowiec**, University of Gdańsk, Poland: *Asymmetry in heart rate and blood pressure manifested in the head-up tilt test*
- 15:30-15:50 **Philine Granitza**, Humboldt University of Berlin, Germany: *Cardiorespiratory coordination in Cheyne-Stokes-Respiration: A case study*
- 15:50-16:10 **Claudio Mazzucco**, Politechnic of Milan, Italy: *Assessment of cardio-respiratory interactions and their stability in anesthetized patients under different mechanical ventilatory modes*
- 11:10-11:40 **Coffee, tea, and refreshments**

(S21) AGEING OF CARDIAC AND VASCULAR REGULATION (LT2)

Alberto Porta, University of Milan, Italy (Chair)

- 16:40-17:00 **Aparecida Catai**, Federal University of São Carlos, Brazil: *Dependence of the cardiovascular control complexity on age and gender*
- 17:00-17:20 **Andreas Voss**, University of Applied Sciences, Germany: *Age and gender dependency of short-term QT indices*
- 17:20-17:40 **Valentina Ticcinelli**, Lancaster University, UK: *Coupling functions between cardiac and myogenic activity in microvascular flow of aged and hypertensive subjects*
- 17:40-18:00 **Alberto Porta**, University of Milan, Italy: *Effects of aging on the redundancy of the cardiovascular control*

S22 CEREBRAL VASCULAR REGULATION (LT3)

David Simpson, University of Southampton, UK & **Antonio Colantuoni**, ‘Federico II’ University Medical School, Italy (Co-Chairs)

- 16:40-17:00 **David Simpson**, University of Southampton: *Cerebral autoregulation: Every normal subject is the average, the rest is noise?*
- 17:00-17:20 **Antonio Colantuoni**, ‘Federico II’ University Medical School, Italy: *Trigemino-cardiac reflex as a long-time modulator of cerebral blood flow*
- 17:20-17:40 **Maria Skytjoti**, University of Oslo, Norway: *Respiratory sinus arrhythmia buffers variability in cerebral blood flow*
- 17:40-18:00 **Dmitry Postnov**, Saratov State University, Russia: *Modeling study of cerebral blood flow redistribution during cortical spreading depression: Tristable fronts and oscillatory vascular responses*

S23 NETWORK PHYSIOLOGY, COMPLEXITY AND TIME-DEPENDENT DYNAMICS (LT4)

Jan Zebrowski, Warsaw University of Technology, Poland (Chair)

- 16:40-17:00 **Chih-Wen Shih**, National Chiao Tung University, Taiwan: *Approximate and identical synchronization in coupled systems*
- 17:00-17:20 **Helen Shiells**, University of Aberdeen, UK: *Network inference in the presence of latent confounders: The role of instantaneous causalities*
- 17:20-17:40 **Michele Orini**, University College London, UK: *A method to estimate unbiased partial time-frequency spectra: Application to repolarization variability changes unrelated to heart rate variability*
- 17:40-18:00 **Yevhen Suprunenko**, University of Liverpool, UK: *Is it always easier to capture time-variable dynamics which resist the influence of external perturbations?*

- 18:30-18:45 **Reception**
- 18:45-20:00 **Concert** in LICA Building, with presentation of poster prizes
- 20:00-21:30 **Conference Dinner** and closing of ESGCO-2016

POSTER PRESENTATIONS

Monday 11th April, 08:00 – Wednesday 13th April, 16:40

1. Y. A. Abdussalam and A. Stefanovska: *Effect of malaria on the dynamics and rheological properties of blood flow in a microvasculature*
2. P. J. Aston, M. Nandi, M. I. Christie, Y. H. Huang and H. B. Mistry: *Continuous information extraction from blood pressure data using attractor reconstruction*
3. O. Mohamoud, I. Kovačić, T. Škorić, N. J. Žigon and D. Bajić: *Entropy relations in infinitely clipped differential time series*
4. M. L. Barabash and A. Stefanovska: *Model of membrane-potential fluctuations*
5. E. Brunetta, P. Mandelli, M. I. S. Achenza, E. Scannella, L. Boccassini, A. Marchi, F. Barbic, P. S. Puttini, A. Porta and R. Furlan: *Vascular sympathetic control in Sjögren syndrome*
6. T. Buchner, T. Sobiech and P. Krzesiński: *Cardiorespiratory coupling interval during tilt-test examination in young healthy males*
7. C. Cammarota and M. Curione: *Amplitude change in R and T waves of electrocardiogram during exercise*
8. C. B. F. Pantoni, A. Porta, J. C. Milan-Mattos, N. M. Perseguini, V. Minatel, P. Rehder-Santos, S. C. G. Moura-Tonello, M. O. Gois, A. C. M. Takahashi, R. A. Gonçalves, V. Bari, A. Marchi, B. De Maria and A. M. Catai: *The influence of aging on the QT interval variability*
9. A.A. Fagundes, A. Porta, N. M. Perseguini, J.C. Milan, V. Minatel, P.R. Santos, A.C.M. Takahashi and A.M. Catai: *Evolution of the complexity of systolic and diastolic blood pressure variabilities with age*
10. J. C. Milan-Mattos, A. Porta, N. M. Perseguini, V. Minatel, P. R. Santos, V. Bari, A. C. M. Takahashi and A. M. Catai: *Phase relation between systolic blood pressure and heart period is age-dependent but gender-independent*
11. G. Cecchini, M. Thiel and B. Schelter: *Improving network inference of oscillatory systems: A novel framework to reliably identify the correct class of network*
12. T. Mastantuono, M. Di Maro, M. Chiurazzi, G. Nasti, D. Lapi, L. Battiloro, N. Starita, M. Cesarelli, G. D'Addio, L. Iuppariello and A. Colantuoni: *Hyposodic and hypocaloric diet effects on oscillatory pattern in newly diagnosed hypertensive people*
13. F. Devalle, D. Pazó and E. Montbrió: *Solvable model for a network of spiking neurons with fixed delays*
14. M. Elstad, I. Zilakos and T. K. Bergersen: *Oscillatory pattern of arteriovenous anastomoses and skin blood flow within thermoneutral zone*
15. A. Gergont, S. Krocicka and M. Kaciński: *Results of cerebral blood flow during autonomic testing in children with migraine*
16. W. A. T. Gibby, D. G. Luchinsky, P. V. E. McClintock, A. Stefanovska and R. S. Eisenberg: *Insights into the potassium selectivity of the KcsA ion channel based on a kinetic model*
17. A. Giczewska, D. Makowiec, J. Wtorek, A. Poliński, D. Wejer, B. Graff, S. Budrejko and Z. R. Struzik: *Interactions between heart rate and blood pressure by cross time-frequency analysis*
18. J. Gierałtowski, M. Petelczyc, G. Siudem and B. Żogała-Siudem: *Observational error in time domain heart rate variability analysis*
19. I. Grzegorzczuk, J. Gierałtowski and P. Krzesiński: *Cardiorespiratory coupling assessment - a new method of monitoring changes in respiratory sinus arrhythmia in time domain*
20. A. Perka and J. Gierałtowski: *ECG player software and data for your own, easy artificial patient*

21. M. Gruszecki, P. J. Winklewski, Y. Tkachenko, K. Mazur, J. Kot, W. Guminski, K. Czuszynski, J. Wtorek, A. F. Frydrychowski: *Sympathetic nervous system does not influence the cardiac and respiratory contribution to the relationship between blood pressure and pial artery pulsation oscillations in healthy volunteers*
22. S. Guzzetti, A. Marchi, R. Colombo, F. Raimondi and A. Porta: *Symbolic analysis of heart rate variability in Trendelenburg position before and after pneumoperitoneum under general anesthesia*
23. A. A. Kamshilin, M. A. Volynsky, I. S. Sidorov and O. V. Mamontov: *Time delay in facial blood pulsations*
24. I. Khovanov, S. Cosseddu, M. Rodger and C. Guardiani: *Dynamics of protein and permeation in KcsA ion channel*
25. M. Kośmider, D. Mieszkowski, S. Żurek, T. Krauze, P. Guzik and J. Piskorski: *The dependence of the ADFA asymmetric effect in RR-intervals time series on the length of the DFA sliding window*
26. J. F. Kraemer and N. Wessel: *Quantification of noise in the electrocardiogram*
27. A. Müller, M. Riedl, J. F. Kraemer, T. Penzel, J. Kurths and N. Wessel: *Ensemble symbolic coupling traces during sleep*
28. P. Laiou and R. G. Andrzejak: *Equivalent couplings in pairs of bidirectionally coupled asymmetric dynamics*
29. M. Zhang, Q. Tan, B. Wang, L. Xu, W. Wang and Z. Li: *Wavelet-based coherence analysis of cerebral tissue oxyhemoglobin and arterial blood pressure signals in healthy subjects during a vigilance task*
30. W. Wang, B. Wang, L. Xu and Z. Li: *Functional connectivity revealed by wavelet-based coherence analysis of near-infrared spectroscopy signals in healthy subjects during vigilance task*
31. A. Loppini, M. G. Pedersen and S. Filippi: *Coupling effects in mouse and human β -cells networks: Emergent dynamics*
32. M. Lucas and A. Stefanovska: *Why we need nonautonomous models and methods*
33. I. Malvestio and R. G. Andrzejak: *Detecting couplings between spike trains with noise*
34. A. Marchi, V. Bari, B. De Maria, G. Bellani, A. Pesenti, F. Barbic, A. Diedrich, R. Furlan and A. Porta: *Quantification of the degree of association between left and right muscle sympathetic nerve activity variability in healthy subjects*
35. I. Mizeva and D. Airikh: *Reaction of blood flow in microvessels on the local heating in patients with diabetes mellitus type 1*
36. I. Mizeva, P. Frick, S. Podtaev: *LDF signal oscillating and average components variations caused by cold pressor test*
37. M. Mojica-Banavides, A. A. Banaeiyan, C. B. Adiels and M. Goksör: *Design and implementation of a microfluidic chamber for synchronization studies of glycolytic oscillations in yeast cells*
38. A. K. Pidde, M. L. Barabash, S. Patel, J. Owen-Lynch, S. Roberts and A. Stefanovska: *Membrane potential of a biological cell: Stochastic or deterministic?*
39. B. Pietras, N. Deschle and A. Daffertshofer: *Coupled networks and networks with bimodal frequency distributions are equivalent*
40. J. Piskorski, T. Krauze and P. Guzik: *Structure of heart rate asymmetry: Duration of monotonic runs*
41. S. Podtaev, A. Parshakov, N. Zubareva and P. Frick: *Assessment of endothelial dysfunction using skin temperature oscillations analysis in patients with peripheral arterial disease*
42. T. Bassani, D. M. Simpson and A. Beda: *Low-frequency respiratory activity correlates strongly with low frequency HRV*
43. M. Volynsky, M. Volkov, N. Margaryants, I. P. Gurov and A. A. Kamshilin: *Modulation of transport speed of red blood cells in capillaries*

44. V. Vuksanović and P. Hövel: *Modelling flexible changes between network configurations in task-free brain activity*
45. D. Wejer, D. Makowiec, B. Graff, S. Budrejko and Z. R. Struzik: *The complexity of cardiac rhythms during head-up tilt test by the entropy of patterns*
46. S. Żurek, M. Kośmider, W. Grabowski, J. Piskorski and P. Guzik: *Complexity distribution in 24h Holter RR time series*

ESGCO 2016
biological oscillations



EVENING PROGRAMME

International Conference on Biological Oscillations and ESGCO–2016

*Wednesday 13th April
Lancaster University*

LICA Building foyer

18:15 Refreshments

LICA Building hall

18:45 Concert part one Jean Spièce (piano) & Maxime Lucas (violin)

19:10 Blood flow circulation P. Furneaux, A. Rosser, J. Spièce & M. Lucas

19:15 Presentation of poster prizes

19:30 Concert part two Phil Furneaux (saxophone) & Alice Rosser (piano)

Private dining room (County College South)

20:10 Conference dinner and closing of ESGCO 2016

CONCERT PART ONE

18:45–19:10 **Jean Spièce** (piano) & **Maxime Lucas** (violin)

A. Vivaldi *L'estro armonico, Op. 3 No. 3 in G major (RV 310), I Allegro*

Published in 1711, the *L'estro armonico*, concertos (12) are among Vivaldi's earliest works. These compositions were tremendously influential in their time, virtually laying the foundations for the concerto form in the eighteenth century. The Allegro first movement is rhythmic and vigorous.

P.I. Tchaikovsky *Souvenir d'un lieu cher - Op. 42, III Mélodie*

Memory of a dear place, Op. 42, was written by Pyotr Ilyich Tchaikovsky in 1878 for for violin and piano. It was presented to Nadezhda von Meck, Tchaikovsky's benefactress, as a token of Tchaikovsky's appreciation for her help and hospitality. *Mélodie*, in E-flat major, is the third and last movement, and a romantic melody of the best kind.

V. Monti *Csárdás*

The term *csárdás* refers to a type of traditional Hungarian folk music, and Monti's *csárdás* is quite possibly the best-known of the kind. Ironically enough, Monti was an Italian who spent most of his life in France. The piece starts with a melancholic section, followed by a much faster dance-like section.

G. Gershwin *Summer time from Porgy and Bess*

Summertime is an aria composed in 1934 by George Gershwin for the 1935 opera *Porgy and Bess*. The song soon became a popular and much recorded jazz standard, recognised as one of the most recorded songs in history. Famous artists who recorded their own version of Summertime include Ella Fitzgerald and Louis Armstrong. The lyrics of the original version are about a child that should not worry "With Daddy and Mammy standin' by" until he is old enough to "spread your wings and [you'll] take to the sky".

19:10–19:15 **P. Furneaux, A. Rosser, J. Spièce & M. Lucas** *Blood flow circulation*

The music will picture one cycle of the blood starting at the heart. It will then go to the arteries up to the capillaries, and then back to heart via the veins. Along the way, the music will change between more turbulence-like and togetherness-like sounds.

CONCERT PART TWO

19:30–20:10 **Phil Furneaux** (saxophone) & **Alice Rosser** (piano)

E. Satie *Gymnopédie Nr 1*

The three *Gymnopédies* are regarded as an important precursor to modern ambient music. Satie's widely reported eccentricity shines through in the title of these pieces, named after a Spartan dance of naked youths. Relaxed yet deliberate, this "furniture music" is now loved worldwide.

F. Chopin *Étude in E-major Op 10 No 3 'Tristesse'*

This popular *étude* is set apart from many of Chopin's *études* by its slower tempo. Whilst the purpose of *études* is primarily to develop certain aspects of technique, Chopin is rumoured to have said about this particular *étude* "In all my life I have never again been able to find such a beautiful melody". It is thought to be a manifestation of his love for his homeland of Poland.

C. Debussy *Clair de Lune*

Clair de Lune (moonlight) is the third and most famous movement of Debussy's "Suite Bergamasque". It was inspired by the poem of the same name by his friend Paul Verlaine, who writes "of your souls ... like landscapes, charming masks and bergamasks, playing the lute and dancing, almost sad in their fantastic disguises".

G. Faure *Après un Rêve Op 7 No 1*

Named "After a Dream", Fauré's grief can be sensed in this piece which he wrote following the breaking off of his engagement. It is one of Fauré's most popular vocal pieces, and was published in 1878, along with "Hymne" and "Barcarolle".

M. Ravel *Pavane pour une Infante Défunte*

Pavane for a Dead Princess was written by Ravel while studying under Gabriel Fauré. He described the piece as "an evocation of a pavane that a little princess might, in former times, have danced at the Spanish court". Ravel dedicated the work to his patron, the Princesse de Polignac. The piece was intended to be played extremely slowly, more so than most modern interpretations.

S. Rachmaninoff *Vocalise Op. 34, No. 14*

This song was composed and published in 1915 as the last of Rachmaninoff's "Fourteen Songs". Written for high voice (soprano or tenor) with piano accompaniment, it contains no words, but is sung using any one vowel (of the singer's choosing).

L. van Beethoven *Moonlight Sonata (extract)*

One of his most popular sonatas, "sonata quasi una fantasia" was completed by Beethoven in 1801 whilst in his early thirties. The nickname "Moonlight" was not applied by Beethoven himself, but by the German critic Ludwig Rellstab, who envisaged moonlight flickering across Lake Lucerne when hearing the opening movement. As evidenced in this work, Beethoven was a revolutionary, refusing to follow the conventional fast-slow-fast pattern of a traditional sonata.

MUSICIANS



Phil Furneaux spent the first part of his life playing rock guitar but was then able to buy a new sax with his mothers bequest at the age of 40, forming a band “Heidi and the Soul Merchants” which toured a rocky style of soul for 4 years. His album “A Real Distraction” was a turning point in his career. Phil has always enjoyed playing with his old and beloved friend Kryz Markowski and is excited about the planned collaboration of a recording and French tour of some jazz standards. FuMar’s (FUrneaux/MARkowski) new album “The Lanercost Sessions” has allowed them to develop their own style of quirky interpretations of some classic standards and will include some original material into the repertoire of their forthcoming tour on September 10–13. Phil worked with Alice Rosser on his new album to reinterpret some of the romantic piano classics, in what he describes as his biggest challenge yet.



Alice Rosser is a classically trained pianist. After obtaining her degree in music performance at Colchester Institute, she studied piano at the North West German Music Academy in Detmold. For many years she ran a private teaching practice in Blackpool and also taught the piano in schools in the area. She is now semi-retired and works part-time, travelling the world as a Music Examiner. She has been working with Phil Furneaux on his “classical project” for the past year.



While doing his PhD in nanoscale heat transfer since October 2014, **Jean Spièce** has carried on his musical passion through diverse collaborations such as conducting the Lancaster University Symphony Orchestra. Immersed in music since his infancy, he then studied piano in St. Petersburg and Brussels conservatories while starting his Physics degree.



Maxime Lucas studied physics in Brussels where he met Jean. He started his PhD in the Nonlinear Biomedical Physics group back in October 2015. Maxime started playing the violin at the age of four and is currently part of the Symphony Orchestra at Lancaster University.

3 Abstracts

3.1 Keynote invited talks

The origin and role of vasomotion including its potential physiological and pathophysiological relevance: from ion channels to the endothelium and smooth muscle cells

Christian Aalkjær

Aarhus University, Copenhagen University, Department of Biomedicine, Aarhus, Copenhagen, Denmark

Oscillations of tension or diameter i.e. vasomotion occurs in the wall of isolated resistance arteries under in vitro conditions (Peng et al., 2001). This vasomotion is independent of and oscillatory input and the oscillations arise within the vascular wall. I will discuss the cellular mechanisms leading to this vasomotion (Peng et al., 2001). Vasomotion requires a synchronized oscillation of the tone of the smooth muscle cells in the vascular wall. This is accomplished through oscillations of the membrane potential and electrical coupling between the smooth muscle cells (Matchkov et al., 2004a), which leads to synchronized oscillations of smooth muscle cell Ca^{2+} and hence smooth muscle tone (Peng et al., 2001). Vasomotion requires that the membrane potential oscillates within a window between about -40 mV and -20 mV, where changes in membrane potential leads to changes in smooth muscle cell Ca^{2+} . In isolated rat mesenteric resistance arteries the oscillation of the membrane potential requires the activity of a cGMP dependent, Ca^{2+} activated Cl^- conductance (Matchkov et al., 2004b; Rahman et al., 2005; Boedtkjer et al. 2008) dependent on two putative Cl^- channel proteins TMEM16A (Dam et al., 2014) and bestrophin (Brogger et al., 2011). The smooth muscle cGMP is provided by a constant tone of NO from the endothelium. Using experimentally determined parameters it is possible to model this vasomotion and obtain oscillations which are similar to those seen experimentally (Jacobsen et al., 2007a; 2007b; 2008). The phase of the oscillations can be reset by input from the sympathetic nervous system (Borovik et al., 2005) and the sympathetic nervous system therefore enhances the prevalence of vasomotion. In conditions where the Ca-ATPase of the sarcoplasmic reticulum is inhibited the vasomotion has a low frequency and high amplitude (Rahman et al., 2007). It is less dependent on NO and more dependent on endothelial derived hyperpolarization. Under these conditions synchronized oscillations of Ca^{2+} in endothelial cells and smooth muscle cells which are 180 degrees phase shifted occur (Rahman et al., 2007).

References

- Boedtkjer DM, Matchkov VV, Boedtkjer E, Nilsson H, Aalkjaer C. Vasomotion has chloride-dependency in rat mesenteric small arteries. 2008 *Pflugers Archives* **457** 389-404.
- Borovik A, Golubinskaya V, Tarasova O, Aalkjær C, Nilsson C. Phase resetting of arterial vasomotion by burst stimulation of perivascular nerves. 2005 *Journal of Vascular Research* **42** 165-173.
- Broegger T, Jacobsen JC, Secher Dam V, Boedtkjer DM, Kold-Petersen H, Pedersen FS, Aalkjaer C, Matchkov VV. Bestrophin is important for the rhythmic but not the tonic contraction in rat mesenteric small arteries. 2011 *Cardiovascular Research* **91** 685-693.
- Dam VS, Boedtkjer DM, Nyvad J, Aalkjaer C, Matchkov V. TMEM16A knockdown abrogates two different Ca^{2+} -activated Cl^- currents and contractility of smooth muscle in rat mesenteric small arteries. 2014 *Pflugers Archives* **466** 1391-409.

Jacobsen JC, Aalkjaer C, Matchkov VV, Nilsson H, Freiberg JJ, Holstein-Rathlou NH. Heterogeneity and weak coupling may explain the synchronization characteristics of cells in the arterial wall. 2008 *Philosophical Transaction Series A Mathematical Physical and Engineering Sciences* **366** 3483-502.

Jacobsen JBC, Aalkjaer C, Nilsson H, Matchkov V, Freiberg J, Holstein-Rathlou NH. Activation of a cGMP-sensitive calcium-dependent chloride channel may cause transition from calcium waves to whole-cell oscillations in smooth muscle cells 2007 *American Journal of Physiology* **293** H215-H228.

Jacobsen JBC, Aalkjaer C, Nilsson H, Matchkov V, Freiberg J, Holstein-Rathlou NH. A model of smooth muscle cell synchronization in the arterial wall. 2007 *American Journal of Physiology* **293** H229-H237.

Matchkov VV, Aalkjær C, Nilsson H: A cyclic-GMP-dependent calcium-activated chloride current in smooth muscle cells from rat mesenteric resistance arteries. 2004b *Journal of General Physiology* **123** 121-134.

Matchkov V, Rahman A, Peng H, Nilsson H, Aalkjær C. Junctional and nonjunctional effects of heptanol and glycyrrhetic acid derivatives in rat mesenteric small arteries. 2004a *British Journal of Pharmacology* **142** 961-972.

Peng HL, Matchkov V, Ivarsen A, Aalkjær C, Nilsson H. 2001 *Circulation Research* **88** 810-815.

Rahman A, Hughes A, Matchkov V, Nilsson H, Aalkjær C. Antiphase oscillations of endothelium and smooth muscle $[Ca^{2+}]_i$ in vasomotion of rat mesenteric small arteries. 2007 *Cell Calcium* **42** 536-547.

Rahman A, Matchkov V, Nilsson H, Aalkjaer C. Effects of cGMP on coordination of vascular smooth muscle cells of rat mesenteric small arteries. 2005 *Journal of Vascular Research* **42** 301-311.

Glycolytic oscillations in isolated yeast cells

**Anna-Karin Gustavsson^{1,6}, David D Niekerk², Caroline B Adiels³,
Bernhard Mehlig¹, Jacky L Snoep^{2,4,5} and Mattias Goksör¹**

¹*Department of Physics, University of Gothenburg, Gothenburg, Sweden*

²*Molecular Cell Physiology, Department of Biochemistry, Stellenbosch University,
Matieland, South Africa*

³*Theoretical Biology, VU University, Amsterdam, The Netherlands*

⁴*Molecular Cell Physiology, VU University, Amsterdam, The Netherlands*

⁵*Manchester Centre for Integrative Systems Biology,
Manchester Interdisciplinary Biocentre, The University of Manchester, UK*

⁶*Department of Chemistry, Stanford University, CA*

Yeast glycolytic oscillations is one of the best known oscillatory system and have therefore been studied since the 1950s in cell-free extracts and intact cells. However, until 2012 sustained oscillations had only been observed at the population level, i.e. for synchronized cultures at high biomass concentrations. Using optical tweezers to position yeast cells in a microfluidic chamber, we were able to observe sustained oscillations in individual isolated cells and determine the precise conditions for autonomous glycolytic oscillations.

Using a detailed kinetic model for the cellular reactions, we simulated the heterogeneity in the response of the individual cells, assuming small differences in a single internal parameter. Hopf bifurcation points were determined experimentally in individual cells as a function of glucose and cyanide concentrations. The results could be interpreted in terms of an oscillatory manifold in a three-dimensional state-space; crossing the boundaries of the manifold coincides with the onset of oscillations and positioning along the longitudinal axis of the volume sets the period. The oscillatory manifold could be approximated by allosteric control values of phosphofructokinase for ATP and AMP.

Cell signaling, gene expression, and metabolism are affected by cell-cell heterogeneity and random changes in the environment. The effects of such fluctuations on cell signaling and gene expression have recently been studied intensively using single-cell experiments. In metabolism heterogeneity may be particularly important because it may affect synchronisation of metabolic oscillations, an important example of cell-cell communication. This synchronisation is notoriously difficult to describe theoretically as the example of glycolytic oscillations shows: neither is the mechanism of glycolytic synchronisation understood nor the role of cell-cell heterogeneity. To pin down the mechanism and to assess its robustness and universality we have experimentally investigated the entrainment of glycolytic oscillations in individual yeast cells by periodic external perturbations. We find that oscillatory cells synchronise through phase shifts and that the mechanism is insensitive to cell heterogeneity (robustness) and similar for different types of external perturbations (universality).

Capturing time-varying dynamics - Lectures from brain dynamics

Klaus Lehnertz

*Department of Epileptology and
Helmholtz Institute for Radiation and Nuclear Physics and
Interdisciplinary Center for Complex Systems, University of Bonn, Germany*

The human brain is a complex network of interacting non-stationary subsystems, whose complicated spatial-temporal dynamics is still poorly understood. Synchronization plays an important role in brain functioning and dysfunctioning. A prominent example for pathophysiologic neuronal synchronization is epilepsy along with its cardinal symptom, the epileptic seizure. Epilepsy affects approximately 1% of the world's population, and in about 25% of individuals with epilepsy seizures cannot be controlled by any available therapy. There is now increasing evidence for the existence of large-scale epileptic networks in which all constituents can contribute to the generation, maintenance, spread, and termination of even focal seizures as well as to the many pathophysiologic phenomena seen during the seizure-free interval. In this talk, I will provide a brief overview of the progress that has been made in understanding the time-varying dynamics of large-scale epileptic networks and will discuss challenging issues associated with the inference of weighted and directed functional networks from multivariate recordings of brain dynamics as well as possible research directions that may help to find better solutions.

References

Lehnertz K. et al. (2009) Synchronization phenomena in human epileptic brain networks. *J. Neurosci. Methods* **183**, 42–48.

Lehnertz K. (2011) Assessing directed interactions from neurophysiological signals—an overview. *Physiol. Meas.* **32**, 1715–1724.

Lehnertz K. et al. (2014) Evolving networks in the human epileptic brain. *Physica D* **267**, 7–15.

An Introduction to the Qualitative Theory of Nonautonomous Dynamical Systems

Martin Rasmussen

Imperial College London, Department of Mathematics, London, United Kingdom

The study of dynamical systems concerns the long-term behaviour of a set of variables (the state of the system) based only on the knowledge of an initial condition and a set of rules (the evolution equations). Most commonly studied examples are differential equations which model large classes of applications such as planetary motion, chemical reactions, population dynamics, consumer behaviour or stock markets.

A breakthrough in the understanding of dynamical systems was initiated by Henri Poincaré and Aleksandr Lyapunov, who developed in the late 19th century an approach that embraced the use of topological and geometrical techniques to the study of dynamical systems, in addition to the traditional analytical side. This development got real momentum in the second half of the 20th century, leading to the now relatively well developed qualitative theory for classical (i.e. autonomous and deterministic) dynamical systems

In contrast to an autonomous dynamical system, the time evolution of a nonautonomous dynamical system is influenced by an independent process (which reflects changes in the rules governing the system). The importance of nonautonomous dynamical systems is illustrated by the fact that a significant number of real-world applications are governed by time-dependent inputs, and the traditional mathematical theory fails to address this. Cardiovascular oscillators, weather phenomena associated to climate change such as El Nino, and the carbon cycle are examples of important dynamical processes that require sophisticated models to take nonautonomous influences in form of changes of parameters into account.

There has been rapid progress concerning the development of a qualitative theory for nonautonomous dynamical systems in the last thirty years. This talk gives an introduction to this theory, and similarities and differences to the autonomous case will be highlighted.

References

Kloeden, P.E., and Rasmussen, M., 2011, *Nonautonomous Dynamical Systems*, vol. 176 of Mathematical Surveys and Monographs, American Mathematical Society, Providence.

3.2 Special talks

Know what you know - Some guidance for efficient experimental and clinical study design

Thomas Jaki¹

¹Medical and Pharmaceutical Statistics Research Unit
Department of Mathematics and Statistics
Lancaster University

Conducting an experiment or clinical study is an elaborate process that is both time consuming and expensive. Yet often only little consideration is given to the way the study is designed and the question of how the resulting data will be analysed is often only considered once the data have been collected.

In this talk we will highlight the importance of good design (which should determine how the study is analysed subsequently) drawing particular attention to the underlying question that one is hoping to answer with the study and discuss general principles of good design. We will discuss so called adaptive designs that allow design modifications on the bases on accumulated data and illustrate their utility as well as their drawbacks on the basis of clinical trial examples.

Psychological and hormonal effects on cardiovascular regulation

Sandra I. Sünram-Lea

Lancaster University, Department of Psychology, Lancaster, UK

The cardiovascular system is subject to various dynamical processes enabling adaptive changes under a wide range of circumstances. The resultant changes allow rapid cardiovascular responses to a number of physiological and psychological factors, including stress. Currently, a wide variety of research avenues are used in the pursuit to better understand the effects and consequences of stress. It is well established that anticipation or exposure to stressors results in activation of two major endocrine systems, the hypothalamic-anterior pituitary-adrenocortical axis and the sympatho-adrenomedullary axis. Together, these systems regulate physiological and behavioral stress processes, which are overall adaptive in the short term, but can be maladaptive in the long-term in vulnerable individuals.

Our social and physical environment exerts strong effects on the brain and the body through the neuroendocrine, autonomic, and immune systems (McEwan, 2007). The ability of the brain and the body to adapt to acute and chronic mental stress is an increasingly important topic in the modern world. Chronic mental stress can have a serious impact on physical as well as psychological health in vulnerable individuals (Cohen, Janicki-Deverts, Miller, 2007). Indeed prolonged mental stress has been linked to several cardiovascular diseases (Dimsdale, 2008; Hjortskov et al., 2004). In this talk, I will provide a brief overview of the evidence pertaining to the patterns of bidirectional communication between the brain, the autonomic, and cardiovascular systems via neural and endocrine mechanisms following stress exposure. In addition, somatic and behavioural response variability that appears to moderate the effects of mental stress on stress systems activation and cardiovascular response will be discussed.

The negative health outcomes associated with mental stress are a matter of growing concern. Large sections of the general public are likely to experience periods of mental stress and this highlights the importance of assessing the effects of stress on multiple systems, including hormonal, cardiovascular and neural responses. A multidisciplinary approach is needed to further our understanding about the effects of stress on various systems and to identify mechanisms and vulnerabilities leading to disease. A more complete understanding of the individual differences in the response to stress will help to explore ways in which resilience can be harnessed to improve individual health outcomes.

References

- McEwan, B.S. (2007) Physiology and neurobiology of stress and adaptation: Central role of the brain. *Physiol Rev* **87**, 873–904.
- Cohen, S., Janicki-Deverts, D., Miller, G.E. (2007) Psychological stress and disease. *JAMA* **298**, 1685–1687.
- Dimsdale, J. E. (2008) Psychological stress and cardiovascular disease. *Journal of the American College of Cardiology* **51**, 1237–1246.
- Hjortskov, N., Rissen, D., Blangsted, A., Fallentin, N., Lundberg, U., and Sjøgaard, K. (2004) The effect of mental stress on heart rate variability and blood pressure during computer work. *European Journal of Applied Physiology* **92**, 84–89.

3.3 Oral presentations

Use of detrended fluctuation analysis for sleep vs wake classification from heart rate variability

M. Aktaruzzaman*, M. W. Rivolta, R. Karmacharya, L. Pugnetti,
M. Garegnani, G. Bovi, M. Ferrarin and R. Sassi

I. INTRODUCTION

Sleep is a dynamic process that plays a significant role in the genesis and insurgence of some pathologies such as cardiac, neurological, and metabolic disorders. The standard assessment of sleep quality is performed professionally in a sleep laboratory using whole night polysomnography (PSG), which requires signals recorded from electroencephalogram (EEG), electrooculogram (EOG), and electromyogram (EMG). According to the American Academy of Sleep Medicine (AASM) [1], at least three EEG, two unipolar EOG, and three EMG recordings are needed for an appropriate sleep staging. An overnight sleep is typically divided into epochs (30 seconds), each of which is categorized as WAKE, non-rapid eye movement (NREM), and rapid eye movement (REM). NREM is again subdivided into sleep stage 1 (NREM1), stage 2 (NREM2), and stage 3 (NREM3). Unfortunately, the use of PSG-based sleep staging is restricted by some serious limitations such as cost of equipments, need of a special sleep laboratory and of trained personnel, and it is also time consuming, which makes PSG unsuitable for monitoring large populations. Moreover, many sleep disorders are not found on daily basis, therefore some sleep disorders might be missed, if one or two nights are assessed only.

Despite the clear utility of PSG in clinical sleep medicine, its limitations have motivated the development of alternative methods for long-term evaluating of sleep at home. Many different studies [2], [3] have demonstrated the strong relationship between sleep and heart rate variability (HRV, the variation in time interval between successive heart beats). It has the advantages of being a low cost and noninvasive method to get insight into autonomic nervous system (ANS) functioning.

In some previous studies [4], [5], fluctuation analysis has been found effective for quantifying changes in HRV as well as sleep stages. Detrended fluctuation analysis (DFA) short term exponent was reported as one of the best relevant features. However, the maximum accuracy was achieved for 10 consecutive epochs (the maximum number considered) (or 5 minutes) from each sleep stage. In fact, the estimation of DFA requires a number of points, which is not always available for a single epoch. One possible way is to re-sample the HRV series [6], and another is to consider a number of surrounding epochs, as commonly done for sleep

classification using acceleration signals [7]. However, there is no standard rule for how many preceding and following epochs should be considered. The objectives of this work are to study: (i) how many epochs are necessary for maximum accuracy? (ii) which is the optimal positioning of the epochs (before/after)? (iii) what is the predictive power of DFA alone? (iv) what together other commonly used features?

II. DATA ACQUISITION

For this study, the ECG data were collected from 5 healthy subjects (average age: 30 ± 2 , 4 male, 1 female). For each subject, a full PSG was recorded using the Xltek Trex HD Ambulatory EEG at home for one night. Proper instructions, about using the device for the PSG, were given to the subjects by neurologists at Don Gnocchi Hospital, Milano, Italy so that they could perform the recordings at home. Then, the sleep scoring was done manually by the same neurologists on each 30-s epoch according to the guidelines of AASM [1]. The ECG signal was collected from the left upper chest using two electrodes with sample frequency 200 Hz. NREM1 is a transition sleep stage and it is typically either discarded or merged into wake (the subject has the feeling of a lack of sleep). In here we followed the second strategy.

III. METHODS

A brief description of the methods applied for automatic SLEEP (REM, NREM2 and NREM3) vs WAKE (WAKE and NREM1) classification from HRV is given in the following subsections:

A. Preprocessing

Beats location and labelling was performed on ECG using the Physionet's algorithm `gqrs`. Then, HRV series of different lengths (3 to 15 epochs) were constructed by starting at 1 epoch before, 1 epoch after and increasing the number of surrounding epochs up to 14 (7 epochs before, 7 epochs after). The selection of the series was shifted by one epoch to the right, so to cover the entire recording (with overlap). Artifacts falling outside the range $Q_1 - 3 \times (Q_3 - Q_1)$ to $Q_3 + 3 \times (Q_3 - Q_1)$ were discarded, where Q_i is the i -quartiles. The segments with more than 50% of the samples detected as artifacts have been discarded from this study.

B. Parameters estimation

A set of linear parameters, like normalized power in low frequency (LF) and high frequency (HF) bands, their ratio LF/HF and sample entropy ($SampEn_{TH}$) [8] were estimated for an AR model fitted to the HRV series. The mean of RR intervals ($mean_{RR}$) normalized by the mean

M. Aktaruzzaman, M. W. Rivolta, R. Karmacharya, and R. Sassi are with Università degli Studi di Milano, Italy (*corresponding author e-mail: md.aktaruzzaman@unimi.it).

L. Pugnetti, M. Garegnani, G. Bovi and M. Ferrarin are with IRCCS S. Maria Nascente, Fond. Don Carlo Gnocchi Onlus, Milano.

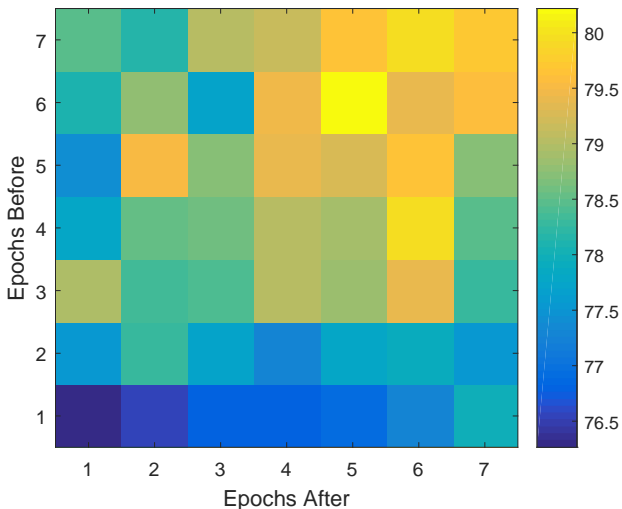


Fig. 1. Mean accuracy of SLEEP vs WAKE classification for different combinations of the surrounding epochs with the current epoch

of the entire series, standard deviation ($SDNN$), root mean square of successive differences ($RMSSD$) along with the DFA short scale exponent ($DFA_{\alpha 1}$), and probability of agreement ($prob_{Agree}$) [5], between sample entropy (SampEn) numerically estimated and the SampEn of the AR model obtained through 200 realizations of the model, were also computed from the series. In fitting the AR model, the order was determined by satisfying the Akaike information criterion (AIC) and Anderson’s whiteness test. To the best of our knowledge, there is no universal indication about m and r . Here, we have considered $m=1$ and $r=0.2 \times STD$ as used in our previous study [5].

TABLE I POWER OF DFA IN DISTINGUISHING SLEEP VS WAKE. TD = TIME DOMAIN / FD = FREQUENCY DOMAIN PARAMETERS.

| | $DFA_{\alpha 1}$ | TD+FD+ $DFA_{\alpha 1}$ | All Features |
|----------------------|------------------|-------------------------|--------------|
| Accuracy | 57.93 | 78.81 | 80.22 |
| Cohen’s Kappa | 0.13 | 0.46 | 0.49 |

C. Sleep vs Wake classification

To the aim of our first and second objective, the set of features (described in section III-B) were used to train and test a support vector machine (SVM), as in [6], using K-fold ($K = 10$) cross-validation technique. The procedure has been repeated 10 times and the average considered as final estimate of the classification accuracy. The best combination of surrounding epochs was selected based on maximizing this average accuracy. The rest of this study was performed on the combination of epochs detected as the best one. To the aim of remaining objectives, we trained and tested the SVM classifier using (i) $DFA_{\alpha 1}$ alone; (ii) $DFA_{\alpha 1}$ with other time and frequency domain parameters; (iii) All extracted features.

D. Results

The mean accuracies for different combinations are depicted in figure 1. The combination of 6 preceding and 5 following epochs has been found as the best one which gives the maximum accuracy of 80.22% (with a reliability measured by Cohens’ Kappa of 0.49) of the SLEEP vs WAKE classification. The predictive power of DFA alone, and also with the other considered features, in SLEEP vs WAKE classification has been reported in table I.

IV. CONCLUSION

The epoch-based SLEEP vs WAKE classification is possible by considering a combination of surrounding epochs, and only a few (6 before and 5 after) are sufficient for getting considerable results. The detrended fluctuation analysis short term exponent itself can predict with more than 50% of accuracy, but it gives significantly higher accuracy (with larger reliability) when combining it with other time and frequency domain features. This method gives slightly better results for SLEEP vs WAKE classification, even with a small number (7) of simple features, than similar studies performed with 10 features [6]. However, subject specific training and testing have been considered in those studies, here we have considered all subjects. So, our results are a more precise estimate of how the method would generalize, when applied to a different population, compared to them.

A limitation of this study is that it has been performed on few subjects only, due to the complex procedure connected to data collection. To extend this result, in future we plan to collect data on more subjects.

REFERENCES

- [1] C. Iber, S. Ancoli-Israel, A. L. Chesson, and S. F. Quan, *The AASM Manual for the Scoring of Sleep and Associated Events*, 1st ed. Westchester, Illinois, U.S.A.: American Academy of Sleep Medicine, 2007.
- [2] A. J. Welch and P. C. Richardson, “Computer sleep stage classification using heart rate data,” *Electroencephalogr Clin Neurophysiol*, vol. 34, no. 2, pp. 145–152, 1973.
- [3] E. Vanoli, P. B. Adamson, n. Ba-Lin, G. D. Pinna, R. Lazzara, and W. C. Orr, “Heart rate variability during specific sleep stages. A comparison of healthy subjects with patients after myocardial infarction,” *Circulation*, vol. 91, no. 7, pp. 1918–1922, 1995.
- [4] T. Penzel, J. W. Kantelhardt, L. Grote, J.-H. Peter, and A. Bunde, “Comparison of detrended fluctuation analysis and spectral analysis for heart rate variability in sleep and sleep apnea,” *IEEE Trans Biomed Eng*, vol. 50, no. 10, pp. 1143–1151, 2003.
- [5] M. Aktaruzzaman, M. Migliorini, M. Tenhunen, S. L. Himanen, A. M. Bianchi, and R. Sassi, “The addition of entropy-based regularity parameters improves sleep stage classification based on heart rate variability,” *Med Biol Eng Comput*, vol. 53, no. 5, pp. 415–425, 2015.
- [6] M. Adnane, Z. Jiang, and Z. Yan, “Sleepwake stages classification and sleep efficiency estimation using single-lead electrocardiogram,” *Expert Syst Appl*, vol. 39, no. 1, pp. 1401–1413, 2012.
- [7] A. Sadeh, K. M. Sharkey, and M. A. Carskadon, “Activity-based sleep-wake identification: an empirical test of methodological issues,” *Sleep*, vol. 17, no. 3, pp. 201–207, 1994.
- [8] M. Aktaruzzaman and R. Sassi, “Parametric estimation of sample entropy in heart rate variability analysis,” *Biomed Signal Process Control*, vol. 14, pp. 141–147, 2014.

Determining Factors for Non-Invasive Fetal ECG Quality: a case study

Fernando Andreotti¹, Alexander Jank², Sophia Schröder²,
Susanne Löther², Julia Kage², Claudia Schmieder², Holger Stepan²,
Hagen Malberg¹ and Sebastian Zaunseder¹

¹*Institute of Biomedical Engineering , TU Dresden, Dresden, Germany*

²*Department of Obstetrics, University Hospital of Leipzig, Leipzig, Germany*

Introduction: The non-invasive fetal electrocardiogram (NI-FECG) offers novel diagnostic possibilities for prenatal medicine. Despite being applicable from the 20th week of gestation (WOG) onwards, few studies have assessed NI-FECG’s feasibility at its early stages (WOG < 28). During this period, the autonomic regulation for healthy fetuses is expected to further develop, thus, NI-FECG can be useful in providing antepartum additional clinical information. In this contribution, we aim at quantifying the usability of NI-FECG recording from 18th to the 28th WOG.

Data Material: Data was acquired at the Department of Obstetrics and Gynecology at the University Hospital of Leipzig (local ethics committee approval 348-12-24092012). Multichannel recordings ($n = 175$, each with 20 min duration, 1 maternal and 7 abdominal channels) from 62 singleton pregnancies (67% physiological) from early stage pregnancies (mean/standard deviation: 24.1 ± 3.4 weeks) were used in this study as described in Andreotti *et al.* (2014). Patients showed different placental positions (42% posterior, 29% anterior, fundal 16%, sideways 2% and 11% others), levels of amniotic fluid (80% normal, 15% under, 5% over norm), fetal presentations (41% vertex, 29% breech, 7% should, 23% unknown) and BMIs (26.3 ± 5.1 kg). Five equidistant 5 s segments extracted from each recording’s channel were carefully annotated by four experts (A, B, C and D) for their FECG amplitude (‘not present’, ‘low’, ‘moderate’, or ‘high’) and SNR levels (‘unacceptable’, ‘bad’, ‘adequate’, ‘good’, ‘excellent’). Observers A and B annotated every segment, while C and D annotated in a complementary manner 72.6% and 37.0% of the data, respectively, so that at least 3 annotations for each segment of the whole data were available. A subset of 500 segments were annotated by every observer twice to evaluate intra-observer reliability.

Methods and Results: Results showed a very good intra-rater (> 0.86) and inter-rater (> 0.90) agreement on average using AC_2 statistics by Gwet (2008). Majority voting was used to generate a consensus for both FECG and SNR criteria in each segment, ties were decided by randomly choosing one of the most voted alternatives. To assess the associations between the clinical information and consensus FECG and SNR annotations a statistical analysis was carried out. Bivariate analysis of effect

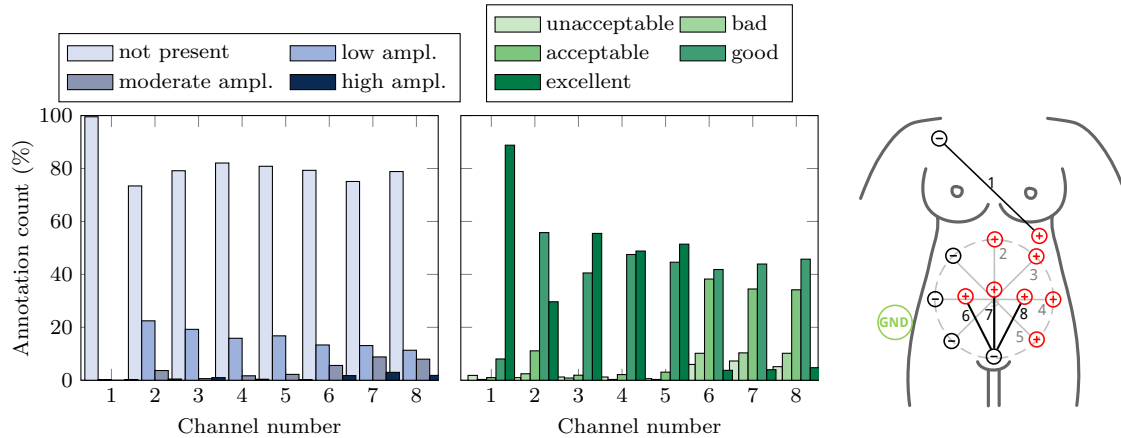


Figure 1: Channel-by-channel overview of consensus FECG (left) and SNR (middle) annotations for this study; electrode configuration on the right.

sizes was performed regarding the independent (interval, ordinal, nominal scaled) and dependent variables (ordinal - FECG/SNR). Strong associations were found for FECG amplitude and channel number ($\eta = 0.78$ - see Fig. 1), between SNR and patient pathophysiological state ($\eta = 0.66$) and fetal presentation ($\eta = 0.63$) and placental position ($\eta = 0.61$). Moderate association was found SNR-channel ($\eta = 0.34$), FECG and fetal/placental position ($\eta = 0.38/0.35$). Weak associations were found between FECG amplitude and patients' state ($\eta = 0.21$). A very significant ($p < 0.001$) association strength (i.e. correlation) was found for most parameters, however, no association was found between FECG/SNR and BMI, amniotic fluid's level or WOG.

Conclusion: Results showed that the quality of NI-FECG recordings between the 18-28th WOG strongly differs from values reported in literature (usually for later stages of pregnancy). Aside from the presented factors, further analyses should take into consideration mother's positioning and skin-electrode impedance.

Acknowledgement

FA thanks the Conselho Nacional de Desenvolvimento Tecnológico (Brazil) for its financial support.

References

Andreotti, F., Riedl, M., Himmelsbach, T., Wedekind, D., Wessel, N., Stepan, H., Zaunseder, S. (2014). Robust fetal ECG extraction and detection from abdominal leads. *Physiol. Meas.*, **35**(8), 15511567.

Gwet, K. (2008). Computing inter-rater reliability and its variance in the presence of high agreement. *Br. J. Math. Stat.* **61**(Pt 1),29-48.

Assessment of Instantaneous Linear and Nonlinear Heartbeat Dynamics During Seizures in Untreated Temporal Lobe Epilepsy

**Riccardo Barbieri^{1,2}, Gaetano Valenza^{2,3}, Luca Citi⁴, Fabio Placidi^{5,6},
Francesca Izzi⁶, Maria Albanese⁶, Maria Grazia Marciani^{5,6},
Andrea Duggento⁵, Maria Guerrisi⁵, Andrea Romigi⁶, Nicola Toschi^{2,5}**

¹*Politecnico di Milano, Milan, Italy*

²*Harvard Medical School, Massachusetts General Hospital, Boston, USA*

³*University of Pisa, Pisa, Italy*

⁴*University of Essex, Colchester, UK*

⁵*University of Rome "Tor Vergata", Rome, Italy*

⁶*Tor Vergata University Hospital, Rome, Italy*

Heart Rate Variability (HRV) changes in epilepsy are known to be associated with both ictal and interictal autonomic cardiac effects [1]. In general, interictal autonomic disorders include a variety of alterations in sympathetic/parasympathetic modulation, including combined inhibition or suppression [2] of both sympathetic and parasympathetic tone, selective suppression of sympathetic or parasympathetic tone, as well as low parasympathetic and high sympathetic tone [3]. While an involvement of the central autonomic network in these disorders has previously been hypothesized, the mechanisms leading to autonomic alterations in epilepsy are not yet well understood. Moreover, while it has been widely accepted that the quantification of Autonomic Nervous System (ANS) dynamics can provide useful information on psychophysiological and pathological states [4], to date, little is known about HRV changes in untreated patients with untreated temporal lobe epilepsy (TLE). In this study, we hypothesize that instantaneous linear, nonlinear, and complexity measures of ANS activity can be employed in characterizing the ANS activity in patients with untreated TLE, particularly immediately preceding ictal events.

Bipolar ECG recordings (sampling frequency: 256 Hz) were collected from 10 patients (age: 40.4±17 years) with at least one seizure originating from temporal regions as recorded by video-EEG monitoring. For each patient, we selected a) a 2-minute long artifact-free interictal period (INT) and b) a 2-minute long artifact-free period immediately preceding a seizure (PRE). After R peak recognition, we investigated linear and nonlinear ANS dynamics through our recently proposed framework related to the inhomogeneous point-process theory [5-7]. To this end, the unevenly sampled RR interval series is modeled through probability density functions, which characterize and predict the time until the next ventricular event occurs as a function of the past history. Within this framework, Laguerre expansions of the Wiener-Volterra autoregressive terms account for long-term nonlinear information. Specifically, we estimated ANS-related metrics defined in the time and frequency domains [5-7], along with measures of instantaneous complexity (dominant Lyapunov exponent and entropy) [7] and higher-order statistics (bispectra) [6].

All time-varying estimates were collapsed across time into measures of central tendency (median) and dispersion (median absolute deviation) and employed for subsequent group comparison as well as single-patient classification. In this context, in order to develop a processing chain in line with the clinical need of single-subject classification, we complemented the study of group-wise statistical differences with the training and validation of an automatic classification algorithm which includes a feature selection procedure. In

particular, we investigated whether feeding our combined linear/nonlinear feature set into a Support-Vector-Machine-based machine learning approach, employed in a leave-one-out validation setting, would be able to discern PRE from INT (hence anticipating the onset of ictal events).

Upon fitting the point-process model to the data, Kolmogorov-Smirnov distance and autocorrelation plot analyses revealed a satisfactory goodness-of-fit - we were therefore able to retain all data originally sampled. No significant differences in HRV metrics (first and second moment orders) were found between preictal events in untreated TLE and interictal periods (Wilcoxon signed rank test: $p > 0.05$). However, when applying a machine learning approach (where data gathered from each subject constitutes one multidimensional point in the full feature space along with its class label) to data from INT and PRE phases, we achieved a satisfactory recognition accuracy when aiming at discerning INT and PRE phases of 73.91%, with a specificity of 84.61% and a sensitivity of 60.00%. When removing features related to variability across time, the classification accuracy dropped to 60.87%, with a specificity of 61.54% and a sensitivity of 60.00%.

In summary, our results point towards subtle autonomic changes which may accompany or precede seizures and can only be detected using an instantaneous, time resolved approach to quantifying ANS activity. The ability to discern (with good sensitivity and specificity) a pre-critical phase in single-patient classification using exclusively ECG recordings indicates the possibility of devising a simple, inexpensive predictive patient monitoring tool targeted to real-time prediction of ictal events.

References

- [1] L. D. Blumhardt, P. E. Smith, and L. Owen, "Electrocardiographic accompaniments of temporal lobe epileptic seizures," *Lancet*, vol. 1, pp. 1051-6, May 10 1986.
- [2] N. Shobha, P. Sathishchandra, T. Sathyaprabha, and K. Udupa, "A study of interictal cardiac autonomic functions in patients with refractory complex partial epilepsy secondary to medial lobe pathology: Before and after surgery.," *Neurology Asia*, vol. 12, pp. 69-80, 2007.
- [3] M. Dutsch, M. J. Hilz, and O. Devinsky, "Impaired baroreflex function in temporal lobe epilepsy," *J Neurol*, vol. 253, pp. 1300-8, Oct 2006.
- [4] H. R. Variability, "Standards of measurement, physiological interpretation, and clinical use. Task Force of the European Society of Cardiology and the North American Society of Pacing and Electrophysiology," *Circulation*, vol. 93, pp. 1043-1065, 1996.
- [5] G. Valenza, L. Citi, E. P. Scilingo, and R. Barbieri, "Inhomogeneous point-process entropy: An instantaneous measure of complexity in discrete systems," *Physical Review E*, vol. 89, 2014/05 2014.
- [6] G. Valenza, L. Citi, E. P. Scilingo, and R. Barbieri, "Point-Process Nonlinear Models With Laguerre and Volterra Expansions: Instantaneous Assessment of Heartbeat Dynamics," *IEEE Transactions on Signal Processing*, vol. 61, pp. 2914-2926, 2013/06 2013.
- [7] G. Valenza, L. Citi, and R. Barbieri, "Estimation of Instantaneous Complex Dynamics through Lyapunov Exponents: A Study on Heartbeat Dynamics," *PLoS ONE*, vol. 9, p. e105622, 2014/08/29 2014.

Conditional joint transfer entropy of cardiovascular and cerebrovascular control systems in subjects prone to postural syncope

Vlasta Bari¹, Andrea Marchi^{2,3}, Beatrice De Maria^{2,4}, Gianluca Rossato⁵, Giandomenico Nollo^{6,7}, Luca Faes^{6,7} and Alberto Porta^{1,8}

¹University of Milan, Department of Biomedical Sciences for Health, Milan, Italy

²Politecnico di Milano, Department of Electronics Information and Bioengineering, Milan, Italy

³San Gerardo Hospital, Department of Emergency and Intensive Care, Monza, Italy

⁴IRCCS Fondazione Salvatore Maugeri, Milan, Italy

⁵Department of Neurology, Sacro Cuore Hospital, Negrar, Verona, Italy

⁶BIOtech, Department of Industrial Engineering, University of Trento, Trento, Italy

⁷IRCS Program, PAT-FBK, Trento, Italy

⁸IRCCS Policlinico San Donato, Department of Cardiothoracic, Vascular Anesthesia and Intensive Care, Milan, Italy

Introduction

Cardiac baroreflex is a short-term reflex adjusting heart period (HP) to changes of systolic arterial pressure (SAP) [1], while cerebral autoregulation modifies mean cerebral blood flow, usually studied through its surrogate, mean cerebral blood flow velocity (mCBFV), in response to changes of mean arterial pressure (mAP) [2]. Respiration (R) disturbs and influences cardiovascular (CV) and cerebrovascular (CBV) interactions [3]. Recently, information-theoretic approaches [4-6] have been proposed to assess the information jointly transferred from a pair of exogenous variables to a target one conditioned on one of the exogenous variables, i.e. the so-called conditional joint transfer entropy (CJTE). In the present study the CJTE was computed, as described in [6], to quantify the CV regulation between HP and SAP and the CBV control between mCBFV and mAP along predefined causal directions and conditioned on the same signal (i.e. R) during head-up tilt test in subjects with recurrent episodes of postural syncope, contrasting results with those derived from healthy individuals.

Experimental protocol and methods of analysis

Thirteen healthy subjects (nonSYNC, age: 27±8 years, 5 males) were studied together with 13 subjects with previous history of unexplained syncope (SYNC, age: 28±9 years, 5 males) at rest in supine position (REST) and during 60 degrees head up-tilt (TILT). The study adhered to the principles of the Declaration of Helsinki and was approved by the local Ethics Committee. ECG, photoplethysmographic arterial pressure (AP), cerebral blood flow velocity (CBFV) through a transcranial Doppler device and R through a thoracic impedance belt were acquired with a sampling frequency of 1 kHz. For a complete description of the protocol we make reference to [3]. HP was derived as the temporal distance between two R-wave peaks on the ECG, SAP as the maximum of AP inside the HP, mAP and mCBFV as the integral of AP and CBFV, respectively, between two consecutive diastolic values (i.e. the minimum of the relative signal inside the HP) divided by the inter-diastolic interval and R was sampled in correspondence of the first R-wave delimiting HP. Sequences of 250 consecutive beats were selected for each series of each subject at REST and during TILT. CJTE from SAP and R to HP given R ($CJTE_{SAP,R \rightarrow HP|R}$), CJTE from HP and R to SAP given R ($CJTE_{HP,R \rightarrow SAP|R}$), CJTE from mAP and R to mCBFV given R ($CJTE_{mAP,R \rightarrow mCBFV|R}$), CJTE from mCBFV and R to mAP given R ($CJTE_{mCBFV,R \rightarrow mAP|R}$) were computed according to [6], accounting for zero-lag effects from SAP to HP and from R to any other variable [7]. Two-way repeated measures

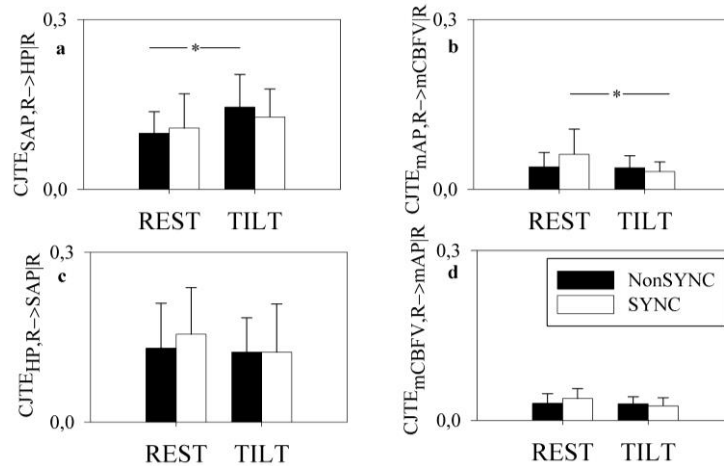


Figure 1. Grouped bargraphs show mean plus standard deviation of $CJTE_{SAP,R \rightarrow HP|R}$ (a), $CJTE_{mAP,R \rightarrow mCBFV|R}$ (b), $CJTE_{HP,R \rightarrow SAP|R}$ (c), and $CJTE_{mCBFV,R \rightarrow mAP|R}$ (d) at REST and during TILT in NonSYNC (black bars) and SYNC (white bars) subjects: The symbol * indicates $p < 0.05$.

analysis of variance (one factor repetition, Holm-Sidak correction for multiple comparisons) was applied to check differences between groups and conditions. A $p < 0.05$ was considered as significant.

Results

Figure 1 reports the CJTE evaluated over CV (Figs.1a,c) and CBV (Figs.1b,d) control systems in NonSYNC (black bars) and SYNC (white bars) subjects as a function of the experimental condition (i.e. REST and TILT). $CJTE_{SAP,R \rightarrow HP|R}$ increased during TILT in NonSYNC subjects, while it was not different either between-conditions in SYNC subjects or between-groups in both conditions. $CJTE_{mAP,R \rightarrow mCBFV|R}$ was significantly reduced in SYNC subjects after TILT with respect to REST but it did not change in NonSYNC ones or between-groups. $CJTE_{HP,R \rightarrow SAP|R}$ and $CJTE_{mCBFV,R \rightarrow mAP|R}$ did not show any between group and between condition differences.

Discussion and conclusions

CJTE applied over CV and CBV variabilities allowed us to determine differences in SYNC and NonSYNC subjects during TILT. In particular, the information jointly transferred from SAP and R to HP conditioned on R increased during TILT only in NonSYNC subjects, thus suggesting the impairment of physiological baroreflex control in SYNC group [3,7]. Conversely, the information jointly transferred from mAP and R to CBFV conditioned on R declined in SYNC individuals during TILT, thus pointing to a derangement of the CBV regulation [7,8]. Remarkably, both findings were detected well before the development of presyncope signs in SYNC patients indicating that CJTE could be exploited for the early detection of syncope. The joint study of CV and CBV control systems could improve the understanding of the interactions among these homeostatic regulations and contribute to the clarification of the process of postural syncope development.

References

- [1] Laude D *et al*, 2004, *Am. J. Physiol.* **286**, R226-R231.
- [2] Aaslid R *et al*, 1989, *Stroke* **20**, 45-52.
- [3] Bari V *et al*, 2016, *Philos. Trans. R. Soc. A*, in press.
- [4] Marinazzo D *et al*, 2012, *Comput. Math. Methods Med.* **2012** 303601.
- [5] Barnett L *et al*, 2009 *Phys. Rev. Lett.* **103** 238701.
- [6] Porta A *et al*, 2015, *Front. Physiol.* **6** 301.
- [7] Faes L *et al*, 2013, *Auton. Neurosci.-Basic Clin.* **178**, 76-82.
- [8] Dan D *et al*, 2002, *J. Am. Coll. Card.* **39**, 1039-1045.

The novel concept of time delay stability and identifying dynamic networks of physiological systems

Ronny P. Bartsch

Bar-Ilan University, Department of Physics, Ramat Gan, Israel

The human organism is an integrated network, where multi-component physiological systems continuously interact through various feedback mechanisms to optimize and coordinate their function. Yet, despite the importance to basic physiology and the broad clinical relevance, the nature of interactions between diverse physiological systems and their collective role in maintaining health is largely unknown. This may be due to the several layers of complexity inherent to the dynamics of organ systems that range from the intermittent and nonlinear behavior of the individual output signals to the continuous alterations in their feedback and coupling. Here, we introduce the novel concept of time delay stability (TDS) to probe interactions among diverse systems. The TDS method determines the time delay with which modulations/bursts in the output dynamics of a given system are consistently followed by corresponding modulations in the signal output of other systems. Utilizing TDS, we distinguish between stable and unstable interactions, characterize coupling strength and identify a physiological network. We find that the network undergoes transitions with changes in physiological state, demonstrating a robust interplay between network and function. These empirical investigations shed new light on the mechanisms of organ interactions and establish first association between patterns of physiological network interactions and specific physiologic states.

Assessing cardiovascular control in children with sleep disordered breathing using predictive information decomposition

Fatima El-Hamad, and Mathias Baumert

University of Adelaide, Electrical and Electronic Engineering, Adelaide, Australia

Introduction

Sleep-disordered breathing (SDB) during childhood may lead to cardiovascular disease in adulthood. Increased blood pressure variability (BPV) and reduced baroreflex sensitivity have been previously reported, indicative of sympathetic activation [1]. In this study we assess cardiovascular control in children with SDB using the information decomposition framework [2].

Methods

We analysed overnight polysomnography (PSG) of 40 children with SDB and 40 healthy non-snoring children matched for age and gender [3]. Event-free beat-to-beat heart period (RR), pulse transit time (PTT) and respiration (R) segments were extracted with a fixed length of 350 samples during non-rapid eye movement sleep (NREM), slow wave sleep (SWS) and deep sleep (REM). PTT was used to indirectly measure BPV [4]. The predictive information in RR (PI_{RR}) was computed as the sum of RR information storage (SE_{RR}), information transfer from respiration to RR ($TE_{R \rightarrow RR}$) and conditional information transfer from PTT to RR given respiration ($TE_{PTT \rightarrow RR|R}$) [2]. Entropies were computed using a linear estimator with uniform embedding ($L = 10$). Independent identically-distributed surrogates approach was used for validation. Mann-Whitney test was used to compare: 1) the control and SDB groups, and 2) sleep stages. Values of $p < 0.05$ were considered statistically significant.

Results

Mean PTT and PTT variance (PTTV) were significantly higher in SDB children, while mean RR (RRm) and RR variance (RRV) did not differ between the two groups. RRm and PTTV were higher in REM compared to NREM only in the control group (Table 1).

Table 1: Mean and variance of RR and PTT.

| Variable | Control [^] | | | SDB [^] | | |
|-------------------------|----------------------|-----------------|-----------------------------|------------------|-----------------|------------------|
| | NREM | SWS | REM | NREM | SWS | REM |
| RRm (ms) | 788 [713 - 856] | 762 [697-847] | 719 ^{§+} [651-787] | 779 [702 - 841] | 730 [673-809] | 713 [671-779] |
| RRV (ms ²) | 2630 [1620-4990] | 2430[1060-5160] | 2335[1353-5190] | 3040[1375-9105] | 2135[1104-6060] | 2220 [1565-6495] |
| PTTm (ms) | 357[339-417] | 353 [339-411] | 355 [328-407] | 422* [382-475] | 423* [378-473] | 415* [388-462] |
| PTTV (ms ²) | 62.3[50-146] | 67.8 [39.2-88] | 118 [§] [6-230] | 135* [76.5-221] | 139* [73.9-299] | 182* [94-372] |

[^] Data are represented as median [25th percentile, 75th percentile]. (*) indicates statistical significance compared to Control. (+) indicates statistical significance compared to NREM. (§) indicates statistical significance compared to SWS.

Results show an increase in the overall PI_{RR} in children with SDB compared to controls (Fig. 1) that is mainly due to the increase in SE_{RR} and the $TE_{PTT \rightarrow RR|R}$, while $TE_{R \rightarrow RR}$ remained unchanged across groups. A trend of decrease in PI_{RR} and $TE_{R \rightarrow RR}$ in REM compared to NREM and SWS sleep stages was observed albeit not statistically significant. Surrogate data (results not shown) demonstrated that entropy decomposition identified non-random dynamics in RR and coupling with R and PTT.

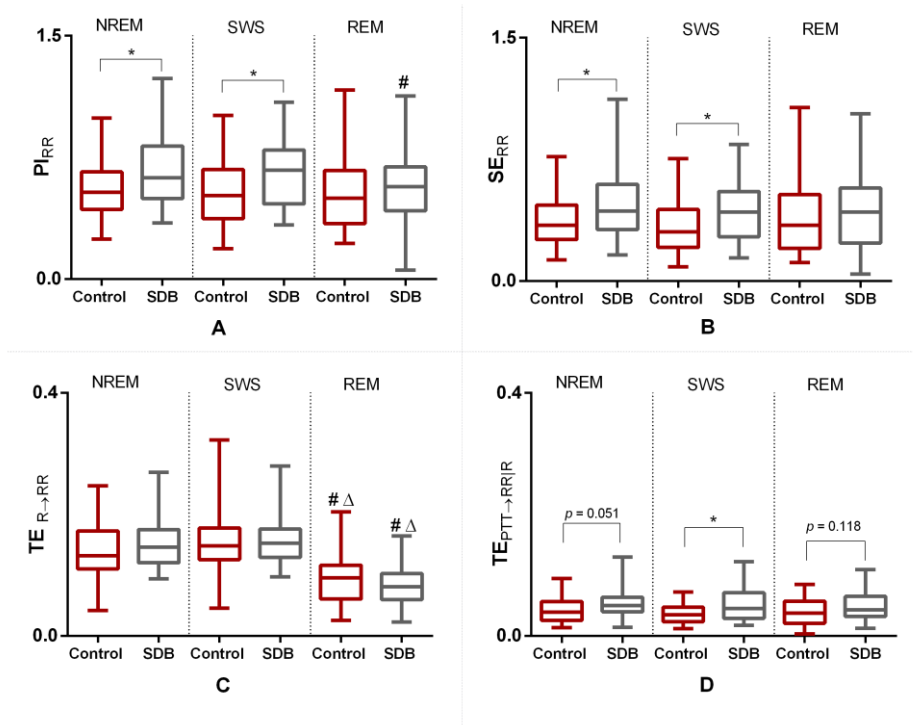


Figure 1: Decomposition of predictive information in RR. (A) Predictive information in RR (PI_{RR}). (B) Information storage in RR (SE_{RR}). (C) Information transfer from R to RR ($TE_{R \rightarrow RR}$). (D) Conditional information transfer from PTT to RR given R ($TE_{PTT \rightarrow RR|R}$). (*) indicates significant difference between control and SDB children. (#) and (Δ) indicate significant difference compared to NREM and SWS, respectively.

Discussion and Conclusion

The increase in PTT variance is consistent with previously reported BPV increase [1], indicating sympathetic activation in children with SDB. Mean RR and RR variance were not different between groups, whereas the predictability of RR was increased in children with SDB. Information decomposition analysis revealed that this increase was due to increase in RR self-regulation and information transfer from PTT to RR ($TE_{PTT \rightarrow RR|R}$), while respiratory sinus arrhythmia ($TE_{R \rightarrow RR}$) remained unchanged. Our results may indicate an increase in BRS gain, which is contrary to findings of decreased BRS gain computed using direct measurement of BP variability [1]. Possibly, PTT is correlated with abrupt changes in BP rather than beat to beat changes in blood pressure, in which case $TE_{PTT \rightarrow RR|R}$ might reflect sympathetic activity rather than cardiac baroreflex control [4].

References

- [1] Nisbet, L. C., et al.,(2014), *Sleep Med Rev*, vol. 18, pp. 179-89.
- [2] Faes, L., et al.,(2015), *Physical Review E*, vol. 91, p. 032904.
- [3] Immanuel, S. A., et al.,(2014), *American Journal of Respiratory and Critical Care Medicine*, vol. 190, pp. 1149-1157.
- [4] Foo, J. Y., et al.,(2006), *Technol Health Care*, vol. 14, pp. 97-108.

Cardiorespiratory interactions: looking at birds for answers

Alona Ben-Tal and Emily Harvey

Massey University, Institute of Natural and Mathematical Sciences, Auckland, New Zealand

Birds and mammals have similar metabolic demands and heart structures but they have evolved strikingly different lungs. In birds, airflow is continuous and unidirectional through rigid tubes where gas exchange occurs. In contrast, mammalian lungs are stretchy with tidal and bidirectional airflow. It has been hypothesized that the unidirectional flow is due to aerodynamic valving during inspiration and expiration, resulting from the anatomical structure and the fluid dynamics involved, however, theoretical studies to back up this hypothesis are lacking. We have constructed a novel mathematical model of airflow in the avian respiratory system that, for the first time, can produce robust unidirectional flow. The model consists of two piecewise linear ordinary differential equations with lumped parameters and discontinuous, flow-dependent resistances that mimic the experimental observations. Using dynamical systems techniques and numerical simulations, we show that unidirectional airflow can be produced by either effective inspiratory or effective expiratory valving, but that both inspiratory and expiratory valving are required to produce the high efficiencies of flows observed in avian lungs. We further show that when the relative airsacs compliances vary, it affects the timing of the airflow across the gas exchange area. Such strong differences in timing are not seen in mammals and are therefore of particular interest for future studies of cardiorespiratory interactions.

References

Harvey EP, Ben-Tal A. 2016 *PLOS Computational Biology* 2016 **12(2)** e1004637

Cardiac repolarisation and heart rate variability during experimental hypoglycaemia in healthy subjects and patients with type 2 diabetes

Alan Bernjak^{1,2}, Elaine Chow³, Emma Walkinshaw², Alexandra Lubina-Solomon², Paul J Sheridan³ and Simon R Heller²

¹University of Sheffield, INSIGNEO Institute for in silico Medicine, Sheffield, UK

²University of Sheffield, Department of Oncology & Metabolism, Sheffield, UK

³University of Sheffield, Department of Cardiovascular Science, Sheffield, UK

Aims: Large trials of intensive blood sugar lowering in type 2 diabetes showed increased frequency of severe hypoglycaemia (low blood sugar), which was later strongly associated with adverse cardiovascular conditions (1) and mortality, including arrhythmic death (2). One mechanism by which hypoglycaemia could promote arrhythmias is through changes in cardiac autonomic activity and cardiac repolarization (indication of the electrical and mechanical activity of the heart). In a recent clinical study involving patients with type 2 diabetes we have reported a higher incidence of cardiac arrhythmia during spontaneous hypoglycaemia versus euglycaemia (normal blood sugar) (3). We attributed these to changes in cardiac autonomic tone during prolonged hypoglycaemia. The aim of this study was to examine in detail the changes in heart rate variability (HRV) and cardiac repolarisation parameters during prolonged experimental hypoglycaemia.

Methods: Twelve subjects with type 2 diabetes and eleven age matched nondiabetic subjects underwent paired hyperinsulinaemic clamps, where insulin and dextrose were infused to change and maintain the subjects' blood sugar at a target level. During the euglycaemia clamp blood glucose was held at a normal level (6mmol/L) and during hypoglycaemia clamp at a low level (2.5mmol/L). The two clamps were separated by 4 weeks. Heart rate (HR) and heart rate variability (HRV) parameters (spectral power of HRV within low frequency (LF: 0.04-0.15Hz) and high frequency (HF: 0.15-0.4Hz) intervals) were assessed at 30 min intervals. Twelve lead electrocardiogram (ECG) was recorded and parameters of cardiac repolarisation (QT interval duration, T wave symmetry) were calculated. Principal component analysis was used to evaluate the complexity of repolarisation (PCA ratio) and heterogeneity of temporal evolution of repolarisation (loop dispersion: LD) across the 12 leads (4). These parameters were previously shown to be predictors of cardiovascular mortality (5,6). Paired and non-paired parametric tests were used to compare differences to baseline and between controls vs diabetes respectively.

Results: No significant changes in HRV parameters occurred in either group during euglycaemic clamps. In the diabetic group, HR increased maximally ($\Delta=5$ bpm, $p=0.04$) after 30 minutes of hypoglycaemia (T90), then fell to baseline level despite maintained hypoglycaemia (T120). High frequency power of HRV decreased at T90 ($p=0.02$), indicating vagal withdrawal, but returned towards baseline at T120. In the control group, the maximal increase in HR ($\Delta=4$ bpm, $p=0.04$) occurred earlier at T60 and HR remained elevated during hypoglycaemia. At the end of the clamp (T120), QT corrected for HR (QTc) significantly increased in both clamps and in both groups. During hypoglycaemia the increase in QTc was bigger in patients with diabetes ($\Delta=76\pm 20$ ms) compared to controls ($\Delta=54\pm 5$ ms) ($p<0.001$). T wave symmetry at T120 decreased in both clamps and both groups ($p<0.01$). In diabetes, the decrease was significantly bigger in hypo ($\Delta=-0.63\pm 0.09$) compared to euglycaemia ($\Delta=-0.19\pm 0.06$), while the changes were similar in controls. The PCA ratio did not change in controls, however it increased in diabetes both during euglycaemia ($\Delta=0.04\pm 0.02$, $p=0.02$) and hypoglycaemia ($\Delta=0.16\pm 0.05$, $p=0.04$). The change was significantly bigger during

hypoglycaemia ($p=0.04$). Loop dispersion significantly decreased in both groups and both clamps. The biggest decrease was during hypoglycaemia in diabetes.

Conclusions: Cardiac autonomic regulation during hypoglycaemia appears time-dependent and different between patients with type 2 diabetes and nondiabetic individuals. In diabetes, the initial increment in HR to hypoglycaemia is delayed. Individuals with type 2 diabetes exhibited greater repolarization abnormalities compared to healthy individuals. These mechanisms could contribute to arrhythmias that have been reported in clinical hypoglycaemic episodes, and provide further evidence to explain the possible relationship between hypoglycaemia and increased cardiovascular mortality in type 2 diabetes.

References

1. Zoungas S, Patel A, Chalmers J, de Galan BE, Li Q, Billot L, Woodward M, Ninomiya T, Neal B, MacMahon S, Grobbee DE, Kengne AP, Marre M, Heller S 2010 *N Engl J Med* **363** 1410-1418
2. Mellbin LG, Ryden L, Riddle MC, Probstfield J, Rosenstock J, Diaz R, Yusuf S, Gerstein HC 2013 *Eur Heart J* **34** 3137-3144
3. Chow E, Bernjak A, Williams S, Fawdry RA, Hibbert S, Freeman J, Sheridan PJ, Heller SR 2014 *Diabetes* **63** 1738-1747
4. Acar B, Yi G, Hnatkova K, Malik M 1999 *Med Biol Eng Comput* **37** 574-584
5. Okin PM, Devereux RB, Lee ET, Galloway JM, Howard BV 2004 *Diabetes* **53** 434-440
6. Perkiomaki JS, Hyytinen-Oinas M, Karsikas M, Seppanen T, Hnatkova K, Malik M, Huikuri HV 2006 *Am J Cardiol* **97** 353-360

Human cardiac systems electrophysiology: from generic models to human stem-cell-derived cardiomyocytes

Etienne Boileau¹, Dimitris Parthimos², Christopher H. Georges²,
Perumal Nithiarasu¹

¹*Biomedical Engineering and Rheology Group, Zienkiewicz Centre for Computational Engineering, Swansea University Bay Campus, Swansea SA1 8EN, United Kingdom, e.boileau@swansea.ac.uk*

²*Cardiff University School of Medicine, Institute of Molecular and Experimental Medicine, Wales Heart Research Institute, Cardiff CF14 4XN, United Kingdom*

1 Abstract

The development of a reliable *in vitro* model for arrhythmia and cardiotoxicity raises a number of important questions such as: (i) how to take into account the *in vivo* complexity of the cardiac tissue, together with its electrical and Ca^{2+} handling properties? and (ii) how to dissociate the role of intercellular communication from that of intracellular processes, when observing the resulting emergent phenomena arising from these interactions? When considering replacements for current animal models, which only approximate human (patho-)physiology, human stem cell-derived cardiomyocytes (hSC-CMs) offer new perspectives for cardiac toxicity screening tests, satisfying the need for physiological relevance [1]. However, study of hSC-CMs is confounded by the heterogeneity of these cells in culture, which recapitulate the developing myocardium, and reveal substantial differences between their electrophysiological, contractile properties, and their Ca^{2+} handling capacity, and those of adult CMs. Accordingly, this brings another question: how answers to questions (i) and (ii) are modulated by ‘spatio-temporal’ variations? In order to contribute to these challenging questions, we present some possible approaches based either on generic mathematical models or more detailed models of cardiac cells, namely human stem cell-derived cardiomyocytes.

1.1 A generic model

Our initial work was concerned with the investigation of questions (i) and (ii), with the aim of providing new insights into the phenomena of tissue synchronisation and the onset of arrhythmogenesis that results from desynchronisation within single cells

and across cell populations. We used a generic model of the heart as an excitable medium to illustrate how changes in the extent of intercellular communication is involved in modulating cell recruitment and synchronization [2].

We studied the effects of two pharmacological agents: *(i)* the Ca^{2+} ionophore ionomycin, that leads to rises in intracellular Ca^{2+} levels by allowing direct Ca^{2+} influx across the plasma membrane and *(ii)* verapamil, a L-type voltage-operated channel antagonist that attenuates the Ca^{2+} influx driven by membrane depolarisation. In addition to parametrizing the effect of these drugs, we also varied the conductance states and gap-junctional permeabilities, producing population level dynamics that are dependent, not only on the strength of the coupling, but most importantly on its variability across the array. Although such an approach is conceptually very simple, it has been used extensively to model ‘wave formation’ and ‘bursting’ phenomena associated with Ca^{2+} dynamics.

1.2 A novel hSC-CM model

Recently, as a first step towards the development of a model of cardiac tissue, we formulated a novel mathematical model of hSC-CM with the objective of complementing the information obtained from temporal patterning of intra- and intercellular calcium signals in spontaneously contractile syncytia of hSC-CMs. The mathematical formulation for the different currents uses the Hodgkin-Huxley formalism, and is based on experimental observations from a wide survey of the existing literature on hSC-CMs. Preliminary results were obtained with the single cell model. We investigated some of the mechanisms underlying automaticity in hSC-CMs, the role of the ‘ Ca^{2+} -clock’, and the effect of known antagonists, such as verapamil and ivabradine.

References

- [1] Lewis, K.J., Silvester, N.C., Barberini-Jammaers, S., Mason, S.A., Marsh, S.A., et al. 2015 *J. Biomol. Screen.* **20** 330–340
- [2] Boileau, E., George, C.H., Parthimos, D., Mitchell, A.N., Aziz, S. and Nithiarasu, P. 2015 *Ann. Biomed. Eng.* **43** 1614–1625

Metastability and collective frequencies in oscillatory brain networks

Joana Cabral, Gustavo Deco and Morten Kringelbach
University of Oxford, Department of Psychiatry, Oxford, UK

MEG studies of spontaneous activity reveal that some brain areas recurrently display the simultaneous emergence and dissipation of oscillations in a limited frequency range. These intermittent collective oscillations lead to correlated amplitude fluctuations of band-limited signals. However, the biophysical mechanism at the genesis of these collective oscillations remains unclear.

We present a novel mechanistic scenario to explain these experimental observations (Cabral et al., 2014). Using a computational model, we show how a system of coupled oscillators (with realistic whole-brain connectivity and conduction delays) can display metastable partially synchronized states (or chimera states). Due to delays, the synchronized units oscillate at reduced collective frequencies. This mechanism originates slow and structured amplitude envelopes of band-limited signals, fairly reproducing MEG data from 10 healthy subjects at rest.

The results show that the large-scale neuroanatomical connectivity provides an optimal network structure to support a robust metastable regime in which band-limited collective oscillations emerge transiently. This mechanism may be at the origin of the correlated envelope fluctuations observed in resting-state MEG data.

References

Cabral J, Luchoo H, Woolrich M, Joensson M, Mohseni, et al. 2014 *Neuroimage* **90** 423-435

Altered HRV fractal dynamics after spinal cord injury as function of lesion level

Paolo Castiglioni¹, Carolina Gambirasio² and Giampiero Merati^{1,3}

¹ *Fondazione Don C. Gnocchi, Milan, Italy;* ² *USU, Osp. Niguarda Ca' Granda, Milan, Italy;*

³ *Università degli Studi di Milano, Milan, Italy*

Background. The cardiovascular system is “complex” because several vascular beds interact each other through local and global regulatory mechanisms. The autonomic nervous system integrates this complex and hierarchical regulation, generating “fractal components” in Heart Rate Variability (HRV). Therefore, aim of this study is to evaluate whether an altered autonomic integrative control can be better identified by fractal- rather than by spectral-analysis of HRV. For this aim, we applied a recently proposed fractal spectrum of HRV scale coefficients [1] in spinal-cord injured (SCI) individuals with lesion level below T4, i.e., the 4th thoracic (T) vertebra.

These SCI individuals represent a model of altered autonomic integrative regulation, in presence of an intact cardiac sympathetic and vagal heart-rate control. In fact, when the lesion is below T4, the cardiac autonomic control is preserved, while the sympathetic regulation is compromised for vascular segments innervated below the lesion.

Methods. We enrolled 28 SCI subjects with lesion below T4, i.e., 14 subjects with lesion between T5 and T11 (SCI_H) and 14 subjects with lesion lower than T11 (SCI_L). We also enrolled 34 able-bodied (AB) controls. The SCI_H, SCI_L and AB groups were matched by age, body mass index and gender composition (see table 1)

Table 1: Anthropometric data in the 3 groups: mean (SD)

| | N | Female/Male | Age [years] | Body Mass Index [kg/m ²] |
|------------------|----|-------------|----------------|---|
| SCI _H | 14 | 1/13 | 37.1 (6.6) | 24.6 (4.1) |
| SCI _L | 14 | 2/12 | 40.9 (10.0) | 25.5 (4.8) |
| AB | 34 | 5/29 | 39.3 (12.1) | 24.7 (2.6) |

The ECG was recorded in all subjects for 10 minutes at rest, in sitting position. The R-R intervals were derived beat by beat, removing premature beats. The HRV power spectrum was estimated between 0.005 and 0.6 Hz with a broadband procedure [2], calculating powers in the very-low frequency (VLF, 0.005-0.04 Hz), low-frequency (LF, 0.045-0.15 Hz) and high-frequency (HF, 0.16-0.40 Hz) bands. The HRV fractal spectrum of self-similarity coefficients, $\alpha(\tau)$, was estimated for scales τ between 5 and 100 s with a DFA based algorithm [1]. Power spectra, after log-transformation, and fractal spectra of SCI_H and SCI_L groups were compared with power and fractal spectra of the AB group at each spectral frequency f and at each temporal scale τ (unpaired t -test, statistical significance at $p < 0.05$).

Results. Table 2 compares spectral powers in the VLF, LF and HF bands. No differences were found between SCI_L and AB power spectra in the three bands and at any frequency f . By contrast, the fractal spectrum was significantly higher in the SCI_L group than in the AB group for scales τ between 12 and 47s (figure 1, left). However, the fractal spectrum preserved the shape described previously in healthy individuals sitting at rest [3], with a relative minimum at $\tau=16$ s and a relative maximum around $\tau=30$ s, as in the AB group of the present study.

Table 2: Comparison of power spectra in the VLF, LF and HF bands

| | AB | SCI _L | | SCI _H | |
|---------------------------------|-------------|------------------|----------|------------------|----------|
| | m (sd) | m (sd) | p vs. AB | m (sd) | p vs. AB |
| VLF ($\log_{10} \text{ms}^2$) | 2.83 (0.40) | 2.94 (0.34) | 0.34 | 2.74 (0.40) | 0.48 |
| LF ($\log_{10} \text{ms}^2$) | 2.84 (0.51) | 2.81 (0.41) | 0.84 | 2.50 (0.64) | 0.06 |
| HF ($\log_{10} \text{ms}^2$) | 2.28 (0.45) | 2.25 (0.46) | 0.83 | 2.03 (0.52) | 0.11 |

By contrast, SCI_H and AB power spectra differed significantly for frequency f falling within the 0.09-0.15 Hz band, and the LF power (Table 2) tended to be lower in the SCI_H group. As to SCI_H and AB fractal spectra, they differed markedly between 10 and 18 s; moreover, the $\alpha(\tau)$ shape was substantially altered in SCI_H individuals, the relative maximum at $\tau=30$ s being missing (figure 1, right).

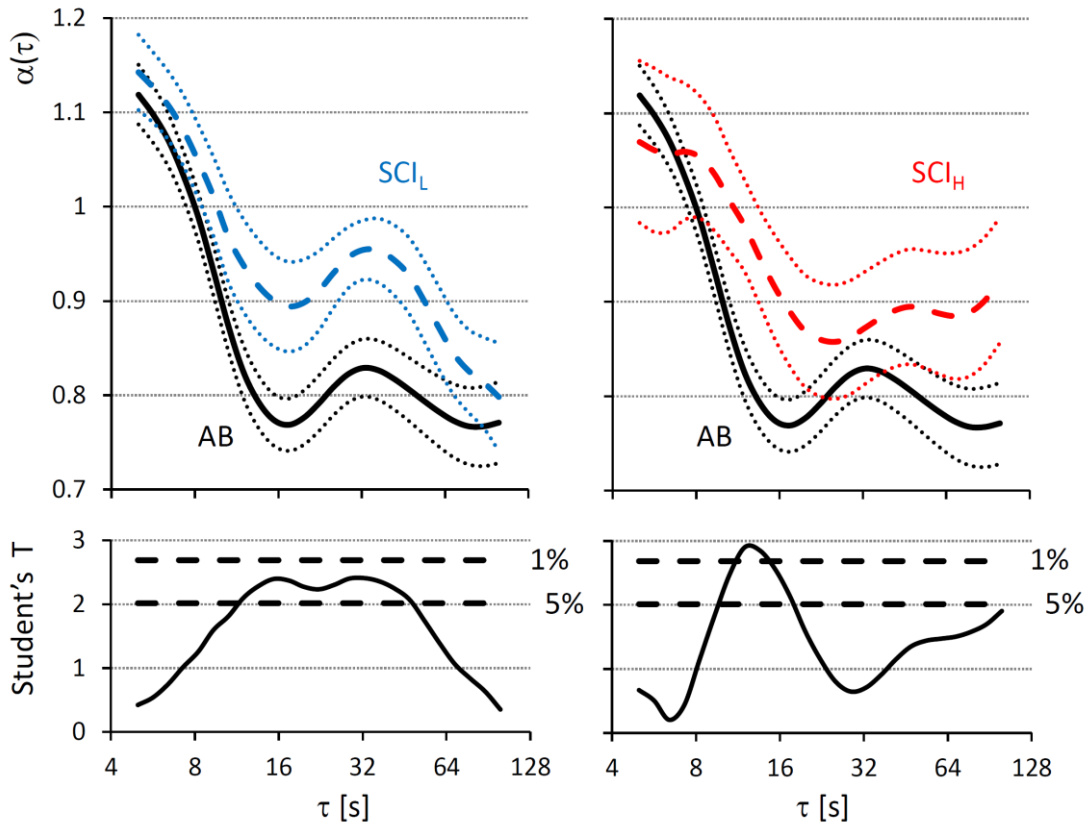


Figure 1. Upper panels: fractal spectra of scale coefficients, function of the temporal scale τ : mean \pm sem. Lower panels: Student's T for the difference between AB and SCI_L groups (left) and between AB and SCI_H groups (right), with 5% and 1% significance levels.

Conclusions. When the lesion compromises the vegetative control of the lower districts only, as in SCI_L individuals, $\alpha(\tau)$ reveals alterations that go undetected in the power spectrum. With higher lesion levels, but intact cardiac autonomic outflows, as in SCI_H individuals, both power and fractal spectra are altered, and appear to provide complementary information, helpful for better understanding alterations in the integrative control of the autonomic nervous system.

References

- [1] Castiglioni P, Parati G, et al, 2011, *J Physiol*, **589** 355-69.
- [2] Di Rienzo M, Castiglioni P, et al, 1996, *Med Biol Eng Comput.*, **34**: 133-41.
- [3] Castiglioni P, Brambilla V et al, 2015, *Conf Proc IEEE Eng Med Biol Soc.* **2015** 290-3.

Dependence of the Cardiovascular Control Complexity on Age and Gender

Aparecida M. Catai¹, Camila B.F. Pantoni and Alberto Porta^{2,3}

¹ Federal University of São Carlos, Department of Physiotherapy, São Carlos, Brazil

² University of Milan, Department of Biomedical Sciences for Health, Milan, Italy

³ IRCCS Policlinico San Donato, Department of Cardiothoracic, Vascular Anesthesia and Intensive Care, Milan, Italy

Introduction

Changes in physiological regulatory mechanisms with aging [1] are mirrored by a reduction in heart period (HP) variability [2], by an increase of systolic blood pressure (SAP) variability [3], and by a reduction in dynamical complexity of the time course of physiological variables [4]. In this context, studies of our group were devoted to investigate the effect of aging on the complexity of the cardiovascular control, focused on HP, SAP and diastolic arterial pressure (DAP) variabilities [5,6]. In this study we present the aging and gender influences on the complexity of HP, SAP and DAP variabilities in our database of healthy humans formed by 110 individuals aged from 21 to 70 years subdivided in 10-years wide bins at rest in supine condition (REST) and during sympathetic activation induced by active standing (STAND).

Experimental Protocol and Data Analysis

The study included in 110 subjects divided into five groups (n=22 for each group, 11 men); age ranges: 21-30; 31-40; 41-50; 51-60; 61-70. Signals were acquired for 15 minutes at REST and during STAND. ECG (modified lead I) and noninvasive continuous arterial pressure (Finometer-PRO, Finapres Medical System, Amsterdam, Netherlands) was acquired and sampled at 400 Hz (Power Lab 8/35, ADInstruments, Sydney, Australia). HP was derived from the ECG as the temporal distance between two consecutive R-wave peaks, SAP, as the maximum of arterial pressure in HP, and DAP, as the minimum of arterial pressure following SAP. Sequences of 256 consecutive HP, SAP and DAP values were extracted randomly inside REST and STAND periods. Indexes of dynamical complexity were estimated via corrected conditional entropy (CCE), as described in [7]. CCE estimates the amount of information carried out by the current sample of the series that cannot be derived from the knowledge of its previous values. A correction strategy prevented the decrease of CCE toward 0 with the number of previous samples and the minimum of the CCE with respect to the number of past values was taken as a complexity index (CI). This index was normalized by the Shannon entropy to obtain a normalized CI (NCI), thus expressing complexity in terms of dimensionless units. NCI ranges from 0 (null information, maximal predictability) to 1 (maximum information, minimal predictability) [8]. Pearson product-moment correlation analysis, or Spearman rank correlation analysis when appropriate, was performed to check the association of any parameter with age. One-way ANOVA (Tukey's post-hoc test) or Kruskal-Wallis ANOVA on ranks (Dunn's post-hoc test), was applied to check the significance of the differences among data in different age groups. The analysis was performed only if a significant difference between the 21-30 and 61-70 was detected. Statistical analysis was performed via a commercial software (Sigmaplot ver.11.0, Systat, USA). A $p < 0.05$ was considered as significant.

Results

Table 1 reports the correlation analysis of NCI_{HP} , NCI_{SAP} and NCI_{DAP} on age, over all subjects and after the separation of the whole group into two subgroups solely formed by

Table 1. Correlations of HP, SAP and DAP complexity indexes on age at REST and during STAND.

| index | REST | | STAND | |
|----------------------------|-----------|--------------|-----------|--------------|
| | r, ρ | significance | r, ρ | significance |
| NCI _{HP} (all) | -0.384 | Yes | 0.107 | No |
| NCI _{HP} (men) | NA | NA | 0.060 | No |
| NCI _{HP} (women) | -0.407 | Yes | 0.149 | No |
| NCI _{SAP} (all) | -0.223 | Yes | -0.015 | No |
| NCI _{SAP} (men) | -0.077 | No | 0.046 | No |
| NCI _{SAP} (women) | -0.360 | Yes | -0.074 | No |
| NCI _{DAP} (all) | -0.223 | Yes | 0.087 | No |
| NCI _{DAP} (men) | -0.090 | No | -0.012 | No |
| NCI _{DAP} (women) | -0.329 | Yes | -0.056 | No |

NCI = normalized complexity index; r, ρ = Pearson product-moment correlation coefficient or Spearman's rank correlation coefficient when appropriate; Yes/No = the variable is/is not men and women. NCI_{HP} decreased with age in the overall population at REST. However, when the groups were divided by gender, a significant negative correlation of NCI_{HP} on age was observed only in women. Indeed, in men no significant changes between 21–30 and 61–70 was detected, thus suggesting that, if present, a trend toward a loss of HP complexity had a quite flat slope. NCI_{SAP} decreased with aging at REST. The same finding was observed in the women group, while no modification of NCI_{SAP} was visible in men, thus confirming HP complexity analysis. Similar findings were found when NCI_{DAP} was considered. During STAND NCI_{HP}, NCI_{SAP} and NCI_{DAP} was unrelated to age regardless of the group.

Discussion and Conclusions

Our findings indicated that the breakdown of complexity of cardiac regulation [1] was associated to a decline of complexity of the vascular control. This breakdown is visible at the level of two different arterial pressure reference values (i.e. SAP and DAP) with DAP value more closely linked to fluctuations of peripheral resistances. Our results stressed that the relation of the complexity of cardiovascular control on age is gender-dependent. At REST, we found that The complexity of HP series decreased with age in the overall population and only women was responsible for this decrease because the decline in men appears to be less steep especially in the older groups. Remarkably, the loss of cardiovascular complexity with age was not detected during STAND, thus suggesting that the decline of complexity observed at REST is mainly due to the increase of sympathetic activity with age that, during STAND, cannot be perceived because the sympathetic activation imposed by the orthostatic challenge tends to mask the trend towards an higher sympathetic drive during senescence.

Grants: FAPESP (2010/52070-4; 2013/07953-3); CNPq (311938/2013-2); (CAPES/CSF/PVE (23038007721/2013-41).

References

- [1] Goldberger AL *et al*, 2002 *Neurobiol Aging* **23** 23-26.
- [2] Catai AM *et al*, 2002 *Braz. J. Med. Biol. Res.* **35** 741-752.
- [3] Mancia G *et al*, 1983 *Circ. Res.* **53** 96-104.
- [4] Takahashi ACM *et al*, 2012 *Intern. Emerg. Med.* **7** 229-235.
- [5] Catai AM *et al*, 2014 *Entropy* **16** 6686-6704.
- [6] Porta A *et al*, 2014 *PLoS ONE* **9** e89463.
- [7] Porta A *et al*, 1998 *Biol. Cybern.* **78** 71-78.
- [8] Porta A *et al*, 2007 *Chaos* **17**, 015117.

Rotors and re-entry in the the human heart: experiments and models

Richard Clayton

University of Sheffield, INSIGNEO institute for in-silico medicine and Department of Computer Science, Sheffield, UK

Ventricular fibrillation (VF) is an arrhythmia that is an important cause of sudden cardiac death. Studies in animal hearts have shown that VF can be sustained by re-entrant mechanisms, and we have confirmed this observation in human hearts by making measurements during cardiopulmonary bypass when the heart is exposed and fibrillating (Nash et al. 2006). Further studies have shown that the complexity of epicardial activity during human VF is modulated by the global cardiac ischaemia that is associated with long duration VF (Bradley et al. 2011). Quantifying the complex spatiotemporal activation patterns observed during VF remains a challenge. Techniques for identifying phase singularities at the pivot point of re-entrant activations offer one option, but must be deployed carefully (Clayton and Nash 2015). Models of electrical activation and recovery in heart tissue provide another tool to investigate re-entry in the heart, but developing patient specific models remains an important challenge.

References

- Nash MP, et al. 2006 *Circulation* **114** 536-542
Bradley CP, et al. 2011 *Circulation Arrhythmia and Electrophysiology* **4** 684-691
Clayton RH, Nash MP, 2015 *Cardiac Electrophysiology Clinics* **7** 49-58

Nonautonomous systems as an inverse problem: Comparison with stochastic and chaotic systems

Philip Clemson and Aneta Stefanovska

Lancaster University, Department of Physics, Lancaster, UK

From the fluctuating membrane potential of a living cell to the changes in an animal's breathing frequency, measured time series play a vital role in the quest to understand function in biological systems. Such systems are inherently complex and as such have been analysed under the frameworks used to analyse similarly-complex stochastic and chaotic systems [Eckmann (1985)]. However, in biological systems this complexity arises from time-dependent interactions rather than an in-built randomness or chaos and are in fact best described as being *nonautonomous* [Kloeden (2011)].

To investigate the performance of different time series analysis methods when applied to nonautonomous systems, three test systems representing chaotic, stochastic and nonautonomous dynamics are considered. Using approaches based on phase space, complexity and frequency domain analysis, one finds that nonautonomous systems often appear stochastic (Fig. 1). In contrast, methods that preserve time-dependent information such as time-frequency analysis and dynamical Bayesian inference reveal these systems to be deterministic [Clemson (2014)].

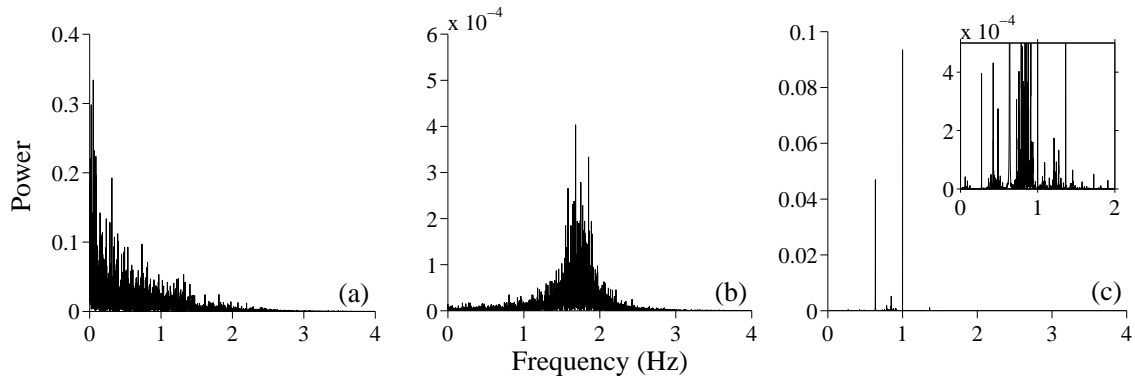


Figure 1: Fourier transforms over the range 0–4 Hz for: (a) The chaotic Lorenz system; (b) The stochastic Duffing system; (c) The nonautonomous Poincaré system, where the inset reveals a broad spectrum of low-power modes.

In the second part, physiological data is analysed, including the peripheral blood flow in the skin from a laser Doppler flowmetry (LDF) probe, an electrocardiogram (ECG) of the heart, and respiration measured using a stretch-sensitive belt

around the chest. Some of the results are shown in Fig. 2, where the values shown on the vertical axis correspond to physiologically meaningful frequency intervals [Shiogai (2010)]. In particular, it can be seen that the heart rate and respiration rate are not constant but vary within the intervals $[0.6\text{--}2\text{ Hz}]$ and $[0.145\text{--}0.6\text{ Hz}]$, which is expected for time-dependent nonautonomous systems. In the continuous time-frequency domain of the LDF signal, lines of high amplitude coincide with the frequencies of the heart and respiration, revealing them to be deterministic by nature. However, if the same signal was viewed without the time axis in only the frequency domain then the time-variability of these components would make them appear the same as a stochastic oscillation. This demonstrates the importance of this new framework of analysis for identifying deterministic properties of biological systems so that they can be optimally characterised, rather than being misrepresented as chaotic or stochastic dynamics.

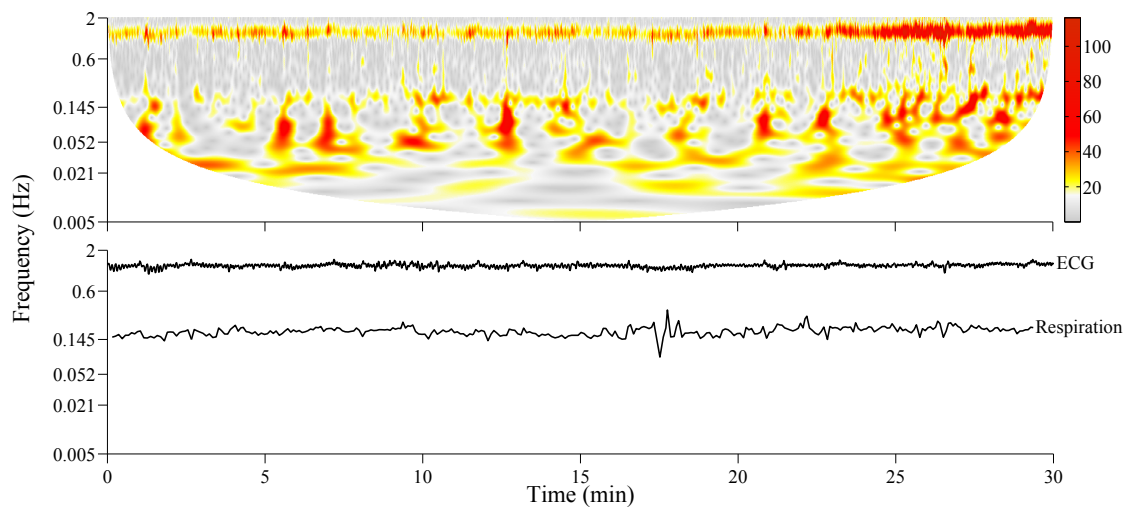


Figure 2: Time-frequency analysis of physiological signals from a single subject recorded over 30 minutes. The continuous wavelet transform of an LDF probe recording is plotted at the top, while instantaneous frequencies of the ECG and respiration signals calculated using marked events are shown below.

References

- Eckmann J. P., Ruelle D., 1983 *Rev. Mod. Phys.* **57** 617–656
 Kloeden P. E., Rasmussen M., 2011 *Nonautonomous Dynamical Systems*, American Mathematical Soc.
 Clemson P. T., Stefanovska A., 2014 *Phys. Rep.* **542** 297–368
 Shiogai Y., Stefanovska A., McClintock P. V. E., 2010 *Phys. Rep.* **488** 51–110

Trigemino-cardiac reflex as a long-time modulator of cerebral blood flow

Dominga Lapi¹, Maurizio Varanini², Cristina Del Seppia², Paolo Orsini³, Antonio Colantuoni¹ and Rossana Scuri³

1 Department of Clinical Medicine and Surgery, "Federico II" University Medical School, Naples, Italy

2 Institute of Clinical Physiology, National Council of Research, CNR, Pisa, ITALY

3 Department of Translational Research on New Technologies in Medicine and Surgery, University of Pisa, Pisa, Italy

The trigemino-cardiac reflex (TCR) represents a physiological mechanism, because within seconds after the initiation of such a reflex there are a powerful and differentiated activation of sympathetic nervous system and a cerebrovascular arteriolar dilation (Sandu et al. 2010). Recently, Lapi et al. demonstrated that in the rat a mandibular extension (ME) able to stimulate the trigeminal nerve induces bradycardia and hypotension causing complex effects on pial microcirculation through the release of endothelial factors. Pial arterioles show a characteristic biphasic response: during ME constrict and successively dilate for about 140 min. The results indicate that vasoconstriction is due to opioid-receptor activation, while vasodilation is related to nitric oxide release (Lapi et al., 2013; Lapi et al., 2014). During the dilation phase the arterioles display rhythmic variations in diameter, where the lowest frequency components related to endothelial activity increase in their spectral density (ranges: 0.005-0.0095Hz and 0.0095-0.021Hz).

The aim of the present experimental study was to assess the effects of two repeated ME on rat pial microcirculation, evaluating the rhythmic diameter changes of the pial arterioles and the corresponding frequency components. Two experimental protocols were accomplished: the second ME was applied 10 or 180 min after the first ME (early repetition and late repetition, respectively). The diameter changes of pial arterioles and the cardiovascular parameters, such mean arterial blood pressure and heart rate, were monitored for the following 240 min after the second ME. Therefore, the main purpose was to assess whether the second ME was effective in promoting further pial arteriolar dilation and decrease in mean arterial blood pressure.

ME was induced by U-shaped device placed between the rat dental arches. Pial microcirculation was visualized by fluorescence microscopy. Video images were recorded by computerized methods and microvascular measurements (diameter and length) were made off-line using a computer assisted imaging software system. The arteriolar network was mapped; the rhythmic variations in diameter were evaluated with computer-assisted methods. Pial arterioles were classified by Strahler's method in five orders (Kassab et al., 1993; Lapi et al., 2008). Spectral analysis was performed on 30 min recordings obtained under baseline conditions; moreover, after the first ME, according to the late repetition protocol, the power spectral analysis was carried out on tracings between 90 and 120 min. Finally, there was spectral evaluation of the recordings between 110 and 140 min after the second ME, according to both early and late repetition protocol. The very long lasting recordings were carried out to implement the resolution of the low frequency components according to the Stefanovska's data in humans (Stefanowska et al., 1999; Kvndal et al., 2003; Kvndal et al.,

2006). The rhythmic diameter changes were analyzed by a computer assisted power spectrum method, based on generalized short time Fourier transform (Varanini et al., 1998; Pradhan et al., 2011; Varanini et al., 2011).

The results show that according to early repetition protocol the second ME was able to induce prolonged pial arteriolar dilation ($20 \pm 3\%$ of baseline) and decrease in systemic mean arterial blood pressure ($15 \pm 5\%$ of baseline). Moreover, spectral analysis showed that the second ME induced a significant increase in the spectral density of the frequency components related to endothelial, neurogenic and myogenic activities (by $10 \pm 2\%$, $8 \pm 3\%$ and $6 \pm 1\%$, respectively) when compared to those observed under baseline conditions. The data obtained during the late repetition protocol indicate that the second ME did not induce pial arteriolar constriction; pial arteriolar dilation, on the contrary, starting during ME lasted up to the end of observation. The pial arteriolar dilation ($25 \pm 5\%$ of baseline) was accompanied by a significant decrease in the systemic mean arterial blood pressure ($10 \pm 2\%$ of baseline). The rhythmic oscillations in diameter showed a further significant increase in spectral density of the frequency components related to the endothelial activity (ranges: 0.005-0.0095Hz and 0.0095-0.021Hz; by $6 \pm 2\%$ and $8 \pm 1\%$, respectively), compared with those observed after the first ME.

In conclusion, repetitive ME extended the effects due to a single ME, inducing a characteristic modulation of the pial arteriolar tone. These effects may contribute to a prolonged redistribution of cerebral blood flow, while can participate to the regulation of the systemic arterial blood pressure.

References

- Kassab GS, Rider CA et al. 1993 *Am J Physiol* **265**: H350–H365.
- Kvandal P, Stefanovska A et al. 2003 *Microvasc Res* **65**: 160-171.
- Kvandal P, Landsverk SA et al. 2006 *Microvasc Res* **72**: 120-127.
- Lapi D, Marchiafava PL et al. 2008 *J Vasc Res* **45**: 69–77.
- Lapi D, Colantuoni A et al. 2013 *Arch Ital Biol* **151**: 11–23.
- Lapi D, Federighi G et al. 2014 *Plos One* **31**: 1-22.
- Pradhan RK, Chakravarthy VS. 2011 *Acta Physiol (Oxf)* **201**: 193-218.
- Sandu N, Cornelius J et al. 2010 *ScientificWorldJournal* **10**: 1416-1423.
- Stefanovska A, Bracic M et al. 1999 *IEEE Trans Biomed Eng* **46**: 120-129.
- Varanini M, De Paolis G et al. 1998 *Computers in Cardiology, IEEE Computer Society Press* **25**: 137-140.
- Varanini M. 2011 *IEEE Press Series on Biomedical Engineering, Wiley* 201-232.

Characterization of photoplethysmographic signal during atrial fibrillation

Valentina D.A. Corino¹, Rita Laureanti¹, Lorenzo Ferranti¹, Federico Lombardi² and Luca Mainardi¹

¹ *Politecnico di Milano, Department of Electronics, Information and Bioengineering, Milan, Italy*

² *Fondazione IRCCS Ca Granda Ospedale Maggiore Policlinico, U.O.C. di Malattie Cardiovascolari, Università degli Studi di Milano, Dipartimento di Scienze Cliniche e di Comunit, Milan, Italy*

Introduction

Identification of paroxysmal atrial fibrillation (AF) can be difficult and undiagnosed AF patients are at high risk of cardioembolic stroke or other complications and even death associated with AF. A screening of the general population would answer the issue of the paroxysmal and asymptomatic nature of AF. Lately, new technologies have been developed to monitor heart rate by means of everyday sensors, as mobile phone cameras, thumb ECG, ballistocardiogram. The aim of this study was to analyze the photoplethysmographic (PPG) signal obtained from a wristband device to explore the possibility of discriminating AF from normal sinus rhythm (NSR).

Study Population

We acquired thirty 10-min long PPG signals, 15 from healthy subjects in NSR, (39 ± 19 years) and 15 from patients with AF (76 ± 10 years). During the acquisition, the subject was required to remain in supine steady state, to reduce motion artifacts, with the Empatica E4 wristband applied on the wrist of the non-dominant arm.

Methods

Pre-processing

To reduce noise interference due to movement artifacts, the information from the built-in accelerometer of the Empatica E4 wristband were used to detect movements and reject noisy segments. Diastolic and systolic values were automatically detected. Briefly, a convolution is performed between the PPG signal and a kernel, providing a smoother signal where the local minima are easily found. These positions are taken as coarse temporal reference for each diastolic peak, whose timing is then refined by searching the minimum on the original signal in a 0.2-s window around it. The systolic peaks were defined as the first local maximum after each diastolic value. From the diastolic peak positions, the inter-diastolic intervals series were obtained, i.e., the time interval between one diastolic peak and the previous one. The inter-diastolic intervals series was used to evaluate the heart rate.

Table 1: Indexes during AF and NSR

| Parameter | NSR | AF |
|---------------|-------------------|------------------------|
| SD (ms) | 71 (45-89) | 210 (156-253) ** |
| rMSSD (ms) | 71 (36-90) | 287 (221-368) ** |
| pNN50 (%) | 15 (7-25) | 80 (72-85) ** |
| AFindex | -121 (-133- -113) | 67 (52-80) ** |
| SampEn (a.u.) | 1.79 (1.57-2.03) | 2.19 (1.99-2.31) * |
| ShEn (a.u.) | 0.42 (0.36-0.43) | 0.60 (0.53-0.62) ** |
| MPW | 0 (0-0.001) | 0.007 (0.003-0.014) ** |
| TPW | 0.003 (0-0.007) | 0.008 (0.001-0.019) * |
| ShapeSim | 0.77 (0.65-0.95) | 0.18 (0.08-0.32) ** |

Data are expressed as median (interquartile range)

p<0.05 AF vs. NSR; ** p<0.001 AF vs. NSR

Signal characterization

Time domain indexes: i) the standard deviation (SD); ii) the root mean square of successive differences (RMSSD); iii) the percentage of successive interval differences greater than 50 ms (pNN50); iv) the AF evidence index [1]; Nonlinear indexes: i) the sample (SampEn) [2] and ii) the Shannon (ShEn) entropy [3]; Shape analysis: i) the detection of multi-peak waves (MPW); ii) two-peak waves (TPW); iii) the shape similarity index (ShapeSim) [4].

Results

All the computed indexes are significantly different when comparing the group of patients with AF and subjects in NSR, as shown in Table 1. Time domain and entropy-based indexes highlight a higher variability and a higher irregularity, respectively, in patients with AF in respect to subjects in NSR. From the shape analysis, it can be noted that waves in NSR are more similar than in AF, and two- and multi-peak waves are more common in AF.

Discussion

In this study, we assessed the ability to discriminate between AF and NSR analyzing the PPG signal obtained from a wristband device. Preliminary results show a marked difference between AF and NSR, further studies will help in assessing the performance of the PPG signal to screen general population.

References

- [1] Sarkar S, Ritscher D, Mehra R 2008 *IEEE Trans Biomed Eng* **55** 219-1224
- [2] Richman JS, Moorman JR 2000 *Am J Physiol* **278** H2039-H2049
- [3] Shannon CE 1948 *Bell System Technical Journal* **27** 379-423
- [4] Faes L, Nollo G, Antolini R, Gaita F, Ravelli F 2002 *IEEE Trans Biomed Eng* **49** 1504-1513

Can binary symbolic dynamics of heart rate variability improve the assessment of fetal functional brain age?

Dirk Cysarz¹, Friedrich Edelhäuser¹, Uwe Schneider², Dirk Hoyer³

1 Integrated Curriculum for Anthroposophic Medicine and Institute of Integrative Medicine, University of Witten/Herdecke, Germany

2 Jena University Hospital, Department of Obstetrics, Jena, Germany

3 Jena University Hospital, Biomagnetic Center, Hans Berger Department of Neurology, Jena, Germany

The development of fetal brain with gestation is accompanied by the development of the autonomic nervous system (ANS). It has been shown that changes of fetal heart rate variability with gestational age reflect the individual fetal development [1]. Recently, a fetal autonomic brain score (fABAS) has been developed to reflect gestational processes of the neuro-vegetative control during gestation [2]. Indices indicating different aspects of the fetal RR tachogram, i.e. fetal heart rate series, (increasing fluctuation amplitude, increasing complexity, pattern formation) contributed to the representation of the development with gestational age. Furthermore, indices derived from binary symbolic dynamics of fetal heart rate have been shown to also reflect individual gestational development [3]. Here, we investigate whether these indices also contribute to fABAS. The analysis comprised $n=168$ magnetocardiographic recordings during quiet sleep and $n=376$ recordings during active sleep (19.9–39.3 weeks of gestation). Furthermore, full length recordings (30 min) were also analysed. Universal gestational aspects of the neuro-functional development were addressed including time domain parameters (median heart rate, pNN5, skewness and fluctuation range of the RR tachogram), frequency domain (total power and power spectral ratios VLF/LF and VLF/HF), complexity (generalized multiscale sample entropy on scales 3 and 4, gMSE3 and gMSE4) and pattern occurrence of the symbolic sequences of length $L=3$ classified according to the amount of variations (no, one or two variations – P0V, P1V, P2V).

In the univariate analysis all indices including the symbolic ones (P0V, P1V and P2V) showed a significant linear regression with respect to gestational age. Multivariate linear regression models including these parameters were calculated and the resulting models constituted the re-evaluated fABAS. fABAS explained 58% (coefficient of determination R^2) of the variance by gestational age in quiet sleep and 52% in active sleep. For quiet sleep one index of symbolic dynamics (P0V) improved the model and was included in the model whereas the model for active sleep was not improved by the parameters of symbolic dynamics. The modelling of fABAS for the full length recordings did also not include symbolic dynamics parameters. In conclusion, functional brain age can be assessed on the basis of single heart rate time series. This time series reflects numerous different aspects of neuro-vegetative development during gestation. In some cases indices of binary symbolic dynamics are able to refine the score and, thus, are helpful for the assessment.

References

- [1] Van Leeuwen P, Cysarz D, Edelhäuser F, et al. 2013 *Auton. Neurosci.* **178**(1) 24-28
- [2] Hoyer D, Tetschke F, Jaekel S, et al. 2013 *PLoS ONE* **8**(9) e74431
- [3] Cysarz D, Edelhäuser F, Van Leeuwen P 2015 *Philos. Trans. A Math. Phys. Eng. Sci.* **373**(2034) 20140087

Nonstationary heart rate dynamics of short time series assessed by symbolic dynamics analysis

Dirk Cysarz¹, Alberto Porta^{2,3} and Friedrich Edelhäuser¹

¹ *Integrated Curriculum for Anthroposophic Medicine and Institute of Integrative Medicine,
University of Witten/Herdecke, Germany*

² *Department of Biomedical Sciences for Health, University of Milan, Milan, Italy*

³ *IRCCS Policlinico San Donato, Department of Cardiothoracic, Vascular Anesthesia and Intensive
Care, Milan, Italy*

Recent epidemiological data clearly show that too much sitting is harmful [1]. Taking into account that the cardiovascular system is designed to be flexible to provide fast adaptation to different activities and demands it can be assumed that the ability to modify cardiovascular regulation seems to be an essential prerequisite for coping appropriately with stressors. These changes are accompanied by nonstationarities in biomedical time series such as the heart rate series. They also contribute to heart rate variability. Hence, if the nonstationary time series is split up into stationary segments [2] e.g. transitions between stationary segments of the heart rate series may contain information complementing information retrieved from stationary time series. The analysis of symbolic dynamics may be applied to short and nonstationary time series [3-5]. Here, we aimed to gain insight into heart rate dynamics during transitions between stationary segments.

The RR interval series obtained from Holter ECG recordings of congestive heart failure patients (N=15, NYHA classes III and IV, 4 female, age range 56±11 years) and young healthy subjects (N=30, 15 female, average age 29±8 years) were investigated. Symbolic dynamics analysis is used to analyze stationary segments of the RR interval series as well as the transitions between successive segments. The data were separately analyzed for daytime (11am to 5pm) and nighttime (sleeping time according to diary or 0 am to 6 am) periods to take into account circadian variations. First, the RR interval series was split into stationary segments (minimum length of segments: 20 RR intervals). For each segment the average RR interval and SDNN were calculated as standard parameters. They were complemented by the interval between the 5% and the 95% percentile of the RR interval series (RRamp) and the calculation of the excursion times, i.e. a surrogate parameter of period lengths calculated as the number of beats between successive zero crossings of the RR interval series after the subtraction of a linear trend. Furthermore, symbolic dynamics was analyzed by two different approaches. The first approach used a percentile base coarse graining procedure with the alphabet {0,1,2,3,4,5} [5]. The resulting symbolic patterns of length L=3 were classified according to the amount of variations (0, 1, 2 like or 2 unlike variations) and the respective occurrences were calculated (0V%, 1V%, 2LV% and 2UV%). The second approach used a binary symbolization reflecting acceleration and deceleration of the instantaneous heart rate. The binary patterns of length L=3 were also classified according to the amount of variations (0, 1 or 2 variations) and the respective occurrences were calculated (0V%, 1V% and 2V%). Transitions were quantified by taking 20 beats before and after each transition between successive stationary segments (l=40 beats). They were analyzed by the same quantities. The comparison of the results of stationary segments and transitions between successive stationary segments was carried out using average values of all segments and average values of all transitions.

During daytime the healthy subjects had stationary segments of 72 beats on average, had similar average RR intervals for the segments and the transitions (687 ms). SDNN, RRamp

and the excursion time increased during the transitions (37 vs. 52 ms, 122 vs. 162 ms, 5.4 vs. 5.5 beats, all $p < 0.05$). The percentile based approach showed an increase of 0V% and 1V% (17.0% vs. 23.5% and 43.4% vs. 45.3%, both $p < 0.05$) whereas 2LV% and 2UV% decreased during the transitions (19.6% vs. 14.6% and 20.0% vs. 16.5%, both $p < 0.05$). The binary patterns showed also an increase of 0V% patterns during the transition (30.2% vs. 32.4%, $p < 0.05$) whereas 1V% and 2V% decreased (50.1% vs. 48.6% and 19.7% vs. 18.9%, both $p < 0.05$). During nighttime the average stationary segment contained 138 beats. Qualitatively, similar results were obtained during nighttime compared to daytime. The CHF patients during daytime had a similar average length of the stationary segments compared to the healthy subjects (78 beats). The patients had similar average RR intervals during the segments and during the transitions (663 ms). SDNN and RRamp increased during the transitions (12 vs. 15 ms and 37 vs. 47 ms, both $p < 0.05$) whereas the excursion times did not change (2.7 beats). Similarly to the healthy subjects, the percentile based approach showed an increase of 0V% and 1V% (7.2% vs. 10.7% and 33.6% vs. 37.2%, both $p < 0.05$) whereas 2LV% and 2UV% decreased (17.0% vs. 14.1% and 42.2% vs. 38.0%, both $p < 0.05$) during the transitions. At the same time the binary patterns showed an increase of 0V% (12.4% vs. 13.1%, $p < 0.05$) and a decrease of 2V% (36.6% vs. 36.1%, $p < 0.05$). During nighttime the length of the stationary segments did not change compared to daytime. Qualitatively, similar results were obtained during nighttime.

The quantification of short stationary and nonstationary segments of RR interval series (length < 100 beats) can be carried out using the presented methods. The quantities expressing the variability show an expected increase of variability during the transition. Dynamical features of these RR interval series can be quantified by means of symbolic dynamics analysis. In contrast to the increase of variability, the dynamics of RR intervals gets simpler in the sense that patterns without (0V%) or only 1 variation (1V%) occur more often during the transitions whereas the patterns with two variations (2LV% and 2UV%) occur less often. These dynamical features can be observed in healthy subjects and CHF patients. Since the appearance of the former patterns are associated with an increase of sympathetic modulations whereas as the latter patterns are associated to parasympathetic modulations [4], transitions seems to be governed mainly by sympathetic modulations. Future studies should concentrate on differentiating the sign of transition and on comparing parameters obtained from two consecutive stationary periods occurring before and after transition.

References

- [1] Levine JA 2014 *Physiology* **29(5)** 300-301
- [2] Bernaola-Galvan P, Ivanov PC, Nunes Amaral LA, et al. 2001 *Physical Review Letters* **87(16)** 168105; Camargo S, Duarte Queiros SM, Anteneodo C 2011 *Physical Review E* **84(4)** 046702
- [3] Guzzetti S, Borroni E, Garbelli PE, et al. 2005 *Circulation* **112(4)** 465-470
- [4] Cysarz D, Porta A, Montano N, et al. 2013 *European Physical Journal – Special Topics* **222(2)** 487-400
- [5] Cysarz D, Edelhäuser F, Javorka M, et al. 2015 *Conference Proceedings of the IEEE Engineering in Medicine and Biology Society* **2015** 286-289

On the relation between interacting networks and networks with multimodal frequency distributions

Andreas Daffertshofer¹, Bastian Pietras¹ and Nicolás Deschle¹

¹ *MOVE Research Institute Amsterdam & Institute for Brain and Behavior Amsterdam, Faculty of Behavioural and Movement Sciences, Vrije Universiteit Amsterdam, van der Boechorststraat 9, Amsterdam 1081 BT, The Netherlands*

The dynamic behavior of coupled networks is a timely and urgent issue. In particular networks of oscillators can display a variety of synchronization patterns dependent on their intrinsic characteristics and the coupling between them. We will discuss to what extent this behavior agrees with the dynamics of a single network of oscillators with natural frequency drawn from a multimodal frequency distribution. We will start with two coupled, symmetric (sub)populations with unimodal frequency distributions and prove that the resulting synchronization patterns resemble those of a single population with bimodally distributed frequencies. The proof of the equivalence of their stability, dynamics, and bifurcations, is based on an Ott-Antonsen ansatz. We will further illustrate that generalization to networks consisting of multiple (sub)populations vis-à-vis networks with multimodal frequency distributions appears difficult if not impossible.

Complexity of vascular control in amyotrophic lateral sclerosis patients is associated with the disease duration

Beatrice De Maria^{1,2}, Laura Dalla Vecchia¹, Kalliopi Marinou¹,
Gabriele Mora¹ and Alberto Porta^{3,4}

¹ IRCCS Fondazione Salvatore Maugeri, Milan, Italy

² Politecnico di Milano, Department of Electronics Information and Bioengineering, Milan, Italy

³ University of Milan, Department of Biomedical Sciences for Health, Milan, Italy

⁴ IRCCS Policlinico San Donato, Department of Cardiothoracic, Vascular Anesthesia and Intensive Care, Milan, Italy

Introduction

Amyotrophic lateral sclerosis (ALS) is a neurodegenerative disease that compromises upper and lower motor neurons. Although the clinical hallmark is a progressive motor weakness, ALS is considered a multisystem disease, causing also autonomic nervous system impairment [1,2]. Traditionally, autonomic nervous system impairment in ALS has been evaluated by means of power spectral analysis of heart period (HP) and systolic arterial pressure (SAP) variabilities [1-3], while complexity analysis has been barely exploited [2]. Complexity analysis has been useful and largely applied in pathological populations to assess the changes induced by the disease [4] and in healthy subjects to assess the effect of autonomic challenges, age, and gender [5]. We hypothesize that the study of ALS patients by complexity analysis of HP and SAP variability may improve the understanding of autonomic nervous system involvement in ALS. The altered cardiovascular neural response to orthostatic challenge and the presence of patients' groups with different autonomic profiles have already been described in ALS [2,3], but it has not been yet investigated whether indexes describing the cardiovascular control complexity could be associated with traditional ALS clinical parameters. Thus, the aim of this study is to correlate the results of complexity analysis of HP and SAP variability with patients' clinical markers of disease severity and progression.

Experimental Protocol and Data Analysis

We studied 51 ALS patients. Patients' functional status was evaluated with the Revised ALS Functional Rating Scale (ALSFRS-R), ranging from 48 (normal) to 0 and the bulbar involvement with ALSFRS-R bulbar subscore (ALSFRS-R BS), ranging from 12 (normal) to 0. The rate of disease progression (RDP) was calculated as the difference between two ALSFRS-R scores at two different evaluation times divided by the months between them. Disease duration (DD) was defined as the number of months from disease onset to clinical evaluation. We acquired electrocardiographic signal (ECG) and non-invasive arterial blood pressure (AP) for 10 minutes at rest in supine position (REST) and during head up tilt test at 75° (TILT). Sampling frequency was 250 Hz. From the ECG and AP signals, HP and SAP beat-to-beat variability series were extracted. HP was defined as the temporal distance between two consecutive R peaks on the ECG signal and SAP as the maximum of the AP signal inside each HP.

Complexity of HP and SAP series was estimated by corrected conditional entropy (CCE), described in detail in [6]. After fixing at 6 the number of the quantization levels, the minimum of the CCE with respect to the number of the past samples utilized to condition the evolution of the current one is taken as complexity index (CI). CI_{HP} and CI_{SAP} refer to CI calculated over HP and SAP series, respectively. CI ranges from 0 (the current value does not carry information given past samples, indicating maximum predictability and null complexity) to the Shannon entropy, representing the maximum information carried by the current value. Normalized CI of HP (NCI_{HP}) and SAP (NCI_{SAP}) series were calculated dividing CI_{HP} and CI_{SAP} by the Shannon entropy of HP and SAP, respectively. NCI_{HP} and NCI_{SAP} range from 0 to 1. CI and NCI indexes were computed over $N=256$ consecutive HP and SAP values for each experimental condition. Pearson correlation coefficient, r , between ALS patients' clinical markers and complexity indexes was calculated. A linear correlation with $p<0.05$ was considered significant.

Table 1. Correlation between clinical parameters and HP and SAP complexity indexes at REST and during TILT.

| REST | | | | | | | | |
|--------------------------|----------|----------|----------|----------|----------|----------|-------------|----------|
| Index | ALSFRS-R | | RDP | | DD | | ALSFRS-R BS | |
| | <i>r</i> | <i>p</i> | <i>r</i> | <i>p</i> | <i>r</i> | <i>p</i> | <i>r</i> | <i>p</i> |
| CI_{HP} | 0.104 | 0.466 | -0.0822 | 0.566 | 0.0539 | 0.707 | 0.11 | 0.444 |
| NCI_{HP} | 0.104 | 0.468 | 0.0296 | 0.837 | -0.0861 | 0.548 | 0.0587 | 0.682 |
| CI_{SAP} | -0.0802 | 0.576 | 0.166 | 0.243 | -0.25 | 0.0768 | -0.164 | 0.25 |
| NCI_{SAP} | -0.0202 | 0.888 | 0.177 | 0.213 | -0.291 | 0.0383* | -0.102 | 0.474 |

| TILT | | | | | | | | |
|--------------------------|----------|----------|----------|----------|----------|----------|-------------|----------|
| Index | ALSFRS-R | | RDP | | DD | | ALSFRS-R BS | |
| | <i>r</i> | <i>p</i> | <i>r</i> | <i>p</i> | <i>r</i> | <i>p</i> | <i>r</i> | <i>p</i> |
| CI_{HP} | 0.0931 | 0.516 | -0.171 | 0.23 | 0.085 | 0.553 | 0.163 | 0.253 |
| NCI_{HP} | 0.0785 | 0.584 | -0.208 | 0.142 | 0.0865 | 0.546 | 0.139 | 0.33 |
| CI_{SAP} | -0.0289 | 0.840 | 0.178 | 0.212 | -0.274 | 0.0518 | -0.126 | 0.38 |
| NCI_{SAP} | 0.0305 | 0.832 | 0.116 | 0.416 | -0.206 | 0.147 | -0.116 | 0.417 |

ALSFRS-R: Revised ALS Functional Rating Scale score; RDP: rate of disease progression; DD: disease duration; ALSFRS-R BS: ALSFRS-R bulbar subscore; *r*: Pearson correlation coefficient; *p*: *p*-value; HP: heart period; SAP: systolic arterial pressure; CI_{HP} and CI_{SAP}: complexity indexes of HP and SAP series; NCI_{HP} and NCI_{SAP}: normalized complexity indexes of HP and SAP series. The asterisk indicates a significant correlation with *p*<0.05.

Results

The results of the correlation analysis between ALS patients' clinical features (i.e. ALSFRS-R, RDP, DD and ALSFRS-R BS) and complexity indexes of HP and SAP series (CI_{HP}, NCI_{HP}, CI_{SAP} and NCI_{SAP}) at REST and during TILT are shown in Tab.1. Pearson correlation coefficient, *r*, and type I error probability, *p*, are reported. A statistically significant correlation was found only between NCI_{SAP} and DD: NCI_{SAP} was negatively correlated with DD at REST with *r*=-0.291 and *p*=0.0383.

Discussion and Conclusions

Complexity indexes were not correlated with ALSFRS-R, ALSFRS-R BS and RDP, thus suggesting that the autonomic nervous system impairment in ALS is not only associated with the disease severity and its rate of progression. However, NCI_{SAP} was negatively correlated to DD. These findings indicate that the ALS degenerative process affects the state of the cardiovascular system, in particular the vascular control. It appears that, while increasing DD, vascular control becomes less and less complex, maybe through a progressive increase of the sympathetic modulation directed to the vessels [7]. This result is in agreement with the positive correlation detected between spectral indexes of SAP and the RDP [3]. Since in our work NCI_{SAP} is not related to age [5], we exclude that the well-known increase of sympathetic activity with age fully explains our finding. In conclusion, the use of complexity indexes of HP and SAP variability in addition to more traditional clinical parameters could be useful to monitor the disease progression in ALS patients.

References

- [1] Pavlovic S *et al*, 2010 *Amyotroph. Lateral Scler.* **11** 272-276.
- [2] Dalla Vecchia L *et al*, 2015 *Physiol Meas* **36** 659-670.
- [3] De Maria B *et al*, 2015 *Conf Proc IEEE Eng Med Biol Soc* 2055-2058.
- [4] Goldberger L *et al*, 2002 *Neurobiol. Aging* **23** 23-26.
- [5] Catai AM *et al*, 2014 *Entropy* **16** 6686-6704.
- [6] Porta A *et al*, 1998 *Biol Cybern* **78** 71-78.
- [7] Porta A *et al*, 2014 *PLoS One* **9** e89463.

Acknowledgement

The study was partially supported by Arisla, Fondazione Italiana di Ricerca per la Sclerosi Laterale Amiotrofica.

Heart rate patterns and cardiac mechanics during sleep in microgravity aboard the International Space Station

Marco Di Rienzo¹, Prospero Lombardi¹, Gianfranco Parati², Emanuele Vaini¹

¹*Fondazione Don Carlo Gnocchi, Dept. of Biomedical Technology, Milano, Italy*

²*Università Milano Bicocca and Istituto Auxologico Italiano, Milano, Italy*

Astronauts often suffer from poor sleep quality during space missions. The causes of this phenomenon have not been clarified yet and past EEG measures during sleep in microgravity did not report significant changes with respect to regular sleep on Earth. With the "*Wearable Monitoring*" experiment, part of the Futura Mission organized and funded by the Italian Space Agency (ASI), we aimed to get a deeper insight into the sleep physiology in microgravity by a multiparametric approach. This was done 1) by validating the applicability of a new smart garment (MagIC-Space) for the unobtrusive and simplified vital signs collection during spaceflights; and 2) by using this device to monitor astronaut's electrocardiogram, autonomic nervous control (by the heart rate variability analysis), heart mechanical activity (by the seismocardiogram, SCG, i.e. the assessment of the precordial vibrations produced by the beating heart), skin temperature and breathing patterns during sleep aboard the International Space Station.

One crewmember participated in this study. Seven in-flight sleep recordings were carried out at regular intervals from January till May 2015. Two pre-flight and two post-flight baseline recordings were also performed on October 2015 and July 2015, respectively. In each experimental session the astronaut worn the smart garment just before going to sleep and took it off the following morning.

The system was reported to be easy to use and not to interfere with the sleep comfort. All recordings were collected as planned. The signal quality was good and 98% of the collected signal was found to be adequate for the subsequent processing. Thus, the first objective of the project, i.e. the validation of the device, may be considered positively concluded. Conversely, the data analysis is still in progress given the large amount of recorded data (about 42 hours in space plus 28 hours on the ground, for a total of about 250,000 heart beats). In particular, the analysis is now focussed on two aspects of sleep in microgravity: 1) on the behaviour of cardiac mechanics, and 2) on the occurrence of non-rhythmic spontaneous activations of the sympathetic nervous system. As to the first aspect, we are now scanning the SCG tracings, and from each heartbeat we identify the specific fiducial points associated with the opening and closure of the aortic and mitral valves. From these data, when coupled with the ECG, we estimate indexes of heart contractility (Pre Ejection Period, Isovolumic Contraction Time, Left Ventricular Ejection Time) and heart relaxation (Isovolumic Relaxation Time) on a beat-to-beat basis. Concerning the second aspect, we are investigating the occurrence of specific non-rhythmic sympathetic activations by the analysis of the RRI profiles during sleep. The rationale behind this analysis is that these activations might reflect the occurrence of autonomic subcortical arousals, being the abnormal rate of the latter a possible co-factor of the poor sleep quality in space. As reported in literature, these sympathetic activations are associated with a specific RRI pattern characterized by a first profound tachycardic phase, lasting several tens of beats, followed by a relatively shorter bradycardic phase that brings the RRI values back to baseline. So far we observed tens of these patterns during sleep in microgravity. The comparison with ground data is in progress.

Reconstructing multivariate causal structure between functional brain networks through a new Laguerre-decomposition based Granger causality approach

Andrea Duggento¹, Gaetano Valenza^{2,3}, Luca Passamonti^{4,5}, Maria Guerrisi¹,
Riccardo Barbieri^{3,6}, Nicola Toschi^{1,7}

¹ *Medical Physics Section, Univ. of Rome “Tor Vergata”, Rome, Italy.*

² *Dep. of Information Engineering and Research Centre “E. Piaggio”, Univ. of Pisa, Pisa, Italy.*

³ *Massachusetts General Hospital and Harvard Medical School, Boston, USA.*

⁴ *Institute of Bioimaging and Molecular Physiology, National Research Council, Catanzaro, Italy.*

⁵ *Dep. of Clinical Neurosciences, University of Cambridge, Cambridge, UK.*

⁶ *Dep. of Electronics, Informatics and Bioengineering, Politecnico di Milano, Milano. Italy.*

⁷ *Dep. of Radiology, A.A. Martinos Center and Harvard Medical School, Boston, USA.*

Introduction and aims. Almost all currently available Granger Causality(GC)-based approaches to the estimation of information flow between brain regions are based on linear bivariate/multivariate autoregressive (MVAR) models. The fMRI signal is an articulate results of convolving neural activity with a locally- and time-varying haemodynamic response function (HRF), – a “pure” MVAR approach hence appears only partially suitable in reconstructing the multiple nonlinearities/time-scales which concur to the BOLD effect. Additionally, employing a linear model to reconstruct complex dynamics necessarily leads to an increase in model order often incompatible with typical fMRI acquisitions. We employ a Volterra-Wiener decomposition using orthogonal Laguerre polynomials as base functions in order to build parsimonious MVAR models which more accurately model BOLD dynamics, and use this framework to estimate Laguerre-based Conditioned Granger Causality (LCGC) in the context of directed functional brain connectivity.

Theory. Estimating LCGC from variable Y_t to the variable X_t ($Y \rightarrow X$) amounts to testing the null-hypothesis that knowledge of the past of Y_t does not improve the prediction of the future of X_t . To this end, in the LCGC approach two models are employed: first, the “restricted” AR model for X_t , which includes the past values of X_t itself and Z_t , which accounts for all other variables except Y_t . Second, the “unrestricted” AR model, which includes all variables X_t , Y_t , and Z_t [1]. Both models are fitted using MVAR systems defined over the components of a Volterra-Wiener expansion with Laguerre polynomials:

$$x_t = \mathbf{A}(\mathcal{L}^{(m)}(x)\mathcal{L}^{(m)}(z)) + \varepsilon_t \quad (\text{restricted model})$$

$$x_t = \mathbf{A}'(\mathcal{L}^{(m)}(x) \oplus \mathcal{L}^{(m)}(y) \oplus \mathcal{L}^{(m)}(z)) + \varepsilon'_t \quad (\text{unrestricted model})$$

Where the discrete-time Volterra-Wiener decomposition with Laguerre polynomials $\mathcal{L}^{(m)}(\cdot)$ over the discrete time signal x_t is defined as $\mathcal{L}^{(m)}(x) = \sum_{n=1}^N \phi_m(n)(x_{N-n} - x_{N-n-1})$, and where the m^{th} -order, discrete time, orthonormal Laguerre polynomial $\phi_m(n)$ is defined as $\phi_m(n) = \alpha^{\frac{n-m}{2}}(1 - \alpha)^{\frac{1}{2}} \sum_{j=0}^m (-1)^j \binom{n}{j} \binom{m}{j} \alpha^{m-j} (1 - \alpha)^j$ and parameter α ($0 < \alpha < 1$) determines the rate of exponential asymptotic decline of $\phi_m(n)$ [2]. The Null-hypothesis that Y_t does not cause X_t , conditioned to Z_t , is rejected if the f_{ratio} of the residual sum of squares (RSS) $f_{\text{ratio}} = \frac{RSS_{\text{r}} - RSS_{\text{ur}}}{RSS_{\text{ur}}} \frac{N_{\text{obs}} - 2m}{m}$ is extreme with respect of its parent distribution (χ^2 -distribution with $N_{\text{obs}} - 2m$ and m degrees of freedom [3]).

Results. We first characterize the ability of LCGC to capture nonlinear/hidden causal relations by simulating multivariate coupling in a network of noisy, driven Duffing oscillators (Figure 1) which interact through integral relationships with different decay constants. The ability of detecting true causal links while rejecting false causal links is quantified as the area under the ROC curve (AUC). Successively, we explore the structure of LCGC -based networks in the human brain in functional

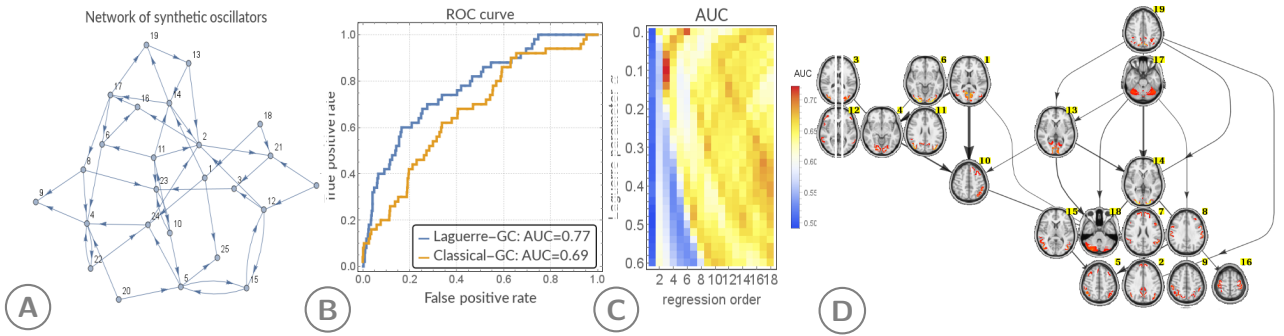


Figure 1: (A) Network graph employed for synthetic simulations. The network has 25 nodes with one periodically driven noisy Duffing oscillator in each node with coupling terms that depend on a build-up function: $\dot{x}_i = y_i + c_{i,j}(\eta_j - x_i) + \xi$; $\dot{y}_i = -\delta y_i - \beta x_i - \alpha x_i^3 + \gamma \cos(\omega_i t + \phi_i)$; $\dot{\eta}_i = -\eta_i/\tau + b x_i$. The direction of the edges indicates the direction of the coupling (causality) between nodes. (B) Example comparison of ROC curves between classical-GC and Laguerre-GC. The ROC curve of both classical- and Laguerre-GC (autoregressive order $p = 3$, Laguerre parameter $\alpha = 0.1$). (C) Example AUC as a function of the MVAR autoregressive order and the Laguerre parameter α . (D) Multivariate Laguerre-GC between functional sub-networks of the brain defined through group ICA in the "HCP-500-Subjects PTN Release" (only representative slices are shown). The thickness of the arrows reflects directed coupling strength.

MRI (fMRI) data from 440 healthy subjects scanned at rest at 3T (4 sessions, 1200 volumes/subject, TR=0.72s) within the "HCP 500-Subjects PTN Release" by employing the subject-specific time-courses of 25 components resulting from spatiotemporal group independent component analysis (ICA). Figure 3 is a graphical summary of the 440 subject directed, between-component brain connectivity network.

Discussion and conclusion. Synthetic validation showed a clear advantage of the LCGC approach in detecting nonlinear, causal links across different timescales at low model order. This is in line with the idea that Laguerre polynomials are smooth basis functions, able to capture damped multiple-frequency oscillations with fewer parameters when compared to linear MVAR models. In turn, overparameterising the MVAR model leads to a degradation of the performance in detecting causality. The within-ICA component LCGC analysis consistently showed that posterior occipital-inferior parietal networks strongly drive the activity in the right dorsolateral prefrontal cortex (PFC)-superior parietal circuits which is consistent with the view of a "bottom-up" information processing flow from the visual systems to the right-lateralized attentional executive system [4]. We also found evidence for a "top-down" information processing flow from the superior parietal networks to the visual systems as well as from the "cognitive" cerebellar regions to the visual networks. This is particularly intriguing in view of the emerging evidence showing the critical role of the posterior lobules of the cerebellum in cognitive control and "coordination" of sensory information processing. While this observation warrants additional validation through specific task-based investigation, in general we have shown that the LCGC method is able to detect in vivo functional interactions and causal dynamics across multiple neural networks while delivering superior performance as compared to classical, linear MVAR-based Granger causality methods.

References

1. Seth A.K. et Al. *J Neuroscience*, 2015. **35**(8): p. 3293-7.
4. Watanabe A. and Stark L.. *Mathematical Biosciences* **27.1** (1975): 99-108.
3. Bressler S.L. and Seth A.K., *Neuroimage*, 2011. **58**(2): p. 323-9.
4. Corbetta M. and Gordon L.S., *Nature reviews neuroscience* **3.3** (2002): 201-215.

Multi-ion Dynamics Dominated by Interactions

Robert Eisenberg

Rush University Medical Center, Dept. of Molecular Biophysics, Chicago IL USA

Ion flow is always constrained by interactions. Maxwell's equations and continuity of current ($\nabla \times \mathbf{B} = \mu_0 \mathbf{J} + \mu_0 \epsilon_0 \partial \mathbf{E} / \partial t$ so $\nabla \cdot (\mathbf{J} + \epsilon_0 \partial \mathbf{E} / \partial t) = 0$, **always**) force **perfect** spatial correlation of current flow everywhere, at all times in all systems. Classical chemical and Markov models do not deal with spatial correlations. Models defined by ordinary differential equations in time do not automatically satisfy spatial conservation laws so they cannot be assumed to satisfy continuity of current. Chemical reaction models depending on the law of mass action, or Markov models of stochastic processes, or ordinary differential equations with rate constants that are constants, or local functions, must then be embedded in a spatial model or simulation if they are to be useful in systems in which current flows or its fluctuations are important. Simulations of such systems are helpful if they satisfy continuity of current as well as conservation of mass and charge. Ionic devices are usually controlled by ions at very high number densities. Number densities in ion channels and enzyme active sites are often more than 30 molar. (Solid Na^+Cl^- is 37 molar for comparison.) Variational methods are the safest way to deal with such crowded interacting charges but they lead to differential equations that are difficult to solve in complex structures like proteins (or electrodes of batteries). Carefully crafted reduced models can give satisfactory results if care is taken to satisfy conservation of charge and current flow while describing steric interactions. Most of electrical engineering is based on such models (including the circuit theory that makes computer science possible) but electrons and holes have zero diameter. Only a handful of ions can fit into biological channels so steric forces and saturation phenomena become vitally important. Fermi like distributions can be linked to Poisson and Nernst Planck partial differential equations so conservation laws are satisfied automatically in saturating systems of crowded spherical ions. This approach successfully describes ionic solutions in bulk, and ions in gramicidin and calcium channels.

Respiratory sinus arrhythmia as a buffer of systemic blood flow

Author: Maja Elstad, University of Oslo, Institute of Basic Medical Sciences, Norway

Background:

Respiratory sinus arrhythmia has been investigated intensively in search of a function/purpose. Several functions have been proposed, some are still disputed, and most of them are not mutually exclusive. One suggested purpose is the ability of respiratory sinus arrhythmia to buffer arterial blood pressure fluctuations (1) but this is still debated (2).

Within intensive care there has been increased focus on the importance of blood flow over blood pressure to maintain organ perfusion (3). In this paper I discuss the findings in support of respiratory sinus arrhythmia in stabilization of the systemic blood flow at respiratory frequency.

Methods:

I reanalysed data from previous experiments in which we modified respiratory sinus arrhythmia and examined cardiac output oscillations at respiratory frequency (4, 5). In both studies respiratory sinus arrhythmia was decreased by atropine medication or positive pressure ventilation. Cardiac output was measured by ultrasound Doppler or estimated from arterial blood pressure curve.

Oscillations in heart rate and cardiac output were quantified as the area under the curve of the power spectrum calculated with Fourier transform algorithm at respiratory frequency (0.15-0.4 Hz). Medians and 95% confidence intervals (95% CI) calculated by Hodges-Lehmann's estimate are reported.

Results:

Atropine medication reduced heart rate variability at 0.15-0.4 Hz by 97%, while cardiac output variability at 0.15-0.40 Hz increased by 207%. Positive pressure ventilation reduced heart rate variability at 0.15-0.4 Hz by 43%, while cardiac output variability at 0.15-0.40 Hz increased by 60%. Combined, when heart rate variability was decreased to a quarter of normal values (27% (95% CI: 8%-43%)), cardiac output variability was more than doubled (231% (95% CI: 148%-313%)).

Conclusion: Respiratory sinus arrhythmia buffer oscillations in systemic blood flow.

References

1. Toska K, Eriksen M. Respiration-synchronous fluctuations in stroke volume, heart rate and arterial pressure in humans. *JPhysiol (Lond)*. 1993;472:501-12.
2. Taylor JA, Eckberg DL. Fundamental relations between short-term RR interval and arterial pressure oscillations in humans. *Circulation*. 1996;93(8):1527-32.
3. Moerman A, Denys W, De Somer F, Wouters PF, De Hert SG. Influence of variations in systemic blood flow and pressure on cerebral and systemic oxygen saturation in cardiopulmonary bypass patients. *Br J Anaesth*. 2013;111(4):619-26.
4. Elstad M, Toska K, Chon KH, Raeder EA, Cohen RJ. Respiratory sinus arrhythmia: opposite effects on systolic and mean arterial pressure in supine humans. *JPhysiol*. 2001;536(Pt 1):251-9.
5. Elstad M, Walloe L, Holme NL, Maes E, Thoresen M. Respiratory sinus arrhythmia stabilizes mean arterial blood pressure at high-frequency interval in healthy humans. *Eur J Appl Physiol*. 2015;115(3):521-30.

Time-resolved characterization of human brain dynamics – noninvasive cognitive neurophysiology

Denis A. Engemann

*Cognitive Neuroimaging Unit, CEA DRF/I2BM, INSERM, Universit Paris-Sud,
Universit Paris-Saclay, NeuroSpin center, 91191 Gif/Yvette, France*

Magneto- and electro-encephalography (M/EEG) enable noninvasive time-resolved neuroimaging. They capture synchronous neural population-level activity of tens of thousands of neurons in real-time by passively measuring electromagnetic events with sensor arrays positioned outside the head. Research has consistently highlighted two broad classes of brain responses: oscillatory and arrhythmic dynamics. Neural oscillations generically describe the rhythmic fluctuations of neural responses over time and can be observed at different functional scales: microscopic membrane fluctuations and intrinsic neural properties lead to resonant properties of the neuron. At the mesoscopic scale, neural oscillations reflect the mean field activity of neural populations. At the macroscopic scale, rhythmic fluctuations capture inter-site synchronisations, reflecting both intrinsic dynamics and neural synchronisations evoked by environmental dynamics. With M/EEG, it is not directly possible to demonstrate that evoked activity results from phase-resetting of ongoing oscillatory activity. Nevertheless, reasonable inferences on the origins of the signal can be motivated by the use of computational and statistical modelling and can provide useful criteria for interpretation. In this context, the notion of neural entrainment can shed light on the propensity of neurons and neural populations to resonate with sensory stimuli. This may not only account for how external temporal structure can be internalised in brain responses but more importantly, how brain responses can dissociate from external temporal cues to represent an individuals autonomous temporal cognition. In this sense, cognitive brain dynamics could motivate a useful functional taxonomy to help reduce the intrinsic complexity of brain-environment interactions.

Prediction and Entropy Measures of Brain-to-Heart Causal Interactions in Patients with Sleep Disorders

Luca Faes¹, Daniele Marinazzo², Alberto Porta³ and Giandomenico Nollo¹

¹*Bruno Kessler Foundation, Trento, Italy*

²*University of Ghent, Department Of Data Analysis, Ghent, Belgium*

³*University of Milan, Department of Biomedical Sciences for Health, Milan, Italy*

Introduction

Sleep dynamically regulates the activity of the brain and cardiovascular systems in a way that is reflected in the nocturnal time course of the spectral components of heart rate variability (HRV) and of EEG activity. This modulation has been recently investigated through dynamical indexes of HRV-EEG variability to assess brain-heart interactions during sleep in both healthy subjects and patients with sleep disorders [1,2]. The present study focuses on the evaluation of causal interactions from the dynamics of different EEG wave amplitudes (δ , θ , α , σ , β) to the variability of cardiac vagal autonomic activity in healthy subjects and patients with severe sleep apnea-hypopnea syndrome (SAHS), both untreated and after continuous positive airways pressure (CPAP) therapy. Measures of the causal coupling from brain to heart and of the interaction between brain rhythms are computed comparing entropy and predictability functionals in relation to their ability to describe the joint brain and cardiovascular regulation during sleep in normal and impaired states.

Methods

We analyzed the polysomnographic recordings of a group of eight patients suffering from severe sleep apneas studied just after the diagnosis of SAHS as well as after prolonged (> 1 year) treatment with nasal CPAP treatment, and a control group of thirteen age-matched healthy subjects (CTRL) [2]. The analyzed time series were the normalized spectral power of the EEG evaluated inside the five conventional bands (δ : 0.5-3 Hz; θ : 3-8 Hz; α : 8-12 Hz; σ : 12-16 Hz; β : 16-25 Hz) for consecutive non-overlapped 60 s windows, and the parasympathetic component of heart rate variability (HRV) assessed as the normalized spectral power in the 0.15-0.4 Hz band computed for consecutive 120 s windows overlapped by half. These six time series were taken as realizations of the cardiac process X , considered in this study as the target, and of the brain processes $Y=\{\delta, \theta, \alpha, \sigma, \beta\}$, considered as sources, and were analyzed in the framework of parametric linear prediction.

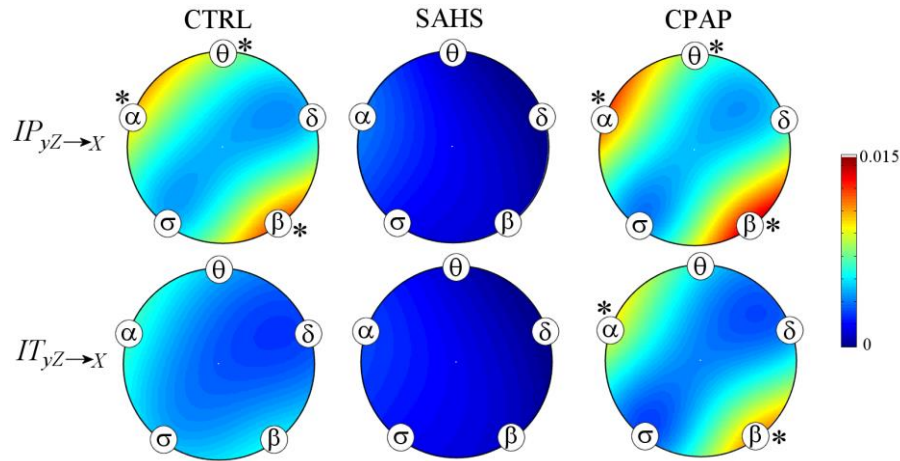
We studied causal interactions from sources to target describing the present sample of the target, X_n , as resulting from a linear combination of its past values, $X_n^-=[X_{n-1} X_{n-2} \dots]$, the past values y_n^- of the assigned scalar source y , and the past values Z_n^- of the remaining sources Z , where $Y=\{y,Z\}$ and y can be any of $\delta, \theta, \alpha, \sigma, \beta$. We considered the prediction error variances of the linear regressions of X_n on X_n^- , on $\{X_n^-, y_n^-\}$, on $\{X_n^-, Z_n^-\}$, and on $\{X_n^-, Y_n^-\}$, denoted respectively as $E_{X|X}$, $E_{X|X,y}$, $E_{X|X,Z}$, and $E_{X|X,Y}$. From these variances, we computed the following measures defined within the framework of Wiener-Granger causality [3]. The *causal predictability* $P_{Y \rightarrow X} = E_{X|X} - E_{X|X,Y}$ measures the portion of the variance of X that can be predicted from the knowledge of Y above and beyond the portion that can be predicted from X considered alone. The *transfer entropy* $T_{Y \rightarrow X} = H_{X|X} - H_{X|X,Y}$ measures the amount of information carried by X that can be explained from the knowledge of Y above and beyond the portion that can be explained from X considered alone (in the linear framework, entropies are estimated directly from prediction error variances: e.g., $H_{X|X} = 0.5 \ln(2\pi e E_{X|X})$ [4]). Then, combining causal predictability or transfer entropy measures we investigated how two sources interact with each other while affecting the dynamics of the target. Specifically, the

interaction predictability was defined as $IP_{yZ \rightarrow X} = P_{y \rightarrow X} + P_{Z \rightarrow X} - P_{Y \rightarrow X}$, and the interaction transfer was defined as $IT_{yZ \rightarrow X} = T_{y \rightarrow X} + T_{Z \rightarrow X} - T_{Y \rightarrow X}$. These measures are positive, denoting redundancy, when the two sources y and Z taken together contribute to the target X with less information than the sum of their individual contribution. The opposite situation, yielding negative values of $IP_{yZ \rightarrow X}$ and $IT_{yZ \rightarrow X}$, denotes synergy between y and Z .

Results and Conclusions

The causal predictability was significantly lower ($p < 0.05$, Mann-Whitney test) in SAHS (median $P_{Y \rightarrow X} = 0.048$) and CPAP ($P_{Y \rightarrow X} = 0.061$) than in CTRL ($P_{Y \rightarrow X} = 0.095$). The transfer entropy showed similar behavior, resulting comparable for SAHS and CPAP ($T_{Y \rightarrow X} = 0.038$ and 0.056) and significantly higher ($p < 0.01$) for CTRL ($T_{Y \rightarrow X} = 0.090$). On the contrary, predictability and information approaches exhibited different behavior when used to estimate the interaction between sources (Fig. 1). According to interaction predictability measures, the processes θ , α and β showed a significant redundant interaction with the other brain processes in CTRL subjects, which was absent in SAHS patients but was restored by CPAP (Fig. 1a). Redundant interactions and their alterations with SAHS were more hardly detected using information measures (Fig. 1b). We ascribe this result to the concave property of the logarithm function that tends to favor the detection of net synergy [5], and in our case blunts the detection of net redundancy.

These results indicate that sleep apneas are associated to a reduced strength of the dynamical causal interactions from the EEG brain rhythms to the cardiac parasympathetic component of HRV that is not fully restored by the CPAP therapy. Moreover, redundancy of interacting brain rhythms seems to be a feature of undisturbed sleep that is lost with apneas and is recovered with treatment; its detection is favored expressing information in terms of reduction in variance rather than reduction in entropy.



Interaction predictability ($IP_{yZ \rightarrow X}$) and interaction transfer ($IT_{yZ \rightarrow X}$) measuring how much each brain process ($y = \delta, \theta, \alpha, \sigma, \beta$) interacts with the other processes (Z) while causing the cardiac process X , computed as median values within CTRL, SAHS, and CPAP groups. * $p < 0.05$ significant interaction (Wilcoxon signed-rank test).

References

- [1] Bashan A, Bartsch RP, Kantelhardt JW, Havlin S, Ivanov PC 2012 *Nature Comm* **3** 702
- [2] Jurysta F, Kempnaers C, Lanquart JP, Nosedà A, van de Borne P, Linkowski P 2013 *Bmc Pulmonary Med.* **13**, 29
- [3] Porta A, Faes L 2016 *Proceedings of the IEEE* **104** (2) 282-309
- [4] Faes L, Porta A, Nollo G 2015 *Entropy* **17** 277-303
- [5] Barrett AB 2015 *Phys Rev E* **91** 052802

Investigating the molecular basis of ion selectivity of NaChBac using the patch clamp technique

Olena A. Fedorenko, Zeyu Zheng and Stephen K. Roberts

Lancaster University, Faculty of Health and Medicine,

Division of Biomedical and Life Sciences, Lancaster, LA1 4YW, UK.

NaChBac is a bacterial voltage-gated sodium channel, which is an important model for structure-function studies of more complex vertebrate Na_v and Ca_v channels¹⁻³. NaChBac is highly Na^+ selective, but it can be converted into Ca^{2+} -selective forms through mutagenesis in its selectivity filter (SF)⁴⁻⁶, which consists of six amino acid residues LESWAS (leucine-glutamate-serine-tryptophan-alanine-serine, respectively)^{4,7}. Key to sodium selectivity is the negatively charged amino acid residue, glutamate (E).

The aim of the present study was to define the role of the charges associated with the amino acid residues in NaChBac's SF. Using site-directed mutagenesis we have generated NaChBac mutant channels, in which the amino acid composition of the SF has been altered. Specifically, we have generated mutant channels with SFs with "neutralised charge" (LEKWAS, in which the neutral residue serine is replaced with a positively charged lysine), "deleted charge" (LASWAS, in which the glutamate is replaced with the electrically neutral alanine) and "added charge" (LEDWAS and LEEWAS, in which the serine is replaced by negatively charged aspartate or glutamate respectively).

To study the permeation and selectivity of wild type and mutant channels we employed the whole-cell patch-clamp technique and solutions, in which extracellular Na^+ was replaced with group I (Li^+ , K^+ , Rb^+ or Cs^+) and group II (Mg^{2+} , Ca^{2+} , Sr^{2+} or Ba^{2+}) elements. The pipette solution contained mainly 20 mM Na-gluconate and 120 mM Cs-methanesulfonate; this solution was designed to isolate Na^+ currents free from contaminating endogenous K^+ and Cl^- currents. Our experiments confirm that wild type NaChBac is a highly selective Na channel with negligible permeability for all other cations tested, except Li^+ (with a permeability ratio, $P_{\text{Li}}/P_{\text{Na}} = 0.8$). The LEKWAS and LASWAS mutant channels (in which the negatively charged glutamate is either neutralised or replaced) exhibited negligible permeability and no significant NaChBac mediated ion currents could be measured for any of the cations tested.

In contrast, the "additional charge" mutant LEDWAS channel conducted both Na^+ and Ca^{2+} (with a permeability ratio, $P_{\text{Ca}}/P_{\text{Na}} \sim 60$) and exhibited a strong anomalous mole fraction effect (AMFE) consistent with LEDWAS being a Ca^{2+} selective channel. We also found that the LEDWAS channel had permeability for Li^+ ($P_{\text{Li}}/P_{\text{Na}} \sim 0.8$), K^+ ($P_{\text{K}}/P_{\text{Na}} \sim 0.2$), Mg^{2+} ($P_{\text{Mg}}/P_{\text{Na}} \sim 2$), Sr^{2+} ($P_{\text{Sr}}/P_{\text{Na}} \sim 25$) and Ba^{2+} ($P_{\text{Ba}}/P_{\text{Na}} \sim 7$), but Rb^+ and Cs^+ were not permeant.

The other "additional charge" channel mutant, LEEWAS, exhibited similar permeability properties for monovalent cations to that observed for LEDWAS. However, the LEEWAS mutant channel revealed reduced permeability for divalent cations compared to that for LEDWAS channels; the relative permeabilities for LEEWAS were: Mg^{2+} ($P_{\text{Mg}}/P_{\text{Na}} \sim 0.1$), Ca^{2+} ($P_{\text{Ca}}/P_{\text{Na}} \sim 17$), Sr^{2+} ($P_{\text{Sr}}/P_{\text{Na}} \sim 5$) and Ba^{2+} ($P_{\text{Ba}}/P_{\text{Na}} \sim 0.2$).

Our experiments demonstrate the importance of negatively charged amino acid residues in the SF in NaChBac ion selectivity. Deletion or neutralisation of the negatively charged glutamate residue leads to loss of the channel's permeability to both mono- and divalent cations. However, addition of negatively charged amino acid residues to the SF results in a

loss of Na⁺ selectivity and increased permeability to a range of cations including Ca²⁺. Furthermore, comparison of the permeability properties of LEEWAS and LEDWAS highlights that the structure of the SF also influences channel ion selectivity. These findings are contributing to collaboration with physicists at the universities of Lancaster (see presentation by Dr. Igor Kaufman) and Warwick (see presentation by Dr. Igor Khovanov) with the aim to understand the molecular basis of ion selectivity and permeability of ion channels.

References

1. Catterall WA. 2001 *Science* **294** (5550) 2306-8
2. Ren D *et al.* 2001 *Science* **294** 2372–2375
3. Koishi R *et al.* 2004 *J. Biol. Chem.* **279** 9532–9538
4. Yue L *et al.* 2002 *J. Gen. Physiol.* **120** 845–853
5. DeCaen PG *et al.* 2014 *eLIFE* **3** e04387
6. Naylor CE *et al.* 2016 *EMBO J* e201593285
7. Charalambous K, Wallace BA 2011 *Biochemistry* **50** 6742-52

Observation of Ionic Coulomb Blockade in Nanopores

Jiandong Feng¹, Ke Liu¹, Michael Graf¹, Dumitru Dumcenco², Andras Kis², Massimiliano Di Ventra³,
& Aleksandra Radenovic¹

¹EPFL School of Engineering, EPFL, Institute of Bioengineering, Laboratory of Nanoscale Biology 1015
Lausanne, Switzerland

²EPFL School of Engineering, EPFL, Institute of Electrical Engineering, Laboratory of Nanoscale Electronics
1015 Lausanne, Switzerland

³University of California, Department of Physics, San Diego, La Jolla, California 92093, USA

Emergent behaviour from electron-transport properties is routinely observed in systems with dimensions approaching the nanoscale. However, analogous mesoscopic behaviour resulting from ionic transport has so far not been observed, most probably because of bottlenecks in the controlled fabrication of sub-nanometre nanopores for use in nanofluidics. transport was also observed in various systems, such as hydrophobic wetting and ion dehydration. In this talk I will provide detailed description of the experimental observation of single-ion transport through the ionic junction of a sub-nm MoS₂ pore.

References

Kaufman, I. K., McClintock, P. & Eisenberg, R. Coulomb blockade model of permeation and selectivity in biological ion channels. *New J. Phys.* **17**, 083021 (2015)

Krems, M. & Di Ventra, M. Ionic coulomb blockade in nanopores. *J. Phys.: Condens. Matter* **25**, 065101 (2013).

Parsegian, A. Energy of an ion crossing a low dielectric membrane: Solutions to four relevant electrostatic problems. *Nature* **221**, 844-846 (1969).

Zhang, J., Kamenev, A. & Shklovskii, B. I. Conductance of ion channels and nanopores with charged walls: A toy model. *Phys. Rev. Lett.* **95** (2005).

Feng et al. Observation of Ionic Coulomb Blockade in Nanopores *Nat. Materials* (2016)

Crisis and stasis: a cellular model of the progressive nature of heart disease-linked Ca²⁺ release dysfunction

Christopher George

Cardiff University, Wales Heart Research Institute, Cardiff, UK

Heart failure (HF) is associated with the progressive loss of heart cell contractility and increased susceptibility to arrhythmias. Both of these aspects of HF pathogenesis involve abnormal Ca²⁺ signalling and specifically, dysfunctional Ca²⁺ release from the sarcoplasmic reticulum (SR), the main Ca²⁺ storage organelle in cardiac cells. Widely referred to in the literature as ‘SR Ca²⁺ leak’, this hallmark abnormal control of SR Ca²⁺ release and sequestration (via defective regulation of ryanodine receptors and SERCA, respectively) represents an important process for normalization in contemporary HF therapy. In order to better understand this process, we developed an in vitro model of Ca²⁺ signalling in heart cell networks. We used the cardiac glycoside ouabain to provoke concentration-dependent disruption of SR Ca²⁺ release in multicellular populations of functionally-coupled mouse cardiomyocytes. Incremental increases in ouabain concentration in the μM range progressively eliminated the spatio-temporal organization of Ca²⁺ signals that characterised normal (drug naïve) cell behaviour. This disruption of intracellular signalling resulted in the desynchronization of intercellular Ca²⁺ signals. In contrast, very low concentrations of ouabain (nM) elicited new steady state Ca²⁺ handling properties that resulted in the decreased susceptibility of these cell populations to subsequent disruption. In this talk, I will describe how these data fit a conceptual model in which the progressive destabilization of Ca²⁺ signalling in heart cell networks proceeds via sequential ‘crises’ and the emergent new steady states (‘stases’). The implications of this model for developing new therapeutic approaches to combat the progressive decline in myocardial performance in HF will be discussed.

Theory of alike selectivity in biological channels

Dmitry G. Luchinsky^{1,2}, Will A.T. Gibby¹, Igor Kh. Kaufman¹, Robert S. Eisenberg³, Peter V.E. McClintock¹

¹*Department of Physics, Lancaster University, Lancaster LA1 4YB, UK*

²*SGT, Inc., Greenbelt, MD, 20770, USA*

We introduce a statistical mechanical model of the selectivity filter that accounts for the interaction between ions within the channel and derive Eisenman equation of the filter selectivity directly from the condition of barrier-less conduction.

Selectivity of the canonical K⁺ filter, formed by a narrow 15 Å-long tunnel holding four K⁺-binding sites, is usually analyzed [1-6] in terms of the difference in the excess chemical potential in the bulk $\bar{\mu}_i$ in and the channel $\bar{\mu}_i^c$ at one binding site

$$\Delta\Delta\bar{\mu}_{K,Na} = (\bar{\mu}_{Na} - \bar{\mu}_{Na}^c) - (\bar{\mu}_K - \bar{\mu}_K^c). \quad (1)$$

The question of how to introduce barrier-less conduction within this formalism elicited a many-voiced debate over decades.

Let n_i^s be a number ions of the i -th type in the solution and n_i their number within the filter. We introduce the free energy of the solution plus the filter in the form

$$G = \sum_i (n_i^s - n_i) kT \ln x_i^s + \sum_i (n_i^s - n_i) \tilde{\mu}_i + \sum_i n_i \tilde{\mu}_i^c + kT \ln \left(\prod_i n_i! \right) + \varepsilon(\{n_j\}, n_f).$$

In treating the filter filled with ions as excited states of the system, we derive the following grand canonical ensemble for the filter (cf [?])

$$P(\{n_j\}) = \mathcal{Z}^{-1} \prod_{i=1}^m \frac{(x_i^s)^{n_i}}{n_i!} e^{\frac{\sum_i n_i \Delta\bar{\mu}_i - \varepsilon(\{n_j\}, n_f)}{kT}}. \quad (2)$$

The current with a constant voltage drop $\Delta\phi = \phi^L - \phi^R$ through the channel in linear response is proportional to the rate of charge fluctuations passing through the channel [7] $J_{steady} = \frac{\Delta\langle Q^2(t) \rangle}{2kT\Delta t} \Delta\phi$.

For discrete conducting ions, charge fluctuations are proportional to fluctuations in the number of ions in the channel. The variance $\sigma_{n_i}^2 = -kT \left(\frac{\partial^2 \Omega}{\partial \Delta\bar{\mu}_i^2} \right)_{T,V}$ of the number of ions in the filter can be found using the grand potential $\Omega = -kT \ln \mathcal{Z}$.

To apply obtained results to the KcsA filter, let us consider two types of conducting ions K⁺ and Na⁺ that can bind to any binding site in the filter, but have to have at

least one water molecule between them. The free energy of the filter filled with n_K and n_{Na} ions (ignoring a prefactor) is $G = -n_K \Delta \tilde{\mu}_K - n_{Na} \Delta \tilde{\mu}_{Na} + \varepsilon(n_K, n_{Na}, n_f)$. The energy of interaction between the ions is $\varepsilon(n_K, n_{Na}, n_f) = \frac{q^2}{2C} (n_K + n_{Na} + n_f)$, where n_f is the number of fixed charges on the channel wall, i.e. the main mutation parameter. The channel capacitance is $C \approx \frac{4\pi\epsilon_0\epsilon_w R^2}{L}$.

The lowest conducting free energy level corresponds to $n_K = 2$. The conditions for fast conduction are: (i) $G(n_K, n_f^*) = G(n_K + 1, n_f^*)$ and (ii) $G(n_K, n_f^*) \approx 0kT$. To tune the selectivity and conductivity of the filter one has to tune: (i) geometry, (ii) $\bar{\mu}_i^c$, and (iii) the n_f . Tuning the filter for fast conduction of K^+ ions gives

$$n_f^* = -(n_K + 1/2) + \frac{C}{q^2} \Delta \mu_K. \quad (3)$$

Substituting this value into the free energy gives the following barrier for Na^+ ion to enter the channel $\Delta G_{Na} = \Delta \mu_K - \Delta \mu_{Na}$, i.e. Eisenman's selectivity relation follows directly from the condition for fast conduction of K^+ ions.

Analysis of the mean and variance for K^+ and Na^+ ions in the filter shows that tuning it for fast conduction of K^+ ions results in effective block of Na^+ conduction if the width of the dispersion peaks is smaller than the separation of the peaks determined by the geometry of the channel and ΔG .

In conclusion, we have introduced a statistical mechanical model for the distribution of alike-charged ions in the K^+ selectivity filter and have shown that the Eisenmann relation for filter selectivity follows directly from the condition for fast barrier-less conduction of K^+ ions in the filter. The results can be extended beyond linear response using a solution of the Nernst-Planck equation. Models of filters with distinguishable binding sites will be considered in future work.

References

1. Zhou Y. et al, Nature 414, 43 (2001)
2. Eisenman G. , in Symposium on Membrane Transport and Metabolism, ed. A. Kleinzeller and A. Kotyk (Academic Press, NY) p. 163 (1961)
3. Bezanilla F. and Armstrong C. M., The J of Gen Physiology 60, 588 (1972)
4. Noskov S. Y. and Roux B., The J of Gen Physiology 129, 135 (2007)
5. Dixit P. D., Merchant S, and Asthagiri D., Biophysical Journal 96, 2138 (2009)
6. Roux B., Biophysical Journal 77, 139 (1999)
7. Liu Y. and Zhu F., Biophysical Journal 104, 368 (2013)

Multiscale Multifractal Analysis - screening examination method presenting highly repetitive HRV multifractal pattern

Dorota Kokosińska, Jan Jakub Gieraltowski and Jan Jacek Żebrowski
Warsaw University of Technology, Faculty of Physics, Warsaw, Poland

The **main goal of our research** was a verification of the hypotheses concerning an effectiveness of Multiscale Multifractal Analysis in screening examination and an existence of highly repetitive heart rate variability multifractal pattern.

The analysis of heart rate variability night-time recordings involved 282 patients in 5 groups: **36 healthy patients**: (7 women and 29 men), **103 with aortic valve stenosis**: (48 women and 55 men), **36 with hypertrophic cardiomyopathy**: (16 women and 20 men), **32 with persistent atrial fibrillation**: (12 women and 20 men), **59 coronary disease**: (8 women and 51 men) and **16 with congestive heart failure** (no information about sex).

In our research, we applied the non-linear method **Multiscale Multifractal Analysis (MMA)**, which is derived from the DFA [1] and MF-DFA [2] methods. MMA yields the scaling properties of fluctuations in many scales at once and allows to analyze long-range correlations. The main result is the Hurst surface - a 3D plot $h(q,s)$ depicting the dependence of the local Hurst exponent h as a function of the magnitude of fluctuations parameter q and the scale of observation s [3].

The Hurst surfaces are characterized by different shapes depending on the medical case analyzed. Because the Hurst surface is difficult to interpret globally in physiological terms, we analyze only the local shape of this surface and we compare the values of the local Hurst exponent for different cases at specific regions of the Hurst surface. Based on the shape of the Hurst surface, 6 general criteria were prepared intended for MMA as a screening examination method. These criteria allow to diagnose subjects as healthy (i.e. when all 6 criteria are fulfilled) and ill patients (at least one criterion is not fulfilled) [4].

In our analysis, we also prepared additional criteria - 2 combinations of the 6 general criteria (where some are fulfilled and other not) indicate that persistent atrial fibrillation is present in heart variability. These combinations of the set of the criteria let us to discern a highly repetitive heart rate variability multifractal pattern for this group of subjects. We noticed also that the Hurst surface for atrial fibrillation has a raised region for large values of s (for very low frequencies) and for small s (low frequencies). This seems to be a very interesting result because other heart rate variability analysis methods are not able to describe the very low frequency band adequately and atrial fibrillation is in general described as 'white noise'.

In order to check the reliability of the method applied and the defined criteria, we calculated sensitivity, specificity, positive predictive value (PPV), negative predictive value (NPV) and accuracy (Table 1). The calculation of an aforementioned diagnostic parameters for healthy subjects is mathematical impossible.

Table 1. The results of test according to criteria based on shape of the Hurst surface.

| Parameter | Coronary disease | Hypertrophic cardiomyopathy | Aortic valve stenosis | Atrial fibrillation | Congestive heart failure |
|-------------|------------------|-----------------------------|-----------------------|---------------------|--------------------------|
| sensitivity | 0,64 | 0,56 | 0,78 | 1,00 | 0,94 |
| specificity | 0,75 | 0,75 | 0,75 | 0,75 | 0,75 |
| PPV | 0,81 | 0,69 | 0,90 | 0,78 | 0,63 |
| NPV | 0,56 | 0,63 | 0,54 | 1,00 | 0,96 |
| accuracy | 0,68 | 0,65 | 0,77 | 0,87 | 0,81 |

The prepared 6 criteria assessing the shape of the Hurst surface $h(q,s)$ show that the Multiscale Multifractal Analysis, applied in this research, can be used as an effective screening examination method. Moreover, the analysis based on MMA allows to distinguish subjects with atrial fibrillation and that a highly repetitive, nontrivial HRV multifractal pattern is obtained, that can be useful for further study concerning this medical condition.

References

- [1] S. Buldyrev, S. Havlin, M. Simons, H. Stanley i A. Goldberger, *Mosaic organization of DNA nucleotides*, Phys Rev E Stat Phys Plasmas Fluids Relat Interdiscip Topics, vol 49, nr 2, pp. 1685-1689, 1994
- [2] J. Kantelhardt, S. Zschiegner, E. Koscielny - Bunde, S. Havlin, A. Bunde i H. Stanley, *Multifractal detrended fluctuation analysis of nonstationary time series*, Physica A, vol 316, pp. 87-114, 2002.
- [3] J. Gierałowski, J. Żebrowski i R. Baranowski, *Multiscale multifractal analysis of heart rate variability recordings with a large number of arrhythmia*, Phys. Rev. E Stat Nonlin Soft Matter Phys., 2012.
- [4] J. Gierałowski, D. Kokosińska, J. Żebrowski *Fractal pattern of heart rate variability revealing unknown very low frequency properties*, Computing in Cardiology 2015, vol 42, pp. 597-600.

Modeling linear and nonlinear properties of night-time heart rate variability

Mateusz Soliński, Jan Gierałtowski and Jan Żebrowski

Warsaw University of Technology, Faculty of Physics, Warsaw, Poland

Modeling heart rate variability is attractive for several reasons. First of all, each new model is an attempt to explain origins of that fascinating phenomenon and could be useful as a generator of realistic RR intervals for testing new algorithms. Night-time heart rate variability (HRV) exhibits different properties in comparison to that during daily activity. The sequences of sleep stages (sleep architecture) that normally occur introduce specific patterns into RR time series. Thus, including the effect of sleep architecture should be a meaningful factor in the modeling of heart rate variability dynamics. We propose a model taking into account both the stochastic properties of heart rate variability and the effect of sleep stages. As a starting point, we used the model by Kantelhardt et al. [1] and introduced a number of modifications. We developed a method for creating synthetic hypnograms based on 30 real EEG recordings (database of the Faculty of Psychiatry, Warsaw University of Medicine, Warsaw, Poland) considering two properties of sleep architecture: the probabilities of transitions between all possible pairs of sleep stages and the probability distributions of sleep stage durations. We tested our model by using 34 RR time series from Institute of Cardiology, Warsaw, Poland each extracted from the nighttime part of Holter recordings. Quantitative comparison using both linear (mean, std, RMSSD, pNN50, LF/HF) and nonlinear (Multiscale Multifractal Analysis) assessment methods [2] showed that the RR time series generated by our model are indistinguishable from the real data (examples of real and generated by our model RR time series are shown in Figure 1).

One of the strengths of the model is a very good reconstruction of the multifractal properties of heart rate variability. We found that 76% of the analyzed synthetic signals are in agreement with the properties observed in real data according to the properties obtained using Multiscale Multifractal Analysis (for criteria see [3,4]) . The results show that stochastic processes and the sleep architecture dynamics used here form a model appropriate for nighttime heart rate variability.

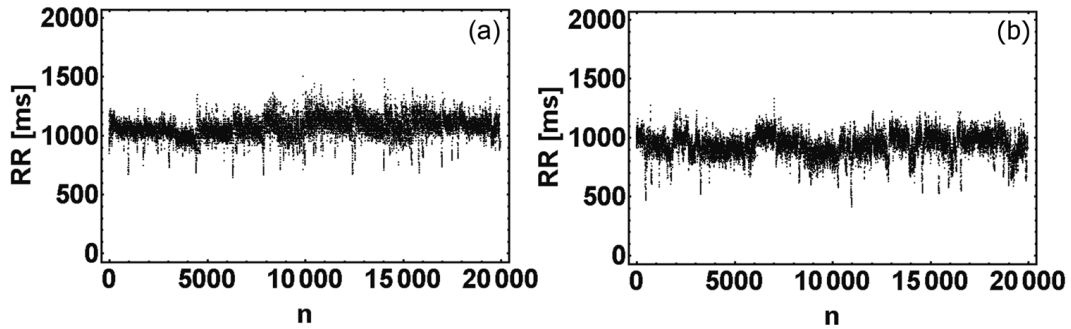


Figure 1: Tachogram obtained for the real data (a) and from our model (b). The characteristic fuzzy structure of the upper envelope, visible in the signals from our model and in real data, reflects human sleep architecture.

References

- [1] Kantelhardt J W, Havlin S, Ivanov Ch, Modeling transient correlations in heart-beat dynamics during sleep, 2003, *Europhys. Lett.* **62**, 147-153.
- [2] Solinski M, Gieraltowski J, Zebrowski J, "Modeling heart rate variability including the effect of sleep stages", 2016, *Chaos* **26**, 023101.
- [3] Gieraltowski J, Żebrowski J, Baranowski R, "Multiscale multifractal analysis of heart rate variability recordings with a large number of occurrences of arrhythmia", 2012, *Phys. Rev. E* **85**, 021915.
- [4] Kokosińska D, Gieraltowski J, Żebrowski J, "Multiscale Multifractal Analysis - a screening examination method yielding highly repetitive HRV multifractal patterns", submitted to ESGCO 2016 program.

Bidirectional information transfer between blood pressure and heart rate and its relation to vascular properties in hypertensive patients

**Beata Graff¹, Grzegorz Graff², Katarzyna Tessmer², Danuta Makowiec³,
Jacek Wolf¹ and Krzysztof Narkiewicz¹**

¹ *Medical University of Gdansk, Department of Hypertension and Diabetology, Gdansk, Poland*

² *Gdansk University of Technology, Faculty of Applied Physics and Mathematics, Gdansk, Poland*

³ *Gdansk University, Institute of Theoretical Physics and Astrophysics, Gdansk, Poland*

Background: The impact of heart rate (HR) on blood pressure (BP) and the influence of blood pressure on heart rate are mediated by distinct mechanisms. Methods which allow the assessment of bidirectional interactions between HR and BP might be especially useful in patients with cardiovascular diseases [1]. Our previous results suggested that Transfer Entropy (TE) method is able to mirror various cardiovascular reactions during head-up tilt in patients with the history of syncope and healthy volunteers [2]. Therefore, we implemented methods based on the information transfer concept also in hypertensive individuals. Our pilot study showed that in patients with hypertension bidirectional HR – BP interaction was decreased compared to healthy volunteers. However, there was a strong relation between age and TE values.

The aim of the present study was twofold: first, to check if hypertension is related to alterations of interactions between HR and BP and second, to test if blood pressure values and vascular properties are associated with the above relation.

Methods: In 24 healthy individuals (CON; 14men, age $43,4 \pm 13,7$ years) and 46 patients with hypertension (HTN, 28 men, age $52,1 \pm 13,9$) Symbolic Transfer Entropy (STE, [3]) was computed. 20-minutes recordings of ECG and beat-to-beat blood pressure (Finometer) in resting – supine conditions were used for the analyses. In all study participants body mass index (BMI), waist-hip ratio (WHR), office blood pressure measurements, 24-hour ambulatory blood pressure monitoring (ABPM) as well as the assessment of vascular properties (diameter and distensibility of carotid artery, intima-media thickness and carotid-femoral pulse wave velocity) were assessed.

Results: 1. In hypertensive subjects STE in both directions was significantly lower than in healthy individuals (RR→BP: $0,06 \pm 0,045$ vs $0,09 \pm 0,041$ and BP→RR: $0,05 \pm 0,03$ vs $0,07 \pm 0,04$; $P=0,0036$ and $P=0,0066$; respectively). However, the compared groups differed significantly with age. When both groups were selected to match each other according to age (14 CON vs 33 HTN, aged 36-65 years) STE differed only for the interaction directed RR→BP.

2. While in younger hypertensive patients (aged 25-44 years) solely transfer in RR→BP direction was decreased ($0,06 \pm 0,02$ vs $0,1 \pm 0,05$; $p=0,045$), in middle-aged patients (45-64 years) both STE BP→RR and STE RR→BP values were lower in patients with hypertension compared to normotensive controls ($0,04 \pm 0,02$ vs $0,07 \pm 0,04$ and $0,05 \pm 0,04$ vs $0,09 \pm 0,06$; $P=0,006$ and $P=0,032$; respectively).

3. In hypertensive patients STE for the direction BP→RR correlated with age ($R= -0.3$; $P=0.041$), carotid artery wall distensibility ($R= 0.45$; $P=0.04$) and carotid-femoral pulse wave

velocity ($R = -0.49$; $P = 0.01$). Further, in HTN group STE $RR \rightarrow BP$ has not correlated with vascular parameters.

4. There was a significant correlation of STE $BP \rightarrow RR$ and standard deviation (SD) of day-time systolic BP as well as SD of day-time diastolic BP in ABPM ($R = -0.44$; $P = 0.002$ and $R = -0.32$, $P = 0.02$; respectively). Similarly, STE in $RR \rightarrow BP$ direction correlated with SD of day-time systolic BP and SD of HR (24-hour and night-time) in ABPM ($R = -0.33$; $P = 0.027$ and $R = 0.35$, $P = 0.018$ and $R = 0.37$, $P = 0.01$; respectively).

Conclusion: In hypertensive patients bidirectional interaction between heart rate and blood pressure seems to be decreased, especially in middle-aged individuals. In HTN patients age and vascular properties are related to the information transfer directed $BP \rightarrow HR$. Heart rate – blood pressure interaction is associated with blood pressure variability and heart rate variability and does not correlate with absolute values of blood pressure and heart rate.

References

- [1] Baumert M, Javorka M, Kabir M 2015 *Phil. Trans. R. Soc. A* **373** 20140097
- [2] Graff B, Wejer D, Faes L, Graff G, Makowiec D, Narkiewicz K 2015 *Autonomic Neuroscience: Basic and Clinical* **192** 101–102
- [3] Staniek M, Lehnertz K 2008 *Phys. Rev. Lett.* **100** 158101

Cardiorespiratory Coordination in Cheyne-Stokes-Respiration a case study

Philine Granitza, Harald Krause, Jan F. Krämer, Niels Wessel
Humboldt-Universität zu Berlin, Department of Physics, Berlin, Germany

Recently Riedl et al. [1] found an increase of cardiorespiratory coordination (CRC) during and after obstructive sleep apnea by introducing the new analysis technique of the coordigram. This technique visualizes the mutual influence of the cardiac and respiratory oscillations on their respective onsets. Their findings on the connection between CRC and the appearance of sleep-disordered events require a substantial extension of the current understanding of obstructive sleep apneas and hypopneas. Moreover, these results call for a further investigation of CRC during central sleep apnea.

In this case study, polysomnographic data of a male, 61-year old patient suffering from Cheyne-Stokes respiration (CSR) was analysed. This data set was chosen from a cohort of patients with CSR because his heart rate was not controlled by an implanted cardiac pacemaker.

An exemplary coordigram with the typical crescendo-decrescendo respiratory pattern is shown in Figure (1) and indicates an increased CRC following the central apneas, which can also be found in most other CSR-episodes of this patient.

As sleep disordered breathing has a high prevalence of up to 70% in heart failure patients as well as adverse prognostic implications [2,3], the coordigram can be a useful tool to estimate the severity of their illness. Prospective studies may show the possible use of the coordigram for risk stratification of CSR-patients as well as investigate the sleep stage as a further influence on CRC.

References

1. Riedl M, Müller A, Krämer JF, Penzel T, Kurths J, Wessel N. Cardio-Respiratory Coordination Increases during Sleep Apnea *PLoS ONE* 2014 **9(4)** e93866
2. Bitter T, Westerheide N, Prinz C, Hossain MS, Vogt J, Langer C, Horstkotte D, Oldenburg O. Cheyne-Stokes respiration and obstructive sleep apnoea are independent risk factors for malignant ventricular arrhythmias requiring appropriate cardioverter-defibrillator therapies in patients with congestive heart failure *European Heart Journal* 2011 **32** 61-74
3. Bradley DT, Floras JS. Sleep Apnea and Heart Failure. Part II: Central Sleep Apnea *Circulation* 2003 **107** 1822-1826

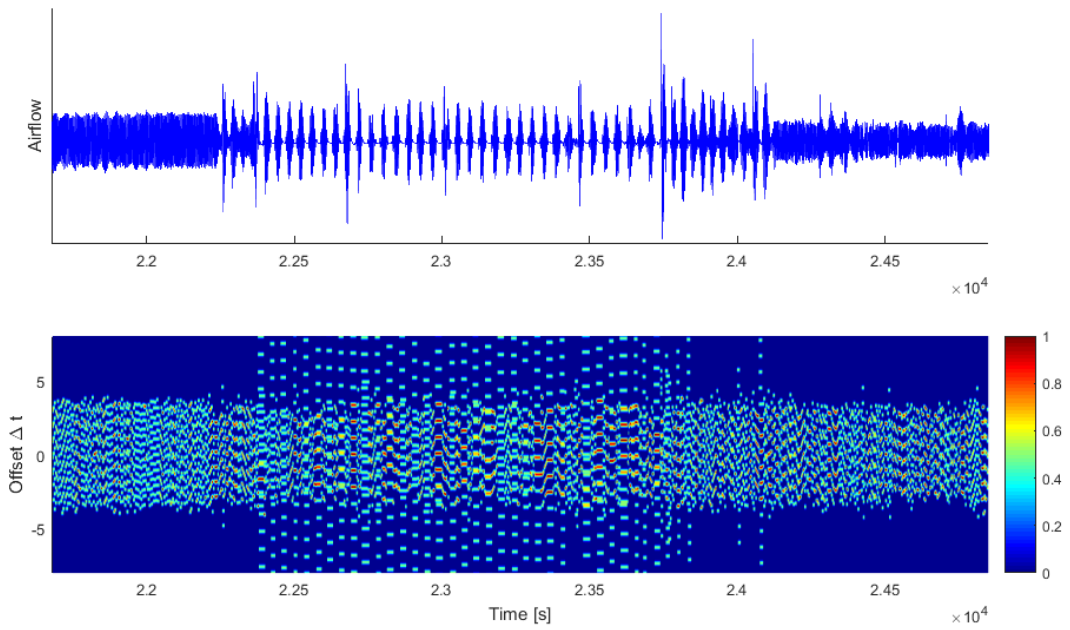


Figure 1: Coordigram of a patient with Cheyne-Stokes respiration. Red horizontal lines indicate cardiorespiratory coordination.

A simulation study of the NaChBac channel: stability, Na^+ binding sites and hydration

Carlo Guardiani, Mark Rodgers and Igor Khovanov

*University of Warwick, School of Engineering and Center for Scientific Computing
, Coventry, UK*

Understanding the structure and functional mechanisms of voltage-gated channels remains a major goal in membrane biophysics. The *Bacillus halodurans* voltage-gated sodium-selective channel NaChBac is an orthologue of mammalian voltage-gated Ca^{2+} (Ca_v) and Na^+ (Na_v) channels. The NaChBac channel is endowed with unique features. In fact, like K_v channels, NaChBac is composed of four identical subunits. It possesses the same selectivity signature sequence as Ca_v channels, but it was experimentally proved to be permeable to Na^+ cations (Yue 2002), similar to Na_v channels. Each of the subunits of NaChBac comprises 6 trans-membrane helices, the first four forming the voltage sensor domain and the last two the channel domain.

Since no crystal structure of NaChBac is currently available, we built a homology model of the pore-only complex using as a template the recently resolved structure of the NavMs channel (McCusker 2012) that features 46% sequence identity with NaChBac. In the model both the selectivity filter and the activation gate are wide open showing a diameter sufficiently large to allow the passage of a fully hydrated sodium ion. The channel model was embedded in a POPC membrane and solvated with 15730 TIP3P water molecules and a 0.5 M concentration of *NaCl*.

The system was then submitted to a 100 ns simulation in the NPT ensemble at the pressure of 1 atm and temperature of 300 °K. Overall, the structure appears to be very stable with RMSD oscillating in a narrow band between 2.0 and 2.5 Å. The analysis of the RMSF profile highlights the rigidity of the selectivity filter since the four corresponding TLESWAS stretches correspond to minima of the profile. The maxima of the RMSF are typically mapped to the initial fragment of helix S5 and the final fragment of helix S6 as well as to the turret loop and the final part of helix P2. The most flexible regions are thus partially unstructured fragments acting as linkers between secondary structure elements.

During the simulation, water molecules and sodium ions enter spontaneously into the selectivity filter. After 5 ns the filter is already occupied by two ions at the level of the EEEE-ring and the LLLL-carbonyl ring respectively. The trajectory then shows several transient entering events of a third ion that are normally short-lived unless the first two ions move to a lower position.

The Potential of Mean Force (PMF) as a function of the axial position reveals the existence of four minima, three of which correspond to the EEEE, LLLL, and TTTT rings respectively, while the fourth one identifies a binding site at the level of the serines above the EEEE ring. The first three minima thus correspond to the HFS, CEN and IN binding sites predicted by Catterall (Payandeh 2011) for NavAb and whose existence was later confirmed by a number of studies (Corry 2012, Stock 2013, Ulmschneider 2013). When sodium occupies the IN or CEN minima it interacts with a single threonine or leucine residue only in 5% of the frames while it is normally surrounded by six water molecules arranged at the vertices of an octahedron, thus occupying an on-axis position. By contrast, in the HFS site, sodium interacts with a glutamate and a serine belonging to the same subunit as well as with four water molecules. As clearly revealed by the 2D-PMF, this results in an off-axis placement.

In order to attain better converged free energy surfaces both 1D and 2D-metadynamics runs are currently underway. Further analysis will concern the behaviour of the system in presence of KCl and $CaCl_2$ to evaluate its selectivity. Simulation of a number of mutants with a different charge on the selectivity filter will finally provide a benchmark for the Coulomb Blockade Oscillations model.

References

Yue L, Navarro B, Ren D, Ramos A Clapham D E, 2002 *J. Gen. Physiol.* **120** 845-853

McCusker E C, Bagnèris C, Naylor C E, Cole A R, D'Avanzo N, Nichols C G, Wallace B A, 2012 *Nature Communications* **3(1102)** 1-8

Payandeh J, Scheuer T, Zheng N, Catterall W A (2011) *Nature* **475** 353-358

Corry B, Thomas M (2012) *J. Am. Chem. Soc.* **134** 1840-1846

Stock L, Delemotte L, Carnevale V, Treptow W, Klein M L (2013) *J. Phys. Chem. B* **117** 3782-3789

Ulmschneider M B, Bagnèris C, McCusker E C, DeCaen P G, Delling M, Clapham D E, Ulmschneider J P, Wallace B A (2013) *Proc. Natl. Acad. Sci. USA* **110(16)** 6364-6369

Rod driven resonance and entrainment in the visual system of the brain

Jens Haueisen

*Institute of Biomedical Engineering and Informatics, Technical University Ilmenau, PF
100565, 98684 Ilmenau, Germany*

Intermittent photic stimulation (IPS) leads to a phenomenon in the human cortex called photic driving: The neural network of the visual system synchronizes with the frequency of the IPS. Two measurable phenomena in electroencephalography (EEG) and magnetoencephalography (MEG) characterize this synchronization: resonance and entrainment. In this talk, I will present a framework to analyse topographic representations of these phenomena and present the results of a study with rod excitation in the retina as an input for photic driving. The hypothesis of a rod driven entrainment and resonance was tested by stimulating 12 healthy volunteers with low intensity light flashes at 20 stimulation frequencies. The frequencies were multiples of the individual alpha frequency (α) of each volunteer in the range from 0.40 to $2.30 \cdot \alpha$. 306-channel whole head magnetoencephalography recordings were analyzed in the time, frequency, and space domain with the topographic matching pursuit algorithm. Entrainment and resonance was found for stimulations at or close to the individual alpha frequency ($0.95-1.10 \cdot \alpha$) and half of the alpha frequency ($0.50-0.55 \cdot \alpha$). No signs of a resonance or entrainment phenomenon were revealed for stimulation frequencies around $2.00 \cdot \alpha$. Instead, on-responses at the beginning and off-responses at the end of each stimulation train were observed at frequencies $1.30-2.30 \cdot \alpha$, indicating that the flicker fusion frequency was reached. Consequently, both cone and rod driven input of the human eye can produce the photic driving effect in the human visual cortex.

Validation of functional Fetal Autonomic Brain Age Score fABAS developed using magnetocardiography for applicability in cardiotocography

¹Hoyer Dirk, ^{1,2}Pytlik Adelina, ³Gonçalves Hernâni, ^{3,4,5}Amorim-Costa Célia, ^{3,4}Bernardes João, ^{3,4,5}Ayres-de-Campos Diogo, ¹Witte Otto W, ²Schleussner Ekkehard, ²Schneider Uwe

¹ Jena University Hospital, Biomagnetic Center, Hans Berger Department of Neurology, Jena, Germany, ² Jena University Hospital, Department of Obstetrics, Jena, Germany, ³ CINTESIS, Faculty of Medicine, University of Porto, Porto, Portugal, ⁴ Department of Obstetrics and Gynecology, Faculty of Medicine, University of Porto, Portugal; Department of Obstetrics and Gynecology, São João Hospital, Portugal; ⁵ INEB — Institute of Biomedical Engineering, Portugal

Introduction

According to the “developmental origins of adult disease (Barker) hypothesis” the early identification of fetal developmental disturbances has implications for health problems in later life which cannot completely be compensated for by later postnatal therapies (Barker 1998). We have previously introduced the functional Fetal Autonomic Brain Age Score (fABAS) using 30 min fetal magnetocardiographic recordings (fMCG, Jena) (Hoyer et al. 2013). The score is based on heart rate pattern indices that are related to universal principles of developmental biology. The present work aims at the validation of the fABAS methodology on cardiotocographic recordings (CTG, Porto).

Methods

Both study data sets include recordings of fetal heart rate patterns during non-stress situation of normally maturing fetuses of a similar range of 24-40 weeks gestational age. Exclusion criteria were: Fetal: known chromosomal abnormalities, sonographically identified malformations, fetal cardiac arrhythmias. Maternal: known heart diseases, diabetes mellitus, medication affecting cardiac function/rhythm, abuse of nicotine, alcohol or drugs, previous administration of synthetic glucocorticoids, uterine contractions during the recording. In both centers the investigations were approved by the Local Ethics Committee and all subjects gave their written informed consent.

From the Jena Fetal Monitoring Data Base 390 MCG recordings over 30 min sampled at 1024 Hz were selected. We investigated the heart beat interval series and the respective time series resampled at 4 Hz. Only normal beat intervals (NN) were considered. The frequency of corrected artificial beats was below 1 % (details see e.g. Hoyer et al. 2013)

The CTG dataset corresponds to 50 normal cases of a longitudinal prospective study acquired at the obstetrics outpatient clinic of a tertiary care hospital (Hospital de S. João, Porto University) and comprises 358 recordings obtained through external monitoring with Hewlett-Packard M1350A or M1351 fetal monitors at 4 Hz sampling. Tracings with signal loss above 33%, or signal quality below 80% were excluded (Amorim-Costa et al 2013).

Fetal behavioural state according to quiet and active sleep (1F, 2F) and active awakeness (4F) were classified based on heart rate patterns as previously described (Hoyer et al. 2013).

Linear regression models were used to recalculate and cross-validated (learning-testing) models of MCG based NN interval series (MCG_{NN}), resampled time series from MCG (MCG_{res}) and CTG using the fABAS factors previously described (Hoyer et al. 2013).

Results, Discussion

From the 390 MCG recordings sections of 1F(142), 2F(346), 4F(24) and from the 358 CTG recordings sections of 1F(153), 2F(294), 4F(23) were classified by clinical experts. Here, only the results of the models of 1F and 2F are reported.

Table 1: Standard error (SE) and coefficient of determinism (R^2) of fitted models (learn sets) and the respective validation sets of MCG based NN (MCG_{NN}), resampled MCG_{NN} (MCG_{res}) and CTG.

| | Learn set | | | Validation (test) set | | |
|--------------|-------------|-------|-------|-----------------------|-------|-------|
| | | SE | R^2 | | SE | R^2 |
| 30min | MCG_{NN} | 2.68 | 0.498 | MCG_{res} | 2.724 | 0.481 |
| | MCG_{res} | 2.647 | 0.510 | CTG | 3.719 | 0.345 |
| | CTG | 3.587 | 0.391 | MCG_{res} | 2.724 | 0.481 |
| 1F | MCG_{NN} | 2.739 | 0.498 | MCG_{res} | 2.742 | 0.497 |
| | MCG_{res} | 2.722 | 0.504 | CTG | 3.891 | 0.294 |
| | CTG | 3.671 | 0.368 | MCG_{res} | 2.721 | 0.505 |
| 2F | MCG_{NN} | 2.929 | 0.395 | MCG_{res} | 2.966 | 0.380 |
| | MCG_{res} | 2.928 | 0.395 | CTG | 3.902 | 0.257 |
| | CTG | 3.766 | 0.308 | MCG_{res} | 3.026 | 0.354 |

The MCG cross-validation (MCG_{NN} - MCG_{res}) shows almost similar goodness in the respective data sets in each state. In both, CTG learn and validation sets, the functional maturation age can significantly be estimated, but with lower goodness (reduced R^2 , increased SE). Interestingly, the applications of CTG based models (learn sets) to MCG resampled time series (validation sets MCG_{res}) result in improved goodness in all data states.

These results indicate that fABAS is applicable to CTG data as well. The reduced goodness of functional maturation age assessment in the CTG data seems to be mainly caused by higher random variability and less precise beat detection underlying the 4 Hz resampled CTG time series.

Conclusion

The cross validation between MCG and CTG showed that fABAS provides a general score of functional fetal autonomic brain age. CTG recordings lack a part of information that can be obtained from MCG recordings, but they are still valuable for the screening of the autonomic maturation in the human fetus. Hence, fABAS was confirmed as being a strong candidate for standardized assessment of functional brain maturation age and developmental disturbances across different recording techniques.

Acknowledgements

DH and US are supported by German Research Foundation: „Development of a clinic suitable marker of fetal autonomic maturation“ (DFG: Ho 1634/15-12, Schn 775/7-1), Hernâni Gonçalves by a post-doctoral grant (SFRH/BPD/69671/2010) from FCT, Portugal.

References

- Barker D J 1998 *Clinical Science* **95** 115-28
Hoyer D, Tetschke F, Jaekel S, Nowack S, Witte O W, Schlessner E and Schneider U 2013 *PLoS One* **8** e74431
Amorim-Costa C, Gonçalves H, Bernardes J, Ayres-de-Campos D 2012 *Int J Gynecol Obstet* **119** (Suppl 3) S735

Temperature regulation of microvascular flow: a multi-dimensional improved EMD-based study of laser speckle contrast images

Humeau-Heurtier Anne¹, Mahé Guillaume,² and Abraham Pierre³

¹*University of Angers, France*

²*University Hospital of Rennes, University of Rennes 1, France*

³*University Hospital of Angers, University of Angers, France*

1 Introduction

Skin plays an important role in the body thermoregulation. This is performed through vasodilation and vasoconstriction of the vessels. Several factors can modify skin temperature, such as fever, exercise, environmental temperature variations. . .

In this work our goal is to study locally, with a recent image processing algorithm, the variations of microvascular perfusion induced by variations of room temperatures. For this purpose, laser speckle contrast imaging (LSCI) data are processed.

2 Materials and Methods

Fifteen healthy volunteers participated in this study which was approved by the local ethics committee of our university hospital (CPP-Ouest II, Angers, France). For each subject, microvascular perfusion on the right forearm was monitored with a laser speckle contrast imager (PeriCam PSI System, Perimed), in two different room temperatures: $17.2 \pm 1.5^\circ\text{C}$ and $31.4 \pm 0.7^\circ\text{C}$. The monitoring of microvascular blood flow was performed at rest, during a 3-minute period of occlusion (biological zero, BZ), and during post-occlusive reactive hyperaemia (PORH). For each subject and for each room temperature, three images have been processed: rest, BZ, PORH.

The interpretation of LSCI data is often difficult. In order to overcome this problem, the multi-dimensional complete ensemble empirical mode decomposition with adaptive noise (MCEEMDAN) algorithm has been recently proposed (Humeau-Heurtier *et al.*, 2015). MCEEMDAN is a fully data-adaptive method that decomposes multi-dimensional data (as images) into components – intrinsic mode functions (IMFs) – that are modulated in frequency and amplitude. IMFs given by MCEEMDAN reveal local textures with characteristic spatial frequencies (Humeau-Heurtier *et al.*, 2015). The first IMF represents the finest textural (the background noise), while the last

one gives only the largest scale of the overall mean trend in intensity of the image. When applied to LSCI data, MCEEMDAN is able to reveal hidden patterns that differ with physiological states (Humeau-Heurtier *et al.*, 2015). In the present work, two IMFs (IMF1 and IMF2) and the residue have been computed for each image. Moreover, the lacunarity of the fractal dimension image for each IMF and residue has been determined.

3 Results and Discussion

The local cutaneous temperatures obtained by the low and high room temperatures were $28.0 \pm 2.0^\circ\text{C}$ and $34.1 \pm 1.3^\circ\text{C}$, respectively. IMFs and residue of LSCI data present local patterns, see examples in Fig. 1. The lacunarity values for each room temperature and for each IMF/residue are shown in Fig. 2. From the latter we observe that, for the finest textural (IMF1 and IMF2), low skin temperature reduces the lacunarity value at rest and at PORH, compared to the high skin temperature. By opposition, for the largest spatial scales (residue), the lacunarity value is the highest for the lowest skin temperature, at PORH. This has to be studied more deeply to understand the physiological phenomena coming into consideration, and to know why different results are observed at different spatial scales.

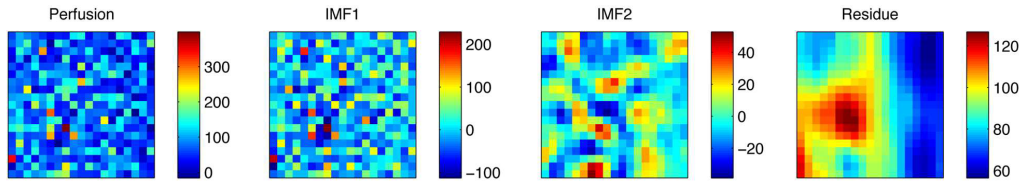


Figure 1: MCEEMDAN results at rest for the high room temperature.

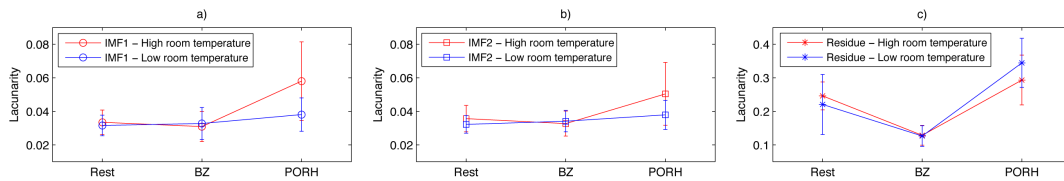


Figure 2: Lacunarity (average and standard deviations computed from 15 subjects) of fractal dimension images for a) IMF1; b) IMF2; c) residue, given by MCEEMDAN.

Reference

Humeau-Heurtier A, Mahé G, Abraham P 2015 *IEEE Trans. Med. Imaging* **34** 2103-2117

Analysing brain dynamics with a novel mutual information estimator: phase and power and their representational interactions

Robin A. A. Ince, Bruno L. Giordano, Christoph Kayser, Guillaume A. Rousselet, Joachim Gross and Philippe G. Schyns

Institute of Neuroscience and Psychology, University of Glasgow, 58 Hillhead Street, Glasgow, G12 8QB, UK

Mutual Information (MI) measures the statistical dependence between two random variables (Cover and Thomas, 1991; Shannon, 1948). It can be viewed as a statistical test against a null hypothesis that two variables are statistically independent, but in addition its effect size (measured in bits) has a number of useful properties and interpretations. A major factor hindering wider practical application of mutual information in experimental science is the difficulty of estimating information theoretic quantities in practice.

We present a novel estimation technique that combines the statistical theory of copulas with the closed form solution for the entropy of Gaussian variables. This results in a general, computationally efficient, flexible, and robust multivariate statistical framework that provides effect sizes on a common meaningful scale and allows for unified treatment of discrete, continuous, uni- and multi-dimensional variables. It also enables direct comparisons of representations from behavioral and brain responses across any recording modality.

A particular challenge in many biological systems is determining the effect of external factors (for example an external stimulus) on oscillatory signals (for example, recorded rhythmic neural activity). In such cases it is often of interest to dissect such modulations and quantify separately the effects on strength (power or amplitude) and timing (the phase) of the oscillation (Schyns et al., 2011). This is particularly true for analysis of brain rhythms recorded via invasive electrophysiology or non-invasive neuroimaging such as Magneto- and Electro-encephalography (M/EEG), since neural oscillations are increasingly thought to underlie many important cognitive processes (Singer, 2013; Thut et al., 2012). However, phase is a circular variable, which presents some technical challenges for statistical analysis. We show how our new MI estimator can be applied to spectral data (or indeed any vector valued signals) to quantify separately, but on a common scale, modulations of oscillatory power and phase. Phase and power MI can be calculated for discrete stimuli (i.e. two experimental conditions) or continuous stimulus features, and it is also possible to condition out (control for) the effect of correlated features or other potentially confounding experimental factors. This approach is applicable to the single-trial outputs of any frequency or time-frequency decomposition including Hilbert transform, Empirical Mode Decomposition, Hilbert-Huang transform or matching pursuit methods (Gross, 2014). Figure 1 demonstrates how this method is able to separate phase vs power modulations with two simulated systems for which the strength of spectral modulation is equal, but the mechanism of the modulation differs (pure phase vs pure power modulation).

A final advantage of the information theoretic framework is the ability to directly relate the information content in different signals. By considering redundant information, it is possible to quantify the representational similarity between, for example, phase and power of an oscillation (in cases where both are informative). If the MI in phase and power is completely redundant, this indicates that both aspects of the signal are likely driven by the same mechanism across trials, and reflect similar aspects of neural processing. On the other hand,

if they convey independent MI, it means that, although they are both modulated by the same experimental or stimulus factor, this modulation occurs in different ways across trials, and therefore indicates that each aspect might reflect a different processing mechanism.

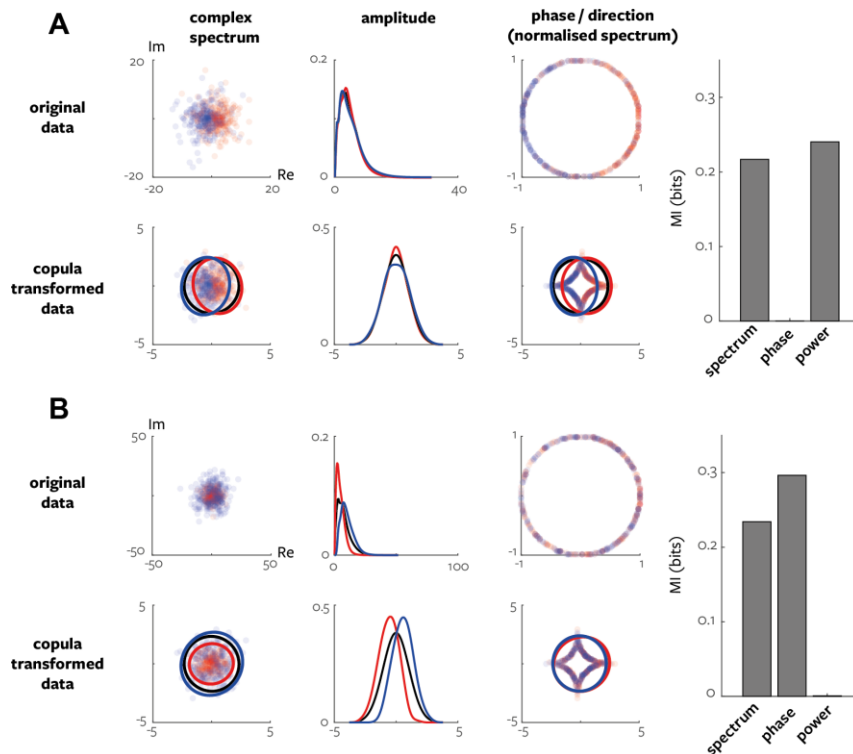


Figure 1 Gaussian-copula MI applied to complex spectral data. Spectral data were generated from two two-class models. **A.** Phase was sampled from von Mises distribution with class specific mean and amplitude was sampled from chi-square distribution (common across classes). **B.** Phase was drawn from von Mises distribution (common across classes) and amplitude was sampled from chi-square distribution with class-specific degrees of freedom. **A,B.** Left plots show generated complex data (top) and with marginal copula transformation (bottom). Solid lines show $p=0.01$ contours of multivariate Gaussian pdf. Centre plots show amplitude (top) and copula transformed amplitude (bottom). Right plots show amplitude-normalized spectrum (top) and copula transformed normalized spectrum (bottom). Far right bar graphs show the MI value in the different data representations.

References

- Cover TM, Thomas JA 1991 *Elements of information theory* Wiley New York
 Shannon CE 1948 *Bell Syst. Tech. J.* **27** 379–423
 Gross J 2014 *J. Neurosci. Methods* **228** 57–66
 Schyns PG, Thut G, Gross J 2011 *PLoS Biol.* **9** e1001064
 Singer W 2013 *Trends Cogn. Sci. Special Issue: The Connectome* **17** 616–626
 Thut G, Miniussi C, Gross J 2012 *Curr. Biol.* **22** R658–R663

Network Physiology: From Brain Dynamics and Plasticity to a first Atlas of organ network interactions

Plamen Ch. Ivanov

Boston University, Department of Physics, Boston, USA

Harvard Medical School, Division of Sleep Medicine, Boston, USA

We systematically study how diverse physiologic systems in the human organism dynamically interact and collectively behave to produce distinct physiologic states and functions. This is a fundamental question in the new interdisciplinary field of Network Physiology, and has not been previously explored. We develop a computational approach to identify and quantify networks of physiologic interactions from long-term continuous, multi-channel physiological recordings. Applying a system-wide integrative approach, we identify distinct patterns in the network structure of organ interactions, as well as the frequency bands through which these interactions are mediated. We establish first maps representing physiologic organ network interactions and discover basic rules underlying the complex hierarchical reorganization in physiologic networks with transitions across physiologic states. These findings demonstrate a direct association between network topology and physiologic function, and provide new insights into understanding how health and distinct physiologic states emerge from networked interactions among nonlinear multi-component complex systems.

Basic cardiovascular signals: mutual interactions explored by information domain analysis

**Michal Javorka¹, Jana Krohova^{1,2}, Barbora Czippelova¹, Zuzana Turianikova¹,
Zuzana Lazarova¹, Ingrid Tonhajzerova¹**

¹*Comenius University, Jessenius Faculty of Medicine, Department of Physiology and Biomedical Centre Martin (BioMed Martin), Martin, Slovakia*

²*VSB – Technical University of Ostrava, Department of Cybernetics and Biomedical Engineering, Ostrava, Czech Republic*

The basic cardiovascular parameters – systolic and diastolic blood pressure (SBP and DBP) and heart rate (HR) oscillate spontaneously on the beat to beat basis. Several mechanisms interconnecting these oscillations are suggested but an analysis of the mutual coupling among basic cardiovascular signals was performed only rarely. The aim of our study was to find the dominant interconnections among SBP, DBP and HR (represented by its reciprocal value – RR interval) oscillations during rest and two different stress conditions. We also compared the strength of the causal coupling between SBP and mean blood pressure (MBP) with heart period (RR) during different states.

Sixty-one young healthy volunteers (37 female and 24 male, mean age 17.5 years (SD = 2.4 years) participated in this study. The continuous finger arterial blood pressure (Finometer Pro, FMS, Netherlands) and ECG signals (CardioFax ECG-9620, Nihon Kohden, Japan) were recorded during study protocol including supine rest, passive orthostasis (head-up tilt) and mental arithmetic test. We analysed the strength of mutual bivariate interactions and trivariate interactions by causality analysis in information domain using non-uniform embedding procedure followed by surrogate (randomly shuffled) data analysis.

Using bivariate approach, we found that the most important connection among SBP, DBP and RR included an influence of the RR oscillations on the SBP and influence of the RR on the DBP variability. In addition, the influence of the DBP on the SBP (much higher than in the opposite direction) was the most dominant during whole protocol. The significant influence of the SBP on the RR was found mostly during orthostatic test. The trivariate approach confirmed the bivariate analysis findings – however, it indicated that the influence of the RR on the SBP is only indirect through the effect of RR on DBP. Although the causal coupling from SBP to RR tended to be higher than coupling MBP – RR, the differences did not reach statistical significance.

We conclude that the multivariate approach is more appropriate to disentangle direct causal interconnections among basic cardiovascular variables. Based on our results, the causal influences cascade RR – DBP – SBP is assumed. The short-term DBP oscillations reflect the heart rate variability effect (run-off phenomenon) and the effect of the SBP oscillations on the DBP variability is only limited. The feedback (baroreflex related) interactions between both blood pressure signals (SBP and MBP) and heart period are of similar strength and relatively weak and become stronger only during orthostasis.

The study was supported by grants APVV-0235-12, VEGA 1/0059/13 and ITMS project “BioMed Martin” no. 26220220187.

Heart rate variability during mental stress versus orthostatic activation in normal subjects

Michal Javorka¹, Mathias Baumert², Barbora Czipelova¹, Zuzana Turianikova¹,
Zuzana Lazarova¹, Michal Mestanik¹, Ingrid Tonhajzerova¹

¹Comenius University, Jessenius Faculty of Medicine, Department of Physiology and
Biomedical Centre Martin (BioMed Martin), Martin, Slovakia

²School of Electrical and Electronic Engineering, The University of Adelaide, Adelaide, SA,
Australia

Introduction: Emotional regulation has been linked to autonomic nervous system activity and emotional dysregulation observed in mental disorders such as major depression or panic disorder has been linked to cardiovascular diseases.

The study was aimed at assessing changes in heart rate variability (HRV) and complexity during mental stress in comparison to physical (orthostatic) stress in healthy subjects and to explore associations with hostility and subjective perception of mental stress.

Methods: Beat-to-beat heart rate signal represented by RR interval from ECG and volume-calibrated respiratory inductance plethysmography (RespiTrace) were noninvasively recorded in 65 healthy volunteers (39f / 26m; age 17.9 (16.9 – 19.0) years) during 5 phases: supine rest (phase 1), head-up tilt test (HUT to 45 degrees, phase 2), supine rest recovery (phase 3), mental arithmetics (MA, phase 4) and supine rest recovery (phase 5). For each phase, linear time (meanRR, SDNN, RMSSD) and frequency domain (LF and HF powers) HRV measures were calculated. In addition, the heart rate complexity (normalized complexity and normalized unpredictability indices – NCI and NUPI) was analysed by a symbolic dynamics approach. For each subject, the hostility was evaluated by Cook-Medley hostility scale and the perceived stress during MA was assessed by visual analogue scale.

Results: Linear HRV measures and heart rate complexity were significantly reduced during both HUT and MA. Tidal volume increased and respiratory rate decreased during HUT. During MA respiratory rate decreased while tidal volume remained unchanged. No significant correlation between hostility score or perceived stress and absolute values of HRV and complexity or respiratory measures was detected. While no correlation between hostility or perceived stress score and a change in linear HRV measures from phase 3 to phase 4 (a response to MA) was found, the change in NCI and NUPI during MA correlated significantly with subjectively perceived stress level during MA. No correlation of HRV and heart rate complexity response to HUT (a change from phase 1 to 2) with either hostility score or perceived stress level during MA was observed. Contrary, the response of respiratory rate to HUT correlated inversely with the hostility score.

Discussion: Our results confirm the well-established reduction of HRV across all domains during orthostatic activation that is characterized by vagal withdrawal and sympathetic activation and paralleled by a reduction in respiratory rate and an increase in tidal volume. Mental stress elicited by arithmetic task also lowers HRV metrics, albeit to a lesser extent, but does not affect tidal volume and increases respiratory rate, demonstrating a differential autonomic response to cortical activation, compared to primarily blood pressure control driven ANS activation following orthostatic challenge.

Interestingly, the individual change in HR complexity during arithmetic task was associated with perceived stress. Subjects who perceived the mental task as more stressful also showed a relatively greater reduction in HRV complexity that might be partly explained by central cortical effects on the insular cortex, projecting to the nucleus tractus solitarius and possibly the overall decrease in ventilation and its modulatory effects on HR.

We conclude that the perceived level of mental stress elicited by arithmetic task is reflected in the change of HR complexity in healthy subjects while hostility is more closely related to autonomic respiratory control.

The study was supported by grants APVV-0235-12, VEGA 1/0059/13, VEGA 1/0087/14 and ITMS project “BioMed Martin” no. 26220220187.

Induced Pluripotent Stem Cell Derived Cardiomyocyte Monolayers as a Model of Cardiac Excitable Networks

Aled R Jones, Annabelle Fricker and David H Edwards
Cardiff University, Wales Heart Institute, Cardiff, UK

Introduction

Historically animal cardiac tissue has been used to develop an understanding of the physiology of the heart in health and disease. However, as our knowledge of myocardial function has advanced, differences between human cardiac tissue and that of experimental animal models are becoming more obvious. The discovery that adult human somatic cells may be reprogrammed into an embryonic-like pluripotent state which may in turn be differentiated to cardiac cells was a significant advancement in the field of cardiac research. These induced pluripotent stem cell derived cardiomyocytes (iPSC-CM) have potential use as cardiac models for drug screening, cardiac regeneration/repair and exploring inherited cardiac disorders. In our study we have set out to explore the potential of a monolayer of iPSC-CM as a model to study complex modes of cell-to-cell interactions via electrical, physical and chemical coupling.

Methods

Monolayers were loaded with the calcium sensitive fluorescent dye, Fluo4-AM (5 μ M), and imaged using confocal microscopy. Custom MatLab® software was used to analyse the patterns of activation. Monolayer images were divided into regions of interest (ROI) and the mean fluorescence intensity time series for each ROI extracted. The phase as a function of time was calculated for each time series and its mean first derivative was plotted as a 'synchronicity image' using a colour map. Areas of similar colour on this image represented areas of the monolayer that activated at a similar frequency with a constant phase difference and were therefore deemed to be synchronous. For regions that were deemed synchronous, isochronal activation maps were produced which illustrated the pattern of activation through the monolayer. A mean time series was also calculated and used to extract relevant statistics such as cycle length and normalised fluorescence amplitude for comparisons between monolayers. Monolayers also underwent pharmacological manipulation and assessment of these interventions were made.

Results

Monolayers of iPSC-CM exhibited spontaneous contraction and stained positive for troponin T cardiac isoform, a marker of cardiac differentiation. The monolayers naturally segregated into separate distinct groups, some exhibited planar waves of cellular calcium spreading across the monolayer in a repeatable fashion, while others exhibited 'spiral waves' in which the wave of activation rotated around a focal point. In some monolayers this focal point could be seen to be a structural discontinuity in monolayer, in others no anchoring structural discontinuity was apparent. Monolayers responded to pharmacological intervention in a

heterogeneous manner. Adrenergic modulation produced cycle length changes in some but not all monolayers. Calcium channel and transporter modulation had a marked effect on transient amplitude and altered the activation pattern in virtually all monolayers.

Conclusions

Monolayer production resulted in distinct phenotypes that varied depending on several culture dependent parameters. The activation patterns that were observed are similar to those thought to underlie arrhythmias in the clinical setting which supports the use of this system as a model of cardiac disease. Pharmacological intervention had a heterogeneous effect on both the fluorescent time series and the 2-dimensional activation patterns. Further work is now required to elucidate the underlying mechanisms of these effects.

Blood pulsations imaging as a tool for studying thermoregulation of skin microcirculation

**Angelica V. Belaventseva¹, Roman V. Romashko^{1,2}, Yuri N. Kulchin^{1,2} and
Alexei A. Kamshilin³**

¹*Institute of Automation and Control Processes of Far-Eastern Branch of Russian Academy of Sciences, Optoelectronics Department, Vladivostok, Russia*

²*Far-Eastern Federal University, School of Natural Sciences, Vladivostok, Russia*

³*ITMO University, Computer Photonics and Videomatics Dept., St. Petersburg, Russia*

Microcirculatory blood flows are known to play a significant role in the pathophysiology of various disorders in such clinical areas as cardiology, dermatology, neurology and ophthalmology. The primary function of microcirculation is referred to the process of blood delivery to the tissue's capillary bed, which is vital for the homeostasis. Non-invasive *in-vivo* techniques capable of visualization microcirculation parameters are beneficial for the user in providing information without disturbing the normal environment. In this report, we present preliminary results, which show that the amplitude of blood pulsations is changing in both time and space after a hand with preliminary cooled fingers has contacted a glass plate of the room temperature.

The measurements were carried out using a Blood Pulsation Imaging (BPI) system [1], which is a kind of imaging photoplethysmography (PPG) technique. Implementation of this technique is quite simple and requires only illumination of a body's part under study by a stable in time light source. A conventional video camera is continuously recording the illuminated part in conditions that the subject refrains from intentional movements during the experiment. Thereafter, the recorded series of frames is processed off-line in a computer. In our particular experiments, a pair of green light emitting diodes (LED) generating light at the wavelength of 530 nm with the spectral width of 40 nm was used as an illuminator. It is known that the PPG signal has the maximal amplitude under illumination by green light [2]. Since the penetration depth of the green light into skin does not exceed 0.6 mm, a recently proposed model of PPG [3] attributes the signal origin with compression of the capillary bed by pulsating arteries. Therefore, BPI system could provide a channel for gathering both spatial and temporal information concerning blood microcirculation.

In our pilot experiment, we asked a volunteer to cool outer phalanges of his hand in cold water down to 16 – 20 °C and then put it into the glass plate at the room temperature of about 23 °C. At the same moment we started warming up the glass plate from another side by an air at the temperature of 40 °C. Video of the palm was recorded through the plate. Contact with the glass plate had a triple goal. First, it provided the conditions for thermoregulation via warming up. Second, it stabilized the image by diminishing movement artefacts. Third, it significantly increased the PPG amplitude due to more efficient modulation of the capillary density by pulsating arteries [4]. In addition, we used polarization filtration to diminish the influence of light reflections from glass interfaces and palm's surface. The temperature of the glass plate and the hand was monitored by two thermocouples installed in different places. Duration of the experiment was 120 seconds. Figure 1 shows the blood pulsation amplitude (BPA) distribution over the palm calculated at the beginning of the experiment (a) and after 100-th second (b). As seen, BPA is not uniformly distributed over the palm. At the beginning, no blood pulsations are observed in the fingers but then the amplitude of pulsations is increased with different rate in different places. Detailed dynamics of the amplitude of pulsations in four region of interests (ROI) chosen in fingers and in the palm is shown in Fig. 2.

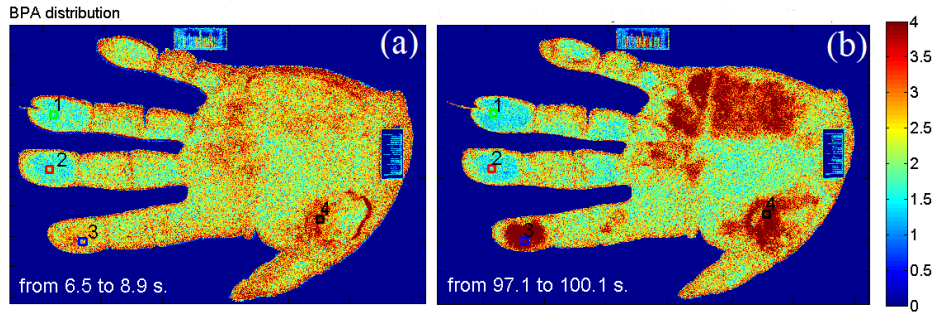


Fig. 1. Distribution of blood pulsation amplitude (BPA) over the palm with preliminary cooled fingers calculated at the beginning (a) and after 100-th second (b) of warming up.

As one can see in Fig.2, all pre-cooled fingers do not show any pulsation at the beginning of the measurement when temperature is low. During warming up the pulsation is recovered but with different speed for different fingers: we cannot see recovering of blood pulsations in the ring finger (Fig.2a), while pulsations in the index finger (Fig.2c) are recovered quite fast. For the comparison Fig.2d shows the PPG signal in the area which was not preliminary cooled (ROI #4). Except for the beginning, blood pulsations are seen in this area during all the measurement while their amplitude is slightly increased due to the warming up. Small amplitude of the PPG signal at first 5 sec after the palm was put into the contact with the glass plate is probably caused by initial difference between temperature of plate and palm which disappears during heating much faster than in pre-cooled areas.

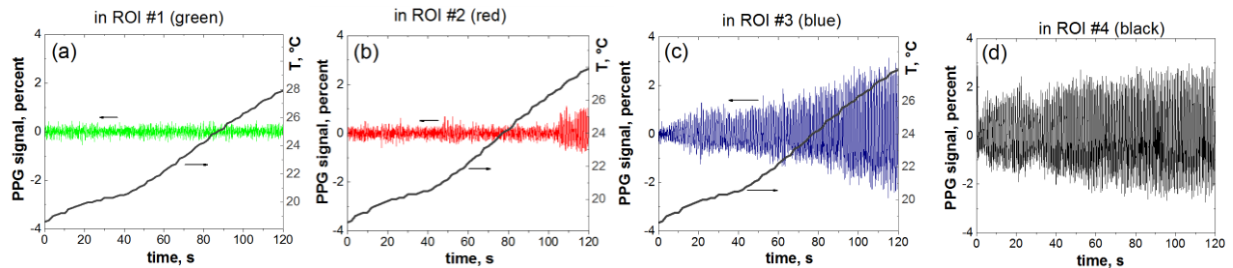


Fig. 2. Temporal evolution of PPG waveform in four different ROIs (shown in Fig.1) during warming up the palm.

Thus, obtained preliminary results demonstrate an applicability of BPI technique for remote studying of thermoregulation of vascular system in live tissues. In the particular experiment, we have shown that dynamics of this process can be different for different tissue regions even if they had originally similar conditions.

AAK acknowledges the financial support provided by the Russian Science Foundation (grant 15-15-20012).

References

- [1] Kamshilin A A, Miridonov S V, Teplov V, Saarenheimo R, Nippolainen E 2011 *Biomedical Optics Express* **2**, 996-1006
- [2] Verkruyse W, Svaasand L O, Nelson J S 2008 *Optics Express* **16**, 21434-21445
- [3] Kamshilin A A, Nippolainen E, Sidorov I S, Vasilev P V, Erofeev N P, Podolian N P, Romashko R V 2015 *Scientific Reports* **5**, 10494
- [4] Kamshilin A A, Mamontov O V, Koval V T, Zayats G A, Romashko R V 2015 *Biomedical Optics Express* **6**, 4326-4334

What is so special about microgravity for blood pressure and heart rate?

John M. Karemaker

Academic Medical Center at the Univ. of Amsterdam, Systems Physiology, The Netherlands

Microgravity was, from the onset of human space exploration, a dreaded condition: could animal/human life survive without harm? What would happen to the vestibular system? Would one be able to orient and not set off into an uncontrollable spin? In our days only a few hundred people have experienced space conditions and came back to tell about it: the conditions are different, indeed, but one can adapt to it.

The only way for 'ordinary people' to experience microgravity is in free fall, like at the turning point of a swing or while jumping on a trampoline, and for longer periods when jumping off a plane, or, slightly safer, in parabolic flight. I have had the privilege of the latter experience and, on top of that, to measure blood pressure (BP) and heart rate (HR) in a series of test subjects while doing so. They went into and out of the parabolas upright or supine and during rest and exercise. This taught us that the BP and HR effects are mainly determined by the baroreceptors in the neck (carotid sinus reflex) and by a sudden increase in venous return when going into the parabola in the upright posture.

However, almost exactly the same responses can be obtained when someone is put on a tilt table and quickly tilted down or up, mimicking going into or out of a parabola, respectively. Only going weightless in the supine posture, where none of the above explanations holds, gave unexpected results.

Finally, most known effects of longer lasting cardiovascular space adaptation have been felt by almost everyone: who hasn't been bedridden for a few days with the flu? Standing up after such a period of fluid loss and being supine for a longer period than just one night, brings the same sense of dizziness and unsteady blood pressure as has been measured in returning astronauts and cosmonauts.

In conclusion: we are all astronauts when it comes to the space effects on blood pressure and heart rate. Microgravity is not so special in this respect.

Coulomb blockade oscillations and AMFE in Calcium ion channels

Igor Kh. Kaufman¹, Dmitry G. Luchinsky^{1,2}, Will A.T. Gibby¹,
Peter V.E. McClintock¹ and Robert S. Eisenberg³

¹ Lancaster University, Dept. of Physics, Lancaster, UK

² SGT Inc., Ames Research Center, Moffett Field, CA, USA

³ Rush University, Dept. of Molecular Biophysics, Chicago, IL, USA

Biological ion channels are protein nanotubes providing for the highly-selective transmembrane transport of physiologically important ions [1]. Reaching an understanding of the selectivity mechanisms of ion channels is a long-standing problem in biophysics.

The conduction and selectivity of calcium/sodium ion channels have recently been described [2] in terms of ionic Coulomb blockade (CB) [3], a phenomenon based on charge discreteness, an electrostatic exclusion principle, and stochastic ion motion through the channel. Von Kitzing earlier revealed a staircase of occupancy for the charged ion channel *vs* site affinity [4]. Similar low-barrier ion-exchange transitions were discovered analytically [5].

Here we demonstrate that strong ionic CB appears for Ca^{2+} ions and manifests itself in divalent blockade and the anomalous mole fraction effect (AMFE).

In what follows e is the proton charge, z the ionic valence, T the temperature, and k_B Boltzmann's constant. The generic electrostatic model describes the selectivity filter of a $\text{Ca}^{2+}/\text{Na}^+$ ion channel as an axisymmetric, water-filled pore of radius $R = 0.3\text{nm}$ and length $L = 1.6\text{nm}$ through the cellular membrane. A centrally-placed, uniform, rigid ring of negative charge Q_f is embedded in the wall.

We approximate the Gibbs free energy G_n as the dielectric self-energy U_n of the excess charge $Q_n = zne + Q_f$, using proper bulk $[\text{Ca}]$ and reference $[\text{Ca}]_0$ calcium concentrations and self-capacitance C_s terms, respectively:

$$G_n = U_n - TS_n = Q_n^2/2C_s - k_B T \ln([\text{Ca}]/[\text{Ca}]_0) \quad (1)$$

CB appears in low- C_s systems from the quantization of (1) at a grid of discrete states, providing a Coulomb energy gap ΔG_n that is large enough ($\Delta G_n \gg k_B T$) to block transitions between neighbouring $\{n\}$ states.

The CB model predicts a periodic pattern of stop/conduction bands (see Fig.1) similar to the electronic CB in quantum dots [6]. We connect selectivity with valence-, concentration-, and hydration-dependent shifts of conduction bands. Fig.1(a) shows

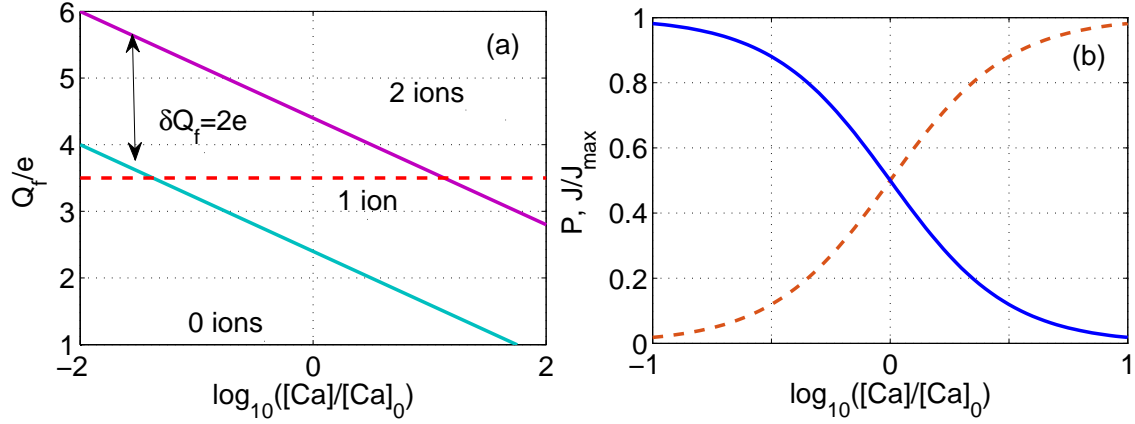


Figure 1: Anomalous mole fraction effect (AMFE) in calcium channels (mixed bath). (a) Phase diagram Q_f vs $\log([Ca])$, switching lines are: 0→1 (green) and 1→2 (violet), AMFE trajectory is shown as red dashed. (b) Attenuation of Na^+ current J (blue line) by Ca^{2+} binding occupancy P (red dashed line).

the switching lines and AMFE trajectory in the “ion exchange phase diagram” [5] for the calcium channel. The first Ca^{2+} ion provides blockade of channel, the second provide knock-on fast Ca^{2+} conduction. Fig.1(b) shows the details of $\{0\} \rightarrow \{1\}$ switching when J/J_{max} vs $[Ca]$ at divalent blockade allows for estimation of occupancy $P([Ca])$ vs U or $\ln([Ca]/[Ca]_0)$ from a simple blockade formula: $J/J_{max} = 1 - P([Ca])$ leading to Langmuir isotherm for $J[Ca]$.

The ionic CB model provides a good account of both the experimental (AMFE and valence selectivity) and the simulated (discrete multi-ion conduction and occupancy bands) phenomena observed in Ca^{2+} channels, including concentration-related shifts of switching lines and conduction bands. The results should also be applicable to biomimetic nanopores with charged walls.

The research was supported by the Engineering and Physical Sciences Research Council UK (grant No. EP/M015831/1).

References

- [1] Hille, B. *Ion Channels Of Excitable Membranes*, 3rd ed. Sinauer Ass. Sunderland, MA, 2001.
- [2] Kaufman, I. K., McClintock, P. V. E., and Eisenberg, R. S., 2015 *New J. Phys.*, **8**, 083021.
- [3] Krems, M., and Di Ventra, M. 2013 *J. Phys. Condens. Matt.* **25** 065101.
- [4] von Kitzing, E. In *Membrane Proteins*, Springer, 1992, 297–314.
- [5] Zhang, J., Kamenev, A., and Shklovskii, B. I. 2006 *Phys. Rev. E* **73** 051205.
- [6] Beenakker, C. W. J. 1991 *Phys. Rev. B* **44** 1646–1656

Molecular and Brownian dynamics simulations of ion transport through outer membrane channels

Ulrich Kleinekathöfer

Jacobs University Bremen, Department of Physics & Earth Sciences , Bremen, Germany

Channels in the outer membrane of Gram-negative bacteria provide essential pathways for the controlled and unidirectional transport of ions, nutrients and metabolites into the cell. At the same time the outer membrane serves as a physical barrier for the penetration of noxious substances such as antibiotics into the bacteria. In this presentation the simulation of ion and substrate transport across such bacterial channels is investigated. To this end we do employ molecular dynamics simulations and will report on results from different channels. Due to electroosmosis, this ion transport can have a significant on the translocation of neutral substrates such as cyclodextrins. A detailed analysis opens the potential to use the electroosmotic effect to distinguish between translocation and channel blocking.

Since the determination of free energy surfaces for ion and substrate transport using MD simulations is computationally very demanding, we developed a hybrid scheme of Brownian and Molecular dynamics which can account for atomic details of a selected set of atoms. The basics of this scheme will be outlined briefly.

References

Pothula K.R., Solano C.J.F. and Kleinekathöfer U. 2016, *Biochimica et Biophysica Acta (BBA) Biomembranes* (review, in press, doi:10.1016/j.bbamem.2015.12.020).

Modi N. , Ganguly S., Bárcena-Uribarri I., Benz R., van den Berg B. and Kleinekathöfer U. 2015 *Biophys. J.* **109** 1429.

van den Berg B., Bhamidimarri P. S., Prajapati D. J., Kleinekathöfer U. and Winterhalter M. 2015 *Proc. Natl. Acad. Sci. USA* **112** E2991.

Pothula K. R. and Kleinekathöfer U. 2015 *Analyst* **140** 4855.

Modi N., Bárcena-Uribarri I., Bains M. , Benz R., Hancock R. E. and Kleinekathöfer U. 2015 *ACS Chem. Biol.* **10**, 441.

Fetal and maternal autonomic interaction in pre-eclampsia

Igor Lakhno

Kharkiv VN Karazin National university, Department of obstetrics and gynecology,

Kharkiv, Ukraine

Parasympathetic nervous regulation increases its activity in the first half of physiological gestation. The above-mentioned increase supports gestational autonomic resetting that leads to hypervolemia and vasodilatation [1]. The absence of the emphasis on vagal-mediated reactions could be associated with failed placentation and it contributes to sympathetic overactivity, hypovolemia and vasoconstriction [1, 2]. Pre-eclampsia (PE) is known as a result of placental ischemia, increased release of vasoconstrictors, endothelial dysfunction and thrombophilia [3]. Since respiratory sinus arrhythmia (RSA) captures parasympathetic impact on the heart rate variability (HRV) the question of the lack of vagal tone in the scenario of PE becomes a rather current issue.

Fetal and maternal hemodynamics are anatomically distinct but periods of the fetal and maternal cardiac synchrony are known. RSA was found as a main instrument of such hemodynamic coupling [4]. It is possible to speculate that maternal RSA-associated hemodynamic fluctuations could penetrate through placental barrier. Fetal RSA plays an important role in its adaptive response to chronic placental insufficiency [5]. The umbilical vein could be approached as a “mirror” of the oscillatory processes in the mother-placenta-fetus system since the cord is not an innervated tissue.

The **aim** of the investigation was to determine the role of RSA in the regulation of fetal circulatory system in the case of healthy pregnancy and in PE.

Materials and methods. Maternal and fetal HRV were studied and umbilical venous blood flow velocity spectral analysis was performed in 106 patients at 32-38 weeks of gestation. 30 of them had a healthy pregnancy and were included in Group I. In Group II, 44 pregnant women with mild-moderate PE were observed. 32 patients with severe PE were monitored in Group III. Maternal and fetal RR-interval time series were obtained in a non-invasive manner from maternal abdominal ECG recordings. HRV was measured in the time and frequency domains in the maternal sitting position. The root mean square of successive heartbeat interval differences (RMSSD) was considered as a RSA-related parameter [5].

Results. Both maternal and fetal HRV in PE demonstrated a total decrease with a relatively increased sympathetic tone. It was found the decreased maternal and fetal RMSSDs in PE. The oscillatory peak at a frequency about $0.5 \frac{1}{113}$ determined in the Doppler spectrograms of the

umbilical vein characterized the participation of the maternal RSA in fetal hemodynamics. Strong relationship between the maternal RMSSD and the amplitude of 0.5 Hz frequency peak ($R=0.62$; $p<0.05$) and between the maternal and the fetal HF's was found in healthy pregnancy ($R=0.48$; $p<0.05$). In this Group, the correlation between the maternal and the fetal RMSSDs was also explored ($R=0.60$; $p<0.05$). No relationship was revealed between the maternal RMSSD and the amplitude of the 0.5 Hz frequency peak ($R=0.20$; $p<0.05$), the maternal and fetal HFs ($R=0.18$; $p<0.05$), the maternal and fetal RMSSDs ($R=0.16$; $p<0.05$) in the patients with a severe PE.

The obtained data confirmed the oscillatory nature of fetal and maternal autonomic interaction. The maternal RSA propagated its influence on the fetal umbilical venous blood flow and the fetal autonomic nervous regulation in a healthy pregnancy. The control of fetal hemodynamics diminished in the mild-moderate PE and even disappeared in severe PE. Placenta was a possible instrument to switch the main frequency of the controlling signal. This speculation could explore the mechanism of the maternal HF band (0.15-0.4Hz) and fetal HF (0.4-1.7 Hz) synchronization. The revealed 0.5 Hz driver in the umbilical venous flow was associated with maternal RSA and it was determined as a main frequency in the system of mother-placenta-fetus.

Conclusion. The interaction between maternal and fetal RSA was a possible mechanism of the fetal well-being. The loss of fetal and maternal hemodynamic coupling could be considered a presumable pathogenetic pathway of the fetal deterioration in PE.

References.

1. Schobel HP, Fischer T, Heuszer K et al. 1996 Preeclampsia – a state of sympathetic overactivity. *N Engl J Med* **335**,1480-1485.
2. Yang CCH, Chao T, Kuo BJK et al. 2000 Preeclamptic pregnancy is associated with increased sympathetic and decreased parasympathetic control of HR. *American Journal of Physiology – Heart and Circulatory Physiology* **278**, 1269-1273.
3. Rosser ML, Katz NT 2013 Preeclampsia: an obstetrician's perspective. *Adv Chronic Kidney Dis* **20**, 287-296.
4. Ivanov PC, Qianli DYM, Bartsch RP 2009 Maternal–fetal heartbeat phase synchronization. *PNAS* **106**, 13641-13642.
5. Arias-Ortega R, Echeverria JC, Gusman-Huerta M et al. 2015 Respiratory sinus arrhythmia in growth restricted fetuses with normal Doppler hemodynamic indices. *Early Hum Dev* **93**, 17-26.

Diagnosis of malignant melanoma based on alterations in blood flow dynamics

Gemma Lancaster¹, Marco Rossi², Margherita Pesce² and Aneta Stefanovska¹

¹*Lancaster University, Department of Physics, Lancaster, UK*

²*University of Pisa, Department of Clinical and Experimental Medicine, Pisa, Italy*

The non-invasive measurement of skin blood flow (SBF) using laser Doppler flowmetry has been used in countless studies as a model for microvascular assessment *in vivo*. The dynamical properties of microvascular blood flow are known to be influenced on multiple scales [1]. As well as systemic oscillations arising from cardiac and respiratory activity, local modulation by vasomotion results in extremely complex, multi-oscillatory blood flow signals. Observing the nature of this modulation provides information about specific myogenic, neurogenic and endothelial processes.

Considering this coupled oscillator model of the cardiovascular system allows the comparison of blood flow regulation mechanisms in healthy and pathological states. This approach has been applied to studies of hypertension [2], diabetes [3] and ageing [4], to name a few.

Here, we investigate blood flow dynamics in skin malignant melanoma, where SBF may be affected both by angiogenesis and by a hostile tumour microenvironment. By applying wavelet analysis to SBF signals in melanoma, atypical naevi, benign naevi and psoriasis lesions, we demonstrate clear differences in wavelet power in the frequency intervals associated with myogenic and neurogenic activity, suggesting alterations in microvascular regulation. We discuss the possible causes for these differences, and show how they can be used as a diagnostic marker for skin melanoma.

References

1. Stefanovska A. 2007 *IEEE Eng. Med. Biol. Mag.* **26** 25–29
2. Rossi M. 2011 *J. Hypertens.* **29** 1569–76
3. Urbančič-Rovan, V. 2006 *Diabetes Res. Clin. Pract.* **73** 166–173
4. Shiogai, Y. 2010 *Phys. Rep.* **488** 51–110

Seizures and chimeras in epileptic brain networks

Klaus Lehnertz

University of Bonn, Department of Epileptology; Helmholtz Institute for Radiation and Nuclear Physics; Interdisciplinary Center for Complex Systems, Bonn, Germany

Epileptic seizures are characterized by an overly synchronized firing of neurons. Knowledge about mechanisms underlying generation, spread, and termination of the extreme event seizure in humans is still fragmentary. There is now increasing evidence for the existence of large-scale epileptic networks in which all constituents can contribute to the generation, maintenance, spread, and termination of even focal seizures as well as to the many pathophysiologic phenomena seen during the seizure-free interval. With model simulations of complex oscillator networks that are based on connection structures seen in human epilepsies we provide evidence that seizures can be regarded as self-initiated and self-terminated chimera states.

Synchronization analysis of cerebral tissue oxygenation and arterial blood pressure signals in post-stroke subjects

Manyu Zhang, Qitao Tan, Bitian Wang, Liwei Xu, Wei Wang, Zengyong Li*

Key Laboratory of High Efficiency and Clean Mechanical Manufacture, School of Mechanical Engineering, Shandong University, Jinan, 250061 P.R. China

*Corresponding authors: zyongli@sdu.edu.cn

Introduction

Cerebral autoregulation (CA) was the ability of the cerebral vasculature to maintain cerebral perfusion relatively constant through myogenic, neurogenic, or metabolic mechanisms despite changes in arterial blood pressure (ABP) (Van Beek et al., 2008). Cerebral infarction (CI) affects brain function among brain areas; however, little information is known about the effects of CI on the CA in various frequency bands in post-stroke subjects.

Near-infrared spectroscopy (NIRS) technique can non-invasively and continuously measure brain activation by monitoring changes in the local oxygenated and deoxygenated hemoglobin concentrations (Ferrari and Quaresima, 2012). The relationship between spontaneous cerebral oscillations (i.e. Delta [O₂Hb]) and cardiovascular parameters (i.e. ABP) is a promising technique for non-invasively assessing the status of CA (Rowley et al., 2007; Van Beek et al., 2008). Wavelet coherence (WCO) and wavelet phase coherence (WPCO) can identify high common power and phase relationships and thereby evaluating the match between the two signals (Bandrivskyy et al., 2004; Sheppard et al., 2011). In this study it can be hypothesized that the dynamic relationship between the Delta [O₂Hb] and ABP signals in elderly subjects would be altered because of CI. This will provides new insight into the regulation mechanisms in the elderly subjects with CI and may be used to assess the motor rehabilitation in post-stroke subjects.

Subjects and methods

A total of 31 elderly subjects were recruited from Shandong University and a local rehabilitation center to participate in this study, in which 16 subjects were patients with cerebral infarction (CI) (age: 77.8 ± 3.8 years; Group CI), and 15 were healthy subjects (age: 73.3 ± 5.1 years; Group Health). Continuous recordings of near-infrared spectroscopy (NIRS) signals in the prefrontal lobes and the motor cortical areas and ABP signals were recorded simultaneously during resting state. The coherence of the Delta [O₂Hb] and ABP signals was analyzed using wavelet coherence (WCO) and wavelet phase coherence (WPCO) methods in six frequency intervals (I, 0.6-2 Hz; II, 0.15-0.6 Hz; III, 0.05-0.15 Hz; IV, 0.02-0.05 Hz; V, 0.0095-0.02 Hz and VI, 0.005-0.0095 Hz).

Results and discussion

The results showed that the WCO of Delta [O₂Hb] and ABP signals exhibited significantly lower level in interval IV ($p < 0.05$) in the motor areas, and in interval III in the prefrontal cortex ($p < 0.05$) in Group CI than in Group Health. Similar results were found in the WPCO of Delta [O₂Hb] and ABP signals between Group CI and Group Health. The lower values of WCO and WPCO in the elderly subjects with CI suggest an enhanced synchronization between Delta [O₂Hb] and ABP and this enhancement might be an indicative of compensatory mechanism. This study provides new insight into the cerebral regulation mechanisms in the elderly subjects with CI and may be used to assess motor rehabilitation and brain plasticity after stroke.

References

- Bandrivskyy, A., Bernjak, A., McClintock, P., & Stefanovska, A., 2004. Wavelet phase coherence analysis: application to skin temperature and blood flow. *Cardiovascular engineering: an international journal*. 4, 89-93.
- Ferrari M, Quaresima V. 2012 A brief review on the history of human functional near-infrared spectroscopy (fNIRS) development and fields of application. *NeuroImage*. 63 (1) :921–935
- Rowley, A. B., Payne, S. J., Tachtsidis, I., Ebden, M. J., Whiteley, J. P., Gavaghan, D. J., ... & Delpy, D. T., 2007. Synchronization between arterial blood pressure and cerebral oxyhaemoglobin concentration investigated by wavelet cross-correlation. *Physiological measurement*. 28, 161-173.
- Sheppard, L. W., Vuksanović, V., McClintock, P. V. E., & Stefanovska, A., 2011. Oscillatory dynamics of vasoconstriction and vasodilation identified by time-localized phase coherence. *Physics in medicine and biology*. 56, 3583-3601.
- Van Beek, A. H., Lagro, J., Olde-Rikkert, M. G., Zhang, R., & Claassen, J. A. , 2012. Oscillations in cerebral blood flow and cortical oxygenation in Alzheimer's disease. *Neurobiology of aging*. 33, 428. e21-428. e31.

Acknowledgements

This study was sponsored by National Natural Science Foundation of China (Grant No. 31371002, 81071223).

Role of temperature and tissue size on nonlinear cardiac dynamics

Christian Cherubini^{1,2}, Flavio H. Fenton³, Simonetta Filippi^{1,2},
Alessio Gizzi¹, & Alessandro Loppini¹

¹*University Campus Bio-Medico of Rome, via A. del Portillo 21, 00128 Rome (IT)*

²*International Center for Relativistic Astrophysics Network - I.C.R.A.Net*
&

³*Georgia Institute of Technology, 837 State Street, Atlanta, Georgia (USA)*
30332-0430

Nonlinear spiral waves in cardiac dynamics are associated with pathological situations. In the heart these conditions have to be treated through fine-tuned defibrillation protocols [1,2]. Cardiac tissue, however, is an active medium whose spatiotemporal dynamics are highly affected by thermal gradients [3,4]. Cardiac hypothermia, in particular, is well known to be pro-arrhythmic though important beneficial effects are exploited during intracardiac surgeries [5]. In the present work, we aim to study the mechanisms that induce fibrillation during hypothermia. A better understanding of the complex spatiotemporal dynamics of heart tissue as a function of temperature will be useful in managing the benefits and risks of hypothermia.

We perform two-dimensional numerical simulations by using a minimal model of cardiac action potential propagation fine-tuned on experimental measurements [4]. The model includes thermal factors acting on the ionic currents and the gating variables to correctly reproduce experimentally recorded restitution curves at different temperatures. Numerical simulations are implemented using Finite Elements and WebGL tools allowing long simulation times running close to real time. We describe and explain (i) why fibrillation is easier to induce at low temperatures, (ii) the minimum size required for fibrillation depends on temperature, (iii) why the frequency of fibrillation decreases with decreasing temperature, and (iv) that regional cooling may be an anti-arrhythmic therapy for small tissue sizes however it may be pro-arrhythmic for large tissue sizes. Implications for model generalization and applications are finally discussed.

References

- [1] Luther S, Fenton FH, et al. 2011. *Nature* **475**:235–239.
- [2] Cherubini C, Filippi S, Gizzi A 2012. *Phys Rev E* **85**:031915.
- [3] Filippi S, Gizzi A, Cherubini C, Luther S, Fenton FH 2014. *Europace*, **16**:424–434.
- [4] Fenton FH, Gizzi A, Cherubini C, Pomella N, Filippi S 2013. *Phys Rev E*, **87**:042717.
- [5] Bigelow WG, Callaghan JC, Hopps JA 1950. *Ann Surg* 132:531–9.

Tensorial self-Transfer Entropy (TsTE) of R-R heart interbeat signals and healthy ageing ¹

Danuta Makowiec^a, Zbigniew R. Struzik^{b,c}

^a*University of Gdańsk, Institute of Theoretical Physics and Astrophysics, Poland*

^b*RIKEN Brain Science Institute, Hirosawa, Japan*

^c*The University of Tokyo, Graduate School of Education, Japan*

Let a Markov chain $\{X(t), t = 0, 1, \dots\}$ be given with a discrete state space $\{\Delta_k : k = 1, 2, \dots, K\}$, and dynamics following a transition matrix

$$T_{jk} = p(\Delta_k | \Delta_j) = \frac{p(\Delta_j, \Delta_k)}{p(\Delta_j)}, \quad (1)$$

in which $p(\Delta_j, \Delta_k)$ describes the probability that $X(t) = \Delta_k$ and $X(t-1) = \Delta_j$, so that $p(\Delta_k | \Delta_j)$ provides the conditional probability of observing $X(t) = \Delta_k$ if $X(t-1) = \Delta_j$ has occurred. Let resulting stationary state μ be nominated by $\mu_k = p(\Delta_k)$. Then the entropy rate S_T of such evolution is defined as:

$$S_T(X) = - \sum_k \mu_k \sum_j T_{jk} \ln T_{jk}, \quad (2)$$

which can be transferred into the formula:

$$S_T(X) = - \sum_{j,k} p(\Delta_j, \Delta_k) \ln p(\Delta_k | \Delta_j). \quad (3)$$

A description of how the entropy rate changes if the history is not one step $X(t-1) = \Delta_j$ but of two-steps, or in general n-steps ($X(t-n) = \Delta_{j_n}, \dots, X(t-1) = \Delta_{j_1}$) is given as:

$$S_T^{n \text{ step}}(X) = - \sum_{j_n, \dots, j_1, k} p(\Delta_{j_n}, \dots, \Delta_{j_1}, \Delta_k) \ln p(\Delta_k | \Delta_{j_1}, \dots, \Delta_{j_n}). \quad (4)$$

Then one can ask if any information is gained when the memory is longer and what kind of information we attain. The answers can be given by considering the difference between (3) and (4), which leads to:

$$S_T(X) - S_T^{n \text{ step}}(X) = - \sum_{j_n, \dots, j_1, k} p(\Delta_{j_n}, \dots, \Delta_{j_1}, \Delta_k) \ln \frac{p(\Delta_k | \Delta_{j_1}, \dots, \Delta_{j_n})}{p(\Delta_k | \Delta_{j_1})}, \quad (5)$$

¹The authors thank for the financial support of the National Science Centre, Poland, UMO: 2012/06/M/ST2/00480

which can be compared to the transfer entropy (TE) notion proposed by Schreiber [1]. Accordingly, let us define the tensorial self transfer entropy as:

$$TsTE(X) = S_T(X) - S_T^{n\ step}(X) = \sum_{j,k} \mathbf{TsTE}_{jk}, \quad (6)$$

where \mathbf{TsTE}_{jk} are tensors given by the formula

$$\mathbf{TsTE}_{jk} = - \sum_{j_n, \dots, j_2} p(\Delta_{j_n}, \dots, \Delta_{j_2}, \Delta_j, \Delta_k) \ln \frac{p(\Delta_k | \Delta_j, \Delta_{j_2}, \dots, \Delta_{j_n})}{p(\Delta_k | \Delta_j)}. \quad (7)$$

In case $n = 2$, we calculate $TsTE$ for RR-signals recorded during the nocturnal rest of healthy individuals at different ages. 194 healthy participants included in the study were classified in age groups: *20's*: 36 subjects (18 female), *30's*: 26 subjects (13 female), *40's*: 36 subjects (16 female), *50's*: 32 subjects (13 female), *60's*: 24 subjects (11 female), *70's*: 22 subjects (10 female), and *80's*: 18 subjects (11 female). In Fig. 1, we show the results. The results are preliminary but promising.

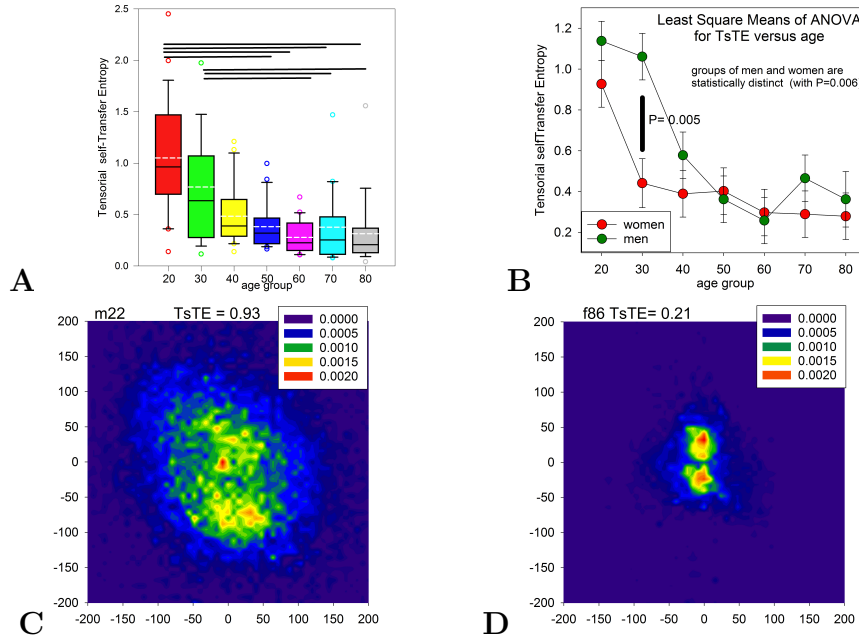


Figure 1: Panels **A** and **B** describe decay of $TsTE$ with advancing age. White dashed lines in **A** denote the group means. Lines over boxes show differences statistically significant (Mann-Whitney test, $p < 0.05$). **B** presents gender influence. Only the difference among the *30's* is statistically significant (Two-way ANOVA, $p < 0.05$). Panels **C** and **D** show tensor \mathbf{TsTE}_{jk} for a typical youngest man and a typical oldest woman.

References

1. Schreiber T, (2000) *Phys.Rev.Lett.* **85** 461–464.

Multifractality of R-R interval signals and healthy ageing ¹

**Danuta Makowiec^a, Marta Żarczyńska-Buchowiecka^b
and Zbigniew R. Struzik^{c,d}**

^a*University of Gdańsk, Institute of Theoretical Physics and Astrophysics, Poland*

^b*Medical University of Gdańsk, 1st Chair and Clinic of Cardiology, Poland*

^c*RIKEN Brain Science Institute, Hirosawa, Japan*

^d*The University of Tokyo, Graduate School of Education, Japan*

RR-intervals are known to be nonstationary, having a $1/f$ spectrum with anti-persistent long-range correlations and multifractality; see [1] and references therein. Alteration of the long-range organization, as well as a loss of complexity, has been reported as people age, although it has been claimed that fractal scale-invariance remains stable with the advance of age [2]. In particular, it has been argued that the sleep phase-based pattern remains unchanged with age [3]. Sleep can be considered to be a period of human activity which is free of external stimulation, and therefore provides an opportunity to observe the state of the autonomic baseline [4]. However, sleep is organized in cycles in which stages of slow wave sleep are followed by rapid eye movement sleep. HRV has been found to be strongly affected by sleep organization [5,3].

Data arising from experiments might not conform to mathematical assumptions about fractal processes with long-range correlations. Therefore there is continuing research into methodologies to estimate complexity in time series. With these, warnings are issued about pitfalls and misinterpretations arising when dealing with real time series [6]. In particular, the required consistency between results obtained from different methods is often missed. Our presentation will concentrate on discussion about consistency and possible reasons for inconsistency among the results describing (multi)fractality of RR-signals obtained by two popular methods: multifractal detrended fluctuation analysis (MDFFA), and wavelet transform modulus maxima method (WTMM). Both methods are known to cope with non-stationary signals, and as such should be able to measure fractal properties also in sleep signals.

Twenty-four hour Holter recordings of, in total 194, healthy participants were included into the study, classified in age groups: *20's*: 36 subjects (18 women), *30's*: 26 subjects (13 women), *40's*: 36 subjects (16 women), *50's*: 32 subjects (13 women), *60's*: 24 subjects (11 women), *70's*: 22 subjects (10 women), and *80's*: 18 subjects (11 women). Multifractal estimators were applied to six-hour signals representing

¹The authors thank for the financial support of the National Science Centre, Poland, UMO: 2012/06/M/ST2/00480

the nocturnal rest which was selected for each subject individually based either on rapid increase in length of RR intervals or on setting 11 pm to 4 am, otherwise.

Results for the basic index of multifractality, capacity exponent h , are shown in Fig. 1. We see that h decreases with age when estimated by WTMM, while MDFA

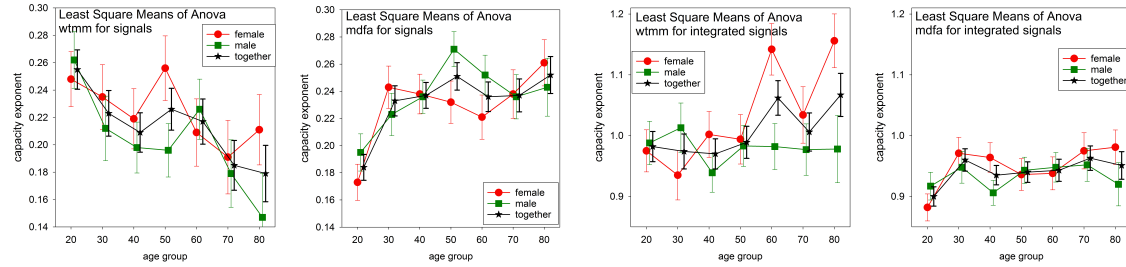


Figure 1: The mean capacity exponents h of multifractal spectra ($h, D(h)$) (i.e., h for which $D(h)$ attains its maximal value) for different age x gender groups. By Two Way ANOVA gender differences are not statistically significant. Differences between age groups are statistically significant in case of MDFA ($p < 0.001$), WTMM ($p = 0.03$) and WTMM for integrated signals ($p = 0.032$).

hints at opposite conclusion. Moreover, for a monofractal signal this exponent corresponds to the Hurst exponent H , or to $1 + H$ in case of integrated signal. Therefore the relation between capacity exponents obtained for integrated signals h^{int} and signals h could be a rough detector of multifractality. From Fig. 1 one can easily evaluate that WTMM shows switch from multi- (up to 60's) to mono-fractality (over 70's). This effect is absent in results given by MDFA.

In our presentation we will discuss possible reasons for described above inconsistency.

References

1. Ivanov PC, Amaral LAN, Goldberger AL, Havlin S, Rosenblum MG, Struzik ZR and Stanley HE (1999) *Nature* **399** 461.
2. Schmitt DT and Ivanov PC (2007) *American Journal of Physiology - Regulatory, Integrative and Comparative Physiology*, 293:R1923–R1937.
3. Schumann AY, Bartsch RP, Penzel T, Ivanov PC and Kantelhardt JW (2010) *Sleep* **33(07)** 943.
4. Stein PK and Pu Y (2012) *Sleep Medicine Review* **16(1)** 47; Chouchou F and Desseilles M (2014) *Frontiers in Neuroscience* **8** (402).
5. Monti A, Medigue C, Nedelcoux H and Escourrou P (2002) *European Journal of Applied Physiology* **87(2)** 174.
6. Gao J, Hu J, Tung W-W, Cao Y, Sarshar N and Roychowdhury VP (2006) *Phys. Rev. E* **73** 016117; Makowiec D, Dudkowska A, Galaska R and Rynkiewicz A (2009) *Physica A* **388(17)** 3486; Eke A, Herman P, Sanganahalli BG, Hyder F, Mukli P and Nagy Z (2012) *Frontiers in Physiology* **3** (417).

Asymmetry in heart rate and blood pressure manifested in the head-up tilt test ¹

Danuta Makowiec^a, Beata Graff^b, Dorota Wejer^a,
and Zbigniew R. Struzik^{c,d}

^aUniversity of Gdańsk, Institute of Theoretical Physics and Astrophysics, Poland

^bMedical University of Gdańsk, Dept of Hypertension and Diabetology, Poland

^cRIKEN Brain Science Institute, Hirosawa, Japan

^dThe University of Tokyo, Graduate School of Education, Japan

Background: Baroreceptor activation or deactivation occurs during transient changes in blood pressure. In response, cardiac period and vascular resistance are modified to maintain the blood pressure homeostasis [1]. These complex multiscale and multilevel interactions are reflected in heart accelerations and decelerations and in drops and rises in blood pressure invoked during the head-up tilt (HUT) test. The Generalized Porta Index (GPI) has been proposed to quantify asymmetry between positive and negative changes in a heart rate period by comparing the role of decelerations and accelerations, combined according to their probability of occurrence [2]. However, this comparative approach is not the only possible one, and the structure of the asymmetry of the roles of decelerations and accelerations can be investigated from an alternative perspective, namely by using a so-called Multistructure Index (MI), which addresses the sizes of events [3]. Here we present a comparison between these complementary indices of the role of decelerations and accelerations in cardiovascular homeostasis dynamics evoked by the HUT test.

Methods: Let $\Delta(i)$ denote a change between subsequent i and $i - 1$ values of either interbeat RR-intervals or values of systolic blood pressure (SBP). Let a positive/negative/non-zero change be denoted as $\Delta^+(i)/\Delta^-(i)/\Delta^{\neq 0}(i)$ if $\Delta(i) > 0/\Delta(i) < 0/\Delta(i) \neq 0$, respectively. Then for any real q , one can define:

$$GPI(q) := \frac{\sum_{\Delta^-} p^q(\Delta^-)}{\sum_{\Delta^{\neq 0}} p^q(\Delta^{\neq 0})}, \quad MI(q) := \frac{\sum_{\Delta^+(i)} (\Delta^+(i))^q}{\sum_{\Delta^{\neq 0}(i)} |\Delta^{\neq 0}(i)|^q}. \quad (1)$$

In particular, when Δ denotes RR-increments, then $GPI < 0.5$ hints at domination of decelerations of less probable $q < 0$ or more probable $q > 0$ events, while $MI < 0.5$ indicates the prevalence of accelerations of smaller $q < 0$ or larger $q > 0$ sizes. Both indices demonstrate a simple relation with the Porta Index (PI): $PI = GPI(1)$ and $PI = 1 - MI(1)$.

Results: Typical distributions of ΔRR or ΔSBP are sharply peaked around zero.

¹The authors thank for the financial support of the National Science Centre, Poland, UMO: 2012/06/M/ST2/00480

Therefore, the smallest increments are usually the most probable events, and the largest changes coincide with the least probable events. As a consequence, the functions $GPI(q)$ and $MI(q)$ are to some degree related to each other, see Fig. 1. Values

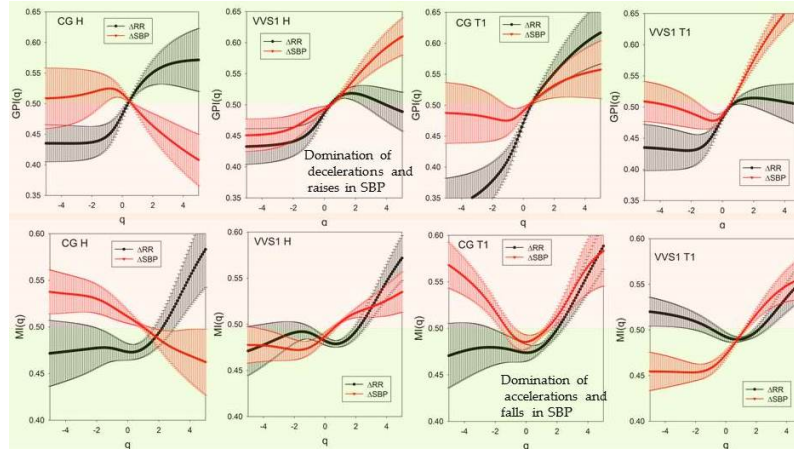


Figure 1: Means of $GPI(q)$ (top) and $MI(q)$ (bottom) with their std errs obtained from signals of healthy people in the control group **CG** (29 subjects: 15 female, age 24.9 ± 1.3 , no history of syncope, no syncope during the HUT test) and vasovagal patients **VVS1** (57 subjects: 40 female, age 26.2 ± 1.0 , mmm, with a history of fainting, who experienced mixed type syncope during the HUT test) in the supine position (H) and just after tilting (T1). The greenish/reddish backgrounds mark regions with opposing dynamics preferences.

of $MI(q)$ or $GPI(q)$ different from 0.5 and, in particular, consistent trends in functional slopes of the respective indices, indicate asymmetric participation of positive and negative increments at scales extracted by the modulatory parameter q . A direct influence on the ΔRR of the sympathetic branch of the autonomic nervous system potentially refers to mid-scales of MI, which are restored within $-2 \leq q \leq 2$, while the vagal activity is likely reflected for the range of $q > 3$. In the case of ΔSBP , a direct effect of the sympathetic activity on the vascular resistance is likely represented by $q > 0$, while an indirect effect (caused via circulating catecholamines and/or local mechanical and chemical reflexes of non-autonomic origin) may be reflected in the acceleration-deceleration balance and captured by the respective indices for $q < 0$.

Conclusions: Although to some extent consistent, the relationship between $GPI(q)$ and $MI(q)$ is not straightforward and captures non-linear dependency and possibly reveals compensatory mechanisms interacting through sizes and probabilities of events. In particular, it indicates fundamental differences in cardiovascular regulatory systems between healthy people and vasovagal patients.

References:

1. Thomas G D 2011 *Adv.Physiol.Educ.*, **35(1)** 28-32.
2. Makowiec D, Graff B, Miklaszewski W, *et al.* 2015 *EPL* **110(2)** 28002.
3. Makowiec D, Graff B, Struzik Z R 2016 *Phys.Rev.E*, under consideration.

Revealing brain-heart interactions with EEG and fMRI

Guo-Rong Wu^{1,2}, Daniele Marinazzo²

[1] *Key Laboratory of Cognition and Personality, Southwest University,
Chongqing, China*

[2] *Department of Data Analysis, Ghent University, Ghent, Belgium*

This contribution will be a review. I will give an introduction to the techniques which can reveal brain-heart interactions using measures of heart rate paired with the two most common neuroimaging techniques: electroencephalography (EEG) and functional magnetic resonance imaging (fMRI). I will first present an overview of the directed dynamical interactions between heart rate variability and the different EEG rhythms, then I will show which regions of the brain, and their interactions, are more influenced by heart rate, circulation and other autonomic parameters.

References

- Bashan A, Bartsch RP, Kantelhardt JW, Havlin S and Ivanov PC 2012 Network physiology reveals relations between network topology and physiological function. *Nat. Communicat.* **3**
- Faes L, Nollo G, Jurysta F and Marinazzo D 2014 Information dynamics of brain-heart physiological networks during sleep. *New J. Phys.* **16** 105005
- Chang C, Metzger CD, Glover GH, Duyn JH, Heinze HJ, Walter M 2013 Association between heart rate variability and fluctuations in resting-state functional connectivity. *NeuroImage* **68** 93-104

Daniele Marinazzo¹, Sebastiano Stramaglia²

[1] *Department of Data Analysis, Ghent University, Ghent, Belgium*

[2] *Department of Physics, University of Bari, Bari, Italy*

One of the key challenges in the study of complex networks is understanding the relation between structure and the collective dynamics stemming from it. This issue is of special relevance in neuroscience, where the question translates to how structurally distinct and distant brain areas dynamically interact [1], both in healthy and pathological conditions. Recent advances in diffusion imaging and tractography methods allow the noninvasive *in vivo* mapping of white matter cortico-cortical projections at relatively high spatial resolution [2], yielding a connection matrix of interregional *structural connectivity* (SC). With the same machines, brain activity is conveniently recorded with a noninvasive technique: functional magnetic resonance imaging (fMRI). Brain connectivity can thus also be investigated by looking at the statistical dependencies between time series of activity recorded at different sites: we talk in this case of *functional connectivity* (FC) [3]. Several studies have shown that SC and FC are closely related [4][5].

The intricate interplay between structure and function can be investigated by simulating spontaneous brain activity on structural connectivity maps. Recent studies [6][7][8][9][10] have implemented models of dynamical oscillators on the connectome structure [11]. These computational models vary from complex, biologically realistic spiking attractor models, describing the firing rate of populations of single neurons, over mean-field models of neuronal dynamics, down to the simple, biologically-naïf Ising model. All these studies agree that the best agreement of simulated functional connectivity with empirically measured functional connectivity can be retrieved when the brain network operates at the edge of dynamical instability. This state has been described as *balanced*, *metastable* or *critical*, and for the Ising model coincides with the maximum value of the heat capacity and of the susceptibility. In particular some studies showed that the resting activity exhibits peculiar scaling properties, resembling the dynamics near the critical point of a second order phase transition, consistent with evidence showing that the brain at rest is near a critical

point [12]; moreover the possible origin and role of criticality in living adaptive and evolutionary systems has recently been ascribed to adaptive and evolutionary functional advantages [13]. In [14] the large scale pattern of empirical brain correlations was compared with those from a large two-dimensional Ising model, showing that the match is optimal when the statistical system is close to the critical temperature. However, the Ising model on brain networks has so far been implemented only according to a spin dynamics in which magnetization is not preserved [15]. Another class of dynamics exists, in which the total magnetization is preserved: it is used to describe for example alloy systems, where the two different spin states naturally correspond to the two component atoms that comprise the alloy [16] and can be implemented via a pair exchange update rule [17]. If we consider the Ising model on the human connectome as a model of neural activity, the conservation of magnetization may be seen as a sort of homeostatic principle for the overall activity of the brain.

The question we address in this work is whether the introduction of a dynamics which conserves magnetization on the human connectome might improve the prediction of functional connectivity based on the structural connectivity between two brain regions, in particular under anesthesia. We show that the answer is positive, at least at the spatial scale examined here.

References

-
- [1] H.-J. Park and K. Friston, *Science* (New York, N.Y.) **342**, 1238411 (2013).
 - [2] O. Sporns, *Networks of the Brain* (2011) p. 412.
 - [3] H. H. Shen, *Proceedings of the National Academy of Sciences* **112**, 14115 (2015).
 - [4] M. P. van den Heuvel, R. C. W. Mandl, R. S. Kahn, and H. E. Hulshoff Pol, *Human brain mapping* **30**, 3127 (2009).
 - [5] A. M. Hermundstad, D. S. Bassett, K. S. Brown, E. M. Aminoff, D. Clewett, S. Freeman, A. Frithsen, A. Johnson, C. M. Tipper, M. B. Miller, S. T. Grafton, and J. M. Carlson, *Proceedings of the National Academy of Sciences of the United States of*

- America **110**, 6169 (2013).
- [6] C. J. Honey, O. Sporns, L. Cammoun, X. Gigandet, J. P. Thiran, R. Meuli, and P. Hagmann, Proceedings of the National Academy of Sciences of the United States of America **106**, 2035 (2009).
 - [7] J. Cabral, E. Hugues, O. Sporns, and G. Deco, NeuroImage **57**, 130 (2011).
 - [8] G. Deco, V. K. Jirsa, and A. R. McIntosh, Nature reviews. Neuroscience **12**, 43 (2011).
 - [9] G. Deco and V. K. Jirsa, The Journal of neuroscience : the official journal of the Society for Neuroscience **32**, 3366 (2012).
 - [10] G. Deco, M. Senden, and V. Jirsa, Frontiers in computational neuroscience **6**, 68 (2012).
 - [11] P. Hagmann, L. Cammoun, X. Gigandet, R. Meuli, C. J. Honey, V. J. Wedeen, and O. Sporns, PLoS biology **6**, e159 (2008).
 - [12] A. Haimovici, E. Tagliazucchi, P. Balenzuela, and D. R. Chialvo, Physical Review Letters **110**, 178101 (2013), arXiv:1209.5353.
 - [13] J. Hidalgo, J. Grilli, S. Suweis, M. A. Muñoz, J. R. Banavar, and A. Maritan, Proceedings of the National Academy of Sciences of the United States of America **111**, 10095 (2014).
 - [14] D. Fraiman, P. Balenzuela, J. Foss, and D. R. Chialvo, Physical review. E, Statistical, nonlinear, and soft matter physics **79**, 061922 (2009).
 - [15] R. J. Glauber, Journal of Mathematical Physics **4**, 294 (1963).
 - [16] P. L. Krapivsky, S. Redner, and E. Ben-Naim, *A Kinetic View of Statistical Physics*, Vol. 18 (Cambridge University Press, 2010).
 - [17] K. Kawasaki, Physical Review **145**, 224 (1966).

Atrioventricular coupling and ventricular interval regularity during atrial fibrillation: a frequency-dependent phenomenon

Michela Masè¹, Marcello Disertori^{2,3}, Massimiliano Marini² and Flavia Ravelli¹

¹University of Trento, Department of Physics, Trento, Italy

²Division of Cardiology, Santa Chiara Hospital, Trento, Italy

³Healthcare Research and Innovation Program, PAT-FBK, Trento, Italy

Background. Despite the importance of rate control therapies in patients with atrial fibrillation (AF), the determinants of ventricular activation during AF are still poorly understood. The ventricular rhythm during AF is the result of the complex interplay between an irregular and high-rate atrial activation and the peculiar conductive and refractory properties of the atrioventricular (AV) node. Recent works have redrawn attention on atrial rate as an important determinant of ventricular rhythm during atrial arrhythmias and AF (Climents A et al. 2010, Masè M et al. 2012, Corino A et al. 2013).

Aim. This study aimed to clarify the role of atrial rate on AV conduction dynamics and ventricular variability and regularity during AF. The task was accomplished by a combined analysis of atrial and ventricular activation time series, acquired during the first minutes of AF, where spontaneous changes in atrial rate are known to occur.

Methods. Atrial and ventricular time series were determined in ten patients during the spontaneous acceleration of the atrial rhythm in the first minutes after AF onset (Ravelli F et al. 2007). The dynamical properties of atrioventricular (AV) coupling were assessed by performing atrioventricular (AV) synchrogram analysis (Masè M et al. 2013). AV synchrogram analysis is an adaption to the atrioventricular conduction system of the analysis of phase synchronization in nonlinear oscillators (Schafer C et al. 1999, Lotric MB et al. 2000, Cysarz D et al. 2004). Specifically, a stroboscopic, beat-to-beat observation of the ventricular phase at the times of atrial activation was performed and instances of AV coupling of different $n:m$ orders (n atrial beats in m ventricular cycles) were automatically identified. A surrogate data approach was used to distinguish significant from background coupling instances (Schreiber T and Schmitz A 2000). AV coupling properties were quantified in terms of the percentage of coupled beats (p_c), the maximal length of coupled epochs (l_{max}) and the average conduction ratios ($CR=m/n$). Ventricular interval variability and regularity were assessed by traditional time domain variability indexes and entropy measures. Specifically, ventricular interval variability was quantified in terms of standard deviation (STD_{RR}), square root of the mean squared differences of subsequent intervals ($RMSSD$) and fraction of interval differences $> 10-90$ ms (pRR_{10} to pRR_{90}). Ventricular interval regularity was assessed by computing Sample Entropy (*SampEn*, Richman JS and Moorman JM 2000) for different embedding dimensions ($m = 1$ and 2), similarity threshold ($r = 0.15, 0.2, 0.25 \times STD_{RR}$) and data length N (50, 100, 150) consistent with the fast evolution of the arrhythmia. The indexes of AV coupling and ventricular interval variability/regularity were compared at the onset versus stabilization of the AF episode.

Results. A significant increase of atrial rate was observed from the onset to the stabilization of the AF episodes, which significantly affected both AV coupling properties and ventricular response. The shortening of atrial intervals from 183 ± 31 ms to 164 ± 25 ms ($p < 0.01$) determined transitions towards AV patterns with progressively decreasing m/n ratios (from $CR = 0.36 \pm 0.08$ to 0.32 ± 0.08 , $p < 0.05$), lower occurrence (from $p_c = 26.6 \pm 8.6$ % to 18.9 ± 5.6 %, $p < 0.01$) and higher instability (from $l_{max} = 4.0 \pm 1.6$ s to 2.8 ± 0.8 s, $p < 0.05$). Despite no global change in ventricular rate was observed, advanced levels of AV block and coupling instability at higher atrial rates were associated with increased ventricular interval variability and irregularity. In terms of variability, STD_{RR} increased from 101.7 ± 30.4 ms to $113.5 \pm$

36.1 ms ($p < 0.05$), *RMSSD* from 137.9 ± 44.7 ms to 156.6 ± 52.5 ms ($p < 0.05$) and *pRR10* from 0.89 ± 0.07 to 0.92 ± 0.05 ($p < 0.01$) passing from AF onset to AF stabilization. In terms of regularity, a significant increase of Sample Entropy at higher atrial rates was consistently observed for different series lengths and similarity thresholds at embedding dimension $m = 2$. In particular, *SampEn* increased from 1.70 ± 0.26 to 2.06 ± 0.28 ($p < 0.001$) from AF onset to stabilization for $N = 100$ and $r = 0.2 \times STD_{RR}$.

Conclusions. These results provide further evidence for the significant dependence of AV coupling and ventricular response on atrial rate during AF. Specifically the increase in atrial rate determines advanced levels of AV block and higher instability of AV coupling, which in turn result in an increased variability and irregularity of ventricular activation. Effects of atrial rate on nodal conduction and ventricular response should be taken into account in the conception of efficacious rate control strategies in AF. In addition, since higher variability and irregularity of ventricular response have adverse effects on hemodynamic regulation (Clark DM et al. 1997), acute changes in atrial rate occurring in the first minutes of AF may be associated with increased hemodynamic risks in AF patients and should be properly monitored.

References

- Clark DM, Plumb VJ, Epstein AE and Kay GN 1997 *J Am Coll Cardiol* **30** 1039-1045
- Climent AM, Guillem MS, Husser D, Castells F, Millet J, Bollmann A 2010 *Pacilectrpng Clin Electrophysiol* **33** 1510-1517
- Corino VD, Cygankiewicz I, Mainardi LT, Stridh M, Vasquez R, Bayes de Luna A, Holmqvist F, Zareba W, Platonov PG 2013 *Ann Noninvasive Electrocardiol* **18** 41-50
- Cysarz D, Bettermann H, Lange S, Geue D, van Leeuwen P 2004 *Biomed Eng Online* **3** 44
- Lotric MB, Stefanovska A 2000 *Physica A* **283** 451-461.
- Masè M, Glass L, Disertori M, Ravelli F 2012 *Am J Physiol Heart Circ Physiol* **303** H1219-1228
- Masè M, Glass L, Disertori M, Ravelli F 2013 *Biomed Sign Proc Contr* **8** 1008-1016
- Ravelli F, Masè M, Del Greco M, Faes L, Disertori M 2007 *J Cardiovasc Electrophysiol* **18** 60-65
- Richman JS, Moorman JR 2000 *Am J Physiol Heart Circ Physiol* **278** 2039-2049
- Schafer C, Rosenblum MG, Abel HH, Kurths J 1999 *Phys Rev E* **60** 857-870
- Schreiber T, Schmitz A 2000 *Physica D* **142** 346-382

Assessment of cardio-respiratory interactions and their stability in anesthetized patients under different mechanical ventilatory modes

Claudio Enrico Mazzucco¹, Andrea Marchi^{1,2}, Sergio Cerutti¹, Vlasta Bari³,
Beatrice De Maria^{1,4}, Carla Amadio⁵, Silvio Cravero⁵, Davide Ottolina⁶,
Tommaso Fossali⁶, Riccardo Colombo⁶ and Alberto Porta^{3,7}

¹*Politecnico di Milano, Department of Electronics Information and Bioengineering, Milan, Italy*

²*San Gerardo Hospital, Department of Emergency and Intensive Care, Monza, Italy*

³*University of Milan, Department of Biomedical Sciences for Health, Milan, Italy*

⁴*IRCCS Fondazione Salvatore Maugeri, Milan, Italy*

⁵*ASST Fatebenefratelli Sacco, Department of Clinical Engineering, Milan, Italy*

⁶*ASST Fatebenefratelli Sacco, Department of Intensive Care, Milan, Italy*

⁷*IRCCS Policlinico San Donato, Department of Cardiothoracic, Vascular Anesthesia and Intensive Care, Milan, Italy*

Introduction

Cardio-respiratory phase synchronization analysis provides indexes relevant to nonlinear interactions between cardiac and respiratory systems complementary to respiratory sinus arrhythmia (RSA). In this context, phase synchronization with a phase locking ratio (PLR) of $m:n$ is defined as a repetitive occurrence of m heartbeats at the same relative phases within n consecutive breathing cycles. In the present study, long-lasting and transient cardio-respiratory interactions were investigated in anesthetized patients under three different mechanical ventilation (MV) modes: i) pressure controlled ventilation (PCV); ii) pressure support ventilation (PSV); iii) neurally adjusted ventilatory assist (NAVA). Previous studies demonstrated [1] that PSV and NAVA modes assures a more physiological ventilation compared to PCV but how different MV modes affect cardio-respiratory phase synchronization is still unknown.

Experimental Protocol and Methods of Analysis

Electrocardiographic (ECG) and airway volume (AWV) signals were acquired from 15 patients (age: 46 ± 12 years, 9 males) at the Department of Intensive Care at the “L. Sacco” Hospital, Milan, Italy. The study was performed according to the Declaration of Helsinki and was approved by the local ethics committee. Written informed consent was provided by all subjects. ECG and AWV signals were acquired at 250 Hz sampling rate. The experimental protocol consisted of three randomized sessions of 30 minutes corresponding to three different MV modes: PCV, PSV and NAVA carried out over the same anesthetized patients. The level of sedation was similar for all subjects and was not varied between-experimental conditions. Detection of phase synchronization episodes was based on the study of cardio-respiratory synchrogram [2,3]. Briefly, the Hilbert transform was applied to AWV signal to estimate the respiration phase [4]. In the synchrogram the phase values of the AWV signal observed in correspondence of the R-wave peak on the ECG was drawn as a function of the cardiac beat number. In order to identify reliable cardio-respiratory interactions, a threshold was set as suggested in [5]. The quantification of cardio-respiratory coupling was assessed by the synchronization (SYNC) index, i.e. the percentage of beats in which it could be observed the most frequent PLR. Furthermore, an index able to track the PLR stability during each MV session was implemented by detecting the most frequent PLR inside a running window of 30 beats [5], by moving the running window beat-by-beat over the entire recording and by generating a PLR series. The number of changes in the PLR series was used to quantify the PRL

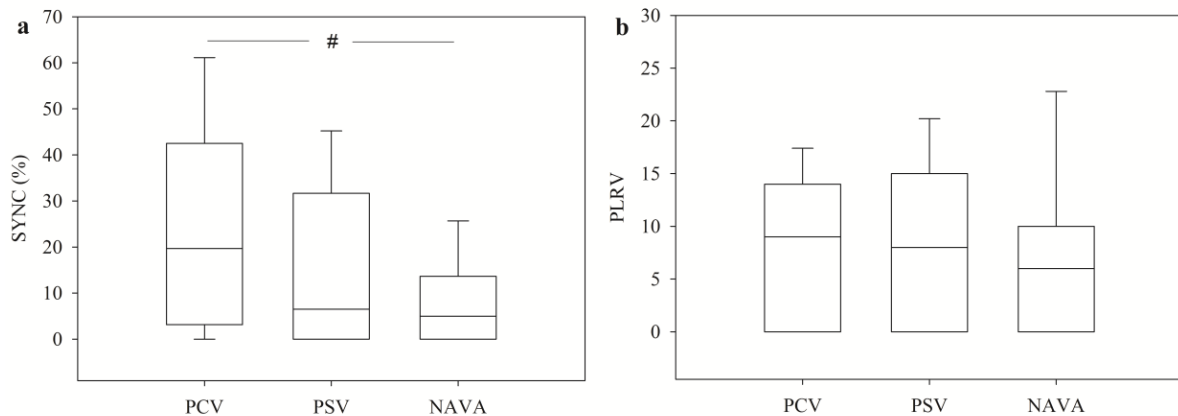


Figure 1. Box-and-whisker plots report the 10th, 25th, 50th, 75th and 90th percentiles of SYNC (a) and PLRV (b) as a function of the MV modes (i.e. PCV, PSV and NAVA). The symbol # indicates $p < 0.05$ vs PCV.

variability (PLRV) and the stability of phase synchronization. Finally, for each respiratory cycle, the difference between the longest and the shortest R-R interval on the ECG was taken as an estimate of RSA amplitude [6]. One way repeated measures analysis of variance (Student-Newman-Keuls test for multiple comparisons) was applied to check differences between experimental conditions. A $p < 0.05$ was considered as significant.

Results

RSA was not able to detect meaningful differences among the three experimental conditions (23 ms, 26 ms and 23 ms for PCV, PSV and NAVA respectively). SYNC index was 25%, 16% and 8% during PCV, PSV and NAVA respectively and the decrease during NAVA was significant compared to PCV (Fig.1a). In addition, we observed that PRLV was stable (8.3, 8.2 and 7 for PCV, PSV and NAVA respectively) regardless of the MV mode (Fig.1b).

Discussion and Conclusions

The reduction of RSA with MV and sedation [6] might be responsible for the inability of RSA to separate the diverse MV strategies. On contrary, SYNC was able to distinguish PCV from NAVA. In particular, large percentage of synchronization detected during PCV is coherent with the results presented in [7], where it was shown a synchronization enhancement under PCV. Both PSV and NAVA were characterized by lower percentage of synchronization than PCV and this percentage was more in keeping with that observed during spontaneous respiration in anesthetized subjects [6]. These findings support the hypothesis that, under paced ventilation with a fixed frequency, the interactions between cardiac and respiratory fluctuations were stronger than in the case of more physiological modes of MV (i.e. PSV and NAVA). Finally, PLRV index did not provide significant differences, thus suggesting that the three MV modes led to similar PLR stability. In future studies, the extension to longer epochs could be useful to check whether PRL stability was manifest for long period of time.

References

- [1] Spahija et al, 2010 *Critical Care Medicine* **38**, 518-526.
- [2] Schafer C et al, 1998 *Nature*, **392**, 239-240.
- [3] Stefanovska A et al, 2000 *Physica A*, **283**, 451–61.
- [4] Sola-Soler J et al, 2015 *Proc. Eng. in Med. and Biology Society*, 7708-7711.
- [5] Bartsch R et al, 2007 *Phys. Rev. Lett.*, **98**, 054102.
- [6] Larsen PD et al, 1999 *British Journal of Anaesthesia*, **82**, 546-550.
- [7] Prokhorov MD et al, 2003 *Phys. Rev. E*, **68**, 041913.

Electrostatic Basis of Selectivity in Biological Ion Channels

Peter V. E. McClintock¹, Robert S. Eisenberg², William A. T. Gibby¹,
Igor Kh. Kaufman¹, and Dmitry G. Luchinsky^{1,3}

¹*Department of Physics, Lancaster University, UK*

²*Department of Molecular Biophysics, Rush University, Chicago, IL, USA*

³*SGT Inc., Ames Research Center, Moffett Field, CA, USA*

It has long been clear that both electrostatics and dehydration must play important roles in the mechanisms that enable ions such as Na⁺, Ca²⁺ and K⁺ to pass, selectively, through the pores of cell membranes¹. The selectivity has been a particular puzzle because the disfavoured ions are selected against so strongly (by a factor of up to 1000×), but without significantly impeding the passage of the selected species.

The physical mechanism underlying this extraordinarily efficient selection process occurs in the channel's selectivity filter, a narrow region that contains protein residues carrying a fixed charge Q_f that varies between different kinds of channel. Although it has been evident that electrostatics, and therefore Q_f , are intimately associated with selectivity, the details remained obscure until recently.

It can now be appreciated², however, that valence selectivity (e.g. of Ca²⁺ over Na⁺) is governed by discrete electrostatic effects analogous to those that control electronic conduction in quantum dots³ and in artificial nanopores⁴, resulting in Coulomb blockade oscillations in all three cases. Coulomb blockade in ion channels means that there are certain values of Q_f for which a current can flow, and blockade points for which ions cannot permeate the channel.

To address this problem we have introduced a general statistical theory of the selectivity filter that takes account of both dehydration and electrostatic interactions. Let n_i^s be the number ions of the i -th type in the solution and n_i their number within the filter. We can introduce the Gibbs free energy of the solution+filter in the form

$$G = \sum_i (n_i^s - n_i) kT \ln x_i^s + \sum_i (n_i^s - n_i) \tilde{\mu}_i + \sum_i n_i \tilde{\mu}_i^c + kT \ln \left(\prod_i n_i! \right) + U(\{n_j\}, n_f),$$

where x_i is the mole fraction, $\tilde{\mu}_i$ and $\tilde{\mu}_i^c$ are the excess chemical potentials in the bulk and at a binding site, T is the temperature and U is the self-energy and the energy of electrostatic (and possibly other types) of interaction between the ions. Treating the filter+ions as excited states $\{n_j\}$ of the system, we can derive the following grand canonical ensemble for the filter (cf ⁵)

$$P(\{n_j\}) = \mathcal{Z}^{-1} \prod_{i=1}^m \frac{(x_i^s)^{n_i}}{n_i!} e^{\frac{\sum_i n_i \Delta \tilde{\mu}_i - \epsilon(\{n_j\}, n_f)}{kT}}.$$

where \mathcal{Z} is the partition function and $\Delta \tilde{\mu}_i = \tilde{\mu}_i - \tilde{\mu}$ is the dehydration energy.

In this presentation we focus on valence selectivity in relatively wide Ca²⁺ channels and consider the distribution for a single species ($n_i = n$). It is then possible to neglect the effects of dehydration and show² that the electrostatic energy of a channel with self capacitance C_s

$$U_n = \frac{(zne + Q_f)^2}{2C_s}$$

has quadratic dependences on both Q_f and n . Here z is the valence of the ion. As a result (ignoring hydration and concentration-related effects), we can show that there are singular points

$$\begin{aligned} Z_n &= -zen \\ M_n &= -ze \left(n + \frac{1}{2} \right) \end{aligned}$$

giving rise to Coulomb blockade, and resonant conduction, respectively. At the M_n points the potential barriers impeding conduction are of negligible height, and so the permeation process can be called “barrierless”.

Consequently, one may expect to see zero conduction at the Z_0 point where $Q_f = 0$, and then a periodic variation in the permeating current as Q_f is increased. Such effects can be seen clearly in Brownian dynamics simulations of a very simple model channel. In this picture, valence selectivity arises because the positions of the maxima and minima in the current depend on z . The magnitude of the Coulomb blockade effect, and hence the selectivity ratio, increase with z : Coulomb blockade for Na^+ is weak but observable, that for Ca^{2+} is very strong, and that for Ba^{3+} is even stronger.

The Coulomb blockade model of selectivity supposes that natural cation-selective channels provide values of Q_f corresponding to the resonant (barrierless conduction) points of the selected ions. The model provides natural explanations of several features of ion channels that had previously been puzzling. In particular, it explains the role of the fixed charge in the selectivity filter. In doing so, it accounts for: valence selectivity; for a range of earlier mutation experiments in which the nature of the selectivity (e.g. for Ca^{2+} or Na^+) was reversed by changing Q_f ; and for the anomalous mole fraction effect (AMFE) in which Na^+ passes easily through a Ca^{2+} channel in a pure Na^+ bath, but is blocked by tiny concentrations of Ca^{2+} .

The effect of dehydration can readily be included within this scheme to account for alike-charge selectivity between univalent ions (e.g. selectivity of K^+ over Na^+ in the KcsA channel), as will be discussed in detail in a separate presentation.

The research was supported by the Engineering and Physical Sciences Research Council UK (grant No. EP/M015831/1).

References

- [1] Hille, B., *Ion Channels Of Excitable Membranes* (Sinauer Associates, Sunderland, MA, 2001), 3rd edn.
- [2] Kaufman, I. K., McClintock, P. V. E. & Eisenberg, R. S., Coulomb blockade model of permeation and selectivity in biological ion channels, *New Journal of Physics* **17**, 083021 (2015).
- [3] Beenakker, C. W. J., Theory of Coulomb-blockade oscillations in the conductance of a quantum dot, *Phys. Rev. B* **44**, 1646–1656 (1991).
- [4] Krems, M. & Di Ventra, M., Ionic Coulomb blockade in nanopores, *J. Phys. Condens. Matter* **25**, 065101 (2013).
- [5] Roux, B., Statistical mechanical equilibrium theory of selective ion channels, *Biophysical Journal* **77**, 139–153 (1999).

Brain, Respiration, and Cardiac Causalities in Anæsthesia

Peter V. E. McClintock¹, Martin Hasler², Juergen Kurths³, Per Kvandal⁴, Svein Landsverk⁴, Dmitri G. Luchinsky¹, Milan Paluš⁵, Arkady Pikovsky³, Zvezdan Pirtošek⁶, Johan C. Ræder⁴, Samo Ribaric⁷, Michael Rosenblum³, Andrew F. Smith⁸, Aneta Stefanovska^{1,9}, and Niels Wessel³

¹*Department of Physics, Lancaster University, UK*

²*School of Computing & Communication Science, EPFL, CH-1015 Lausanne, Switzerland*

³*Institute of Physics, University of Potsdam, D-14469 Potsdam, Germany*

⁴*Department of Anæsthesiology, Oslo University Hospital, 0407 Ullevål, Oslo, Norway*

⁵*Institute of Computer Science, Academy of Sciences, Prague Czech Republic*

⁶*Department of Neurology, University Medical Centre, Ljubljana*

⁷*Institute of Pathophysiology, Faculty of Medicine, University of Ljubljana, Slovenia*

⁸*Department of Anæsthesia, Royal Lancaster Infirmary, Lancaster LA1 4RP, UK*

⁹*Faculty of Electrical Engineering, University of Ljubljana, Slovenia*

By the turn of the 21st century it had become clear that physiological oscillations may be used to characterise many states of the body¹, both in health and disease. One such state is anæsthesia, and there was already strong evidence that there were corresponding characteristic changes in cardiovascular, respiratory, and brain oscillations compared to the conscious state. It had been established that heart-rate-variability (HRV) changes² in human anæsthesia, and that the synchronisation ratio³ and direction of influence (directionality) between cardiac and respiratory oscillations⁴ in rats changes according to depth of anæsthesia. The FP6 BRACCIA (Brain, Respiratory and Cardiac Causalities in Anæsthesia) project was intended to investigate these changes, including alterations in the interactions between the different oscillations.

The main motivation was to understand the nature of the interactions between brain, cardiac and respiratory causalities in the awake state, and to establish how they change with two of the most frequently applied anæsthetics in humans and their equivalents in rats. We also wanted to characterise the two states, awake and anæsthetised, so that any new case can be classified easily, whence we can aim at generating a method/device for measuring depth of anæsthesia. The device in question will rely, not just on the state of the cardiovascular system, nor on the state of the brain, as do the majority of present-day devices. Rather, it is to combine knowledge about the states of both systems and their interactions. The underlying philosophy of the enterprise has been discussed by the BRACCIA Coordinator⁵.

Data were recorded in two hospitals (Oslo and Lancaster) for human subjects, and for rats (Ljubljana), and passed to a central database in Lancaster, from whence they could be downloaded by the analysis groups in Lausanne, Potsdam and Prague as well as in Lancaster.

Completion of the analysis has been a challenging task involving the development of new methods for time series analysis, but it is now coming to fruition^{6,7,8} as will be described in subsequent presentations. It should perhaps be emphasized that the author list above reflects the team on the original BRACCIA proposal. Inevitably, for a variety of reasons, including retirement, not all team members are still with the project; similarly, others joining the project later have made immense and crucially important contributions to its eventual success, as will be described.

This work was supported by the European Union as a NEST (New and Emerging Science and Technology) Project, No. 517133, “Brain, Respiratory and Cardiac Causalities in Anæsthesia” (BRACCIA), by the Engineering and Physical Sciences Research Council (EPSRC) UK (grant No. EP/100999X1) and in part by the ARRS Slovenia (program No. P20232).

References

- [1] Stefanovska, A. & Bračić, M., Physics of the human cardiovascular system, *Contemp. Phys.* **40**, 31–55 (1999).
- [2] Pomfrett, C. J. D., Barrie, J. R. & Healy, T. E. J., Respiratory sinus arrhythmia – an index of light anesthesia, *Brit. J. Anaesth.* **71**, 212–217 (1993).
- [3] Stefanovska, A., Haken, H., McClintock, P. V. E., Hožič, M., Bajrović, F. & Ribarič, S., Reversible transitions between synchronization states of the cardiorespiratory system, *Phys. Rev. Lett.* **85**, 4831–4834 (2000).
- [4] Musizza, B., Stefanovska, A., McClintock, P. V. E., Paluš, M., Petrovčič, J., Ribarič, S. & Bajrović, F. F., Interactions between cardiac, respiratory, and EEG- δ oscillations in rats during anaesthesia, *J. Physiol. (London)* **580**, 315–326 (2007).
- [5] Stefanovska, A., Coupled oscillators: Complex but not complicated cardiovascular and brain interactions, *IEEE Eng. Med. Bio. Magazine* **26**, 25–29 (2007).
- [6] Kenwright, D., Bernjak, A., Draegni, T., Dzeroski, S., Entwistle, M., Horvat, M., Kvandal, P., Landsverk, S., McClintock, P., Musizza, B., Petrovčič, J., Raeder, J., Sheppard, L., Smith, A., Stankovski, T. & Stefanovska, A., The discriminatory value of cardiorespiratory interactions in distinguishing awake from anaesthetised states: a randomised observational study, *Anaesthesia* **70**, 1356–1368 (2015).
- [7] Stankovski, T., Petkoski, S., Ræder, J., Smith, A. F., McClintock, P. V. E. & Stefanovska, A., Alterations in the coupling functions between cortical and cardio-respiratory oscillations due to anaesthesia with propofol and sevoflurane <http://dx.doi.org/10.1098/rsta.2015.0186>, *Phil. Trans. R. Soc. A* 20150186 (2016).
- [8] Stefanovska, A., McClintock, P. V. E., Ræder, J. & Smith, A. F., (Editors) *Nonlinear Dynamics of Anaesthesia: From Theory to Clinical Application*, to be published (Springer, Berlin, 2017).

Human whole-ventricle simulations of transmural reentry promoted by early afterdepolarizations in acute myocardial ischaemia

**Ana Mincholé,¹ Sara Dutta,¹ Ernesto Zacur,² T. Alexander Quinn,³ Peter Taggart,⁴
Blanca Rodriguez¹**

¹ *Department of Computer Science, University of Oxford, Oxford, United Kingdom*

² *Institute of Biomedical Engineering, University of Oxford, Oxford, United Kingdom*

³ *Department of Physiology and Biophysics, Dalhousie University, Canada*

⁴ *Institute of Cardiovascular Science, University College London, Barts Heart Centre, UK*

Acute ischemia is a major cause of sudden arrhythmic death, and increased mortality in ischemic patients was reported following administration of potassium current blockers (Waldo, 1996), which reduce the repolarization reserve. Pro-arrhythmic mechanisms of acute ischemia have been extensively investigated in animal models (Janse, 1989) rather than in human ventricles. Reentry around the ischemic region is the main mechanism, but in addition, electrotonic current flow, due to gradients in membrane potential in heterogeneous tissue, could promote the occurrence of repolarization abnormalities such as early afterdepolarizations (EADs) in acute ischemia (Verkerk, 2000). EADs have been shown primarily in single cells, whereas, in the coupled tissue, the propensity of EAD formation is greatly decreased (Weiss, 2010). Therefore, the conditions needed for EADs to be triggered by electrotonic currents in ischaemia are still unclear.

In this study, we constructed an anatomically-based biophysically-detailed human ventricles model to investigate the multiscale mechanisms of increased arrhythmic risk in acute myocardial ischemia for different degrees of potassium channel block. The human ventricular biophysically-detailed model was developed by integrating experimental data on the electrophysiological ionic alterations caused by coronary occlusion (Dutta, 2016). In order to investigate mechanistic implications of reduced repolarization reserve in acute ischemia, we considered three scenarios represented by 0%, 30% and 50% decrease of the rapidly activating delayed rectifier potassium current (IKr) conductance. Arrhythmic risk was evaluated by determining the vulnerable window (VW) for reentry following ectopy at the ischemic border zone. High performance computer multiscale simulations were conducted in the supercomputer HECTOR. Macro-reentry around the ischemic region is the main reentrant mechanism in the ischemic human ventricle, in agreement with experiments in animals.

30% IKr reduction results in prolongation of refractoriness by 4%, which counteracts the establishment of macro-reentry and reduces the VW for reentry by 23.5%. However, a further decrease in repolarization reserve (50% IKr reduction) is less anti-arrhythmic despite further prolongation of refractoriness. Simulations enable the identification of the underlying mechanisms: electrotonically-triggered EADs facilitate transmural reentry near the ischemic border zone under conditions of reduced repolarization reserve (see Fig 1). We further investigated the ionic mechanisms underlying the formation of EADs in the acutely-ischemic human ventricles, showing that a prolonged low amplitude electrotonic current injected during the repolarization phase may trigger EADs due to reactivation of the L-type calcium current gates.

Electrotonically-triggered EADs have been identified as a potential mechanism of increased arrhythmic risk and re-entry maintenance in the human ischaemic ventricles affected by potassium channel block.

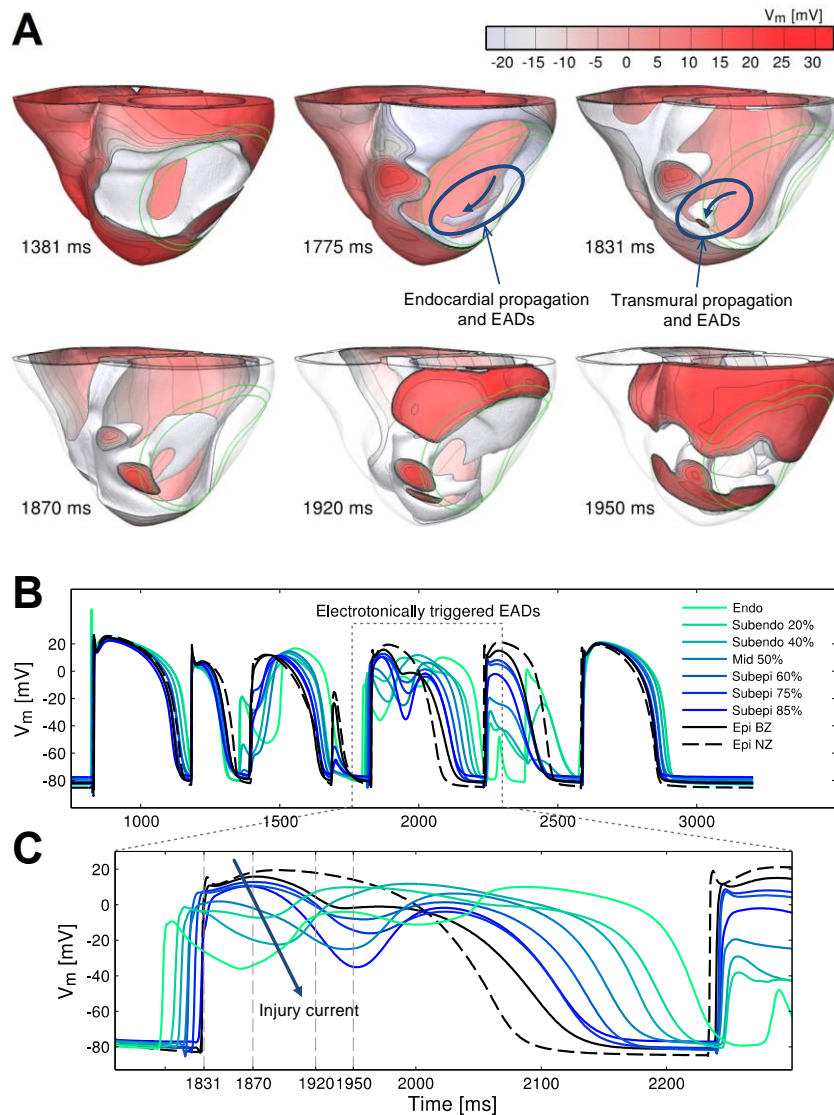


Figure 1. Human whole-ventricle simulations of arrhythmia mechanisms in acute myocardial ischaemia. **A.** Distribution of V_m throughout the ventricles at different timings following ectopic excitation resulting initially in macroreentry, but failure to support retrograde propagation (1381 ms), followed by propagation through the endocardial BZ (1775ms) and transmurally (1831ms), leading to EAD formation and intramural re-entry (1831-1950ms). Depolarized cells with V_m above -20mV are shown in colors, and cells with $V_m < -20$ mV are transparent. **B.** Time course of the AP revealing EAD formation transmurally from endo to epicardium in the area marked with a blue circle in panel A. **C.** Zoom in time of panel B to highlight EAD formation and V_m gradients. Legend indicates the transmural location corresponding to each action potential time course with % indicating transmural distance from the endocardium.

References

- Janse, M.J., Wit, A.L., 1989. *Physiol. Rev.* 69, 1049–1169.
- Verkerk, A.O., Veldkamp, M.W., de Jonge, N., et.al., 2000. *Cardiovasc. Res.* 47, 124–132.
- Weiss, J., Garfinkel, A., Karagueuzian, Chen, Qu, Z., 2010. *Heart Rhythm* 7, 1891–1899.
- Waldo, A.L., Camm, A.J., deRuyter, H., Friedman, P.L., et.al, 1996. *Lancet* 348, 7–12.
- Dutta, Minchole, Zacur, Quinn, Taggart, Rodriguez, 2016, *Progress in Biophysics and Molecular Biology*, <http://dx.doi.org/10.1016/j.pbiomolbio.2016.01.008>

Quasiperiodic and chaotic partial synchronization in populations of inhibitory neurons with delay

Ernest Montbrio

University Pompeu Fabra, Spain

We investigate the dynamics of a large network of oscillatory quadratic integrate and fire neurons. The neurons interact all-to-all via synaptic, time delayed excitation or inhibition. For identical neurons, time delays in synaptic connectivity induce collective synchronization or asynchronous states, for both excitatory and inhibitory networks. However, for inhibitory networks, and for certain time delays, the system sets into a state between full order and disorder: a so-called quasiperiodic partially synchronized (PS) state.

In this state, reported here for the first time in an inhibitory network, neurons fire quasiperiodically, while the macroscopic, firing rate dynamics of the network displays periodic, fast oscillations ($>90\text{Hz}$). Moreover, as inhibition is further increased, quasiperiodic PS may undergo a cascade of period-doubling bifurcations leading to a totally novel state, that we call chaotic PS, in which the population firing rate becomes chaotic.

Using the so-called Lorentzian Ansatz, we obtain the exact firing rate equations for a spiking neuron network with time delays. This allows us to find exact formulas for the stability boundaries of the network's macroscopic states. The resulting phase diagram for excitatory neurons closely resembles that of the Kuramoto model of coupled oscillators, with stereotyped regions of incoherence and synchronization alternating as time delay is increased. In contrast, the phase diagram for inhibitory networks differs from that of the Kuramoto model, revealing the presence of quasiperiodic and chaotic PS.

Dynamical criticality in the collective activity of a neural population

Thierry Mora

*Ecole normale supérieure and CNRS, Laboratoire de physique statistique, Paris,
France.*

The past decade has seen a wealth of physiological data suggesting that neural networks may behave like critical branching processes. Concurrently, the collective activity of neurons has been studied using explicit mappings to classic statistical mechanics models such as disordered Ising models, allowing for the study of their thermodynamics, but these efforts have ignored the dynamical nature of neural activity. I will show how to reconcile these two approaches by learning effective statistical mechanics models of the full history of the collective activity of a neuron population directly from physiological data, treating time as an additional dimension. Applying this technique to multi-electrode recordings from retinal ganglion cells, and studying the thermodynamics of the inferred model, reveals a peak in specific heat reminiscent of a second-order phase transition.

Physiological Oscillations and Health

Moser, M.

Medical University Graz and Human Research Institute, Weiz, Austria.

Oscillations of physiological parameters contain valuable information about body regulation and homeostasis and hence, health. Modern medicine has developed a multitude of methods to differentiate between different diseases, a procedure, that is called diagnosis, but, interestingly, has few tools available to determine the state of health of a subject. In medicine, a healthy subject usually is entitled “results negative” or “NAD” (nothing abnormal detected).

During a space medical project together with the Russian Institute for Biomedical Problems in Moscow we developed a health diagnosis program based on biological rhythms. Cosmonauts in space should never become sick, due to the high costs of a possible unscheduled return to earth. So an early warning system quantifying the state of health was requested.

Later, we transferred this system to the framework of a rehabilitation clinic in Austria and investigated patients during their return to health after a larger surgical procedure. Again, the determination of the amount and components of biological rhythms proved astonishingly indicative of the state and prognosis of the patients, which was followed for at least one year after surgery. The resulting “health guide system” provides orthogonal information about different aspects of health and is based on the occurrence and strength of biological oscillations present in heart rate variability as well as the results of psychometric questionnaires.

References

- Moser M¹, Frühwirth M, Penter R, Winker R.: 2006, *Cancer Causes and Control* **17 (4)** pp 591 -9
- Moser M¹, Frühwirth M, Kenner, T.: 2008, *IEEE Eng Med Biol Mag.*; 27(1) pp 29-37

Bioelectronic Central Pattern Generators for Cardiorespiratory Disease

Alain Nogaret

Department of Physics, University of Bath, Bath BA2 7AY

We report on the construction of biological models from the large scale assimilation of electrophysiological recordings of biological neurons. By applying a primal-dual interior point filter to a multichannel conductance model, we are able to extract the ion channel conductances, reversal potentials as well as parameters underpinning the nonlinear activation and kinetics of individual ion gates. The system of nonlinear equations incorporating the extracted parameters form completed models which we use to predict the neurons' response to arbitrary current protocols. The assimilation-prediction sequence is fully automated and treats all data points as equal quantities in contrast to methods which require arbitrary fitting objectives. We will present examples of the remarkable predicting power of nonlinear optimization and discuss the biological relevance of the completed models. The method is extended to making accurate models of biological central pattern generators such as those that control cardiorespiratory activity in the medulla. We will present hardware models of such central pattern generators we have constructed in the laboratory. These devices have successfully induced heart rate variability modulated by the respiratory rhythm in animal models of heart failure.

References

- L.Zhao, A.Nogaret (2015), *Physical Review E* **92**, 052910
C.D. Meliza et al. (2014), *Biological Cybernetics* **108**, 495
D.V. Vavoulis et al. (2012), *PLoS Computational Biology* **8**, e1002401
A. Nogaret et al. (2015), *J. Physiology* **593**, 763

A Method to Estimate Unbiased Partial Time-Frequency Spectra: Application to Repolarization Variability Changes Unrelated to Heart Rate Variability

Michele Orini¹ and Pier Lambiase¹

University College London, Institute of Cardiovascular Science, London, UK
Barts Heart Centre, St Bartholomews Hospital, London, UK

Introduction: The cardiovascular system should continuously adjust to an ever-changing environment in order to maintain blood pressure and supply. Therefore, cardiovascular signals are non-stationary and dynamically interacting. The study of these interactions, and the assessment of their temporal changes, is relevant to the understanding of pathophysiology and it may have clinical applications.

Time-frequency (TF) analysis has been applied to the study of these interactions [1]. Recently, partial TF spectra have been proposed to separate the variability of a given cardiovascular signal into two components: one showing local linear coupling with a second signal (characterized by a coherent TF spectrum), and another locally unrelated to this second signal (characterized by a conditioned TF spectrum). This methodology has been applied to study cardio-respiratory interactions [2] and to estimate QT variability unrelated to heart rate variability [3]. However, the TF partial spectrum may be inaccurate, because it is proportional to the TF coherence function, which is a biased estimator [1, 5]. In this work, we present a simple scheme to correct for this bias and improve the accuracy of TF partial spectra estimates.

Methods: The proposed methodology applies to systems that can be modeled as the sum of two single-input/output models [4], with uncorrelated inputs (Fig. 1). The function g that maps theoretical, $\gamma_0(t, f)$, to estimated, $\hat{\gamma}(t, f)$, coherence, i.e. $\hat{\gamma}(t, f) = g(\gamma_0(t, f))$, is empirically derived by calculating the coherence between random processes characterized by a known $\gamma_0(t, f)$. The inverse function of g is then used to compute corrected TF coherence estimates, i.e. $\tilde{\gamma}(t, f) = g^{-1}(\hat{\gamma}(t, f)) \approx \gamma_0(t, f)$.

ECG lead V4 from 16 healthy subjects undergoing a tilt table test were analyzed and QT and RR variability (QTV and RRV) were estimated [3]. The proposed scheme was implemented to estimate the TF coherence between QTV and RRV, and the TF partial spectrum representing QTV unrelated to RRV.

Results: In a simulation study where TF analysis was applied to random processes $y(t)$, $x_1(t)$ and $x_2(t)$ (Fig. 1) characterized by controlled coherence function, both $\hat{\gamma}_{y,1}(t, f)$ and partial powers $P_{y:1}(t)$ and $P_{y:2}(t)$, i.e. power of $y(t)$ related to $x_1(t)$ and $x_2(t)$, respectively, were biased (Fig. 2 left panels). The proposed correction completely removed this bias and provided accurate estimates $\tilde{\gamma}_{y,1}(t, f)$, $\tilde{P}_{y:1}(t, f)$ and $\tilde{P}_{y:2}(t, f)$ (Fig. 2 right panels).

In the studied population, mean TF coherence between QTV and RRV was 0.57 ± 0.15 before and 0.40 ± 0.21 after correction ($P < 0.0005$, Fig. 3 left), while the proportion of spectral power of QTV unrelated to RRV with respect to total QTV power, i.e. $P_{QTV/RRV}(t)$ divided by $P_{QTV}(t)$, was 0.38 ± 0.19 before and 0.46 ± 0.21 after correction ($P < 0.0005$,

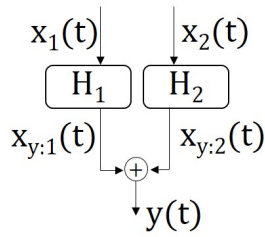


Figure 1: Model

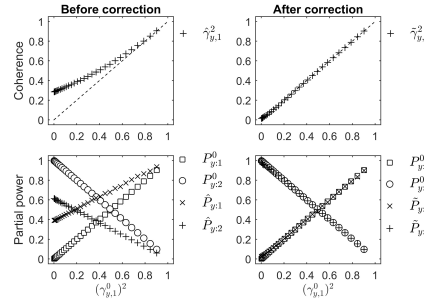


Figure 2: Simulation

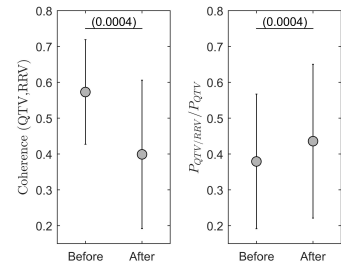


Figure 3: Tilt-table test.

Fig. 3 right).

Conclusion: In this study, a simple scheme to correct the bias of TF coherence and obtain unbiased TF partial spectra is proposed. The analysis of ECGs from healthy volunteers undergoing a tilt table test revealed that QTV unrelated to RRV estimated by means of unbiased TF partial spectra was about 20% higher than that estimated without correcting for the bias.

The proposed methodology improves the accuracy of cardio-respiratory and cardiovascular markers, and can provide a better tracking of changes of QTV unrelated to RRV.

References

- [1] M. Orini et al, Characterization of dynamic interactions between cardiovascular signals by time-frequency coherence. *IEEE Trans Biomed Eng*, 59(3):663–673, Mar 2012.
- [2] D. Widjaja et al, Cardiorespiratory dynamic response to mental stress: A multivariate time-frequency analysis. *Computational and Mathematical Methods in Medicine*, 2013:12, 2013.
- [3] M. Orini et al, A multivariate time-frequency approach for tracking QT variability changes unrelated to heart rate variability. *Conf Proc IEEE Eng Med Biol Soc*, Submitted:–, 2016.
- [4] J. Bendat and A. Piersol. Multiple-input/output relationships. In *Random Data*, pages 201–247. John Wiley & Sons, Inc., 2012.
- [5] K. Keissar et al. Coherence analysis between respiration and heart rate variability using continuous wavelet transform. *Philos Trans A Math Phys Eng Sci*, 367(1892):1393–1406, 2009.

Respiratory sinus arrhythmia: what is this oscillation good for?

Julian F.R. Paton

University of Bristol, School of Physiology, Pharmacology & Neuroscience, Bristol, UK

The healthy heart exhibits many rhythms of different frequencies from its diurnal rhythm to a frequency modulated by breathing. It is the latter I would like to focus on. A major component of heart rate variability (a prognostic indicator of good health) is respiratory sinus arrhythmia or RSA. Typically RSA comprises a slight acceleration during inhalation and a slowing of heart beat during expiration. The slowing is also associated with a reduction in force of contraction. Archers and riflemen fire their weapons on breathing out, which softens and slows the heart beat to improve their aim. RSA has withstood the test of evolutionary time as it is present in cartilaginous fish as well as Amphibia, Reptiles and man. It is exaggerated in youth and the physically trained but lost in many disease states. But what is the physiological function of RSA? There have been many suggestions including optimising ventilation perfusion of the lungs (Hayano et al.1996), cardiac energy saving and control of the arterial tension of carbon dioxide (Ben-Tal et al. 2012) and regulating output from both the left and right heart (Elstad 2012). I will present recent data that has tested the possibility that RSA improves cardiac output and coronary blood flow. I will show how we are planning to use RSA to treat conditions of congested heart failure. Using a novel silicon rhythm generator (Nogarte et al. 2013; O'Callaghan et al. 2016), I will describe how we are able to induce RSA in small and large animals and how there may be therapeutic benefit from harnessing RSA in conditions of heart failure, a condition in which RSA is lost. Whether this approach can be translated to humans awaits testing but we propose that reinstating RSA might form the basis of the world's first physiological pacemaker device.

References

- Ben-Tal, A., S. S. Shamilov and J. F. Paton (2012). Evaluating the physiological significance of respiratory sinus arrhythmia: looking beyond ventilation-perfusion efficiency. *J Physiol.* 590, 1989-2008.
- Elstad, M. (2012). Respiratory variations in pulmonary and systemic blood flow in healthy humans. *Acta Physiol (Oxf)* 205, 341-348.
- Hayano, J., F. Yasuma, A. Okada, S. Mukai and T. Fujinami (1996). Respiratory sinus arrhythmia. A phenomenon improving pulmonary gas exchange and circulatory efficiency. *Circulation* 94, 842-847.
- Nogaret A, Zhao L, Moraes DJ, Paton JF. (2013). Modulation of respiratory sinus arrhythmia in rats with central pattern generator hardware. *J Neurosci Methods.* 212, 124-132.
- O'Callaghan EL, Chauhan AS, Zhao L, Lataro RM, Salgado HC, Nogaret A, Paton JF. (2016). Utility of a novel biofeedback device for within-breath modulation of heart rate in rats: A quantitative comparison of vagus nerve vs. right atrial pacing. *Front Physiol.*7, 27.

Spatial distribution of time delays determines the synchronization of coupled oscillators

Spase Petkoski^{1,2}, and Viktor K. Jirsa¹

1 Aix-Marseille University, Institut de Neurosciences des Systèmes, Marseille, France

2 Aix-Marseille University, Institut des Sciences du Mouvement, Marseille, France

Network couplings of oscillatory large-scale systems, such as the brain, have a space-time structure composed of connection strengths and signal transmission delays. The latter are often considered a nuisance affecting the proper system functioning and can be mostly ignored when they are small with regard to the characteristic time scale of the system. In a number of systems though, foremost in the brain, the delays (10 to 200 ms) are on the same scale as the signal operation (10 to 250 ms) and contribute critically to the system's spatiotemporal organization. As the spatial distribution of the connection strengths affects the network dynamics, so does the spatial distribution of time delays. We provide a theoretical framework [1], which allows treating the space-time structure of network couplings with regard to synchronization, as one of the key mechanisms of brain function.

With the advance of non-invasive structural brain imaging [2], large-scale brain modelling approaches have become feasible using biologically realistic connectivity, the so-called connectome [3]. For each pair of brain regions it defines weights as numbers of individual tracts between them, whereas the lengths are averaged over the existing tracts. Upon analysis of experimental data [4], the results imply that the lengths of connection routes, and thereafter the time-delays, are bimodally distributed, Fig. 1. This insight suggests that the complex space-time structure of the connectivity maybe approximated by a less complex mode decomposition.

Assuming for simplicity bimodal- δ distributed delays, three delay-imposed architectures, Fig. 1, are analyzed: (i) random; and two spatial subpopulations, with (ii) identical internal and external delays, model A, and (iii) different internal and randomly, equally-distributed external delays, model B. Besides representing distinct phenomenological structures, these are motivated from the connectome. Its simplest decomposition on a left and a right hemisphere leads to model A, while other more complex divisions of the brain network could possibly identify patterns corresponding to the other two architectures, or their combination.

A common idealization for the study of synchronization is the Kuramoto Model (KM) [5]. Time delays appear explicitly in it as a canonical model for weakly delay-coupled oscillators for delays of same order as the inverse of the coupling strengths

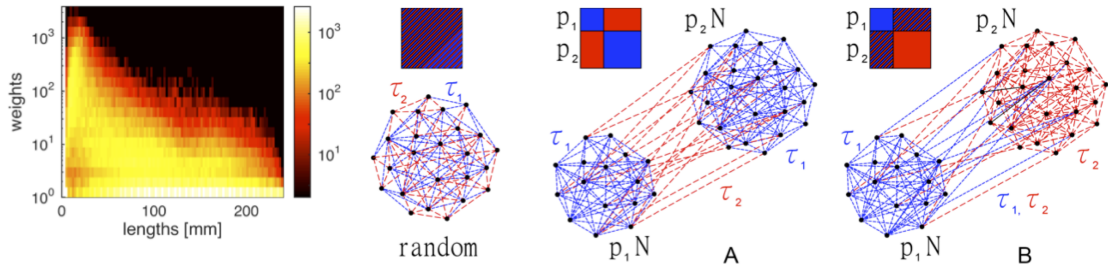


Figure 1: Joint distribution of tract lengths and weights from 1120 regions brain parcellation averaged for 4 healthy subjects, and sketch of a random and two delay-imposed structure and connectivity matrices (A and B)

and natural frequencies [6]. Hence we analyze KM with symmetric, link-dependent delays, whose dynamics is reduced using the Ott and Antonsen ansatz [7]. By decomposing the distribution of time delays into patterns, we reduce the stability analysis into the tractable problem of a finite set of delay-coupled differential equations, allowing analytical computation of the synchronization characteristics of the network. We find that depending on the architecture the oscillators group in phase-shifted, anti-phase, steady, and non-stationary clusters, and analytically compute their stability boundaries.

The regions of synchronizability are calculated at realistic frequency range, for the suggested delay structures. The obtained critical couplings differ by nearly 2 orders of magnitude depending on the frequency and the architecture. A relevant real-world example for these results is found in clinical neuroscience, where the reshaping of the distribution of time delays is common in neurodegenerative diseases such as multiple sclerosis, but also known to be critical in ageing and neuroplasticity.

References

1. Petkoski S, Spiegler A, Proix T, Aram P, Temprado JJ, Jirsa VK 2016 *in review*
2. Johansen-Berg H, Rushworth MFS 2009 *Annu. Rev. Neurosci.* **32**, 75
3. Sanz-Leon P, Knock SA, Spiegler A, Jirsa VK 2015 *Neuroimage* **111**, 385
4. Van Essen DC, Smith SM, Barch DM, Behrens TEJ, Yacoub E, Ugurbil K, W-M H Consortium, et al. 2013 *Neuroimage* **80**, 62
5. Kuramoto Y 1984, *Chemical Oscillations, Waves, and Turbulence* (Springer-Verlag, Berlin)
6. Izhikevich E 1998, *Phys. Rev. E* **58** 905
7. Lee WS, Ott E, Antonsen TM 2009 *Phys. Rev. Lett.* **103** 044101

Stochastic Spontaneous Calcium Release Events Trigger Premature Ventricular Complexes by Overcoming Electrotonic Load

Ferando O. Campos^{1,2}, Gernot Plank¹

¹*Medical University of Graz, Department of Biophysics, Graz, Austria*

²*German Heart Institute Berlin, Department of Congenital Heart Diseases and Pediatric Cardiology, Berlin, Germany*

Arrhythmias continue to be the leading cause of sudden death in adults. Premature ventricular complexes (PVCs) are believed to disrupt the regular beating of the heart and precipitate a variety of these arrhythmias¹. PVC formation has been associated to spontaneous calcium (Ca) release (SCR) events at the cell level². Experimental studies with isolated myocytes have shown that SCR events activate Ca-sensitive inward currents leading to transient delayed afterdepolarizations (DADs) in the diastolic phase of the cardiac cycle³. While such DADs may reach the threshold to trigger an action potential (AP) in isolated myocytes, this is not necessarily the case in tissue where myocytes are coupled via gap junctions to quiescent neighboring myocytes. In order for a DAD to form a PVC in the intact heart, SCR events must synchronize across many cells to produce sufficient depolarizing current to overcome the electrotonic source-sink mismatch⁴. However, the mechanism by which spatiotemporal synchronization of stochastic SCR events is achieved in tissue remains not well understood.

The aim of this study was to investigate the conditions under which DADs resulting from stochastic subcellular SCR events can summate to overcome tissue electronic load and initiate a PVC. We hypothesized that a critical diastolic Ca threshold in the sarcoplasmic reticulum (SR) exists above which PVCs emerge without the need for a mechanism to synchronize stochastic SCRs across cells. We further hypothesized that electrotonic loading conditions in structurally healthy ventricles favor the origin of the first DAD-induced PVC in the Purkinje system (PS).

To test these hypotheses, a stochastic subcellular-scale mathematical model of SCR was incorporated in a realistic model of the rabbit ventricles and PS. Elevated levels of diastolic SR Ca (CaSR) were imposed until triggered activity was observed, allowing us to compile statistics on probability, timing, and location of PVCs. At $\text{CaSR} \geq 1500 \mu\text{mol/L}$ PVCs originated in the PS. When SCR was incapacitated in the PS, PVCs also emerged in the ventricles, but at a higher CaSR ($\geq 1550 \mu\text{mol/L}$) and with longer waiting times. For each model configuration tested, the probability of PVC occurrence increased from 0% to 100% within a well-defined critical CaSR range; this transition was much more abrupt in organ-scale models

($\approx 50 \mu\text{mol/L}$ CaSR range) than in the tissue strand ($\approx 100 \mu\text{mol/L}$) or single-cell ($\approx 450 \mu\text{mol/L}$) models. Among PVCs originating in the PS, $\approx 68\%$ were located near Purkinje-ventricular junctions ($\leq 1 \text{ mm}$).

Using an anatomically accurate computer model of rabbit ventricles and His-Purkinje system, we found that SCR events overcome source-sink mismatch to trigger PVCs at a critical CaSR threshold. Above this threshold, PVCs emerge due to increased probability and reduced variability in timing of SCR events, leading to significant diastolic depolarization. Sites of lower electronic load, such as the PS, are preferential locations for triggering.

References

1. Nuyens D, Stengl M, Dugarmaa S, Rossenbacker T, Compernelle V, Rudy Y, Smits JF, Flameng W, Clancy CE, Moons L, Vos MA, Dewerchin M, Benndorf K, Collen D, Carmeliet E, Carmeliet P 2001 *Nat Med.* **7(9)** 1021-7.
2. Cerrone M, Noujaim SF, Tolkacheva EG, Talkachou A, O'Connell R, Berenfeld O, Anumonwo J, Pandit SV, Vikstrom K, Napolitano C, Priori SG, Jalife J 2007 *Circ Res.* **101** 1039-48.
3. Schlotthauer K, Bers DM 2000 *Circ Res.* **87** 774-780.
4. Campos FO, Shiferaw Y, Prassl AJ, Boyle PM, Vigmond EJ, Plank G 2015 *Cardiovasc Res.* **107(1)** 175-83.

Effects of aging on the redundancy of the cardiovascular control

Alberto Porta^{1,2}, Vlasta Bari¹, Andrea Marchi^{3,4}, Beatrice De Maria^{3,5},
Natália M. Perseguini⁶, Juliana Milan⁶, Vinícius Minatel⁶,
Anielle C.M. Takahashi⁶ and Aparecida M. Catai⁶

¹ *University of Milan, Department of Biomedical Sciences for Health, Milan, Italy*

² *IRCCS Policlinico San Donato, Department of Cardiothoracic, Vascular Anesthesia and Intensive Care, Milan, Italy*

³ *Politecnico di Milano, Department of Electronics Information and Bioengineering, Milan, Italy*

⁴ *San Gerardo Hospital, Department of Emergency and Intensive Care, Monza, Italy*

⁵ *IRCCS Fondazione Salvatore Maugeri, Milan, Italy*

⁶ *Federal University of São Carlos, Department of Physiotherapy, São Carlos, Brazil*

Introduction

Aging strongly affects cardiovascular control [1]. Indeed, the complexity of the spontaneous variations of heart period (HP) declines with age as a likely result of the vagal withdrawal reducing the respiratory sinus arrhythmia during senescence [1]. The influence of aging on cardiovascular control is detectable through the assessment of the magnitude of the interactions along predefined temporal directions via Wiener-Granger causality analysis as well [2]. For example, when respiration (R) is conditioned out, the strength of the dependence of systolic arterial pressure (SAP) on HP decreases with age and this finding was taken as an indication of the progressively increased exploitation of the mechanical properties of the heart compared to other mechanisms of SAP regulation (e.g. the diastolic run-off) [2]. Recently, joint transfer entropy (JTE) decomposition strategies [3-5] allowed one to decompose the information jointly transferred from a pair of exogenous sources to a target variable (i.e. the JTE) into quotes genuinely transferred from each exogenous variable to the destination one, the so-called conditional TEs (CTEs) from one exogenous signal to the destination given the other exogenous variable, and a term, the so-called interactive transfer entropy (ITE), describing the joint contribution of the two drivers to the information carried by the target. A negative ITE indicates that JTE is larger than the sum of the information transfer from the exogenous sources (i.e. the two drivers act in synergy because their contemporaneous presence generates genuine information transfer to the target), while a positive ITE points to the reverse situation (i.e. the drivers behave redundantly because the information transfer from the exogenous sources to the destination features duplicated parts) [4]. The aim of this study is to track changes of the redundant/synergistic contributions to cardiac and vascular control systems with age. Target variables such as HP and SAP are taken as descriptors of the cardiac and vascular control systems respectively, while pairs of variables such as {SAP,R} and {HP,R} are considered as sources of variability for the two control systems respectively. We hypothesised that redundancy/synergy varies during senescence and its monitoring may provide new clues about aging process.

Experimental Protocol and Data Analysis

We studied 100 nonsmoking healthy humans (54 males, aged from 21 to 70 years, 20 subjects for each 10 years-wide bin) [2]. ECG (lead I), continuous plethysmographic arterial pressure and respiratory movements via thoracic belt were acquired and sampled at 400 Hz. The experimental session consisted of two periods of 15 minutes: i) resting in supine position (REST); ii) active standing (STAND). The subjects breathed spontaneously and they were not allowed to talk. The study was performed according to the Declaration of Helsinki and

Table 1. JTE decomposition terms and their relation with age at REST and during STAND.

| JTE term | REST | | | STAND | | |
|------------------------------|--------|----------------------|----------|--------|----------------------|----------|
| | r_p | p | $p<0.05$ | r_p | p | $p<0.05$ |
| $CTE_{SAP \rightarrow HP R}$ | -0.048 | $6.38 \cdot 10^{-1}$ | No | -0.176 | $7.94 \cdot 10^{-2}$ | No |
| $CTE_{R \rightarrow HP SAP}$ | 0.028 | $7.85 \cdot 10^{-1}$ | No | -0.002 | $9.98 \cdot 10^{-1}$ | No |
| $ITE_{SAP,R \rightarrow HP}$ | -0.255 | $1.04 \cdot 10^{-2}$ | Yes | -0.154 | $1.27 \cdot 10^{-1}$ | No |
| $CTE_{HP \rightarrow SAP R}$ | -0.208 | $3.77 \cdot 10^{-2}$ | Yes | -0.268 | $7.09 \cdot 10^{-3}$ | Yes |
| $CTE_{R \rightarrow SAP HP}$ | -0.241 | $1.57 \cdot 10^{-2}$ | Yes | -0.223 | $2.59 \cdot 10^{-2}$ | Yes |
| $ITE_{HP,R \rightarrow SAP}$ | -0.107 | $2.91 \cdot 10^{-1}$ | No | 0.127 | $2.08 \cdot 10^{-1}$ | No |

r_p = Pearson product-moment correlation coefficient; p = probability of the type-I error; Yes/No = the variable is/is not significantly related to age with $p<0.05$.

was approved by the Ethics Committee of the Federal University of São Carlos. HP was derived as the temporal distance between two consecutive R-wave peaks and SAP as the maximum of arterial pressure inside HP. R was picked up from the R signal at the occurrence of the first R-wave delimiting HP. Stationary sequences of 256 HP, SAP and R consecutive values were analyzed [2]. CTE from SAP to HP given R ($CTE_{SAP \rightarrow HP|R}$), CTE from R to HP given SAP ($CTE_{R \rightarrow HP|SAP}$), CTE from HP to SAP given R ($CTE_{HP \rightarrow SAP|R}$), CTE from R to SAP given HP ($CTE_{R \rightarrow SAP|HP}$), ITE from SAP and R to HP ($ITE_{SAP,R \rightarrow HP}$) and ITE from HP and R to SAP ($ITE_{HP,R \rightarrow SAP}$) were computed according to the model-based linear approach set in [4]. Traditional linear correlation analysis of the abovementioned parameters on age was carried out. A $p<0.05$ was deemed as significant.

Results

$CTE_{SAP \rightarrow HP|R}$ and $CTE_{R \rightarrow HP|SAP}$ were unrelated to age both at REST and during STAND, while $CTE_{HP \rightarrow SAP|R}$ and $CTE_{R \rightarrow SAP|HP}$ were negatively correlated with age both at REST and during STAND (Tab.1). Both $ITE_{SAP,R \rightarrow HP}$ and $ITE_{HP,R \rightarrow SAP}$ were significantly larger than 0. The percentages of subjects with negative $ITE_{SAP,R \rightarrow HP}$ were 4% and 5% at REST and during STAND respectively, while those with negative $ITE_{HP,R \rightarrow SAP}$ were 9% and 17%. $ITE_{SAP,R \rightarrow HP}$ was negatively correlated with age at REST and unrelated to age during STAND, while $ITE_{HP,R \rightarrow SAP}$ was unaffected by age both at REST and during STAND (Tab.1).

Discussion and Conclusions

We confirmed that the information transfers from HP to SAP given R and from R to SAP given HP were negatively correlated with age, thus indicating a tendency toward the more important use of cardiac mechanics to control arterial pressure and the augmentation of the arterial stiffness during senescence [2]. Remarkably, this result was obtained using a different Wiener-Granger causality index compared to the one exploited in [2]. The original finding of this study is that SAP and R contributed redundantly to the cardiac control and the amount of SAP-R redundancy gradually declined with age, thus suggesting that its reduction might contribute to increase the cardiac frailty in old people. Conversely, the redundant contribution of HP and R to vascular control was unrelated to age, thus indicating that the maintenance of HP-R redundancy with age might contribute to the resilience of the vascular system to senescence process.

References

- [1] Beckers F *et al*, 2006 *Am. J. Physiol.* **290** H2560-H2570.
- [2] Porta A *et al*, 2014 *PLoS ONE* **9** e89463.
- [3] Stramaglia S *et al*, 2012 *Phys. Rev. E* **86** 066211.
- [4] Porta A *et al*, 2015 *Front. Physiol.* **6** 301.
- [5] Barrett AB, 2015 *Phys. Rev. E* **91** 052802.

Modeling study of cerebral blood flow redistribution during cortical spreading depression: tristable fronts and oscillatory vascular responses

Dmitry Postnov¹, Andrey Verisokin² and Darya Verveyko²

¹*Saratov State University, Department of Physics, Saratov, Russia*

²*Kursk State University, Department of Theoretical Physics, Kursk, Russia*

Cortical spreading depression (CSD) along with migraine waves and spreading depolarization events (SDE) at stroke or injuries are the front-line examples of extreme physiological behaviours of brain cortex, that manifest itself via the onset and spreading of localized areas of neuronal hyperactivity. Since discovery of CSD by Leao [1] more than 70 years ago it was believed that CSD and other spreading depolarization events are the artifacts produced in animal experiments and do not directly applicable for human neurological conditions, mostly due to the difficulty in detecting the brief and localized depolarization waves noninvasively. At present there is the increased evidence that CSD and SDE appear to be a pathophysiological mechanism for the group of acute neurological disorders in humans [2] and the detailed study of its mechanisms is still very relevant in a view of possible implications for treatment strategies, in order to minimize the neuronal damage in acutely injured human brain cortex caused by repeating SDEs.

It is well established, that CSD and SDE are accompanied by the considerable alterations in cerebral blood flow (CBF), see [3] and table therein. Being triggered by excessively high neuronal activity, the redistribution of CBF provides the attractive possibility to detect and monitor CSD and SDEs by means of noninvasive measurements using, say functional magnetic resonance imaging (fMRI) based on blood oxygen level dependent (BOLD) signal. However, it appears to be a challenge since the BOLD signal depends on neurovascular coupling (NVC) by which neurons control the local blood supply from the surrounding vasculature. NVC, in turn, acts as nonlinear regulatory pathway and might work differently in normal ageing and disease [4]. Moreover, it has been shown experimentally that blood vessels dilation and constriction can appear even ahead of the leading edge of CSD wave [5]. It suggests the existence of spatial coupling between different locations in cortex via the cerebral blood flow (CBF) redistribution. Note, there is the well established experimental evidence that the local increase of blood vessel radius may propagate both upstream and downstream in order to provide the demanded increase of blood supply. This is known as functional hyperemia [6,7]. Such conducted vasodilation provides the spatial coupling in a distance range up to 2 mm showing the exponential decay with distance [8] or the less studied non-decaying pattern [9]. Spatially synchronized local vascular responses, in turn, cause blood redistribution in tree-like vascular structures: if some location consumes more blood then the neighbors

will receive less. This type of flow-mediated coupling in kidney was considered in [10,11]. In brain cortex such *hemodynamic coupling* is much less studied.

In a view of all above, there is the need for better understanding of how the reciprocal interaction between the neuronal activity and CBF can affect their behavior. Along with experimental studies, this problem might be addressed by means of modeling of discussed above mechanisms at a functional (simplified) level with focus on dynamical mechanisms rather than on physiological details. We propose such computational model which is based on our previous work [9], but additionally counts the basic effects of neurovascular coupling and cerebral blood flow redistribution. Testing the model behavior, we focus on the main dynamical consequences of implemented pathways, such as changes in formation and propagation speed of CSD front and the pattern formation features in 2D. Our main findings are concerned with nature of CSD front, as well as with controversial contribution of CBF changes to dynamics. Namely, the transition of modeled neuronal tissue from normal excitable state to the abnormal and energy consuming persistent depolarization occurs through the third state, being the collective but locally asynchronized self-sustained firing. Depending on the choice of parameters that govern the neurovascular coupling rate and perfusion-dependent dissipation of extracellular potassium, our model shows different types of vascular responses that are consistent with previously reported experimental results. The most intriguing model predictions are the transient oscillations of blood vessel diameter that entail the propagated CSD front and may form the stationary patterns those spatial scale is governed by the the hemodynamic coupling parameters.

References

1. Leao, A.A.P., 1944. *J. Neurophysiol.* **7**, 359-390
2. Lauritzen M., Dreier J.P., Fabricius M., Hartings J.A., Graf R., Strong A.J., 2011, *Journal of Cerebral Blood Flow & Metabolism* **31**, 1735
3. Busija D.W., Bari F., Domoki F., Horiguchi .T, Shimizu K., 2008, *Prog Neurobiol.*, **86**, 379-95.
4. D'Esposito, M, Deouell, L.Y., Gazzaley, A., 2003, *Nat Rev Neurosci*, **4**, 863 - 872.
5. Brennan, K.C., Beltran-Parrazal, L., Lopez-Valdes, H.E., Theriot, J., Toga A.V., Charles, A.C., 2007, *J Neurophysiol* **97**, 4143 - 4151.
6. Gustafsson, F., and Nolstein-Rathlou, N.H., 1999, *Acta Physiol. Scand.*, **167**, 11-21.
7. Hill, C.E., 2012, *Microcirculation*, **19** , 379 - 390.
8. Crane, G. J., Neild, T.O., Segal, S.S, 2004, *Microcirculation*, **11**, 425 - 433.
9. Figueroa, X.F. et al. 2007), *Am. J. Physiol. Heart Circ. Physiol.*, **293**, H1371 - H1383.

10. Marsh, D.J. et al., 2013, *Am J Physiol Renal Physiol*, **304** F88F102.
11. Postnov D.D. et al. , 2012, *Bulletin of Mathematical Biology*, **74**, 2820 - 4110
12. Postnov, D. E., Postnov D.D., and Schimansky-Geier, L., 2012, *Brain Research*, **1434**, 200 -211.

ABSTRACT:

The discriminatory value of combining signals from brain, cardiovascular system, respiration and skin in distinguishing awake from anaesthetised states: a randomised observational study

J.Raeder ¹, A. Bernjak, ¹ T. Draegni, ² S. Dzeroski, ³ (M. Entwistle, ⁴) M. Horvat, ⁵ D.A. Kenwright ¹, P. Kvandal, ⁶ S.A. Landsverk, ⁶ P.V. E. McClintock, ⁷ B. Musizza, ⁸ S.Petkoski, J. Petrovčič, ⁹ J. Raeder, ¹⁰ L.W. Sheppard, ¹ A.F. Smith, ⁴ T. Stankovski, ¹ A. Stefanovska ¹¹

Background:

Most present commercial technologies on so called depth of anesthesia monitoring use one or two sources of physiological signals. None of them do so far report 100% sensitivity and specificity. In the present study we wanted to use a high number of different physiological signals and develop new methods on analyzing raw data, oscillation and coupling in order to achieve optimal prediction for the state of general anesthesia.

Methods:

In two institutions a total of 26 healthy patients were analyzed in the awake state and 29 in the non-stimulated state of general anesthesia with either propofol or sevoflurane as the only anesthetic drug. Continuous sampling was done on: EEG, ECG, respiration, temperature, pulse transit time and skin conductivity. The signals were analyzed for raw output, frequency distribution and variability, power of oscillations, wavelet phase coherence, wavelet phase synchronization, coupling strength and coupling functions

Results:

A total of 28 different physiological outputs were tested. With a best selection of 11 attributes, 9 from the EEG, 1 from ECG and 1 from respiratory rate we were able with 97% precision to distinguish the state of being awake from the state of general anesthesia. For the distinction between general anesthesia caused by either sevoflurane or propofol the precision was 87%.

Conclusions:

The combination of sophisticated analyses on EEG, ECG and respiration rate may provide a useful approach in the further strive for increased precision on monitoring depth of anesthesia with objective means.

Characterization of ventricular response during atrial fibrillation using a network model of the AV nodal function

Frida Sandberg and Mikael Wallman

*Lund University, Department of Biomedical Engineering, Lund, Sweden
Fraunhofer FCC, Gothenburg, Sweden*

The atrioventricular node (AVN) plays an important role during atrial fibrillation (AF) since it prevents the heart from racing by blocking atrial impulses. Anatomically and functionally the AVN consists of two pathways, referred to as the slow pathway (SP) and the fast pathway (FP), running in parallel to the bundle of His [1]. The FP has a faster conduction time and a longer refractory period than the SP, giving rise to the complex rate dependent properties observed in the AVN function [2]. These properties in turn influence the ventricular response during AF.

Here we fit a network model of the AVN to intracardiac data obtained from a patient in AF. The present model is a modified version of the model presented in [3] consisting of 21 nodes; an FP branch with 10 nodes and an SP branch with 10 nodes ending with one common node. The refractory time R_n and conduction delay D_n of the n :th node is assumed depend on the time from the end of the last refractory period until the new stimulation arrives t_n :

$$R_n = R_{min} + \Delta R(1 - e^{-t_n/\tau_R}), \quad (1)$$

$$D_n = D_{min} + \Delta D e^{-t_n/\tau_D}, \quad (2)$$

The model parameters R_{min} , D_{min} , ΔR , ΔD , τ_R and τ_D are shared between all nodes in the FP branch and the SP branch including the common node, respectively. To simulate conduction through the model, we assume that the outermost nodes of SP and FP are simultaneously activated by atrial impulses. We then employ a modified Dijkstra's algorithm, as described in [4], to compute arrival times of the impulses in all nodes while dynamically updating the R_n and D_n .

The model is fitted to data from the intracardiac atrial fibrillation database [5], consisting of simultaneous endocardial recordings from the right atria and surface ECG recordings. An atrial electrogram obtained close to the tricuspid valve annulus was selected due to its proximity to the AV node entrance. Following ventricular far field cancellation and standard preprocessing, atrial activations were detected using an iterative method [6]. The corresponding R peaks were detected from the ECG signals.

Using the series of detected atrial activations, the model is repeatedly fitted to the RR interval series 1000 times using a genetic algorithm. In the genetic algorithm,

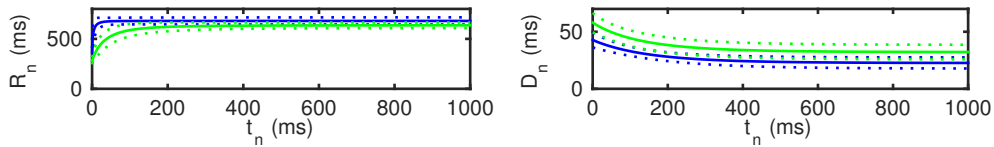


Figure 1: Mean \pm std of R_n and D_n for SP (green) and FP (blue).

populations of 500 individuals were used, with a survival rate of 10%. Populations were initiated with R_{min} and ΔR in the range $[10, 300]$, D_{min} and ΔD in the range $[0, 30]$, and τ_R and τ_D in the range $[20, 300]$. At each generation, 450 pairs of "parents" were selected, with selection probability inversely proportional to individual fitness. Using these 450 pairs, 450 new individuals were produced via random crossover, with equal probability of a given parameter being inherited from either parent. For each new individual, each parameter had a 10% chance of mutation, consisting of the parameter being resampled from the initial range. The algorithm was set to terminate when no improvement of the fittest individual occurred for 10 consecutive generations. The fitness function employed combines the mean square error between closest true and modeled R peak timings with a penalty for missing beats and extra beats in the simulated RR series. Additionally, a large penalty term was added for parameter sets which allowed either 1) the FP delay to become longer than the SP delay, or 2) the FP refractory time to become shorter than the SP refractory time.

The mean \pm std of the R_n and D_n curves corresponding to the resulting 1000 sets of fitted model parameters are displayed in Fig. 1. It can be noted that the R_n curve is steeper for FP than for SP, corresponding to significantly smaller values of τ_R . It can also be noted that the std of all curves are relatively small. The std of D_n is smaller for FP than for SP for all values of t_n , suggesting that the FP delay can be more accurately determined from the available data. The std of R_n increases at small values of t_n for FP and decreases at small values of t_n for SP, suggesting that the SP refractory period can be more accurately determined at these values of t_n from the available data.

References

- Kurian T, Ambrosi C, Hucker W, Fedorov VV, Efimov IR. 2010 *PACE* **33** 754-762
 Billette J, Tadros R. 2014 *Am J Physiol Heart Circ Physiol* **306** H173-83
 Wallman M, Sandberg F, 2015, *In Proc. CinC* **42** 477-480
 Wallman M, Bueno-Orovio A, Rodriguez B. 2013 *In Proc. CinC* **40** 711-714
 Goldberger A et al. 2000, *Circulation* **101** e215-e220
 Ng J, et al. 2014, *IEEE Trans Biomed Eng* **61** 273-278

Permutation entropy and its parametric estimation in heart rate variability analysis

Md Aktaruzzaman¹, George Manis², Roberto Sassi¹

¹*Università degli Studi di Milano, Dipartimento di Informatica, Italy*

²*University of Ioannina, Department of Computer Science and Engineering, Greece*

Entropy has been extensively used in the analysis of heart rate variability (HRV), and other time series in many scientific fields. Approximate Entropy and Sample Entropy are the two most common metrics, and a large number of research papers have been based on their descriptive and discriminating power. Both methods depend on two essential parameters: the dimension m of the space in which we look for similar vectors, and the threshold r used for testing similarity. The applicative results rely (sometimes significantly) on them, making the existence of these parameters a limit. Permutation Entropy (PE) [3] embodies a practical complexity metric which does not rely on the threshold r . Differently from ApEn and SampEn, which are estimates of the entropy rate of a stochastic process possibly underlying the time series, PE measures the (Shannon) entropy of the ranks of the elements composing the m dimensional vectors. The popularity of this metric has rapidly increased, and has been widely employed in biological time series [7]. Analytical expressions for permutation entropy do exist for *e.g.*: Gaussian, fractional Brownian, and autoregressive moving-average (ARMA) processes [2]. Autoregressive (AR) processes play a central role in the analysis of HRV, given the fact that they are routinely employed for maximum entropy estimate of the series power spectrum. Bandt & Shiha [4] provided expressions for PE of ordinal pattern derived from AR-generated series up to $m = 4$, while they are unavailable for longer patterns.

In this work, we show how to efficiently compute theoretical values of PE for ordinal patterns derived from AR-generated series for $m > 4$. In fact, in practical applications, values of m up to 7 are typically explored [7] (larger values are uncommon for data limitations). These theoretical values might then be employed effectively with, at least, two different objectives: i) to verify if the length of a series is suitable for a proper estimate of PE at a given m , by testing its convergence to the theoretical value on surrogate series generated through AR models fitted on the data; ii) to obtain estimate of PE with very short time series, using a parametric approach based on AR models (as done for spectral analysis and SampEn [1] of HRV).

Computing PE involves, as a first step, the computation of the probability mass function, for each of the possible $m!$ ordinal patterns of length m (avoiding the possibility that two or more elements are identical, as in [3]). While “there is no hope to get closed formulas” [4], this probability can be still assessed integrating numerically a multivariate normal cumulative distribution function $\mathcal{N}(\mathbf{x}, \mu = \mathbf{0}, \Sigma_{\mathbf{m}})$ in an efficient manner (*e.g.*, the algorithm `qsimvnr` [5]). This is simple to illustrate with an example. Let’s consider the ordering (2, 5, 4, 3, 1) for $m = 5$. Then

$$P(x_2 < x_5 < x_4 < x_3 < x_1) = \int_{-\infty}^{\infty} \int_{x_2}^{\infty} \int_{x_5}^{\infty} \int_{x_4}^{\infty} \int_{x_3}^{\infty} \mathcal{N}(\mathbf{x}, \mathbf{0}, \Sigma_{\mathbf{5}}) dx_1 dx_3 dx_4 dx_5 dx_2,$$

where Σ_5 is the 5×5 autocorrelation matrix of the AR process. The integral is challenging to evaluate directly. However, with the affine transformation

$$\mathbf{n} = \begin{bmatrix} n_1 \\ n_2 \\ n_3 \\ n_4 \end{bmatrix} = \begin{bmatrix} 0 & 1 & 0 & 0 & -1 \\ 0 & 0 & 0 & -1 & 1 \\ 0 & 0 & -1 & 1 & 0 \\ -1 & 0 & 1 & 0 & 0 \end{bmatrix} \begin{bmatrix} x_1 \\ x_2 \\ x_3 \\ x_4 \\ x_5 \end{bmatrix} = \mathbf{B}\mathbf{x}$$

the probability $P(x_2 < x_5 < x_4 < x_3 < x_1) = P(n_1 < n_2 < n_3 < n_4)$, and

$$P(n_1 < n_2 < n_3 < n_4) = \int_{-\infty}^0 \int_{-\infty}^0 \int_{-\infty}^0 \int_{-\infty}^0 \mathcal{N}(\mathbf{n}, \mathbf{0}, \mathbf{B}\Sigma_5\mathbf{B}^T) dn_1 dn_2 dn_3 dn_4.$$

The procedure can be extended to any permutation. Being any AR process time-reversible, at most $m!/2$ probabilities need to be estimated [4], but other symmetries, induced by the Toeplitz correlation matrix, can also be exploited to reduce further the computational load. Finally, PE is obtained as the Shannon entropy of the probability mass function, or more recently, as its Rényi entropy of order 2 [6].

We first tested the approach by simulating the AR model $x_n = 0.2x_{n-1} - 0.1x_{n-2} + w_n$ with $w_n \sim \mathcal{N}(0, 0.01)$, and then comparing the expected values of PE and those computed from realizations of the model. The average differences, for $m = 5$ and series length $N = 150, 300, 1000$ and 10000 , were 9.59%, 4.37%, 0.82% and 0.13% for permutation entropy, and 1.41%, 0.50%, 0.11% and 0.01% for permutation Rényi entropy of order 2 (RPE2), respectively.

Second, we considered RR series of length $N = 100, 300$ and 1000 , extracted at the beginning of each of the 54 long-term recordings contained in the Physionet's Normal Sinus Rhythm RR Interval Database (`nsr2db`). After artifacts removal, an AR model (of order $p = 9$) was fitted to each series and used to generate 40 synthetic series (with different realizations of white noise as input). Then, for each of them, values of permutation entropy were numerically assessed. Finally, we counted the number of times that the value of permutation entropy of the real series was within the 95% standard range of the synthetic ones. The agreement was remarkable, with a percentage at $m = 5$ and $N = 300$ of 77.8% and 79.6% for PE and RPE2, respectively. In future, we plan to extend the approach to further metrics, like conditional permutation entropy.

References

- [1] Aktaruzzaman M. and Sassi R. 2014 *Biomed. Signal Process. Control* **14**, 141–147
- [2] Amigó J. *Permutation Complexity in Dynamical Systems*. Springer Berlin Heidelberg, 2010
- [3] Bandt C. and Pompe B. 2002 *Phys. Rev. Lett.* **88**, 174102
- [4] Bandt C. and Shiha F. 2007 *J. Time Ser. Anal.* **28**, 646–665
- [5] Genz A. 1992 *J. Comput. Graph. Stat.* **1**, 141–149
- [6] Liang Z., et al. 2015 *Front. Comput. Neurosci.* **9**, 16
- [7] Riedl M., Müller A. and Wessel N. 2013 *Eur. Phys. J. Spec. Top.* **222**, 249–262

Risk stratification by means of HRV fractal methods: where we are

Roberto Sassi⁽¹⁾, Sergio Cerutti⁽²⁾, Federico Lombardi⁽³⁾, Marek Malik⁽⁴⁾

⁽¹⁾ Università degli Studi di Milano, Dipartimento di Informatica, Italy

⁽²⁾ Dipartimento di Elettronica, Informazione e Bioingegneria, Politecnico di Milano, Italy

⁽³⁾ UOC Malattie Cardiovascolari, Fondazione I.R.C.C.S. Ospedale Maggiore Policlinico, Dipartimento di Scienze Cliniche e di Comunità, Università degli Studi di Milano, Italy

⁽⁴⁾ St. Paul's Cardiac Electrophysiology, University of London, and Imperial College, UK

In the last three decades, the study of Heart Rate Variability (HRV) has been widely employed to noninvasively derive information about the functioning of the Autonomic Nervous System (ANS). Clearly, the technological advances in electrocardiology progressively fostered the widespread adoption of HRV analysis, with more reliable and not intrusive devices. In 1996, a joint effort of the European Society of Cardiology and the North American Society of Pacing and Electrophysiology set up a Task Force on HRV. The document then published [1] reported the consensus reached on “standards of measurement, physiological interpretation, and clinical use” of HRV (still as of March 2016 the 5th most cited paper in *Circulation*). Since then, several thousand papers were published either describing new methodologies for HRV analysis, or reporting HRV-related results obtained in a variety of different physiological and clinical conditions.

In 2012, the e-Cardiology Working Group of the European Society of Cardiology considered that it was time for an update to the 1996 recommendations, and therefor decided to initiate the process for a new consensus document. In particular, the objective was that of considering those new techniques, which had been developed meanwhile and had proven clinically effective. The European Heart Rhythm Association agreed to participate to the effort and the Asia Pacific Heart Rhythm Society co-endorsed the document, which was finally published in 2015 [2].

In this presentation, which acts as introduction to the session on fractal analysis of HRV series, we will present an overview of the results highlighted in the 2015 consensus document [2], with special focus on those methods, which characterizes long-range correlation and fractal scaling in heart rate variability.

References

[1] Task Force of the European Society of Cardiology and the North American Society of Pacing and Electrophysiology. Heart rate variability standards of measurement, physiological interpretation, and clinical use. 1996 *Circulation* **93** 1043–65.

[2] Advances in heart rate variability signal analysis: joint position statement by the e-Cardiology ESC Working Group and the European Heart Rhythm Association co-endorsed by the Asia Pacific Heart Rhythm Society. 2015 *Europace* **17** 1341–1353.

Advanced time-variant, non-linear approaches for analysing brain dynamics

Karin Schiecke, Diana Piper, Britta Pester, Lutz Leistriz and Herbert Witte

Institute of Medical Statistics, Computer Sciences and Documentation, Jena University Hospital, Friedrich Schiller University Jena, 07740 Jena, Germany

The detection and quantification of directed (causal) interactions within the brain and their time course are of highest interest in neuroscience. Different measures exist to define directed interactions between time series X and Y , the most popular are based on the concept of the Granger Causality (GC). Multivariate generalizations exist (Milde et al. 2010), partial directed coherence (PDC) allows time-variant and frequency-selective investigations (Leistriz et al. 2013). The Transfer Entropy (TE) (Schreiber 2000) is a model-free measure of information transfer. Comparison of both approaches can be found in (Faes et al. 2015). Convergent Cross Mapping (CCM) (Sugihara et al. 2012) defines interactions between time series X and Y in terms of non-linear stability. We present an investigation of non-linear interactions within the EEG and specific EEG components before, during and after an epileptic seizure in children with temporal lobe epilepsy (TLE). Linear AR modeling and therefore time-variant multivariate PDC analyses failed for these data. Aim of our study is to demonstrate potentials and limitations of CCM by applying it to clinical highly relevant data.

Basic idea of CCM is to test for causation between time series X and Y by looking at the correspondence between so-called shadow manifolds constructed from lagged coordinates of the time series values of X and Y . Contrary to intuition (and the concept of GC) the causality concept of CCM is that when causation is unilateral (' X drives Y '), then it is possible to estimate X from Y , but not Y from X . CCM correlation defined by the Pearson correlation coefficient between the original time series X and an estimation of X using the convergent cross mapping with Y quantifies interaction from time series X to Y (definition from Y to X respectively). For a pair of time series X and Y both values are compared to determine the directed bivariate CCM causality. To be able to investigate also time-varying causal interactions, an interval-based estimation can be performed by using a sliding window of an appropriate data length.

We investigated 18 children with TLE. For each child one recording was analyzed containing 5 minutes before and 5 min after the seizure onset (23 channels EEG, sampling frequency 256 Hz). Multivariate empirical mode decomposition preserving non-linearity of data was performed. Intrinsic mode functions (IMFs) were selected which are of most interest for our analysis (IMF4: δ -EEG band; IMF2: α -EEG band, Piper et al. 2015). Bivariate CCM analyses were performed for two different EEG areas (Fig. 1 A and Fig. 2 A) and all children: (1) T3 and T4 is investigated as "focus" and "no-focus" area (children with left side seizure: focus T3 / no-focus T4; for right side seizure: focus T4 / no-focus T3), and (2) T3 (T4 for right seizure) and Fp1 (Fp2 for right seizure) as "focus" and "far away" area. The same investigations were performed for IMF4 (δ -EEG-activity) and IMF2 (α -EEG-activity). For non-linear state space reconstruction, an embedding dimension of $D=16$ and a time lag $\tau=5$ were used. A time window of 4 s was adapted for interval-based analysis (sliding window approach).

The time courses of CCM between "focus" and "no-focus" (Fig. 1) reveal highest interactions in the δ -EEG band (blue line) and lowest in the α -EEG band (red line) in the pre-ictal period. With seizure onset CCM of EEG clearly increases (black line). The increase of CCM in the δ -EEG band is less pronounced. Both remain increased in the post-ictal period. CCM in the α -EEG band slightly increases with seizure but clearly decreases in the post-ictal period. The time courses of CCM between "focus" and "far away" (Fig. 2) replicate these results. The main difference is that modified interactions occur in the α -EEG band: CCM is lower during pre-ictal period, does not increase during seizure and does not drop in the post-ictal period

(red line). For all investigations, no differences in the direction of CCM (Fig. 1/ Fig. 2 B vs. Fig. 1/ Fig. 2 C) were found possibly revealing the generalized character of such a seizure.

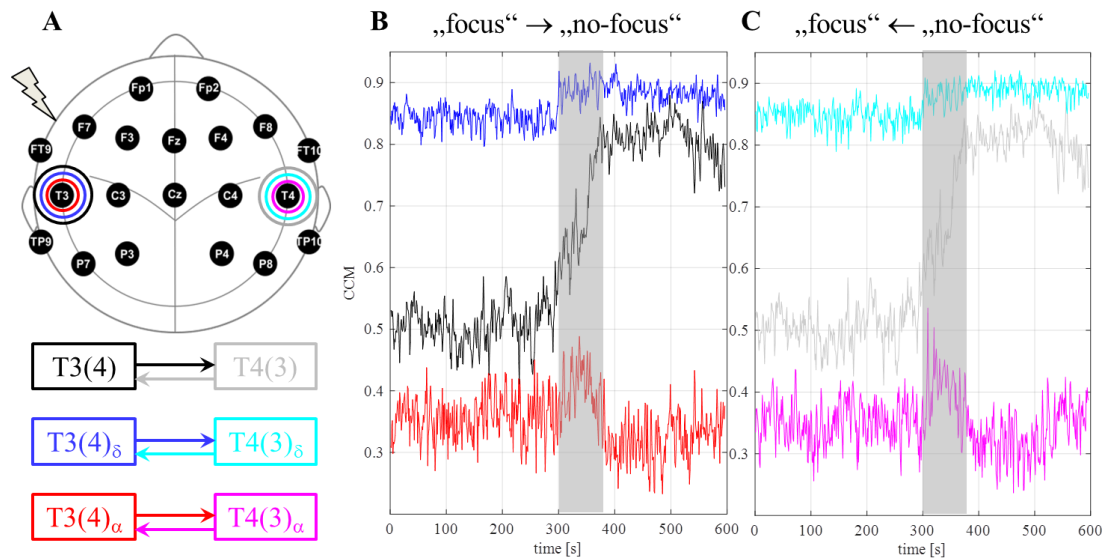


Figure 1 CCM analysis in the “focus” and “no-focus” area. **A)** depicts locations and investigated interaction schemes, in **B)** and **C)** both directions of interval-based results of CCM are shown (mean result over all children, color code according to A). Gray rectangle marks onset and median length of seizure.

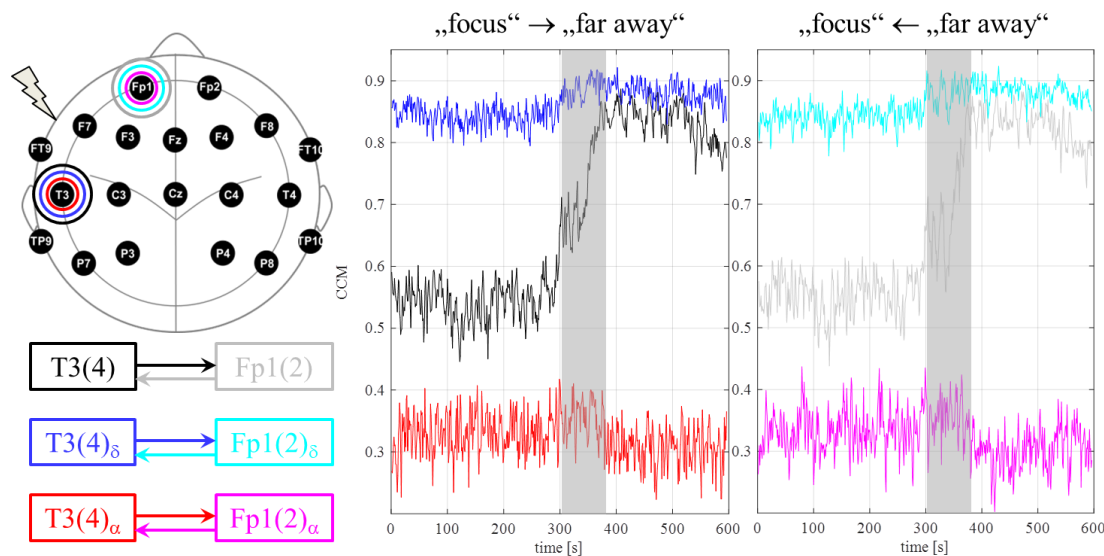


Figure 2 CCM analysis in the “focus” and “far away” area. **A)** depicts locations and investigated interaction schemes, in **B)** and **C)** both directions of interval-based results of CCM are shown (mean result over all children, color code according to A). Gray rectangle marks onset and median length of seizure.

In summary, the advantage of CCM is to reveal clear time pattern of non-linear interactions thereby possibly contributing to the further understanding of complex behaviour of the brain during TLE, but the limiting factor in the application of CCM is its bivariate implementation. This work was supported by the DFG under Grant Wi 1166/12-2 and Le 2025/6-2.

References

- Faes L, Marinazzo D, et al. 2015 *Physiological Measurement* **36** 683-698
- Leistritz L, Pester B, et al. 2013 *Philos Trans A Math Phys Eng Sci* **371** 20110616
- Milde T, Leistritz L, et al. 2010 *Neuroimage* **50** 960-969
- Piper D, Schiecke K, et al. 2014 *New Journal of Physics* **16** 115012
- Schreiber T 2000 *Physical Review Letters* **85** 461-464
- Sugihara G, May R, et al. 2012 *Science* **338** 496-500

**Fetal Heart Rate Regulation reflecting autonomic maturation –
Listening comprehension in the communication with the unborn child.**

**Uwe Schneider¹, Alexander Schmidt², Eva-Maria Dölcker², Susann Jaekel¹, Samuel
Nowack², Dirk Hoyer²**

Study Group ‘Prenatal Monitoring of Autonomic Maturation’

*1 Jena University Hospital, Department of Obstetrics, Division of Prenatal Diagnostics and
Fetal Physiology, Jena, Germany*

*2 Jena University Hospital, Biomagnetic Center, Hans Berger Department of Neurology,
Jena, Germany*

Developing the autonomic ability to adapt to varying amounts of supply and demand is one of the key necessities during fetal maturation. This maturational process of autonomic regulation in utero reaches a pace that may never be observed again later in life. We only start to anticipate that this maturation deems to be highly sensitive to acute and chronic influences with long-lasting consequences and one may assume that any disturbance of normal intrauterine development inevitably leads to changes in autonomic capacities. The exposition to synthetic steroids in utero leads to an acute suppression of sympathetic regulatory capabilities that wears off after about 48-72 hours [1]. The consequences of chronic placental insufficiency depend on the state of maturation at the time the disturbance becomes manifest [2].

Autonomic aptitude is mirrored in cardiovascular regulation. Considering the limitations of the fetus to adapt the single stroke volume owing to the small size of the heart in comparison to later extrauterine life, one may anticipate that the fetal heart rate (fHR) is not only the major continuous regulative of the developing autonomic nervous system (ANS) but the access point to understand fetal autonomic maturation.

Continuous antenatal heart rate tracing is based on two physical principles: Doppler ultrasound based cardiotocography (CTG) delivering a reasonable temporal resolution for daily clinical practice, i.e. to apply computerized analysis according to the Dawes/Redman algorithm and calculating the short-term variation (STV) [3]. In comparison to the CTG, electrophysiological methods such as fetal electrocardiography or fetal magnetocardiography (fMCG) are able to enhance the temporal acuity of fHR monitoring. The temporal resolution of the QRS complex detection enables precise fetal beat-to-beat heart rate variability (fHRV) analysis which is of particular advantage in resolving fast vagal activity and in the analysis of complexity measures of the fetal heart rate pattern (fHRP).

Besides the physiological changes with increasing gestational age (GA), the fetal neuro-behavioral state (state of fetal activity) must be taken into account when interpreting fHRP. Rest/activity cycles have been described from about 23 weeks GA onwards and the progressive synchronization of neuro-behavioral variables like fHRP, body movements and eye-movements are markers of developmental integrity of the fetus. Our results demonstrate increasing synchronization of coordinated movement – heart rate patterns and a reasonable

assessment of the apparent fetal neuro-behavioral state by visual expert assessment of the heart rate traces [4]. Further phenomena like fetal respiratory sinus arrhythmia (RSA) in association with thoracic movements and changes in the series of heart – beats due to the increasing size of the fetal heart have been accounted for by reasonable choice of fHRV parameters [5].

fHRV increases with increasing GA. Characteristic intervals of maturation appear: The transitional period between the second and the third trimesters of pregnancy is characterized by the appearance of physiological decelerations, a steeply enhancing vagal regulation followed by an increase in overall variability and complexity [5].

Beyond 30 weeks GA development is characterized by the diversification of fHRV parameters according to the stabilization of the fetal neuro-behavioural states and a strong relation between heart rate accelerations and intentional body movements. Both sympathetic activation and vagal modulation increase with increasing fetal age [6].

The ‘active awake’ fetal neuro-behavioral state marks a different quality of sympathetic activation that is characterized by a significantly higher mean fetal heart rate, a shift in sympatho-vagal balance and reduced complexity of the time series of heartbeats (sympathetic triad) [4]. fHRV inversely correlates with mean fetal heart rate [7].

We conclude that fetal autonomic development follows universal principles of maturation like increasing variability, increasing complexity and the formation of typical patterns. These phenomena qualify for further assessment of functional autonomic brain age and may be explored in clinical situations to help discriminating the impaired from the healthy fetus [8].

References

- [1] Schneider U, Arnscheidt C, Schwab M, Haueisen J, Seewald HJ, Schleussner E. Steroids that induce lung maturation acutely affect higher cortical function—a fetal magnetoencephalography study. *Reprod Science*, 18 (2011) 99-106.
- [2] Schneider U, Fiedler A, Liehr M, Kähler C, Schleussner E. Fetal heart rate variability in growth restricted fetuses. *Biomed Tech* 2006, 51: 248 – 250.
- [3] Seliger G, Stenzel A, Kowalski EM, Hoyer D, Nowack S, Seeger S, Schneider U. Evaluation of standardized, computerized Dawes/Redman heart-rate analysis based on different recording methods and in relation to fetal beat-to-beat heart rate variability. *J Perinat Med*. 2015 Nov 19. pii: /j/jpme.ahead-of-print
- [4] Schneider U, Frank B, Fiedler A, Kaehler C, Hoyer D, Liehr M, Haueisen J, Schleussner E. Human fetal heart rate variability-characteristics of autonomic regulation in the third trimester of gestation. *J Perinat Med*. 2008, 36, 433-441.
- [5] Hoyer D, Heinicke E, Jaekel S, Tetschke F, Di Pietro Paolo D, Haueisen J, Schleußner E, Schneider U: Indices of fetal development derived from heart rate patterns. *Early Hum Dev*. 85 (2009) 379-386.
- [6] Schmidt A, Schneider U, Witte OW, Schleußner E, Hoyer D. Developing fetal motor-cardiovascular coordination analyzed from multi-channel magnetocardiography. *Physiol Meas*. 2014 Sep 17;35(10):1943-1959.
- [7] Lange S, Van Leeuwen P, Schneider U, Frank B, Hoyer D, Geue D, Grönemeyer D. Heart rate features in fetal behavioral states. *Early Human Development*, 2009, 85: 131-135.
- [8] Hoyer D, Tetschke F, Jaekel S, Nowack S, Witte OW, Schleußner E, Schneider U. Fetal functional brain age assessed from universal developmental indices obtained from neuro-vegetative activity patterns. *PLoS One*. 2013 Sep 18;8(9):e74431.

Testing and interpreting coherence in biological fluctuations

Lawrence W. Sheppard¹, James R. Bell², Richard Harrington², Emma Defriez³, Philip C. Reid⁴, Vesna Vuksanovic⁵, Peter V.E. McClintock⁶, Aneta Stefanovska⁶, and Daniel C. Reuman^{1,7}

1. *University of Kansas, Department of Ecology and Evolutionary Biology and Kansas Biological Survey, Lawrence, USA*
2. *Rothamsted Research, Rothamsted Insect Survey, Harpenden, UK*
3. *Silwood Park, Imperial College London, UK*
4. *SAHFOS, The Laboratory, Plymouth, UK*
5. *Bernstein Center for Computational Neuroscience, Berlin, Germany*
6. *Lancaster University, Physics Department, Lancaster, UK*
7. *Rockefeller University, Laboratory of Populations, New York, USA*

In biophysical systems multivariate data is often autocorrelated and cross correlated and incorporates a number of different spectral components. Wavelet coherence methods can be used to evaluate the strength of statistical relationships between the fluctuations found in these signals. Examples include blood flow and temperature fluctuations in human skin [1], fluctuations in human blood pressure and skin conductivity during anaesthesia [2], and the ecological relationships between the different plankton species found in the North Sea [3].

Determining the statistical significance of apparent phase relationships in spatio-temporal data requires careful testing. We must test against a properly constructed distribution of possible coherence values consistent with the null hypothesis that no actual phase relationship exists between variables, but including the properties of spatial and temporal autocorrelation that are present in the data. This distribution depends on the frequency of the wavelet component under consideration, and on how its rate of phase growth varies over time [4].

We apply Fourier-phase-shuffled-surrogate based methods [5] to testing large spatio-temporal data sets for wavelet coherence. A method is described for testing wavelet coherence with a high degree of computational efficiency, exploiting the relationship between the Fourier and Morlet wavelet transforms. In this way we can robustly demonstrate relationships between paired timeseries (for example, fluctuations in abundance of two plankton species [3]) drawn from a large number of locations. The methods could also be applied to purely physical variables or biomedical timeseries drawn from multiple measurement sites on the human body.

References

1. Sheppard LW, Vuksanović V, McClintock PVE, Stefanovska A 2011 *Phys Med Biol* **56** 3583–3601
2. Kenwright DA, Bernjak A, Drægni T, Dzeroski M, Entwistle M, Horvat M, Kvandal P, Landsverk S, McClintock PVE, Musizza B, Petrovčič J, Ræder J, Sheppard LW, Smith AF, Stankovski T, Stefanovska A 2015 *Anaesthesia* **70** 1356-1368
3. Sheppard LW, Defriez E, Reid PC, Reuman, DC 2016 *In preparation*
4. Sheppard LW, Stefanovska A, McClintock PVE 2013 *Phys. Rev. E* **85** 046205
5. Prichard D, Theiler J 1994 *Phys. Rev. Lett.* **7** 951-954

Network Inference in the Presence of Latent Confounders: The Role of Instantaneous Causalities

Helen Shiells, Heba Elsegai, Marco Thiel and Björn Schelter

*University of Aberdeen, Institute for Complex Systems and Mathematical Biology,
Aberdeen, Scotland*

Detecting causal interactions in multivariate systems, in terms of Granger-causality, is of major interest in Neuroscience. Typically, it is almost impossible to observe all components of a measured system. Missing certain important components can lead to the appearance of spurious interactions. The aim of this study is to demonstrate the effect of these spurious interactions and to demonstrate that distinction between latent confounders and volume conduction is possible in some cases.

Our new method uses a combination of renormalised partial directed coherence to detect directed interactions and analysis of the (partial) covariance matrix of residual noise process to detect instantaneous instantaneous, both spurious and non-spurious. Sub-network analyses are then performed to infer the true network structure of the underlying system. We have used the modelling framework of vector autoregressive processes, in which past values of one process regress on to current values of another,

$$\mathbf{X}_i(t) = \sum_{r=1}^p \mathbf{a}(r)\mathbf{X}_j(t-r) + \epsilon(t), \quad (1)$$

this is an approach independent of phase. Renormalised partial directed coherence - essentially the Fourier transform of the coefficients of the VAR process - is a technique to infer Granger causal influences in multivariate networks, unencumbered by the breaking down of the phase locking index with increasing dimension.

We provide evidence that it is possible to distinguish between instantaneous interactions that occur as a result of a latent confounder and those that occur as a result of volume conduction.

Our novel approach demonstrates to what extent inference of unobserved important processes as well as the distinction between latent confounders and volume conduction is possible. We suggest a combination of measures of Granger-causality and covariance selection models to achieve this numerically.

Sub-network analyses enable a much more precise and correct inference of the true underlying network structure in some cases. From this it is possible to distinguish

between unobserved processes and volume conduction when measuring, among other things, biological oscillatory systems such as EEG networks. The numerical complexity of our novel approach increases with the number of nodes in the network, therefore a naïve application of our approach to large networks is infeasible. Conceivably, probabilistic concepts could guide the choice of links for investigation and the finding of motifs in larger networks in order to facilitate the application of this method to larger networks. Our approach is straightforwardly adaptable to various measures of Granger-causality emphasising its ubiquitous successful applicability.

References

- Elsegai. et al 2015 *Journal of Neuroscience Methods* **245** 91-106
Ramb. et al 2013 *Philosophical Transactions of the Royal Society A* **371** 20110612
Schelter. et al 2009 *Journal of Neuroscience Methods* **179(1)** 304-313
Eichler. 2005 *Philos. Trans. R. Soc. Lond. B. Biol. Sci.* **360** 953-967

Approximate and Identical Synchronization in Coupled Systems

Chih-Wen Shih

Department of Applied Mathematics

National Chiao Tung University

Hsinchu, Taiwan

We have established a framework for investigating approximate synchronization of coupled systems under general coupling scheme with delays [2]. The units comprising the coupled systems are allowed to be non-identical. In this lecture, we present this framework for the general coupled network system which comprises N subsystems:

$$\dot{\mathbf{x}}_i(t) = \mathbf{F}_i(\mathbf{x}_i^t, t) + \sum_{j \in \mathcal{N}} \omega_{ij}(t) \mathbf{G}_{ij}(\mathbf{x}_i^t, \mathbf{x}_j^t, t), \quad t \geq t_0, \quad i \in \mathcal{N},$$

where $\mathcal{N} := \{1, \dots, N\}$, and $\mathbf{x}_i(t) = (x_{i,1}(t), \dots, x_{i,K}(t)) \in \mathbf{R}^K$. Time delays in the range $[0, \tau_M]$, $\tau_M \geq 0$, are considered. For an $n \in \mathbf{N}$, denote by $\mathcal{C}([-\tau_M, 0]; \mathbf{R}^n)$ the set of continuous functions from $[-\tau_M, 0]$ to \mathbf{R}^n . The intrinsic dynamics of the i th subsystem is governed by $\mathbf{F}_i = (F_{i,1}, \dots, F_{i,K})$ which is a continuously differentiable function of $\mathbf{x}_i^t \in \mathcal{C}([-\tau_M, 0]; \mathbf{R}^K)$, with $\mathbf{x}_j^t(\theta) = \mathbf{x}_j(t + \theta)$ for $\theta \in [-\tau_M, 0]$. Coupling functions $\mathbf{G}_{ij} = (G_{ij,1}, \dots, G_{ij,K})$ are smooth functions. $\omega_{ij}(t)$ are bounded smooth functions of t , which represent the time-dependent connection weights from node j to node i , and $W(t) := [\omega_{ij}(t)]_{N \times N}$ is referred to as the connection matrix for the system. Herein, $(\mathbf{x}_1^t, \dots, \mathbf{x}_N^t)$ denotes the evolution of the system at time t from the initial condition $(\mathbf{x}_1^{t_0}, \dots, \mathbf{x}_N^{t_0}) \in \mathcal{C}([-\tau_M, 0], \mathbf{R}^{KN})$ at $t = t_0$, and $(\mathbf{x}_1(t), \dots, \mathbf{x}_N(t))$ is the state of the system at time t . This system reduces to ordinary differential equations if $\tau_M = 0$. Both delay-dependent and delay-independent criteria for approximate synchronization are derived, based on an approach termed sequential contracting.

Sequential contracting is an iterative argument for concluding asymptotic behaviors in dynamical systems [3, 4, 5, 6, 7]. With a preliminary estimation on the globally attracting set for the coupled system, the dissipative structure or degradation terms in the equations is utilized to estimate the attracting interval for each component of the system successively and iteratively. Analyzing the asymptotic behavior will then be converted into solving a linear system of algebra equations. Condition for the convergence of Gauss-Seidel iteration for this linear system will lead to synchronization criteria.

We shall show how the synchronization error, the distance between the asymptotic state and the synchronous set, decreases with respect to the differences between

subsystems and some factors in the coupling structure. This error vanishes when these factors decay to zero, and approximate synchronization becomes identical synchronization for the coupled system. Applications of the present theory to a model on segmentation clock genes and coupled FitzHugh-Nagumo neurons are illustrated.

The framework for identical synchronization of coupled systems via sequential contracting was reported in [3]. Approximate synchronization and asymptotic synchronization have been studied by Hale in [1].

References:

1. J. Hale, 1997, Diffusive coupling, dissipation, and synchronization, *J. Dynamics and Differential Equations*, **9**, No. 1, 1-52.
2. C.-W. Shih and J.-P. Tseng, 2016, From approximate synchronization to identical synchronization in coupled systems, preprint.
3. C.-W. Shih and J.-P. Tseng, 2013, A general approach to synchronization of coupled cells, *SIAM J. Appl. Dyn. Syst.*, **12**, 1354-1393.
4. C.-W. Shih and J.-P. Tseng, 2011, Global synchronization and asymptotic phases for a ring of identical cells with delayed coupling, *SIAM J. Math. Anal.*, **43**, no. 4, 1667–1697.
5. K.-L. Liao, and C.-W. Shih, 2011, Snapback repellers and homoclinic orbits for multi-dimensional maps, *J. Math. Anal. Appl.*, **381**, no. 1, 387–400.
6. A. Friedman, C.-Y. Kao, and C.-W. Shih, 2012, Asymptotic limit in a cell differentiation model with consideration of transcription, *J. Differential Equations*, **252**, no. 10, 5679–5711.
7. K.-L. Liao, C.-W. Shih, and J.-P. Tseng, 2012, Synchronized oscillations in a mathematical model of segmentation in zebrafish, *Nonlinearity*, **25**, no. 4, 869–904.

**Cerebral autoregulation: every normal subject is the average,
the rest is noise?**

**David M. Simpson¹, Dragana Nikolic¹, Emmanuel Katsogridakis² and
Ronney B. Pannerai²**

1. University of Southampton, Institute of Sound and Vibration Research, UK

2. University of Leicester, Department of Cardiovascular Sciences, UK

Cerebral autoregulation (CA) refers to the ability of the brain to maintain blood flow approximately constant, when blood pressure changes. The assessment of CA presents many challenges and often leads to considerable dispersion among CA measures even within groups of healthy adults. This results in great difficulty in setting a clear border between normal and impaired CA. The current work considers if the diversity of results seen in normal subjects is just "noise", or might provide useful information that could be exploited in developing more robust clinical assessment methods. In this paper we ask how between- and within-subject variability in CA compare, and how this changes between rest and a protocol with augmented variability in blood pressure. The latter was motivated by the previous observation that increased variability (unsurprisingly) leads to more robust estimates of the relationship between blood pressure and flow. In the current work, random inflations of thigh-cuffs (TC) were used to provoke this increased challenge to the CA system.

The study was performed on 28 normotensive volunteers with two recordings made on separate occasions. Arterial blood pressure (ABP) was measured with a servo-controlled finger cuff device, while the subject was in supine position. Cerebral blood flow velocity (CBFV) was recorded from the left and right middle cerebral arteries with a transcranial Doppler ultrasound held in place with an elastic head-band. The power of the blood pressure (P_p) and flow velocity (P_{v_L} , P_{v_R}) was estimated and the phase in the low frequency (LF) range [0.07-0.20] Hz (ϕ_{pv_L} , ϕ_{pv_R}) was found by transfer function analysis [Claassen, 2016]. Consistency of estimates was assessed using the intra-class correlation coefficient (ICC) and the between- and within-subject variability (σ_{bs}^2 , σ_{ws}^2) calculated from the variabilities of the sum and difference between two measurements (σ_{Σ}^2 and σ_{Δ}^2 respectively).

The results (Table 1) show that there is significant between-subject variability in P_p at baseline (BL) which cannot be explained by measurement error or other within-subject effects (as given by the difference between repeated measurements in each individual). For P_{v_*} , within-subject variability can explain all dispersion in measurements at BL – though, of course, that does not indicate that there is no significant between-subject variability which more repeated and extended measurements may reveal. The TC achieved the expected increase in ABP and CBFV variability, but only decreased the coefficient of variation (CoV) for ABP, not for CBFV. In that

Table 1: The between- and within-subject variability of the phase and the power of pressure and flow velocity. The units for variabilities correspond to the units for pressure power [mmHg²Hz⁻¹], flow velocity power [cm²s⁻²Hz⁻¹] and phase [°].

| | | ICC | CoV | σ_{Σ}^2 | σ_{Δ}^2 | σ_{bs}^2 | σ_{ws}^2 | $\frac{\sigma_{bs}^2}{\sigma_{ws}^2}$ |
|--------------|----|-----------------------|------|---------------------|---------------------|-----------------|-----------------|---------------------------------------|
| P_p | BL | 0.69 ^(a) | 0.98 | 1213.79 | 231.65 | 245.54 | 115.82 | 2.12 |
| | TC | 0.54 ^(b) | 0.56 | 2863.77 | 802.79 | 515.25 | 401.40 | 1.28 |
| P_{vL} | BL | 0.13 ^(ns) | 0.91 | 748.75 | 640.10 | 27.16 | 320.05 | 0.08 |
| | TC | 0.78 ^(a) | 0.83 | 7962.35 | 1020.51 | 1735.46 | 510.25 | 3.40 |
| P_{vR} | BL | 0.21 ^(ns) | 0.88 | 1274.45 | 846.23 | 107.05 | 423.12 | 0.25 |
| | TC | 0.78 ^(a) | 0.72 | 4558.80 | 582.81 | 994.00 | 291.41 | 3.41 |
| ϕ_{pvL} | BL | 0.32 ^(b) | 0.51 | 386.15 | 227.93 | 39.55 | 113.97 | 0.35 |
| | TC | 0.81 ^(a) | 0.29 | 333.60 | 35.90 | 74.42 | 17.95 | 4.15 |
| ϕ_{pvR} | BL | -0.05 ^(ns) | 0.37 | 292.30 | 324.75 | -8.11 | 162.38 | -0.05 |
| | TC | 0.72 ^(a) | 0.29 | 343.37 | 56.15 | 71.81 | 28.07 | 2.56 |

a) p -value $<5 \cdot 10^{-5}$, b) p -value $<5 \cdot 10^{-2}$, ns) not significant (p -value $>5 \cdot 10^{-2}$)

sense, the TC did not lead to more consistent results for CBFV. However, the ICC for CBFV did increase, linked to the greatly increased between-subject variability compared to that for the within-subject component. There are some outliers in this distribution (due to unusually large values in both measurements), which may have biased results – this further underlines the challenges that between-subject variability introduces when considering the "average" taken from normal subjects.

It is interesting to note that the effect of TC on CBFV is not entirely consistent with that on ABP and may indicate that the TC had an effect on the physiology not mediated directly through ABP, but could include other effects such as the mental state (e.g. sleepiness, attention) and thus cerebral metabolic activity and flow. While the initial motivation for using TC was to increase ABP variability within each session and thus provide a more robust and consistent challenge to CA, the impact of this and other protocols on the physiological state may be equally as important. Thigh-cuffs did lead to greatly reduced within-subject variability in CA (phase in LF) and a reduced coefficient of variation. It, however, did not reduce the between-subject variability which became the dominant component in CA estimates in normal subjects. Future efforts to find CA measures that are more robust thus need to focus on between-subject differences, not only aim to reduce the errors and dispersion within each measurement.

Acknowledgement: The authors gratefully acknowledge the support of EPSRC (UK) on projects EP/K036157/1, EP/G010420/ and EP/K036181/1.

References

Claassen JAHR, et. al. (2016) Transfer function analysis of dynamic cerebral autoregulation: A white paper from the International Cerebral Autoregulation Research Network, *Journal of Cerebral Blood Flow and Metabolism*, in press.

Using skewness and the first-digit phenomenon to detect dynamical transitions in cardiac arrhythmia

**Pavithraa Seenivasan, Soumya Easwaran, Seshan Sridhar and
Sitabhra Sinha**

¹ *Theoretical Physics Group, The Institute of Mathematical Sciences, Chennai, India.*

² *Scimergent Analytics and Education Pvt Ltd., Chennai, India.*

Arrhythmias, which are disruptions in the normal rhythmic functioning of the heart, often result from qualitative changes in the excitation dynamics of the organ. The transitions between different types of arrhythmia are accompanied by alterations in the spatiotemporal pattern of electrical activity that can be measured by observing the time-intervals between successive excitations of different regions of the cardiac tissue. Using biophysically detailed models of cardiac activity we show that the distribution of these time-intervals exhibit a systematic change in their skewness during such dynamical transitions. Further, the leading digits of the normalized intervals appear to fit Benford's law better at these transition points. This raises the possibility of using these observations to design a clinical indicator for identifying changes in the nature of arrhythmia. More importantly, our results reveal an intriguing relation between the changing skewness of a distribution and its agreement with Benford's law, both of which have been independently proposed earlier as indicators of regime shift in dynamical systems.

References

Seenivasan P, Easwaran S, Sridhar S, Sinha S 2016 *Front. Physiol.* **6** 390

RESPIRATORY SINUS ARRHYTHMIA BUFFERS VARIABILITY IN CEREBRAL BLOOD FLOW

Maria Skytjoti¹, Signe Søvik², Maja Elstad¹

¹University of Oslo, Division of Physiology, Institute of Basic Medical Sciences, Oslo, Norway

²Dept. of Anaesthesia and Intensive Care, Akershus University Hospital, Norway

Background: Respiration is one main source of cardiovascular and cerebral blood flow (CBF) variability in the high-frequency range. Respiratory sinus arrhythmia (RSA) has been shown to stabilize mean arterial blood pressure at the respiratory frequency by buffering changes in SV^{1,2}. The purpose of this study was to investigate the interrelation between respiration-induced heart rate (HR) oscillations (RSA) and blood flow to the brain. We hypothesized that a reduction in RSA would increase the respiration-induced variability in CBF. We examined CBF variability at rest and during the combination of mechanical ventilation and simulated hypovolemia which both reduce RSA^{2,3}.

Methods: Mean velocity in internal carotid artery (ICA) was recorded beat-by-beat using Doppler ultrasound in 10 healthy volunteers. While spontaneous respiration was substituted with positive pressure ventilation (PPV), a lower body negative pressure (LBNP) chamber was used to induce simulated hypovolemia. HR (electrocardiogram), MAP (Finometer), respiratory frequency and end-tidal CO₂ were also recorded. Beat-by-beat ICA blood volume (ICA BV, ml) and ICA blood flow (ICA BF, ml min⁻¹) were calculated from the velocity, ICA diameter and angle of insonation. Power density spectra were computed by the Fast Fourier Transform algorithm for all variables along 2 min of successful recording at rest and during PPV+LBNP. The integral under the curve of the power spectra was calculated around the peak respiratory frequency (peak RF \pm 0.03Hz), as an estimate of respiration-induced variability of HR, MAP and ICA BF. The interaction between cardiovascular variables was examined by computing phase angles and coherences from the cross-spectra at the peak RF \pm 0.02Hz. Median phase angles and confidence intervals were calculated using circular variance. Medians and 95% confidence intervals for the integrals and coherence between signals were calculated by Hodges-Lehmann's estimate. For testing statistical significances the Wilcoxon matched-pairs signed-rank test was used.

Results: The combination of PPV+LBNP decreased HR variability (from 4.1 bpm² (2.0-5.9) to 1.1 bpm² (0.4-1.5), p=0.01) and decreased ICA BV variability (from 0.042 ml² (0.013-0.062) to 0.009 ml² (0.004-0.012), p=0.013). In contrast, ICA BF variability increased from 14.0 ml² min⁻² (5.1-19.4) at rest to 29.1 ml² min⁻² (7.6-43.4) during PPV+ LBNP, (p=0.03). ICA BF variability during PPV+LBNP also demonstrated an increased oscillatory pattern around the RF, which was absent at rest. During spontaneous breathing and normovolemia, respiration-induced HR oscillations were in antiphase (median phase angle: 3.28 rad, 95% CI: 3.16-3.50) and highly coherent with ICA BV oscillations (median coherence 0.90, 95% CI: 0.80-0.97), demonstrating the respiratory component of CBF variability. During PPV+LBNP,

the phase angle between HR and ICA BV tended to increase (median: 3.77 rad, 95% CI: 3.15-4.71, $p=0.16$) and a reduction in coherence was observed (median: 0.65, 95% CI: 0.30-0.76, $p=0.01$). The coherence between MAP and ICA BF was lower than 0.5 during both conditions.

Conclusion: Respiration-synchronous ICA BV oscillations were in antiphase and closely related to HR oscillations at rest. Loss of coherence indicated dissociation between ICA BV and HR oscillations during PPV+simulated hypovolemia; this resulted in a more fluctuating ICA BF. Coherence between MAP and ICA BF remained low, suggesting that respiration-induced MAP fluctuations were not transmitted linearly to ICA BF. RSA seem to buffer CBF oscillations around the respiratory frequency. Increased variability in CBF was introduced during mechanical ventilation and simulated hypovolemia even though spontaneous cardiovascular and cerebrovascular respiratory variability was reduced. Challenges such as mechanical ventilation and hypovolemia may affect patient outcome in a clinical setting⁴⁻⁶ as increased CBF variability has been proposed to cause cerebrovascular pathology that involves disordered brain perfusion⁷.

References

1. Toska K, Eriksen M. Respiration-synchronous fluctuations in stroke volume, heart rate and arterial pressure in humans. *The Journal of physiology*. 1993;472:501-12.
2. Elstad M, Walloe L, Holme NL, Maes E, Thoresen M. Respiratory sinus arrhythmia stabilizes mean arterial blood pressure at high-frequency interval in healthy humans. *Eur J Appl Physiol*. 2015;115(3):521-30.
3. Elstad M, Walloe L. Heart rate variability and stroke volume variability to detect central hypovolemia during spontaneous breathing and supported ventilation in young, healthy volunteers. *Physiological measurement*. 2015;36(4):671-81.
4. Tatasciore A, Renda G, Zimarino M et al. Awake systolic blood pressure variability correlates with target-organ damage in hypertensive subjects. *Hypertension*. 2007;50(2):325-32.
5. Soehle M, Czosnyka M, Chatfield DA, Hoeft A, Pena A. Variability and fractal analysis of middle cerebral artery blood flow velocity and arterial blood pressure in subarachnoid hemorrhage. *Journal of cerebral blood flow and metabolism : official journal of the International Society of Cerebral Blood Flow and Metabolism*. 2008;28(1):64-73.
6. Nagata K, Sasaki E, Goda K et al. Differences in heart rate variability in non-hypertensive diabetic patients correlate with the presence of underlying cerebrovascular disease. *Clinical physiology and functional imaging*. 2006;26(2):92-8.
7. Tzeng YC, MacRae BA. Interindividual relationships between blood pressure and cerebral blood flow variability with intact and blunted cerebrovascular control. *Journal of applied physiology (Bethesda, Md : 1985)*. 2013;114(7):888-95.

BRACCIA: methodology and cardio-respiratory interactions

Andrew Smith on behalf of the BRACCIA investigators

Royal Lancaster Infirmary, Lancaster, UK

Depth of anaesthesia monitors usually analyse cerebral function with or without other physiological signals; noninvasive monitoring of the measured cardiorespiratory signals alone would offer a simple, practical alternative. We aimed to investigate whether such signals, analysed with novel, non-linear dynamic methods, would distinguish between the awake and anaesthetised state. We recorded ECG, respiration, skin temperature, pulse and skin conductivity before and during general anaesthesia in 27 subjects in good cardiovascular health, randomly allocated to receive propofol or sevoflurane. Mean values, variability and dynamic interactions were determined. Respiratory rate ($p = 0.0002$), skin conductivity ($p = 0.03$) and skin temperature ($p = 0.00006$) changed with sevoflurane, and skin temperature ($p = 0.0005$) with propofol. Pulse transit time increased by 17% with sevoflurane ($p = 0.02$) and 11% with propofol ($p = 0.007$). Sevoflurane reduced the wavelet energy of heart ($p = 0.0004$) and respiratory ($p = 0.02$) rate variability at all frequencies, whereas propofol decreased only the heart rate variability below 0.021 Hz ($p < 0.05$). The phase coherence was reduced by both agents at frequencies below 0.145 Hz ($p < 0.05$), whereas the cardiorespiratory synchronisation time was increased ($p < 0.05$). A classification analysis based on an optimal set of discriminatory parameters distinguished with 95% success between the awake and anaesthetised state. We suggest that these results can contribute to the design of new monitors of anaesthetic depth based on cardiovascular signals alone.

References

- Kenwright, D. A., Bernjak, A., Draegni, T., Dzeroski, S., Entwistle, M., Horvat, M., Kvandal, P., Landsverk, S. A., McClintock, P. V. E., Musizza, B., Petrovčič, J., Raeder, J., Sheppard, L. W., Smith, A. F., Stankovski, T. and Stefanovska, A. (2015), The discriminatory value of cardiorespiratory interactions in distinguishing awake from anaesthetised states: a randomised observational study. *Anaesthesia*, 70: 1356–1368. doi: 10.1111/anae.13208
- Kurata, J. (2015), Mining the hidden dysrhythmia - can machines get smarter at defining the anaesthetised state?. *Anaesthesia*, 70: 1338–1341. doi: 10.1111/anae.13314

Location-dependent microvascular response to thermal stimulation

Michele Sorelli, Leonardo Bocchi, Zlatka Stoyneva and Irina Mizeva

Univ. of Florence, Dept. Information Engineering, Italy

Univ. Hosp. St. Ivan Rilsky, Clinic of Occupational Diseases, Bulgaria

Russian Acad. of Sciences, Inst. Continuous Media Mechanics, Russia

Pathological alterations of the blood microcirculatory system are identified by measuring temporal and spectral properties of the blood flow and its variations caused by physiological stimuli. However a large variability of stimulation patterns (i.e. occlusive, temperature, orthostasis) and measurement location (glabrous and non glabrous skin, different extremities and so on) are observed. As concerns the stimulation patterns, most researchers focus on non-invasive stimulations, typically post-occlusive hyperemia, cold test, and local heating. A thermal stimulation elicits a complex response in the local microcirculatory system. In the temporal domain, two effects have been described [1]: a fast transient response, correlated to a neural activation, named axon reflex, and a slower plateau mediated by release of nitric oxide. Parameters describing this response, in turn, depends on the characteristics of stimulation, as maximum temperature, rise time, duration of the heating phase.

Moreover, recent investigations demonstrated that different locations present different reaction on the physiological provocations [2]. At the moment no consensus has been reached on the optimal location of the probes, on the selected stimulation pattern, and on the physiological parameter of interest.

The aim of this work is quantitatively evaluate the local response to the local heating for different locations. The study, thus, may contribute to the definition of a standardized measurement procedure, in dependence of the pathological condition of the subject and of the physiological parameter of interest.

Data recordings pertaining to control subjects were selected from preexisting data that involve analogous acquisition protocols in different anatomical positions, namely the forearm, the finger, and the toe. The selected stimulation pattern consists of a pre-heating phase, lasting 60s, where the baseline flow is measured, followed by heating at 43°C for 360s, and by a post-heating phase, where the temperature returns to equilibrium. The microcirculatory flow was measured by using a laser Doppler instrument, and mathematically modeled to extract a set of quantitative parameters. The signal has been low-pass filtered to remove the heart beat-related oscillations using a median filter on a span of 2.5s. The resulting average blood flow signal has been modeled using a mathematical function F composed of two terms representing the components of the physiological response: a Gaussian bell, modeling the axon peak, and a sum of exponentials, representing the NO-mediated activation [3]. The resulting function F is expressed as:

$$F(t) = a_1 e^{\frac{(t-b_1)^2}{c_1}} + a_2 (e^{-b_2 t} - e^{-c_2 t}) + k$$

where k represents the baseline flow, and the parameters (a_1, b_1, c_1) and (a_2, b_2, c_2) are the parameters, to be determined, describing the axon peak, and the NO activation, respectively. The parameters describing the model are thus related to the physiological or pathological alterations of the subject and to the measurement location, and they have been determined by fitting each curve using a least squares procedure, based on gradient descent. The average results, obtained on a preliminary data set, for the different locations are reported in Tab. 1.

Table I: Average and standard deviation of the curve parameters (superscripts mark statistically different elements in each column)

| Parameter | a_1 (AU) | b_1 (s) | c_1 (s) | a_2 (AU) | b_2 ($10^{-3}s^{-1}$) | c_2 ($10^{-3}s^{-1}$) | a_1/a_2 |
|-----------|----------------|---------------|------------------|--------------------|------------------------------|------------------------------|-------------------|
| Forearm | 112 ± 97^a | 62 ± 19^a | 68 ± 23^{ab} | 545 ± 396^{ab} | 1.6 ± 1.5 | 5.5 ± 2.5 | 0.50 ± 0.34^a |
| Toe | 202 ± 104 | 35 ± 37^a | 149 ± 50^a | 632 ± 492^a | 1.3 ± 0.5 | 3.9 ± 3.1 | 0.33 ± 0.30 |
| Finger | 266 ± 45^a | 23 ± 19 | 133 ± 49^b | 1494 ± 775^b | 1.4 ± 1.7 | 2.0 ± 2.0 | 0.26 ± 0.24^a |

Discussion

In all records we observed biphasic perfusion–time curve, which peculiarities were quantified by parameters of the fitting model. We obtained that local heating provokes a larger increase in blood flow in the finger than in the forearm and toe, and a significant difference in the axon reflex in the three sites. Firstly, this peak occurs much earlier in toe and finger than in forearm (parameter b_1 is twice larger for the forearm). Secondly, perfusion-time curve has a pronounced peak caused vasodilation in the forearm ($c_1 = 68s$) with a width twice broader than in finger and toe records. The NO mediated vasodilation is described by the second term of the model. The balance of axon reflex and NO mediated peaks (a_1/a_2) is very different for toe and finger. We do not see any significant difference for the b_2 parameter. So the character of the curve relaxation is not dependent from the region of data collecting. On the contrary NO mediated vasodilation rate is sensitive to the region of data collecting.

Results indicate that parameters, describing this curve are significantly different in these three regions. In future we plan to compare spectral behaviour as well.

This work was partly supported by the Russian Science Foundation under project No 14-15-00809.

References

- [1] Johson M., Kellog D. 2010 *J Appl Phys.*, **109** (2010), 1229-1238
- [2] Balaz D, Komornikova A, *et al*, 2015, *Vasa* **44(6)** 458-65
- [3] Bandini *et al*, 2013, *MVR*

Analysis of network states in large-scale brain models with an application to brain stimulation

Andreas Spiegler

Aix Marseille Universit, Institut de la Sant et de la Recherche Mdical, Institut de Neurosciences des Systmes UMR-S 1106, 13005, Marseille, France

To study the emergence of spatiotemporal brain activity, such as resting-state like patterns in fMRI, a whole human brain model can be composed based on experimentally derived information about the brain structure (e.g., white matter), the so-called connectome. The question arises whether and which qualitatively new states result from a large-scale network given the temporal description of each network node (e.g., brain area). To identify network effects, the network states due to systematic scaling of the connectome were compared to the node's repertoire (i.e., intrinsic dynamics). The results show how the network is using the node's repertoire but also how this network introduces new states. Furthermore, the analysis was performed for the biased network using a spatially distributed input, which represents brain stimulation. The results show how stimulation can alter the network states.

The Virtual Brain: Selective activation of resting state networks following focal stimulation

Andreas Spiegler¹, Anthony R. McIntosh², Viktor K. Jirsa¹

1 Aix Marseille Universit, Institut de la Sant et de la Recherche Mdical, Institut de Neurosciences des Systmes UMR-S 1106, 13005, Marseille, France

2 Rotman Research Institute of Baycrest Center, University of Toronto, Toronto, M6A 2E1, Canada

Imaging studies suggest that the functional connectivity patterns of resting state networks (RS-networks) reflect underlying structural connectivity (SC). If the connectome constrains how brain areas are functionally connected, the stimulation of specific brain areas should produce a characteristic pattern of activity ultimately resolving into RS-networks. To systematically test this hypothesis, we use TVB and systematically activate all possible brain areas with focal stimulation patterns and confirm that the stimulation of specific areas evokes network patterns that closely resemble RS-networks. Our results confirm that the brain is operating at the edge of criticality, wherein stimulation produces a cascade of functional network recruitments, collapsing onto a smaller subspace that is constrained in part by the anatomical short-range and long-range SCs. We suggest that stimulus-induced brain activity, which may reflect information and subsequent cognitive processing, follows specific routes imposed by connectome features, and that these routes explain the emergence of RS-networks.

Cardiovascular and Brain Coupling Functions in Anaesthesia

Tomislav Stankovski^{1,2}, Spase Petkoski^{3,4}, Andrew F. Smith⁵, Johan Raeder⁶, Peter V. E. McClintock¹ and Aneta Stefanovska¹

¹*Department of Physics, Lancaster University, Lancaster, UK*

²*Faculty of Medicine, Ss Cyril and Methodius University, Skopje, Macedonia*

³*INS UMR-S 1106, Aix-Marseille Universit, Marseille, France*

⁴*ISM UMR 7287, Aix-Marseille Universit, Marseille, France*

⁵*Department of Anaesthesia, Royal Lancaster Infirmary, Lancaster, UK*

⁶*Department of Anaesthesiology, Oslo University Hospital, Oslo, Norway*

General anaesthesia has a very important role in many surgical procedures, for which it has a big impact on human health. However, the precise mechanisms underlying the anaesthesia are still not fully understood and there are number of open questions. To address some of them, we have studied general anaesthesia induced by the widely-used (intravenous) propofol and (inhalational) sevoflurane anaesthetics, computing cross-frequency coupling functions between brain, cardiac, and respiratory oscillations in order to determine their mutual interaction mechanisms [1].

The undesirable consequences of overdose or unintended awareness in general anaesthesia [2] might in principle be made better or avoided to some extent by improved control if we could understand better the changes in function [3] that occur during general anaesthesia, in particular the dynamical brain states [4, 5], the dynamics of cardiovascular oscillations [6], and their mutual interactions [3].

We applied a novel methodology based on the analysis of phase *coupling functions* which prescribe the physical rule specifying how the inter-oscillator interactions occur. The coupling functions offer a unique means of describing mechanisms in a unified and mathematically precise way. Recently much progress has been made on the theory and methods which are able to extract and reconstruct the coupling functions between interacting oscillations from data, leading to useful applications in cardiorespiratory interactions [7–9], chemistry [10], and communications [11].

We used a method based on dynamical Bayesian inference [7, 12] to identified and analyzed the coupling functions for six significant relationships, including the δ - α , θ - γ , α - γ , respiratory- θ , cardiac- θ and cardio-respiratory coupling. The δ - α coupling function (Fig. 1) that was very low, not significant and unstable for awake, was greatly affected by propofol and especially by sevoflurane anaesthesia showing a stronger and well defined coupling functional form, depending and changing predominantly along the δ -axis. Fig. 2 shows a quantitative measure ρ of how much the forms of the coupling functions were similar [8], irrespectively of their strength. The *anaesthesia had opposite effects* on

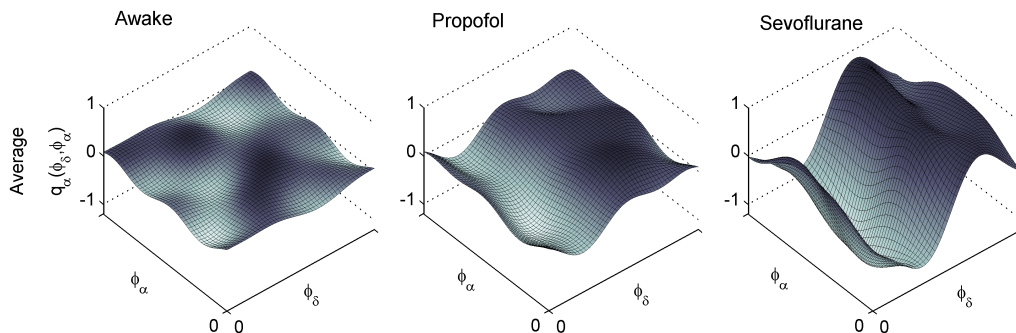


Figure 1: Cross-frequency coupling functions between δ and α brain oscillations. Average coupling functions from all subjects within the group, (left to right) for *Awake*, *Propofol* and *Sevoflurane* state.

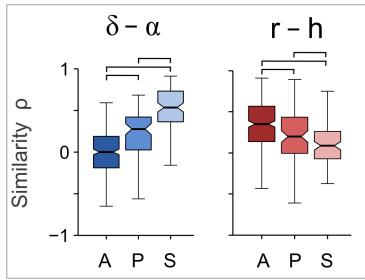


Figure 2: Effect of anaesthesia on the form of the coupling functions. The similarity of functional forms as the correlation coefficient ρ for two coupling relationships: (left) δ - α and (right) r - h , for the awake (A), propofol (P) and sevoflurane (S) states as indicated on the abscissa. The line connectors on the tops indicate where the difference between two distributions was statistically significant.

the similarity of the functional forms for the significantly increasing delta-alpha and the significantly decreasing cardio-respiratory coupling functions.

Coupling functions have enabled us to unveil a new perspective on how the neurophysiological mechanisms are affected by general anaesthesia. The application of this novel methodology was in a sense overwhelming in that we have identified six important and very illuminating coupling relationships. By quantitative assessment of the forms and strengths of the couplings, we have revealed how these relationships are changed by general anaesthesia, also showing that some of them are differently affected by propofol and sevoflurane. Coupling functions can also be used to study the mechanisms of other neurophysiological interactions, states and diseases in order to reconstruct the underlying functional mechanisms.

Acknowledgments

This work was supported by the EU project, No. 517133, BRACCIA, by the EPSRC, UK grant EP/100999X1 and in part by the ARRS Slovenia No. P20232.

References

- [1] T. Stankovski, S. Petkoski, J. Raeder, A. F. Smith, P. V. E. McClintock, and A. Stefanovska, *Phil. Trans. R. Soc. A* – <http://dx.doi.org/10.1098/rsta.2015.0186> **20150186** (2016).
- [2] M. T. Alkire, *Science* **322**, 876 (2008).
- [3] A. Stefanovska, *IEEE Eng. Med. Bio. Magazine* **26**, 25 (2007).
- [4] B. Musizza, A. Stefanovska, P. V. E. McClintock, M. Paluš, J. Petrovčič, S. Ribarič, and F. F. Bajrović, *J. Physiol. (London)* **580**, 315 (2007).
- [5] T. Stankovski, V. Ticcinelli, P. V. E. McClintock, and A. Stefanovska, *New J. Phys.* **17**, 035002 (2015).
- [6] A. Stefanovska and M. Bračič, *Contemp. Phys.* **40**, 31 (1999).
- [7] T. Stankovski, A. Duggento, P. V. E. McClintock, and A. Stefanovska, *Phys. Rev. Lett.* **109**, 024101 (2012).
- [8] B. Kralemann, M. Frühwirth, A. Pikovsky, M. Rosenblum, T. Kenner, J. Schaefer, and M. Moser, *Nat. Commun.* **4**, 2418 (2013).
- [9] D. Iatsenko et al., *Phil. Trans. R. Soc. Lond. A* **371**, 20110622 (2013).
- [10] I. Z. Kiss, C. G. Rusin, H. Kori, and J. L. Hudson, *Science* **316**, 1886 (2007).
- [11] T. Stankovski, P. V. E. McClintock, and A. Stefanovska, *Phys. Rev. X* **4**, 011026 (2014).
- [12] A. Duggento, T. Stankovski, P. V. E. McClintock, and A. Stefanovska, *Phys. Rev. E* **86**, 061126 (2012).

Interactions between oscillatory cardiac muscle cells

Tomislav Stankovski^{1,2}, Philip T. Clemson¹, David D. Edwards³ and Aneta Stefanovska¹

¹*Department of Physics, Lancaster University, Lancaster, UK*

²*Faculty of Medicine, Ss Cyril and Methodius University, Skopje, Macedonia*

³*Institute of Molecular and Experimental Medicine, School of Medicine, Cardiff University, Cardiff, UK*

Individual cells constitute and contribute to the overall structure and function of biological organs. What is usually accessible and mostly analyzed is the average measurement of an entire population of cells that work in coordination to form a physiological function. An important example of that kind is the widely accessible electrocardiogram (ECG) signal used to assess the cardiac electrical activity, which is known to have pronounced oscillatory nature. If assessed properly, however, the different cardiac cells as building blocks could bring deeper insight into the cardiac structure, and more importantly its function. In this direction we analyzed the oscillatory interactions between individual cardiac muscle cells (also called cardiac myocytes). In this direction we analyzed the oscillatory interactions between individual cardiac muscle cells (cardiomyocytes derived from human induced pluripotent stem cell (iPSC-CM)). Cells were loaded with a calcium sensitive fluorescent dye, imaged using confocal microscopy and the fluorescence intensity time series for each region of interest extracted.

We applied comprehensive analysis for assessment of the oscillations and the interactions between them [1,2]. The existence and the strengths of the oscillations were analyzed through wavelet power [3]. Next, to investigate the coordination between the oscillations we calculated the wavelet phase coherence and its windowed version for following the time-varying coherence [4,5]. In a similar way, we also tested if the oscillations are phase synchronized in different frequency ratios, and if there are any synchronization transitions [6,7]. To find the functional mechanisms that underlay the interactions we calculated the coupling functions between the cells oscillations using a dynamical Bayesian inference of the phase dynamics [8-10].

The wavelet transform in Fig. 1 demonstrates a *strong power of oscillations* with frequencies around 0.25 Hz and 0.5 Hz in the first 170 s, and then there is a transition, much

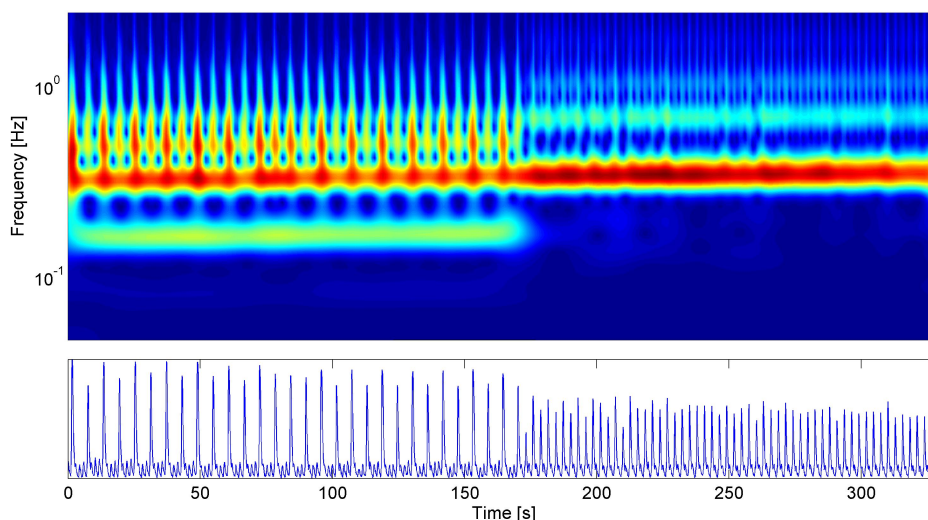


Figure 1: Wavelet transform (top) of a cardiac muscle cell signal (bottom).

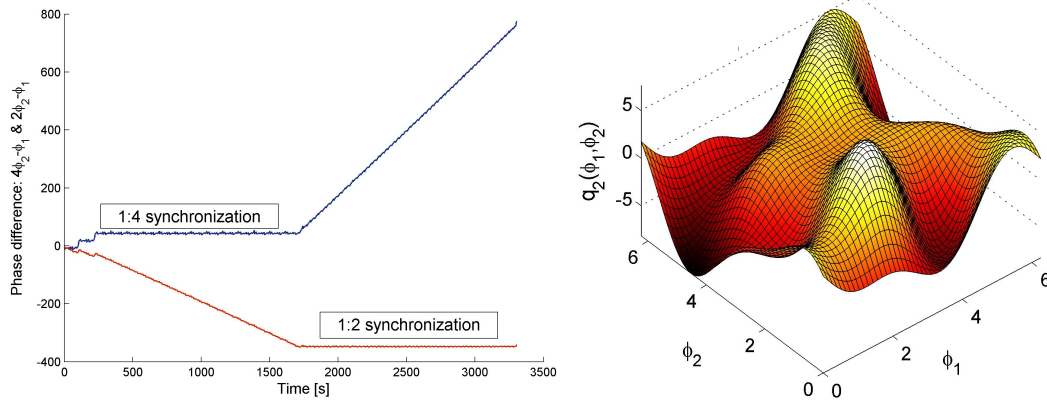


Figure 2: Phase difference as a measure of phase synchronization in 1:2 and 1:4 frequency ratios (left). Coupling function between phases of two cardiac cells (right).

like a period-doubling event, where the wavelet power predominantly stays only around the 0.5Hz oscillation. This change is also noticeable in the time domain evolution of the signal.

The investigation of phase synchronization between two cell signals, one which had transition (as shown on Fig. 1) and other signal which had single oscillation is shown on Fig. 2 (left). The (horizontal-like) bound phase difference indicates regions where the two cells are phase synchronized in a particular frequency ratio. From the figure, one can see that there is a 1:4 to 1:2 *synchronization transition* at around 1700 s. The wavelet phase coherence revealed similar results.

The coupling function Fig. 2 (right) demonstrates a complex form which describes the mechanism of the interactions. The form is predominantly diagonal, which indicates that the *coupling is either due to common influence or due to indirect influence from other oscillations*.

These preliminary results demonstrate that there is indeed a rich oscillatory dynamics in the cardiac muscle cells and that the interactions are well defined with occasional qualitative transitions of synchronization.

References

- 1 P. T. Clemson and A. Stefanovska, *Phys. Rep.* **542(4)**: 297 (2014).
- 2 Y. Shiogai, A. Stefanovska and P. V. E. McClintock, *Phys. Rep.* **488**: 51 (2010).
- 3 A. Stefanovska, M. Bračić and H. D. Kvernmo, *IEEE Trans. Bio. Med. Eng.* **46**: 1230 (1999).
- 4 A. Bandrivskyy, A. Bernjak, P. V. E. McClintock and A. Stefanovska, *Cardiovasc. Engin.* **4**: 89 (2004).
- 5 L. W. Sheppard, A. Stefanovska and P. V. E. McClintock, *Phys. Rev. E* **85**: 046205 (2012).
- 6 A. Pikovsky, M. Rosenblum and J. Kurths, *Synchronization – A Universal Concept in Nonlinear Sciences*, Cambridge University Press, Cambridge (2001).
- 7 P. Tass, *et all*, *Phys. Rev. Lett.*, **81**: 3291 (1998).
- 8 T. Stankovski, A. Duggento, P. V. E. McClintock and A. Stefanovska, *Phys. Rev. Lett.* **109**: 024101 (2012).
- 9 A. Duggento, T. Stankovski, P. V. E. McClintock and A. Stefanovska, *Phys. Rev. E* **86**: 061126 (2012).
- 10 T. Stankovski, V. Ticcinelli, P. V. E. McClintock and A. Stefanovska, *New J. Phys.* **17**: 035002 (2015).

IUGR detection from Doppler based HRV markers in low resource environments

Lisa Stroux¹, Christopher Redman², Antoniya Georgieva², Stephen Payne¹ and Gari D Clifford³

1 University of Oxford, Institute of Biomedical Engineering, UK

2 University of Oxford, Nuffield Department of Obstetrics & Gynaecology, UK

3 Emory University and Georgia Institute of Technology, Departments of Biomedical Informatics and Biomedical Engineering, USA

Introduction: Intrauterine growth restriction (IUGR) is a pathological decrease in fetal growth rate associated with significantly increased mortality and morbidity [1]. Developing countries carry the highest burden of perinatal mortality (98%) [2], of which a significant proportion can be attributed to IUGR-based complications [3]. Key reasons for this include lack of systematic screening and robust referral. Insight into the developmental status of the fetus would provide valuable decision support to frontline healthcare workers. The fetal cardiac signal is the most accessible source of information on the physiological control and development of the fetus. 1D Doppler ultrasound is a low-cost method for estimating the fetal heart rate variations. This work presents a retrospective investigation of the utility of Doppler-based heart rate variability (HRV) risk markers for antenatal IUGR detection.

Database: An extensive cardiotocography (CTG) archive of fetal heart rate variables, collected at the John Radcliffe hospital in Oxford, UK, was analysed. The control group of normal fetuses was matched for both gender and gestational age. The resultant study dataset of 2326 IUGR cases and controls, recorded between the 23rd and 42nd week of gestation (wGA), is the largest of its kind by a factor of 10.

Methods: A logistic regression classifier was trained to classify fetuses as IUGR or normal for gestational age. HRV markers included in the analysis were long-term variability (LTV) and short-term variability (STV) computed by the CTG system according to Dawes and Redman [4], averaged over episodes identified as of high or low variability (associated with active or quiet sleep) to avoid bias dependent on the trace composition of fetal sleep states. Metrics characterising the sleep state distribution within a trace were also considered. The data were split randomly 70:30 for testing and training. A five fold cross validation approach was taken to select features and optimise the logistic regression classifier. Only one recording per patient was used, so no patients appeared in both the testing and training sets or in any more than one fold. The associated AUC was computed for comparison of the predictive power of the risk markers and their combinations.

Given the anticipated implementation in low-resource environments, the trace length

required in order to make meaningful predictions is important. Recordings of 60 minutes, the standard maximum trace length in CTG monitors, may not be feasible. Experiments have shown that variability measures are better predictors of IUGR when derived from active sleep episodes. The time of onset of the first high HRV episode in recorded traces was therefore investigated.

Results: Early-onset IUGR (≤ 34 wGA) and late-onset IUGR (>34 wGA) do not impact the fetal cardiovascular system in the same way. Models for gestational ages over 34 weeks performed only poorly. Studied risk markers are therefore not suitable for the classification of late-onset IUGR. The difficulty of detecting late-onset IUGR has been previously noted in relation to other monitoring modalities [5]. However, the out of sample AUC for fetuses between 23 and 34 wGA was found to be 0.76. The best performing multivariate model included the features gestational age, LTV and STV in high variation episodes, the average duration in high variation and the number of high episodes in the trace. The AUC improved to over 0.80 for gestational ages ≤ 31 weeks.

In 61% of IUGR and 84% of normal traces an episode of high heart rate variability occurred within 30 minutes of starting the recording. When taking into account the percentage of fetuses that did not enter a period of active sleep at all within 60 minutes (27% IUGR, 6% normal), monitoring for only 30 minutes would capture 83% of the expected high variability episodes in IUGR and 89% in healthy fetuses.

Conclusion: Analysis confirmed that the distribution of HRV markers differs significantly in IUGR fetuses compared to normal controls, also when averaging over periods of active and quiet sleep. The results suggest that HRV markers together with information on sleep states can contribute to the detection of early-onset IUGR, which is of particular importance in settings where IUGR prevalence is high due to addressable factors such as malnutrition or substance abuse. This investigation confirms the dependence of HRV markers on gestational age, which has been reported in the literature using magnetocardiogram data [6]. By using 1D ultrasound we demonstrate a promising, accurate, but simple and low-cost, screening approach for IUGR detection, that requires a recording length of no more than 30 minutes.

References

- [1] Resnik R 2002 *Obstetrics & Gynecology* **99(3)** 490–496
- [2] World Health Organization 2006 *Neonatal and perinatal mortality : country, regional and global estimates*
- [3] Black R E, Allen L H, Bhutta Z A, Caulfield L E, De Onis M, Ezzati M, Mathers C, Rivera J 2008 *The Lancet* **371(9608)** 243–260
- [4] Pardey J, Moulden M, Redman C 2002 *Am J Obstet Gynecol* **186(5)** 1095–1103
- [5] Baschat A A 2010 *J Perinat Med* **38(3)** 239–246
- [6] Schneider U, Fiedler A, Liehr M, Kähler C, Schleussner E 2006 *Biomedizinische Technik* **51(4)** 248–250

Should Physicists Analyse Heart Rate?

Zbigniew R. Struzik^{1,2}

¹*RIKEN Brain Science Institute, Hirosawa, Japan*

²*The University of Tokyo, Graduate School of Education, Japan*

Physicists are trained to deal with non-living matter and until recently, it was considered detrimental to physics training and practice to depart from a strictly material philosophy of physical science. This status quo began to change rapidly around the turn of the millennium, when physicists started to embrace elements of physics of complexity, biology, systems, networks and living systems in general. Physicists were looking for new terrains offering new chances for physics methods of science to be applied, but also challenging scientists established in their own disciplines of biological origin to explore rigorous methodologies of physics in their fields.

The particular trend to apply methods of physics to other disciplines of science can perhaps be traced back to the success of physics methodology in offering tractable, simplified models of complex phenomena. One such paradigm was offered by the statistical physics of phase transitions. The 'translational' success of universality observed in phase transition phenomena and, in particular, at criticality was a breakthrough in physics – it offered a unifying view of inaccessible system-level complexity, using tractable, low-dimensional models. Suddenly, physics became capable of approaching and successfully treating a multitude of system scales and degrees of freedom. Indeed, a multiscale view of phenomena, in physics and beyond, flourished following the pioneering, breakthrough work on statistical physics of phase transitions and criticality.

It is perhaps no wonder that physicists deeply involved in the theory of universality approached the challenge of systemic complexity of biological origin, that of heart rate regulation. The dynamic complexity of our own life-perpetuating system – the cardiovascular regulatory system, consisting of intertwined feedback loops involving cardiac and baroregulation – is inherently non-trivial. Elucidation of fundamental molecular, cellular and biological mechanisms involved in this particular complex dynamical system is done by physiologists and put into practice by medical doctors. Yet physicists pursued the challenge from their own perspective – that of identifying possible universal laws governing the dynamics of the cardiac regulatory system [1].

The insights gathered in recent years all point towards the view that the cardiac regulatory system works in the critical regime [2]. A plausible, albeit not proven hypothesis would be that this criticality is of a self-organised nature. Indeed, in terms of Zipfian distribution of the probabilities of states, Kalda [3] contributed to

the body of evidence that heart rate follows Zipf statistics. The Zipfian distribution of states has recently been established as a hallmark of self-organised criticality in complex systems, including biological systems [4].

The origin of these laws, however, remains somewhat of a mystery. The inherently multiscale, self-organising and adaptive regulatory feedback scenario still remains the most plausible paradigm of complexity of heart rate [5]. Recently, this evidence has been strengthened by contributions from non-physicists who adopted the phenomenological view mainly purported by physicists [6, 7]. This is an exciting development, which may both signal an emerging trend of the acceptance of physicists' findings, and lead to a whole new way for physiologists and medical doctors to embrace the work and findings of physicists and apply them in their own research and practice. Going back to the question posed in the title, the benefits in fact work both ways. By tackling a real-life problem, physicists have to learn to adapt their methodology and mindset to cope with reasoning with the uncertainties and poor statistics for which life science research is known.

References

- [1] P. Ch. Ivanov, L. A. N. Amaral, A. L. Goldberger, S. Havlin, M. G. Rosenblum, Z. R. Struzik, H. E. Stanley, "Multifractality in human heartbeat dynamics," *Nature*, vol. 399, pp. 461–465, 1999.
- [2] K. Kiyono, Z. R. Struzik, N. Aoyagi, S. Sakata, J. Hayano, and Y. Yamamoto, "Critical scale-invariance in healthy human heart rate," *Phys. Rev. Lett.*, vol. 93, pp. 178103-1–4, 2004.
- [3] J. Kalda, M. Sakki, M. Vainu, M. Laan, "Zipf's law in human heartbeat dynamics," arXiv:physics/0110075v1, 2001.
- [4] T. Mora, W. Bialek, "Are Biological Systems Poised at Criticality?," *J. Stat. Phys.*, vol. 144, pp. 268–302, 2011.
- [5] Z. R. Struzik, "Is heart rate variability dynamics poised at criticality?" In: *ES-GCO. 8th Conference of the European Study Group on Cardiovascular Oscillations; 25-28 May 2014; Trento, Italy* IEEE: doi: 10.1109/ESGCO.2014.6847599
- [6] J.-O. Fortrat, C. Gharib, "Self-organization of blood pressure regulation: Clinical evidence", *Frontiers in Physiology* 2016 to appear.
- [7] J.-O. Fortrat, T. Levrard, S. Courcinous, J. Victor, "Self-Organization of Blood Pressure Regulation: Experimental Evidence", *Frontiers in Physiology* 2016.

Is it always easier to capture time-variable dynamics which resist the influence of external perturbations?

Yevhen F. Suprunenko, Philip T. Clemson, Aneta Stefanovska

University of Liverpool, Institute of Integrative Biology, Department of Evolution, Ecology and Behaviour, Liverpool, UK

It is much harder to treat time-variable oscillatory dynamics than the autonomous oscillatory dynamics, especially when using data from real life systems. As a result, time-varying oscillatory dynamics can often be misinterpreted as autonomous stochastic or chaotic when observed. External perturbations, which are unavoidable in real systems, represent one of reasons of such a misidentification of time-variable systems. External perturbations can make dynamics look more complex, hiding time-variable deterministic component. Recently, a subclass of non-autonomous oscillatory systems has been introduced and called chronotaxic to stress that their dynamics are ordered in time (from chronos time and taxis order). Such an ordering in time makes the chronotaxic dynamics capable of resisting external perturbations while preserving its time-variability. Using the definition of chronotaxic systems and theoretically generated examples, we study to what extent chronotaxicity helps to identify time-variability of the dynamics. The case of chronotaxicity in time-variable cardio-respiratory dynamics is also discussed.

References

Suprunenko Y F, Clemson P T, Stefanovska A 2013 *Physical Review Letters* **111**, 024101.

Suprunenko Y F, Clemson P, Stefanovska A 2014 *Physical Review E* **89**, 012922.

Clemson P T, Suprunenko Y F, Stankovski T, Stefanovska A 2014 *Physical Review E* **89**, 032904.

Suprunenko Y F, Stefanovska A 2014 *Physical Review E* **90**, 032921.

Lancaster G, Clemson P T, Suprunenko Y F, Stankovski T, Stefanovska A 2015 *Entropy* **17**, 4413-4438.

Investigation of cerebral venous outflow in microgravity

**Angelo Taibi, Giacomo Gadda, Mauro Gambaccini, Erica Menegatti,
Francesco Sisini, Paolo Zamboni**
University of Ferrara, Ferrara, Italy

Since the gravitational gradient is the major component to face when considering the physiology of venous return, there is a growing interest in understanding the mechanisms ensuring the heart filling in the absence of gravity for astronauts who perform long-term space missions. One of the most serious problems produced by microgravity is a fluid shift from lower to upper body. Indeed, this cephalad fluid shift may change the hemodynamics in the brain. Furthermore, cerebral drainage has been recognized as a factor of great importance for the regulation of cerebral functions, and has also been related to symptoms like headache and chronic fatigue without pathogenetic evidence, as well as to neurodegenerative diseases.

The purpose of the *Drain Brain* experiment [1], sponsored by the Italian Space Agency (ASI), was to monitor the venous return of the astronaut during the space mission, so as to study the compensatory mechanisms that facilitate this essential physiological action in subjects living in a microgravity environment. In particular, in-flight sessions consisted of:

- Plethysmography and basal spiromery measurements as a function of vital capacity to assess the physiology of venous return.
- Repetition of above measurements during the same day for chronobiology studies (circadian rhythm).
- Ultrasound (US) examination to measure cross section area of the internal jugular vein (IJV). The US device is integrated within the Human Research Facility (HRF), available on the ISS.

We have collected plethysmography data in different gravitational conditions so as to analyze brain outflow in relation to physiological variations such as respiration and posture. Preliminary results show that the respiratory pump could become a compensatory mechanism in the space, i.e. capable to attract blood toward the heart [2]. Moreover, comparison between plethysmography data and US data will be presented. Indeed, it has been suggested that the jugular venous pulse (JVP) can be used to investigate IJV drainage function and to obtain valuable information about cardiac hemodynamics through the analysis of its waveform [3].

References

- [1] http://www.nasa.gov/mission_pages/station/research/experiments/1278.html
- [2] Zamboni P, Menegatti E, Pomidori L, Morovic S, Taibi A, Malagoni AM, Cogo AL, Gambaccini M 2012 *J. Appl. Physiol.* **112** 904-910.
- [3] Sisini S, Tessari M, Gadda G, Di Domenico G, Taibi A, Menegatti E, Gambaccini M, Zamboni P 2015 *Ultrasound Med. Biol.* **41** 1334-1341.

Wavelet phase coherence analysis of polyfrequency skin blood flow oscillations under normal conditions in human

**Arina V. Tankanag, Andrey A. Grinevich, Irina V. Tikhonova
and Nikolay K. Chemeris**

Institute of Cell Biophysics, Russian Acad. Sci., Pushchino, Moscow region, Russian Federation

Despite the numerous thorough studies of the phenomenon of spontaneous oscillations in the microvascular blood flow (flowmotions) in the last decades, the localization of the mechanisms responsible for the generation of oscillations in the skin peripheral blood flow remains undetermined. Some researchers have hypothesized that skin blood flow is exclusively under local control, whereas others have suggested both general (central) adjustments and baroreflex-induced changes. It is known that oscillations in the microvascular blood flow are determined by the effects of endothelial, neurogenic, myogenic, respiratory and cardiac processes. Apparently, part of the oscillatory processes in the microvascular blood flow are of central origin, since the fluxomotion-generating source is located external to the microvascular flow, while the other part is determined by both local and central mechanisms of blood flow regulation in a tissue or an organ. The central factors of fluxomotion generation include the changes in blood flow velocity due to the influence of the respiratory function (respiratory rhythm) and pulse wave passage (cardiac rhythm), whereas endothelium-dependent, neurogenic and myogenic oscillations, conditioned by the intrinsic contractive activity of vascular smooth muscle cells (vasomotions) represent local factors. Early we found that in many subjects, the frequency intervals related to the local control are characterized by high values of the cross-correlation function for the oscillations of the peripheral blood flow in contralateral sites of forearm skin, which might be indicative of high phase synchronization of oscillations in these frequency intervals. In the present study an approach based on the calculation of wavelet phase coherence and evaluation of reliability for the obtained phase relationships was applied as a measure of synchronicity of the peripheral blood flow oscillations. On the assumption that the regulation is of a local nature we suggested that the microvascular blood flow oscillations in similar skin sites should have weak phase correlation. In contrast to that, the blood flow oscillations of central origin might possess high and reliable phase coherence in different regions of the blood vascular system. Thus the aim was to determine the frequency intervals for the peripheral blood flow oscillations in contralateral sites of forearm skin with high (> 0.5) statistically reliable degree of wavelet phase coherence.

The wavelet phase coherence of oscillations in the peripheral blood flow of contralateral skin sites was studied in volunteers. 20 healthy normotensive young women with normal constitution aged from 18 to 22 years (weight 60 ± 11 kg, height 166 ± 5 cm, arterial blood pressure $119 \pm 7/69 \pm 7$ mm Hg, heart rate 73 ± 11 bpm, menstruation phase was not accounted) participated in the study. The participants had not taken any drugs for at least one week before the study. None of the participants smoked and they abstained from any alcohol- or caffeine-containing drinks for at least 12 hours before the study. The exclusion criteria were previous history of cardiovascular diseases, diabetes and other acute and chronic illnesses. The study was approved by the local Committee for Human Biomedical Research Ethics and was carried out in accordance with the principles outlined in the 2002 Declaration of Helsinki of the World Medical Association.

The parameters of microcirculation were recorded using laser Doppler flowmetry (LDF) technique by dual-channel flowmeter LAKK-02 ('LAZMA', Russia) with two identical channels (wavelength 0.63 μm , emission power 0.5 mW). The registered characteristic of

the capillary blood flow is a microcirculation index, which reflects the volumetric flow rate of erythrocytes per time unit, measured in relative units.

The study was initiated following a 20-minute adaptation period. During the measurements the subjects were in sitting position in a quiet room at constant room temperature of 23 ± 1 °C. The LDF probes were fixed above the outer surface of the right and left forearms close to the wrist on the skin sites with similar blood flow levels. These zones were chosen because skin of the external forearm surface is characterized by a small number of anastomoses and demonstrates mainly nutritive blood flow. The duration of recording of skin blood perfusion was 750 sec. The sampling frequency of the LDF signal was 16 Hz.

The method of adaptive wavelet transform was used for data analysis. We chose the complex valued Morlet wavelet. The degree of correlation between the phases of the analyzed signals was estimated from the value of the wavelet phase coherence. We applied the method of surrogates to exclude the influence of autocorrelation and determine the significance of the obtained phase correlation relationships. For surrogate generation we employed the method of amplitude-adjusted Fourier transform, which produces surrogates having original values retained in the time series but rearranged in a way that largely preserves the spectrum while destroying temporal information. Two surrogate sets were produced for the LDF signals of the left and right forearms to estimate the degree of reliability for the observed correlations. For each set of surrogates we obtained the mean values and standard errors. The significance thresholds were determined as mean values and double standard errors. Only phase coherence function values which exceeded the threshold values for the surrogates of both the left and right forearms simultaneously were considered significantly reliable. Fig. represents reliable values of the phase coherence function only. If the values did not exceed the threshold values for the surrogates, i.e. were unreliable, such values were not taken into account. The obtained reliably significant values were analyzed statistically.

High median values (0.63 and 0.59) of the wavelet phase coherence were obtained for the frequency intervals of respiratory (0.145 – 0.6 Hz) and cardiac (0.6 – 2 Hz) rhythms in 18 and 20 participants, respectively. In all the 20 participants we detected high and reliable values (Me = 0.72) of the wavelet phase coherence for skin blood flow oscillations in the myogenic interval (0.052 – 0.145 Hz). Additionally, we demonstrated high wavelet phase coherence in the neurogenic (0.021 – 0.052 Hz) and endothelial (0.0095 – 0.021 Hz) intervals in 8 and 7 participants, respectively. The corresponding medians of the reliable wavelet phase coherence values for these intervals were 0.74 and 0.82.

We believe that high phase coherence of blood flow oscillations in respiratory and cardiac intervals is due to the central generation mechanisms: respiratory excursions and cardiac output, respectively. The reliable high phase coherence detected in blood flow oscillations in myogenic interval in all the participants of the study allows us to hypothesize that there exist central mechanisms in the peripheral blood flow regulation, which apparently synchronize the oscillations in this frequency interval throughout the whole cardiovascular system. The high phase correlation of blood flow oscillations in neurogenic and endothelial intervals discovered in approximately 30-40% participants of the analysis might presumably be explained by the effect from the central mechanisms of blood flow regulation (neurogenic and/or humoral regulation) in these frequency intervals.

The study is supported by the Russian Foundation for Basic Research (RFBR grant # 15-04-03429).

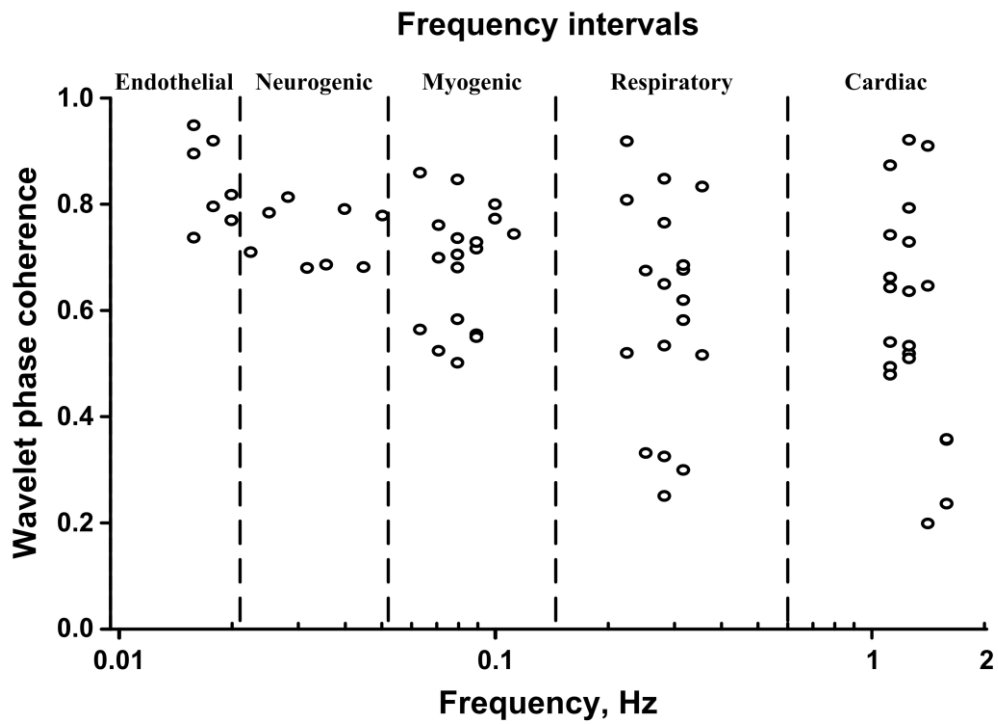


Figure. Reliable values of the wavelet phase coherence function for the intervals examined. The frequency axis is presented in logarithmic scale. Vertical dash lines indicate the boundaries of frequency intervals.

The role of perfusion in the oxygen extraction capability of skin and skeletal muscle

Clare Thorn and Angela Shore

University of Exeter Medical School, Diabetes and Vascular Medicine, Exeter, United Kingdom

The viability of all human cells is dependent upon two separate fundamental processes: the ability of the cardiovascular system to supply nutrients in close proximity to the cell via the microcirculation and the ability of the cell to uptake and metabolise these products. Crucial to all tissue health is the ability to couple together these two processes and match local blood flow with changing metabolic demands. Key to the classic model of the metabolic blood flow regulation is that as a feedback system by definition, regulation will only occur when homeostasis is perturbed. This leads to a cyclical behaviour fluctuating between normoxic and hypoxic states. In this study the role of blood flow in regulating oxygen extraction (OE) in skin and skeletal muscle was investigated in 12 lean and 12 obese men. OE was derived by two optical reflectance spectroscopy techniques. Firstly, from the rate of fall in mean blood saturation during a 4 minute below knee arterial occlusion and thus no blood flow, in calf skin and skeletal muscle. Secondly in the perfused, unperturbed calf and forearm skin of these 24 subject. This novel technique uses the spontaneous falls in mean blood saturation in skin induced by vasomotion and attributed to endothelial function¹ to derive a measure of oxygen extraction². OE in perfused skin was significantly higher in lean compared to obese subjects in forearm (Mann Whitney, $p < 0.004$) and calf ($p < 0.001$) and did not correlate with OE in unperfused skin ($\rho = -0.01$, $p = 0.48$). With arterial occlusion and thus no blood flow, skin OE in lean and obese subjects no longer differed ($p = 0.23$, ns). In contrast in skeletal muscle with arterial occlusion and no blood flow, the difference in OE between lean and obese subjects occurred, with obese subjects exhibiting significantly higher OE ($p < 0.012$). In skin, oxygen extraction is dependent upon unhindered perfusion that can fluctuate as demand exceeds supply. The reduced OE observed in the skin of obese compared to lean subjects and attributed, at least in part, to impaired functional capillary density is no longer observed during an arterial occlusion. In contrast, in this study resting muscle does not appear to exhibit these fluctuations between normoxic and hypoxic states suggesting other non-perfusion related regulatory mechanisms. These ensure that resting muscle is sufficiently perfused to match demand.

References

¹ Kvernmo H.D, Stefanovska A, Kirkebøen K.A, Kvernebo K. 1999 *Microvasc. Res.*, **5** 298–309

² Thorn C.E, Kyte H, Slaaf D.W, Shore A.C. 2011 *Am J Physiol Heart Circ Physiol* **301**(2) H442-9.

Coupling functions between cardiac and myogenic activity in the microvascular flow of aged and hypertensive subjects

Valentina Ticcinelli¹, Tomislav Stankovski^{1,2}, Peter V. E. McClintock¹
and Aneta Stefanovska¹

¹Lancaster University, Physics Department, Lancaster, UK

² Faculty of Medicine, Ss. Cyril and Methodius University, Skopje, Macedonia

Introduction We have computed coupling functions between the phases of myogenic and cardiac activities in skin blood flow in order to investigate the effects of ageing and hypertension on the microcirculation.

Couplings. The balance and functionality of the human body, in common with many other natural systems [1], are maintained by a network of couplings between the different oscillations involved [2, 3]. Factors that disrupt the dialogue between processes taking place within a particular subsystem can therefore undermine the overall health of the entire organism. As exemplars, we will see that the crucially important mechanisms of microcirculatory dynamics are altered by the changes in coupling induced by ageing and hypertension.

Materials and methods Laser Doppler flowmetry signals from three groups of subjects were analysed: 29 (14F) young healthy (aged 24.4 ± 3.4 years), 22 (13F) aged healthy (71.1 ± 6.6 years) and 22 (10F) treated-hypertensive aged subjects (70.3 ± 6.7 years). Signals were recorded on the forearm for 30 minutes. By applying dynamical Bayesian inference¹, we computed coupling functions [4–6] between the phases of the propagated cardiac pulse (~ 0.1 Hz) [7] and the slower myogenic oscillation (~ 0.1 Hz) caused by the contractions of vessels' walls [8]. The phases were extracted by nonlinear mode decomposition² [9]. By calculating the correlation $|\rho_q|$ of a coupling function q with a bank of numerically generated forms Q having specific shape features, one can determine which of those features is predominant in q [6, 10]. The numerical set simulates the shape of a direct coupling from the slower oscillation to the faster.

Results and discussion Comparison of Fig. 1-A with Fig. 1-B shows that ageing alone reduces the amplitude of the average form, but without modifying its shape, that is, it does not affect the mechanism underlying the coupling. This shape is completely lost in the surrogate group reported in Fig. 1-D, which has significantly lower similarity moduli compared to data from both young and aged subjects. Moreover, the box-plot in Fig. 1-E shows that most subjects from the healthy-aged group preserve a considerable $|\rho_{m,c}|$, not different statistically from that of the healthy-young group. In treated hypertension, however, the average form of the coupling between ϕ_m and ϕ_c (Fig. 4-C) becomes more randomly buckled, generating a smaller $|\rho_{m,c}|$, as shown by the orange box of Fig. 1-E: the distribution is similar to that of the surrogates (grey), with an even lower median value. An impaired efficiency of myogenic activity within the vascular system in treated hypertension has already been suggested by studies based on post-occlusive hyperaemia [7]. In contrast, the innovative approach used here enables us to assess the effective coupling by analysis of unperturbed baseline signals.

Conclusion Ageing attenuates the coupling functions between myogenic and cardiac oscillatory activity in skin blood flow whereas hypertension, even when treated, both attenuates and severely distorts them thus indicating a more serious impairment of function.

¹toolbox at <http://py-biomedical.lancaster.ac.uk/>

²toolbox at <http://www.physics.lancs.ac.uk/research/nbmphysics/diats/nmd>

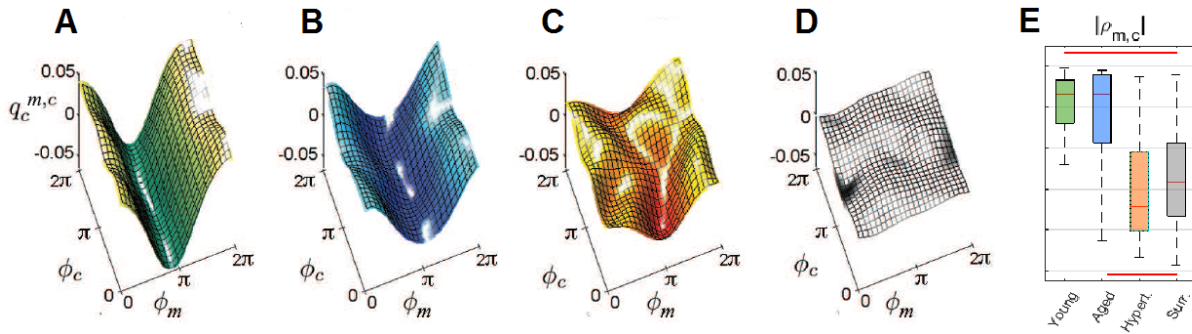


Figure 1: Average forms of the coupling function between myogenic and cardiac phases for (A) healthy young, (B) healthy old, (C) treated hypertensive and (D) surrogate groups. (E) Boxplots of the similarity moduli

References

- [1] S. H. Strogatz, “Exploring complex networks,” *Nature* **410**, 268–276 (2001).
- [2] A. Stefanovska, “Coupled oscillators: Complex but not complicated cardiovascular and brain interactions,” *IEEE Eng. Med. Bio. Magazine* **26**(6), 25–29 (2007).
- [3] A. Bashan, R. P. Bartsch, J. W. Kantelhardt, S. Havlin, and P. C. Ivanov, “Network physiology reveals relations between network topology and physiological function,” *Nat. Commun.* **3**, 702 (2012).
- [4] B. Kralemann, A. Pikovsky, and M. Rosenblum, “Reconstructing phase dynamics of oscillator networks,” *Chaos* **21**, 025104 (2011).
- [5] T. Stankovski, A. Duggento, P. V. E. McClintock, and A. Stefanovska, “Inference of time-evolving coupled dynamical systems in the presence of noise,” *Phys. Rev. Lett.* **109**, 024101 (2012).
- [6] T. Stankovski, V. Ticcinelli, P. V. McClintock, and A. Stefanovska, “Coupling functions in networks of oscillators,” *New J. Phys.* **17**, 035002 (2015).
- [7] M. Rossi, A. Carpi, C. Di Maria, F. Galetta, and G. Santoro, “Spectra analysis of laser Doppler skin blood flow oscillations in human essential arterial hypertension,” *Microvasc. Res.* **72**, 34–41 (2006).
- [8] T. Söderström, A. Stefanovska, M. Veber, and H. Svenson, “Involvement of sympathetic nerve activity in skin blood flow oscillations in humans,” *Am. J. Physiol.: Heart. Circ. Physiol.* **284**, H1638–H1646 (2003).
- [9] D. Iatsenko, *Nonlinear Mode Decomposition*, Springer, Berlin, 2015. See especially Chap. 4.
- [10] B. Kralemann, M. Frühwirth, A. Pikovsky, M. Rosenblum, T. Kenner, J. Schaefer, and M. Moser, “In vivo cardiac phase response curve elucidates human respiratory heart rate variability,” *Nat. Commun.* **4**, 2418 (2013).

Causal brain correlates of autonomic nervous system (ANS) outflow: a 7T study

**Andrea Duggento¹, Marta Bianciardi², Lawrence L. Wald², Luca Passamonti^{3,4},
Gaetano Valenza^{5,6}, Maria Guerrisi¹, Riccardo Barbieri^{7,6}, Nicola Toschi^{1,2}**

¹ *Medical Physics Section, University of Rome "Tor Vergata", Italy.*

² *Department of Radiology, A.A. Martinos Center and Harvard Medical School, Boston, USA.*

³ *Department of Clinical Neurosciences, University of Cambridge, Cambridge, UK.*

⁴ *Institute of Bioimaging and Molecular Physiology, National Research Council, Catanzaro, Italy.*

⁵ *Department of Information Engineering, and Research Centre "E. Piaggio", University of Pisa, Italy.*

⁶ *Massachusetts General Hospital and Harvard Medical School, Boston, USA.*

⁷ *Department of Electronics, Informatics and Bioengineering, Politecnico di Milano, Milano. Italy.*

The study of central correlates of autonomic nervous system (ANS) activity (i.e. directed brain-heart information flow) presents considerable challenges due to limited spatial and temporal resolution of current neuroimaging techniques. Also, the application of Granger Causality (GC - a method to analyze directed information transfer) to functional MRI is difficult due to the high inter-dependance of brain-derived signals, which can lead to the appearance of spurious causal links [1]. The aim of this study was to provide the first causality-based investigation of directed brain-heart interactions in the resting state, and to associate our results with estimates of directed, globally conditioned brain-brain resting state networks.

Nine subjects (283y) underwent 7T MRI (32-channel receive coil-array, TE/FA/SMS/ repetitions = 26ms/40°/3/300, TR=1.5 s, isotropic 1.8 mm³ voxel) with simultaneous physiological signal acquisition (1 kHz) at the Martinos Center for Biomedical Imaging (MGH). After slice timing-, motion- and RETROICOR correction, 116 ROI-wise BOLD signals (AAL atlas) were extracted. A time-varying, point-process based probabilistic model for cardiac pulsations was employed to estimate instantaneous ANS indexes (HF: sympathetic (SA), LF: SA and parasympathetic (PSA), Bal: simpthovagal balance). We computed globally (i.e. to all other brain regions) conditioned within-brain (i.e. brain-brain) causality (GCGC) between locally averaged brain signals as well as conditioned brain-heart causality between locally averaged brain signals and the point-process-derived dynamical band-specific powers (LF, HF, BAL). For each directed connection between any two brain regions as well as for each connection between each brain region and every ANS regressor the p-value of the connection was evaluated. Successively, for each connection the number of subjects with p-value < 0.01 and < 0.05 was counted (Figure 1).

Figure 2 shows the result of combining globally conditioned within-brain and brain-heart networks. Brain-brain networks are taken out of anatomical space in order to improve legibility. The resulting graph spans most brain regions while retaining a certain degree of simplicity given the high redundancy of brain signals even in the resting state, it is plausible that the high percentage of connections which are removed through the use of the globally conditioned approach correspond to spurious/indirect causalities which should not be interpreted as direct within-brain causal influences.

In conclusion, while the limited number of subjects employed in this study necessarily warrants some caution in casting strong physiological hypothesis based on our globally conditioned networks, in this feasibility study we have shown that 7 Tesla functional imaging coupled with globally conditioned Granger causality estimates is able to quantify directed brain-heart interactions, which can be interpreted in terms of central modulation of ANS outflow while correctly disentangling the high redundancy between locally aggregated brain signals.

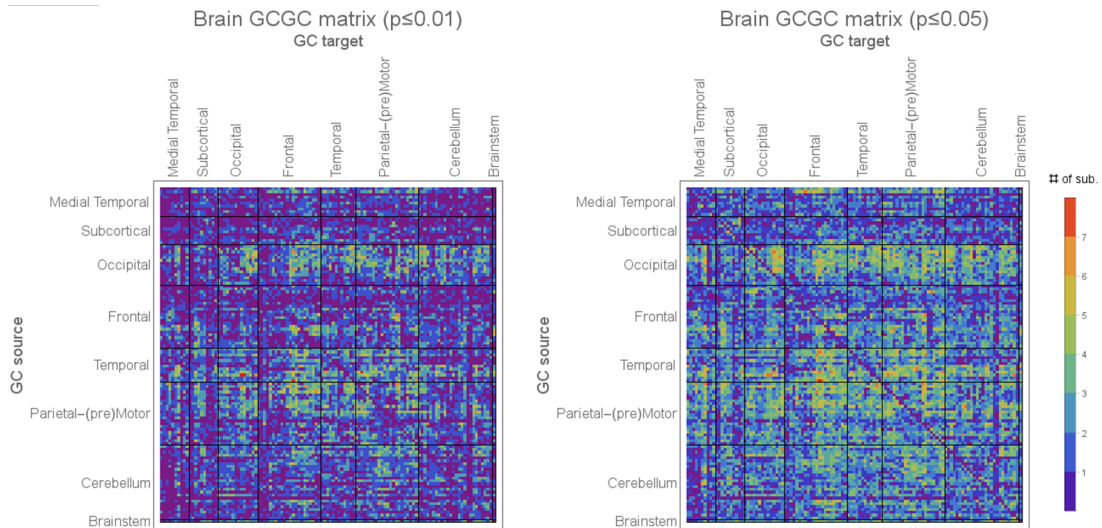


Figure 1: Group-wise count of significant connections in globally conditioned GC. For each directed connection the number of subjects where that particular connection is statistically significant with a p -value < 0.01 (left) and a p -value < 0.05 (right) is shown. Rows label brain regions (GC sources) G-Causing the brain regions labelled by columns (GC target).

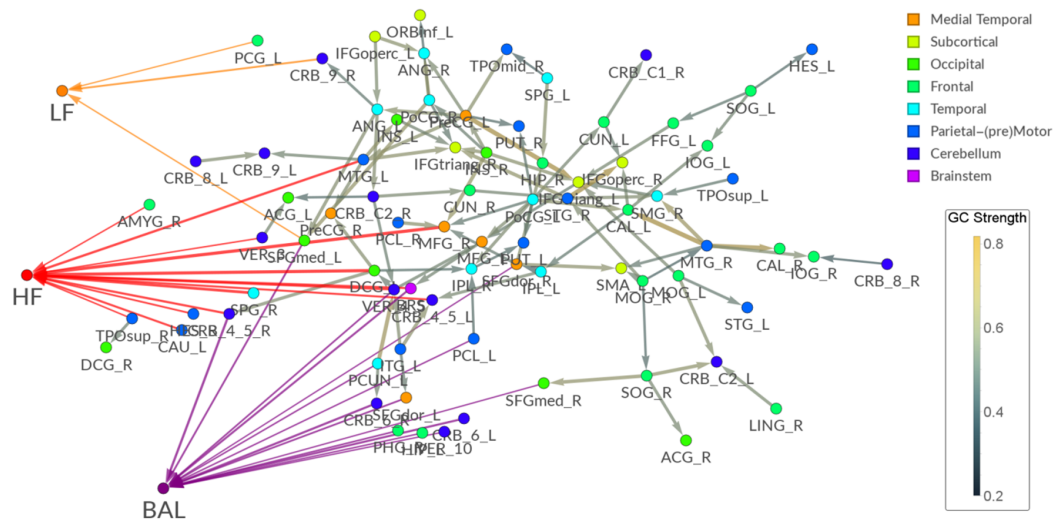


Figure 2: Group-wise directed resting state brain-brain (cutoff at p -value < 0.01) and brain-heart network graphs as inferred using globally conditioned GC (right) (brain nodes arranged accordingly to a spring embedding).

References

1. Duggento A. et Al. *Phil. Trans. of Royal Soc.*, 2016. Theme issue: "Uncovering brain-heart information through advanced signal and image processing"; *in press*; DOI:10.1098/rsta.2015.0185.

Diabetic foot ulcers: improved microcirculation after low-energy laser irradiation

V. Urbančič-Rovan^{1,2}, A. Bernjak^{3,4}, B. Sedej⁵ and A. Stefanovska^{3,4}

¹University Medical Centre, Dept of Endocrinology, Ljubljana, Slovenia; ²University of Ljubljana, Faculty of Medicine, Ljubljana, Slovenia; ³University of Ljubljana, Faculty of Electrical Engineering, Ljubljana, Slovenia; ⁴Lancaster University, Dept Physics, Lancaster, UK; ⁵University Medical Centre, Centre for Medical Rehabilitation, Ljubljana, Slovenia

Background and aims: Alterations in microvascular blood flow dynamics play a role in the development of diabetic neuropathic ulceration. Resting laser-Doppler skin blood flow in diabetic patients is significantly higher than in non-diabetic individuals (high perfusion microangiopathy). On the other hand, the amplitude of the blood flow oscillations is lower than in healthy population [1]. Low-energy laser beam irradiation has been demonstrated to augment wound healing in conditions of reduced microcirculation [2, 3]. Athermic laser irradiation on one foot in people with diabetes with angiopathy causes a significant increase in skin circulation in both feet and points to the possibility of systemic effects. We sought to investigate the influence of low-energy laser beam irradiation on microvascular blood flow.

Patients and methods: 12 diabetic patients with chronic foot ulceration (D) and 9 healthy controls (C) participated in the study. Laser-Doppler flowmetry was performed at the ulcerated site at baseline and after 5 sessions of pulsatile laser irradiation. The wavelet transform was applied to the flowmetry signal to evaluate its spectra within 6 characteristic frequency intervals: 0.005-0.0095Hz and 0.0095–0.021Hz (endothelium-related); 0.021–0.052Hz (sympathetic nerve activity); 0.052–0.145Hz (myogenic activity); 0.145–0.6Hz (respiration-related); 0.6–1.6Hz (heart rate-related).

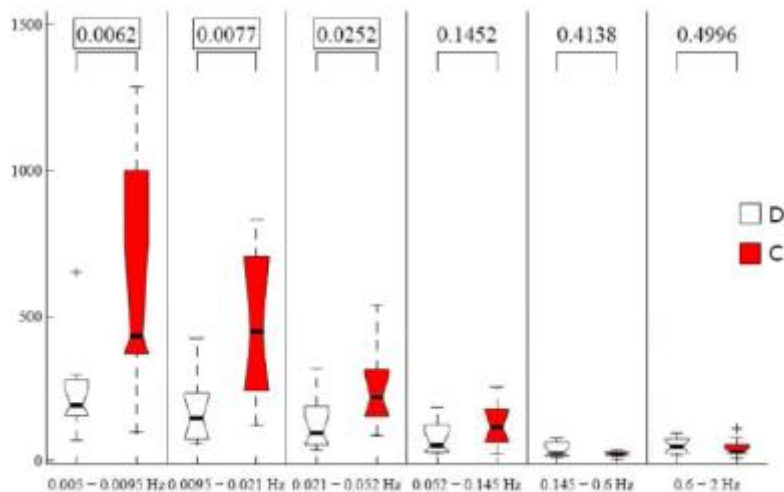


Figure 1. Absolute amplitudes at baseline.

Results: At baseline, mean flow was higher in D than in C ($p=0.0077$), the amplitudes of the low frequency oscillations were lower (all $p<0.05$) (Figure 1). One session of laser irradiation in D decreased the mean flow ($p=0.3408$, ns) and the contribution of the heart rate to the total flow (Figure 2, interval 0.6-2Hz). At the same time the normalised amplitudes below 0.145Hz increased, indicating increased contribution of the low frequency components to the total flow ($p<0.05$) (Figure 2). After 5 sessions, mean flow in D, although lower than at baseline ($p=0.806$, ns), remained higher than in C ($p=0.9048$, ns). The amplitudes of the low frequency oscillations in D increased insignificantly, but remained lower than in C ($p<0.05$) (Figure 3).

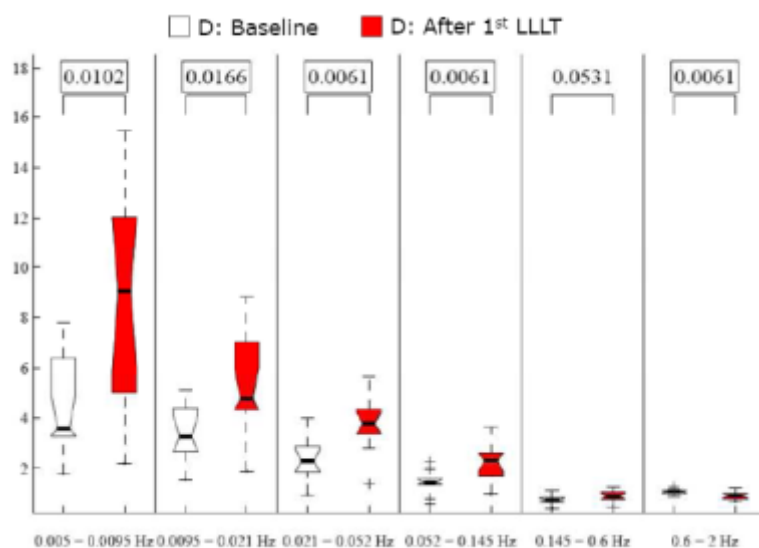


Figure 2. Normalised amplitudes after 1 session of low-level laser therapy.

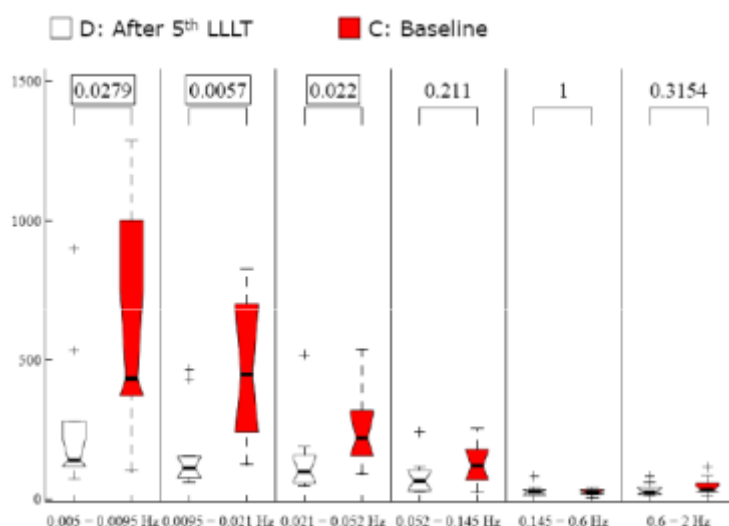


Figure 3. Normalised amplitudes after 5th session of low-level laser therapy.

Conclusion: Our results indicate that laser irradiation enhances wound healing through a favourable influence on microvascular flow dynamics: decreased mean laser-Doppler skin blood flow and increased amplitude of the low-frequency oscillations (endothelial and sympathetic nerve activity).

References:

1. Edmonds ME, Roberts VC, Watkins PJ: Blood flow in the diabetic neuropathic foot. *Diabetologia*; **22**:9–15 (1992).
2. Schindl A, Schindl M, Schön H, Knobler R, Havelec L, Schindl L. Low-intensity laser irradiation improves skin circulation in patients with diabetic microangiopathy. *Diabetes Care*; **21**:580-4 (1998).
3. Schindl A, Heinze G, Schindl M, Pernerstorfer-Schön H, Schindl L. Systemic effects of low-intensity laser irradiation on skin microcirculation in patients with diabetic microangiopathy. *Microvasc Res*; **64**: 240-6 (2002).

An Instantaneous Estimation of Transfer Entropy using Point-Process Models with Application to Cardio-Respiratory Dynamics

Gaetano Valenza^{1,2}, Luca Faes³, Luca Citi⁴, Michele Orini⁵, and
Riccardo Barbieri^{2,6}

¹*University of Pisa, Italy*

²*Harvard Medical School, Massachusetts General Hospital, Boston, MA, USA*

³*IRCS-FBK and BIOtech, University of Trento, Italy*

⁴*University of Essex, Colchester, UK; ⁵University College London, London, UK*

⁶*Politecnico di Milano, Milan, Italy*

Nonlinear physiological systems are characterized by complex interactions among multiple sub-system variables, whose dynamics show peculiar nonlinear coupling properties. To this extent, transfer entropy [1] is a mathematical construct devised to measure the nonlinear directional amount of information transfer from one physiological variable to the other. Transfer entropy measures derived from heart rate variability (HRV) analysis have been proven to be effective indicators of baroreflex functions and of aging-related changes, involving also respiratory dynamics, at different frequency bands. In this domain, important limitations are mainly related to a finite, single non-parametric estimation of transfer entropy involving cardiovascular and respiratory dynamics, and they can be summarized as follows: i) estimation of probability density functions (PDFs) using experimental data whose observation is limited within a relatively short time window; ii) assumption of stationarity of the time series; iii) presence of outliers originating from either noise sources or underlying physiology (e.g., ectopic beats); iv) inability to track time-varying changes in nonlinear coupling with a sufficiently high resolution in time. Moreover, when dealing with HRV estimates, the intrinsic unevenly sampled nature of heartbeat events observation has to be taken into account. To overcome these limitations, this study proposes a new definition of transfer entropy having time varying properties and being suitably applicable to HRV series. In previous studies we demonstrated that it is possible to model the unevenly spaced heartbeat intervals as a probabilistic point process. Here we embed the standard definition of transfer entropy within the point-process framework, obtaining *instantaneous transfer entropy* estimates of heartbeat dynamics, namely inhomogeneous point process transfer entropy, $ipTransfEn(t)$. This measure inherits all the advantages of the point process modeling, so that it is possible to characterize the heart events' probabilistic generative mechanism and to obtain continuous estimates, even considering short recordings, under nonstationary conditions, and without using any interpolation method. The choice of PDF refers to the inverse Gaussian family of functions [2], parametrized in a monivariate and bivariate autoregressive structure linked to cardiovascular and respiratory dynamics.

The proposed instantaneous transfer entropy estimation is performed through proper combination of monivariate heartbeat dynamics modeling, and bivariate heartbeat-respiratory dynamics modeling. As a general aim, $ipTransfEn$ refers to the instantaneous estimation of the Kolmogorov-Smirnov distances between PDFs from these

mono- and bivariate models. As such, it follows the general principle of Granger of measuring the information that the past of the driver brings to the present of the destination above and beyond the information that is brought by its own past. We show the estimates of *ipTransfEn* (time resolution of 5ms) in exemplary data gathered from healthy subjects undergoing postural changes. Moreover, we integrate *ipTransfEn* dynamics with recently defined instantaneous measures of entropy, the inhomogeneous point process approximate and sample entropy measures [2], which are defined through monovariate analysis of heartbeat dynamics data, and are also embedded within a point process framework. Given a generic index variable, all results in this study are referred to inter-subject analyses. In order to demonstrate the applicability to real cases, we have performed the instantaneous analysis in a RR-interval time series recorded from 16 healthy subjects undergoing a tilt-table protocol where each subject, initially lying horizontally in a supine position, is then passively tilted to the vertical position. The study, fully described in [3], comprises sixteen subjects (10 males, 24–34 yr, 28.6+/-2.9 yr, no known history of cardiovascular disease) who underwent a head-up tilt table test according to the following protocol: 4 min in early supine position, 5 min tilted head-up to an angle of 70° and 4 min back to later supine position.

Results show how *ipTransfEn* measures perform fast tracking of the tilting events and low variability during the standing phase. *ipApEn*, the monovariate version of *ipTransfEn*, shows a similar dynamics as *ipTransfEn* during the resting phases, whereas differences exist during the tilting phase. In this phase, in fact, more pronounced oscillations are present in the *ipApEn* dynamics, possibly showing that other mechanisms than cardiorespiratory information transfer underlie the complexity of heartbeat dynamics. From a physiological point of view, we have shown that *ipTransfEn* promisingly provides helpful multivariate time-varying and adaptive assessment for real-time monitoring of sympathovagal dynamics, which has also been proven in agreement with previous works. Furthermore, *ipTransfEn* is here applied to cardio-respiratory dynamics, and it can consequently be linked to respiratory sinus arrhythmia. To conclude, the proposed methodology offers a promising mathematical tool for the dynamic analysis of a wide range of applications and to potentially study any physical and natural stochastic discrete process.

References

- [1] K. Hlaváčková-Schindler, et al., “Causality detection based on information-theoretic approaches in time series analysis,” *Physics Reports*, vol. 441, no. 1, pp. 1–46, 2007.
- [2] G. Valenza et al. “Inhomogeneous point-process entropy: An instantaneous measure of complexity in discrete systems,” *Physical Review E*, vol. 89, no. 5, p. 052803, 2014.
- [3] M. Orini et al. “A multivariate time-frequency method to characterize the influence of respiration over heart period and arterial pressure,” *EURASIP Journal on Advances in Signal Processing*, vol. 2012, no. 1, pp. 1–17, 2012.

Maximal Information Coefficient to Estimate Brain-Heart Dynamics during Visual Emotional Elicitation

G. Valenza¹, A. Greco¹, C. Gentili², A. Lanata¹, N. Toschi³, R. Barbieri⁴,
L. Sebastiani¹, D. Menicucci¹, A. Gemignani¹, E.P. Scilingo¹

¹*University of Pisa, Pisa, Italy*, ²*University of Padua, Padua, Italy*

³*University of Roma Tor Vergata, Rome, Italy*

⁴*Politecnico di Milano, Milan, Italy*

The so-called “brain-heart axis” refers to anatomical and functional links interconnecting the Autonomic and Central Nervous Systems (ANS, CNS) [1]. A paradigmatic brain-heart interaction occurs during an emotional experience. Previous studies investigated the coupled brain-heart dynamics during healthy and pathological emotional responses. Nonetheless, how such a brain-heart dynamics is further modulated by the specific kind of emotional stimuli is still unknown.

In this study, we present a novel approach to study brain-heart interactions quantifying the linear and nonlinear brain-heart coupling mechanisms through the calculation of the Maximal Information Coefficient (MIC) index, a statistical method for detecting linear and nonlinear associations between pairs of variables. MIC calculations were performed at a single-subject level, between time-varying estimates of high-resolution (128 channels) EEG power spectra and instantaneous heart rate, during visual emotional elicitation. Twenty-two healthy volunteers were emotionally elicited through passive viewing of pictures taken from the International Affective Picture System (IAPS), associated to 25 different combinations of arousal and valence levels, including neutral elicitations. Combinations of valence (how pleasant/unpleasant is an emotion) and arousal (intensity of the emotional stimuli), which are intended as orthogonal dimensions, are associated to specific emotions. As a proof of concept of the proposed methodology, we particularly focus on the experimental results gathered analyzing EEG oscillations in the θ band (4-8 Hz), and its coupling with instantaneous heartbeat measures. Instantaneous cardiovascular dynamics was estimated through inhomogeneous point-process models of RR interval series [2], which were gathered from the ECG. The use of inhomogeneous point-process on heartbeat dynamics allows to obtain instantaneous time domain and spectral estimates, which can be considered as covariate measures of brain-heart interaction during emotional processing. The recording paradigm related to this work has been previously described in [2]. Briefly, a homogeneous population of 22 healthy subjects (aged from 21 to 24) was recruited to participate in the experiment. The affective elicitation was performed by visualizing the IAPS pictures onto a PC monitor. Then, the slideshow started, being comprised of 9 sessions, alternating neutral sessions (from N_1 to N_5) and arousal sessions (from A_1 to A_4).

Differences between resting state sessions were found in coupling with μ_{RR} , σ_{HR} , and HF only. Differences in all of the couplings between EEG θ band and HRV features, instead, were found between all neutral, and between all arousing sessions. In particular, major differences between neutral sessions occurred in the prefrontal cortex, mainly due to significant changes occurring in the neutral session 5, whereas major differences between arousal sessions occurred in the prefrontal cortex and parietal lobes, mainly due to significant changes occurring in the intermediate arousal session 3. Note that, in the experimental protocol timeline, arousal level 3 follows neutral session 5. Negative elicitation sessions showed arousal-dependent differences, occurring exclusively on the coupling between EEG θ - μ_{RR} , and EEG θ - HRV LF/HF ratio in the prefrontal cortex region. To conclude, we demonstrated that a point-to-point linear and nonlinear correlation measure between instantaneous heartbeat dynamics and EEG time-varying spectra may be a feasible method to understand the coupling between ANS and CNS. We show how EEG oscillations in the θ band are the promising metrics to be used in such an evaluation. However, it is possible to hypothesize that different EEG bands couple with different aspects of ANS dynamics. As expected, we found that prefrontal cortex plays a crucial role in brain-heart coupling modulation during visual emotional elicitation. In particular, a strong coupling between prefrontal cortex activity and heartbeat dynamics was found at intermediate arousal (arousal level 3). In such an arousing elicitation, we also found a significant EEG θ - HRV-LF coupling in the left temporal region. As a matter of fact, generic and reactive medial prefrontal cortex processes are parsimoniously reflected by EEG θ band activities, which also showed different patterns of coherence between the distinct brain regions in response to social and fearful stimuli [3]. Further studies should address whether any early/late phenomena as a response of affective stimuli can be identified in brain-heart dynamics. Moreover, quantification of the exact amount of nonlinear coupling occurring in brain-heart dynamics should also be performed.

References

- [1] A. Craig, “Pain mechanisms: labeled lines versus convergence in central processing,” *Annual review of neuroscience*, vol. 26, no. 1, pp. 1–30, 2003.
- [2] G. Valenza, L. Citi, A. Lanatá, E. P. Scilingo, and R. Barbieri, “Revealing real-time emotional responses: a personalized assessment based on heartbeat dynamics,” *Scientific reports*, vol. 4, 2014.
- [3] A. Tendler and S. Wagner, “Different types of theta rhythmicity are induced by social and fearful stimuli in a network associated with social memory,” *eLife*, vol. 4, p. e03614, 2015.

Linear and nonlinear causal coupling analyses between the central and autonomic nervous system in schizophrenia

Steffen Schulz¹, Aniol Serra Juhé², Beatriz Giraldo², Karl-Jürgen Bär³, Mathias Bolz⁴
and Andreas Voss¹

¹ *University of Applied Sciences, Institute of Innovative Health Technologies IGHT, Jena, Germany*

² *Universitat Politècnica de Catalunya, CREB, Barcelona, Spain*

³ *University Hospital, Department of Psychiatry and Psychotherapy, Pain and Autonomics-Integrative Research, Jena, Germany*

⁴ *University Hospital, Department of Child and Adolescent Psychiatry, Jena, Germany*

1. Introduction

Schizophrenia is considered to be one of the most severe mental disorders in the world associated with higher cardiac mortality rates and up to triple the risk of attaining cardiovascular disease compared to the general population (Hennekens et al., 2005). The autonomic nervous system (ANS) dysfunction has been well described in schizophrenia. However, the coupling between the ANS and central brain activity in schizophrenia has been only partly investigated until now (Schulz et al., 2016). The interactions between the central nervous system (CNS) and ANS need to be considered as a feedback-feedforward system which supports flexible and adaptive responses to specific demands acting in a linear and nonlinear way. Different studies have been revealed that autonomic regulation (cardiovascular) mainly involves the prefrontal lobe. The aim of this study was to investigate the short-term instantaneous central-autonomic coupling (CAC) in the frontal lobe in 17 patients suffering from paranoid schizophrenia (SZ; 2 females, 37.5±10.4 years) and in 17 age-gender matched healthy controls (CO; 4 females, 37.7±13.1 years) applying the causal coupling approaches normalized short-time partial directed coherence (NSTPDC) and multivariate transfer entropy (MuTE).

2. Materials and methods

Patients

Patients had been treated with depot antipsychotic medication (77% being atypical neuroleptics, and 23% being a mixture of antidepressant and atypical neuroleptics). All participants (SZ and CO) provided their written informed consent to a protocol approved by the local ethics committee of the Jena University Hospital. This study complies with the Declaration of Helsinki.

Data recordings and pre-processing

From all patients and controls, a 3-channel short-term ECG (500 Hz), the non-invasive continuous blood pressure (200 Hz) and a 64-channel EEG (500 Hz) were recorded for 15 minutes under resting conditions. Participants remained seated and their eyes were closed during this recording. The following time series were extracted from the raw data records: heart rate (consisting of successive beat-to-beat intervals - BBI), successive systolic blood pressure amplitudes - SYS) and the mean power P_{EEG} from the EEG (in relation to each RR-interval). Three different brain regions (the frontal area, the left frontal area, and the right frontal area) were investigated.

Central-autonomic coupling approaches

To quantify the causal coupling strength between the CNS- and ANS time series, the NSTPDC approach was applied (Schulz et al., 2015), based on an m -dimensional multivariate autoregressive model with model order p to determine linear Granger causality in the frequency domain. Furthermore, the MuTE with the nearest neighbour estimator and non-

uniform embedding (NN NUE) was applied to quantify the nonlinear interactions (Montalto et al., 2014).

Statistics

The nonparametric exact two-tailed Mann-Whitney U-Test (SPSS 21.0) was performed to evaluate differences in CAC indices between SZ and CO. The significance level was set to $p < 0.01$ (*) and $p < 0.00625$ (Bonferroni-Holm adjustment, **).

3. Results and discussion

In general, we found significantly reduced linear as well as nonlinear CAC (strength) in SZ compared to CO.

In detail, (table 1) the nonlinear influences (MuTE) from ANS to CNS (BBI→EEG, SYS→EEG) as well as from CNS to ANS (EEG→BBI, EEG→SYS) were reduced in SZ compared to CO. Furthermore, the linear coupling (NSTPDC) from ANS to CNS (SYS→EEG) was stronger in CO than in SZ, whereas the linear influence from CNS to ANS (EEG→SYS) was higher in SZ than in CO.

Table 1: Results of CAC analysis applying NSTPDC and MuTE (frontal, left, right hemispheres)

| | coupling strength | all frontal | left frontal | right frontal | CO mean ± SD | SZ mean ± SD | CO_left mean ± SD | SZ_left mean ± SD | CO_right mean ± SD | SZ_right mean ± SD |
|--------|-------------------|-------------|--------------|---------------|-----------------|-----------------|----------------------|----------------------|-----------------------|-----------------------|
| MuTE | BBI→EEG | ** | ** | ** | 0.012 ± 0.011 | 0.007 ± 0.009 | 0.013 ± 0.012 | 0.007 ± 0.009 | 0.010 ± 0.010 | 0.007 ± 0.009 |
| | EEG→BBI | ** | ** | ** | 0.012 ± 0.009 | 0.007 ± 0.008 | 0.013 ± 0.009 | 0.006 ± 0.008 | 0.012 ± 0.009 | 0.006 ± 0.007 |
| | SYS→EEG | ** | ** | ** | 0.012 ± 0.011 | 0.006 ± 0.008 | 0.013 ± 0.011 | 0.007 ± 0.009 | 0.012 ± 0.010 | 0.005 ± 0.008 |
| | EEG→SYS | ** | ** | n.s. | 0.008 ± 0.008 | 0.006 ± 0.008 | 0.008 ± 0.008 | 0.006 ± 0.008 | 0.008 ± 0.008 | 0.006 ± 0.008 |
| NSTPDC | BBI→EEG | n.s. | n.s. | n.s. | 0.10 ± 0.05 | 0.09 ± 0.06 | 0.10 ± 0.05 | 0.09 ± 0.06 | 0.10 ± 0.05 | 0.09 ± 0.06 |
| | EEG→BBI | n.s. | n.s. | n.s. | 0.23 ± 0.16 | 0.26 ± 0.17 | 0.22 ± 0.15 | 0.25 ± 0.16 | 0.23 ± 0.17 | 0.28 ± 0.18 |
| | SYS→EEG | ** | ** | ** | 0.13 ± 0.07 | 0.10 ± 0.06 | 0.13 ± 0.07 | 0.10 ± 0.06 | 0.13 ± 0.08 | 0.09 ± 0.07 |
| | EEG→SYS | ** | ** | ** | 0.14 ± 0.10 | 0.20 ± 0.13 | 0.14 ± 0.10 | 0.19 ± 0.12 | 0.14 ± 0.10 | 0.21 ± 0.14 |

The central-cardiac coupling seems to be of nonlinear nature and are significantly reduced in each direction in SZ. These diminished closed-loop interaction in SZ are probably caused by the known significant heart rate changes. It is presumed that lesions within the CNS may result in profound alterations in cardiac regulation and may even result in potentially fatal cardiac arrhythmias or sudden cardiac death (due to cardiovascular dysfunctions) (Foster and Harrison, 2004). Furthermore, CAC results suggest that the linear closed-loop regulation process of central-vascular regulation is more pronounced than the nonlinear one in SZ and strongly focused on maintaining the blood pressure regulation. For SZ, the central part of this closed-loop seems to influence more strongly the autonomic system (SYS, BBI) than the autonomic system the central one.

This study shows for the first time an impaired complex brain-heart network between central activity and cardiovascular regulation in SZ patients. In addition, this study provides a more in-depth understanding of the interplay of neuronal and autonomic regulatory processes in SZ and most likely greater insight into the complex relationship between psychotic stages and autonomic activity.

References

- Foster PS, and Harrison DW, 2004. *Int J Psychophysiol* **52**, 239-255.
Hennekens CH, Hennekens AR, Hollar D, and Casey DE, 2005. *Am Heart J* **150**, 1115-1121.
Montalto A, Faes L, and Marinazzo D, 2014. *PLoS One* **9**, e109462.
Schulz S, Bär KJ, and Voss A, 2015. *Entropy* **17**, 483-501.
Schulz S, Bolz M, Bär KJ, and Voss A, 2016. *Philos Trans A Math Phys Eng Sci* **374**, in press.

Age and gender dependency of short-term QT indices

Andreas Voss¹, Sarah Radon¹, Claudia Fischer¹, Mireia Valero², Montserrat Vallverdú², Rico Schroeder¹, Annette Peters³ and Siegfried Perz³

¹ University of Applied Sciences, Institute of Innovative Health Technologies IGHT, Jena

² Universitat Politècnica de Catalunya, CREB, Barcelona, Spain

³ Helmholtz Zentrum München - German Research Centre for Environmental Health, Neuherberg, Germany

1. Introduction

QT variability (QTV) (Baumert et al., 2016) and heart rate variability (HRV) are risk stratifiers for patients with different heart diseases. In contrast to long-term analysis, short-term investigations (<30 min) provide a test result almost immediately. The data on QTV age dependency are more consistent than those on QTV gender dependency.

The objective of this study was to determine general age- and gender-related influences on short-term QT indices in a large and representative cohort of 1801 healthy subjects from the KORA S4 study.

2. Methods

Patients and pre-processing

In 1906 healthy subjects from the KORA S4 trial (Cooperative Research in the German Region of Augsburg, investigated under resting conditions in supine position) (Holle et al., 2005) the analysis of QT and HRV indices were performed based on 5 min ECGs (sampling frequency 500Hz, Einthoven lead II). For each subject, information about medical history, lifestyle, medications, etc. were raised and documented in a database. All subjects provided their written informed consent to a protocol approved by the local ethics committee of the Bavarian Medical Association. This study complies with the Declaration of Helsinki.

QT and HRV Indices

QT and heart rate time series were extracted applying an algorithm developed by Berger et al. (Berger et al., 1997). After defining a typical QT pattern for each ECG recording, the algorithm detects all QT intervals within the ECG automatically determining how much each beat must be scaled in time to best match the pattern. Estimated indices from QT analysis were: QTintmean - mean QT interval (s), QTVI_log = $\log((\text{QTvar}/\text{QTintmean}^2)/(\text{NNvar}/\text{meanNN}^2))$ where QTvar is the variance of all QT intervals, NNvar is the variance of NN intervals, and meanNN is the mean NN interval, QTc is the Bazett corrected QT interval $\text{QTc} = \text{QTintmean}/(\text{meanNN})^{1/2}$. The following linear HRV indices were computed: meanHR - mean heart rate (bpm), SDNN - standard deviation of beat-to-beat [NN] interval time series (ms), RMSSD - square root of the mean squared differences of successive NN intervals (ms), pNN50 - percentage derived by dividing the number of interval differences of successive NN intervals > 50 ms by the total number of NN intervals (%), and LFn - low frequency power divided by the sum of low and high frequency power.

Statistics

Statistics was performed using IBM SPSS 21. General age and gender dependencies of individual QT and HRV indices were investigated considering young subject groups 25-49 years old (YF - young females and YM - young males) and elderly subject groups 50-74 years old (EF - elderly females and EM - elderly males) applying the Mann-Whitney U test for two independent samples (table 1). The significance levels were set to $p < 0.01$ (*), $p < 0.0012$ (Bonferroni-Holm adjustment, **) and $p < 10^{-10}$ (***).

3. Results and discussion

With the exception of meanHR all calculated indices were significantly depending on age if comparing YM vs. EM and YF vs. EF (table 1). Diminished mean values of SDNN, RMSSD and pNN50 and increased mean values of the QT indices and LFn were associated with ageing, irrespectively of the gender. In comparison to the age group tests, the number of significant different indices in the gender group tests (YF vs. YM and EF vs. EM) was lower (n=4 vs. n=7) indicating a lower influence of the gender. The indices LFn and QTc differed more between the younger groups YF and YM than the elderly ones. The significance levels of the indices were higher in the test YF vs. YM compared to EF vs. EM indicating also an age- and gender-dependency. In comparison to females, in males the indices meanHR and QTc were lower and LFn was higher. Interestingly, the QTVI_log index retains unaffected by gender.

Table 1: Limited results of general dependence of age and gender on QT and HRV indices; *p<0.01, **p<0.0012 (Bonferroni criterion), ***p<10⁻¹⁰, NS - no significance.

| Statistical tests Indices | Mann-Whitney-U test | | | |
|------------------------------|---------------------|----------|----------|----------|
| | YM vs EM | YF vs EF | YF vs YM | EF vs EM |
| meanHR | NS | NS | ** | * |
| SDNN | *** | *** | NS | NS |
| RMSSD | *** | *** | NS | NS |
| pNN50 | *** | *** | NS | NS |
| LFn | ** | ** | *** | ** |
| QTVI_log | *** | *** | NS | NS |
| QTc | *** | *** | *** | ** |
| QTintmean | ** | * | ** | NS |

According to Baumert et al. (Baumert et al., 2016) and Bonnemeier et al. (Bonnemeier et al., 2003) this study shows a general rise of the QTV (QTVI_log) and according to Voss et al. (Voss et al., 2015) a decrease of the heart rate variability (SDNN) with increasing age, which suggests the differences in the cardiovascular structure and function with ageing.

For the first time we could show in this representative study that there are also gender differences in the QT indices QTintmean and QTc and especially in younger ages. They might be justified by the suggested hormonal changes among males and females in adolescence caused by testosterone and menopause.

These age and gender differences in healthy subjects should be considered in further research when analysing QTV and HRV.

References

- Baumert M, Porta A, Vos MA, Malik M, Couderc JP, Laguna P, Piccirillo G, Smith GL, Tereshchenko LG, and Volders PG, 2016. *Europace*.
- Berger RD, Kasper EK, Baughman KL, Marban E, Calkins H, and Tomaselli GF, 1997. *Circulation* 96, 1557-1565.
- Bonnemeier H, Wiegand UK, Braasch W, Brandes A, Richardt G, and Potratz J, 2003. *Pacing Clin Electrophysiol* 26, 377-382.
- Holle R, Happich M, Lowel H, Wichmann HE, and Group MKS, 2005. *Gesundheitswesen* 67 Suppl 1, S19-25.
- Voss A, Schroeder R, Heitmann A, Peters A, and Perz S, 2015. *PLoS One* 10, e0118308.

Oscillatory behaviour of skin blood flow in response to local temperature change

Vesna Vuksanović¹, Lawrence W Sheppard², Peter VE McClintock³,
Aneta Stefanovska³

¹ *Aberdeen Biomedical Imaging Centre, The University of Aberdeen, Aberdeen, UK*

² *Kansas Biological Survey, The University of Kansas, Lawrence, US*

³ *Department of Physics, Lancaster University, Lancaster, UK*

Background Thermal homeostasis in humans is mainly achieved by regulation of the level of blood flow in the skin. Accordingly, blood perfusion through the vessels in the skin surface constantly adjusts to the skin temperature, and the skin temperature and heat loss rate changes as a result. This enables us to examine the dynamics of thermoregulation from the point of view of the associated timescales of fluctuation. In this way, fluctuations of less than 0.1 Hz in skin blood flow are attributed to thermoregulatory control mechanisms.

Methods Simultaneous, continuous recordings of skin blood flow and skin temperature, with the sensors placed together on the volar aspect of the forearm, were performed for 30 min (basal recording), then under conditions of skin cooling (30 min) or heating (30 min). Two 1h datasets were collected from each of the ten subjects participating in the study. In each case basal recording was followed by a step change in temperature-controlled metal plate ($\approx 10 \text{ cm}^2$), to either 24°C or 42°C. We apply wavelet-based time-localized phase coherence to investigate the relationship between blood flow and skin temperature provoked by local cooling or heating. In our time-series we identified six different oscillatory components. Each of these components is recognized as different physiological process: (I) cardiac (0.6-2.0 Hz); (II) respiratory (0.145-0.6); (III) myogenic(0.145-0.052); (IV) neurogenic (0.021-0.052); (V) NO endothelial related activity (0.0095-0.021) and (VI) non-NO endothelial related activity (0.005-0.0095 Hz).

Results There was a significant ($p < 0.05$) decrease in the average frequency of myogenic blood flow oscillations and the myogenic spectral peak became more prominent. During heating, there was a significant ($p < 0.05$) general increase in spectral energy, associated with vasodilation, except in the myogenic interval. Weak phase coherence between temperature and blood flow was observed for unperturbed skin, but it increased in all frequency intervals as a result of heating.

Conclusion The mechanisms of vasodilation and vasoconstriction, in response to temperature change, are oscillatory in nature and are independent of central sources of variability.

References

- Sheppard LW, Vuksanović V, McClintock PVE, Stefanovska A 2011 *Phys Med Biol* **56** 35833601
Vuksanović V, Sheppard LW, Stefanovska A 2008 *Biophys J* **94** 78-80

Cardiovascular interactions during head-up tilt test by transfer entropy between ordinal patterns of heart rate and blood pressure¹

Dorota Wejer¹, Danuta Makowiec², Luca Faes³, Beata Graff⁴, Szymon Budrejko⁵ and Zbigniew R. Struzik⁶

¹ *University of Gdańsk, Inst. of Experimental Physics, Gdańsk, Poland*

² *University of Gdańsk, Inst. of Theoretical Physics and Astrophysics, Gdańsk, Poland*

³ *University of Trento, BIOTech Center, Dept. of Industrial Engineering, Trento, Italy
Bruno Kessler Foundation, Healthcare Research and Innovation Program, Trento, Italy*

⁴ *Medical University of Gdańsk, Dept. of Hypertension and Diabetology, Gdańsk, Poland*

⁵ *Medical University of Gdańsk, Dept. of Cardiology and Electrotherapy, Gdańsk, Poland*

⁶ *RIKEN Brain Science Institute, Wako-shi, Japan*

University of Tokyo, Graduate School of Education, Tokyo, Japan

Introduction: The coupling between cardiac and vascular systems is realized by the mechanical interactions and the neural reflexes which are responsible for maintaining homeostasis. The baroreflex is assumed to be the main control mechanism because it provides a relatively fast negative feedback.

The head-up tilt (HUT) test is a method to provoke changes in the human cardiovascular system caused by a rapid change in the body position. Heart periods and systolic blood pressure were recorded during the HUT test and have provided a noninvasive way to get insights into couplings between cardiac and vascular systems.

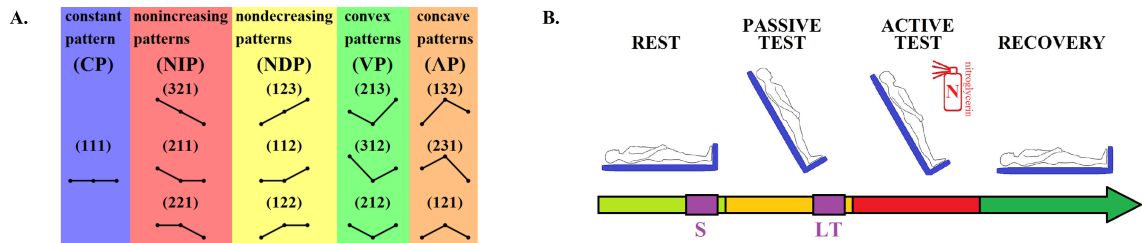


Figure 1: **A.** The categories of ordinal patterns use to calculate transfer entropy between RR and SBP series. **B.** A scheme of the HUT test. S and LT denote time-windows selected for the further analyzes related to supine position and late tilt.

Methods: The series of RR-intervals and systolic blood pressure (SBP) values were obtained by the HUT test with the controlled breathing regime, see fig. 1B. The HUT test was performed on healthy volunteers (CG: 14 males, 14 females; age: 20-39 yr, median: 23 yr; the HUT test: negative) and patients suffering from vasovagal faints

¹This work was supported by the National Science Centre, Poland, UMO: 2012/06/M/ST2/00480.

(VVS: 17 males, 42 females; age: 18-44 yr, median: 23 yr; the HUT test: positive). Transfer entropy (TE) with non-uniform embedding is used to estimate the coupling between cardiac and vascular systems [1]. The method is applied to symbolic series, where each symbol denotes one of the category of ordinal patterns [2]. Ordinal patterns are grouped into five categories, see fig. 1.A. Different signal resolutions (Δ_{RR} , Δ_{SBP}) applied to signals before mapping them into ordinal patterns series enhances the capabilities of analysis [2], because we could observe interactions between signals in different scales.

Results:

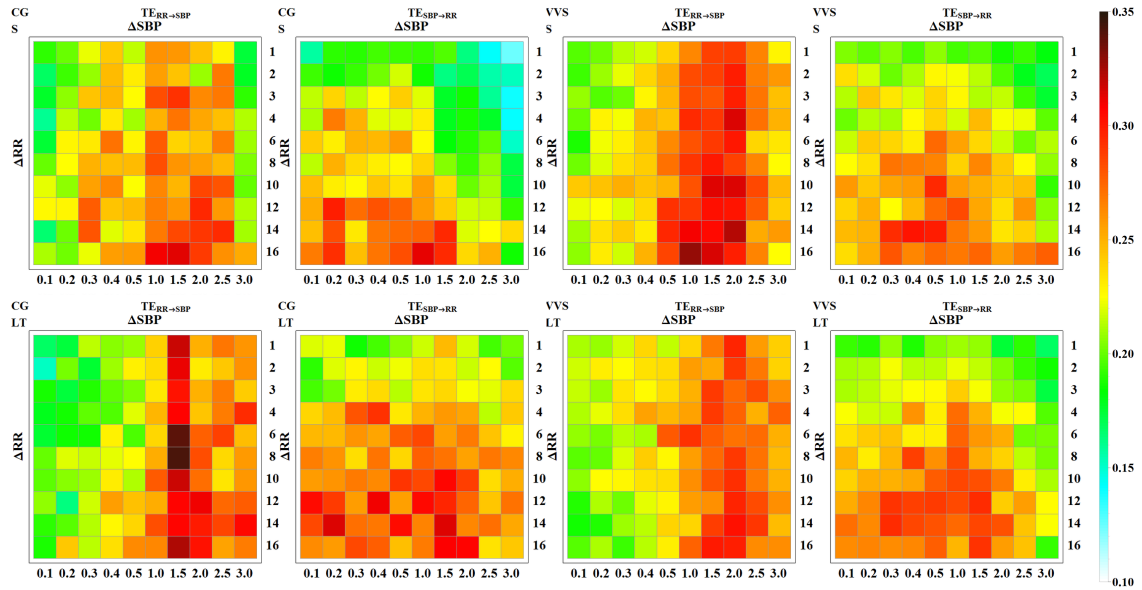


Figure 2: The values of transfer entropy for healthy people (CG) and vasovagal patients (VVS) in supine position (S - top row) and during late tilt (LT - bottom row) in both direction between patterns of RR-intervals and patterns of SBP values for the various of signal resolutions: $\Delta_{RR} = \{1, 2, 3, 4, 6, 8, 10, 12, 14, 16\}$ and $\Delta_{SBP} = \{0.1, 0.2, 0.3, 0.4, 0.5, 1.0, 1.5, 2.0, 2.5, 3.0\}$.

Conclusions: The transfer entropy between series representing RR-intervals and SBP values does not change significantly in case of vasovagal patients. Significant changes of $TE_{RR \rightarrow SBP}$ and $TE_{SBP \rightarrow RR}$ are obtained for healthy people during HUT test. Therefore our approach provides a way to observe the proper and improper interactions in cardiovascular system.

References

- [1] Faes L, Marinazzo D, Montalto A, Nollo G 2014 *IEEE Trans Biomed Eng.* **61(10)** 2556-2568
- [2] Makowiec D, Kaczkowska A, Wejer D, Żarczyńska-Buchowiecka M, Struzik Z.R 2015 *Entropy* **17** 1253-1272

Recap: 20 Years of Task Force Heart Rate Variability

Niels Wessel 1, Ljudmila Sidorenko 1,2,3, Jan F. Kraemer 1, Gert Baumann 3
and Jürgen Kurths 1

1 Humboldt-Universität zu Berlin, Department of Physics, Berlin, Germany

2 State University of Medicine and Pharmacy "Nicolae Testemitanu", Department of
External Relations and European Integration, Chişinău, Republic of Moldova

3 Charité - Universitätsmedizin Berlin, Department of Cardiology and Angiology, Berlin,
Germany

Twenty years ago the Task Force of The European Society of Cardiology and The North American Society of Pacing and Electrophysiology published the heart rate variability (HRV) standards of measurement, their physiological interpretation, and the clinical use [1]. In the Web of Science today we find more than 64000 articles dealing with HRV, the original Task Force paper [1] now has more than 10000 citations. Recently, the e-Cardiology ESC Working Group and the European Heart Rhythm Association co-endorsed by the Asia Pacific Heart Rhythm Society wrote a joint position statement about advances in HRV signal analysis [2]. They present a critical review of newly developed HRV methodologies developed after publication of the initial Task Force HRV overview [1] and their applications in different physiological and clinical studies. These novel approaches improved the technical understanding of the HRV signal, however, their success in clinical applications, such as in the identification of high-risk patients, have been rather limited.

Therefore, we present here one possible explanation for this limited success that merits additional attention: The importance of monitoring respiration for the interpretation of standard HRV analysis and the need to address its complexities using improved signal processing methods. In a case report [3] we introduced a 20-year-old woman who had a non-sustained ventricular tachycardia (VT). Cardiac autonomic function was evaluated via standard heart rate variability analysis which found a remarkably increased power in the low frequency (LF) band in the resting state. Standard interpretation would suggest an increased sympathetic activity (cf. Fig. 1a).

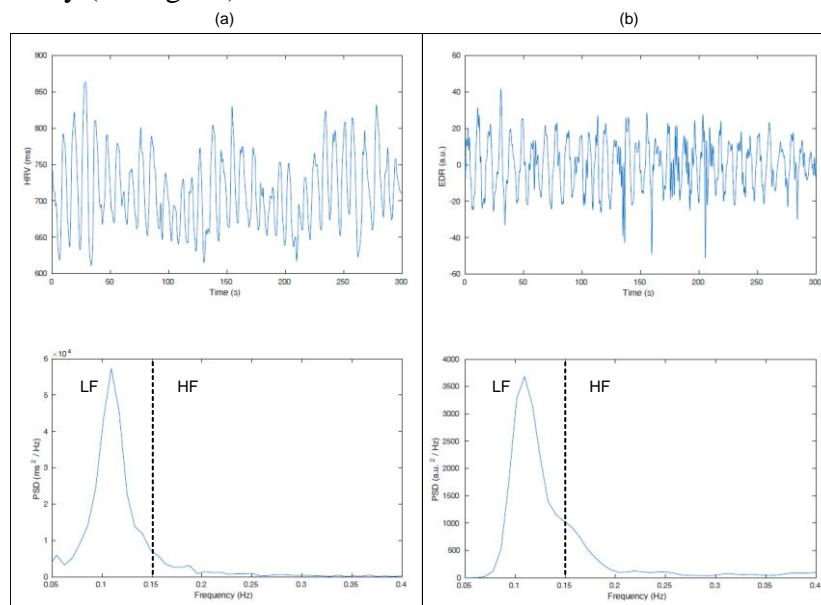


Fig. 1: (a) Five minute HRV recording of a 20-year-old woman with previously diagnosed non-sustained ventricular tachycardia while recording sinus rhythm with the corresponding power spectral density and (b) the EDR estimated from the ECG morphology as well as its power spectral density.

In this case report we additionally looked for respiration. This arose from our experience in this matter that also led to us answering the question raised by Lean Glass ‘Is the normal heart rate chaotic?’ (Reference 45 in [2]) with another question ‘Is the normal heart rate "chaotic" due to respiration?’[4]. There we demonstrated the principal influence of respiration in short-term HRV recordings. In the current case report [3], the power spectra of both the respiration and HRV showed an almost identical picture (cf. Fig. 1); leading to the conclusion that respiration is clearly dominating the HRV. It follows that the 20-year-old woman does not have a sympathetic overactivation, but a situational changed respiratory pattern, shifting the whole spectrum to the LF band. Hence, β -blockers are not the appropriate therapy.

Baumert et al. [5] advocated the inclusion of respiratory rate as a covariate of respiratory sinus arrhythmia in sleep studies. We suggest that respiration has to be considered as a covariate for all HRV analyses. The respiratory signal can be measured very easily and where the measurement is not possible the signal can be estimated indirectly from the ECG with high precision regarding the respiratory rate. This offers the possibility to apply more complex signal processing methods such as cardiorespiratory synchronization or coordination [6] which will very likely improve the success in clinical application. Finally, it avoids mistakes in the interpretation of the cardiac autonomic function of the heart.

Looking at the huge expertise of the members of the European Study Group of Cardiovascular Oscillations we suggest publishing a position statement about methodological advances in the recent years with clear recommendations for clinical application.

References

1. Malik M, Camm J, Bigger JT, Breithardt G, Cerutti S, Cohen RJ, et al. Heart rate variability: standards of measurement, physiological interpretation and clinical use. Task Force of the European Society of Cardiology and the North American Society of Pacing and Electrophysiology. *Circulation* 1996; 93: 1043-1065.
2. Sassi R, Cerutti S, Lombardi F, Malik M, Huikuri HV, Peng CK, et al. Advances in heart rate variability signal analysis: joint position statement by the e-Cardiology ESC Working Group and the European Heart Rhythm Association co-endorsed by the Asia Pacific Heart Rhythm Society. *Europace* 2015; 17: 1341-1353.
3. Sidorenko L, Kraemer JF, Wessel N, Standard heart rate variability spectral analysis: Does it purely assess cardiac autonomic function? *Europace* 2016, in press.
4. Wessel N, Riedl M, Kurths J. Is the normal heart rate "chaotic" due to respiration? *Chaos* 2009; 19: 028508.
5. Baumert M, Pamula Y, Porta A, Immanuel SA. Towards a more accurate analysis of respiratory sinus arrhythmia during sleep. *Sleep Med*. 2016, in press.
6. Riedl M, Müller A, Kraemer JF, Penzel T, Kurths J, Wessel N. Cardio-respiratory coordination increases during sleep apnea. *Plos One* 2014; 9: e93866.

Cardio-respiratory coordination during sleep

M Riedl, Department of Physics, Humboldt-Universität zu Berlin, Germany, maik.riedl@physik.hu-berlin.de

A Müller, Department of Physics, Humboldt-Universität zu Berlin, Germany, andreas.mueller@physik.hu-berlin.de

J F Kraemer, Department of Physics, Humboldt-Universität zu Berlin, Germany, jkraemer@physik.hu-berlin.de

T Penzel, Department for Cardiology, Charité Universitätsmedizin Berlin, Germany, thomas.penzel@charite.de

J Kurths, Department of Physics, Humboldt-Universität zu Berlin, Germany, juergen.kurths@physik.hu-berlin.de

N Wessel, Department of Physics, Humboldt-Universität zu Berlin, Germany, wessel@physik.hu-berlin.de

Obstructive apnoeas and hypopnoeas (AHE) are defined by reduced or disrupted ventilation which is caused by obstructions of the upper airways during sleep. In order to characterise the autonomic regulation during AHE, we concentrate on the mutual influence of the cardiac and respiratory oscillations on their respective onsets, the cardio-respiratory coordination (CRC). We find not only that the occurrence of CRC is significantly more frequent during AHE than in normal respiration but also more frequent after these events.

Increased inspiratory resistance alters the cardiac contribution to the dynamic relationship between blood pressure and pial artery pulsation oscillations in healthy subjects

Pawel J. Winklewski¹, Jacek Wolf^{2,3}, Magdalena Wszedybyl-Winklewska¹, Ewa Swierblewska², Katarzyna Kunicka³, Kamila Mazur⁴, Marcin Gruszecki⁵, Wojciech Guminski⁶, Andrzej F. Frydrychowski¹, Leszek Bieniaszewski², Krzysztof Narkiewicz^{2,3}

¹ *Institute of Human Physiology, Medical University of Gdansk, Gdansk, Poland*

² *Department of Hypertension and Diabetology, Medical University of Gdansk, Gdansk, Poland*

³ *Department of Cardiovascular Diseases, International Clinical Research Center, St. Annes University Hospital in Brno (FNUSA), Brno, Czech Republic*

⁴ *Department of Biomedical Engineering, Faculty of Electronics, Telecommunications and Informatics, Gdansk University of Technology, Gdansk, Poland*

⁵ *Department of Radiology Informatics and Statistics, Medical University of Gdansk, Gdansk, Poland*

⁶ *Department of Computer Communications, Faculty of Electronics, Telecommunications and Informatics, Gdansk University of Technology, Gdansk, Poland*

Aim

There is increasing evidence that heart performance directly influences cerebral perfusion. We hypothesised that increased inspiratory resistance will affect the cardiac contribution to the relationship between blood pressure and pial artery pulsation oscillations.

Methods

Experiments were performed in a group of 20 healthy volunteers undergoing controlled intermittent Mueller Manoeuvres (Figure 1). Blood pressure and heart rate were measured using continuous finger-pulse photoplethysmography; oxyhaemoglobin saturation with an ear-clip sensor; end-tidal CO₂ with a gas analyser; cerebral blood flow velocity, pulsatility and resistive indices with Doppler ultrasound. Changes in the pial artery pulsation and in the width of subarachnoid space were recorded with a new method called near-infrared transillumination/backscattering sounding. Wavelet transform analysis was used to assess the relationship between blood pressure and pial artery pulsation oscillations.

Results

Initiating Mueller manoeuvres evoked pial artery pulsation decline, blood pressure

Table 1: Effects of a 60s Mueller manoeuvres series on wavelet coherence and wavelet phase coherence between blood pressure and pial artery pulsation oscillations at cardiac frequency. Data are presented as mean values and standard deviations. The minimum and maximum correspond to wavelet coherence minimum and maximum values during the Mueller manoeuvres series.

| | Base. | Min. | Min. vs. Base. (%) | Max. | Max. vs. Base. (%) | Max. vs. Min. (%) |
|------------|-------------|-------------|--------------------|-------------|---------------------|---------------------|
| WCO left | 0.65 ± 0.15 | 0.44 ± 0.30 | 67.7* | 0.67 ± 0.22 | 103.1 ^{NS} | 152.3** |
| WCO right | 0.52 ± 0.18 | 0.28 ± 0.26 | 54.0** | 0.64 ± 0.17 | 123.1 ^{NS} | 228.6*** |
| WPCO left | 0.86 ± 0.36 | 0.85 ± 0.36 | 98.8 ^{NS} | 0.78 ± 0.42 | 90.7 ^{NS} | 91.8 ^{NS} |
| WPCO right | 0.87 ± 0.35 | 0.83 ± 0.35 | 95.4 ^{NS} | 0.93 ± 0.26 | 106.9 ^{NS} | 112.0 ^{NS} |

* P<0.05; ** P<0.01; *** P<0.001; WCO – wavelet coherence; WPCO – wavelet phase coherence; cc-TQ – cardiac component of transillumination quotient (pial artery pulsation); left – left hemisphere; right – right hemisphere; SD – standard deviation

and heart rate increase. By the end of Mueller manoeuvres, pial artery pulsation and heart rate did not change, but blood pressure was elevated. A decrease in wavelet coherence between blood pressure and pial artery pulsation oscillations at cardiac frequency found in the first half of the Mueller manoeuvres was followed by recovery by the end of Mueller manoeuvres. Wavelet phase coherence was high at baseline and did not change throughout the Mueller manoeuvres (Table 1; Figure 2, Figure 3).

Conclusions

Increased inspiratory resistance is associated with swings in the cardiac contribution to the dynamic relationship between blood pressure and pial artery pulsation oscillations. Impaired cardiac performance reported in Mueller manoeuvres may be transmitted to the cerebral microcirculation.

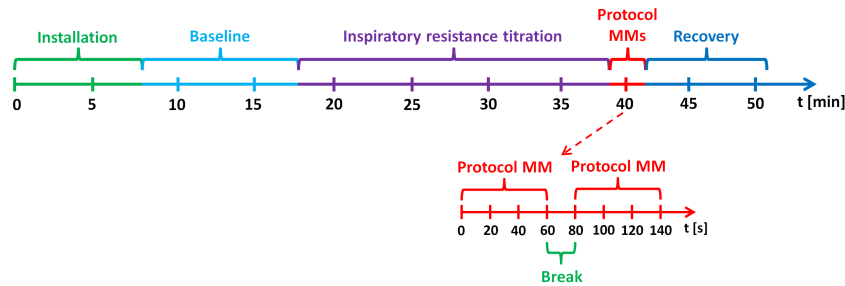


Figure 1: Schematic representation of the study design.

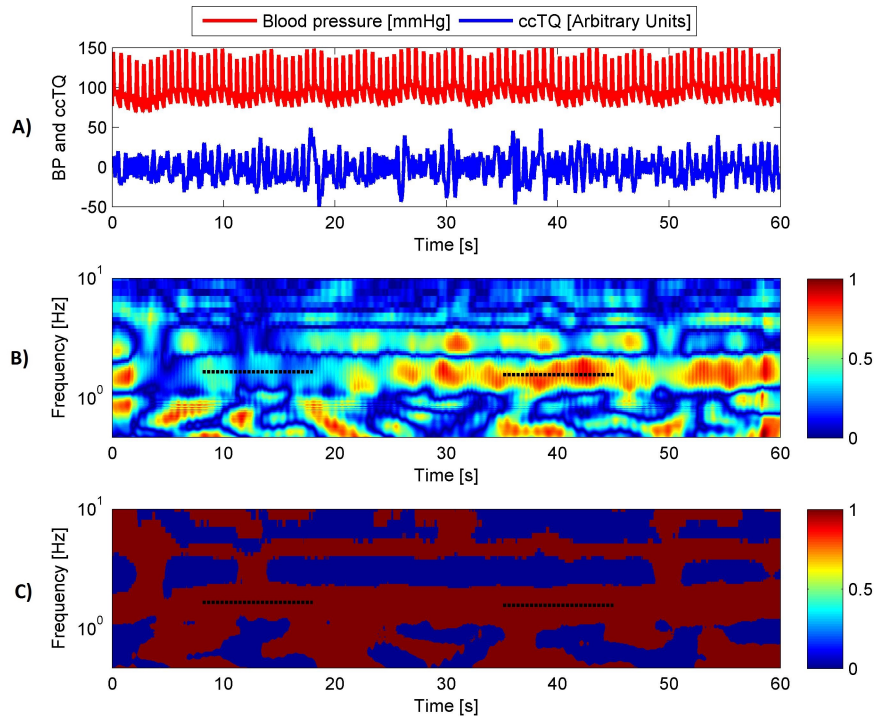


Figure 2: Representative wavelet coherence (WCO, panel B) and wavelet phase coherence (WPCO, panel C) tracings. Blood pressure (BP, red) and pial artery pulsation (cc-TQ, blue) signals are provided in the panel A. Wavelet coherence reaches its minimum between 8 and 18s of the Mueller manoeuvres, and later upon recovery, reaches its maximum between 35 and 45s for cardiac frequency. Wavelet phase coherence remains stable. Cardiac frequency is indicated by horizontal dotted lines.

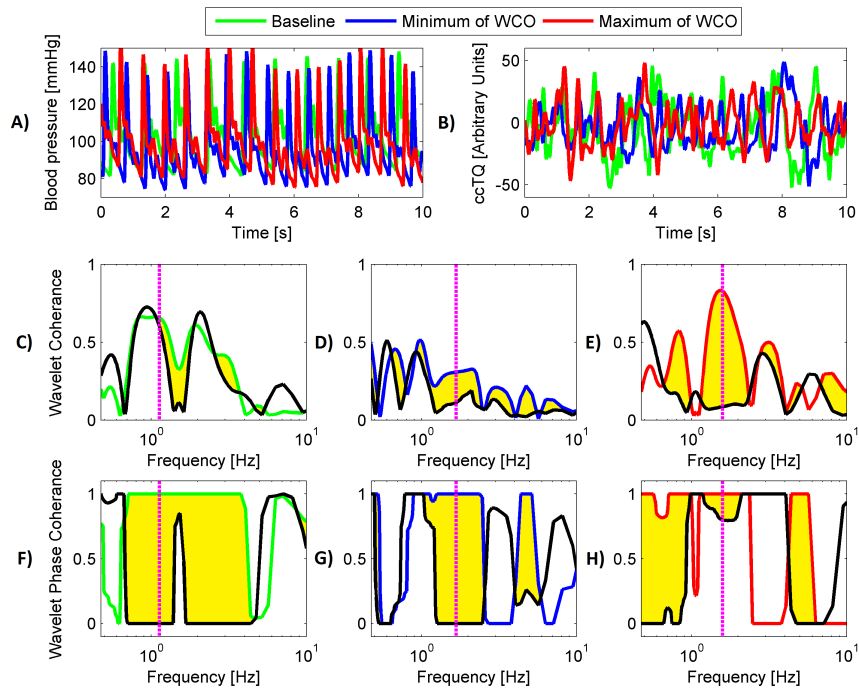


Figure 3: Representative tracings of 10s signals of baseline (in green), 10s of minimum wavelet coherence (WCO, in blue) and 10s of maximum wavelet coherence (WCO, in red). Blood pressure oscillations (BP, panel A), pial artery pulsation oscillations (cc-TQ, panel B), wavelet coherence (WCO, panels C, D and E) and wavelet phase coherence are shown (WPCO, panels F, G and H). Cardiac frequency is indicated by vertical, magenta, dotted lines.

Recurrence plot and multifractal analysis of fetal heart rate variability – dependence on gestational age

Jan J. Żebrowski 1, Jan Gieraltowski 1, Uwe Schneider 2, and Dirk Hoyer 3

1 Cardiovascular Physics, Faculty of Physics, Warsaw University of Technology, Warsaw, Poland

2 Jena University Hospital, Department of Obstetrics, Friedrich Schiller University, Jena, Germany

3 Jena University Hospital, Biomagnetic Center, Hans Berger Department of Neurology, Friedrich Schiller University, Jena, Germany

During gestation the autonomic nervous system develops which results in changes of the fetal heart rate variability. We have previously published results on multiscale entropy and multiscale multifractal analysis indicating dependencies of fetal heart rate variability (HRV) on gestational age (GA) [1,2]. Here, we present new results on fetal heart rate variability development with GA using recurrence plot analysis.

Data: We analyzed normal singleton fetuses, healthy according to standard obstetric observation methods, in a non-stress situation. All magnetocardiographic (MCG) recordings were taken by a vector-magnetograph in a magnetically shielded room at the Biomagnetic Center at gestation age 18-39 weeks. The pregnant women were positioned supine or with a slight twist of the body. The MCG signal was recorded over a period of 30 minutes with a sampling rate of 1024 Hz. The fetal heart beats were automatically detected. The data consisted of 360 recordings over 30 min, 10 min sections were extracted from the 30 min recordings which had a well defined sleep state: quiet ($n = 92$) and active ($n = 292$).

Methods: Recurrence plots (RP) were computed for each 30 min recording without windowing. Standard Recurrence Quantitative Analysis (RQA) was calculated using the Matlab package [3]: recurrence rate RR, determinism Det, entropy of diagonal lines Entropy, the length of vertical lines V and trapping time TT were calculated. For each recording, the Takens delay was found using mutual information and the embedding dimension – using the False Nearest Neighbors method. The recurrence diagram tolerance parameter was set empirically at 20 (no normalization was used) from a range of 10-40.

An Activity Index, enabling to distinguish a fetus in the quiet state from an active one, was found by calculating, for each 10 min recording, the recurrence diagrams using a 100 data point sliding window shifted by its length, embedding dimension 10, Takens delay = 5 and tolerance parameter = 10. Next, a histogram of the recurrence rate in each window was found. There were always a number of windows for which a 0 was obtained for the recurrence rate. The activity index is defined as the ratio of the number of windows with RR=0 to the number of all other windows – with a nonzero RR value.

The Multiscale Multifractal Method of [2] was applied to the complete set of 30 min recordings ($n = 360$) and the correlation surface between the Hurst surface and gestation age of the fetuses was obtained.

Results: Of all the RQA parameters only Det and Entropy yielded interesting results. The first step was to check whether the active and quiet sleep fetal HRV may be distinguished by RQA. It was found that both for Det vs GA and Entropy vs GA the results calculated using the 10 min recordings, for the two sleep states, practically coincide. This opened the possibility to analyze the 30 minute recordings for which the state may have been active, quiet or mixed.

It was then found that both Det and Entropy for the 30 min recordings decrease with GA. However, at the week 30-32, Det evidently begins to decrease more slowly while Entropy

definitely levels out (Fig.1). There is a rather large spread between the results of the RQA measures obtained for a given gestation week.

The new Activity Index is able to discern between active and quiet fetal states based on 10 min recordings. Despite the large spread in the results the Activity Index values are well separated. The results for the multiscale multifractal analysis of the 30 min recordings are similar to the results obtained for a different group of recordings in [2]. Similar scale and q-parameter values yielding the largest correlation of the local Hurst exponent $h(q,s)$ with GA were obtained.

Conclusions: RQA Determinism is a measure of the occurrence of unstable periodic orbits (UPO) in the data – a feature of deterministic dynamics of the system. Entropy of the diagonal lines in the RP is a measure of the disorder of the UPOs. The observed behavior of the RQA parameters indicates that, as the autonomic nervous system (ANS) regulation of heart rate variability grows with GA, the initial simple (deterministic) properties of the heart rate variability due to the self-oscillatory conduction system of the fetal heart become dominated by a more complex (disordered) variability due to the effect of the ANS on the fetal heart rate. At the same time, entropy of the diagonal lines decreases indicating a less complex structure of the UPOs. This effect seems to be in keeping with the increase of long term correlations observed at later GA [4]. The process appears to be complete at about GA 30 weeks after which the entropy stays approximately constant. The results seem to confirm earlier findings indicating a transition in the properties of fetal heart rate variability at about the gestation age of 30 weeks [4,5].

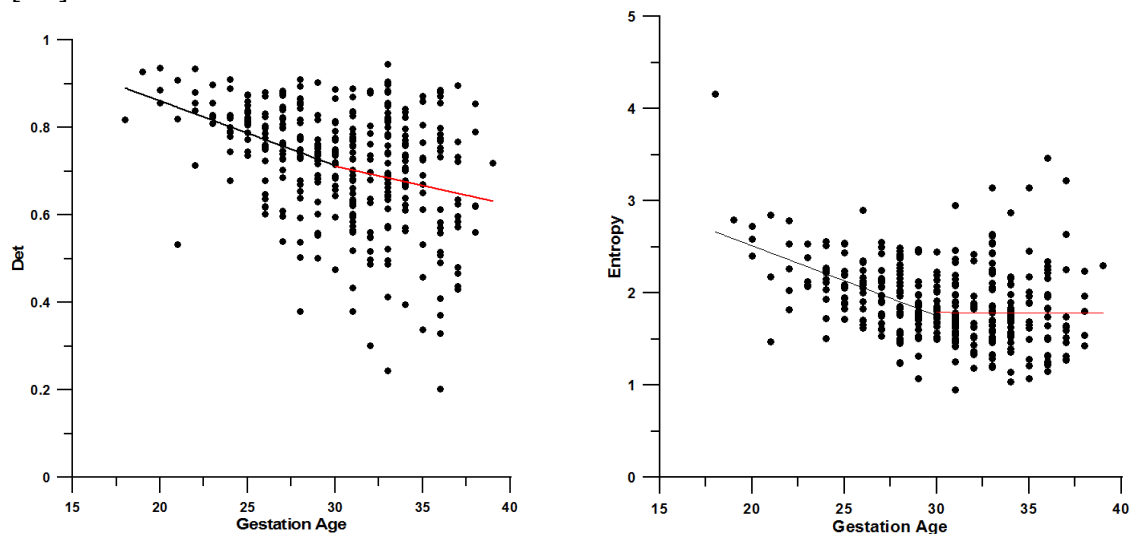


Figure 1 Left panel: Determinism vs Gestational Age; Right panel: Entropy vs Gestational Age

References

- [1] Hoyer, D., Nowack, S., Bauer, S., Tetschke, F., et al., 2013 *Am. J. Physiol. Regul. Integr. Comp. Physiol.* **304**, R383-R392.
- [2] Gierałowski J, Hoyer D, Schneider U, Żebrowski JJ, 2015 *Autonomic Neuroscience* **190**, 33-39
- [3] <http://tocsy.pik-potsdam.de/CRPtoolbox> by Norbert Marwan
- [4] Hoyer D , Nowack, S., Bauer, S., Tetschke, F., et al., 2012 *Computers in Biology and Medicine* **42** 335–341
- [5] Van Leeuwen P, Geue D, Lange S, Hatzmann W, Grönemeyer D, 2003 *Prenat Diagn*; **23** 909–916.

3.4 Poster presentations

Effect of malaria on the dynamics and rheological properties of blood flow in a microvasculature

Yunus Abdulhameed Abdussalam and Aneta Stefanovska

Physics Department, Lancaster University, Lancaster, United Kingdom

Blood is circulated through a closed system of vessels. The ultimate goal of the circulation is transport of nutrients and oxygen to every cell in the body. Thus, one can consider blood circulation as consisting of two main parts: (i) blood flow through large vessels, with relatively high velocities and under high pressure difference, and (ii) blood perfusion that happens in small vessels that form microvascular beds, with small velocities of flow and small pressure differences [1,2,3].

While the blood flow in the large vessels can be modelled by Navier-Stokes equations, the assumptions needed for their applications to model blood perfusion are difficult to meet. Mechanical assumptions in the description of blood flow have neglected many important physiological properties that manifest in this blood flow [3,5].

Noninvasive measurement of blood perfusion, using e.g. laser Doppler flowmetry (LDF), or blood oxygenation, using e.g. near infrared spectroscopy, provides insights into the dynamic properties of microvascular flow. A number of studies have demonstrated that the measured signals are characterised by complex oscillations spanning the frequency interval from the cardiac pulse (around 1 Hz in healthy humans in repose) down to 0.005 Hz which include endothelial-related oscillations [1,4].

High deformability is a prerequisite for healthy red blood cells (RBCs) because, in order to facilitate adequate transport of oxygen to the various parts of the body they must squeeze their way through narrow capillaries. In the onset of malaria, the Plasmodium parasite invades the red blood cells (RBCs) right from the erythrocytic stage and strongly influence the mechanical behaviour of the RBC [2,6]. The essential consequence of malaria from the mechanistic perspective is the significant increase in stiffness and cytoadherence of the Plasmodium parasitized RBCs to the inner linings of the Capillaries. This causes them to sequester themselves in the microvascular bed [6]. It may therefore be postulated that the net result will be an impairment of blood flow oscillations and, especially, of the oscillatory processes associated with microvascular dynamics (the myogenic, neurogenic and endothelial activities). It therefore seems reasonable to hypothesize that both the blood flow oscillatory components, the deformability and adhesion of RBCs are markedly affected in malaria and hence, that the biorheological properties of blood will be changed.

In this work we will review the biomechanics and hemodynamics models of microvascular flow and compare the existing models with the information extracted from measured data, thus demonstrating the relevance of biomechanics in studying malaria. In particular, we will investigate the effect of malaria on microvascular flow. The variations in hemorheological properties in malaria on account of the spatial distributions of erythrocytes, the increased blood viscosity, the altered flow resistance and wall shear stress in blood vessels, and associated high velocity component at the vessel wall have already been documented [6]. We will seek evidence of manifestation of these changes on endothelial-related oscillations observed in the LDF signal. Hence a detailed understanding of the relationship between the hemorheological and hemodynamic properties will be established.

References

1. Stefanovska A., Bračič M. 1999 Physics of the human cardio-vascular system. *Contemp. Phys.* **40(1)**: 31-55.
2. Popel A. S., Johnson C. P. 2005 Microcirculation and hemorheology. *Annu. Rev. Fluid Mech.* **37(1)**: 43-69.
3. Fung Y. C., Zweifach B. W. 1971 Microcirculation: mechanics of blood flow in capillaries. *Annu. Rev. Fluid Mech.* **3(1)**: 189-210.
4. Jayanthi A. K., Sujatha N, Ramasubba M. R. 2011 Measuring blood flow: Techniques and applications – A review. *Int. J. Res. Review Appl. Sci.* **6**: 203-216.
5. Thiriet M. 2008 *Biology and mechanics of blood flows: Part II: Mechanics and medical aspects*. Springer New York, pp 11-30.
6. Yeom E., Kang Y. J. Lee S. J. 2014 Changes in velocity profile according to blood viscosity in a microchannel. *Biomicrofluidics*, **8**: 034110.

Continuous Information Extraction From Blood Pressure Data Using Attractor Reconstruction

Philip J. Aston¹, Manasi Nandi², Mark I. Christie², Ying H. Huang¹
and Hitesh B. Mistry³

¹*Department of
Mathematics
University of Surrey
Guildford
UK*

²*Institute of
Pharmaceutical Science
King's College London
London
UK*

³*Manchester Pharmacy
School
University of Manchester
Manchester
UK*

The cardiovascular system keeps blood in continuous motion around the body and must be able to adapt to changes in the body's physiology such as sleep, postural changes, exercise and of course disease. The blood pressure signal is an approximately periodic waveform which is affected by many of the physiological processes in the body and therefore contains a lot of information, but it is also irregular, strongly non-stationary and noisy. Advances in monitoring technology allow blood pressure waveforms to be collected at sampling frequencies of up to 1000Hz which results in large quantities of data when monitoring over many days. The classic problem, having collected all the data, is to derive useful information from it.

Commonly derived features of the blood pressure signal are the systolic and diastolic pressures. The beat-to-beat intervals provide the foundation for the many methods that consider Heart Rate Variability [1]. However, all of these approaches ignore the wealth of information that is contained in the varying waveform profile.

We describe a new approach for extracting useful information from such large and complex data. We use Takens' method of delay coordinates to reconstruct an attractor [2]. Conventionally, when Takens' method is used, the first step is to find the optimal embedding dimension using, for example, the method of false nearest neighbours [3]. Our aim is to use properties of a reconstructed attractor to provide information regarding key features of the data and for this purpose we choose an embedding dimension of $n = 3$ which provides us with an attractor in a three dimensional phase space that is easily visualised. The time delay τ that separates the three delay coordinates is chosen to be one third of the average cycle length, so that the points are evenly spaced across each cycle.

The naturally occurring baseline variation in the signal results in a noisy attractor. Many methods have been proposed for removing baseline wander, but we show that simply viewing the attractor in the three dimensional phase space down the

$x = y = z$ axis results in the elimination of constant shifts in the vertical direction, and is surprisingly effective at removing baseline wander. This projection onto a plane gives us a two dimensional attractor. In order to extract more information from the mass of lines that make up this attractor, we compute a density on a square grid, as shown in Fig. 1, that we refer to as a ‘cardiomorph’.

We extract particular features of this density (e.g. maximum density, angle of rotation of the attractor) which, in many cases, relate to particular features of the waveform. Using this approach on a window of data, and moving the window through a long dataset gives us a collection of time traces that show the variability of the chosen features of the density.

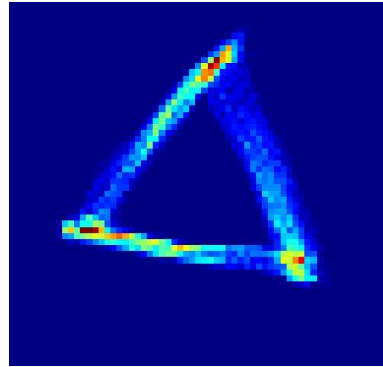


Figure 1: A density derived from a reconstructed attractor after removal of baseline variation.

We have previously shown that this approach is capable of detecting changes in blood pressure data that HRV methods cannot detect [4]. More recently, we have shown that this approach can provide very early detection of sepsis infection in mice.

References

- [1] U.R. Acharya, K.P. Joseph, N. Kannathal, C.M. Lim and J.S. Suri. Heart rate variability: a review. *Med. Bio. Eng. Comput.* **44**, 1031–1051, 2006.
- [2] F. Takens. Detecting strange attractors in turbulence. *Dynamical Systems and Turbulence*, Warwick 1980, Lecture Notes in Mathematics 898, 366–381, 1981.
- [3] H.D.I. Abarbanel, R. Brown, J.J. Sidorowich and L.S. Tsimring. The analysis of observed chaotic data in physical systems. *Rev. Mod. Phys.* **65**, 1331–1392, 1993.
- [4] P.J. Aston, M. Nandi, M. Christie and Y. Huang. Comparison of attractor reconstruction and HRV methods for analysing blood pressure data. *Computing in Cardiology* **41**, 437–440, 2014.

Entropy relations in infinitely clipped differential time series

Omer Mohamoud¹, Ivana Kovacic¹, Tamara Skoric¹, Nina Japundzic Zigon² and Dragana Bajic¹

¹University of Novi Sad, Faculty of Technical Sciences-CEVAS, Novi Sad, Serbia

²University of Belgrade, School of Medicine, Belgrade, Serbia

Continuous monitoring ceased to be a privilege of medical doctors: development of sensors and communications equipment initiated extensive implementation of monitoring during sleep, walk, fitness, recreation etc. The amount of collected data is huge, approaching the boundaries of “big data, but the data are non-stationary, polluted by artefacts and consequently unsuitable for blind automatic analysis. The consumers, on the other hand, are unwilling to perform the signal pre-processing, expecting statistics to effortlessly appear at the display.

The effects of non-stationarity and most of the errors would be attenuated, if the data have been differentiated and binary coded. Unfortunately, the coarseness of binary coding reduce the information content as well. But, long ago, it was shown that speech signal, if infinitely clipped, preserves the intelligibility [1]. Motivated with this, we set the hypothesis that information content, preserved in binary coded signal, is sufficient to allow (cross) approximate entropy estimation. We have chose $(X)ApEn$ as it is approved in many clinical studies, with more than 4000 quotations [2]. Its straightforward application in this context is impossible, as it requires stationarity, it is sensitive to errors, and due to complexity $\sim O(N^2)$ it is time consuming. We tested the proposed $(X)BinEn$ – i.e, $(X)ApEn$ applied to a series of binary differential time series - against the known results [3], where the laboratory animals of two kinds (normotensive and borderline hypertensive rats) were exposed to restraint and to shaker stress.

The complexity of $(X)BinEn$ estimation is linear: it is sufficient to find the histograms $N_Y(n)$ and $N_X(k)$ of all binary vectors of length m in the observed time series \mathbf{x} and \mathbf{y} . The distances are calculated in a Hamming sense (details in the full text).

$$\hat{p}_k^m(r) = \Pr\{d(\mathbf{X}_m^{(k)}, \mathbf{Y}_m) \leq r\} = \frac{1}{N - (m-1) \cdot \tau} \sum_{n=0}^{2^m-1} N_Y(n) \cdot \mathbb{I}\{h_{kn}^{(m)} \leq r\} \quad (1)$$

$$d(\mathbf{X}_m^{(i)}, \mathbf{Y}_m^{(j)}) = \sum_{k=0}^{m-1} x_{i+k \cdot \tau} \oplus y_{j+k \cdot \tau} = \sum_{k=0}^{m-1} \mathbb{I}\{x_{i+k \cdot \tau} \neq y_{j+k \cdot \tau}\}, \quad i, j = 1, \dots, N - (m-1) \cdot \tau \quad (2)$$

The concept of Joint symbolic dynamics [4] is also defined over the differential binary time series. We show that, if the threshold value is set to zero, $(X)BinEn$ is actually equal to a difference between JSDsh entropies for symbols of different length.

References

- [1] Fawe A, Interpretation of infinitely clipped speech properties, 1966, *IEEE Transactions on Audio and Electroacoustics*, VOL 14-4: 178–183.
- [2] Yentes J.M, Hunt N, Schmid K.K, Kaipust J.P, Mcgrath D, Stergiou N, The appropriate use of approximate entropy and sample entropy with short data sets, 2013, *Annals of Biomedical Engineering*, VOL 41: 349–365.
- [3] Boskovic A, Loncar-Turukalo T, Sarenac O, Japundzic-Zigon N, Bajic D, Unbiased entropy estimates in stress: a parameter study, 2012, *Computers in Biology and Medicine*, VOL 42: 667–679, 2012.
- [4] Baumert M, Baier V, Truebner S, Schirdewan A, Voss A, Short- and Long-Term Joint Symbolic Dynamics of Heart Rate and Blood Pressure in Dilated Cardiomyopathy, 2005, *IEEE Transactions on biomedical engineering*, VOL 52: 2112-2115.

Model of membrane-potential fluctuations

Miraslau L. Barabash and Aneta Stefanovska

Lancaster University, Physics Department, Lancaster, LA1 4YB, UK

Introduction

The existence of a biological cell is impossible without K^+ , Na^+ and Cl^- ions. Their transport through a membrane can be enhanced or inhibited by additional factors, for instance by calcium or ATP. The role of all mentioned substances in the evolution of excitable cells, especially in temporal evolution of the membrane potential, has been well investigated (see e.g. [1]). In nonexcitable cells, however, temporal behaviour of the membrane potential is usually overlooked. Here we argue that properties of this behaviour may provide useful indicators of cellular dynamics, and propose a mathematical model to describe them.

Modern modelling techniques usually focus on single ion channels. Standard models include the Poisson-Nernst-Planck (PNP) approach, Brownian dynamics (BD), molecular dynamics (MD) [2, 3], and phenomenological methods [4]. The PNP approach deals with ion diffusion in an electric field, the charges and fields being space-continuous functions. Applicability of PNP retains as long as the diffusion approximation holds. BD treats the motion of discrete ions in a continuous bulk; the stumbling-block are approximations for the interionic potential. MD considers all particles (including the bulk and channel) as discrete entities; its computational demand to date does not allow the prediction of the main property of an ion channel (and consequently the membrane) — its conductance.

One of the semimechanical approaches, the Hodgkin-Huxley model, operates in terms of the transmembrane current and voltage. This model is unable to self-consistently account for the effects from the spatial domain near the membrane. For instance, one requires auxiliary methods such as the Goldman-Hodgkin-Katz equation to estimate the reversal potentials. Ion-ion interactions are also not taken into consideration, thus excluding charge screening and hydration effects.

Thus, one or several of the following issues is usually missed: coupling between the concentration gradient and voltage, active transport, gating mechanisms, hydration, and time-variability of membrane constituents. To grasp these crucial points simultaneously, we expand the PNP model which itself consistently couples ionic concentrations and the electric potential. In our model of whole-cell potential dynamics, an explicit current term introduces the active transport, while effects of gating, hydration and time-variability are comprised by the corresponding sensitivities of the diffusivity.

Model

We employ the following Poisson-Nernst-Planck equations

$$\frac{\partial c_m}{\partial t} = -\nabla \mathbf{J}_m, \quad \mathbf{J}_m = -D_m \left(\nabla c_m + \frac{z_m e}{k_B T} c_m \nabla \phi \right) + \mathbf{j}_m, \quad \nabla(\varepsilon \nabla \phi) = -4\pi \rho,$$

where dynamics of m^{th} ion species' concentration c_m is coupled with its flux \mathbf{J}_m via the electric potential ϕ with the local charge density $\varrho(c_1, \dots, c_N)$. The equations are fulfilled in three compartments: bulk A, membrane M, and bulk B. Matching of solutions follows from the conditions of continuity at each boundary:

$$c|_{\mathbf{r}-0} = c|_{\mathbf{r}+0} \quad (\text{concentration continuity}), \quad (1)$$

$$(D\nabla c_m)|_{\mathbf{r}-0} = (D\nabla c_m)|_{\mathbf{r}+0} \quad (\text{flux continuity}). \quad (2)$$

A membrane consists of a number of ion-channels species [5], therefore, all their transport properties are naturally reflected by the parameters of our model. Electrodiffusion is described by the diffusivity D_m , specific for each compartment. This specificity effectively reflects ion hydration in a bulk so that the diffusion constant is smaller for hydrated ions. Membrane permeation properties, stemming from the ion channel's properties, are explicitly incorporated by the functional dependence of D_m on the corresponding stimulus (see e.g. [5]). This includes gating effects (e.g. from calcium or voltage), but as well can include the influence of ion-channel blockers (e.g. tetrodotoxin). For instance, for the membrane being impermeable to some ion species Eq. (2) transforms to zero. The explicit flux \mathbf{j}_m , existing only in compartment M, introduces active transport mechanisms such as \mathbf{j}_K and \mathbf{j}_{Na} for the ubiquitous Na/K exchanger. Finally, time-variability of membrane constituents is described by the explicitly time-dependent diffusivity $D_m = D_m(\mathbf{r}, t)$ for the ions in compartment M.

Summary

We introduce a model which self-consistently describes ion transport and voltage dynamics across the whole membrane, and includes effects of K^+ , Na^+ , Cl^- , Ca^{2+} and ATP. Predictions for voltage fluctuations and their spectral properties will be compared with these received from the human T-lymphocytes [6, 7]. In our analysis we discuss possible candidates for the fluctuation source, canvass the goals of the model and its discrepancies with experimental data. To conclude, consideration of voltage dynamics allows us to capture the dynamics of membrane transport properties, and thus can be a useful tool in analysing the properties of its constituents.

References

- [1] B. Hille, *Ion Channels of Excitable Membranes*, University of Washington, 3 edition, 2001.
- [2] S. Kuyucak, O. S. Andersen, and S.-H. Chung, Rep. Prog. Phys. **64**, 1427 (2001).
- [3] S.-H. Chung and B. Corry, Soft Matter **1**, 417 (2005).
- [4] J. Zheng and M. C. Trudeau, editors, *Handbook of ion channels*, Taylor & Francis Group, LLC, 2015.
- [5] M. D. Cahalan and K. G. Chandy, Immunol Rev. **231**, 59 (2009).
- [6] S. Patel, *The role of membrane potential dynamics in cell behaviours: investigating the membrane potential dynamics in the Jurkat and HMEC-1 cell lines using the continuous wavelet transform*, PhD thesis, Division of Biomedical and Life Sciences, Lancaster University, 2015.
- [7] A. K. Pidde et al., Membrane potential of a biological cell: stochastic or deterministic?, in *ESGCO*, Lancaster University, 2016.

Vascular Sympathetic Control in Sjögren Syndrome

Enrico Brunetta¹, Pietro Mandelli¹, Maria Italia Sara Achenza¹, Emanuela Scannella¹,
Laura Boccassini², Andrea Marchi³, Franca Barbic¹, Piercarlo Sarzi Puttini^{2,4},
Alberto Porta^{4,5}, Raffaello Furlan^{1,6}

¹ Internal Medicine, Humanitas Research Hospital, Rozzano, Italy

² Rheumatology, L. Sacco Hospital, Milan, Italy

³ Politecnico di Milano, Department of Electronics Information and Bioengineering, Milan, Italy

⁴ University of Milan, Milan, Italy

⁵ IRCCS Policlinico San Donato, Department of Cardiothoracic, Vascular Anesthesia and Intensive Care, Milan, Italy

⁶ Humanitas University, Rozzano, Italy

Introduction

Sjögren Syndrome (SS) is a chronic autoimmune systemic disease affecting salivary and lacrimal glands. In addition, there are extraglandular systemic pathological manifestations, including purpura, glomerulonephritis, peripheral neuropathies and middle vessel vasculitis. [1]

Of interest, gland fibrosis is affecting only a minimal part of the tissue, in spite of remarkable loss of secretory function. [2] Moreover, the amount of lymphocytic infiltrate is unrelated to secretory deficit. [3] This rises the possibility that the secretory deficit might be related to an autonomic peripheral neuropathy, which in turn might be reflected in an altered systemic vasomotor neural control.

The aim of the present study was to assess the sympathetic vasomotor control in a group of patients with SS by using power spectrum analysis of blood pressure variability and the direct recording of the post-ganglionic sympathetic nerve activity (Muscle Sympathetic Nerve Activity, MSNA). A group of age- and gender-matched healthy subjects served as controls.

Experimental Protocol and Data Analysis

We studied 7 female patients affected by SS according to AECG criteria, [4] aged 35-75 years. The patients were recruited from the outpatient clinics of Clinical Immunology of Humanitas Research Hospital, Rozzano, Italy and of Rheumatology of L. Sacco Hospital, Milan, Italy. A control group of seven healthy age-matched females was also studied.

In every subject, we recorded ECG, beat-by-beat non invasive arterial pressure (AP), respiratory activity and both raw and integrated MSNA, in recumbent position. MSNA was obtained by microneurography technique from the left peroneal nerve, as already described in [5]. Variables were sampled at 400 Hz and stored on a PC for off-line analysis.

In the present study we focused on the analysis of both AP variability and integrated MSNA recordings but we extracted also mean heart period, as the time interval between two consecutive R-wave peaks (RR), the mean of systolic arterial pressure (SAP), the variance of SAP (σ^2_{SAP}) and the respiratory frequency (f_{RESP}).

Power spectrum analysis of systolic arterial pressure (SAP) variability provided the power in the low frequency (LF, from 0.04 to 0.15 Hz) indicated as LF_{SAP} and considered an indirect marker of sympathetic modulation directed to the vessels. [6] The sympathetic drive directed to the vessels was assessed directly via the burst rate of the integrated MSNA expressed in burst/min.

Table 1. Time and frequency domain parameters

| | Patients | Controls | p |
|--|--------------|---------------|------|
| HR (beats/min) | 67.71 ± 4.33 | 66.17 ± 2.88 | 0.79 |
| f _{RESP} (cycles/min) | 20.14 ± 2.80 | 17.67 ± 2.51 | 0.53 |
| SAP (mmHg) | 125.4 ± 7.73 | 119.41 ± 4.47 | 0.53 |
| σ^2_{SAP} (mmHg ²) | 15.74 ± 3.79 | 17.27 ± 11.09 | 0.89 |
| LF _{SAP} (mmHg ²) | 2.64 ± 0.94 | 2.56 ± 1.69 | 0.96 |
| MSNA (burst/min) | 30.57 ± 2.75 | 20.71 ± 3.29* | 0.04 |

p: type I error probability. The symbol * indicates $p < 0.05$ vs. patients.

Results

Table 1 summarizes the hemodynamic profile of the two groups. It is worth noting that that heart rate, systolic arterial pressure and respiratory activity were similar in patients and controls.

The spectral index of sympathetic activity to the vessel (LF_{SAP}) was similar in the two groups, whereas the sympathetic neural firing (MSNA) was significantly greater in patients compared to controls.

Discussion and Conclusions

In the present study the combined use of power spectral analysis technique and direct sympathetic neural recording enabled us to reveal subtle alterations in the vascular autonomic control in SS which were hidden by simple analysis of the hemodynamic profile of the two groups. Indeed, in spite of the similar heart rate and blood pressure values, we observed a greater sympathetic nerve burst activity in SS, compared to healthy individuals. This was accompanied by similar values in the spectral index of sympathetic vasomotor control (LF_{SAP}). Therefore, in SS we observed a potentially contradictory finding: the spectral index of sympathetic vascular modulation was similar to controls, whereas the direct recording of the neural sympathetic activity to the vessel was greater.

How can these apparently conflicting findings be reconciled?

It is important to point out that LF_{SAP} is a comprehensive index that takes into account both the neural vasomotor control and the arterial smooth muscle responsiveness. Conversely, MSNA is a direct measure of the neural vasoconstrictor firing to the arterial vessels.

It is likely that a chronic subclinical vasculitis, already described in SS, [1] might result in a blunted vessel response to sympathetic vasoconstrictor stimuli.

Therefore, we hypothesize that, in SS patients, in a setting of potential arterial damage, there is the need of an enhanced neural sympathetic drive to the vessel to obtain a proper vasoconstriction and maintain adequate blood pressure values.

References

- [1] Fox RI 2005 *Lancet* **366** 321-331
- [2] Humphreys-Beher MG *et al*, 1999 *Scand J Immunol* **49** 7-10
- [3] Jonsson R *et al*, 1993 *Br J Rheumatol* **32** 578-581
- [4] Vital C *et al*, 2002 *Ann Rheum Dis* **61** 554-558
- [5] Diedrich A *et al*, 2009 *Am J Physiol* **296** H1758-H1765
- [6] Furlan R *et al*, 2000 *Circulation* **101** 886-892

Cardiorespiratory coupling interval during tilt-test examination in young healthy males

Teodor Buchner (1), Tomasz Sobiech (1) and Paweł Krzesiński (2)

(1) Cardiovascular Physics Group, Faculty of Physics, Warsaw University of Technology Warsaw, Poland (2) Department of Internal Diseases and Cardiology, Military Institute of Health Services, Warsaw, Poland

The idea of cardiorespiratory coupling has been studied since the cardiodepressive role of vagal nerves has first been observed, in XIX century. The most pronounced idea is the one that the heart action is affected by cardiac vagal activity, which modulates the activity of the sinus node (Anrep 1936). However, there exists a still growing evidence, that at least equally important is the opposite direction of coupling. Galletly and Larsen have observed coupling of spontaneous ventilation to heart beat during anaesthesia (Galletly, Larsen 1997). Then, they formulated a model, in which the inspiration is, under certain conditions triggered by heart beat (Galletly, Larsen 2001). This observation has been supported by brain research, where an experimental and numerical analysis of the dynamics of pre-Boetzing complex has revealed, that the somatic input of phasic type may entrain the respiratory rhythm (Potts 2005). Such a phasic input is the sympathetic drive, which at rest exhibits mainly the periodicity of the heart, introduced by baroreflex and chemoreflex. If the sympathetic drive is dominated e.g. by a strong locomotive rhythm, this rhythm may also entrain the respiratory rhythm: in horses during canter, breathing is 1:1 synchronized with the locomotor cycle (Lafortuna et al 1996). A quantitative analysis has shown, that the histogram of intervals between the preceding R wave and the following inspiration (the cardiorespiratory coupling interval) exhibits a clear maximum at $T=0.5$ s. This fact has been observed in sedated (Galletly, Larsen 1997) as well as in resting subjects (Tzeng et al 2003). The position of this maximum does not depend on the instantaneous heart rate. The original name of the interval was the RI interval and the definition of I point (inspiration onset) was based on the airflow measurement (Galletly, Larsen 1997).

The aim of this study was to find if the constant cardiorespiratory coupling interval can be observed under various types of physiological stress in healthy subjects. We also wanted to verify this result with the use of a suitable choice of test signals, such as signals with random shuffling of heart intervals and signals with pairwise channel shuffling (ECG of one patient versus ventilation of another patient).

We have examined a group of 40 healthy and well-trained young males, who underwent a tilt-test examination along the Italian protocol. Using Porti device (Porti 5,

TMSI, The Netherlands), we have recorded blood pressure, two channels of ECG and the respiratory signal measured using the thoracic belt. All signals were sampled at 200 Hz. The tilt test table protocol consisted of: 1) control breathing test (CBT) at a constant rate, 2) hand grip test, 3) tilt, 4) nitroglycerine administration followed by 5) fainting, which was observed either during passive (before nitroglycerine) or active phase of the test. All the fiducial points, both in ECG and in respiratory signal were extracted using custom Python algorithms. Since the position of the minimum of the chest diameter was taken as an instant I point, we denote the interval as the cardiorespiratory coupling interval. We verified the validity of results obtained by random visual inspection and careful analysis of outliers.

We calculated an averaged (over all subjects) and normalised histogram of the distance between the bottom of the expiration valley and both the preceding and the following R wave for all phases of the examination. The histogram exhibits a clear maximum at $T=-0.5$ s: i.e. the presence of the bottom of the expiration valley is the most probable at 0.5 s after the preceding R wave. The standard deviation of a peak of distance for the R wave following the expiration valley is considerably larger, which suggests weaker coupling in this direction. The shape of the histogram is qualitatively constant in all conditions studied, however it is less eminent in states of increased sympathetic activity (after tilt and during hand grip test). Next, we have verified if such a histogram may be mimicked by any test signals. We have used three types of signals: a) two uncoupled random spike trains with a Gaussian distribution, of a certain mean value and a certain variance, b) pairwise shuffled channels and c) random shuffled RR intervals combined with the original respiratory intervals. In any of the above conditions we were not able to obtain the similar shape of the experimental distribution. We noted, that the artificial distribution may be nonuniform and even multimodal, for a very specific choice of parameters of two Gaussian distributions.

In conclusion, we can confirm, that a certain percentage of heart beats seems to be directly triggered by the heart action. It also means, that kicked rotator models (Buchner 2010) may be a good choice for modelling the cardiorespiratory coupling.

References

- Anrep GV, Pascual W, Rossler R 1936 *Proc. Royal Soc. B* **119** 191-222
Galletly DC and Larsen PD 2001 *Br J of Anaesth.* **86** 777-88
Buchner T 2010, *Acta Phys Pol B* **41** 1111-1126
Galletly DC and Larsen PD 1997 *Br J Anaesth* **78** 100-101
Lafortuna CL, Reinach E 1996 *J Physiol* **492** 587-96
Potts JT, Rybak IA, Paton JFR 2005 *J. Neurosci.* **25** 1965-1978
Tzeng YC, Larsen PD and Galletly DC 2003 *Experimental Physiology* **88** 775-782

Amplitude Change in R and T Waves of Electrocardiogram during Exercise

Camillo Cammarota and Mario Curione

University La Sapienza, Rome, Italy

Dep. of Mathematics and Dep. of Internal Medicine and Medical Specialties

The electrocardiogram (ECG) recorded during the exercise test is used to evaluate the presence of myocardial ischaemia [1]. During the test the patient on a bicycle ergometer is subjected to a workload increasing in time. The exercise is stopped when the heart rate reaches a maximum (acme), usually 85% of the estimated top heart rate based on the patient's age. After achieving peak workload the patient spends some minutes at rest until its heart rate recovers its basic value. The R and T waves occur respectively at the end of the ventricular diastolic phase and at the end of the systolic phase, which are the times of maximum and minimum ventricular filling. The series of the RR intervals, of the R and T waves amplitudes extracted from the ECG of 65 healthy subjects during exercise are in fig. 1.

The RR series is characterized by a V-shaped profile, in which the minimum corresponds to the acme. We first estimate the acme location in each tachogram (RR series), then we synchronize all the series extracting a window of $m = 600$ beats centered at the acme, in such a way that the acme occurs at beat number 300. The data are affected by a large inter individual variability, due to amplitude variations across the subjects that affects proportionally the amplitudes of the R and T waves. Since we are interested in relative variation of these variables during time, we normalize each series dividing by its temporal mean. The mathematical model of the rescaled R and T series is $Y_i(t) = \mu(t) + Z_i(t)$, $i = 1, \dots, n$; $t = 1, \dots, m$; where i is the index of the subject, $\mu(t)$ is the population profile and the $Z_i(t)$'s are i.i.d. random variables with zero mean for each t and i and $\text{Var } Z_i(t) = \sigma_i(t)^2$. The $Z_i(t)$'s account for individual deviations from the population mean. The mean of the above equations over the n individuals is $\bar{Y}(t) = \mu(t) + \bar{Z}(t)$, $t = 1, \dots, m$.

In this model the data series $\bar{Y}(t)$ is decomposed into a deterministic component $\mu(t)$ plus the noise $\bar{Z}(t)$. In order to construct a confidence band for $\mu(t)$ we use the R package `SiZer` [3,4]. This package performs a locally weighted polynomial regression centered at each point t_j , $j = 1, \dots, k$ of a grid, a suitable subset of the time values; for each grid point the estimated parameters provide the local trend and slope. The weight is $w_j(t) = K((t - t_j)/h) / \sum_t K((t - t_j)/h)$ where K is a Gaussian kernel, and h is the bandwidth. We use a second order polynomial $P_j(t) = \beta_0^{(j)} + \beta_1^{(j)}(t - t_j) + \beta_2^{(j)}(t - t_j)^2$ and the parameters $\beta_0^{(j)}$, $\beta_1^{(j)}$, $\beta_2^{(j)}$ are estimated minimizing

for any j the quantity $\sum_t (\bar{Y}(t) - P_j(t))^2 w_j(t)$. The value of h acts as a smoothing parameter. The theory of multivariate linear models provide both an estimate and a confidence interval for the polynomial coefficients $\beta^{(j)}$. The coefficients of zeroth order $\beta_0^{(j)}$, $j = 1, \dots, k$ provide an estimator of the level; similarly the coefficients of first order $\beta_1^{(j)}$ provide an estimator of the derivative.

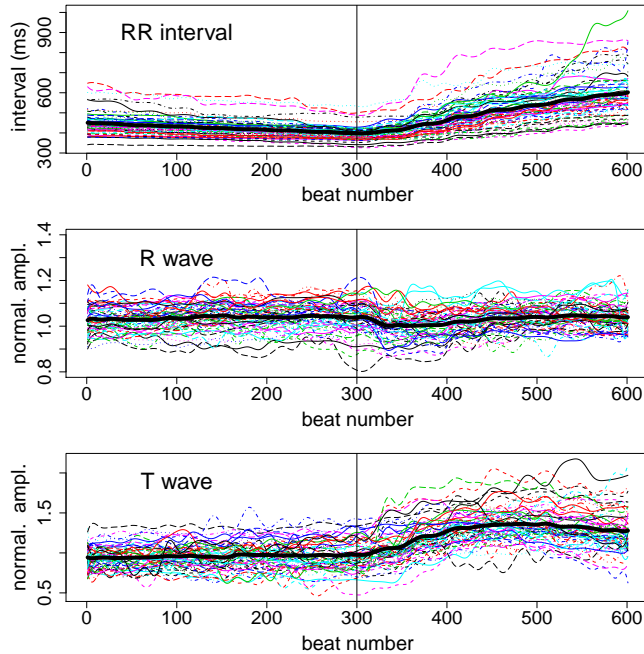


Fig. 1. Time-mean rescaled and aligned series of a group of 65 normal subjects and their population mean (thick black line) of RR interval (top), R amplitude (centre) and T amplitude (bottom) during the exercise test. The vertical line denotes the acme. The series are restricted to a window of 600 beats centered at the acme. Adimensional units on vertical axis. Color on line.

The 95% confidence band for the population mean $\mu(t)$ allows to conclude that the two main features of the population mean of R and T series, i.e. the dip of R and the bump of T, occurring just after the acme (fig. 1), are significant. This result [5] extends the previous one obtained by the authors on the R amplitude [2]. Amplitude changes of R and T waves seem to reflect the changes of electrical resistivity due to the number of red cells in the left ventricular chamber. Opposite trends in R and T wave amplitude after the acme present a specular behavior according to the Frank-Starling law.

References

1. Gibbons and Balady (2002) *J. Am. Coll. Cardiol.* **40** 1531 – 1540.
2. Curione, Cammarota et al. (2008) *Archives of medical science* **4** 51–56.
3. R Development Core Team (2008) *R: A Language and Environment for Statistical Computing*.
4. Sonderegger (2011) *SiZer: Significant Zero Crossings*. <http://CRAN.R-project.org>
5. Cammarota and Curione (2016) *arXiv:1602.05907*.

The influence of aging on the QT interval variability

Camila B. F. Pantoni¹, Alberto Porta^{2,3}, Juliana C. Milan-Mattos¹,
Natália M. Perseguini¹, Vinícius Minatel¹, Patrícia Rehder-Santos¹,
Sílvia C.G. Moura-Tonello¹, Mariana O. Gois¹, Anielle C.M. Takahashi¹, Renata A.
Gonçalves¹, Vlasta Bari², Andrea Marchi^{4,5}, Beatrice De Maria⁶ and
Aparecida M. Catai¹

¹ Federal University of São Carlos, Department of Physiotherapy, São Carlos, Brazil;
² University of Milan, Department of Biomedical Sciences for Health, Milan, Italy; ³ IRCCS
Policlinico San Donato, Department of Cardiothoracic, Vascular Anesthesia and Intensive
Care, Milan, Italy; ⁴ Politecnico di Milano, Department of Electronics Information and
Bioengineering, Milan, Italy; ⁵ San Gerardo Hospital, Department of Emergency and
Intensive Care, Monza, Italy; ⁶ IRCCS Fondazione Salvatore Maugeri, Milan, Italy

Introduction

Aging is associated with modifications of electrical and mechanical properties of the cardiac muscle. Moreover, autonomic nervous system impairment [1] and a drop of the complexity of cardiovascular control [2,3] are observed. Heart rate variability (HRV) has been widely used in many different conditions in healthy and pathological individuals to typify cardiac activity and autonomic nervous system state. In particular in aging studies HRV analysis, carried out via linear and nonlinear methods, suggested a decrease of the parasympathetic modulation and an increase of the sympathetic one with age [4,5]. Also the variability of the time interval between Q-wave onset and T-wave end (QT) provided important information on temporal repolarization lability [6] and cardiac control [7]. The amount of QT variability (QTV) has been used as a risk predictor for sudden cardiac death [6] and higher values of QTV have been related to a more pronounced sympathetic modulation directed to ventricles [7]. Scanty data are present in literature on the dependence of QTV on age. Therefore, the aim of this study is to evaluate the evolution of QTV during aging and compares it with the well-known trend of HRV.

Experimental Protocol and Data Analysis

We studied 116 subjects that were divided into five groups according to the age ranges: 20-29; 30-39; 40-49; 50-59; 60-69. All subjects were apparently healthy based on a previous evaluation. The ECG signal (modified lead I) was acquired by a bioamplificator (BioAmp FE132, ADInstruments, Sydney, Australia) with a sampling rate of 1000 Hz. The experimental session consisted of 15 minutes at rest in the supine position. The subjects breathed spontaneously and they were not allowed to talk. The study protocol adhered to the principles of the Declaration of Helsinki and was approved by the ethical committee of the Federal University of São Carlos, Brazil. ECG recordings were pre-processed to limit broadband noise and cancel baseline wandering. Heart period was measure as the time distance between two consecutive R-wave peaks (RR). The temporal distance between the R-wave peak and T-wave end (R_{Te}) was taken as an approximation of QT interval automatically measured from the ECG recording [7]. Sequences of 256 consecutive RR and R_{Te} measures were considered. After the computation of the RR and R_{Te} means (μ_{RR} and $\mu_{R_{Te}}$), the RR and R_{Te} series were linearly detrended and, then, the RR and R_{Te} variances (σ_{RR}^2 and $\sigma_{R_{Te}}^2$) were calculated. Autoregressive power spectral density was computed. The power of the RR series in high frequency (HF, from 0.15 to 0.5 Hz) band, expressed in absolute units and indicated as HF_{RR}, and the power of the R_{Te} series in the low frequency (LF, from 0.04 to 0.15 Hz) band, expressed in absolute units and denoted as LF_{R_{Te}}, were calculated [7]. One way analysis of variance, or Kruskal–Wallis one way analysis of variance

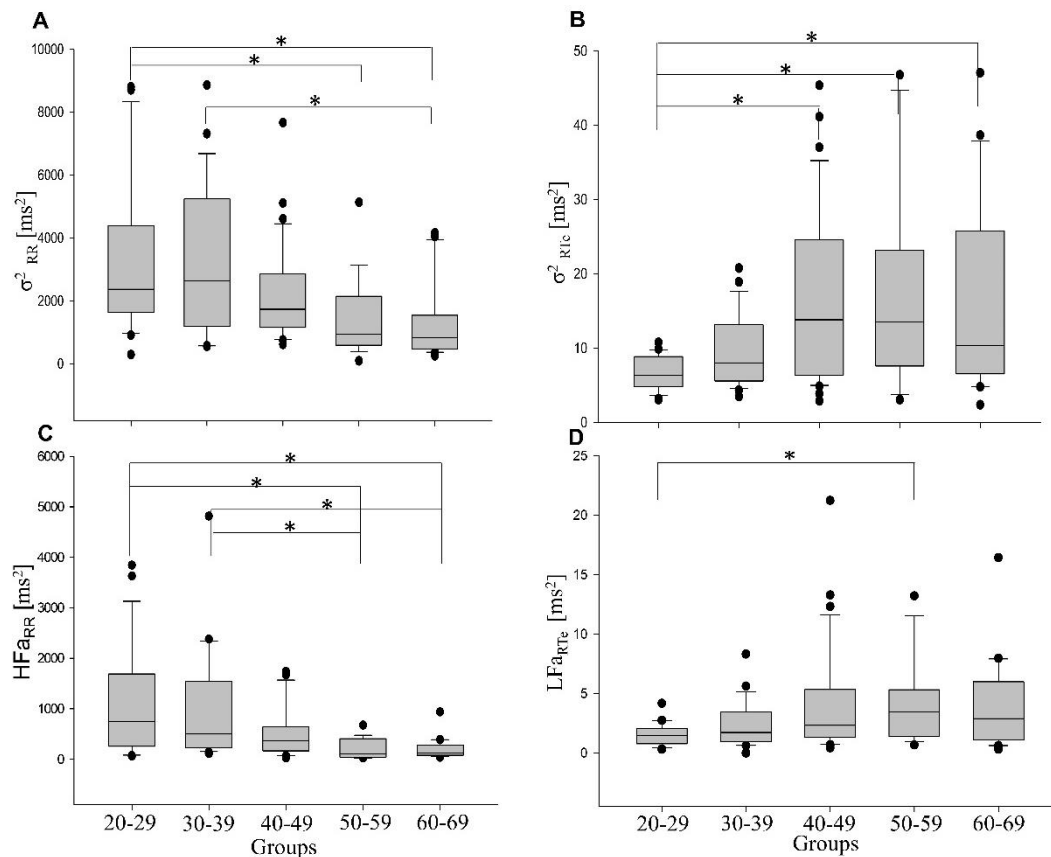


Figure 1. Box-and-whisker plots report the considered time and frequency domain parameters: σ^2_{RR} (A), σ^2_{RTc} (B), HFaRR (C) and LFaRTc (D). The symbol * indicates a between-group difference with $p < 0.05$.

on ranks when appropriate, was applied to check the significance of differences among the groups. A $p < 0.05$ was deemed as significant.

Results

Results relevant to time and frequency domain parameters as a function of the groups are reported in Fig.1. The σ^2_{RR} was significant lower in 50-59 and 60-69 compared to 20-29 and in 60-69 compared to 30-39 (Fig.1A). The HFaRR was lower in 50-59 and 60-69 compared to 20-29 and 30-39 (Fig.1C). The σ^2_{RTc} was higher in 40-49, 50-59 and 60-69 compared to 20-29 (Fig.1B) and LFaRTc power was higher in 50-59 compared to 20-29 (Fig.1D). Between-group differences were not observed in the case of μ_{RR} and μ_{RTc} .

Discussion and Conclusions

We demonstrated that the QTV at REST in healthy subjects depends on age with the greatest modifications occurring above 40 years old. As higher QTV values were related to a more pronounced sympathetic control [7], we suggest that the increase of sympathetic modulation during senescence is the more likely cause of the observed dependence of QTV with age.

Grants: CAPES-CSF-PVE: 23038.007721/2013-41; FAPESP: 2010/52070-4.

References

- [1] Pikkujämsä SM *et al*, 1999 *Circulation*. **100** 393-399.
- [2] Catai AM *et al*, 2014 *Entropy*. **16** 6686-6704.
- [3] Voss A *et al*, 2015 *PLoS One*. **10**: e0118308.
- [4] Natália MP *et al*, 2015 *Int. J. Cardiol*. **178** 79–81.
- [5] Takahashi AC *et al*, 2012 *Intern. Emerg. Med*. **7** 229-235.
- [6] Berger RD, 2009 *J. Am. Coll. Cardiol*. **54** 851-852.
- [7] Porta A *et al*, 2015 *J. Am. Coll. Cardiol*. **65** 367-374.

Evolution of the complexity of systolic and diastolic blood pressure variabilities with age

Alessandra A. Fagundes^{1,2}, Alberto Porta^{3,4}, Natália M. Perseguini¹, Juliana C. Milan¹, Vinicius Minatel¹, Patricia R. Santos¹, Anielle C.M. Takahashi¹ and Aparecida M. Catai¹

¹ Federal University of São Carlos, Department of Physiotherapy, São Carlos, Brazil; ² Vale do Paraíba University, Health Science Faculty, São José dos Campos, Brazil; ³ University of Milan, Department of Biomedical Sciences for Health, Milan, Italy; ⁴ IRCCS Policlinico San Donato, Department of Cardiothoracic, Vascular Anesthesia and Intensive Care, Milan, Italy

Introduction

Aging process is associated with modifications of the cardiovascular system and its control mechanisms that cause a progressive breakdown of the physiological complexity [1,2]. Previous studies reporting the effect of aging on the complexity of the cardiovascular control are limited to the evaluation of the heart period and SAP complexity [3]. However, it would be interesting to investigate the evolution of complexity on age from the analysis of diastolic arterial pressure (DAP) variability as well and to check whether the trend of DAP complexity with age is analogous to that of SAP. Thus, the aim of this study is to investigate the evolution of DAP complexity with age and compare it to the modifications of SAP complexity during senescence.

Experimental Protocol and Data Analysis

The study was carried out in 110 subjects divided into five groups (n=22 for each group, 11 men, 11 women) according age ranges: 21-30; 31-40; 41-50; 51-60; 61-70. The database used was exactly the same presented in [3]. Signals were acquired for 15 min at rest in supine position (REST) and in standing position (STAND). Noninvasive continuous blood pressure (AP) was obtained from the middle of the right hand finger (Finometer-PRO, Finapres Medical System, Amsterdam, Netherlands). The right hand was maintained at the level of the heart at REST and during STAND. All signals were sampled at 400 Hz (Power Lab 8/35, ADInstruments, Sydney, Australia). After detecting SAP and DAP values from the AP recordings, sequences of 256 consecutive SAP and DAP values were extracted randomly at REST and during STAND. Indexes of dynamical complexity were estimated via corrected conditional entropy (CCE), as described in [4]. CCE estimates the amount of information carried out by the current sample of the series that cannot be derived from the knowledge of its previous values. A correction strategy prevented the decrease of CCE toward 0 with the number of previous samples and the minimum of the CCE with respect to the number of past values was taken as a complexity index (CI). This index was normalized by the Shannon entropy to obtain a normalized CI (NCI), thus expressing complexity in terms of dimensionless units. NCI ranges from 0 (null information, maximal predictability) to 1 (maximum information, minimal predictability) [5]. Spearman correlation analysis was performed to check the association of any parameter with age at REST and during STAND. A $p < 0.05$ was considered as significant.

Results

Table 1 reports the results of correlation analysis of NCI_{SAP} and NCI_{DAP} on age over all subjects and after the separation of the whole group into two subgroups solely formed by men and women. NCI_{SAP} decreased with aging at REST. The same finding was observed in the women group, while no modification of NCI_{SAP} was visible in men. During STAND NCI_{SAP} was unrelated to age regardless of the group. Similar findings were found when NCI_{DAP} was considered.

Table 1. Correlations of SAP and DAP complexity indexes on age at REST and during STAND.

| index | REST | | STAND | |
|----------------------------|--------|--------------|--------|--------------|
| | ρ | significance | ρ | significance |
| NCI _{SAP} (all) | -0.223 | Yes | -0.015 | No |
| NCI _{SAP} (men) | -0.077 | No | 0.046 | No |
| NCI _{SAP} (women) | -0.360 | Yes | -0.074 | No |
| NCI _{DAP} (all) | -0.223 | Yes | 0.087 | No |
| NCI _{DAP} (men) | -0.090 | No | -0.012 | No |
| NCI _{DAP} (women) | -0.329 | Yes | -0.056 | No |

NCI = normalized complexity index; ρ = Spearman's rank correlation coefficient; Yes/No = the variable is/is not significantly related to age with $p < 0.05$.

NCI_{SAP} and NCI_{DAP} were similar in men and women at REST regardless the age bin. During STAND, NCI_{DAP} was higher than NCI_{SAP} in 41-50 group in women compared to men.

Discussion

Previous studies proved the reduction of SAP complexity with age [1-3,6,7], but no information was given about the DAP complexity. This study confirmed the decrease in NCI_{SAP} with age [3] and demonstrated that complexity of DAP behaved exactly in the same way. The decrease of SAP complexity has been interpreted as the result of an increased sympathetic drive directed to the vessels synchronizing more efficiently the oscillatory activity of microvasculature [8] and producing rhythmical modifications of peripheral resistance that can be detected at the level of a systemic variable such as SAP [9]. The observed decrease of DAP complexity with age corroborates this interpretation because DAP is more directly related to variations of peripheral resistances. Since NCI_{SAP} in men was unrelated to age, we can confirm that women are the main responsible of the negative correlation of NCI_{SAP} on age observed at the level of the entire population. The decrease of SAP complexity in women might be triggered by a decline of estrogen levels during the menopausal period [3]. This result was confirmed at the level of DAP series, thus again suggesting that the loss of complexity of the vascular control with age in women might be strictly related to an increase of sympathetic activity related to the fall of estrogen levels. Similar behaviors of SAP and DAP complexities was detected during STAND.

Conclusions

Complexity of the vascular control is gender-dependent and the observed decline could be linked to the synchronizing action of sympathetic activity on vasomotion at the level of peripheral vascular districts.

Financial Support: FAPESP (2010/52070-4); CAPES/CSF/PVE (23038007721/2013-41).

References

- [1] Lewis A *et al*, 1992 *JAMA* **13** 1806-1809.
- [2] Porta A *et al*, 2014 *PLoS ONE* **9** e89463.
- [3] Catai AM *et al*, 2014 *Entropy* **16** 6686-6704.
- [4] Porta A *et al*, 1998 *Biol. Cybern.* **78** 71-78.
- [5] Porta A *et al*, 2007 *Chaos* **17**, 015117.
- [6] Perseguini NM *et al*, 2011 *Braz. J. Med. Biol. Res.* **44** 29-37.
- [7] Nemati S *et al*, 2013 *Respir. Physiol. Neurobiol.* **189** 27-33.
- [8] Baselli G *et al*, 2006 *IEEE Trans. Biomed. Eng.* **53** 53-64.
- [9] Porta A *et al*, 2012 *J Appl Physiol.* **113** 1810-1820.

Phase relation between systolic blood pressure and heart period is age-dependent but gender-independent

Juliana C. Milan-Mattos¹, Alberto Porta^{2,3}, Natália M. Persegui¹, Vinicius Minatel¹, Patricia R. Santos¹, Vlasta Bari², Anielle C. M. Takahashi¹ and Aparecida M. Catai¹

¹Cardiovascular Physical Therapy Laboratory, Department of Physical Therapy, Federal University of São Carlos, São Paulo, Brazil

²Department of Biomedical Sciences for Health, University of Milan, Milan, Italy

³Department of Cardiothoracic, Vascular Anesthesia and Intensive Care, IRCCS Policlinico San Donato, Milan, Italy

Introduction

The natural human aging causes a series of alterations in cardiac autonomic control including vagal withdrawal, sympathetic activation and baroreflex sensitivity decrease [1-3]. In the recent years, cross-spectral analysis carried out over the spontaneous fluctuations of heart period (HP) and systolic arterial pressure (SAP) has been mainly utilized for the assessment of baroreflex sensitivity and the evaluation of the degree of HP-SAP association [4-7]. The same methodology can be utilized to assess the phase relation between HP and SAP variabilities. Even though with relevant methodological limitations, mainly related to the presence of phase multiples [8], phase is historically utilized to interpret directionality of the interactions in bivariate approaches [5]. For example, assigned the conventions for the computation of the cross-spectrum a negative phase might indicate that HP variations lag behind SAP changes and, thus, information flows from SAP to HP along the so-called cardiac baroreflex. However, due to the difficulty of interpreting phase, it is scarcely exploited to derive information about cardiovascular control and mainly utilized to test the prerequisites for the reliable computation of the baroreflex sensitivity via transfer function methods [4,9]. Therefore, the aim of this study was to check whether phase between HP and SAP can provide information about the senescence process in healthy individuals and whether this information is gender-dependent.

Experimental Protocol and Data Analysis

We evaluated 110 apparently healthy volunteers divided into 2 groups (n=55 each) and divided into age subgroups (21-30; 31-40; 41-50; 51-60; 61-70). The study was approved by the Ethics Committee on Human Research of the Federal University of São Carlos (n°. 328472) and all participants signed an informed consent. The ECG (BioAmp FE132, ADInstruments, Australia), arterial pressure (AP) via a plethysmographic arterial pressure device (Finometer Pro, Finapres Medical Systems, Amsterdam, Netherlands) with the cuff placed on the middle finger of the right hand and the respiratory signal via thoracic belt (Marazza, Monza, Italy) were contemporaneously acquired. Signals were sampled by a commercial device (PowerLab 8/35, ADInstruments, Australia) and sampled at 400 Hz. The simultaneous collection of the signals was performed for 15 minutes at rest in supine position (REST) and in orthostatic position STAND). The participants were instructed to breath spontaneously without talking. HP was derived as the temporal distance between two consecutive R-wave peaks from the ECG and SAP was taken as the maximum of the AP inside each HP. Stable sequences of 256 HP and SAP consecutive values were analyzed at REST and during STAND [10]. Less than 5% of measures coming from ectopic beats was corrected via linear interpolation.

The cross-spectral analysis was performed according to a bivariate autoregressive model [9]. The phase of the cross-spectrum represents the phase relation between HP and SAP (Ph_{HP-SAP}). According to the convention for the computation of the cross-spectrum a negative phase indicated that HP changes lagged behind SAP variations. Ph_{HP-SAP} was computed in the low frequency (LF, from 0.04 Hz to 0.15 Hz) and high frequency (HF, from

0.15 to 0.4 Hz) bands [10] and hereafter indicated as $Ph_{HP-SAP}(LF)$ and $Ph_{HP-SAP}(HF)$ respectively. One-way ANOVA (Tukey's post-hoc test) or Kruskal-Wallis ANOVA on ranks (Dunn's post-hoc test) were used to analyze differences between 21-30 and the other groups. The Spearman rank correlation analysis was carried to assess the degree of association of $Ph_{HP-SAP}(LF)$ and $Ph_{HP-SAP}(HF)$ with age. It was performed only if a significant difference between the 21-30 and 61-70 was found. Statistical analysis was performed via a commercial software (Sigma Plot 11.0, Systat, USA, 2011). A $p < 0.05$ was considered as significant.

Results

At REST the $Ph_{HP-SAP}(LF)$ showed a negative and significant correlation with age when all volunteers were taken together regardless of the gender ($r = -0.490$, $p < 0.05$). The same findings held when men and women were separated ($r = -0.515$ and $r = -0.486$, respectively both with $p < 0.05$). During STAND results were similar (i.e. $r = -0.497$, $r = -0.525$ and $r = -0.491$, respectively, all with $p < 0.05$). The $Ph_{HP-SAP}(HF)$ in REST and STAND did not exhibit differences between 21-30 and 61-70 groups.

Discussion and Conclusions

This study showed that phase between HP and SAP in the LF band is age-dependent but gender-independent. In healthy subjects the phase shift in the LF band became more and more negative as a function of the age in both men and women. This finding is in disagreement with [11] who detected no significant changes in phase between HP and SAP when a slow controlled breathing at 0.1 Hz was utilized. This disagreement might be related to the use of slow controlled breathing at 0.1 Hz to solicit cardiovascular control in [11], while in the present study spontaneous variations in the LF band have been exploited. Conversely, results are in agreement with [11] in the HF band when controlled breathing at a rate more in keeping with the usual breathing frequency in healthy volunteers was utilized. The dependence of the phase between HP and SAP on age cannot be simply explained as an effect of the increase of sympathetic activity with age that might increase the latency of the baroreflex. Indeed, the increase of the sympathetic activity induced by graded head-up tilt test did not affect the phase between HP and SAP in the LF band but made more negative the phase in the HF one [8]. Therefore, the dependence on phase between HP and SAP with age should be considered a hallmark of senescence of the cardiovascular control that is gender-independent that deserves additional, ad-hoc, studies to better understand its physiological correlates and practical implications.

Financial Support: FAPESP (2010/52070-4); CNPq (140164/2015-4); CAPES/CSF/PVE (23038007721/2013-41).

References

- [1] Voss A *et al*, 2012 *Physiol Meas* **33** 1289-311.
- [2] Fauvel JP *et al*, 2007 *Hypertension* **50** 543-546.
- [3] Barantke M *et al*, 2008 *J Cardiovasc Electrophysiol* **19** 1296-1303.
- [4] Laude D *et al*, 2004 *Am J Physiol* **286** R226-R231.
- [5] Saul JP *et al*, 1991 *Am J Physiol* **261** H1231-H145.
- [6] Wichterle D *et al*, 2000 *Pacing Clin Electrophysiol PACE* **23** 1425-1430.
- [7] Gulli G *et al*, 2005 *Clin Auton Res.* **15** 92-98.
- [8] Porta A *et al*, 2011 *Am J Physiol* **300** R378-R386.
- [9] Porta A *et al*, 2000 *Am J Physiol* **279** H2558-H2567.
- [10] Task Force, 1996 *Circulation* **93** 1043-1065.
- [11] Halánek J *et al*, 2003 *Circulation* **22** 292-297.

Improving Network Inference of Oscillatory Systems: A Novel Framework To Reliably Identify the Correct Class Of Network

Gloria Cecchini, Marco Thiel and Björn Schelter
University of Aberdeen
Institute for Complex Systems and Mathematical Biology
Aberdeen, Scotland

Recently, many research groups have focused on the inference of networks from time series data such as brain networks from observed electroencephalography or functional magnetic resonance imaging data. Particular emphasis is on understanding the normal functioning as well as malfunctioning of these networks. In the example of the brain, this promises to disclose information about how the brain processes signals and how alterations thereof cause specific diseases. A key hypothesis is that important characteristics are not specific to individual subjects but rather common in a given population. This is reflected by the fact that brain networks but also other networks are typically classified into main prototypic networks, i.e., Erdos-Renyi, Small World and Scale Free Networks.

These prototypical models for networks are characterised by few parameters and clear procedures have been described to generate these networks with their well established characteristics. Some of their key features are the vertex degree distribution, the global clustering coefficient and the average of the shortest path. In the Inverse Problem, the challenge is to infer the network topology from data. Two challenges are particularly relevant: (i) to reliably obtain the links in the network once the nodes have been fixed, (ii) to use the characteristics above to uniquely determine the type of network.

For oscillatory systems several cutting-edge methods have been suggested in the literature to address problem (i). Usually these techniques rely on statistical inference. The correct reconstruction of networks is therefore hampered by mis-estimation of links due to statistical uncertainties, unobserved processes, noise contamination to name just a few. Mis-estimated links in a network typically alter the key characteristics; this makes it particularly difficult to infer the correct type of network.

We investigated to which extent classical statistical approaches to estimate links in a network are reliable; furthermore, we investigated if common rules of type I and type II errors should be modified to achieve a reliable inference of the correct type of network. Our approach is based on the topological analysis of the detected networks taking into account the role of two important parameters: false positive and false negative decisions about the presence and absence of links.

In this work we suggest a novel procedure to optimally balance false positive conclusions about links in a network for a given analysis technique and characteristics of the networks. This enables us to obtain, e.g., the best estimate for the average shortest path length or degree distribution for a given analysis technique. Standard alpha values for statistical inference turn out to be suboptimal when for instance the degree distribution is to be estimated.

For example, let G_p be an Erdos-Renyi random graph with parameter p . Setting, for instance, $\alpha = \frac{10^{-3}}{\beta}$ – an arbitrary choice motivated by the fact that this reflects an analysis technique that has high sensitivity and specificity – we analysed how the degree distribution is influenced by $\beta \equiv \beta(\alpha)$. Distance here refers to the difference between the means of the two distributions. For some values of p the distance is negligible, but the optimal p to minimize this distance changes if β is modified. Marginalising out the influence of p , the integral with respect to p is taken for each β ; the sum respectively in the discrete case. We call this quantity the total distance. In this case, it's possible to conclude that the best value for $\beta \simeq 0.03$ and consequently $\alpha \simeq 0.033$. These values are pretty close to standard values for α and β , the latter for a well-powered analysis technique. Standard alpha values turn out to be suboptimal when the type of network is different. In our work we will present results that provides evidence for this assumption.

Based on these improved estimates we can infer the correct type of network with high probability.

References

Fronczak A., Fronczak P., Holyst J.A.. Average path length in random networks. *Physical Review*. **E 70**, pag. 056110. 2004.

Newman M. *Networks: An Introduction*. Oxford University Press, Inc., New York, NY, USA, 2010.

Hyposodic and hypocaloric diet effects on oscillatory pattern in newly diagnosed hypertensive people

Teresa Mastantuono¹, Martina Di Maro¹, Martina Chiurazzi¹, Gilda Nasti¹, Dominga Lapi¹, Laura Battiloro¹, Noemy Starita¹, Mario Cesarelli², Gianni D'Addio³, Luigi Ippariello² and Antonio Colantuoni¹.

¹“Federico II” University, Dept Clinical Medicine and Surgery, Naples, Italy;

²“Federico II” University, Dept Biomedical, Electronics and TLC Engineering, Naples, Italy;

³IRCCS S. Maugeri Foundation, Telese, Benevento, Italy.

Introduction

Obesity is associated with elevated arterial blood pressure, because of interactions between dietary, genetic, epigenetic and environmental factors. Obesity-related hypertension contributes to increased cardiovascular risk in obese people, representing an important cause of morbidity and mortality [1]. Moreover, obesity complicated by hypertension is associated with structural and functional changes in microcirculation, such as impairment of vasomotor tone, decrease in arteriolar diameters and increase in wall-to-lumen ratio of resistance arterioles with resulting capillary rarefaction [1-2].

Therefore, the aim of the present study was to investigate skin microvascular blood flow (SBF) in newly diagnosed hypertensive obese adults using laser Doppler perfusion monitoring (LDPM) technique. In particular, the main purpose was to analyze the oscillations in blood flow by spectral methods. Finally, the effects of hyposodic and hypocaloric diet on oscillatory patterns were evaluated in hypertensive patients.

Materials and methods

Sixty normotensive (30 females, group NT) and sixty hypertensive people (30 females, group HT) were recruited from the Outpatient Clinic of the Department of Clinical Medicine and Surgery, “Federico II”, University of Naples.

All patients were required to be 50-64 years old and obese [body mass index (BMI) ≥ 30 Kg/m²]. Exclusion criteria were: presence of disease influencing body composition (cancer, osteoporosis and muscular dystrophia), heart failure, hyperglycemia and microangiopathy; treatment with drug influencing microvascular blood flow (such as vasodilators and anti-inflammatory drugs), antihypertensive therapy and smoking.

Nutritional status was evaluated by anthropometric measurements: weight, body mass index (BMI), waist circumference (WC), hip circumference (HP) and triceps skinfold (TS). Bioimpedance analysis (Akern RJL, BIA 101) was carried out to evaluate Fat Mass (FM), Fat Free Mass (FFM) and Muscle Mass (MM). Finally, arterial blood pressure was measured.

Microvascular blood flow evaluation was performed on the patients in supine position in a quiet and temperature-controlled room (22 ± 2 °C). SBF was recorded using a laser Doppler perfusion monitoring apparatus (PeriFlux 4001 System, Perimed, Stockholm, Sweden), connected with a computer. The LDPM probe (PF 408, Perimed, Stockholm, Sweden) was placed on the right forearm volar surface. After 10 min of acclimatization period, digital blood flow was recorded for 30 min by a Perisoft software. The SBF mean value was expressed as arbitrary perfusion units (PU), while the power spectral density (PSD) of laser Doppler signals was reported as PU²/Hz. Finally, skin blood flow oscillations were analyzed by Wavelet transform [3].

The study was approved by “Federico II” University Institutional Ethical Committee and all patients gave their informed consent at the moment of the recruitment.

All data were expressed as mean \pm standard error of the mean (SEM). Data were tested for normal distribution with the Kolmogorov-Smirnov test. Parametric (Student's t tests, ANOVA and Bonferroni post hoc test) or nonparametric tests (Wilcoxon, Mann-Whitney and Kruskal-

Wallis tests) were used. The statistical analysis was carried out by SPSS 14.0 statistical package. Statistical significance was set at $p < 0.05$.

Results

Under baseline conditions, the patients recruited for this study presented BMI values higher than 30 Kg/m^2 ; while, high levels of mean arterial blood pressure were detected in hypertensive group.

According to LDPM measurements, SBF mean value was lower in the hypertensive patients than in normotensive people, as well as total PSD. Furthermore, spectral analysis showed blood flow rhythmic oscillations in the interval 0.0095-2.0 Hz. In particular, in normotensive patients the frequency component in the range 0.052-0.15 Hz was the most representative in the total PSD. Conversely, in hypertensive patients the frequency component in the range 0.021-0.052 Hz was the highest when compared to normotensive subjects.

After 3 months of treatment with hyposodic and hypocaloric diet, BMI was significantly reduced in females (34.3 ± 1.2 vs $36.6 \pm 1.5 \text{ Kg/m}^2$, $p < 0.01$ vs baseline) and males (34.3 ± 0.5 vs $36.7 \pm 0.5 \text{ Kg/m}^2$, $p < 0.01$ vs baseline) belonging to HT group, as well as mean arterial blood pressure.

The improvement in nutritional status was accompanied by changes in microvascular blood flow and oscillatory patterns. In particular, SBF mean value significantly increased in females (10.6 ± 0.4 vs $7.8 \pm 0.6 \text{ PU}$, $p < 0.01$ vs baseline) and males (11.6 ± 0.4 vs $7.5 \pm 0.3 \text{ PU}$, $p < 0.01$ vs baseline) belonging to HT group, as well as total PSD: 142.2 ± 2.3 vs $103.4 \pm 2.7 \text{ PU}^2/\text{Hz}$ ($p < 0.01$ vs baseline) and 204.9 ± 5.9 vs $102.4 \pm 2.5 \text{ PU}^2/\text{Hz}$ ($p < 0.01$ vs baseline) in females and males, respectively, of HT group. Furthermore, the frequency component in the range 0.052-0.15 Hz appeared to be the highest in the spectral density in females (37.7 ± 1.4 vs $32.1 \pm 1.5 \%$, $p < 0.01$ vs baseline) and males (35.6 ± 2.1 vs $28.3 \pm 2.0 \%$, $p < 0.01$ vs baseline) HT group after 3 months of dietary treatment.

Discussion and conclusions

Our data demonstrate that microvascular blood flow was impaired in hypertensive patients. Furthermore, spectral analysis of LDPM signals in the range 0.0095-2.0 Hz revealed six frequency components, due to six mechanisms regulating microvascular blood flow. It has been demonstrated that the frequency components in the range 0.021-0.052 Hz and 0.052-0.15 Hz are related to the sympathetic nervous system and the intrinsic myogenic activity of vascular smooth muscle cells, respectively [4-5]. In the normotensive patients, the frequency component related to myogenic activity was the most representative in the total PSD. Our results show that this activity was impaired by hypertension, while the sympathetic nervous system-related frequency component appeared increased in spectral density. It has been previously reported an adrenergic hyperactivity in the early hypertensive stages [6]. However, both activities were improved after the treatment with hyposodic and hypocaloric diet, indicating a recovered function of the vascular smooth muscle cells and the sympathetic nervous system discharge.

References

- [1] DeMarco VG, Aroor AR, Sowers JR (2014). *Nat Rev Endocrinol*; **10(6)**:pp364-76.
- [2] De Boer MP, Meijer RI, Wijnstok NJ, Jonk AM, Houben AJ, Stehouwer CD, Smulders YM, Eringa EC, Serné EH (2012). *Microcirculation*; **19(1)**:pp5-18.
- [3] D'Addio G, Cesarelli M, Bifulco P, Iuppariello L, Faiella G, Lapi D, Colantuoni A (2014). *IFMBE Proceedings*; **Volume 41**:pp 647-650.
- [4] Mastantuono T, Lapi D, Battiloro L, Cesarelli M, D'Addio G, Iuppariello L, Colantuoni A (2014). *ESGCO Proceedings*, pp191-192.
- [5] Kvandal P, Landsverk SA, Bernjak A, Stefanovska A, Kvernmo HD, Kirkebøen KA (2006). *Microvasc Res*; **72(3)**:pp120-7.
- [6] Mancina G, Grassi G (2014). *Circ Res*; **114(11)**:pp1804-14.

Solvable model for a network of spiking neurons with fixed delays

Federico Devalle^{1,2}, Diego Pazó³ and Ernest Montbrió¹

¹*Universitat Pompeu Fabra, Center for Brain and Cognition, Barcelona, Spain*

²*Lancaster University, Department of Physics, Lancaster, United Kingdom*

³*CSIC-Universidad de Cantabria, Instituto de Física de Cantabria (IFCA), Santander, Spain*

We analyse the dynamics of a network of quadratic integrate-and-fire neurons in their excitable (or quiescent) dynamical regime. We fix our analysis at the population level, investigating mesoscopic brain dynamics. The neurons are coupled all-to-all via time-delayed excitatory (or inhibitory) synaptic interactions. The fixed time-delays are introduced to model the discrete time needed by the neurons to hyperpolarize, due mainly to synaptic kinetics and dendritic processing [1,2]. Using the so-called Lorentzian Ansatz [3], we obtain the following firing rate equations for a spiking neural network with time delays:

$$\begin{cases} \dot{r} = 2rv & (1a) \\ \dot{v} = v^2 + \bar{\eta} + Jr(t - D) - \pi^2 r^2 & (1b) \end{cases}$$

The first equation describes the evolution of the firing rate, while the second the evolution of the mean membrane potential across all neurons. D is the fixed time delay, J the weight of the synaptic interaction and $\bar{\eta}$ the parameter determining the dynamics of the single neuron.

This allows us to find exact formulas for the stability boundaries of the network asynchronous states, not only for self-oscillatory neurons [4], but also for populations of neurons in the excitable regime. For identical neurons, synchronization boundaries are also analytically obtained. The resulting phase diagram for excitatory, identical neurons shows three qualitatively different regions of collective behaviour. At low excitatory coupling a globally-excitable state with zero firing rate is the only attractor of the system. As excitatory coupling is increased, the presence of time delay creates a self-sustained global oscillatory state (via a saddle node bifurcation of cycles), in which all neurons fire in perfect synchrony. In addition, for small (but finite) time delays, excitation creates (via a saddle node bifurcation) a self-sustained, asynchronous state, with a high firing rate, which coexists with either the excitable state, or with both excitable and synchronized states. As excitatory coupling is increased the asynchronous state destabilizes in a (subcritical) Hopf bifurcation.

Finally, we observe that the frequency range of the oscillations we detected for inhibitory networks correspond to fast brain oscillations ($f > 100$ Hz).

References

- [1]Brunel N, Hakim V 1999 *Neural Comput.* **11** 1621-1671
- [2]Roxin A, Montbrió E 2011 *Physica D* **240** 323-345
- [3]Montbrió E, Pazó D, Roxin A 2015 *Phys. Rev. X* **5** 021028
- [4]Pazó D, Montbrió E, *submitted*

Oscillatory pattern of arteriovenous anastomoses and skin blood flow within thermoneutral zone

Authors: Maja Elstad, Ilias Zilakos, Tone Kristin Bergersen

Division of Physiology, Institute of Basic Medical Sciences, University of Oslo

Background:

Core temperature regulation is a key mechanism for homeostasis and within the thermoneutral zone, it is probably maintained stable with adjusting oscillations in acral skin blood flow. The acral skin contains arteriovenous anastomoses (AVA), which are shunts between arterial and venous circulation in hands and feet. The blood flow through AVAs is adjusted by sympathetic vasoconstrictor nerves. The AVAs constrict simultaneously in hands and feet. The vasoconstrictions appear at a frequency of 2 to 3 per minute (0.03-0.05 Hz) while the subject is thermoneutral (1). By changing frequency of this vasomotor activity the AVAs may regulate body temperature within the thermoneutral zone at low energy expenditure. In this study we describe the AVA vasomotion from upper to lower thermoneutral zone in healthy subjects. We hypothesized that from 32°C to 18°C of ambient temperature, the oscillatory pattern shifts from higher to lower frequency.

Methods:

Twelve young, healthy volunteers participated in an experimental protocol with changing ambient temperature (2). In this study we reanalyze the data by wavelet analysis. The subject was supine in a climate chamber. Laser Doppler fluxes were obtained from pulp of the right and left third fingers as a measure of acral skin blood flow (moorVMS, Moor instruments, Devon, UK). The ambient temperature went from 32°C to 18°C with three plateaus; 32°C, 25°C and 18°C.

The wavelet transform technique, a time-frequency method with logarithmic frequency resolution, was used to analyze the acral blood flow oscillations. The time-frequency analysis tools employed in our study have been developed by the Department of Physics, Lancaster University, UK (3). The Morlet wavelet (4) was selected for the wavelet transform analysis of the acral skin blood flow at five distinct time intervals - of approx. 800 s each - including three plateaus and their corresponding transition zones. For each time interval and for both right and left fingertips signals, the time averaged wavelet spectral power were calculated and were divided to two frequency intervals of 0.02-0.05 Hz and 0.05-0.08 Hz respectively. For each of the aforementioned time intervals the integral under the curve of the wavelet spectral power at both frequent intervals was estimated along with the coherence and the phase lag of the two fingertip signals. The data are reported as Hodges-Lehmann estimates of median with 95% confidence interval (5). The significance levels of differences were tested by Wilcoxon method between adjacent intervals.

Results:

The laser Doppler flux integrals from the two finger tips were similar and their oscillations were in phase and thus only the values from the right fingertip are reported.

The fluctuations in laser Doppler flux at 0.02-0.05 Hz were stable at 32°C, during the transition 32°C-25°C, and at 25°C (figure 1). During the transition 25°C-18°C the fluctuations decreased ($p=0.005$) and then decreased further at 18°C ($p=0.0005$) (figure 1). At this frequency the coherence between the oscillations of the signal from right and left finger tips was high during the transition 32°C-25°C, at 25°C (figure 1) and during the transition 25°C -18°C, while lower at 32°C ($p=0.02$) and 18°C ($p=0.03$) (figure 1).

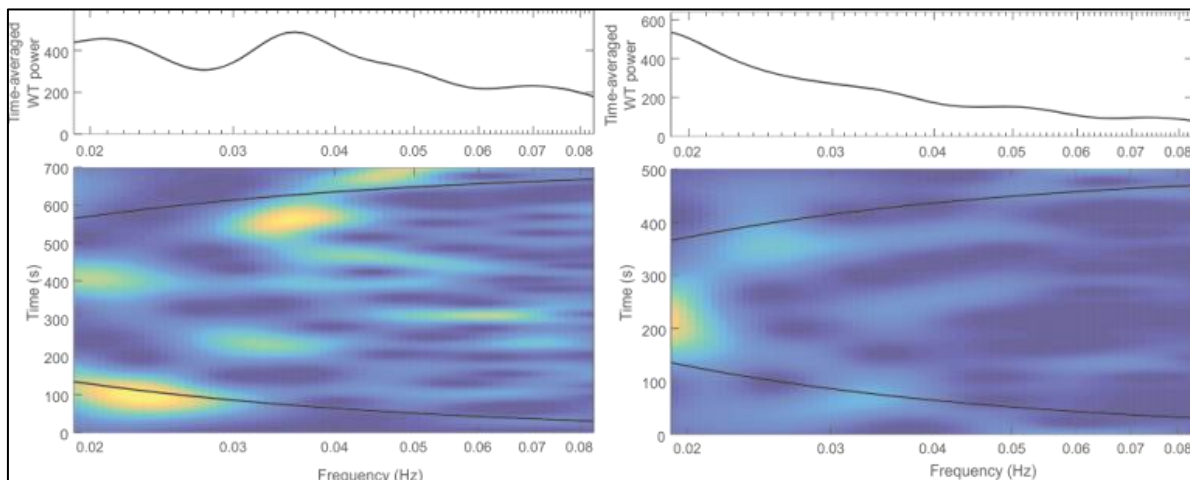
The fluctuations in laser Doppler flux at 0.05-0.08 were stable at 32°C, during the transition 32°C-25°C and at 25°C, whereas decreased during the transition 25°C-18°C ($p=0.002$) and decreased further at 18°C ($p=0.0005$). At this frequency the coherence between the oscillations of the signal from right and left finger tips was high at 25°C and during the transition 25°C-18°C, whereas lower at 32°C ($p=0.003$), during the transition 32°C -25°C ($p=0.04$) and at 18°C ($p=0.007$).

Table 1 Hodges-Lehmann Estimates of Median with 95% confidence interval.

| | | 32°C | 32°C -25°C | 25°C | 25°C -18°C | 18°C |
|--|--------------|------------------------|------------------------|------------------------|----------------------|----------------------|
| Integral Right finger (au^2) | 0.02-0.05 Hz | 10.11 (3.05, 18.74) | 12.17 (6.68, 16.63) | 10.87 (5.04, 17.69) | 5.00 (0.50, 8.05) | 1.28 (0.22, 2.87) |
| | 0.05-0.08 Hz | 7.43 (3.43, 12.34) | 11.37 (5.95, 14.57) | 7.60 (3.63, 10.26) | 3.85 (0.54, 6.04) | 0.84 (0.08, 1.58) |
| Coherence between right and left fingertip | 0.02-0.05 Hz | 0.77 (0.64, 0.83) | 0.87 (0.80, 0.89) | 0.89 (0.84, 0.92) | 0.87 (0.82, 0.89) | 0.82 (0.66, 0.85) |
| | 0.05-0.08 Hz | 0.73 (0.57, 0.80) | 0.85 (0.80, 0.88) | 0.91 (0.81, 0.92) | 0.85 (0.79, 0.87) | 0.77 (0.65, 0.80) |

The integrals of the laser Doppler flux from the right fingertip at 0.02-0.05 Hz was higher at 25°C ($p=0.002$) and 18°C ($p=0.02$) as compared to the corresponding integrals at 0.05-0.08 Hz. We did not find a shift from higher to lower oscillatory frequencies when reducing ambient temperature from 32°C to 18°C.

Figure 1 Wavelet power and contour plots from right fingertip at 25°C and 18°C (n=1)



Conclusion

The AVA vasomotion is modified by ambient temperature within the thermoneutral zone. The oscillatory pattern of AVA is more stable at 0.02-0.05 Hz as compared to 0.05-0.08 Hz. At 25°C ambient temperature, the laser Doppler flux integrals was high at 0.02-0.05 Hz, while lower values were observed at 0.05-0.08 Hz.

References

1. Thoresen M, Walloe L. Skin blood flow in humans as a function of environmental temperature measured by ultrasound. *Acta Physiol Scand.* 1980;109(3):333-41.
2. Elstad M, Vanggaard L, Lossius AH, Walloe L, Bergersen TK. Responses in acral and non-acral skin vasomotion and temperature during lowering of ambient temperature. *J Therm Biol.* 2014;45:168-74.
3. Iatsenko D, McClintock PVE, Stefanovska A. Linear and synchrosqueezed time-frequency representations revisited: Overview, standards of use, resolution, reconstruction, concentration, and algorithms. *Digit Signal Process.* 2015;42:1-26.
4. Stefanovska A, Bracic M, Kvernmo HD. Wavelet analysis of oscillations in the peripheral blood circulation measured by laser Doppler technique. *IEEE Trans Biomed Eng.* 1999;46(10):1230-9.
5. Hollander M, Wolfe DA. *Nonparametric Statistical Methods*: John Wiley & Sons, Inc.; 1999.

Results of cerebral blood flow during autonomic testing in children with migraine

Aleksandra Gergont, Sławomir Krocza, Marek Kaciński
Jagiellonian University Medical College, Krakow, Poland

Background: Transcranial monitoring (TCD) of cerebral blood flow velocity at the middle cerebral artery (MCA) has been found to be a useful method to investigate vascular changes, which may have a role in migraine pathogenesis. There are also signs of involvement of autonomic nervous system (ANS) in migraine patients. One of methods to assess the autonomic function by analyzing heart rate variability (HRV) is to establish low frequency (LF) to high frequency (HF) ratio, LF/HF ratio. Little is known about the relationship of HRV and parameters of the blood flow in MCA in children with migraine.

Aims: The aim of the study was to establish blood flow parameters in MCA as well as LF/HF ratio in children with migraine, during rest, passive tilting and also active standing. Prospective research, approved by Bioethical Commission of Jagiellonian University.

Material and methods: The examination was performed in 86 children with migraine (39 without and 47 with aura) during a headache-free period and in 32 children without headaches and syncope, constituting an age-matched control group. TCD and electrocardiogram monitoring was simultaneously performed during rest, during a 10-min 70 degrees head-up passive tilting and during 3-min active standing test (using Nicolet Companion III and Task Force Monitor 3030i/3040i). *Results:* In 47 children with migraine with aura head-up tilt test was negative for syncope. Postural orthostatic tachycardia syndrome (POTS) was diagnosed in 4 children with migraine with sensory aura and in 1 child with migraine without aura. In 2 children with migraine without aura and in 2 controls head-up tilt-induced syncope occurred. Results of LF/HF ratio did not differ between control group and migraine patients, however LF/HF ratio was significantly higher in a group of 24 children with migraine with sensory aura during passive tilting. Active standing did not reveal differences of LF/HF ratio between any groups. The correlation between parameters of TCD and HRV will be presented at the Conference.

Conclusions: Predominance of sympathetic nervous system activity during passive head-up tilt test, as well as more common POTS in patients with migraine with sensory aura as compared with children with migraine without aura and healthy volunteers indicate differential autonomic reactivity. In spite of poor orthostatic tolerance reported by patients

with migraine, active standing did not reveal differences of sympathovagal balance between migraine patients and healthy volunteers.

1. Matei D, Constantinescu V, Corciova C, Ignat B, Matei R, Popescu CD Autonomic impairment in patients with migraine 2015 *Eur Rev Med Pharm Sci* 19 3922-3927
2. Manzoni GC, Torelli P Migraine with and without aura: a single entity ? 2008 *Neurol Sci* 29 S40-43
3. Domingues RB, Fonseca KB, Ziviane LF, Domingues SA, Vassalo D Altered cardiovascular reactivity to mental stress but not to cold pressure test in migraine 2010 *Headache* 50 133-137
4. Shechter A, Stewart WF, Silberstein SD, Lipton RB Migraine and autonomic nervous system function: a population-based case-control study 2002 *Neurology* 58 422-427
5. Yerdelen D, Acil T, Goksel B, Karatas M Heart rate recovery in migraine and tension type headache 2008 *Headache* 48 221-225
6. Peroutka SJ Migraine: a chronic sympathetic nervous system disorder 2004 *Headache* 44 53-64
7. Vollono C, Gnoni V, Testani E, Dittoni S, Losurdo A, et al. Heart rate variability in sleep-related migraine without aura 2013 *J Clin Sleep Med* 9 707-711

Insights into the Potassium Selectivity of the KcsA Ion Channel Based on a Kinetic Model

William A.T. Gibby¹, Dmitry G. Luchinsky^{1,2}, Peter V.E. McClintock¹,
Aneta Stefanovska¹ and Robert S. Eisenberg³

¹ Lancaster University, Dept. of Physics, Lancaster, UK

² SGT Inc., Ames Research Center, Moffett Field, CA, USA

³ Rush University, Dept. of Molecular Biophysics, Chicago, IL, USA

Ion channels can be highly selective between monovalent ions, and simultaneously allow for conduction at nearly the rate of free diffusion $10^8 s^{-1}$. We introduce a kinetic scheme for KcsA, that includes multiple species, hydration energy and ultimately strong selectivity between K^+ and Na^+ ions.

The occupancy configurations (or states) of the filter are described by considering the four charged indistinguishable binding sites; however we only consider the regime of optimum ion transport i.e. the transition between 2 and 3 ions. We only consider the lowest energy states for K^+ and Na^+ transitions and we denote this reduced set of states $\{n_s\}$ as: $\{\{2K^+\}, \{3K^+\}, \{2K^+1Na^+\}\}$.

The mixed species Master equation solved at steady state coupled to probability conservation, gives us occupancy and current (see Fig 1) of the filter.

Transition rates Γ are calculated following (Im 2000). At equilibrium between the filter and respective bulk (j) for each species (i), we find detailed balance. Since we know the Grand equilibrium distribution function (derived in Luchinsky 2016) we solve these relations subject to the constraint that permeation time $\leq D_i/L^2$

$$\Gamma_{23}^i = \sum_j \frac{D_i/L^2 \cdot \exp[(-\Delta G_j)/kT]}{1 + \exp[(-\Delta G_j)/kT]}, \quad \Gamma_{32}^i = \sum_j \frac{D_i/L^2}{1 + \exp[(-\Delta G_j)/kT]}. \quad (1)$$

The summation is over bulks (von Kitzing 1992); importantly in limiting we recover Kramers rate at large free energy barriers and diffusion with free energy wells: $\Delta G \lesssim kT$. Gibbs free energy G present in exponents, is given below for n_i ions in the filter

$$G_j(\{n_s\}, n_f) = \mathcal{E}(\{n_s\}, n_f) + \sum_i n_i (\mu_i^c - \mu_i^b) + \sum_i n_i q (\phi^c - \phi_j^b) - kT \ln \left(\prod_i (x_{ij}^{n_i}/n_i!) \right). \quad (2)$$

Principal terms present are: electrostatic energy in the filter \mathcal{E} , activity of ions in the bulk x_{ij} and excess chemical potential $\Delta\mu_i$. The excess chemical potential is of

importance because it describes the change in energy required to move an one ion from the bulk to filter, and hence a measure of dehydration

$$\Delta\mu_i = \mu_i^c - \mu_i^b. \quad (3)$$

The solution to the Master equation gives us current peaks (Fig 1) and a probability staircase of occupancy similar to (Kaufman 2015,von Kitzing 1992). Inclusion of multi-species demonstrates strong selectivity with a peak in K^+ current of $\sim 40pA$ as compared to the blocked Na^+ current at least 3 orders of magnitude smaller.

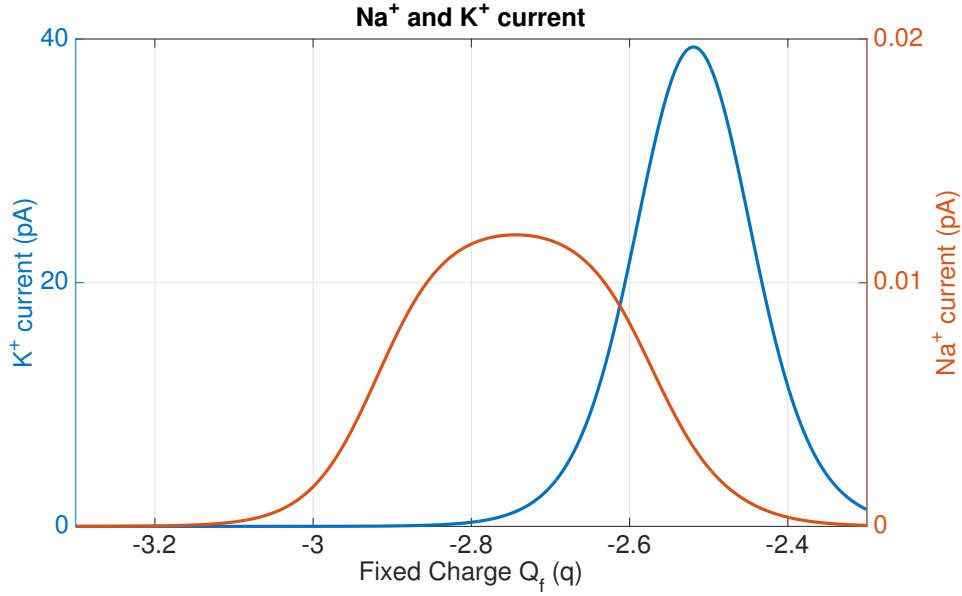


Figure 1: Resonant current peaks under conditions of intra-extra cellular voltage drop of $50mV$ and symmetric mole fractions for both species of 0.1.

In conclusion we have introduced a kinetic model for selective conduction between monovalent ions through a biological filter. This model accounts for the dehydration of ions and interactions in the filter. The model predict high conductivity of K^+ ions and their strong selectivity over Na^+ ions under physiological conditions. In future work we will extend our kinetic model to discuss its relation to that of Eisenman and try to calculate his sequences (Eisenman 1960).

References

- Im, W, Seefeld S, Roux B, 2000 *Biophysical Journal*, **79**, 788-801.
Luchinsky, D. G., Gibby, W. A. T., Eisenberg, R. S., McClintock, P. V. E., 2016 abstract ESGCO.
von Kitzing, E., 1992 In *Membrane Proteins* , Springer, 297-314.
Kaufman, I. K., McClintock, P. V. E., and Eisenberg, R. S., 2015 *New J. Phys.*, **8**.
Eisenman, G., 1960 *Symposium on Membrane Transport and Metabolism*, Academic Press, p. 163.

Interactions between heart rate and blood pressure by cross time-frequency analysis ¹

Anna Giczewska^A, Danuta Makowiec^B, Jerzy Wtorek^A, Artur Poliński^A,
Dorota Wejer^C, Beata Graff^D, Szymon Budrejko^E
and Zbigniew R. Struzik^F

^A Gdańsk University of Technology, Dept. of Biomedical Engineering, Gdańsk, Poland

^B University of Gdańsk, Inst. of Theoretical Physics and Astrophysics, Gdańsk, Poland

^C University of Gdańsk, Inst. of Experimental Physics, Gdańsk, Poland

^D Medical University of Gdańsk, Dept. of Hypertension and Diabetology, Gdańsk, Poland

^E Medical University of Gdańsk, Dept. of Cardiology and Electrotherapy, Gdańsk, Poland

^F RIKEN Brain Science Inst., Wako-shi, Japan

University of Tokyo, Graduate School of Education, Tokyo, Japan

Introduction: Analysis of heart rate (RR) and systolic blood pressure (SBP) variability yields fascinating information and represent a useful instrument for the study of the mechanisms involved in cardiovascular regulation, mainly affected by the autonomic nervous system with its parasympathetic and sympathetic components. This paper presents the characterization of RR and SBP signals in frequency domain and coherence analysis between RR and SBP signals in two groups of subjects undergoing the orthostatic stress.

Methods: The study was conducted on patients aged 18 to 39 years. All respondents (breathing at a fixed rate of 0.25Hz) underwent a (60°) head-up tilt table (HUT) test. Two groups of subjects were considered: *CG*- a control group of healthy people (19 people), *NEG*- a group of vasovagal patients who did not faint during the test(31 people). Methods described in [1] were used to obtain spectrum of counts for RR signals with large accuracy. For SBP signals spline interpolation was performed and linear trends were removed (following [2]). The idea of analysis those two signals is inovative part of study. Furthermore both signals were passed through an ideal low-pass filter with cutoff frequency 2Hz. Then the frequency analysis was carried out, namely: wavelet transform (WT), synchrosqueezed wavelet transform (SWT)[3] and wavelet coherence (WTC)[4].

Results: Evident frequency response to breathing fixed rate is observable in spectra as well as in coherence computations in all analyzed signals. Among 9 subjects from *CG* group, explicit increase in low frequencies (LF): 0.04 – 0.15 Hz, was noticed during tilt test. However, the second group of vasovagal patients (in 19 for 31 patients) is characterized by noticeable presence of power of spectrum in LF band in resting state in contrast to healthy people. Furthermore, analysis with SWT provides a fine

¹The authors AG, DM, DW, BG and ZRS acknowledge the financial support of the National Science Centre, Poland, UMO: 2012/06/M/ST2/00480.

line which follows a main course of the wavelet transform which enhances the significance of the WT plots. Also coherence plots are consistent with these observations. The analysis of phases (represented by arrows) indicates at the leading role of RR signals which oscillate in case of healthy people in anti-phase to SBP, but in case of vasovagal patients the phase of oscillations is changing.

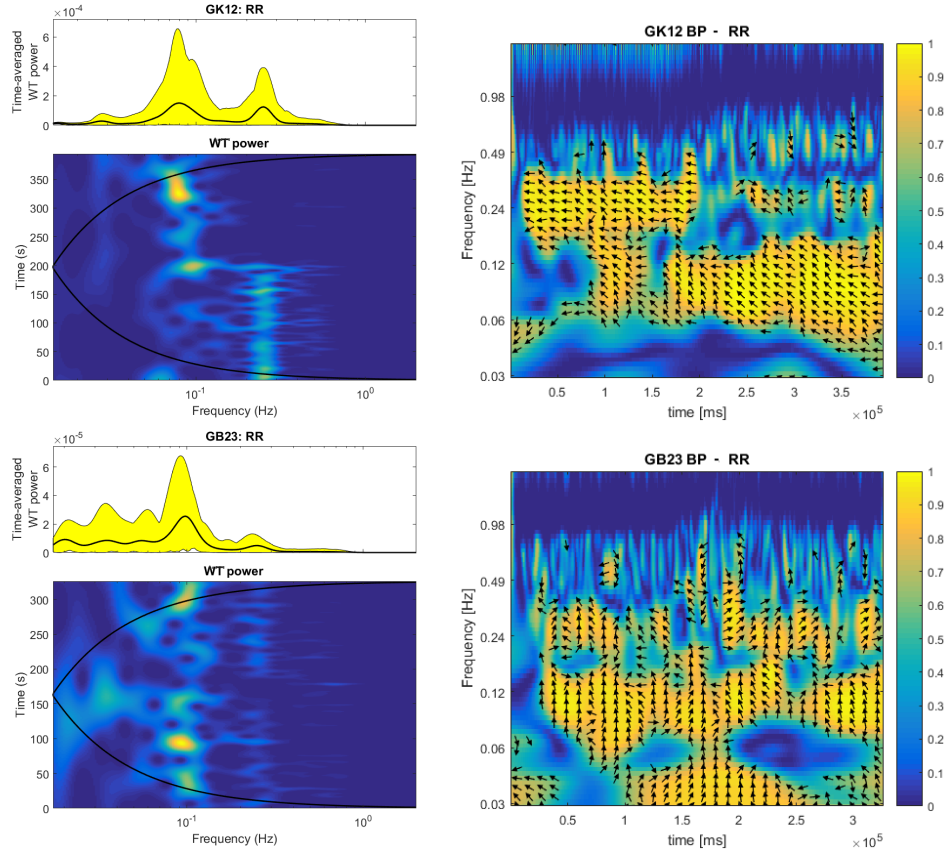


Figure 1: Examples of time-frequency analysis of a regular response to the HUT in a healthy individual (GK12, first row) and dissimilar response to HUT in a vasovagal patient (NEG23, second row). Pictures present CWT between RR and SBP signals and WT for RR signals which represent last 200 beats before tilting and 300 beats after tilting.

Conclusions: Differences in LF band between healthy people and vasovagal patients indicate at different characterization of the cardiovascular response to the orthostatic stress. Our qualitative findings presented above are preliminary, however the computations are intensively performed and the results will be shown.

References

- [1] DeBoer RW, Karemaker JM, Strackee J, 1984, *IEEE Trans.Biomed.Eng.* **31** 384-387.
- [2] Orini M, Laguna P, Mainardi LT, Bailon R, 2012, *Physiol.Meas.* **33** 315-331.
- [3] Iatsenko D, McClintock PVE, Stefanowska A, 2015 *Dig.Sig.Proc.* **42** 1-26.
- [4] Grinsted A, Moore JC, Jevrejeva S, 2004, *Nonlinear Process.Geophys.* **11** 561-566.

Observational error in time domain heart rate variability analysis

Jan Gierałowski¹, Monika Petelczył¹, Grzegorz Siudem¹ and Barbara Żogała-Siudem²

¹Warsaw University of Technology, Faculty of Physics, Warsaw, Poland
²Systems Research Institute, Polish Academy of Sciences, Warsaw, Poland

Introduction

The accuracy of determination of many popular heart rate variability (HRV) parameters is usually not discussed in the literature. There are limited studies dedicated for impact of low sampling frequency on time and frequency domain and also nonlinear measures (Hejjel 2004, Ziemssen 2008). Note, that especially nonlinear methods are composed of many complex transformations. Multiple steps of computations propagate the observational error, which magnitude in final result is usually unknown or at least is difficult to predict. Therefore the results might have doubtful statistical reliability.

Objectives

The main goal of our work presented here is to estimate the impact of observational error on basic time domain parameters of HRV: *mean RR*, *SDNN* (the standard deviation of NN intervals), *SDSD* (standard deviation of successive differences), *RMSSD* (root mean square of successive differences), *pNN50* (the proportion of pairs of successive NN intervals that differ by more than 50 ms) (Malik et al 1996). Note, that we focus on observational errors associated to the ECG sampling rate only. We do not remove or replace arrhythmias in our simulations, because this procedure influences on magnitude of general error of the method. Therefore we use *pRR50* instead *pNN50*, *SDRR* instead of *SDNN*. We assume that each RR interval is burdened by observational errors and postulate its form. We decided to show the relation between observational error and general error of the time domain method, which results from propagation of measurement error in computations. For that purpose we present Monte Carlo (MC) simulations. Additionally for three parameters (*mean RR*, *SDNN*, *pNN50*), we suggest the exact analytical calculations for supporting our numerical results.

Methods

The random variable X_i instead of the RR_i interval is proposed:

$$X_i = RR_i + \zeta_i \quad (1),$$

where ζ_i is observational error. We assume that errors ζ_i for RR interval are independent and are normally distributed with zero mean and standard deviation σ : $N(0; \sigma)$. Note that each RR interval is characterized by the noise component with the same statistics features. Therefore we assume constant σ with range of milliseconds. Such range of values is caused by standard sampling frequency of ECG recorders. In result the X_i distribution is also normal: $N(RR_i; \sigma)$ with mean equals RR_i .

We perform computations on real data from MIT-BIH Arrhythmia Database –the most popular collection of signals used for scientific tests (Golberger 2000). The MIT-BIH database contains 48 half-hour excerpts of two-channel ambulatory ECG recordings, studied by the BIH Arrhythmia Laboratory between 1975 and 1979. According eq. (1), for each real RR interval we add random Gaussian variable from distribution with $\sigma \in \{1, 2, 3 \dots 11, 12\} ms$. In effect we obtain new data with artificial observational noise. In Monte Carlo simulations we repeat this procedure 1000 times. For each “noisy” time series we computed five basic parameters: *mean RR*, *SDRR*, *SDSD*, *RMSSD*, *pRR50*. Each time domain parameter is then characterised by own distribution. We introduce the standard deviation β of such distribution as the magnitude of general time domain parameter error.

Results

Because of limited length of abstract we present MC simulation results for $pRR50$ in two forms (Fig.1a,b) for three different examples. In Fig. 1a we show percentage change of $pRR50$ in comparison to original data - separately for different measurement error σ . In Fig 2a we present the standard deviation β as general method error. We observe an nonlinear increase of $pRR50$ with increasing magnitude of observational error. The standard deviation β of distribution of $pRR50$ from MC simulations are also sensitive to observational error σ magnitude – note that this dependence is not clearly linear.

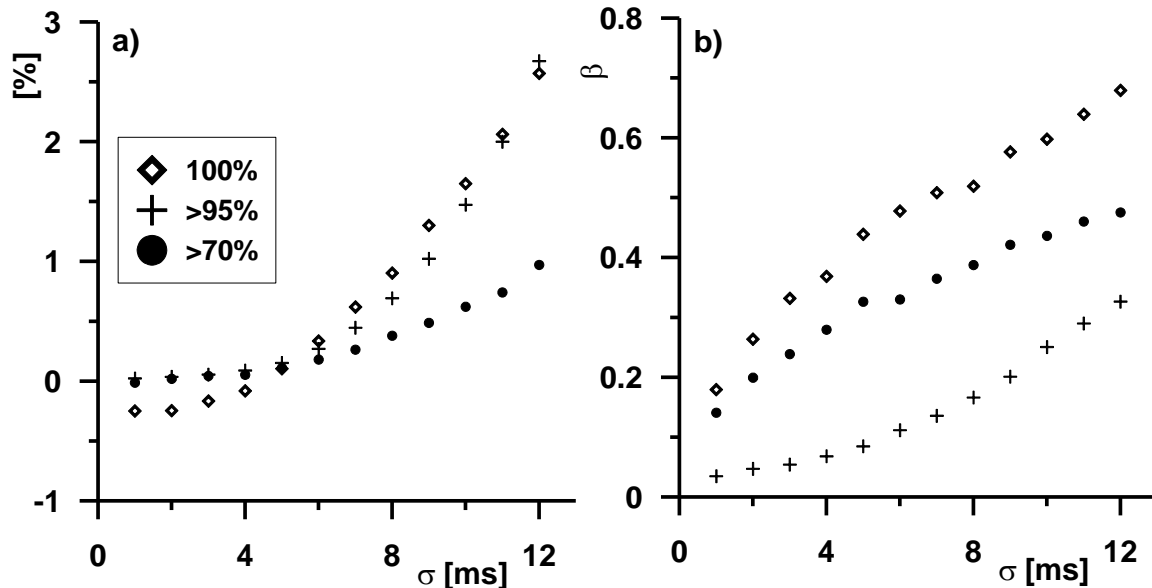


Fig. 1a) Percentage change of the mean of $pRR50$ in comparison to original data for increasing measurement error σ b) the general time domain parameter error presented as β (standard deviation) of distribution presented in a) panel. Examples of data consisting of: 100% N intervals (empty diamonds), more than 95% N intervals (crosses), more than 70% N intervals (circles).

For other HRV time domain parameters their mean values does not depend on the magnitude of observational error σ . However, the β increases linearly with observational error σ .

Discussion

For assessment of accuracy of time domain parameters burdened by observational error associated from sampling rate, we introduce the standard deviation β . β is a magnitude of general parameter error, which occurs as result of measurement error σ propagation in computations of time domain method. *Mean RR*, *SDRR*, *SDSD*, *RMSSD* are not sensitive for measurement error. We present the most interesting results for $pRR50$, in which the increase of β with increase of measurement error σ is not regular. Note that our test database was MIT-BIH Arrhythmia Database, which represents the real clinical study. We are preparing similar computations for nonlinear methods, which we suppose will be characterized by larger β error.

References

- Hejjel L, Roth E, *Phys Meas* (2004) **25(6)** 1405-11
 Ziemssen T, Gasch J, Ruediger H, *J Clin Monit Comput* (2008) **22(2)** 159-68
 Malik et al *Circulation* (1996) **93(5)**:1043-65
 Goldberger AL, Amaral LAN, Glass L, Hausdorff JM, Ivanov PCh, Mark RG, Mietus JE, Moody GB, Peng CK, Stanley HE. *Circulation* (2000) **101(23)** e215-e220

Cardiorespiratory Coupling Assessment - a new method of monitoring changes in Respiratory Sinus Arrhythmia in time domain

Iga Grzegorzczuk¹, Jan Gierałtowski¹ and Paweł Krześciński²

¹ *Warsaw University of Technology, Department of Physics, Warsaw, Poland*

² *Military Institute of Medicine, Department of Cardiology and Internal Diseases, Warsaw, Poland*

The cardiovascular and respiratory systems are both controlled by the Autonomic Nervous System (ANS). Analysis of interrelation in functioning of these two systems might provide a valuable insight into quality of ANS performance. The best known representative of this phenomena is Respiratory Sinus Arrhythmia (RSA). It causes the accelerations of the heart rate during inspirations and decelerations in expirations. Some measures to analyze the RSA effect already exist i.e. peak to valley estimate [1], which is easily applicable but tends to omit samples when there are less than two of them per expiratory or inspiratory period and does not change over the time. Same problem applies to other methods e.g. the spectral coherence [2]. There is also a method designed to define a RSA pattern by phase averaging [3]. It measures changes in the time domain, but classifies remarkable amount of respiratory cycles as outliers throughout the averaging process. The aim of this study was to create a more precise and easily interpretable method allowing to analyze the coupling between Heart Rate Variability (HRV) and respiratory rhythm. The method should also fulfill some basic requirements, i.e. statistical ones. When both signals are constant the RSA effect does not occur, so the result should be equal to zero. Moreover, the created algorithm ought to acknowledge the fundamental laws of physiology.

The proposed Cardiovascular Coupling Assessment (CCA) method enables to determine the changes in strength of the Respiratory Sinus Arrhythmia (RSA) over the time, which is obtained by using a moving window of 1 minute length. The method's advantage is that it does not dismiss any samples or respiratory cycles. The measure is calculated as a median of differences of RR intervals (RRI) detected during expiration and inspiration in each window. It can be described by the following equation:

$$CCA(t) = \text{median}(RRI_{exp}(k)) - \text{median}(RRI_{insp}(k)),$$

where RRI_{exp} and RRI_{insp} are the matrices of RRI detected consecutively in expiratory and inspiratory phase of breathing in the k -th window. First, the method

efficiency was tested on the generated synthetic dataset. Its task was to verify whether the result depends entirely on the changes in RRI, e.g. it equals zero when the RRI set is constant. Then the analysis with the CCA method on the real data was executed. Provided data consisted of recordings of ECG and respiratory signals, each 5 minutes long. The signals were registered for 70 healthy, exceptionally fit male subjects (37 ± 12 years) during the spontaneous breathing phase followed by the controlled breathing test with frequency of 15 – 20 breaths per minute. The examination was carried out in Military Institute of Medicine in Warsaw.

The performed analysis proved the CCA method to be accurate to observe the changes in the strength of the RSA effect in time domain. When the CCA is positive it implies that the RSA is present and its strength increases with the value of the CCA. The equality to zero means that the RSA effect does not occur in the analyzed period. It might be caused by the poor condition of the patient's ANS or just signalize the stress or physical activity. The negative values of the parameter are rather a new concept in RSA analysis. They indicate the reversed RSA effect, which has been already mentioned in the literature but is still not fully understood. It suggests the delay in the transfer of information in the organism. The results obtained by the presented method confirm the previous knowledge about the RSA effect. The calculations of the differences between maximum and minimum value of the CCA measure (amplitude) for each subject during the controlled breathing phase of examination, when patients were breathing faster (about 20 breaths per minute), equaled to $77,14 \pm 53,04$ msec. For the spontaneous breathing phase it was $106,61 \pm 55,54$ msec. That indicates that even with not perfectly maintained breathing rate during CBT there was smaller variability as expected. These results were confirmed also by computation of the standard deviation of CCA for each subject and for the CBT phase it was $21,33 \pm 12,13$ msec and for the spontaneous breathing phase $16,16 \pm 12,19$ msec. In the near future the way of the methods interpretation should be improved, with more variants of synthetic data. Furthermore, its reaction to the trends in RR time series as well as to the different types of noises has to be verified.

References

- [1] Lewis G.F., Furman S.A., McCool M.F. Et al. (2012) , Statistical strategies to quantify respiratory sinus arrhythmia: Are commonly used metrics equivalent? . *Biol Psychol.* **89(2)**: 349-364.
- [2] Grossman P., Janssen K. H. L., Vaitl D. (2013) Cardiorespiratory and Cardiosomatic Psychophysiology *Springer Science & Business Media* 105-117
- [3] Gilad O., Swenne C.A., Davrath L.R. and Akselrod S. (2005) Phase Averaged Characterization of Respiratory Sinus Arrhythmia Pattern *AJP-Heart Circ Physiol* **288**: H504 – H510.

ECG player – software and data for your own, easy artificial patient

Anna Perka and Jan Gierałtowski

Warsaw University of Technology, Department of Physics, Warsaw, Poland

On the market there are available simulators of ECG signals, which are used to control the quality and proper functioning of electrocardiographs. These artificial patients enable to perform such tests without need of participation of a living person, to avoid potential risk. Nevertheless, they produce synthetic signal, which is deformed and does not reflect the actual morphology of the ECG, thus are not sufficient for testing of more advanced functions of modern ECG equipment.

We prepared an alternative artificial patient based on the simplest possible assumption, which was using an easily accessible and cheap device (in our case it was a portable mp3 audio player). For this purpose, we developed software for converting raw ECG signals into audio files using Matlab. Next we converted files from the MIT-BIH Arrhythmia Database [1] to waveform audio file format in order to play these signals on audio player. The function which allowed us to do this is `audiowrite`, which is one of core Matlab functions. Resulting audio files have 8 kHz sampling, 16 bit resolution and have two channels (stereo). Then we checked compatibility of original and modified signals, especially checking if standard audio players are capable of preserving low-frequencies of ECG signal (audio signals are usually in the range from 20 Hz to 20 kHz whereas ECG is in the range from 0.15 Hz to 40 Hz [2]) and results were highly sufficient. Adjusting the volume of the player turned out to be adequate to receive signals with amplitude comparable to real ECG signals and there was no need to use voltage divider.

The main goal of our work was to obtain signals which would be the most realistic without need for involvement of the patient. We have already used our solution to test highly advanced medical equipment, for which usage of the standard ECG simulator was not enough. Preliminary tests show that ECG signals from our generator are in a very good correspondence with real recordings (see Fig. 1). Additional, necessary numerical tests presenting agreement between reconstructed and real signals are in preparation and will be provided during the Conference. Our solution gives an opportunity to have an artificial patient, which may be used to scientific or industrial purposes and is available for anyone who has a reliable audio player (even this one in laptop can be used). Moreover, it offers very broad prospects for its application at zero cost and time of implementation.

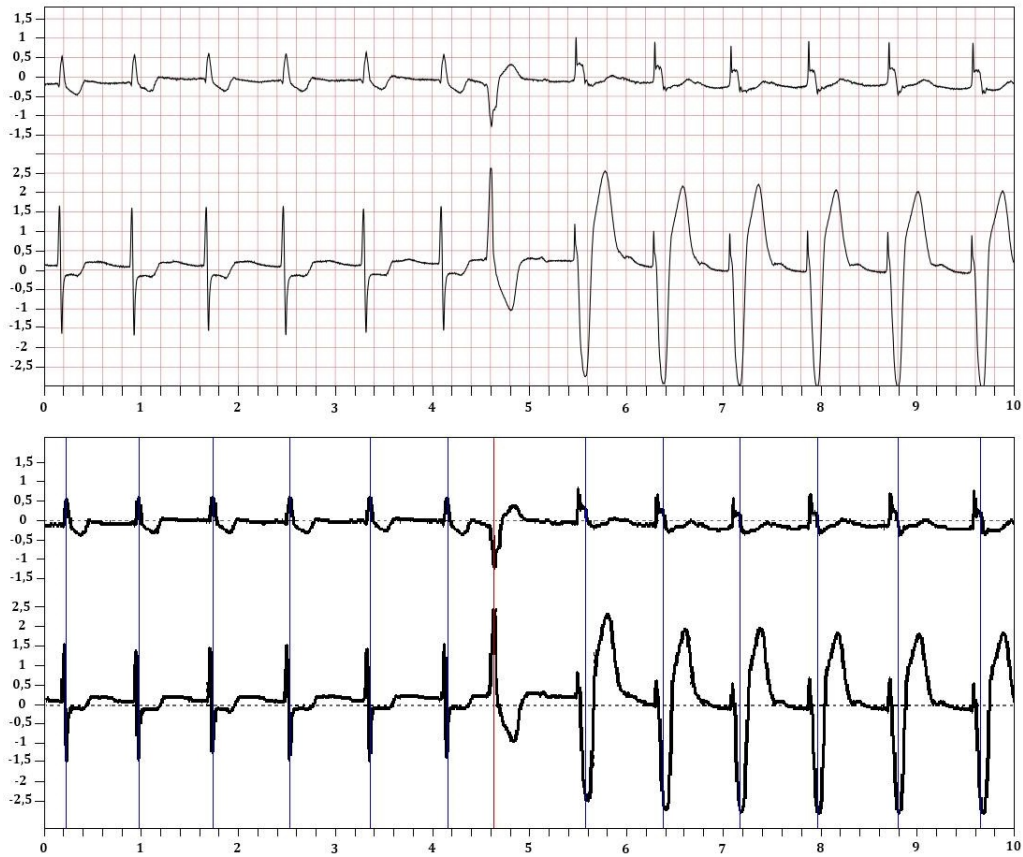


Figure 1 Plots presenting fragments of ECG signals: on top – signal from the MIT-BIH Arrhythmia Database displayed with the official PhysioNet Lightwave browser, the bottom: signal registered by Holter-ECG recorder from the audio player files viewed by using Sentinel software.

References

- [1] Moody GB, Mark RG. (2001) The impact of the MIT-BIH Arrhythmia Database. *IEEE Eng in Med and Biol* **20(3)**:45-50.
- [2] Clifford GD, Azuaje F, McSharry PE (2006) *Advanced Methods And Tools for ECG Data Analysis* Artech House Publishing.

Sympathetic nervous system does not influence the cardiac contribution to the relationship between blood pressure and pial artery pulsation oscillations in healthy volunteers

**Marcin Gruszecki¹, Pawel J. Winklewski², Yurii Tkachenko³, Kamila Mazur⁴,
Jacek Kot³, Wojciech Guminski⁵, Krzysztof Czuszyński⁴, Jerzy Wtorek⁴,
Andrzej F. Frydrychowski²**

¹ *Department of Radiology Informatics and Statistics, Medical Univ. of Gdansk*

² *Institute of Human Physiology, Medical Univ. of Gdansk*

³ *National Centre for Hyperbaric Medicine, Medical Univ. of Gdansk*

⁴ *Department of Biomedical Engineering, Gdansk Univ. of Technology*

⁵ *Department of Computer Communications, Gdansk Univ. of Technology*

Evidence accumulates that variation in cardiac output either acutely or chronically leads to a change in cerebral blood flow [1, 2]. However, the mechanisms linking cardiac output with brain haemodynamic remains largely unrecognized. The aim of this study was to assess changes in heart generated relationship between blood pressure (BP) and subarachnoid space width (SAS) oscillations. Non-invasive assessment of SAS oscillations became possible due to a recently developed method based on infrared radiation called near-infrared transillumination/backscattering sounding (NIR-T/BSS). Based on our previous experiments [3, 4] we speculated that sympathetic nervous system (SNS) may tend to stabilize BP-SAS coupling in extreme conditions while do not affect the relationship between these signals during more physiological stimuli. Therefore, we hypothesised that both handgrip test (HGT) and cold test (CT) would not affect the cardiac contribution to the relationship between BP-SAS oscillations, regardless of the fact that the stimuli evoked by the tests are likely transmitted by different central sympathetic circuits.

The pial artery and subarachnoid width response to HGT and CT were studied in 20 healthy subjects. SAS was measured using NIR-T/BSS; cerebral blood flow velocity was measured using Doppler ultrasound of the left internal carotid artery; heart rate (HR) and beat-to-beat mean BP were recorded using a continuous finger-pulse photoplethysmography; respiratory rate, minute ventilation, end-tidal CO₂ and end-tidal O₂ were measured using a metabolic and spirometry module of the medical monitoring system. Wavelet transform analysis was used to assess the relationship between BP and SAS oscillations.

In time domain HGT and CT evoked typical changes [5]. To assess BP-SAS coupling we used wavelet transform analysis. Compared with autoregressive estimation, wavelet transform is calculated directly from data, and the limitations of linear modelling and the choice of model order are thus avoided [6]. No statistically significant difference with respect to wavelet coherence (WCO) and wavelet phase coherence (WPCO) was found between the BP and SAS oscillations (Fig. 1).

We believe that combination of NIR-T/BSS with advanced signal analysis tools most likely

represents a promising approach in describing the interrelations and pathways involved in heart failure, obstructive sleep apnoea and related cerebrovascular diseases. The presented results establish therefore reference for future clinical studies which are warranted. We have shown that SNS activation does not affect the cardiac contribution to the relationship between the BP and SAS oscillations in healthy subjects. In fact, it seems that a high sympathetic drive tends to stabilise the relationship between the analysed signals.

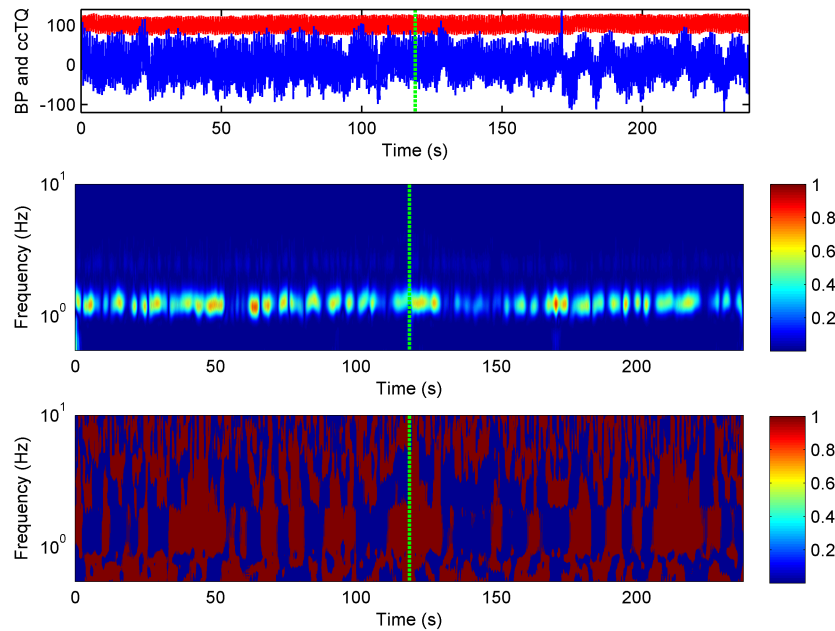


Figure 1: Representative WCO (middle panel) and WPCO (lower panel) tracings. BP (red) and cc-TQ (blue) signals are provided in the upper panel. The green dashed line separate baseline and cold test period. WCO and WPCO remains relatively stable throughout baseline and cold test.

References

- [1] Brassard P, Gustafsson F., *Can J Cardiol.*, 2015, doi: 10.1016/j.cjca.2015.12.021
- [2] Meng L, Hou W, Chui J, Han R, Gelb A.W., *Anesthesiology*, 2015, 123, 1198
- [3] Winklewski P.J., Gruszecki M., Wolf J. et al., *Microvasc Res.*, 2015, 99, 86
- [4] Winklewski P.J., Barak O., Madden D. et al., *PLoS One*, 2015, 10, e0135429
- [5] Winklewski P.J., Tkachenko Y., Mazur K. et al., *PLoS One*, 2015, 10, e0135751
- [6] Shiogai, Y., Stefanovska, A., McClintock, P.V., *Phys. Rep.*, 2010, 488, 51

Symbolic analysis of heart rate variability in Trendelenburg position before and after pneumoperitoneum under general anesthesia

Stefano Guzzetti¹, Andrea Marchi^{2,3}, Riccardo Colombo⁴,
Ferdinando Raimondi⁵ and Alberto Porta^{6,7}

¹ Emergency Department, Azienda Ospedaliera Luigi Sacco – Polo Universitario, University of Milan, Milan, Italy

² Politecnico di Milano, Department of Electronics Information and Bioengineering, Milan, Italy

³ Department of Anesthesia and Intensive Care, San Gerardo Hospital, Monza, Italy

⁴ Department of Anaesthesiology and Intensive Care Unit, Azienda Ospedaliera Luigi Sacco – Polo Universitario, University of Milan, Milan, Italy

⁵ Department of Anaesthesiology and Intensive Care Unit, Istituto Clinico Humanitas IRCCS, Rozzano, Italy

⁶ University of Milan, Department of Biomedical Sciences for Health, Milan, Italy

⁷ IRCCS Policlinico San Donato, Department of Cardiothoracic, Vascular Anesthesia and Intensive Care, Milan, Italy

Introduction

Prostatectomy in the Trendelenburg position with pneumoperitoneum is a challenge for the anaesthesiologist, in particular for possible bradycardic and hypotensive episodes. We evaluated the cardiovascular autonomic control in two groups of patients undergoing elective laparoscopic prostatectomy. In all patients anesthesia was induced with propofol plus remifentanyl via infusion pump. In the first group (41 patients) the patients lay in head-down tilt position at -25° (Trendelenburg) and underwent the pneumoperitoneum, insufflated with CO₂ at 12-14 mmHg through a surgically inserted trocar. In the second group (25 patients) we reversed pneumoperitoneum and Trendelenburg maneuver. Symbolic analysis of heart rate variability (HRV) was exploited to track cardiac autonomic regulation [1-3] and might suggest countermeasures to better deal with hypotensive episodes. The physiological plausibility of symbolic analysis is based on the observation that sympathetic and parasympathetic systems have different latencies that are responsible for different dynamical features on HRV signal [4].

Experimental Protocol and Data Analysis

The symbolic analysis was fully described and validated previously [1,2]. Briefly, the full range of each RR sequences was uniformly spread on 6 levels (from 0 to 5), and patterns of length of 3 beats were constructed. Therefore, each subject and each experimental condition had its own level. All the patterns were grouped without any loss into four families according to the number and types of variations from one symbol to the next one. The pattern families were: i) patterns with no variation (0V, all the symbols were equal, e.g. (2,2,2) or (4,4,4); ii) patterns with one variation (1V, two consecutive symbols were equal and the remaining one is different, e.g. (4,2,2) or (4,4,3); iii) patterns with two like variations (2LV, the three symbols formed an ascending or descending ramp, e.g. (1,3,4) or (5,4,2); iv) patterns with two unlike variations (2UV, the three symbols formed a peak or a valley, e.g. (3,5,3) or (4,1,2). We evaluated the rates of occurrence of these families labeled as %0V, %1V, %2LV and %2UV. These indices were computed simply by counting the number of times that a pattern belonging to a specific family and by expressing them as percentage of the overall amount of patterns. An increase in sympathetic modulation and a vagal withdrawal elicits a significant increase of %0V and a decrease of %2V over HRV data, whereas parasympathetic activity dominance induces the opposite effect [1].

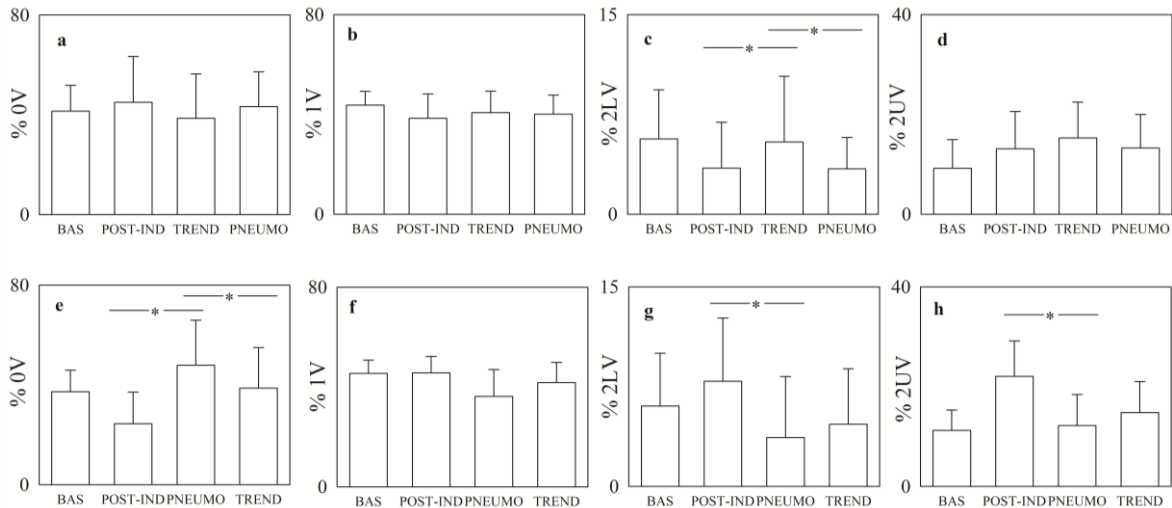


Figure 1. Bargraphs (upper row) show mean plus standard deviation of %0V (a), %1V (b), %2LV (c), and %2UV (d) as a function of the four different experimental sessions (BAS = baseline, POST-IND = post-induction of anesthesia, TREND = Trendelenburg; PNEUMO = pneumoperitoneum). Bargraphs (lower row) show the same parameters after reversing the sequence of PNEUMO and TREND. The symbol * indicates $p < 0.05$.

The patients were recorded at rest in supine horizontal position (BAS), after the induction of general anesthesia and the onset of mechanical ventilation in horizontal position (POST-IND), after pneumoperitoneum (PNEUMO) after Trendelenburg with a table inclination of -25° (TREND). All sessions lasted 5 minutes. PNEUMO was in horizontal position if it occurred before TREND, while it was at -25° if it occurred after TREND.

Results

As reported in Fig.1c, the group of patients with TREND before PNEUMO exhibited an increase of %2LV from POST-IND to TREND and a decrease of the percentage of this symbolic pattern during PNEUMO following TREND. This change can be interpreted as an increase of vagal modulation with TREND and a reduction of this modulation with PNEUMO. In the other group of patients featuring PNEUMO before TREND, an increase of %0V suggests an initial increase of sympathetic modulation followed by a decrease of %0V% with TREND (Fig.1e).

Discussion and Conclusions

Reversing TREND with PNEUMO led to a completely different final condition during prostatectomy surgery that can be detected via symbolic analysis of HRV data. Thus, symbolic analysis seems an appropriate method to study the complexity of the cardiac autonomic nervous control during different sequences of laparoscopic surgery maneuvers under a condition of depressed autonomic function such as during general anesthesia and might give helpful suggestions to eventually modify clinical procedures.

References

- [1] Guzzetti S *et al*, 2005, *Circulation* **112**, 465-470.
- [2] Porta A *et al*, 2001, *IEEE Trans Biomed Eng* **48**, 1282-1291.
- [3] Porta A *et al*, 2007, *Am J Physiol* **293**, H702-708.
- [4] Warner HR *et al*, 1962, *J Appl Physiol* **317**, 349-355.

Time delay in facial blood pulsations

Alexei A. Kamshilin¹, Maxim A. Volynsky¹, Igor S. Sidorov¹ and Oleg V. Mamontov^{1,2}

¹ITMO University, Computer Photonics and Videomatics Dept., Saint Petersburg, Russia

²V. A. Almazov North-West Federal Medical Research Centre, Saint Petersburg, Russia

Face is a subject's area to which one can easy access by an optical technique for non-contact and non-invasive measurements of the important physiological signals of a human body. Imaging photoplethysmography (IPPG) technique has become very popular among researchers because of its simplicity and potentially low cost. Even though interpretation of IPPG signal is still a matter of debate, the technique was proposed to be used for heart rate monitoring, measurements of the heart rate variability, and estimations of oxygen saturation. In this work we report on measurements of facial blood pulsations with IPPG system carried out synchronously with electrocardiographic (ECG) recordings. It is shown for the first time to the best of our knowledge that pulsations revealed by the IPPG system stem from the previous (not the nearest in the time scale) R-peak of ECG.

Experiments were carried out with 24 healthy subjects aged 19 – 64 years. Each subject was asked to take a comfort sitting position and lean his head on a properly adjusted support. Video recording of subject's face was done during 30 – 50 s. We used a custom-made IPPG system in which video was recorded by digital black-and-white CMOS camera at the framerate of 39 fps while subject's face was illuminated by green light at the wavelength of 530 nm with the spectral bandwidth of 40 nm. Video and ECG recordings were synchronized so that the difference between the beginning of ECG and the first recorded frame did not exceed 1.0 ms. Recorded frames and ECG were processed off-line by using custom software implemented in the MATLAB® platform. No image stabilization was applied. In a core of the algorithm, we calculated PPG waveforms by averaging pixels values in a Region of Interest (ROI) sizing 11×11 pixels (3×3 mm²), which was moveable over both cheeks. In each ROI we detected positions of the PPG-waveform minima, which correspond to the beginning of each pulsation. Duration of each cardiac cycle was estimated from the delay between two consecutive peaks in ECG. Further, only the ROIs in which the number of cardiac cycles defined from the ECG recording is the same as from PPG were taken in consideration. Figure 1 shows an example of the frame with the positions of the ROIs satisfied to the conditions of equality of the number of the cardiac cycles.

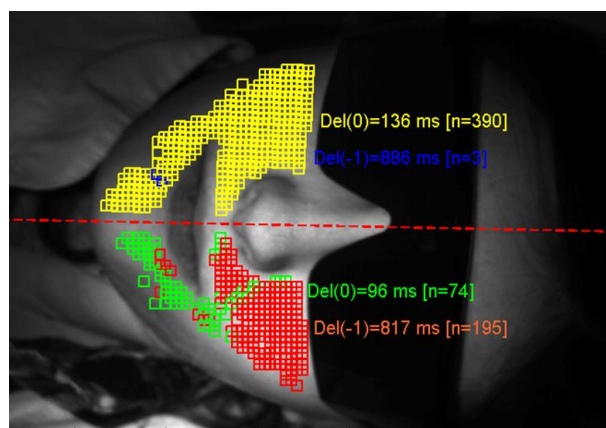


Fig. 1. One of the raw frames from the recorded video with ROIs in which the number of cardio cycles defined from ECG coincides with that from PPG waveforms. Numbers show the delay time between R-peaks of ECG and minima of PPG-signal averaged within the groups of ROIs of the same colour.

A fragment of the typical PPG waveform from one of the ROI chosen in the red group is shown in Fig. 2a by the blue curve. Black curve in Fig. 2a shows simultaneously recorded

ECG. Estimations show that the mean delay of the PPG signal from the nearest R-peak is about 0.12 s. We took advantage of the natural heart rate variability to evaluate correctness of this approach of the delay calculation. The period of each cardiac cycle defined from the ECG recording is shown in Fig. 2b by black curve for each respective sequential cycle. Similar sequence of the periods defined from the minima of the PPG waveform is shown in Fig. 2b by blue curve. It is seen that the blue curve is delayed by one cycle in respect to black curve resulting in the correlation coefficient of 0.36. Figure 1c illustrates excellent coincidence (correlation = 0.91) of both curves when the PPG curve is shifted by one cycle backward. Therefore, the PPG waveform stems from the previous R-peak. Consequently, the correct delay of the PPG signal in this particular case is 0.82 s.

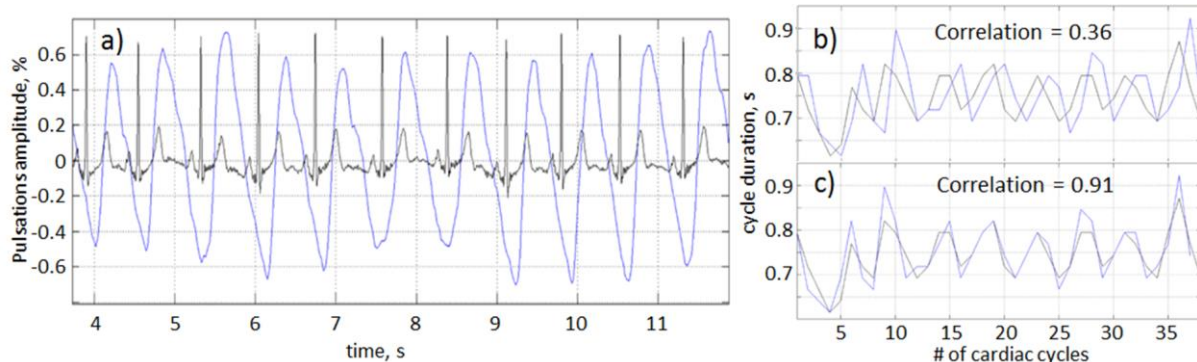


Fig. 2. a) PPG waveform recorded simultaneously with ECG in one of the chosen ROIs in the red group of the lower cheek shown in Fig. 1. b) Cardiac-cycle period as a function of the cycle's sequential number directly calculated from the data (part a) of ECG (black curve) and PPG (blue curve). c) Same dependences as in the part b but the PPG-curve is shifted for one cycle backward.

Our algorithm automatically estimates the best correlation between PPG and ECG signals in each ROI and calculates the delay of pulsations taking into account this correlation. As seen in Fig.1, both types of ROIs (PPG signal correlates with nearest, Del(0), or previous, Del(-1), R-peak) coexist in the same face. Different types of correlation are marked by different colours in Fig.1. The ratio of different ROI types strongly varies from one subject to another and it depends on the subject's position: sedentary or recumbent. For all 24 studied subjects we found several ROIs in which the time delay between the PPG minimum and R-peak is larger or comparable with the duration of the cardiac cycle. This finding again rises up the question: where does PPG waveform come from? According to the classical PPG model, the light is modulated in time due to direct interaction with the pulsatile arterial blood [1]. Since the speed of the pulse wave in arteries is known to be high (4 – 6 m/s), pulse propagation time from the heart to face should not exceed the 0.2 – 0.4 s. Observed longer delay time contradicts the classical theory. It is also not completely consistent with the recently proposed alternative model in which the PPG signal is linked to local changes in absorption and light scattering within the capillary bed in the dermis rhythmically compressed by a changeable arterial pressure [2]. Possible explanation of new observations will be discussed during the presentation.

Financial support by Russian Scientific Foundation (Grant 15-15-20012) is acknowledged.

References

- [1] Allen J 2004 *Physiological Measurement* **28** R1-R41
- [2] Kamshilin A A, Mamontov O V, Koval V T, Zayats G A, Romashko R V 2015 *Biomedical Optics Express* **6**, 4326-4334

Dynamics of protein and permeation in KcsA ion channel

Igor Khovanov¹, Salvatore Cosseddu², Mark Rodger¹ and Carlo
Guardiani¹

¹ *University of Warwick, Centre for Scientific Computing, Coventry, UK*

² *VU University, Division of Theoretical Chemistry, Amsterdam, The Netherlands*

MD simulations are aimed to provide a mechanistic picture of the permeation of an ion through a channel. Typically, such a picture is build up via calculating the potential of mean force (free energy) by using so-called biased techniques. In such approach dynamics (oscillations) of the protein are averaged out whereas ion's dynamics considered as pure stochastic. First we discuss the relationship between an external artificial bias and dynamics of the protein and show generic pitfalls of 'standard' biased methods. Then we consider modifications of the standard procedure and provide a picture of the permeation and selectivity in KcsA channel. Finally the role of ions' dynamics and ions' interactions in the permeation and selectivity is discussed.

The dependence of the ADFA asymmetric effect in RR-intervals time series on the length of the DFA sliding window

Marcin Kořmider¹, Dawid Mieszkowski¹, Sebastian Źurek¹, Tomasz Krauze², Przemysław Guzik², Jarosław Piskorski¹

¹*University of Zielona Gora, Institute of Physics, Zielona Gora, Poland*

²*Poznan University of Medical Sciences, Department of Cardiology-Intensive Therapy and Internal Diseases, Poznan, Poland*

Introduction Asymmetric Detrended Fluctuation Analysis (ADFA) is an asymmetric extension of the classical DFA algorithm. It consists of the same steps as the standard DFA, except it defines scaling components for rising and falling trends separately. The existence of Heart Rate Asymmetry leads one to suspect that the scaling properties of accelerating and decelerating trends may have different scaling properties.

Unlike in standard DFA, two, rather than one, types of root square errors are defined: one for the noise on the rising trends and one for the noise on the falling trends

$$F^+(n) = \sqrt{\frac{1}{M_n^+ \cdot n} \sum_{k=1}^{M_n^+} (y(k) - y_n(k))^2}, \quad F^-(n) = \sqrt{\frac{1}{M_n^- \cdot n} \sum_{k=1}^{M_n^-} (y(k) - y_n(k))^2}, \quad (1)$$

M_n^\pm is the number of boxes of length n with rising/falling trend, respectively, and $y_n(k)$ is the linear fit to the data in the window.

These quantities are used to check for the existence of power law

$$F^\pm(n) \sim n^{\alpha^\pm}, \quad (2)$$

separately for rising and falling trends. The α^\pm exponents are derived from the plots of $\log_{10} F^\pm(n)$ on $\log_{10}(n)$. For more details and motivation see Rivera-Castroa *et al.*

One last modification of the standard DFA developed by Rivera-Castroa *et al* is the local approach to ADFA. In this approach ADFA is calculated for a sliding window of a set length moving along the recording.

Recently we showed (see Mieszkowski *et al*) that there is a highly statistically significant effect with $\alpha^- > \alpha^+$. The aim of this study is to check whether the length

of the sliding window influences this result, and, if so, in which way and to what extent.

Materials and methods One hundred and ten healthy volunteers were enrolled in the study, 48 women, aged between 20 and 40 years. In each subject standard 30-minute, 12-lead ECG was recorded at 1600 Hz. The RR intervals with annotations were exported to text files which were further analyzed by the in-house software written in python and cython for local ADFA (see link to the software in the References). The length of the sliding window was changed from 40 to 1000 RR intervals and the percentage of recordings with $\alpha^- > \alpha^+$ was calculated for each length. Then the proportions were compared to the theoretical value of 50% (proportion 0.5) with the binomial test.

Results We have found that the shortest lengths cases (40 and 50) does not exhibit any significant asymmetry, then there is a rising tendency with increasing window length which peaks at 150 and then drops off slightly and stabilizes. These results, along with the statistical significance, are demonstrated in figure 1.

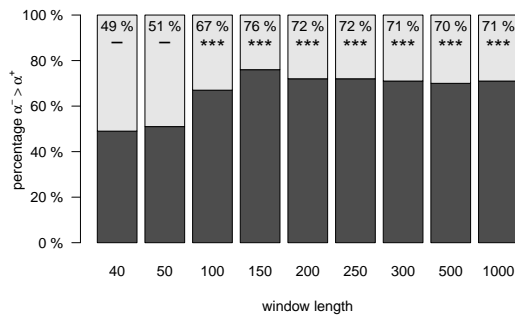


Figure 1. The percentages of recordings with $\alpha^- > \alpha^+$ with the statistical significance of the test for the percentage to be different from 50%. The symbols have the following interpretation for the p -value: *** - (0.–0.001), ** - [0.001 – 0.01), * - [0.01 – 0.05), . - [0.05 – 0.1), - - [0.1 – 1.0).

Conclusion The present paper demonstrates that there is a strong relation between the length of the sliding window in the local version of ADFA and the asymmetric effect in the RR-intervals time series. For the shortest windows the effect is absent, and for a wide range of lengths it is very clear and significant. The physiological and mathematical significance of both the existence of the $\alpha^- > \alpha^+$ effect require further study.

References

- Ramirez J.A., Rodrigues E., Echeverria J.C 2009 *Physica A* **388** 22632270;
 Rivera-Castroa M.A., Mirandaa J.G.V., Cajueirob D.O., Andradea R.F.S 2012 *Physica A* **391** 170179;
 Peng C.K., Havlin S., Stanley H.E., Goldberger A.L. 1995 *Chaos* **5** 82-87;
<https://github.com/kosmo76/adfa>;
 Mieszkowski D., Kośmider M., Krauze T. Guzik P., Piskorski J. *J. App. Math. and Comp. Mech.* in print

Quantification of Noise in the Electrocardiogram

Jan F. Kraemer and Niels Wessel

Humboldt-Universität zu Berlin, Institut für Physik, Berlin, Germany

All endeavors working with computational cardiology, from trying to understand the relationship between respiration and the cardiovascular system through the cardiogram, to expanding the capabilities of prognosis for significant events in a hospital setting, share the problem of not only having to provide results, but making sure that the provided input data is of sufficient quality that the results can be trusted.

In a research setting this can be easily achieved through manual examination. "I know it when I see it," is an easy rule to follow, but hinders repeatability through the inclusion of unquantifiable subjective measures and is inherently unscalable. The following will describe an approach to create a specific measure of electrocardiogram (ECG) quality usable to select high-quality stretches of sinus rhythm in ECG signals.

The quality measure is produced from an noise color-corrected signal-to-noise ratio (SNR) derived from a measured ECG signal. We estimate a noise signal in two stages: first baseline wander and power-line interference is estimated, after which the self-similarity of the manifestations of the heart beat is used to segregate noise and signal from the filtered ECG upon which a QRS-detector has been run. The power of noise and signal is calculated and combined to a signal-to-noise ratio, which is then adjusted to account for the varying degrees of influence different colors of noise have on the quality of feature detection in ECG signals.

Powerline interference is the result of the power distribution system acting as a transmitter and inducing a signal on the ECG-cables acting as antenna. This source of noise can drastically reduced through the simple use of a notch filter around the local, to the location of measurement, frequency of the power system, mostly either 16.6, 50 or 60 *Hz*. Baseline wander results from varying influences such as static charges resulting from friction during movement or changes of the relative distance between electrodes and the heart due to body position. It can be estimated through a low-pass filter, but in our work an implementation based on the work of de Chazal et al. [*deChazal2004*] works very well if slowly, due to the involvement of a median-filter.

These preparatory steps produce a signal that, while not noise-free, is acceptable to most QRS detection algorithms, in our case an implementation of work by Benitez [*Benitez2001*]. The resulting indices of QRS complexes are most probably, in all but toy examples, incomplete and contains false positives. Since we mostly do not need the full time of the recording but a limited segment, for example 5 min for heart-rate-variability (HRV) analysis, it is sufficient to select a continuous segment of the desired length where we minimize the risk for misclassification and noise induced detection inaccuracies.

This can be achieved by using the principle component analysis (PCA) method on segments of the ECG, aligned on the QRS complex, to separate highly self-similar parts of the signal from the non-correlated noise as described by [Moody1989, Clifford2006]. Using 300 beats per PCA operation, windowed so that only the middle 100 beats are used for the noise reconstruction (from all but the first 5 eigenvalues) performs well with regard to adaptation to morphological changes in the ECG signal, while still providing good separation from misclassified beats. Reconstruction into a single estimated noise signal is performed by realigning the segments and, where overlap exists, fading between segments according to a sigmoidal cosine based function. Areas where no QRS complex was detected are classified as wholly consisting of noise.

Calculating the continuous-time power of the signal (i.e. the original) and the noise through short-time Fourier transform (STFFT) we can calculate a signal-to-noise ratio with a lower limit of 1, since in segments where no beat was detected the segments of signal and noise are equal. ECG feature detection is less precise in the presence of high-frequency noise [?], which we acknowledge by introducing a color-corrected signal-to-noise (ccSNR) ratio. Using the noise color quantification β , the linear slope of a log-log regression of the noise Fast-Fourier-Transform (FFT), we define identity of SNR and ccSNR at $\beta = 1$. Noise with a $\beta < 0.25$ will receive a multiplier of 0.2, while noise with $\beta > 1.75$ is multiplied by 5. In our work, selecting a segment with a continuous ccSNR > 7 has proven to provide a high certainty of error-free QRS detection and ability to detect further ECG features and use the resulting data to provide high quality analysis.

In our contribution we will show further details and applications of this method, used to provide reliable source data for the estimation of respiration frequency and power, calculation of coordigramms on the basis of ECG-derived respiration and creating repeatable methods for statistical analysis of large ECG derived datasets.

References

- Benitez D, Gaydecki PA, Zaidi A, Fitzpatrick AP, 2001, The use of the Hilbert Transform in ECG Signal Analysis, *Computers in Biology and Medicine* **31** 399–406
- de Chazal P, Penzel T, Heneghan C, 2004, Automated Detection of Obstructive Sleep Apnoea at Different Time Scales using the Electrocardiogram, *Physiological Measurement*, **25**, 967–983
- Clifford GD, Azuaje F, McSharry P, 2006, Advanced Methods and Tools for ECG Data Analysis, *Artech House Inc.*
- Moody GB, Mark RG, 1989, QRS Morphology Representation and Noise Estimation using the Karhunen-Loeve Transform, *Computers in Cardiology*, **1989**, 269–272

Ensemble Symbolic Coupling Traces during Sleep

A Müller 1, M Riedl 1, JF Kraemer 1, T Penzel 2, J Kurths 1, N Wessel 1

1 Institut für Physik, Kardiovaskuläre Physik, Humboldt-Universität zu Berlin

2 Interdisziplinäres Schlafmedizinisches Zentrum, Charité Berlin

wessel@physik.hu-berlin.de

The analysis of different events like apneas, hypopneas and various types of arousals during sleep plays a central role when diagnosing and trying to understand sleep related disorders and possible secondary diseases. Often, only the occurrence of such events is regarded instead of putting them into context with other cardiovascular variables and characterizing their mutual interactions.

In this paper, we present a new method of cardiorespiratory coupling analysis: The ensemble symbolic coupling traces. It is applied to a case study of a subject with frequent arousals as well as to nocturnal measurements of 27 males suffering from obstructive sleep apnea syndrome.

By means of the case study the possibilities of the new tools are shown in order to quantify the autonomous reaction on sleep disturbances: The effects originating in the vagal feedback (diametric $\tau = -2$), the Frank-Starling mechanism (symmetric $\tau = -1$), and in the mechanical influence of the respiratory movements ($\tau = 0$) are clearly significant ($p < 0.05$). With the beginning of the arousals the heart rate increases at first, followed by an increase in the blood pressure (diametric effect). About five heart beats later the heart rate goes down again while the blood pressure is still rising (symmetric effect).

The ensemble symbolic coupling analysis offer an effective, easily applicable method to understand a systems reaction to very short but notable events.

Equivalent couplings in pairs of bidirectionally coupled asymmetric dynamics

Petroula Laiou and Ralph G. Andrzejak

Universitat Pompeu Fabra, Department of Information and Communication Technologies , Barcelona, Spain

The characterization of interdependence among interacting dynamics is an important aspect to understand the topology of complex networks. The elementary components of these networks are pairs of coupled dynamics. Therefore, for the understanding of network structure it is important to analyze pairs of coupled dynamics X and Y . An open problem is the assessment of bidirectional couplings when the coupled dynamics are non-identical. Is it possible to define a symmetric interaction in such cases? To study this question, we use a data-driven approach and analyze signals from interacting dynamics. We use the directional measure L (Chicharro and Andrzejak 2009) to detect the interdependence between the coupled dynamics. This measure belongs to the category of the state space measures and quantifies the degree to which spatial close neighbors of one dynamics are mapped to spatial close neighbors of the other dynamics. The measure was designed to estimate the overall coupling strength and predominant direction of the coupling. The aim of our study is not to evaluate the accuracy of the measure L , but to use it as a tool in order to detect symmetric interactions among bidirectionally coupled dynamics. Our results show that in pairs of identical dynamics, equal estimates of interdependence in both directions, as judged by L are indeed obtained when the coupling strength from X to Y is the same as the one from Y to X . However, in pairs of non-identical dynamics, equal estimates of interdependence in both directions, are obtained for asymmetrical values of the coupling strength. The stronger the asymmetry in the dynamics, the stronger is this effect. To address this problem we propose the notion of coupling impact. For this purpose, we estimate the energy of the individual dynamics from the variance of the signals of X and Y . The coupling impact is then straightforwardly determined by normalizing the coupling strength with the variance. Our results show that the measure L estimates the interdependence to be the same in both directions when the values of coupling impact (from X to Y versus Y to X) are approximately equal. This holds for both identical and non-identical pairs of dynamics. The remaining deviations are always smaller than the ones found in the non-normalized, original values of the coupling strength. We conclude that the coupling impact can help to better assess the real influence between the interacting dynamics. Accordingly, a potential criterion in the evaluation of a newly developed directional measure for interdependence is whether equal values of interdependence in both directions are obtained when the values of coupling impact (from X to Y

versus Y to X) are equal. We should note that the notion of coupling impact is best suited to study model systems. In contrast to such systems with controlled conditions, in real-world data we do not know in general the values of the coupling strength connecting the dynamics underlying the signals. The measure L , however, was already applied successfully to experimental data. It was applied to EEG recordings from epilepsy patients and it was shown that it is able to localize the epileptic focus (Andrzejak et al. 2011] as well as to assess the nonlinear interdependence in the brain (Andrzejak et al.2012).

References

- Chicharro D.,Andrzejak R.G., 2009, *Phys. Rev.E*, **80**, 026217
Andrzejak, R. G., Chicharro, D., Lehnertz, K. and Mormann, F., 2011, *Phys. Rev.E*, **83**, 046203
Andrzejak, Ralph G., Schindler, Kaspar and Rummel, Christian, 2012, *Phys. Rev.E*, **86**, 046206

Wavelet-based coherence analysis of cerebral tissue oxyhemoglobin and arterial blood pressure signals in healthy subjects during a vigilance task

Manyu Zhang, Qitao Tan, Bitian Wang, Liwei Xu, Wei Wang, Zengyong Li*
*Key Laboratory of High Efficiency and Clean Mechanical Manufacture, School of
Mechanical Engineering, Shandong University, Jinan, 250061 P.R. China*

*Corresponding authors: zyongli@sdu.edu.cn

Introduction

Spontaneous oscillations are generally found in the spectral analysis of changes in Delta [O₂Hb] signals measured using near-infrared spectroscopy (NIRS) as well as in arterial blood pressure (ABP) signals (Cui et al., 2014, Rowley et al., 2007). The bivariate relationship between the spontaneous oscillations in ABP and Delta [HbO₂] can be used to assess the state of cerebral autoregulation (CA) (van Beek et al., 2012). CA is considered to be the cooperative action of both sympathetically mediated and local myogenic or metabolic mechanisms (Rowley et al., 2007). Wavelet coherence (WCO) identifies high common power, and wavelet phase coherence (WPCO) finds locally phase-locked behavior (Bandrivskyy et al 2004; Sheppard et al 2011). In this study, the WCO and WPCO were used to assess the CA in various frequency bands during a vigilance task. This study aims to explore the physiological mechanism of the influence of the mental load on the CA.

Subjects and methods

A total of 20 healthy adults were recruited from Shandong University to participate in this study. All participants were right-handed and had normal or corrected vision. The experiment studies were performed in a quiet room. The participant consisted of 10 min of resting state (sitting in a chair) followed by a 20 min of task state (performing a vigilance task). A vigilance task was designed to simulate mental load in real car driving. The participant was asked to press the foot pedal when three different odd appeared on the screen during a vigilance task. Data for the Delta [O₂Hb] and ABP signals were recorded simultaneously during each session. The continuous ABP waveform was monitored by a transducer attached to the wrist and using an ABP analysis system (FDP-1, Shanghai Science Teaching Co., China) at a sampling of 1000 Hz. The Delta [O₂Hb] signals in the left and right prefrontal cortex (PFC) areas of the subjects were recorded with a cerebral tissue saturation monitor (TSAH-200, developed by Tsinghua University, China). Additionally, the Delta [O₂Hb] signals were obtained from the left and right motor areas with 4 channels bilaterally in subjects using Oxymon (developed by the Netherlands) at a sampling of 10 Hz. The four detectors and four sources were plugged into the optode holders and arranged into a 2×2 array bilaterally to cover the left and right motor areas by referring to the international 10–20 electrode system. The wavelet coherence (WCO) and wavelet phase coherence (WPCO) of Delta [O₂Hb] and ABP signals were analyzed in the four frequency intervals (I, 0.6-2 Hz; II, 0.15-0.6 Hz; III, 0.05-0.15 Hz; IV, 0.02-0.05 Hz).

Results and discussion

In this study, the WCO in intervals I and II in the PFC, and in interval III in both the PFC and the sensorimotor areas exhibited significantly lower level in task state than in resting state ($p < 0.01$). Also, the WPCO in interval III was significantly lower in the PFC in task state than

in resting state ($p < 0.05$). The lower WCO and WPCO values indicated reduced synchronization in amplitude and phase between the Delta [O₂Hb] and ABP signals. The reduced synchronization in interval III indicates an enhanced CA in the vigilance task state. This enhancement might reflect a spontaneous physiology response of CA to mental stress. This study provides new insight into the fundamental mechanisms of CA and may be useful to assess the brain function.

References

- Bandrivskyy A, Bernjak A, McClintock P, Stefanovska A 2004 Wavelet Phase Coherence Analysis: Application to Skin Temperature and Blood Flow Cardiovascular Engineering: An International Journal. 4(1): 89-93
- Cui R, Zhang M, Li Z, Xin Q, Lu L, Zhou W, Han Q, Gao Y 2014 Wavelet coherence analysis of spontaneous oscillations in cerebral tissue oxyhemoglobin concentrations and arterial blood pressure in elderly subjects Microvascular Research 93:14–20
- Rowley AB, Payne SJ, Tachtsidis I, Ebdon MJ, Whiteley JP, Gavaghan DJ, Delpy DT 2007 Synchronization between arterial blood pressure and cerebral oxyhaemoglobin concentration investigated by wavelet cross-correlation. Physiological measurement, 28(2), 161.
- Sheppard LW, Vuksanovic V, McClintock PVE, Stefanovska A 2011 Oscillatory dynamics of vasoconstriction and vasodilation identified by time-localized phase coherence, Phys. Med. Biol. 56: 3583–3601.
- van Beek AH, Lagro J, Olde-Rikkert MG, Zhang R, Claassen JA (2012). Oscillations in cerebral blood flow and cortical oxygenation in Alzheimer's disease. Neurobiology of aging, 33(2), 428-e21.

Acknowledgements

This study was sponsored by National Natural Science Foundation of China (Grant No. 31371002, 81071223).

Functional connectivity revealed by wavelet-based coherence analysis of near-infrared spectroscopy signals in healthy subjects during vigilance task

Wei Wang, Bitan Wang, Liwei Xu, **Zengyong Li***

Key Laboratory of High Efficiency and Clean Mechanical Manufacture, School of Mechanical Engineering, Shandong University, Jinan, 250061 P.R. China

**Corresponding authors: zyongli@sdu.edu.cn*

Introduction

The mechanism behind performance decline in attention-related task is still far comprehensive. Functional connectivity (FC) is characterized by a strong correlations among spontaneous fluctuations of distinct regions of the brain in the low frequency range (<0.1 Hz) (Biswal et al 1995), which has been well reproduced in many studies using functional magnetic resonance imaging (fMRI) (Damoiseaux et al 2006; Fox and Raichle 2007) and near-infrared spectroscopy (NIRS) (White et al 2009; Zhang et al 2010). NIRS is a non-invasive neuroimaging technique for recording brain activity. Wavelet coherence (WCO) identifies high common power, and wavelet phase coherence (WPCO) finds locally phase-locked behavior (Bandrivskyy et al 2004; Sheppard et al 2011). In this study, it was hypothesized that the FC would change in various frequency bands in the vigilance task. The objective of this study was to evaluate the FC using wavelet-based coherence analysis of NIRS signals during an attention-related task.

Subjects and methods

Twenty young healthy subjects (24.9 ± 3.3 years) were recruited from Shandong University to participate in this study. Continuous recordings of NIRS signals were obtained from the prefrontal cortex (PFC) and sensorimotor cortical areas during 20-min resting state and 20-min vigilance task state. The WCO and WPCO of six channel pairs were calculated in five frequency intervals: I, 0.6–2 Hz; II, 0.145–0.6 Hz; III, 0.052–0.145 Hz; IV, 0.021–0.052 Hz; V, 0.0095–0.021 Hz.

Results and discussion

The results show that the WCO in interval III exhibits significant lower level during task than in at rest in the four channel pairs, including the left prefrontal region, left sensorimotor area, left prefrontal regions and the right sensorimotor areas ($p < 0.05$). The WPCO in frequency interval I was significantly lower in attention state than in resting state ($p < 0.01$). Also, the WPCO in interval II was significant lower in task than in resting state between the right prefrontal region and the right sensorimotor area ($p < 0.05$). However, the WPCO level in interval V was a little higher in attention state than in resting state between the left prefrontal regions and the left sensorimotor area. Our findings suggest that the vigilance task induced lower connectivity level in interval I and III between the prefrontal and sensorimotor areas. This study provides us a new insight on the mechanism of performance decline in attention-related task.

References

Bandrivskyy A, Bernjak A, McClintock P, Stefanovska A 2004 Wavelet Phase Coherence Analysis: Application to Skin Temperature and Blood Flow Cardiovascular Engineering: An International Journal. 4(1): 89-93

- Fox MD, Raichle ME 2007. Spontaneous fluctuations in brain activity observed with functional magnetic resonance imaging. *Nat. Rev. Neurosci.* 8: 700–711.
- Sheppard LW, Vuksanovic V, McClintock PVE, Stefanovska A 2011 Oscillatory dynamics of vasoconstriction and vasodilation identified by time-localized phase coherence, *Phys. Med. Biol.* 56: 3583–3601.
- White BR, Snyder AZ, Cohen AL, Petersen SE, Raichle ME, Schlaggar BL, Culver JP, 2009. Resting-state functional connectivity in the human brain revealed with diffuse optical tomography. *Neuroimage* 47:148–156.
- Zhang H, Zhang Y, Lu C, Ma S, Zang Y, Zhu C 2010. Functional connectivity as revealed by independent component analysis of resting-state fNIRS measurements. *Neuroimage* 51: 1150–1161.

Acknowledgements

This study was sponsored by National Natural Science Foundation of China (Grant No. 31371002, 81071223).

Coupling effects in mouse and human β -cells networks: emergent dynamics

Alessandro Loppini¹, Morten Gram Pedersen² and Simonetta Filippi¹

¹*Nonlinear Physics and Mathematical Modeling Laboratory, Campus Bio-Medico University of Rome, I-00128, Rome, Italy*

²*Department of Information Engineering, University of Padua, I-35131, Padua, Italy*

β -cells in the endocrine pancreas are a typical example of coupled biological oscillators. Gap junction connections, in particular, form complex cellular networks which coordinate and release insulin [1-2]. Pathological conditions, such as diabetes, affect β -cells architecture resulting in different emerging behaviour [3].

In the present work, we analyse the emergent dynamics of different β -cell architectures in terms of bursting oscillations robustness and synchronisation properties. A compact cubic cluster, mimicking the compact arrangement of β -cells in mouse islets, is analysed in comparison with a sparse cluster obtained from a site-bond percolation performed on a compact architecture. A linear arrangement of cells is also studied to analyse a degenerate case of cellular connectivity.

The electrophysiological behaviour of β -cells is reproduced via a generalised stochastic model fine-tuned on mouse data [4]. Synchronisation phenomena are analysed with the use of functional networks tools based on the correlation indices of cells electrical activity.

We show that compact clusters induce strongly synchronised and robust electrical activities not observed in linear chain configurations. In addition, percolated clusters resembling human pancreatic architectures show a limited synchronisation and out-of-phase bursting oscillations. In this case, functional networks are characterised by scale-free properties and modularity. Our observations are in line with experimental studies performed on mouse and human islets, showing a global and a limited synchronised cells activity, respectively [5]. Moreover, functional connectivity based on calcium imaging data shows optimal cell synchronisation at proper glucose conditions [6].

We complete the work quantifying the gap junction coupling conductance between human β -cells. In this case, a mathematical model fine-tuned on human electrophysiology is considered [7]. We show that synchronisation in the electrical activity can be obtained in small heterogeneous β -cell clusters, further affecting fast bursting oscillations. Specifically, an enhancement of the bursting oscillation period can be

observed in the estimated range of junctional conductance, in line with published results obtained on mouse electrophysiological models. The coupling also affects the slow bursting patterns driven by heterogeneous glycolytic oscillators. In this case, in agreement with human data, glycolytic oscillations are not able to synchronise causing a fragmentation of the action potential. When the metabolic coupling is also considered, regular emergent oscillations arise underlying that emergent electrical activities can be significantly altered by gap junction coupling [8].

References

- [1] Salomon D, Meda P 1986 *Experimental Cell Research* **162** 507-520.
- [2] Jonkers FC, Henquin JC 2001 *Diabetes* **50** 540-550.
- [3] Ravier MA, Güldenagel M, Charollais A, Gjinovci A, Caille D, Söhl G, Wollheim CB, Willecke K, Henquin JC, Meda P 2005 *Diabetes* **54** 1798-1807.
- [4] Portuesi R, Cherubini C, Gizzi A, Buzzetti R, Pozzilli P, Filippi S 2013 *Diabetes/metabolism research and reviews* **29** 194-203.
- [5] Cabrera O, Berman DM, Kenyon NS, Ricordi C, Berggren PO, Caicedo A 2006 *PNAS* **103** 2334-2339.
- [6] Cherubini C, Filippi S, Gizzi A, Loppini A 2015 *Physical Review E* **92** 042702.
- [7] Riz M, Braun M, Pedersen MG 2014 *PLoS Computational Biology* **10** e1003389.
- [8] Loppini A, Braun M, Filippi S, Pedersen MG 2015 *Physical Biology* **12** 066002.

Why we need nonautonomous models and methods

Lucas Maxime and Stefanovska Aneta

Lancaster University, Physics Department, Lancaster, UK

Introduction

From the respiration to cells membrane potential or circadian rhythms, oscillations are ubiquitous in living systems [1]. Moreover, living systems need to interact with their environments – e.g. energy and matter are continuously supplied to the heart – and continuously adapt that interaction – more supply is needed for the heart to pump faster in case of danger. In other words, living systems are open and nonautonomous [2]. Nonautonomicity can arise from an explicit dependence on time of the dynamics of the system or from the unidirectional influence of an other (external) dynamical system [4].

Traditionally, oscillations in living systems are modelled either by an autonomous limit-cycle [1] or a stochastic model [3]. Whilst the latter does not allow the existence of a time-varying attractor on the limit-cycle, the former does not provide much insight about the internal structure and dynamics of the system at hand.

This is why the theory of chronotaxic systems was proposed in 2013 [2]: a deterministic but nonautonomous description of oscillations that exhibit stable amplitude and stable phase dynamics. The mathematical theory of nonautonomous dynamical systems has been developed in the last decades (see for example [4]). However, nonautonomous models are still rare outside the mathematical community. We show why we need nonautonomous models and why reducing them to autonomous ones is not satisfactory.

Problem statement

One may argue that, mathematically, any nonautonomous system of dimension n evolving in state space $\mathcal{M} \subseteq \mathbb{R}^n$

$$\begin{aligned}\dot{x}_1(t) &= f(x_1, \dots, x_n, t) \\ \dot{x}_2(t) &= f(x_1, \dots, x_n, t) \\ &\vdots \\ \dot{x}_n(t) &= f(x_1, \dots, x_n, t)\end{aligned}$$

can be turned into an autonomous one by adding an extra dimension $x_{n+1} = t$ and its corresponding differential equation $\dot{x}_{n+1}(t) = 1$, the whole system now living in the extended state space $\mathcal{M} \times \mathbb{R} \subseteq \mathbb{R}^{n+1}$. This is the approach suggested in [5] for example.

Results

We will show that while the previous argument holds, it is not of much use. Hence, we stress the importance of a truly nonautonomous description of living systems. In [4], Rasmussen and Kloeden briefly state that such an extended $n + 1$ -dimensional system has no equilibrium points and no bounded solutions in the extended state space; and that it is sufficient to move away from the extended state space approach. Indeed, from the extended set of $n + 1$ ODEs, one sees that the $n + 1$ th equation prevents the extended system to have a fixed point. Furthermore, solutions of the extended system are unbounded in general since x_{n+1} is unbounded. However, we add that, if the nonautonomous component of the system is periodic, periodic solutions are possible as in synchronisation by external forcing phenomena.

We aim at using a minimalist theoretical model to show theoretically, graphically and conceptually why the approach of the extended state space is not useful. Possible models include simple models that exhibit properties that do not exist in autonomous systems. For example, a toy pullback attractor as $\dot{x} = 2xt$, and a simple model for a time-evolving fixed point. Those systems involve finite-time attractivity. Finally, we will discuss the analysis of cardiac activity data, and compare an autonomous and nonautonomous approach for that analysis.

References

- [1] Albert Goldbeter *Biochemical oscillations and cellular rhythms*. Cambridge University Press, Cambridge, 1997.
- [2] Yevhen F. Suprunenko, Philip T. Clemson, and Aneta Stefanovska. *Phys. Rev. Lett.*, 111(2):024101, 2013.
- [3] Didier Gonze, José Halloy, and Albert Goldbeter. *Int. J. Quant. Chem.*, 98(2):228–238, 2004.
- [4] Peter E. Kloeden and Martin Rasmussen. *Nonautonomous dynamical systems*. Amer. Math. Soc., Providence, 2011.
- [5] Steven H. Strogatz. *Nonlinear dynamics and chaos: with applications to physics, biology, chemistry, and engineering*. Westview Press, Boulder, 2nd edition, 2014.

Detecting couplings between spike trains with noise

Irene Malvestio and Ralph G. Andrzejak

Universitat Pompeu Fabra, Department of Information and Communication Technologies, Barcelona, Spain

We study the method for detecting directional couplings between point processes, developed by Andrzejak and Kreuz (2011). This method is derived from a state space approach (Chicharro and Andrzejak (2009)) based on the principle of asymmetric state similarity conditioning. It uses the nonlinear interdependence measure L and a spike train distance. The midterm goal of our work is to determine if the coupling detection method is suitable for application to neuronal data. We present here the first stage in which we analyze exclusively signals from models generated under controlled conditions. In particular, we analyze spike trains derived from coupled Hindmarsh-Rose model neurons. We study the degree to which the coupling between the model neurons can be detected under noisy conditions. The noise types include measurement noise such as random removal and/or addition of spikes, or dynamical noise, caused by random terms in the equations used to generate the neurons dynamics. We apply different noise levels and define the performance of the measure in detecting the coupling and its direction. We compare the results obtained with two spike distances, the so-called ISI and SPIKE distance (Kreuz et al. (2007)). Our results indicate that the performance decreases gradually with the noise level for all types of noise, showing the robustness of this method. Furthermore, we find that ISI-distance performs better than the SPIKE. We conclude that this method is suited to study real data, which will be the next step in our studies.

References

- Andrzejak R. G., Kreuz T. 2011 *EPL* **96** 50012.
Chicharro D. and Andrzejak R. G. 2009 *Phys. Rev. E*, **80** 026217.
Kreuz T., et al. 2007 *Journal of neuroscience methods* **165** 151-161.

Quantification of the degree of association between left and right muscle sympathetic nerve activity variability in healthy subjects

Andrea Marchi^{1,2}, Vlasta Bari³, Beatrice De Maria^{1,4}, Giacomo Bellani^{2,5},
Antonio Pesenti^{2,5}, Franca Barbic⁶, André Diedrich⁷,
Raffaello Furlan⁶ and Alberto Porta^{3,8}

¹ Politecnico di Milano, Department of Electronics Information and Bioengineering, Milan, Italy

² Department of Anesthesia and Intensive Care, San Gerardo Hospital, Monza, Italy

³ University of Milan, Department of Biomedical Sciences for Health, Milan, Italy

⁴ IRCCS Fondazione Salvatore Maugeri, Milan, Italy

⁵ Department of Health Science, University of Milan-Bicocca, Monza, Italy

⁶ Internal Medicine, Humanitas Research Center, Humanitas University, Rozzano, Italy

⁷ Autonomic Dysfunction Center, Division of Clinical Pharmacology, Departments of Medicine,
Vanderbilt University, Nashville, Tennessee, USA

⁸ IRCCS Policlinico San Donato, Department of Cardiothoracic, Vascular Anesthesia and Intensive
Care, Milan, Italy

Introduction

The sympathetic neural control of the cardiovascular system is influenced by cortical hemisphere laterality [1]. The potential dissimilarity between neural efferent sympathetic activities can be addressed by recording simultaneously muscle sympathetic nerve activity (MSNA) from both left and right peroneal nerves in humans. Previous studies found similar burst rate in left MSNA (lMSNA) and right MSNA (rMSNA) [2,3], while the presence of right lateralization was identified by using normalized burst amplitude and area [4]. The aim of the study was to assess the degree of association between lMSNA and rMSNA variability as a function of the frequency. Therefore, in addition to traditional MSNA analysis over lMSNA and rMSNA recordings, we computed the squared coherence function between lMSNA and rMSNA variability (K^2). Analysis was carried out at rest in supine position during spontaneous breathing (SB) and control breathing (CB). The significance of the detected coupling was tested via a surrogate approach [5].

Experimental Protocol and Data Analysis

We studied 10 right-handed volunteers (age: 33 ± 9 years, 5 women) without evidence of disease. Raw MSNA was recorded from the peroneal nerve of the right and left leg simultaneously. The raw MSNA was band-pass filtered, amplified, rectified and integrated to obtain traditional integrated MSNA signals [4,6]. Integrated MSNA [4,6] was sampled at 300 Hz. The experimental sessions consisted of two periods of 15 minutes during SB and CB at 15 breaths/minute. The study was performed according to the Declaration of Helsinki and was approved by the Vanderbilt University Institutional Review Board. Written informed consent was provided by all subjects. From the integrated MSNA signal we computed traditional parameters such as burst frequency (bf), burst incidence (bi), burst amplitude (ba) and burst area (ba^2). MSNA variability series was obtained from the integrated MSNA signal by counting the number of MSNA bursts inside a moving time window of 5 s and by dividing the count by the length of the time window, thus obtaining a time series expressed in burst/s [9]. Subsequently, the MSNA variability series was obtained by low-pass filtering the count signal with a cut-off frequency of 0.5 Hz and down-sampling the resulting signal once per cardiac beat [9]. Mean (μ) and variance (σ^2) of MSNA variability were computed. Autoregressive spectral analysis provided an estimate of the power in the low frequency band (LF, from 0.04 to 0.15 Hz). K^2 was computed via a bivariate autoregressive approach [5] and averaged in LF and high frequency (HF, from 0.15 to 0.5 Hz) bands to obtain $K^2(\text{LF})$ and $K^2(\text{HF})$ respectively. The computation of the threshold to test the hypothesis of lMSNA-

Table 1. Traditional parameters from IMSNA and rMSNA signals and their variabilities.

| Indexes | SB | | CB | |
|---|---------------|---------------|---------------|---------------|
| | rMSNA | IMSNA | rMSNA | IMSNA |
| bf [bursts/min] | 19.7 ± 6.7 | 20.9 ± 6.2 | 20.8 ± 5.6 | 21.1 ± 6.1 |
| bi [bursts/100 beats] | 28.9 ± 7.1 | 30.8 ± 6.4 | 28.7 ± 6.2 | 29.1 ± 5.9 |
| ba [a.u.] | 72.4 ± 43.2 | 51.9 ± 22.5 | 65.4 ± 41.3 | 48.5 ± 19.0 |
| ba ² [a.u. ²] | 21.2 ± 13.4 | 16.5 ± 8.6 | 21.9 ± 15.8 | 16.3 ± 7.6 |
| μ [bursts/s] | 0.32 ± 0.11 | 0.34 ± 0.10 | 0.34 ± 0.10 | 0.34 ± 0.10 |
| σ ² [bursts ² /s ²] | 0.039 ± 0.013 | 0.037 ± 0.010 | 0.033 ± 0.012 | 0.037 ± 0.008 |
| LFa [bursts ² /s ²] | 0.025 ± 0.015 | 0.023 ± 0.007 | 0.022 ± 0.011 | 0.023 ± 0.011 |

bf = burst frequency; bi = burst incidence; ba = burst amplitude; ba² = burst area; μ = mean of the MSNA variability; σ² = variance of the MSNA variability; LFa = low frequency power of the MSNA variability expressed in absolute units; SB = resting in supine position during spontaneous breathing; CB = resting in supine position during control breathing; a.u. = arbitrary units. Values are expressed as mean±standard deviation. The symbol * indicates $p < 0.05$ vs. SB.

rMSNA coupling was based on the construction of a set of 100 uncoupled isospectral isodistributed surrogates via iteratively-refined amplitude-adjusted Fourier transform method [7]. $K^2(\text{LF})$ and $K^2(\text{HF})$ were deemed as significant if they were larger than the 95th percentile of the $K^2(\text{LF})$ and $K^2(\text{HF})$ distribution computed over the uncoupled surrogates respectively [5,8]. Two way repeated measures analysis of variance (one factor repetition, Holm-Sidak test for multiple comparisons) was applied to check differences between sides and conditions. A $p < 0.05$ was deemed as significant.

Results

None of the traditional parameters (Tab.1) showed significant differences in relation to sides or conditions. During SB a significant IMSNA-rMSNA coupling was identified in 80% and 100% of the subjects in LF and HF bands respectively, while these percentages decreased to 60% during CB in both bands.

Discussion and Conclusions

Since no difference between traditional parameters was detected during both experimental sessions, we can support the hypothesis that sympathetic nerves directed to skeletal muscles projected the activity of a common central drive. Accordingly, a large percentage of subjects during SB exhibited a significant IMSNA-rMSNA coupling in both frequency bands. However, these percentages were importantly reduced during CB, thus allowing us to hypothesize the existence of a certain degree of independence between left and right sympathetic controls. Respiration seems to play a key role in governing the degree of association between IMSNA and rMSNA variabilities. The quantification of the coupling between IMSNA and rMSNA variabilities might deepen our understanding on the functioning of the sympathetic control in humans.

References

- [1] Oppenheimer SM *et al*, 1992 *Neurology* **42** 1727-1732.
- [2] Sundlof G and Wallin BG, 1977 *J Physiol* **272** 383-397.
- [3] Sverrisdottir YB *et al*, 1998 *Clin Auton Res* **8** 95-100.
- [4] Diedrich A *et al*, 2009 *Am J Physiol* **296** H1758-H1765.
- [5] Porta A *et al*, 2002 *Biol Cybern* **86** 241-251.
- [6] Furlan R *et al*, 2003 *Circulation* **108** 717-723.
- [7] Schreiber T and Schmitz A, 2000 *Physica D* **142** 346-382.
- [8] Faes L *et al*, 2004 *IEEE Trans Biomed Eng* **51**, 1156-1166.
- [9] Marchi A *et al*, 2016 *Am J Physiol Regul Integr Comp Physiol* [Article in Press].

Reaction of blood flow in microvessels on the local heating in patients with diabetes mellitus type 1

Irina Mizeva, Darya Airikh

Institute of continuous media mechanics, Perm, Russia

Microcirculation plays a significant role in the diabetic complications development, especially in diabetic neuropathy and diabetic foot syndrome. We present the results of experiments examining the human skin microcirculatory response to local heating obtained by laser Doppler flowmetry (LDF) of health subjects and patients with diabetes mellitus (DM1). One of the approach of LDF study is based on the determination of the average skin perfusion and its changes in response to physiological tests [1]. To the best of our knowledge, the issue of changing skin perfusion in response to local heating is nowadays elucidated in sufficient detail [2] and it depends on the regime of heating (rate, maximum value). The perfusion – time curve demonstrates several phases observed during the physiological test. Fast increasing of the blood flow for the first few minutes after heater turning on is associated with the axon-reflex, on prolonged heating at the same temperature, the LDF signal has a local minimum, accompanied by an increase of the perfusion, driven by another physiological mechanism – local synthesis of vasodilator agent NO).

The study was carried out on the control group of 12 healthy nonsmoking volunteers (*CG*) and 8 subjects with DM1 without vascular complications (*DM*). The diagnosis of DM1 was clinically identified, the duration of the disease was longer than 5 years. Subjects were caffeine free for 12 hours before start of the test and were for 15 minutes under comfort laboratory conditions. For the analysis of blood flow changes in the skin area exposed to heating, a two-channel laser Doppler flow meter (Moor Instruments, UK) was used. A skin heater unit (heat control accuracy $\pm 1^\circ\text{C}$) was mounted on the volar site of the forearm of the left hand of each volunteer using a double sided adhesive disk. A laser Doppler flowmeter sensor was installed into the heater through the hole. Measurements of temperature and LDF were recorded continuously. During the first 10 minutes the heating element was turned off, and recordings of the basal blood flow were made. In the eleventh minute the heating element was turned on (heating to 40°C during 1 minute was performed gradually - 1°C per 15 seconds). Then at the temperature of 40°C the perfusion parameters were recorded during 40 minutes. 50 minutes after the start of the experiment the heating element was turned off, and the cooling phase was recorded during 15 minutes. For the statistical analysis we apply moving average procedure to data with the scale of averaging 5 s. After this procedure we obtain smooth curve for LDF, and find maximum value of LDF in the phase of axon-reflex and mean value during plateau phase. Mann-Whitney test was used to compare intergroup results.

The baseline perfusion was (9.5 ± 0.75) p.u. for *CG* and 7.5 ± 1.4 for the *DM*, the difference is not statistically meaningful ($p=0.3$). The mean value of maximum perfusion during the first phase of vasodilation for the *CG* is (190 ± 90) p.u. and for *DM* is (110 ± 50) p.u. The increase of the blood flow due to axon-reflex is lower in the *DM* but the difference is not significant ($p=0.06$). The mean value of blood flow caused by NO dependent vasodilation for *CG* (250 ± 100) p.u. is much higher than *DM* (140 ± 70) p.u., $p=0.03$. We estimated the relative changes of the perfusion caused by axon-reflex to the baseline and perfusion during NO dependent vasodilation to the baseline and didn't find any significant difference between groups. Linear correlation analysis was provided for mean values of perfusion in the tree time intervals under consideration. We observed moderate anticorrelation of perfusion in basal conditions and in time of the axon-reflex mediated vasodilation (-0.44 for *CG* and -0.40 for *DM*) and in time of basal conditions and NO mediated vasodilation (-0.65 for *CG* and -0.46 for *DM* subjects). Correlation of perfusion during axon-peak and NO-mediated plateau was high (0.96) for both groups.

Healthy and DM1 subjects demonstrated similar two phase reaction on the local heating. Significant difference between these two groups is founded only in the second phase of vasodilation which is caused by NO synthesis. This fact indirectly proves the dysfunction of endothelium of subjects with DM1 without vascular complications. The similar results was obtained in [3], in [4] it was suggested that early impairment of low-frequency flow motion (a measure of endothelium-dependent microvascular regulation) correlates closely with the presence of sudomotor dysfunction as a manifestation of autonomic neuropathy. The study is limited by poor statistic of the groups and it will be useful to study together results of physiological tests and endothelial function markers. We plan to study contribution of microvascular tone regulation mechanisms separately using the wavelet analysis of the LDF signals [5,6,7]. (This work was supported by the Russian Science Foundation under project No 14-15-00809.)

References

1. Roustit M., Cracowski J. 2012 *Microcirculation* **16** (2012) 47-64
2. Johson M., Kellog D. 2010 *J Appl Phys.*, **109** (2010), 1229-1238
3. Khan F. , Elhadd T.A., Greene S.A., Belch J.J. 2000 *Diabetes Care* **23**, 215-20
4. Sun P., Chen C., Kuo C., Lin H., Chan R., Kao M. 2012 *Microvasc Res* **83** 2438
5. Tankanag A. and Chemeris N. 2008 *Phys. Med. Biol.* **53** 5967-5976
6. Mizeva I.A., Vetrova D.V. 2014 *Russian Journal of Biomechanics* **18** 447-454.
7. Stefanovska A. Bracic M. and Kvernmo H. 1999 *IEEE transactions on bio-medical engineering.* **46**, 1230–1239

LDF signal oscillating and average components variations caused by cold pressor test

Irina Mizeva, Peter Frick, Sergey Podtaev

Institute of continuous media mechanics, Perm, Russia

Laser Doppler flowmetry (LDF) has become an attractive technique for the intravital studies of cutaneous blood flow. It enables simple, real-time monitoring of the relative changes of red blood cell flux in cutaneous microvascular bed, which consists of nutritive capillaries and deeper elements of the skin vascular tree. LDF signals beside the average, slowly varying component, also includes an oscillating component [1], which reflects the cardiac, respiratory, neurogenic, myogenic and endothelial activities [2,3]. However, in the majority of clinical studies, the pulsations are typically smoothed by data preprocessing and only the mean blood flow is taken into consideration.

To reveal the relationship between average and oscillating components of LDF signal we studied the microvascular response to the contralateral cold pressor test (CPT) [4] on two different sides of the hand. CPT excludes a direct influence on the vessels of the hand and indirectly provides strong vasoconstriction, described for the first time by Lewis in 1930. In the study fourteen healthy volunteers were involved aged 35 ± 5 years. Data was collected continuously during 23 minutes from the right hand of a subject, sitting in the relaxed position. LDF probes (Moor instruments) were attached to the tissue pulp of index finger and to the dorsal part of the palm. The left hand was immersed on the tenth minute to the tank with ice-water mixture for three minutes. So continuous LDF signal contains record in basal conditions, under contralateral cooling and recovery of the blood flow.

By means of wavelet coefficients technique [6] we traced variations of amplitude of pulsations in four frequency bands, corresponding to cardiac, respiratory, myogenic and neurogenic activities [2]. It is obtained, that while the average perfusion always decreases during cooling, the oscillating components in all four frequency bands demonstrates a multidirectional reaction [5]. It is established that the LDF pulsatile component is nonlinearly related to the average perfusion. Under low perfusion, the amplitude of pulsation is proportional to its mean value, and this dependence the same linear law for both sides of the arm - glabrous and non glabrous skin. Such low and moderate perfusion is in the basal conditions on the dorsal part of the hand and under cooling conditions on the fingertip. As perfusion increases, the amplitude of pulsations becomes lower, oscillating component converges to zero at high perfusion. The type of reaction is defined by the initial perfusion in basal

state and the degree of vasoconstriction caused by cooling. This relation manifests itself as a positive correlation an average and pulsatile component under moderate perfusion ($< 300p.u.$) and its autocorrelation for high perfusion. Using wavelets correlation analysis, we demonstrated that the average and pulsatile components are noticeably correlated in phase under low perfusion, while it is in contraphase under high perfusion.

In the majority of measurements, the perfusion of the acral skin was high, > 300 p.u., and the low amplitude of pulsations was observed. We assume that these weak oscillations of the LDF signal are provided by the large input of capillary blood flow the LDF signal. The blood flow in the capillaries is stationary with a low oscillating component, so the oscillating component in the resulting LDF signal becomes low.

This work gives rise to a number of potential research tasks that could widen our knowledge on the functional state of microcirculation system. It would be interesting to study the dependence of average and pulsatile components for individuals, especially for subjects with abnormalities of the microvascular system.

This work was supported by the Russian Science Foundation under project No 14-15-00809.

References

1. Aalkjer C., Boedtkjer D., and Matchkov V., 2011 *Acta Physiologica* **202**, 253–269.
2. Rossi M., Carpi A., Galetta F., Franzoni F., and Santoro G., 2008 *Biomedicine and Pharmacotherapy* **62**(8), 541–545.
3. Stefanovska A., Bracic M., and Kvernmo H. D. 1999 *IEEE transactions on bio-medical engineering*. **46**, 1230–1239.
4. Isii Y., Matsukawa K., Tsuchimochi H., and Nakamoto T. 2007 *Journal of Physiological Sciences* **57**, 241–248.
5. Mizeva I., Frick P., and Podtaev S. 2015 *Engineering in Medicine and Biology Society (EMBC)*, 7382–7385.
6. Podtaev S., Stepanov R., Smirnova E., and E. Loran, 2015 *Microvascular Research* **97**(0), 109 – 114.

Design and implementation of a microfluidic chamber for synchronization studies of glycolytic oscillations in yeast cells.

Martin Mojica-Benavides, Amin A. Banaeiyan, Caroline B. Adiels and Mattias Goksör

University of Gothenburg, Physics Department , SE-41296 Gothenburg, Sweden

It has been well proven that single yeast cells can present sustained oscillations under the presence of a cyanide-glucose solution and that periodic variations of this solution entrain the oscillations causing a phase shift (Gustavsson A-K et al., 2015). Acetaldehyde (Aca) has been shown to be a possible mediator for cell-cell synchronization given its fast membrane transportation dynamics and its role in the NAD-NADH cycle during glycolysis (Bier Martin et al., 2000). Previous studies have focused on synchronization between two out-of-phase cell populations when mixed together, showing a macroscopic response. We designed a microfluidic device to observe possible entrainment on a cell-cell level, where a phase shift is triggered on single yeast cells by means of diffusion and the response of the neighboring cells can be tracked. Thorough understanding of cell-cell communication gives insight into oscillatory behaviours in biological systems, such as energy metabolism fluctuations and insulin secretion from pancreatic β -cells (Tornheim K., 1997).

Conjointly with the attenuation of the respiration process in mitochondria during glucose metabolism, it has been shown that cyanide reacts with Aca producing lactonitrile (Danø Sune et al., 2007). This reaction must have direct influence on phase shifts in the oscillations based on the Aca-cyanide concentration ratio inside and in the surroundings of the cells. In previous experiments, three and four-channel devices allowed to control flow rates of stress solutions for single cell analysis during metabolic oscillations (Gustavsson A-K et al., 2015). In this way, phase shifts were controlled by the external trigger of a cyanide-glucose solution covering a yeast cells array, affecting all of the cells at the same time and washing away the Aca secreted after each glycolytic period. This, however, limited the study of the intercellular phase relation and the control of the cyanide and secreted Aca reaction. Designing a device that circulates a flow of stress solution around an array of packed cells, by means of diffusion channels, allows cyanide to interact radially with the outer yeast cells. This enables the examination of cell-cell phase relation due to the exchange of Aca during the metabolic oscillations in a quasi static environment.

Flow velocity and diffusion of species were simulated for two devices with different geometries in order to characterize the diffusion of the stress solution and thus assure a dominant cell-to-cell interaction over the external phase triggering (see Figure 1.). The chambers were fabricated using photolithography and PDMS replica molding techniques. For the data acquisition, NADH autofluorescence allowed us to follow the oscillatory responses of the yeast cells and together with signal processing, cell-cell synchronization was evaluated. The study is currently in an optimization and experimental replication stage.

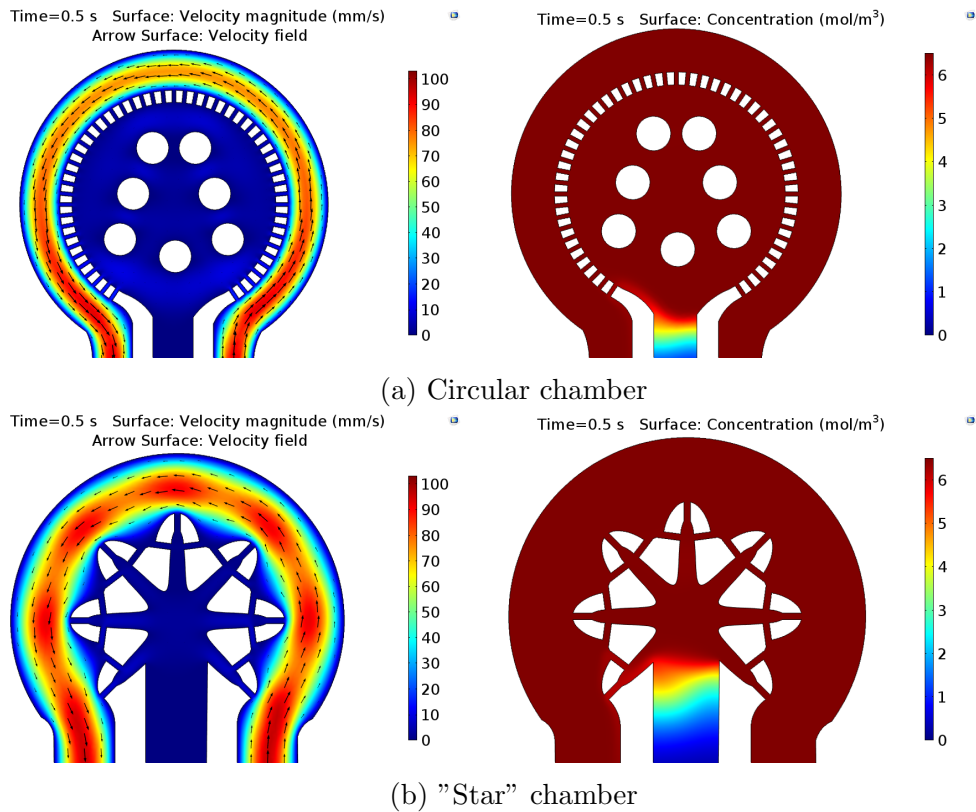


Figure 1: Flow and diffusion simulations for the a) Circular microfluidic chamber and b) "Star" shape chamber. Both of the devices were designed with 50 μm channel width and 5 μm diffusion channels with a height profile of 5 μm

References

- Bier, Martin and Bakker, Barbara M and Westerhoff, Hans V. 2000. *Biophysical Journal* **78** 1087-1093.
- Danø, Sune and Sørensen, Preben Graae and others. 2007. *Proceedings of the National Academy of Sciences* **104** 12732-12736.
- Gustavsson, Anna-Karin and Adiels, Caroline B. and Mehlig, Bernhard and Goksör, Mattias. 2015. *Scientific Reports* **5** 9404 EP.
- Tornheim, K. 1997. *Diabetes* **46** 1375-1380.

Membrane potential of a biological cell: stochastic or deterministic?

Aleksandra K. Pidge^{1, 2}, Miraslau L. Barabash¹, Shakil Patel³,
Jane Owen-Lynch³, Stephen Roberts³ and Aneta Stefanovska¹

¹Lancaster University, Physics Department, Lancaster, UK

²Universitat Pompeu Fabra, Barcelona, Spain

³Lancaster University, Division of Biomedical and Life Sciences, Lancaster, UK

Introduction

Every living cell continuously maintains its membrane potential by carefully adjusting the concentrations of potassium, sodium, chloride and other ions inside thus to avoid the osmotic pressure increase. Two basic types of transmembrane ion transport can be distinguished: passive transport-ion channels, and active transport-ion pumps. Most of widely used models do not take into account the contribution of active transport, explaining significant part of time recordings as noise. This suggests that the cell membrane voltage should be considered as stochastic rather than deterministic. We argue that traditional approach may be insufficient. The role of K^+ , Cl^- , Ca^{2+} , and ATP, in voltage behaviour and possible indications of their deterministic impact in non-excitable cells will be presented.

Methods

The Jurkat cells (human T-lymphocytes) were analysed. The cells were grouped based on the response of the resting membrane potential to the extracellular perturbations in the concentration of either K^+ , Cl^- or Na^+ . The cohorts of potassium- and chloride-sensitive cells were chosen for further analysis. Membrane voltage recordings were obtained from free-running voltage-patch clamp experiment in whole-cell mode [1]. Experiments included recordings of potential in standard bath (SB) and non-standard bath solutions (non-SB: high-potassium or low-chloride) [1]. In addition, in a group of experiments, the intracellular contents were altered by adding $1\mu M$ Ca and/or $4mM$ ATP. Each group contained at least 6 recordings and each of them lasted for 10 min maximum. Data were preprocessed by downsampling, third-order polynomial extraction, and filtering to remove irrelevant low-frequency trends [2]. Living systems indicate time-variability, therefore data were analysed in the time-frequency domain using wavelet-based techniques: power spectra, bispectra and biphases [2]. Wavelet transform, in contrast to short-time Fourier transform, gives optimal time-frequency resolution which is achieved by using an adaptive time window and logarithmic frequency scale [2]. Bispectrum arises from third-order statistics in the frequency domain. It is able to provide a measure of the coupling between two oscillations in a time series. Surrogate testing [3] included phase randomisation and random permutation in time domain. All analysis has been done for 0.01-10Hz frequency band. For statistical tests the confidence level was assumed to be 5% except where otherwise stated.

Results

K⁺-sensitive cells: Increasing external potassium depolarised membrane significantly, Tables 1, 2. Fluctuation magnitudes, measured as standard deviations, were greatly reduced in non-SB; similar observation was made for the time-averaged wavelet powers. Adding Ca^{2+} decreased voltage significantly only when ATP was already in the pipette. Similarly, adding ATP had no impact on the mean voltage, except decreasing it when Ca^{2+} was already in the pipette. Adding Ca^{2+} and/or ATP increased time-averaged wavelet power significantly (within range of interest).

Cl⁻-sensitive cells: Reducing external Cl^- elevated the voltage significantly, with the fluctuation magnitude increase at 10% level of significance. Adding ATP to intracellular solution magnified

the membrane voltage and its fluctuations. In contrast, adding Ca^{2+} altered neither voltage nor its fluctuations. Wavelet spectral analysis indicated that adding either Ca^{2+} , or ATP, or both, increased the spectral amplitudes within most frequency ranges. However, the significant increase was observed only after adding ATP in cells already containing Ca^{2+} ions.

| | SB K^+ | high K^+ | SB Cl^- | low Cl^- |
|----------------------------|---|---|---|---|
| intrapipette | $\langle V \rangle \pm \langle \sigma \rangle [mV]$ | $\langle V \rangle \pm \langle \sigma \rangle [mV]$ | $\langle V \rangle \pm \langle \sigma \rangle [mV]$ | $\langle V \rangle \pm \langle \sigma \rangle [mV]$ |
| i | -32.6 ± 1.7 | -9.22 ± 0.37 | -3.71 ± 0.96 | 14.6 ± 1.43 |
| i + Ca^{2+} | -31.1 ± 2.9 | -9.28 ± 0.71 | 0.61 ± 0.68 | 23.2 ± 1.23 |
| i + ATP | -32.3 ± 2.1 | -9.15 ± 0.51 | -6.07 ± 1.28 | 8.71 ± 2.15 |
| i + Ca^{2+} + ATP | -35.2 ± 1.5 | -13.0 ± 0.5 | -15.1 ± 1.37 | 4.84 ± 2.08 |

Table 1: Means and mean standard deviations for SB and non-SB solutions for K^+ and Cl^- , *i* stays for the basic intrapipette solution.

| | SB K^+ | high K^+ | SB Cl^- | low Cl^- |
|----------------------------|-----------------------------|-----------------------------|-----------------------------|-----------------------------|
| intrapipette | WP [$10^{-7} \times V^2$] |
| i | 2.22 | 0.108 | 1.67 | 2.35 |
| i + Ca^{2+} | 6.25 | 0.703 | 0.57 | 1.68 |
| i + ATP | 4.88 | 0.293 | 2.13 | 6.05 |
| i + Ca^{2+} + ATP | 2.43 | 0.253 | 2.23 | 5.31 |

Table 2: Time-averaged wavelet power (WP) within 0.01-10Hz frequency band for SB and non-SB solutions for K^+ and Cl^- , *i* stays for the basic intrapipette solution.

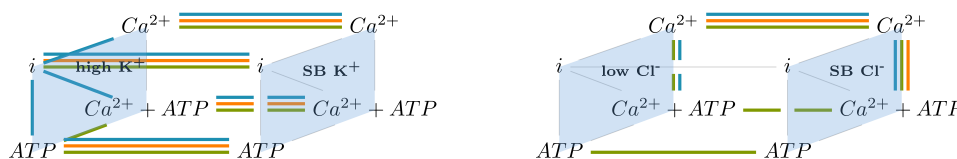


Figure 1: Diagram with significant changes in voltage, standard deviation, time-average wavelet power for SB and non-SB for K^+ and Cl^- experiments.

In addition, the wavelet analysis indicates possible low-frequency oscillations (below 0.1Hz). For some datasets wavelet bispectra and time courses of biphasic, compared with surrogates, indicated possible coupling at low frequencies.

Summary

We have investigated the impact of potassium, chloride and calcium ions, and ATP, on cellular voltage dynamics. We have shown that increasing the extracellular potassium concentration significantly depolarises the membrane and decreases the voltage fluctuations, while decreasing the extracellular chloride depolarises the membrane and increases the fluctuations. Time-frequency analysis indicates possible low-frequency dynamics. Longer recordings in combination with ion channel blocking substances could help to further elucidate the dynamics of the membrane potential and help build a new mathematical model to describe the resting state of a cell far from thermodynamic equilibrium.

References

- [1] S. Patel, *The role of membrane potential dynamics in cell behaviours: investigating the membrane potential dynamics in the Jurkat and HMEC-1 cell lines using the continuous wavelet transform*, PhD thesis, Division of Biomedical and Life Sciences, Lancaster University, 2015.
- [2] P. T. Clemson and A. Stefanovska, *Physics Reports* **542**, 297 (2014).
- [3] J. Theiler, S. Eubank, A. Longtin, B. Galdrikian, and J. D. Farmer, *Physica D: Nonlinear Phenomena* **58**, 77 (1992).

Coupled networks and networks with bimodal frequency distributions are equivalent.

Bastian Pietras, Nicolás Deschle and Andreas Daffertshofer
*Vrije Universiteit Amsterdam, MOVE Research Institute Amsterdam,
The Netherlands*

Populations of oscillators can display a variety of synchronization patterns. This depends on the coupling between oscillators and on intrinsic properties like the oscillators' natural frequency. If two symmetric (sub)populations with unimodal frequency distribution are coupled to one another, the resulting dynamics may resemble that of a single population with bimodally distributed frequencies; see, e.g., [3],[4] for related conjectures. Using an Ott-Antonsen ansatz [1], we show that both networks - the coupled version of two subpopulations and the single one with a bimodal frequency distribution - are equivalent and indeed exhibit the same properties as regards stability, dynamics, and bifurcations. To do so, we use the seminal work by Martens and co-workers [2] as a reference point, as they analyzed a network of all-to-all coupled Kuramoto oscillators, Eq.(1), whose natural frequencies followed a symmetric bimodal frequency distribution $g(\omega)$. Next we consider two separate Kuramoto networks, Eq.(2), also all-to-all coupled each of strength $K_{\text{int}} = K_{\sigma,\sigma}$, but with a unimodal frequency distribution $g_{\sigma}(\omega_{\sigma})$. Introducing also all-to-all coupling *between* the two populations $K_{\text{ext}} = K_{\sigma,\tau}$, we arrive at the same governing equations as in [2] but now with an additional bifurcation parameter, which represents the ratio of (weaker) external to (stronger) internal coupling. However, the latter does not lead to bifurcations of higher co-dimension, but leaves our system topologically equivalent to the bimodal case.

$$(1) \dot{\theta}_k = \omega_k + \frac{K}{N} \sum_{j=1}^{2N} \sin(\theta_j - \theta_k) \text{ vs. } (2) \dot{\theta}_{\sigma,k} = \omega_{\sigma,k} + \sum_{\tau=1}^2 \frac{K_{\sigma,\tau}}{N} \sum_{j=1}^N \sin(\theta_{\tau,j} - \theta_{\sigma,k}) .$$

Two variations of the subpopulation-approach will further be considered. First, we address the question whether introducing a time delay in the coupling term has an influence on the effective coupling strength between the subpopulations. For small delay, i.e. as long as a phase lag parameter approximation is valid, this change does not lead to a change of the coupling strength. Second, the equivalence considered above strongly suggests a generalization to networks consisting of multiple subpopulations compared to networks with multimodal frequency distributions. As it turns out this step is no trivial. The governing equations even for the three-population and the trimodal network, respectively, reveal that (a) both systems coincide only for frequency distributions that no longer permit the Ott-Antonsen manifold to exhibit the whole dynamics of the system (cf. [6]), and that (b) we have to deal with first and second

harmonics in the coupling terms. This may lead to different synchronization patterns, e.g. 2 : 1-synchronization, or even to chaotic states (cf. also [5]). Hence, a proper investigation of the link between multimodal and multiple subpopulation-networks remains a challenging task and their dynamics need to be treated analytically more carefully. Similarly, refraining from the symmetries in the frequency distributions will arise new insights into the interaction of networks.

A natural question may also be whether the equivalence described above also applies for finite-sized networks. In the two population-approach, finite-size effects occur as low-frequency modulation of the oscillating local order parameters, and the transients become longer. Future numerical investigations shall shed more light on a proper comparison of both approaches. Likewise, they also bring theory closer to application, e.g. when exploring the interaction of cortical networks at distinct frequency bands. We believe that our work will be relevant seeing that (biomedical) data is rather available on a macroscopic level, i.e. in form of local/global order parameters, than on the oscillator level. Hence, specific features, e.g., an oscillating order parameter at the edge of a (Hopf) bifurcation, may hint at interacting (hidden) networks.

This project has received funding from the European Union's Horizon 2020 research and innovation programme under the Marie Skłodowska-Curie grant agreement No 642563.

References

- [1] E. Ott, T.M. Antonsen. Low dimensional behavior of large systems of globally coupled oscillators, *Chaos* 18 (3) pp. 037113, 2008.
- [2] E. A. Martens, E. Barreto, S.H. Strogatz, E. Ott, P. So, T.M. Antonsen. Exact results for the Kuramoto model with a bimodal frequency distribution, *PRE* 79 (2) pp. 026204, 2009.
- [3] E. Barreto, B. Hunt, E. Ott, P. So. Synchronization in networks of networks: The onset of coherent collective behavior in systems of interacting populations of heterogeneous oscillators, *PRE* 77 (3) pp. 36107, 2008.
- [4] D. Anderson, A. Tenzer, G. Barlev, M. Girvan, T.M. Antonsen, E. Ott. Multiscale dynamics in communities of phase oscillators, *Chaos* 22 (1) pp. 013102, 2012.
- [5] M. Komarov, A. Pikovsky. Effects of nonresonant interaction in ensembles of phase oscillators, *PRE* 84 (1) pp. 016210, 2011.
- [6] E. Ott, T.M. Antonsen. Long time evolution of phase oscillator systems, *Chaos* 19 (2) pp. 023117, 2009.

Structure of heart rate asymmetry: duration of monotonic runs

Jaroslav Piskorski¹, Tomasz Krauze² and Przemyslaw Guzik²

¹*University of Zielona Gora, Institute of Physics, Zielona Gora, Poland*

²*Poznan University of Medical Science, Department of Cardiology Intensive Therapy, Poznan, Poland*

Introduction Heart rate asymmetry (HRA) is the physiological phenomenon by which the contributions of accelerations and decelerations to the variability and structure of the RR-intervals time series is different. This phenomenon was first described for heart rate variability (HRV) by partitioning short- and long-term as well as total variability into parts contributed by decelerations and accelerations only. It turns out that the contributions of decelerations to short-term variability are bigger and smaller to long-term and total variability than those of accelerations (see references).

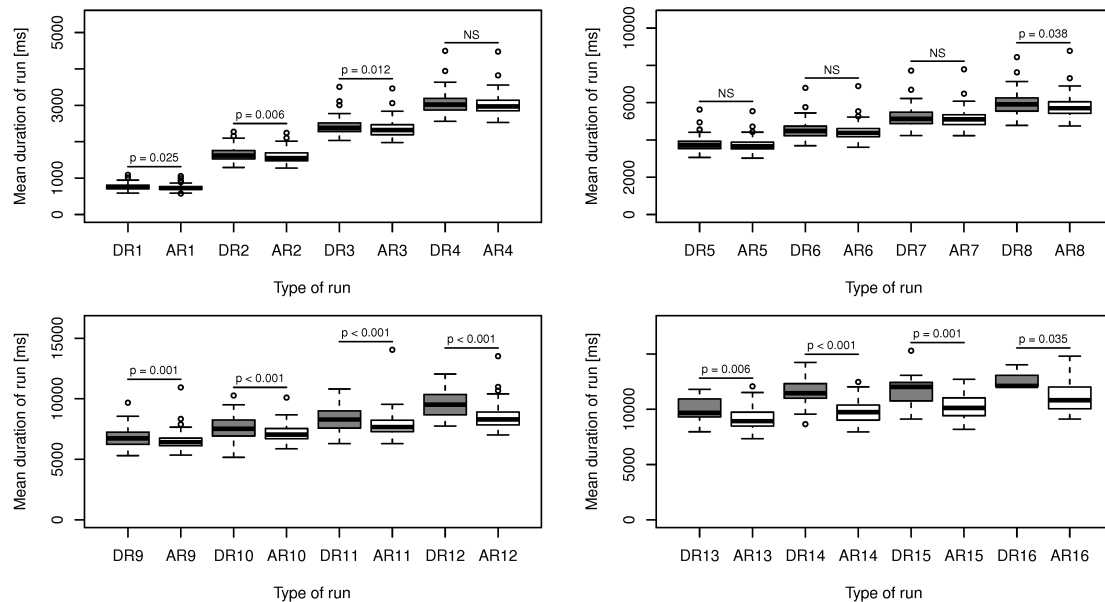
Another approach to studying HRA is the monotonic runs method which analyses the structure of HRV. In this method the lengths and numbers of monotonic (purely accelerating or decelerating) runs are studied. By *length* we mean the *number of beats in a run*. It has been found that the acceleration runs are longer and more numerous than deceleration runs - runs of accelerations of all lengths, with the exception of lengths 3 and 4, are more numerous than those of decelerations. Also, the longest runs in 24-hour recordings are almost exclusively runs of accelerations. The runs method has an independent predictive value in post-infarction patients. For the precise definition of the above runs and other details see references.

It is reasonable to expect that this mechanism must be compensated by a different distribution of the *duration* of the various runs. By *duration* of a run we mean the sum of all *RR* intervals in a run expressed in units of time. The aim of this paper is to study this distribution.

Materials and methods Eighty seven 24 hour ECG recordings were recorded in a group of healthy volunteers 25-41 years of age, 41 women. All of them reported to be healthy, were in sinus rhythm with resting heart rate 50-90 bpm, all had normal blood pressure, under 140/90 mmHg.

The runs analysis was carried out with in-house software written in python. The durations of runs of corresponding lengths were compared with the one-sided unpaired Wilcoxon test. Unlike in the case of runs lengths analysis, only recordings in which specific runs were actually represented were used in the analysis.

Results As expected, deceleration runs of length 1, 2 and 3 have highly significantly longer duration, runs 4 to 7 do not differ in duration and for the remaining lengths, 8 – 16 deceleration runs are again longer than acceleration runs. It is impossible to calculate the p -value for longer runs, because many of them were not represented in the analyzed recordings. For details see the figure below.



Conclusions The greater length of acceleration runs is compensated for by a greater duration of deceleration runs. This is evidence of a mechanism which keeps the heart rhythm within a certain set of values balancing two processes - more dynamic deceleration runs and gradual and more numerous accelerations (by *more dynamic* we mean changing the heart rhythm more than acceleration runs within the same number of runs). In this paper we have established the existence of such a phenomenon as well as finding the distribution of the duration of the runs.

References

Guzik P, Piskorski J, Krauze T, Wykretowicz A, Wysocki A, Heart rate asymmetry by Poincare plots of RR intervals 2006 *Biomedizinische Technik (Berlin)* **51** 272 - 275; Piskorski J, Guzik P, Geometry of the Poincar plot of RR intervals and its asymmetry in healthy adults 2007 *Physiological Measurement* **28** 287 - 300; Piskorski J, Guzik P, The structure of heart rate asymmetry: Deceleration and acceleration runs 2011 *Physiological Measurement* **32** 1011 - 1023; Guzik P, Piskorski J, Barthel P, Bauer A, M:uller A, Junk N, Ulm K, Malik M, Schmidt G, 2012 *Heart rate deceleration runs for post-infarction risk prediction Journal of Electrocardiology* **45** 70 - 76

Assessment of endothelial dysfunction using skin temperature oscillations analysis in patients with peripheral arterial disease

Sergey Podtaev^{1*}, Aleksey Parshakov², Nadezhda Zubareva², Peter Frick¹

¹*Institute of Continuous Media Mechanics, 614013, Academician Korolev Str., 1, Perm, Russian Federation*

²*Perm State Medical University, 614600, Petropavlovskaya Str., Perm, Russian Federation*

* Corresponding author, e-mail address: spt802@gmail.com

Objective: The purpose of this study was to examine correlations between laboratory markers of endothelial dysfunction (ED) and the degree of endothelium-dependent vasodilation using wavelet analysis of skin temperature (WAST) during a local heating test in patients with peripheral arterial disease (PAD). The studies were conducted before and after lower extremity bypass surgery.

Materials and methods: All the participants were distributed over 5 groups.

The first group included 17 healthy individuals (8 males and 9 females) aged 44-61 years (55.1 ± 8.1 years).

The second group contained 12 patients (11 male and 1 female) aged 52-81 years (64.1 ± 7.2) with PAD and chronic limb ischaemia (CLI) at stage II (CLI II).

The third group comprised 8 patients (6 males and 2 females) aged 63-86 years (74.5 ± 7.6) with stage III CLI (CLI III).

The fourth group consisted of 9 patients (7 males and 2 females) aged 63-80 years (68.5 ± 6.4) with PAD complicated by toe necrosis (CLI IV-N).

The fifth group included 9 patients (7 males and 2 females) aged 62-75 years (70.5 ± 4.7) with PAD complicated by foot gangrene (CLI IV-G). The duration of disease was 18.7 ± 4.1 years..

The ST on the plantar surface of the first toe was measured using a Microtest recorder (FM Diagnostics LLC, Russia) with an accuracy of 0.1°C and temperature resolution of 0.001°C . The inverse wavelet transform was applied to reconstruct the ST signals in three frequency bands corresponding to myogenic (0.052-0.145 Hz), neurogenic (0.021-0.052 Hz) and endothelial (0.0095-0.021 Hz) mechanisms of vascular tone regulation. The response of each vascular tone regulation mechanism was estimated by comparing the root-mean-square (r.m.s.) amplitudes of the temperature fluctuations obtained during and after the local heating test. We calculated the relative changes in r.m.s. amplitudes (vasodilation indexes) for myogenic (K_m), neurogenic (K_n) and endothelial (K_e) frequency ranges.

Results: In healthy subjects, a local increase in temperature up to 42°C caused a greater than three-fold increase in the amplitudes of foot ST oscillations. In the patients with PAD, the levels of amplitudes of skin temperature foot oscillations during the local heating test increased, remaining lower than the values obtained for the healthy subjects ($p < 0.05$). The levels of amplitudes of skin temperature foot oscillations during the local heating test in the endothelial, neurogenic and myogenic frequency ranges reached the largest values in the patients in group 2 ($p < 0.05$). In the endothelial frequency range, the levels of amplitudes of skin temperature oscillations obtained for patients in groups 2 and 3 were comparable and appeared to be sufficiently higher than the levels detected in the patients with necrosis of the lower extremities.

The plasma level of endothelin reached a maximum value in patients with toe necrosis and foot gangrene, which correlated positively with femoral artery stenosis ($R_s=0.94$; $p=0.048$) and correlated negatively with the vasodilation indexes in the endothelial frequency range ($R_s=-0.76$; $p<0.001$). The plasma level of vWF increased with the progression of trophic disorders, reached a maximum in patients with foot gangrene and correlated negatively with the vasodilation indexes in the endothelial frequency range ($R=-0.52$, $p<0.001$). The plasma homocysteine level increased with the progression of the disease, correlated strongly with the magnitude of tibial artery stenosis ($R_s=0.84$; $p=0.008$), correlated positively with the level of thrombocytes ($R_s=0.88$; $p=0.008$), and correlated negatively with the vasodilation indexes in the endothelial frequency range ($R=-0.52$, $p<0.001$).

Discussion and Conclusion: The principal finding of the study is that in the healthy subjects, a local increase in temperature up to 42°C caused a greater than three-fold increase in the amplitudes of foot skin temperature oscillations in the myogenic, neurogenic, and endothelial ranges. In patients with PAD, the response to local heating was much weaker in all frequency ranges, which suggests the presence of dysfunction in regulation mechanisms. The level of vasodilation dysfunction correlated with the level of artery stenosis in the lower extremities and with the progression of CLI.

The secondary finding of our study is that vasodilation indexes (relative changes in temperature oscillations during local heating) in the endothelial range were well correlated with the laboratory markers of endothelial dysfunction: endothelin, homocysteine and vWF. Increased vWF levels in PAD patients indicate arterial endothelial cell damage by atherosclerotic and revascularisation processes.

From the obtained results, it can be concluded that WAST is a useful technique for the non-invasive assessment of endothelium-dependent vascular dysfunction and can be applied to identify subclinical microvascular dysfunction in patients. The main advantages of WAST technology over expensive and labour-intensive ultrasound technology are its simplicity, low cost, portability and ease of use in clinical testing.

This work was supported by the Russian Science Foundation under project No 14-15-00809

Low-frequency respiratory activity correlates strongly with low frequency HRV

Tito Bassani^{1,3}, David M. Simpson² and Alessandro Beda³

¹*IRCCS Istituto Ortopedico Galeazzi, Milan, Italy,* ²*ISVR, University of Southampton, UK,*

³*DEE, Federal University of Minas Gerais, Belo Horizonte/MG, Brazil*

One of the most common approaches in heart-rate variability (HRV) analysis consists of estimating the power spectral density of the heart period time series and then taking the total power in different frequency bands as indices of autonomic control (Berntson et al., 1997). The power of the high-frequency band (HF: 0.15-0.5 Hz), usually dominated by respiratory sinus arrhythmia has been commonly associated with vagal modulation of cardiac activity, while the low frequency band (LF: 0.05-0.15 Hz) is considered to reflect a strong (but not exclusive) sympathetic influence (Berntson et al., 1997). The association of the power of HRV in the HF band (HRVHF) with vagal modulation and of HRV in the LF band (HRVLF) with sympathetic modulation have been the interpretative paradigm in many studies, especially in psychophysiology. However, there is considerable evidence that this paradigm might be inappropriate when the respiratory pattern deviates from the 'ideal' condition of regular spontaneous breathing with a respiratory rate within the HF band and little variability in respiratory volume and rate (Berntson, 1997).

The impact of respiration on HRV analysis is of particular concern when the respiration rate falls within the LF band – which is not uncommon (Beda et al., 2007). In the latter case, the respiration-related sinus arrhythmia affects primarily HRVLF rather than HRVHF. One consequence, which has been repeatedly highlighted, is that differences in the respiratory pattern between subjects and tasks can result in differences in the spectral indices of HRV that might be unrelated to changes in autonomic control (Beda et al., 2007). For instance, it is possible that the same cognitive tasks performed with two different breathing patterns (e.g. answering sequence of question verbally rather in written form) might produce discrepant results in terms of HRVLF and HRVHF that are mainly the effect of differences in breathing. Furthermore, the gain between respiratory volume and heart period is known to increase for lower frequencies, a trend that can continue to frequencies well below 0.1 Hz. At low respiratory rates both vagal and sympathetic effects can drive HRV (Berntson et al., 1997). In addition, even if the average respiratory frequency is located within the HF band, HRVLF can potentially be affected by respiratory activity due to breath-by-breath variability. The latter leads to a spectral spread of respiratory activity. We recently showed (Beda et al., 2014) that LF activity in the respiratory volume signal is strongly correlated with HRVLF ($r=0.77$) for a series of five psychophysiological protocols, some of which involved speaking. As pointed out by anonymous reviewers at the time, autonomic activity may however still be the underlying cause, if it leads to both changes in HRV and respiration. In the current work we will probe this further.

From a systems analysis point of view, one may consider HRV as an output, with respiration (and other signals) as inputs. The gain of the system has been associated with autonomic control (Berntson et al., 1997). The objective of the current work is to assess if it is primarily the change in RESP input signal or the model that determines HRVLF.

The data used is the same as analysed in Beda et al. (2007), but only the 20 subjects whose respiratory frequency at rest was above 0.15 Hz are considered. Systolic blood pressure (SAP) was derived from instantaneous blood pressure recorded with a Finapres device, respiratory volume (RESP) was estimated from a pneumotachograph and heart-period (RR interval - HP) from the ECG. Each subject undertook the following protocols: baseline rest—relaxed and without talking; read—reading a text aloud; talk—talking about a topic of choice; maths silent—performing a series of subtractions, writing the answers; maths aloud—same as maths

silent, but reading and answering questions aloud. Each task had a duration of 5 minutes. The interaction among HP and SAP was modelled with a parametric closed-loop system with RESP as an exogenous input affecting both HP and SAP (Baselli et al, 1988). Model parameters were estimated using a least-squares approach for each of the 20 subjects and each of the five tasks. Each model was then driven by the corresponding RESP signals and the resulting normalized HRVLF estimated from the power of the output as $HRVLF_n = HRVLF / (HRVHF + HRVLF)$. In order to test if this output is determined primarily by the 'system' (the model) or the input signal (RESP), we then drove the model for each task with the four RESP signals corresponding to the other tasks in the same subject, and correlated the results (subject by subject) with the correctly matched model and RESP signals. Correlations were calculated for each individual subject and then averaged across the 20 subjects.

The correlation between $HRVLF_n$ obtained by driving only the model of maths silent with RESP of the other tasks, with the results from the correctly matched model-RESP signals was 0.88 ± 0.13 (mean \pm standard deviation across all subjects). For the other models the mean value varied between 0.44 and 0.83. On the other hand, the correlation between $HRVLF_n$ obtained applying only the RESP signal for maths silent to the remaining tasks with the results of the correct model-RESP matching was only 0.08 ± 0.66 , and for the remaining RESP signals the corresponding mean correlation coefficient was less than 0.17. The results thus clearly indicate that between-tasks changes in $HRVLF_n$ is primarily associated with the RESP input, with the differences in models only playing a very minor role, in this set of data from mental challenges. When repeating the correlation analysis with the recorded values of $HRVLF_n$ rather than the values predicted by the correct model-RESP matching, the correlation coefficients were between 0.82 and 0.87, showing that all models predicted $HRVLF_n$ well. Furthermore, when correlating the measured normalized LF power of RESP with $HRVLF_n$ the correlation coefficient was 0.82 ± 0.22 confirming the previous results that within each subject, the relative HRVLF is highly correlated with LF RESP activity across the protocols.

These results thus further underline the strong association between LF RESP activity and HRVLF. The new results strongly support the hypothesis that if a task elicits a non negligible change in respiration, this may be the primary determinant of the associated changes in HRVLF, rather than a change in the 'system' driving respiratory sinus arrhythmia.

What remains open and requires further studies in psychophysiology is whether it is autonomic drive that is changing this respiratory input such that HRVLF still represents a valid measure of autonomic function, even with varying respiratory activity. However, if this is the case, the study of LF RESP activity directly rather than the potentially indirect route via HRVLF might be more appropriate. If it is not the case, then the interpretation of HRVLF as reflecting autonomic function could be quite misleading (Berntson, 1997) when respiration varies.

References

- Baselli, G. et al. 1988, *IEEE Trans. Biomed. Eng.* **35**, 1033–1046
Beda A, et al 2007 *Psychophysiology* **44**, 767–778
Beda A et al. 2014 *Psychophysiology* **51**, 197-205
Berntson, GG et al., 1997, *Psychophysiology* **34**, 6230 648

Acknowledgements

Funding support was received from CNPq and FAPEMG (Brazil), the University of Southampton and EPSRC (UK) and data was collected at COPPE/UFRJ (Rio de Janeiro, Brazil) with the support of Prof. A. Gianella Neto and colleagues.

Modulation of transport speed of red blood cells in capillaries

Maxim Volynsky, Mikhail Volkov, Nikita Margaryants, Igor P. Gurov,
and Alexei A. Kamshilin

ITMO University, Computer Photonics and Videomatics Dept., Saint Petersburg, Russia

Capillaries are the smallest blood vessels responsible for nutrition of human organs. Nailfold capillaries have distinguished feature that they can be directly viewed in a microscope allowing direct measurement of the red-blood-cells (RBC) speed [1]. The aim of this study was comparative study of blood pulsations dynamics assessed in a subject by three different techniques for clarifying the origin of light modulation by subcutaneous blood vessels. We carried out simultaneous recordings of high-speed microscopic video of a capillary together with the electrocardiography (ECG) and imaging photoplethysmography (PPG) of the fingers. On the one hand, ECG is commonly used method to study the cardiovascular system. On the other hand, according to commonly accepted model [2], PPG waveform describes change of cutaneous blood volume caused by pulsatile arteries. We have found that the speed of RBC is modulated in time similarly as the PPG signal but there is significant true delay between these signals.

Experiments were carried out with 5 healthy volunteers of different age (22 – 64 years). A digital black-and-white CMOS camera (8-bit model GigE uEye UI-5220SE of Imaging Development Systems GmbH) was used to record an image of nailfold capillary provided by 12^x optical microscope with long focal-length eyepiece. The frames (size of 400×400 pixels) were recorded at the rate of 146 frames per second (fps) under illumination of the finger with light-emitting diode (LED) at the central wavelength of 460 nm. PPG waveforms were recorded from other fingers by a custom-made imaging PPG system [3], which consisted of another similar CMOS camera and LED illuminator at 530 nm. The frames sizing 752×480 pixels were recorded at the rate of 32.5 fps. Both video systems were synchronized with ECG recordings so that the difference in the time scale of all recordings did not exceed 1.0 ms.

The whole set of the recorded data was processed offline. Advanced algorithm of video frames processing developed in our group [4] allowed us to detect both borders and a middle line of the capillary, and calculate the RBC speed as a function of the cell position in the track and time of the measurement (frame number). Typical example of the RBC-speed map is shown in Fig. 1. As it is seen in Fig. 1, even though the average speed is smaller in the venous part (C-D) compare to the arterial part (A-B), the RBC-speed is periodically modulated in time along the complete capillary length. Notably that with accuracy of one pixel, we have found no modulation of capillaries borders in all our recordings.

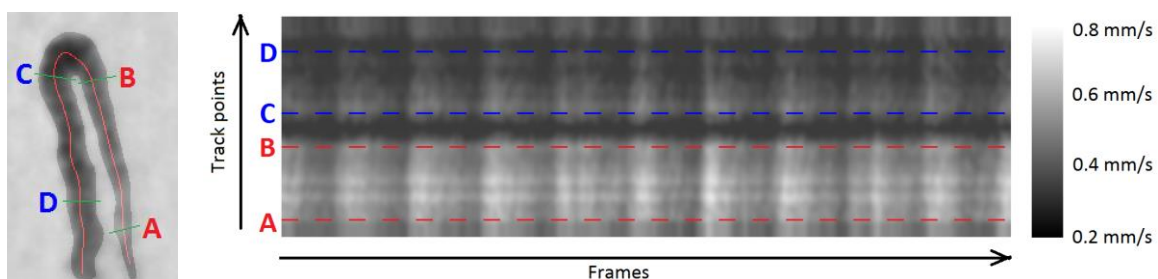


Fig. 1. An example of a capillary image with the middle track (right part), and RBC-speed map as a function of the position in the track (Y-axis) and frame number (X-axis).

Oscillations of the mean RBC-speed in the part A-B of the capillary are shown in Fig. 2 by the red curve. Simultaneously recorded PPG and ECG signals are plotted in Fig. 2 by the blue and black curves, respectively. As one can see, the number of minima in the red and blue curves is the same as the number of R-peaks in ECG. Moreover, the shape of the RBC-speed

signal is similar with the PPG signal, and both resemble oscillations of the pulsatile arterial pressure. Minima positions were chosen for the comparison because R-peak occurs just before contraction the left ventricle (beginning of the systole phase), which corresponds to the smallest arterial pressure and it is physiologically similar to the minimum of RBC speed and minimum of the PPG waveform. At a glance, the minima of the PPG signal (blue curve) occur earlier than that of RBC-speed (red curve) in Fig. 2. However, taking advantage of the natural heart rate variability, we can find out which oscillation of the signals correspond to which R-peak. Correlation analysis shows that the sequence of the RBC-speed minima positively correlates (Pearson coefficient = 0.87, $p < 10^{-3}$) with the sequence of R-peaks as they shown in Fig. 2. In contrast, the sequence of PPG minima positively correlates with that of R-peaks when the latter is shifted backward by one cardiac cycle (Pearson coefficient = 0.98, $p < 10^{-3}$). It means that the observed oscillations of the RBC speed originate from the nearest R-peaks, while each pulsation of the PPG signal – from the previous R-peak. Consequently, the delay time between R-peaks and RBC-speed oscillations is estimated as 0.25 ± 0.04 s but the delay time of the PPG signal is 0.92 ± 0.05 s.

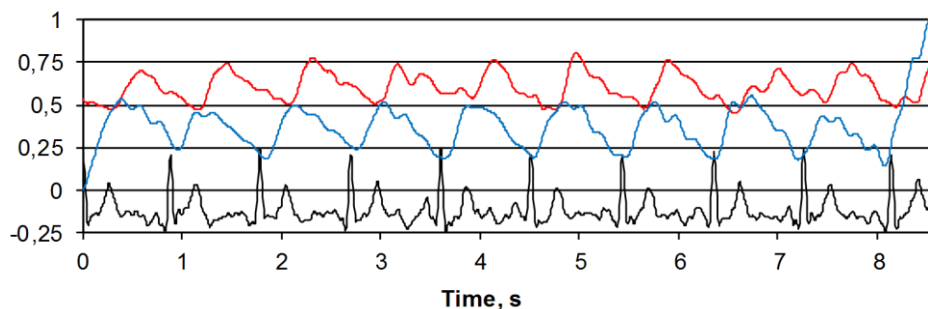


Fig. 2. Oscilloscope traces of simultaneously recorded speed of RBC in the nailfold capillary (red curve, in mm/s), PPG waveform (blue curve, in a.u.) in another finger, and ECG signal (black curve, in a.u.).

While the delay of RBC-speed oscillations is explained by the time needed for the propagation of the pulse wave from the heart to a finger, no explanation can be given at the moment to the observed significant delay of the PPG signal. Nevertheless, we can conclude that observed PPG oscillations do not directly stem from the arterial blood volume pulsations although have the shape similar to variations of the blood pressure. These experimental findings require further detailed study and analysis. Future understanding of the physiological mechanism behind the formation of the observed oscillations and their relative delay would allow development of new tools and methods for study microcirculation and diagnosis of various diseases.

To summarize, we found that (i) RBC speed in a capillary is modulated in time at the heart bit frequency; (ii) size of the capillaries remains unchangeable during this modulation; and (iii) there is significant delay between oscillations of the RBC speed and those in the PPG waveform.

Acknowledgment. The work was financially supported by the Russian Science Foundation (Grant No. 15-15-20012).

References

- [1] Hahn M, Klyscz T, Jünger M 1996 *The Journal of Investigative Dermatology* **106** 1256-1259
- [2] Allen J 2007 *Physiological Measurement* **28** R1-R40
- [3] Kamshilin A A, Mamontov O V, Koval V T, Zayats G A, Romashko R V 2015 *Biomedical Optics Express* **6**, 4326-4334
- [4] Karimov K, Volkov M 2015 *Proceedings of SPIE* **9528** 952810

Modelling flexible changes between network configurations in task-free brain activity

Vesna Vuksanović¹ and Philipp Hövel²

¹ *Aberdeen Biomedical Imaging Centre, The University of Aberdeen, Aberdeen, UK*

² *Institute of Theoretical Physics, Technical University Berlin, Berlin, Germany*

Background Brain imaging methods allow a non-invasive assessment of structural connections and their functional interactions, representing either instantaneous or (task-specific) causal relations. However, the mechanisms of how functional brain interactions arise on top of structural backbone is as yet poorly understood. Here, we use a modelling approach to interpret these experimental findings, with reference to the whole-brain dynamics and functional connectivity between segregated brain areas in task-free brain state.

Methods By linking the brain regions (nodes) by their structural connections (edges) and modelling the functional (temporal) interactions arising from it, we explore how dynamically organised neural ensembles work in concert to enable functional interactions underlying cognitive functions. Neural activity and the inferred hemodynamic response of the network nodes are modelled as sets of self-sustained oscillators, which are embedded in topologies of complex structural and functional brain interactions. The coupling topology of such interactions is based on connectivity maps derived from task-free (i.e. in the absence of any external input) functional magnetic resonance imaging (fMRI) and diffusion weighted MRI (dMRI) experiments. By combining brain structural and functional data the architecture of complex brain functional interactions is additionally reduced to its main structural pathways.

Results We characterize brain network dynamic properties by synchrony and variability in synchrony (metastability). We demonstrate that fast flexible changes in neural network synchrony contribute to the emergence of correlated activity between remote brain regions. We show that such changes reflect alternations between network synchronized and less synchronized state. We also show that the level of synchrony between remote network nodes strongly correlates with the corresponding number of shared connections.

Conclusion Our results show that functional brain interactions may arise from the network dynamics which allow for flexible changes between different network configurations.

References

Vuksanović V and Hövel P 2015 *Chaos* **25** 023116.

Vuksanović V and Hövel P 2014 *NeuroImage* **97** 1-8.
Cabral J, Kringelbach ML, Deco G 2014 *Prog Neurobiol* **114** 102-31.
Park HJ and Friston K 2013 *Science* **342** 1238411-5.

The complexity of cardiac rhythms during head-up tilt test by the entropy of patterns¹

Dorota Wejer¹, Danuta Makowiec², Beata Graff³, Szymon Budrejko⁴
and Zbigniew R. Struzik⁵

¹ *University of Gdańsk, Inst. of Experimental Physics, Gdańsk, Poland*

² *University of Gdańsk, Inst. of Theoretical Physics and Astrophysics, Gdańsk, Poland*

³ *Medical University of Gdańsk, Dept. of Hypertension and Diabetology, Gdańsk, Poland*

⁴ *Medical University of Gdańsk, Dept. of Cardiology and Electrotherapy, Gdańsk, Poland*

⁵ *RIKEN Brain Science Institute, Wako-shi, Japan*

University of Tokyo, Graduate School of Education, Tokyo, Japan

Introduction: Shannon entropy of a pattern distribution has been proposed for quantifying complexity of the heart rhythm and blood pressure response to a rapid change in a body position caused by the head-up tilt (HUT) test^[2]. Two sets of patterns have been considered, so-called, permutation patterns^[1] and deterministic patterns^[2]. However patterns of these sets often overlap each other what makes the comparison difficult, see fig. 1A. Therefore we propose a family of patterns, called ordinal, which separates events considered within the permutation and deterministic sets of patterns. Then we test how this new approach influences on estimation of complexity of signals of healthy subjects and patients with vasovagal syncope undergoing the HUT test, see fig. 1B.

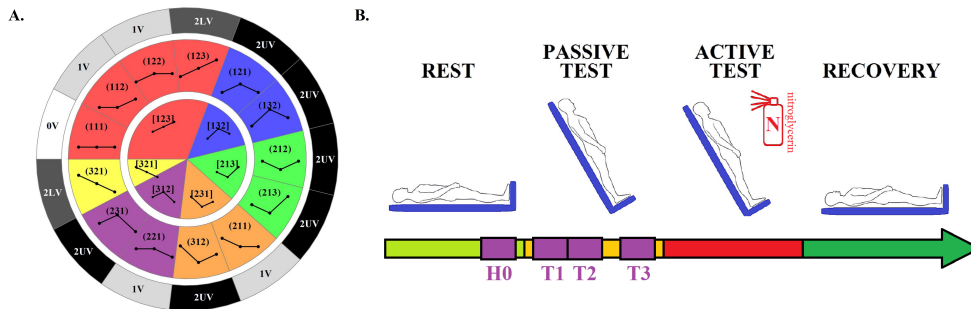


Figure 1: **A.** Relationships between permutation patterns (the center of the pie chart), ordinal patterns (the middle ring of the pie chart) and deterministic patterns (the external ring of the pie chart). Ordinal patterns describe all possible patterns and they are a bridge between permutation and deterministic patterns. **B.** A scheme of the HUT test. H0, T1, T2, and T3 denote time-windows selected for the further analyzes.

Methods: Time series (RR-intervals and systolic blood pressure (SBP)) were obtained in the HUT test under the paced breathing regime. The HUT test was performed on healthy volunteers without syncopes in the past and with a negative HUT test (CG: 14 males, 14 females; age: 20-39yr, median: 23yr) and patients suffering from vasovagal faints with positive HUT test (VVS: 17 males, 42 females; age:

¹This work was supported by the National Science Centre, Poland, UMO: 2012/06/M/ST2/00480.

18-44yr, median: 23yr). Two types of preprocessing data were used: mapping each signal into 6-value series^[2] and using different signal resolutions Δ_{RR} and Δ_{SBP} .

Results:

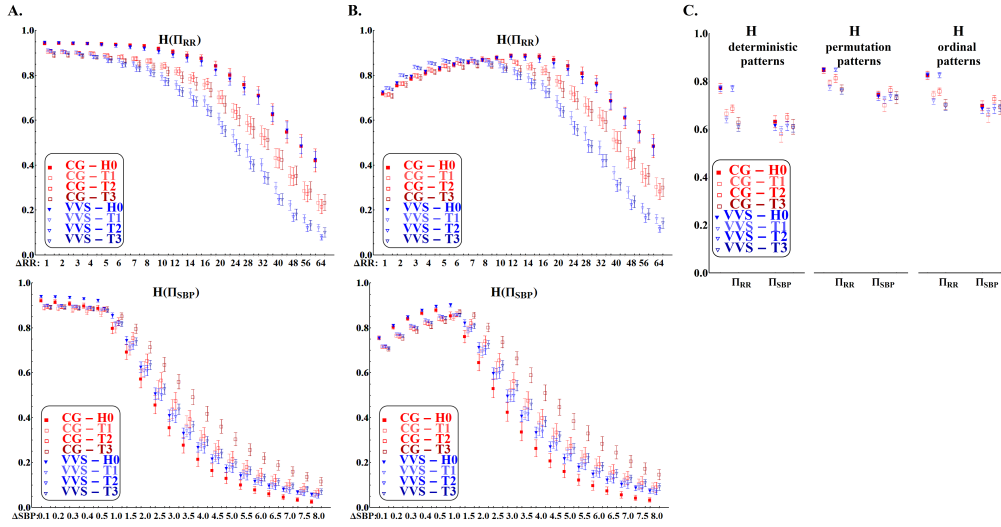


Figure 2: Graphs show the values of entropy normalized by $\log N$ (N - number of patterns in a given approach) for healthy people (CG) and patients suffering from vasovagal faints (VVS) in time-windows: H0, T1, T2, and T3. The entropy of **A.** permutation patterns and **B.** ordinal patterns was calculated for signals with the various of resolution $\Delta_{RR} = 1, \dots, 64$ ms and $\Delta_{SBP} = 0.1, \dots, 8$ mmHg. **C.** The entropy of permutation, ordinal and deterministic patterns calculated following the preprocessing schema described in [2].

Conclusions:

There is a statistical significant increase in the value of entropy of ordinal patterns when the resolution of Δ_{RR} and Δ_{SBP} changes. It corresponds to increasing occurrence of patterns with same values which are absent at the highest resolution. At the maximum, the entropy for different groups of signals do not differ from each other. Then in time windows T1, T2, and T3, the signal complexity of the healthy people is always higher than vasovagal patients, independently of the signal resolution. This last observation refers also to the entropy of permutation patterns.

In case of the entropy calculated from signals represented by 6 symbols, the ordinal pattern approach provides a lower value of entropy than the permutation one. As expected, the deterministic patterns give the lowest value of entropy. However, the relations between entropy of deterministic patterns of different groups are the same as among entropy found for ordinal patterns.

References

- [1] Bandt C, Pompe B 2002 *Phys. Rev. Lett.* **88** 174102:1-174102:4
- [2] Porta A, Guzzetti S, Montano N, Furlan R, Pagani M, Malliani A, Cerutti S 2001 *IEEE Trans Biomed Eng.* **48(11)** 1282-1291
- [3] Makowiec D, Kaczkowska A, Wejer D, Żarczyńska-Buchowiecka M, Struzik Z.R 2015 *Entropy* **17** 1253-1272

Complexity distribution in 24h Holter RR time series

Sebastian Żurek¹, Marcin Kośmider¹, Waldemar Grabowski¹
Jarosław Piskorski¹, Przemysław Guzik²

¹*Institute of Physics, University of Zielona Góra, Zielona Góra, Poland*

²*Department of Cardiology, Intensive Therapy and Internal Diseases,
Poznań University of Medical Sciences, Poznań, Poland*

Sample Entropy (SampEn) is a popular method for assessing the regularity of RR intervals. The $SampEn(N, m, r)$ estimates the entropy of a series of N data points by calculating the probability that segments of m samples which are similar, i.e., within a given distance r , remain similar when the segments length increases to $m + 1$. The parameter m is called the embedding dimension, and the threshold distance is often expressed as a fraction d of the standard deviation (SD) of the time series: $r = d \cdot SD$. In most studies SampEn for a series of N points is calculated as a single point selected for $m = 2$ and $d = 0.2$. These values are suggested by Pincus who introduced the *Approximate Entropy* - entropy estimator that later evolved to SampEn. Effects of different r and m values on SampEn have been rarely assessed, because of the high computational burden of this task. Recently, however, a fast Norm Component Matrix (NCM) algorithm for estimating correlation sums has been proposed that allows calculating SampEn quickly.

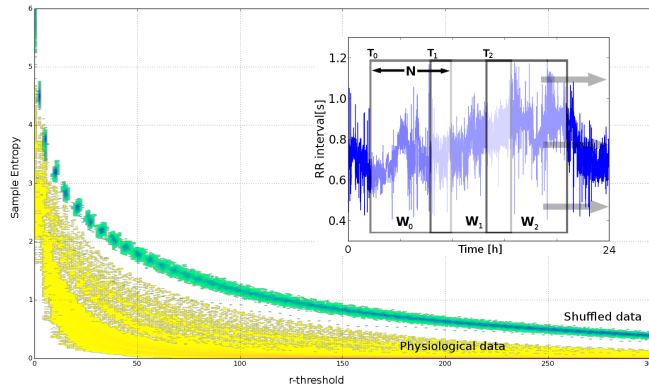


Figure 1: The SampEn distribution for the individual subject physiological (yellowish) and shuffled (bluish) data. The inset explains how the time windows W containing N samples were defined, located at the time T and moved.

The aim of our work was to describe, how $SampEn(N, m, r)$ curves calculated for a real heart rate (HR) data of healthy people are distributed over the time. The

rationale for this approach was to verify, that the HR data complexity measured with *SampEn* is changing during the day-to-night and that these changes are significant, however constrained. This supports the suggestion to evaluate *SampEn* as a whole curve - not only as a single point calculated for a specific (m, d) pair. For this goal we applied the NCM algorithm on RR intervals extracted from 24h Holter ECGs, estimating SampEn over wide ranges of r and fixed m . **The data** we analysed have been collected in 79 healthy volunteers (41 men, age 35 ± 7.4 years, mean \pm SD). They were all in sinus rhythm (55-90 bpm) without chronic or acute disease within the last 3 months. No one was taking any medications or was into endurance training. To analyse the consecutive updates of the RR complexity the SampEn was calculated for the set of time-windows moving along the signal (Fig. 1 inset). Each window W had a fixed length ($N = 5000 \approx 1h$) and was located at the time T . The distribution of SampEn values calculated for a set of ~ 1000 overlapping windows W in an individual RR time series is presented in Fig. 1. We have also calculated the overall distribution of SampEn values calculated for the whole set of recordings taken in the group of 79 volunteers - almost 80000 one hour long windows of RR data - Fig. 2.

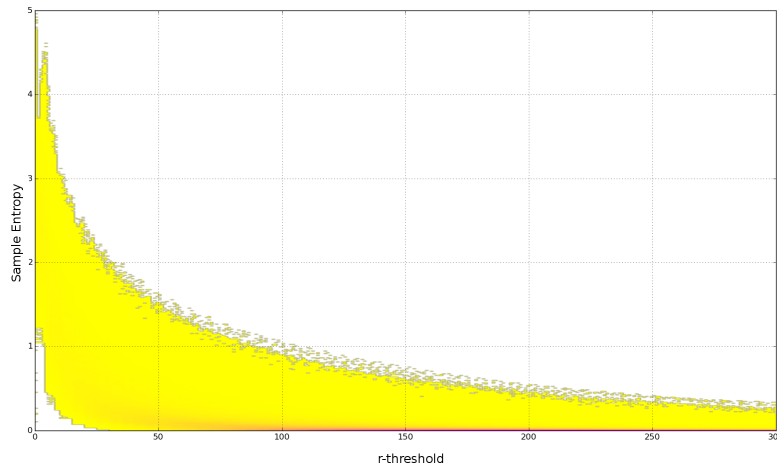


Figure 2: The overall SampEn distribution - calculated for 79 volunteers.

Results indicate that the SampEn values are distributed over the fixed area defined by smooth boundary lines (Fig. 2). The circadian rhythm gradually shifts the individual SampEn curves (i.e. calculated for a specific W) within the pattern - between the low and the high complexity regimes. The geometry of this distribution is an intriguing subject – its detailed analysis might give some insights into the heart rate complexity dynamics. While the entropy changes during the day-to-night cycle is a known phenomenon, this is the first report on the constraints to these changes. Physiological and clinical meaning of these findings as well as the detailed analysis

of day vs. night and healthy vs. pathological populations require further studies.

References

Richman JS, Moorman JR, 2000, *Am J Physiol Heart Circ Physiol*, **278**, 2039-2049
Żurek S, Guzik P, Pawlak S, Kośmider M, Piskorski J., 2012, *Physica A*, **391 (24)**, 6601-6610

4 List of Participants

ESGCO 2016 Participants

| Name | Surname | Affiliation | Country | email |
|-------------|----------------|--|----------------|--|
| Christian | Aalkjær | Department of Biomedicine, Aarhus University | Denmark | ca@biomed.au.dk |
| Yunus | Abdulhameed | Department of Physics, Lancaster University | UK | yunusabhamid@yahoo.com |
| Fernando | Andreotti | Institute Of Biomedical Engineering, TU Dresden | Germany | fernando.andreotti@mailbox.tu-dresden.de |
| Philip | Aston | Department of Mathematics, University Of Surrey | UK | P.Aston@surrey.ac.uk |
| Dragana | Bajic | Faculty Of Technical Science, University of Novi Sad | Serbia | dragana.bajic@gmail.com |
| Miraslau | Barabash | Department of Physics, Lancaster University | UK | m.barabash@lancaster.ac.uk |
| Vlasta | Bari | Department of Biomedical Sciences for Health, University of Milan | Italy | vlasta.bari@grupposandonato.it |
| Ronny | Bartsch | Department of Physics, Bar-Ilan University | Israel | bartsch.ronny@gmail.com |
| Mathias | Baumert | Electrical and Electronic Engineering, University Of Adelaide | Australia | mathias.baumert@adelaide.edu.au |
| Alona | Ben-Tal | Institute of Natural and Mathematical Sciences, Massey University | New Zealand | A.Ben-Tal@massey.ac.nz |
| Alan | Bernjak | INSIGNEO Institute for in silico Medicine, University Of Sheffield | UK | a.bernjak@sheffield.ac.uk |
| Leonardo | Bocchi | Information Engineering, University Of Florence | Italy | leonardo.bocchi@unifi.it |
| Etienne | Boileau | Zienkiewicz Centre for Computational Engineering, Swansea University | UK | e.boileau@swansea.ac.uk |
| Enrico | Brunetta | Internal Medicine, Humanitas Research Hospital | Italy | enrico.brunetta@humanitas.it |
| Teodor | Buchner | Faculty of Physics, Warsaw University of Technology | Poland | buchner@if.pw.edu.pl |
| Joana | Cabral | Department of Psychiatry, University Of Oxford | UK | joana.cabral@psych.ox.ac.uk |
| Camillo | Cammarota | Department of Mathematics, University La Sapienza | Italy | cammar@mat.uniroma1.it |
| Paolo | Castiglioni | Fondazione Don C. Gnocchi | Italy | paolo.castiglioni@gmail.com |
| Aparecida | Catai | Department of Physiotherapy, Federal University of São Carlos | Brazil | amcatai50@gmail.com |
| Gloria | Cecchini | Institute for Complex Systems and Mathematical Biology, University Of Aberdeen | UK | r01gc15@abdn.ac.uk |
| Richard | Clayton | INSIGNEO Institute for in silico Medicine, University Of Sheffield | UK | r.h.clayton@sheffield.ac.uk |
| Philip | Clemson | Department of Physics, Lancaster University | UK | phil.clemson@cardiocity.com |
| Antonio | Colantuoni | Department of Clinical Medicine and Surgery, "Federico II" University Of Naples | Italy | antonio.colantuoni@unina.it |
| Valentina | Corino | Department of Electronics, Information and Bioengineering, Politecnico Di Milano | Italy | valentina.corino@polimi.it |
| Dirk | Cysarz | Integrated Curriculum for Anthroposophic Medicine, University Of Witten/Herdecke | Germany | d.cysarz@rhythmten.de |
| Beatrice | De Maria | Department of Electronics, Information and Bioengineering, Politecnico Di Milano | Italy | beatrice.demaria@polimi.it |
| Nicolas | Deschle | MOVE Research Institute, Vrije Universiteit Amsterdam | Netherlands | n.deschle@abdn.ac.uk |
| Federico | Devalle | Center for Brain and Cognition, Universitat Pompeu Fabra | Spain | federico.devalle@upf.edu |
| Marco | Di Rienzo | Department of Biomedical Technology, Fondazione Don C. Gnocchi | Italy | mdirienzo@dongnocchi.it |
| Andrea | Duggento | Medical Physics Section, University Of Rome "Tor Vergata" | Italy | duggento@med.uniroma2.it |
| David | Edwards | Institute of Molecular and Experimental Medicine, Cardiff University | UK | edwardsdh@cf.ac.uk |

| | | | | |
|-------------|-----------------|---|---------------|-----------------------------------|
| Robert | Eisenberg | Department of Molecular Biophysics, Rush University | United States | bob.eisenberg@gmail.com |
| Mahmoud | Eissa | Department of Physics, Lancaster University | UK | m.eissa@lancaster.ac.uk |
| Maja | Elstad | Division of Physiology, University Of Oslo | Norway | maja.elstad@medisin.uio.no |
| Mandy | Engelsma | Handfast Point | Netherlands | zbignewstruzik@yahoo.co.uk |
| Denis | Engemann | Cognitive Neuroimaging Unit, Universit Paris-Sud | France | denis.engemann@gmail.com |
| Luca | Faes | Bruno Kessler Foundation | Italy | faes.luca@gmail.com |
| Olena | Fedorenko | Division of Biomedical and Life Sciences, Lancaster University | UK | o.fedorenko@lancaster.ac.uk |
| Jiandong | Feng | Laboratory of Nanoscale Biology, EPFL School of Engineering | Switzerland | jiandong.feng@epfl.ch |
| Phil | Furneaux | Department of Physics, Lancaster University | UK | p.furneaux@lancaster.ac.uk |
| Christopher | George | Wales Heart Research Institute, Cardiff University | UK | christopher.george.home@gmail.com |
| Aleksandra | Gergont | Jagiellonian University Medical College | Poland | agergon@cm-uj.krakow.pl |
| William | Gibby | Department of Physics, Lancaster University | UK | w.gibby@lancaster.ac.uk |
| Anna | Giczewska | Department of Biomedical Engineering, Gdańsk University of Technology | Poland | anna.giczewska@yahoo.com |
| Jan | Gierałtowski | Faculty of Physics, Warsaw University of Technology | Poland | gieraltowski@if.pw.edu.pl |
| Mattias | Goksör | Physics Department, University Of Gothenburg | Sweden | mattias.goksor@physics.gu.se |
| Beata | Graff | Department of Hypertension and Diabetology, Medical University Of Gdańsk | Poland | bgraff@gumed.edu.pl |
| Grzegorz | Graff | Faculty of Applied Physics and Mathematics, Gdańsk University Of Technology | Poland | graff@mif.pg.gda.pl |
| Philine | Granitza | Department of Physics, Humboldt-Universität Zu Berlin | Germany | granitza@physik.hu-berlin.de |
| Marcin | Gruszecki | Department of Radiology Informatics and Statistics, Medical University Of Gdańsk | Poland | mgruszecki@gumed.edu.pl |
| Carlo | Guardiani | Centre for Scientific Computing, University Of Warwick | UK | c.guardiani@warwick.ac.uk |
| Stefano | Guzzetti | Emergency Department, Azienda Ospedaliera Luigi Sacco, University of Milan | Italy | guzzetti.stefano@hsacco.it |
| Jens | Haueisen | Institute of Biomedical Engineering and Informatics, Technical University Ilmenau | Germany | jens.haueisen@tu-ilmenau.de |
| Dirk | Hoyer | Jena University Hospital Biomagnetic Center | Germany | dirk.hoyer@med.uni-jena.de |
| Anne | Humeau-Heurtier | LARIS, University Of Angers | France | anne.humeau@univ-angers.fr |
| Robin | Ince | Institute of Neuroscience and Psychology, University Of Glasgow | UK | robin.ince@glasgow.ac.uk |
| Plamen | Ivanov | Department of Physics, Boston University | United States | plamen@buphy.bu.edu |
| Thomas | Jaki | Department of Mathematics and Statistics, Lancaster University | UK | t.jaki@lancaster.ac.uk |
| Michal | Javorka | Jessenius Faculty Of Medicine, Comenius University | Slovakia | mjavorka@jfmed.uniba.sk |
| Aled | Jones | Wales Heart Research Institute, Cardiff University | UK | jonesa110@cardiff.ac.uk |
| Alexei | Kamshilin | Computer Photonics and Videomatics Department, ITMO University | Russia | alexei.kamshilin@yandex.ru |
| John M. | Karemaker | Academic Medical Center, University Of Amsterdam | Netherlands | karemaker@ijnnet.nl |
| Igor | Kaufman | Department of Physics, Lancaster University | UK | i.kaufman@lancaster.ac.uk |
| Igor | Khovanov | Centre for Scientific Computing, University Of Warwick | UK | i.khovanov@warwick.ac.uk |

| | | | | |
|------------|------------------|--|-------------|--|
| Ulrich | Kleinekathöfer | Department of Physics and Earth Sciences, Jacobs University Bremen | Germany | u.kleinekathoefer@jacobs-university.de |
| Marcin | Kosmider | Institute of Physics, University of Zielona Gora | Poland | kosmo@codelab.pl |
| Jan | Krämer | Institute of Physics, Humboldt-Universität Zu Berlin | Germany | jkraemer@physik.hu-berlin.de |
| Petroula | Laiou | Department of Information and Communication Technologies, Universitat Pompeu Fabra | Spain | petroula.laiou@upf.edu |
| Igor | Lakhno | Department of Obstetrics and Gynecology, Kharkiv V N Karazin National University | Ukraine | igorlakhno71@gmail.com |
| Gemma | Lancaster | Department of Physics, Lancaster University | UK | g.lancaster1@lancaster.ac.uk |
| Klaus | Lehnertz | Interdisciplinary Center for Complex Systems, University of Bonn | Germany | Klaus.Lehnertz@ukb.uni-bonn.de |
| Zengyong | Li | School of Mechanical Engineering, Shandong University | China | zyongli2000@aliyun.com |
| Harri | Lindholm | NokiaTech | Finland | harri.lindholm@nokia.com |
| Alessandro | Loppini | Nonlinear Physics and Mathematical Modeling Laboratory, University Of Rome | Italy | a.loppini@unicampus.it |
| Maxime | Lucas | Department of Physics, Lancaster University | UK | m.lucas@lancaster.ac.uk |
| Carol | Luscombe | Cambridge Research Systems | UK | carol.luscombe@crsltd.com |
| Marek | Makowiec | Accompanying | Poland | fizdm@univ.gda.pl |
| Danuta | Makowiec | Institute of Theoretical Physics and Astrophysics, University of Gdańsk | Poland | fizdm@univ.gda.pl |
| Irene | Malvestio | Department of Information and Communication Technologies, Universitat Pompeu Fabra | Spain | malvestio.irene@gmail.com |
| Andrea | Marchi | Department of Electronics, Information and Bioengineering, Politecnico Di Milano | Italy | andrea.marchi@polimi.it |
| Daniele | Marinazzo | Department of Data Analysis, University Of Ghent | Belgium | daniele.marinazzo@ugent.be |
| Michela | Masè | Department of Physics, University Of Trento | Italy | mase@science.unitn.it |
| Claudio E. | Mazzucco | Department of Electronics, Information and Bioengineering, Politecnico Di Milano | Italy | claudioenricomazzucco@gmail.com |
| Peter | McClintock | Department of Physics, Lancaster University | UK | p.v.e.mcclintock@lancaster.ac.uk |
| Ana | Minchole | Department of Computer Science, University Of Oxford | UK | anamin@cs.ox.ac.uk |
| Irina | Mizeva | Institute Of Continous Media Mechanics | Russia | mizeva@icmm.ru |
| Martin | Mojica-Benavides | Physics Department, University Of Gothenburg | Sweden | martin.mojica@physics.gu.se |
| Ernest | Montbrio | Department of Information and Communication Technologies, Universitat Pompeu Fabra | Spain | ernest.montbrio@upf.edu |
| Thierry | Mora | Ecole Normale Supérieure And CNRS | France | thierrymora@yahoo.com |
| Max | Moser | Medical University of Graz and Human Research Institute | Austria | max.moser@medunigraz.at |
| Patrick | Neary | Faculty of Kinesiology and Health Studies, University Of Regina | Canada | patrick.neary@uregina.ca |
| Alain | Nogaret | Department of Physics, University Of Bath | UK | A.R.Nogaret@bath.ac.uk |
| Michele | Orini | Institute of Cardiovascular Science, University College London | UK | michele.orini.maculotti@gmail.com |
| Julian | Paton | School of Physiology, University Of Bristol | UK | Julian.F.R.Paton@Bristol.ac.uk |
| Spase | Petkoski | Institut De Neurosciences Des Systèmes, Aix-Marseille University | France | spase.petkoski@univ-amu.fr |
| Aleksandra | Pidde | Department of Physics, Lancaster University | UK | a.pidde@lancaster.ac.uk |
| Bastian | Pietras | MOVE Research Institute, Vrije Universiteit Amsterdam | Netherlands | b.pietras@vu.nl |

| | | | | |
|--------------|-------------|--|---------------|------------------------------------|
| Jaroslav | Piskorski | Institute of Physics, University of Zielona Gora | Poland | jaropis@zg.home.pl |
| Gernot | Plank | Department of Biophysics, Medical University of Graz | Austria | gernot.plank@medunigraz.at |
| Sergey | Podtaev | Institute of Continuous Media Mechanics | Russia | spt802@gmail.com |
| Alberto | Porta | Department of Biomedical Sciences for Health, University Of Milan | Italy | alberto.porta@unimi.it |
| Dmitry | Postnov | Department of Physics, Saratov State University | Russia | postnov@info.sgu.ru |
| Aleksandra | Radenovic | Laboratory of Nanoscale Biology, EPFL School of Engineering | Switzerland | aleksandra.radenovic@epfl.ch |
| Johan | Raeder | Institute of Clinical Medicine, University Of Oslo | Norway | johan.rader@medisin.uio.no |
| Martin | Rasmussen | Department of Mathematics, Imperial College London | UK | m.rasmussen@imperial.ac.uk |
| Flavia | Ravelli | Department of Physics, University Of Trento | Italy | ravelli@science.unitn.it |
| Jos | Reulen | Maastricht University Medical Centre | Netherlands | jos.reulen@mumc.nl |
| Stephen | Roberts | Division of Biomedical and Life Sciences, Lancaster University | UK | s.k.roberts@lancaster.ac.uk |
| Jonathan | Ruffle | IOP Publishing | UK | angela.gage@iop.org |
| Frida | Sandberg | Department of Biomedical Engineering, Lund University | Sweden | frida.sandberg@bme.lth.se |
| Roberto | Sassi | Department of Computer Science, University Of Milan | Italy | roberto.sassi@unimi.it |
| Karin | Schiecke | Institute Of Medical Statistics, Computer Sciences And Documentation, JUH | Germany | karin.schiecke@med.uni-jena.de |
| Uwe | Schneider | Department of Obstetrics, Division of Prenatal Diagnostics and Fetal Physiology, JUH | Germany | uwe.schneider@med.uni-jena.de |
| Steffen | Schulz | Institute Of Innovative Health Technologies IGHT, University of Applied Sciences | Germany | steffen.schulz@fh-jena.de |
| Lawrence | Sheppard | Kansas Biological Survey, University of Kansas | United States | lwsheppard99@hotmail.com |
| Helen | Shiells | Institute for Complex Systems and Mathematical Biology, University Of Aberdeen | UK | r01hcs14@abdn.ac.uk |
| Chih-Wen | Shih | Department of Applied Mathematics, National Chiao Tung University | Taiwan | cwshih@math.nctu.edu.tw |
| Maria G. | Signorini | Department of Biomedical Engineering, Politecnico Di Milano | Italy | mariagabriella.signorini@polimi.it |
| David M. | Simpson | Institute of Sound and Vibration Research, University of Southampton | UK | ds@isvr.soton.ac.uk |
| Maria | Skytjoti | Division of Physiology, University Of Oslo | Norway | maria.skytjoti@medisin.uio.no |
| Andrew | Smith | Royal Lancaster Infirmary | UK | andrew.f.smith@mbht.nhs.uk |
| Michele | Sorelli | Department of Information Engineering, University Of Florence | Italy | michele.sorelli@gmail.com |
| Andreas | Spiegler | Institut de la Santé et de la Recherche Médical, Aix-Marseille Université | France | andreas.spiegler@univ-amu.fr |
| Tomislav | Stankovski | Faculty Of Medicine, Ss Cyril And Methodius University | Macedonia | toshomail@gmail.com |
| Aneta | Stefanovska | Department of Physics, Lancaster University | UK | aneta@lancaster.ac.uk |
| Lisa | Stroux | Institute of Biomedical Engineering, University Of Oxford | UK | gari@alum.mit.edu |
| Zbigniew | Struzik | Graduate School of Education, University Of Tokyo | Japan | zbigniewstruzik@yahoo.co.uk |
| Sandra-Ilona | Sunram-Lea | Department of Psychology, Lancaster University | UK | s.sunram-lea@lancaster.ac.uk |
| Yevhen | Suprunenko | Institute of Integrative Biology, University Of Liverpool | UK | y.suprunenko@liverpool.ac.uk |
| Angelo | Taibi | University Of Ferrara | Italy | taibi@fe.infn.it |

| | | | | |
|-----------|----------------|--|----------|------------------------------|
| Arina | Tankanag | Institute of Cell Biophysics, Russian Academy of Sciences | Russia | tav@icb.psn.ru |
| Jakob | Thomassen | Cambridge Research Systems | UK | jakob.thomassen@crsltd.com |
| Clare | Thorn | Diabetes and Vascular Medicine, University Of Exeter | UK | C.E.Thorn@exeter.ac.uk |
| Valentina | Ticcinelli | Department of Physics, Lancaster University | UK | v.ticcinelli@lancaster.ac.uk |
| Vilma | Urbančič-Rovan | Department of Endocrinology, University Medical Centre | Slovenia | vilma.urbancic@kclj.si |
| Gaetano | Valenza | University Of Pisa/ Harvard Medical School | Italy | g.valenza@ieee.org |
| Maxim | Volynsky | Computer Photonics and Videomatics Department, ITMO University | Russia | maxim.volynsky@gmail.com |
| Andreas | Voss | Institute Of Innovative Health Technologies IGHT, University of Applied Sciences | Germany | andreas.voss@fh-jena.de |
| Vesna | Vuksanović | Aberdeen Biomedical Imaging Centre, University Of Aberdeen | UK | vesna.vuksanovic@abdn.ac.uk |
| Eric | Weber Jensen | Quantium Medical S.L | Spain | gf@quantiummedical.com |
| Dorota | Wejer | Institute of Experimental Physics, University Of Gdańsk | Poland | dorota.wejer@ug.edu.pl |
| Jou-Mei | Wen | Accompanying | Taiwan | cwshih@math.nctu.edu.tw |
| Niels | Wessel | Department of Physics, Humboldt-Universitaet Zu Berlin | Germany | wessel@physik.hu-berlin.de |
| Pawel | Winklewski | Institute of Human Physiology, Medical University Of Gdańsk | Poland | pawelwinklewski@gumed.edu.pl |
| Jan | Żebrowski | Faculty of Physics, Warsaw University of Technology | Poland | zebra@if.pw.edu.pl |
| Ilias | Zilakos | Division of Physiology, University Of Oslo | Norway | izilakos@gmail.com |
| Sebastian | Żurek | Institute of Physics, University of Zielona Gora | Poland | s.zurek@if.uz.zgora.pl |

With special thanks to our sponsors

Faculty of Science
& Technology

Lancaster
University



IOPscience

EPJ.org



your physics journal



moor instruments

innovation in microvascular assessment



CAMBRIDGE RESEARCH SYSTEMS

Section Editors-in-Chief

Interdisciplinary Topics:



Włodzimierz Klonowski
Polish Academy of Sciences

Physics of Biological Systems and Their Interactions:



Aneta Stefanovska
University of Lancaster

Physics of Cancer and Oncology:



Jack Tuszynski
University of Alberta

Systems Biology and Dynamical Diseases:

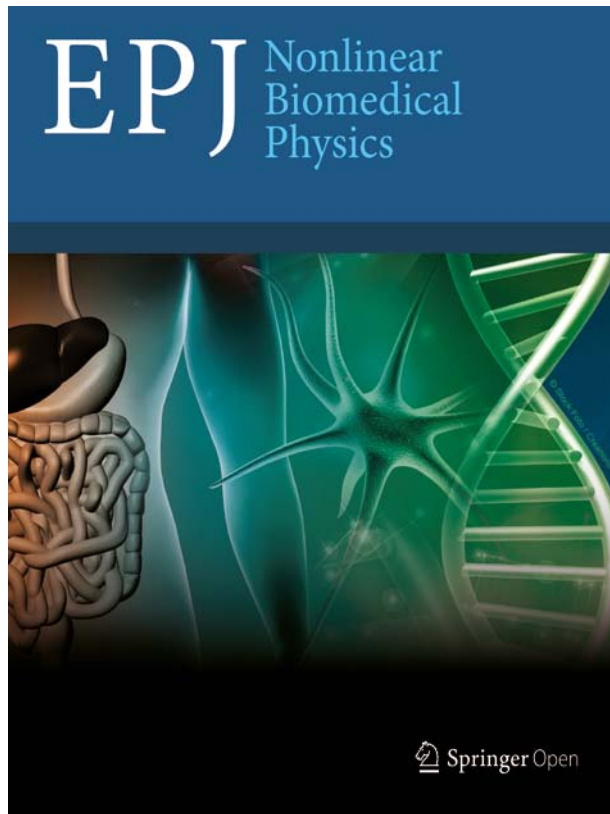


Marc-Thorsten Hütt
Jacobs University

Systems Neurosciences and Integrative Brain Research:



Viktor Jirsa
University of Aix-Marseille



- **Open Access**
- **Peer-reviewed**
- **Research Articles, Letters, Reviews, Commentaries, Topical Issues**

EPJ Nonlinear Biomedical Physics is a peer-reviewed, open access journal promoting the field of quantitative biomedical complexity science.

It is specifically devoted to the dissemination of knowledge about the applications of nonlinear dynamics and complexity-inspired integrative systems science, to the quantitative modeling and understanding of how structure, function and/or dysfunctions and diseases, often concomitantly, emerge in complex biomedical matter, systems and processes.

The focus will be on the application-driven development of theoretical, experimental and computational techniques. This includes the development of relevant methodologies, instrumentation, and related advanced technology. *EPJ Nonlinear Biomedical Physics* publishes in sections based on subject area.

Authors may choose at submission one of the following sections:

Interdisciplinary Topics

This section is devoted to the exploration of a number of relevant topics including but not limited to psychophysics, fractals in medicine, methods of physical therapy, structure-function relationships, network topology, dynamics of anesthesia, nonlinear signal and image analysis, anatomopathology and virtual patient simulations.

Physics of Biological Systems and Their Interactions

This section is concerned with the fundamental physical principles that

Editorial Board

Interdisciplinary Topics

Irena Cosic
 Luigi Fortuna
 Franco Orsucci
 Sadasivan Puthusserypady
 Michael Small
 Jiri Wackermann

Physics of Biological Systems and Their Interactions

Plamen Ivanov
 Christophe Letellier
 Alberto Porta
 M Carmen Romano
 Michael Rosenblum
 Niels Wessel
 Jan J. Zebrowski

Physics of Cancer and Oncology

Heiko Enderling
 Robert A. Gatenby
 Michael R. King
 Luigi Preziosi

Systems Biology and Dynamical Diseases

Oliver Ebenhoeh
 Thilo Gross
 Annick Lesne
 Nikolaus Sonnenschein

Systems Neurosciences and Integrative Brain Research

Ingo Bojak
 Andreas Daffertshofer
 Gustavo Deco
 Stefan Kiebel
 Lilianne R. Mujica-Parodi
 John Terry
 Wilson Truccolo
 Krasimira Tsaneva-Atanasova

Scientific Advisory Committee

Kazuyuki Aihara, Tokyo
 Eshel Ben-Jacob, Tel-Aviv
 Wlodzislaw Duch, Singapore
 Jürgen Kurths, Potsdam
 Michael Mackey, Montreal
 Peter V. E. McClintock, Lancaster
 Péter Érdi, Kalamazoo & Budapest

govern functional units of living systems (such as organs and organ systems) at intermediate and macroscopic scales. Emphasis is on the investigation of biological transport systems and networks (such as e.g. the cardiovascular system) and their couplings to similar or other type of functional units (e.g. biological information processing systems). In contrast to the goal of efficient mathematical modelling in systems biology, the focus of this section is on the search for basic principles and operating mechanisms.

Physics of Cancer and Oncology

Cancer research is a multidisciplinary effort in which physical methods and concepts have been playing an increasingly prominent role. In this section all aspects of experimental, computational and theoretical physics with applications to cancer research and oncology in general will be given a forum for the dissemination of latest results. Areas of research of particular interest include: quantitative models of tumor initiation and progression, mechanical and electrical properties of cancer cells, ionizing radiation effects on sub-cellular structures, nanotechnology applications in oncology, tumor imaging techniques, pharmacokinetics of chemotherapeutic agents, models of metabolic and genomic instabilities, evolutionary models of cancer.

Systems Biology and Dynamical Diseases

In this section, methods and results from systems biology, their underlying physical principles and their potential medical applications are explored. Relevant topics include (but are not limited to) the analysis of system-wide data, modeling strategies in systems biology, metabolic diseases, mathematical models of biological systems or of disease dynamics, physical insights into biological systems or into disease dynamics, methods from nonlinear dynamics applied to topics in systems biology.

Systems Neurosciences and Integrative Brain Research

The section is devoted to the development, exploration and application of integrative concepts in systems neuroscience and nonlinear brain dynamics. Its scope ranges from theoretical, experimental, informatics to methodological research.

For more information and to submit your manuscript, please visit epjnonlinearbiomedphys.com

Co-published by Società Italiana di Fisica, EDP Sciences and Springer.

